Geological Interpretation of Aeromagnetic Data

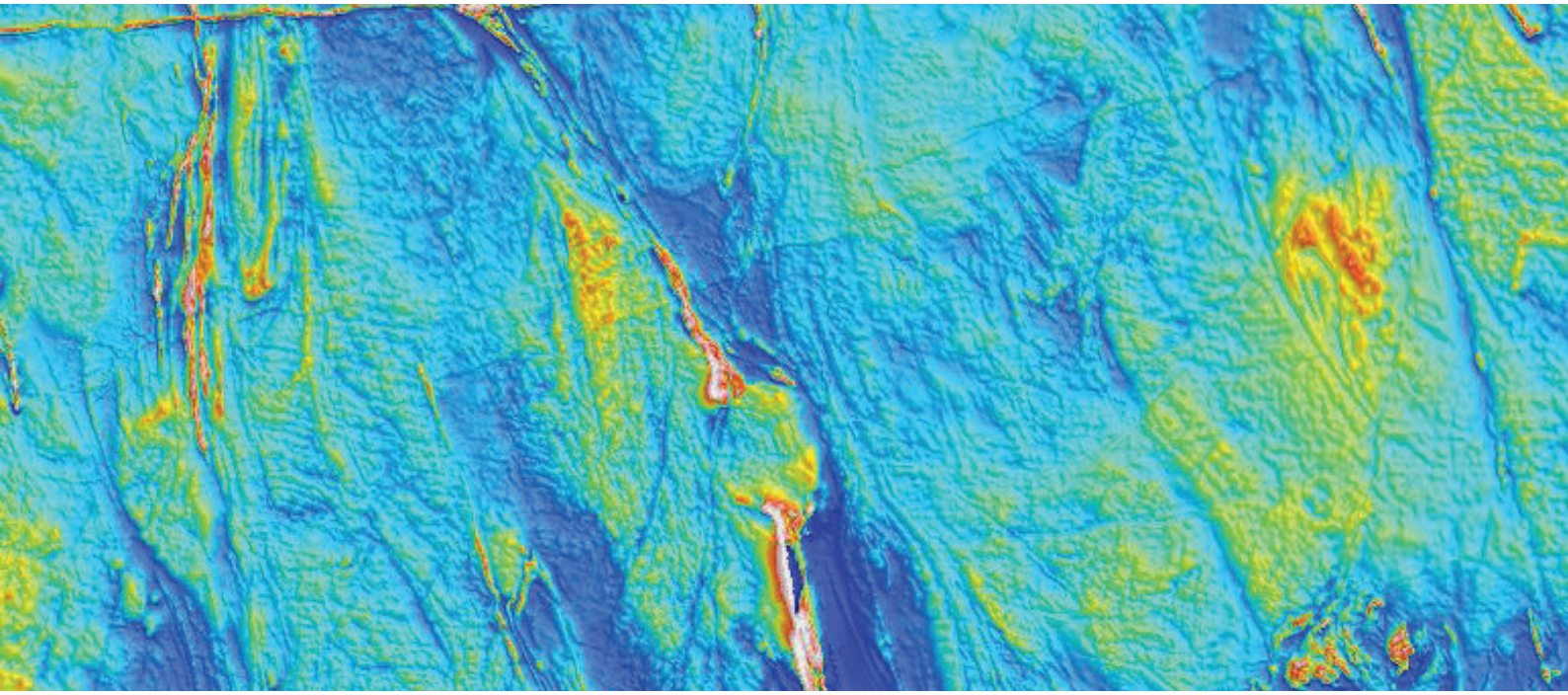

David J. Isles and Leigh R. Rankin

SEG

CSIRO PUBLISHING

National Library of Australia Cataloguing-in-Publication entry

Isles, D. J., author.

Geological interpretation of aeromagnetic data / by
David J. Isles and Leigh R. Rankin.

9780643098091 (CD-ROM)

Includes bibliographical references.

Aeromagnetic prospecting – Data processing.

Rankin, L. R. (Leigh Ronald), 1959– author.

622.153

Published by
Australian Society of Exploration Geophysicists
PO Box 8463
Perth Business Centre WA 6849
Australia

Telephone: +61 8 9427 0838
Fax: +61 8 9427 0839
Email: aseg@casm.com.au
Website: http://www.aseg.org.au

Produced by
CSIRO PUBLISHING
150 Oxford Street (PO Box 1139)
Collingwood VIC 3066
Australia

Telephone: +61 3 9662 7666
Local call: 1300 788 000 (Australia only)
Fax: +61 3 9662 7555
Email: publishing.sales@csiro.au
Website: www.publish.csiro.au

Front cover: Aeromagnetic image of the Kalgoorlie Region in Western Australia. The image is approximately 150 km × 60 km and comprises 200 m line spacing data flown as 'multiclient' surveys by Aerodata Holdings and World Geoscience Corporation between 1986 and 1995. The data was further marketed by Fugro Airborne Surveys after their acquisition of WGC and in 2012 it became freely available through the Geological Survey of WA and Geoscience Australia. The course on which this book is based was founded using early surveys from this data base.

Set in 11/14 Adobe Minion Pro and ITC Stone Sans
Edited by Adrienne de Kretser, Righting Writing
Cover and text design by James Kelly
Typeset by diacriTech, Chennai, India

Contents

Preface – why this book is for you

This book aims to help you to extract maximum value from aeromagnetic survey data. It shows how to integrate these data with geological data to build an interpretation that matches the objectives of your project. The book is as much for geologists as geophysicists and is written by two consulting geoscientists who deal with complex geophysical and geological interpretation problems in their day-to-day work.

We have prepared the book in response to the frequently cursory analysis of high-quality aeromagnetic data, usually caused by the absence of geologists' active participation in the integration and interpretation process. We have seen the value of many superb datasets seriously eroded by under-use. Surveys costing $500 000 or more sometimes attract only a handful of days of interpreter time for assessment. We believe that aeromagnetic data contain a wealth of geological information that may be overlooked if the analysis is constrained to the 'geophysical' aspects and confined to geoscientists with predominantly geophysical training and a predominant focus on the physics and mathematics of the data. The examples in this book show the level of geological detail and consequent exploration value that can be gained from adequate, well-focused time spent analysing aeromagnetic data.

Our backgrounds exemplify our approach. Dave Isles is a geophysicist by training who has spent most of his 40-year career using aeromagnetic data (and many other geophysical tools) to facilitate mineral exploration programs. His grasp of geology has grown through the need to fully understand the geological environment of each new exploration project. Leigh Rankin is a geological mapper with specialist structural skills. He began using aeromagnetic data in South Australia during the 1980s when he discovered that just beneath the vast expanses of sand dunes, swamps and alluvial plains, there were rocks with readily measurable magnetisation. Beneath the paddocks of wheat and sheep, these rocks could be mapped both individually and collectively by using aeromagnetic data, thus aiding the assembly of geological interpretations at all scales. Our experience underlies the focus of this book.

We emphasise that the main ingredients in a high-quality interpretation are astute use of the geoscientist's brain and adequate time, not only to digest diverse clusters of data, but to integrate these into a working map that drives our project forward. The rewards for this (usually modest) effort and time can be substantial – a resource discovery, a quantum leap in understanding of local geological evolution or a new direction and momentum in exploration, to name a few.

The book has evolved from a short course created to address the demand from exploration geologists who, faced with an explosion of high-resolution aeromagnetic data in the Australian gold and base-metal provinces in the early 1990s, recognised the need to take ownership of the interpretation function on their project areas. Simply put, there were too few suitably experienced geoscientists then, to assist with the exciting task of integrating this wealth of new data into exploration programs. Hence the book has its roots mainly in gold exploration in Australia (as reflected in much of the imagery used in the examples), but the authors have since expanded the methodology to embrace the interpretation of aeromagnetic surveys in a wide range of 'hard-rock' and 'soft-rock' applications. We believe that the methodology is appropriate for mineral and hydrocarbon explorers, as well as groundwater explorers, and in fact all those involved in producing and using integrated geoscientific maps.

Integration is the key word for our approach; not only of geological and aeromagnetic data, but also radiometric, satellite imagery, aerial photo, gravity, electromagnetic and of course seismic reflection data where these are accessible for the project. Because of the diverse and consistent range of geological information it provides, our prime focus in this book is on 'aeromagnetics'.[1] We stress, however, that all available data should be considered when compiling a working interpretation. The cornerstones of the integration process

1 The colloquial abbreviation 'aeromagnetics' is commonly used in reference to aeromagnetic survey data, as are 'aeromag', 'airmag' and occasionally 'AMAG'. In this book we stick to the accepted industry term 'aeromagnetic data'.

are formed by the wonderful GIS, imaging and modelling tools at our disposal for enhancing and cross-referencing datasets, but the diligent and experienced human brain is the tool that shapes the end result and determines its quality. The tasks of observation, integration and interpretation that we describe in this book involve mostly simple and qualitative steps, using much more geological reasoning than heavy-duty physical or numerical analysis.

We encourage you to 'jump in at the deep end' – to gather, observe and consider, and begin to experience the adventures that the addition of aeromagnetic data to your project will initiate.

Acknowledgements

We warmly thank and acknowledge Fugro Airborne Surveys and one of its predecessor companies, World Geoscience Corporation, which have provided data and ongoing support for this book and the short course on which the book is based. Alasdair Cooke and Pat Cunneen (both formerly of World Geoscience Corporation) provided the inspiration that led to the development of the course. Rick Valenta and Helen Anderson have made significant contributions to the methodology presented in this book and have continued to provide assistance with new data and ideas.

We sincerely thank David H. Moore who engaged with the authors at an early stage of this project and provided astute guidance on the structure and content of the book as well as an enormous amount of time in the editorial process. We believe that David's input has greatly helped to make the book readily usable by aspiring interpreters.

Zhiqun Shi (FrOG Tech) and Ian Campbell (Austerra) conducted specialist modelling and data processing for Chapters 10 and 13. Their willing and substantial contribution in time and expertise is gratefully acknowledged.

Phil Schmidt and Michael Asten actively promoted ASEG's involvement in the project and provided considerable encouragement during its long gestation period. Phil is also thanked for editorial guidance and technical guidance on magnetisation matters. The late Peter Elliott, while President of ASEG, initiated its involvement in the project. Koya Suto and Phil Harman are also thanked for mustering and shoring up ASEG's support for the project.

V.J.S. (Tien) Grauch, Alan Reid, Rosemary Hegarty, Cathy Norman and Tony D'Orazio gave invaluable input to the content of the book. Tien and Alan, as SEG's reviewers, have been particularly helpful in smoothing many of the 'rough edges' in early drafts and adding important aspects of their own experience to the content.

We thank Southern Geoscience Consultants for contributing the re-processing of two of our main teaching datasets and producing modern imaging products.

Many companies and organisations have allowed us to present their data in the book. These are acknowledged in the course of the book, but we take this opportunity to reiterate our thanks to:

Lundin Mining,(Dick West, Ciara Talbot and Andy Bowden), Roc Oil, Normandy Mining (Mike Sexton), GPX Surveys (Greg Reudavey, Katherine McKenna), UTS Geophysics (Micheal Lees, David Abbott), Barrick Gold (Barry Bourne and Lee Sampson), Newmont Mining (Terry Hoschke), Rio Tinto Exploration (Stephen MacIntosh and Theo Aravanis), Anne Tomlinson (nee Morrell), Duncan and Sheila Cowan, and Steve Webster. We also thank David Pratt, Clive Foss and Dean Hillan for valuable technical guidance on modelling and magnetisation matters, and for permission to use illustrations from their work in the book.

Most of the data used in this book can now be sourced free, on-line from the Geoscience Australia 'GADDS' website (http://www.geoscience.gov.au/gadds). The ready accessibility of these data has facilitated a much wider range of examples than would have otherwise been possible, and we gratefully acknowledge Geoscience Australia and the State Geological Surveys in Western Australia, South Australia, Victoria, Tasmania, New South Wales, Queensland and the Northern Territory for their cooperative efforts in assembling this amazing data resource and for permission to reproduce their data in this book. In this regard, we must also acknowledge the critical contribution of Dr Ross Fardon who, in several guises, not only drove the acquisition and advanced processing of detailed aeromagnetic and radiometric data by many governments, but also rekindled the strategy of making such data freely available to all interested users. This strategy has been at the core of many major resource discoveries.

Our respective partners, Heather Isles and Cate Newton, not only gave unquestioning support and showed inestimable patience, but also provided considerable assistance in the preparation and editing of the manuscript.

Cartography and GIS services were provided by Bill Hitch and Robert Nicol.

Finally, we thank our 'guru' Prof. David Boyd, who was mentor in matters aeromagnetic to both authors during their student days at Adelaide University and who has been a source of inspiration ever since.

1 Introduction

1.1 WHAT CAN WE *DO* WITH AEROMAGNETIC SURVEY DATA?

Finding magnetic ore bodies is not the only use for aeromagnetic surveys. It is, however, a good place to start. Without the extensive coverage of aeromagnetic surveys, the world-class Olympic Dam and Cannington mines would not have been found and the same applies to many ore bodies worldwide. Aeromagnetic surveys extend our vision of geology way beyond the realm of surface mapping and drilling. They allow us to 'see' key aspects of the geology through much of the Earth's crust (including the surface) and provide a cornerstone for building 3-dimensional geological models. The geological environments where aeromagnetic data add value are broad, to the point where many governments worldwide either have, or are planning to have, complete coverage of their countries with semi-detailed (500 m spacing or better) surveys. Although well established in and best known for its contributions to mineral exploration, aeromagnetic surveying had its origins in oil exploration, and is now making a 'comeback' in this domain as measurement sensitivities and the understanding of low-order magnetisation in sediments allow us to map in environments previously considered to be 'non-magnetic'. This has greatly enhanced our ability to integrate aeromagnetic and seismic data.

By far the largest modern use of aeromagnetic surveys is in routine government-sponsored mapping. The extraordinary return on investment in such surveys in Canada and Australia, dating from the 1950s, has inspired many other countries, especially those in Africa, to gather quality data from which a broad range of Earth resource projects can be instigated or accelerated (e.g. Hutchins *et al.* 2007). Boyd and Isles (2007) outline both the progress of the aeromagnetic method and the range of applications which give it a unique status in the armoury of the explorer and the geological mapper.

1.2 OBJECTIVE

The main aim of this book is to enable users of aeromagnetic survey data to integrate these data with field geological information. The visual (and subsequent laboratory) observations made by geologists in the field can be greatly enhanced and extended with the addition of information from the 'eye' of the magnetometer. It is important to recognise that aeromagnetic data maps a key aspect of geology: the variation (potentially in 3-D) of magnetic minerals. These data are integral to the understanding of the geology in many environments and authors such as Grant (1985a) and Ishihara (1977) have proposed geological classification schemes based on the opaque mineralogy which can be broadly inferred using aeromagnetic surveys. This book presents a methodology for recording observations made from aeromagnetic imagery and relating these to conventional geological mapping data to produce integrated solid geology maps and 3-dimensional interpretations.

1.3 GEOLOGICAL TRAINING IS THE MOST IMPORTANT ATTRIBUTE FOR AN AEROMAGNETIC INTERPRETER

Our book is based on the premise that interpreters should be the geoscientists most familiar with the geology of the project. This parallels the practice in seismic interpretation where interpreters need to have the best possible knowledge of the local geology and the 'play styles' – and may equally be geologists or geophysicists by training. In times past, many geologists leading mapping and exploration teams were reluctant to take personal responsibility for the integration of aeromagnetic data into projects, and preferred to engage specialist geophysicists (who frequently had little knowledge of the local geological environment) to perform this function. We contend that this often limits the quality and value of the end result, and that a better way to proceed is to have the on-site project geoscientists conduct the major phases of integration and interpretation.

The parallels between aeromagnetic interpretation and geological mapping are both striking and logical. The field geologist's observations of rock type, strike, dip etc. have equivalents in our work with aeromagnetic data. The assembly of many and varied (but often incomplete) observations to form an interpretive geological map is exactly the methodology required in aeromagnetic interpretation. While there is no substitute for the spectrum of information that can be gained by a skilled geologist mapping on an outcrop, the geologist's observations are usually limited by access to fresh rock (either due to cover or physical inaccessibility) resulting in datasets characterised by a 'feast or famine' of information. We cannot hope to gain the same detailed information from aeromagnetic data, but the fact that we are mapping a single geological parameter, the distribution of magnetic minerals, greatly simplifies the task. The value of integrating geological mapping and aeromagnetic survey data is plainly apparent when we consider the role that magnetic minerals play in mineralogy and in the alteration and mineralisation processes. The fact that aeromagnetic surveys allow us to see and map these minerals in 3-D makes them a powerful geological mapping tool. A particular strength of aeromagnetic surveys is that we can and do cover very large areas with uniform (and often highly detailed) sampling. This can be done rapidly and cost-effectively, adding greatly to the geologist's 'feast' of surface information and providing key information in areas of 'famine'.

Despite the proliferation of extensive (and often government-sponsored) aeromagnetic surveys in recent years, we find that the integration and interpretation of these surveys with available geological data is typically cursory. It is the authors' experience that full or even fair value from aeromagnetic surveys is rarely achieved because too little time and effort is allocated to the integration and interpretation process. We believe that this situation can be readily rectified by developing observation, integration and interpretation skills in the geoscientists most closely involved at the coal-face of mapping or exploration. Hence, this book is designed to provide a practical step-by-step guide for non-specialists to integrate aeromagnetic data with geology.

1.4 HOW TO USE THIS BOOK

The cornerstone of this book is a set of worked examples of 'real-life' aeromagnetic interpretations compiled by the authors for their established short course workshop (Isles and Rankin 2011). Three quite different geological environments are represented in these examples and the work is presented at both regional and detailed scales. We encourage readers to follow the steps described in the worked examples and apply these to aeromagnetic survey data that is pertinent to their projects.

Convention dictates that we present a substantial body of background information and essential theory before getting to the practical descriptions in the worked examples. While a firm understanding of most of this information is important for the interpretation process, new interpreters may find it more effective to 'jump in the deep end' and absorb the worked examples at an early stage, rather than wade systematically through the 'shallow end' containing the less exciting technical basis for interpretation. The theory chapters provide the new interpreter with ample reference material to support their growth in experience with aeromagnetic projects in most geological environments, but they may not be the best place to start the highly stimulating journey.

2 Basic physics

2.1 THE EARTH'S MAGNETIC FIELD, INDUCTION AND THE CURIE POINT

The Earth's magnetic field, sourced in its core, effectively magnetises susceptible rocks in the Earth's crust. While there is a range of processes by which this can occur, the phenomenon of magnetic induction is by far the most important, accounting for the great majority of magnetic variations evident in aeromagnetic surveys.

Magnetic behaviour of rocks at laboratory scale is complex and, for the most part, these complexities need not be addressed when undertaking basic aeromagnetic interpretation. The physics and chemistry of magnetisation in rocks is outlined in Chapter 3. In this chapter we emphasise the relationships between magnetic rock bodies and the magnetic anomalies we observe in aeromagnetic surveys.

The Earth's magnetic field, the Curie Point of rocks and the phenomenon of magnetic induction are the starting point for these discussions.

The Earth's magnetic field behaves remarkably like a bar magnet located in the Earth's core (Fig. 2.1). It is dipolar, having a north pole in the Arctic and a south pole in the Antarctic. Notably the magnetic poles do not coincide with the geographic poles and they are not stationary. The magnetic poles are where the field orientation is vertical and its strength is close to its maximum. The strength and orientation of the field vary relatively smoothly across the globe, reaching minimum strength and having a horizontal orientation in equatorial regions. The 'magnetic equator' is the line where the Earth's field inclination changes from 'upward-pointing' to 'downward-pointing'. Like the poles, the magnetic equator is not coincident with the geographic equator; Figure 2.2 shows how the variations in field inclination deviate markedly from geographic latitude.

The magnetic field definitions of north, south, upward and downward are scientific conventions; the key point for the aeromagnetic interpreter is that magnetic anomalies due to rock bodies will vary according to their location on the globe because the Earth's field is the principal cause of magnetisation in the crust.

Magnetic susceptibility is a physical property of rocks which allows them to be magnetised by the Earth's field. This process is called **magnetic induction**. The magnetic field induced in the rock is parallel to the Earth's field and its strength is proportional to the local strength of the Earth's field. Figure 2.3 shows how the vector equation $\underline{\mathbf{M}} = \boldsymbol{k}\underline{\mathbf{H}}$ describes this situation. The magnetic susceptibility ($\boldsymbol{k}$) is readily measurable with a simple hand-held device and, importantly, is usually a reliable indicator of the magnetic mineral content in the rock.

The **Curie Point** of a rock is a temperature/pressure point across which the rock's magnetic behaviour changes. Being largely driven by temperature, the Curie Point surface within the Earth's crust is usually described as an isotherm; this occurs at depths of tens of kilometres in the crust where temperatures around 550°C prevail. At temperatures greater than the Curie Point rocks lose their magnetic properties; when cooler than the Curie Point they become susceptible and may also attain permanent 'remanent' magnetisation. In areas of very high heat flow the Curie Point may occur at depths of less than 10 km, while under normal geothermal gradients it may be as deep as 40 km.

The magnetic variations we seek to observe in aeromagnetic surveys are therefore sourced exclusively from the middle and upper crust, and are controlled by the local strength and direction of the Earth's field as well as the amount of magnetic mineral in the rocks. There are many intriguing aspects of the Earth's field, magnetic induction and the Curie Point which have little impact on the day-to-day interpretation of aeromagnetic surveys. The reader is referred to the following references for more robust descriptions of the physics of magnetic induction and the detailed nature of the Earth's magnetic field:

a) Reeves (2005) succinctly covers much of the nitty-gritty material on the physics of the aeromagnetic method and the acquisition and processing of aeromagnetic data;
b) Grant and West (1965) is a geophysical text which provides a solid grounding on the theory behind the aeromagnetic method;
c) Merrill and McElhinny (1983) does not deal with aeromagnetic data but gives a thorough outline of the Earth's magnetic field;
d) Moskowitz (1991) is a useful rapid guide to rock magnetism;
e) Shive (1986) outlines the basic entities in rock magnetism studies and their preferred SI units.

We address the crucial topic of magnetisation in rocks in some detail in Chapter 3.

2.1.1 What do we measure?

Aeromagnetic surveys measure the (scalar) strength of the local Earth's field. As outlined in Reeves (2005) (see Section 1.5), this measurement is a combination of the Earth's core field (documented worldwide as the International Geomagnetic Reference Field, IGRF) and the field induced in crustal rocks. We call this measurement the Total Magnetic Intensity (TMI), but readers should be aware that the TMI images that are the basic product of an aeromagnetic survey are usually the difference between the measured field and the IGRF. This residual field is often referred to as the 'IGRF Residual' and in some cases (particularly crustal scale images) the 'Magnetic Anomaly'. In this book we follow the commonly used, if not strictly technically correct abbreviation, TMI because of its wide use in the airborne geophysical industry.

The vector components of the field are often measured on board the aircraft but are rarely used as survey products. The nanoTesla (nT) is the unit of field strength used and, as shown in Figure 2.1, the strength varies from around 70 000 nT near the poles to around 25 000 nT in equatorial regions. Modern surveys should readily detect and define geological signals of less than 0.25 nT and, where special attention is given to low noise acquisition, minimum signal levels of 0.05 nT are achievable. Variations in the field due to magnetic rocks are commonly in the order of thousands of nT and occasionally (over large, massive magnetite bodies) may be as large as 50 000 nT.

2.2 MAGNETIC ROCK BODIES

The variations in magnetisation through a geological formation and the geometry of the formation are frequently complex. Our task as aeromagnetic interpreters is to decipher this geometry (and the magnetisation variations) as best we can from remote TMI measurements. The initial geophysical approach is to consider the TMI patterns as being caused by simple geometric shapes ('models') which approximate the shape of the geological formation, and to assume the magnetisation to be uniform throughout this model. We refer to these models as magnetic rock bodies and, despite their simplicity, they provide remarkably useful insights into the actual geology. In this chapter we use a range of model studies to illustrate basic physical concepts.

A recurring model (**'pblock'**) will be a rectangular prism 800 m long ('strike length'), 200 m wide and 500 m in vertical extent. The magnetic susceptibility is 0.03 SI, which roughly equates to 1% 'magnetite' (see Chapter 3). This model magnetic rock body might represent a deformed volcanic flow, a zone of alteration in a fault complex or a small intrusive body. For interpreters with predominantly geological training it is important to appreciate that these simple models provide an effective means of estimating depths, shapes, sizes, orientations and magnetic properties of actual subsurface geological formations. They are not designed to literally represent the geological formations themselves. Interested readers can (freely) download the pblock software from www.geoss.com.au.

2.2.1 Dipoles and magnetic field asymmetries

Like the Earth's inducing field, the magnetic fields in rock bodies will be dipolar. Hence, the magnetic field measured at the surface across a buried rock body will have both positive and negative parts. The degree of asymmetry in this measured profile will depend on the orientation of the body with respect to the local Earth's field and, as mentioned above, the orientation of the Earth's field. As illustrated in Figure 2.3, the same rock body will yield a different magnetic field profile at different magnetic field inclinations. Figure 2.4 shows how the profile shape also changes when we change the strike direction of the body. We will see that the asymmetry evident in the profile is as much a function of the Earth's field inclination as it is of the rock body's orientation. It is critical to recognise that profile asymmetry rarely has a simple relationship to the dip and plunge of rock bodies, and we should expect that every TMI 'high' will be accompanied by a 'low' in some form (see Fig. 2.4). While there are numerical processes which simplify this situation and transform the measured data into a form where the magnetic field asymmetries more closely reflect the real geological dips and plunges, it is important to be aware of, and be prepared to deal with, the inherent dipolar nature of the measured magnetic field.

2.2.2 Magnetic rock body location

The TMI anomaly profile caused by a rock body will always be wider than the body itself. Where the profile is roughly symmetrical (as is often the case), **a simple measure of the width of the anomaly is the distance between the maximum gradients of the field profile**. As illustrated in Figures 2.5 and 2.6, the maximum gradient position can be located from profiles, contour plans or images, and the (plan view) location of the body causing the anomaly can be assumed to lie within the bounds of the maximum gradient position. More commonly, where anomalies have positive and negative components, the body location is a little harder to gauge. Figure 2.7 shows how the positive and negative components 'migrate' away from the body location, especially in regions where the Earth's field inclination is low (equatorial regions). We can safely infer that the body lies within the confines of the combined magnetic high and low, but this is not a precise guide to the location of the upper edges of the body. This situation worsens as the depth to the top of the body increases. In the simple case of the symmetrical anomaly (Fig. 2.5), the maximum gradient locus, while still enclosing the body position, becomes increasingly broad.

2.2.3 Depth effects

As a magnetic rock body becomes deeper (and further away from our magnetometer sensor) the observed magnetic field diminishes, as does the clarity with which we are able to delineate the shape of the body. The lengths of the magnetic gradients near the edges of the body provide a rough measure of this clarity and also a means of estimating depth to the 'top' or 'nearest edge' of a magnetic rock body. Figure 2.5 shows that the shape of the magnetic anomaly approximates the shape of the rock body where the depth is much smaller than the longest lateral dimension, but the anomaly shape becomes increasingly blurred as the body becomes deeper. While the body still lies within the maximum gradient locus, our ability to resolve the shape diminishes rapidly when the depth to top approaches the body's longest lateral dimension. In the extreme cases (Fig. 2.6), the body shape is sharply outlined when the depth is a small fraction of the lateral dimensions, but when the depth to top is the same as the longest dimension, the anomaly becomes an equi-dimensional 'blob'.

Depth estimation

Simple graphical constructions and rules of thumb based on careful observation of the magnetic gradients can rapidly provide approximate but very useful depth information. We stress that these approximations do not replace the quantitative modelling tools that we discuss in Chapter 8, but they do provide a reliable means of obtaining 'ball-park' depths during the qualitative process of observing and assessing aeromagnetic imagery.

The first step in estimating depth is to consider the lateral dimensions of the anomaly. Where the anomaly is much longer in one direction than the other, we can regard the magnetic rock body as 2-dimensional (2-D); this can greatly simplify the interpretation process. The depth to the top of simple body shapes can be estimated using the 'straight slope distance' (ss), as shown in Figures 2.8 and 2.10. **For 2-D bodies, ss is approximately equal to the depth to top**. For anomalies which appear equi-dimensional, a multiplier must be applied to the measured ss to estimate the depth to top. As shown in Figure 2.10, where the lateral anomaly dimensions are of the same order as the ss distance and a large vertical extent is inferred for the magnetic source (e.g. a steep-sided, pipe-like body), the depth to top will be ~2 × ss. For bodies with lateral dimensions equal to or smaller than ss and limited depth extent, the depth to top will be around 3 × ss. Figure 2.10 also shows the changing rate at which anomaly amplitude 'falls off' as the different body shapes become deeper. Note particularly that for 2-D bodies the fall-off rate is linear, so doubling the depth will halve the anomaly amplitude.

A second graphical construction is the 'anomaly width' also shown in Figures 2.9 and 2.10. This is generally less reliable as an estimator of depth to top than ss, particularly where anomalies are strongly asymmetric, but it can provide a useful check. A very useful aspect of this construction is that the full-width distance $x^{1/2}$ is the maximum possible depth to top irrespective of the shape of the body. For the mathematically inclined, $x^{1/2}$ is exactly the depth to a point dipole (Grant and West 1965).

There are numerous powerful quantitative schemes for modelling magnetic rock bodies and for automatically estimating depth to top (see Chapter 8). These have an important role to play where maximum precision and confidence are sought on depth and shape parameters for particular magnetic bodies of interest. However, in the general flow of aeromagnetic interpretation the simple, rapid graphical methods enable the user to obtain very useful ball-park (around ± 25%) estimates of depth, and in many cases these estimates are more than sufficient to constrain the interpretation.

2.2.4 Dip and plunge effects

As stressed above, shape of the magnetic profile over a rock body is as much a function of the local Earth's field inclination (I) as the shape and orientation of the body itself. Our simple pblock model illustrates this (Fig. 2.11). We observe that even at moderate field inclinations (I = –50°) the anomaly shape does not reliably reflect the shape and orientation of the model body. However, in the same model set calculated at polar inclinations (Fig. 2.12, calculated for I = –90°), the asymmetry in the anomaly is a direct reflection of the dip in all cases. This is because the Earth's magnetising field is vertical and the relationship between I and the body orientation is simple and does not change with changing strike direction.

The plunging fold model in Figure 2.13, which uses material from Jessell's *Atlas of Structural Geophysics* (Jessell 2002), provides another clear illustration of the complexities of anomaly shape as strike, dip and plunge direction vary. The TMI model study is calculated at mid latitudes in the southern hemisphere (I = –50°). Readers who prefer to view northern hemisphere (I = 50°) variations may simply rotate Figure 2.13 by 180° and read north as up the page. Carefully considering the models from the northward plunge progressively through to the southward plunge we note the strong dipolar character of the magnetic anomalies and, with the exception of the north-plunging set, asymmetry in the contour patterns is a poor reflection of the subsurface geometry of the model. The south-plunging set shows limited asymmetry and if we assumed that this asymmetry reflected subsurface geometry we would infer a very steep plunge to the north!

The model is also calculated for I = –90° from northerly to southerly plunge at 45° intervals (Fig. 2.14). Note that the model anomalies are identical apart from their strike orientation and, more importantly, the anomaly asymmetries intuitively reflect the subsurface geometry of the fold sets. We will see in Chapter 5 that there is a mathematical transformation known as Reduction to the Pole (RTP) which allows us to present aeromagnetic

data measured from any field inclination as if it were measured at the poles. This largely removes the dipolar effects seen in TMI imagery and greatly assists our perception of the subsurface geometry of magnetic rock units.

The conclusion we reach from Figures 2.11 to 2.14 is that attempting to read dip and plunge from TMI imagery or profiles is not practicable; however, we will see that if we are able to apply the RTP transformation, the task is more readily achievable.

2.2.5 Anomaly superposition

At laboratory scale, interactions between strongly magnetic bodies can be complex but at geological field scales where aeromagnetic surveys are applied, such interactions can be ignored. (There may be mine scale situations involving massive ironstones where detailed modelling of such interactions has some application.) Our general assumption is that the individual magnetic field profiles from neighbouring magnetic rock bodies simply add up to form the total anomalous field. This is well illustrated in Figure 2.15, which shows the effect of near-surface magnetic basalts which overlie 1–2 km of non-magnetic sediments, these sediments in turn overlying an older magnetic basement. The additive nature of the fields allows us to read the different depths from the basalts and the basement via simple straight slope approximations.

2.2.6 Resolution

Several factors can create situations where it becomes impossible to resolve certain characteristics of magnetic rock bodies from magnetic surveys. The further the magnetic sensor is from the magnetic rock body, the poorer will be our ability to observe and resolve its shape. Empirical studies show that the distance from the magnetic sensor to the nearest edge of the magnetic rock body controls our ability to resolve shape. Where this distance is much less than body's lateral dimensions we are able to clearly resolve the shape (in plan view). Where it is much greater than the lateral dimensions, the body's magnetic anomaly appears as an equidimensional 'blob', as illustrated in the depth study (Figs 2.5 and 2.6). Recalling that the sensor to source distance can be estimated using the straight slope graphical construction (ss) and the maximum lateral dimensions of the body can be traced via the steepest gradient locations around the anomaly, we can gauge the degree to which the actual shape of the magnetic rock body can be resolved.

Two very important manifestations of this are illustrated in Figures 2.16, 2.17 and 2.18. The first situation concerns resolution of width on a long linear 2-D body. In practice, the minimum resolvable width is approximately the sensor to source distance. Where the body width is less than this, the anomaly shape is essentially unchanged and we can have situations where a narrower body with a stronger magnetisation will have the same magnetic anomaly as a wider body with a weaker magnetisation (Fig. 2.16). This is a common form of ambiguity in aeromagnetic interpretation, whereby different magnetic bodies produce essentially the same magnetic anomaly. In this case our sensor–source distance limits our determination of width and, without control on the width, we cannot determine the strength of magnetisation. We will discuss ambiguity further in the next section.

The second manifestation of resolution concerns our ability to recognise the presence of multiple bodies. Once again the source–sensor distance, which we can estimate using ss, is the critical factor. Empirical studies (e.g. Haederle 1992) show that where two bodies are much further apart than the source–sensor distance, they will be readily resolved as separate bodies. If they are closer together than the sensor–source distance their anomalies will merge into one and the anomaly profile will appear to be from a single source (Fig. 2.17). The model study in Figure 2.18 illustrates this and the real data example in Figure 2.19, compiled using upward continuation (see Chapter 5) to simulate increasing depth-to-source, clearly demonstrates the loss of spatial resolution with depth.

The issues of resolution illustrated above, impact heavily on the choice of flying height in aeromagnetic surveys, as we will see in Chapter 4.

2.2.7 Ambiguity

We have seen that as our magnetic sensor becomes more distant from the geology, anomaly shapes become increasingly vague and it becomes increasingly possible to interpret these shapes in a variety of ways. It is an inflexible rule that where the sensor–source distance is larger than the distances and dimensions we attribute to our magnetic rock body models, those distances and dimensions will be ambiguous.

The other important expression of ambiguity in aeromagnetic data concerns the estimation of dips and plunges. The equations for the dipping dyke (or layer), reproduced in Reeves (2005) after Reford and Sumner (1964), tell us that if we know the magnetisation direction and the strike direction of a 2-D tabular body we can unambiguously determine its dip from the anomaly profile. As we discover in the next chapter, the great majority of magnetic rock bodies have induced magnetisation which is aligned parallel to the Earth's field. The strength and direction of the Earth's field are quite accurately known and monitored from field and satellite observations. The strike direction of a body should be readily evident where the survey covers a sizeable area. Hence in most cases, estimation of a dip for this simple magnetic rock unit shape is achievable.

However, if the body's magnetisation direction is unknown, our ability to estimate dip from the magnetic profile vanishes. In essence we have two unknowns but only one equation relating them. This situation often occurs where the magnetisation of the body is dominated by remanence, self-demagnetisation or (more rarely) anisotropic susceptibility. In most aeromagnetic interpretations there will not be pre-existing rock property measurements alerting us to the presence of these less common forms of rock magnetisation. Hence any inferences we make on dip (irrespective of rock body shape) should be qualified by stating that induced magnetisation is assumed. Figure 2.20 clearly illustrates this concept of non-uniqueness. To reiterate, where the less common and more complex forms of rock magnetisation do occur, we **cannot determine dip** with any confidence unless we have adequate laboratory rock property measurements. These less common forms magnetisation will be discussed and illustrated at some length in the next chapter.

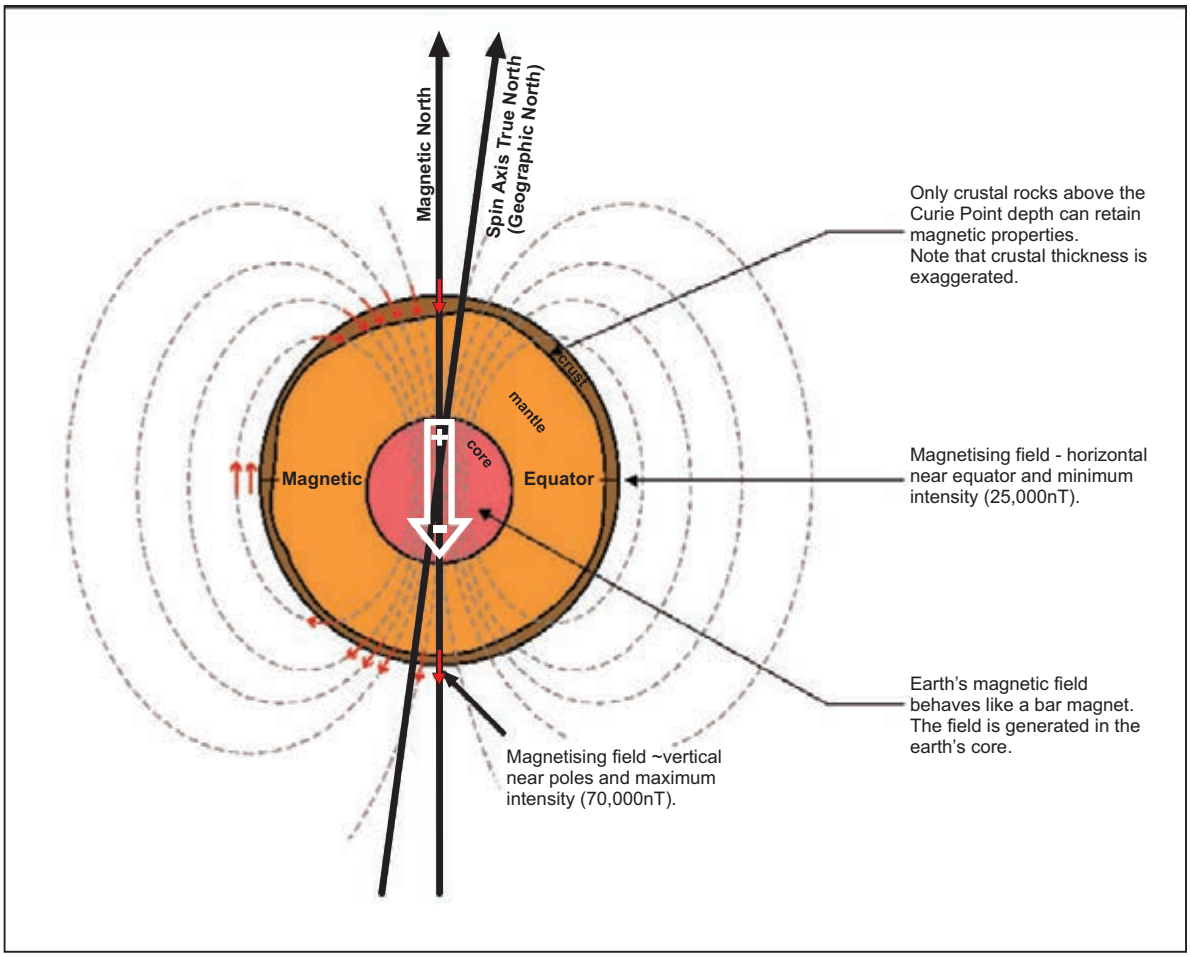

Figure 2.1: Schematic section through the Earth showing the main features of its magnetic field.

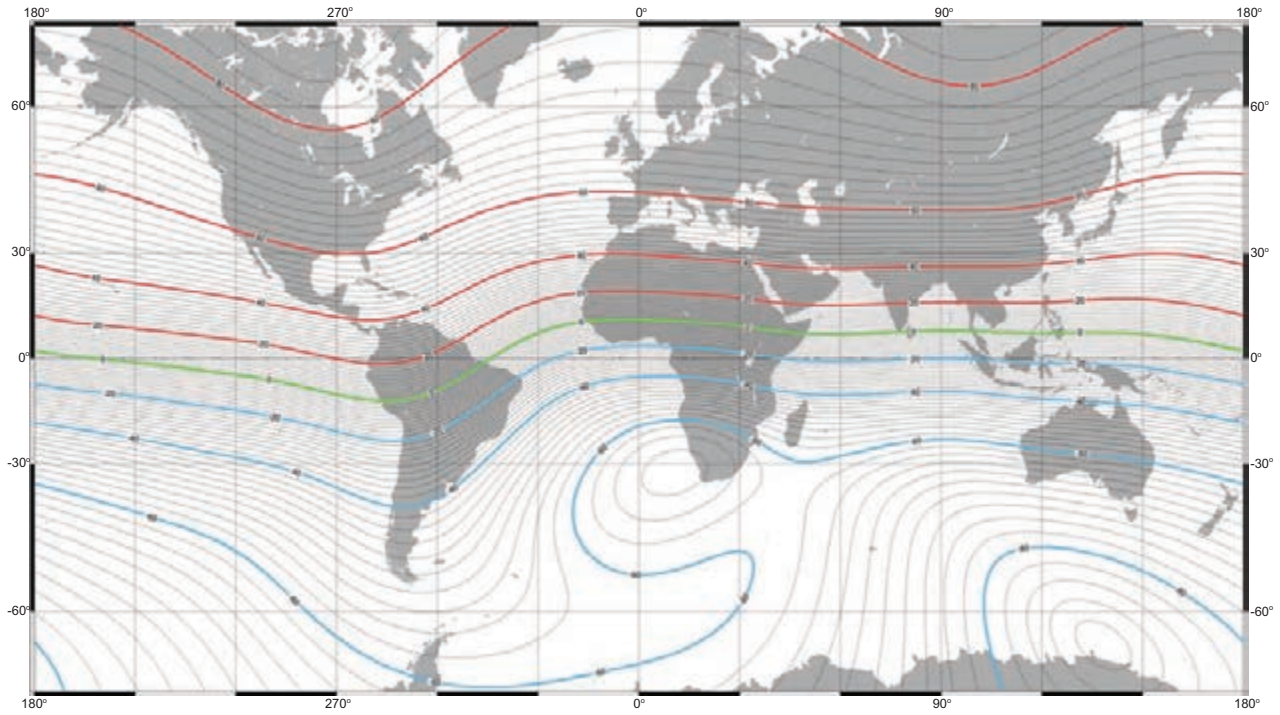

Figure 2.2: World Magnetic Model Epoch 2005.0, Main Field Inclination. Source NOAA/NGDC and CIRES, http://www.ngdc.noaa.gov/geomag. Note that all the latest WMM parameters can be sourced from this website.

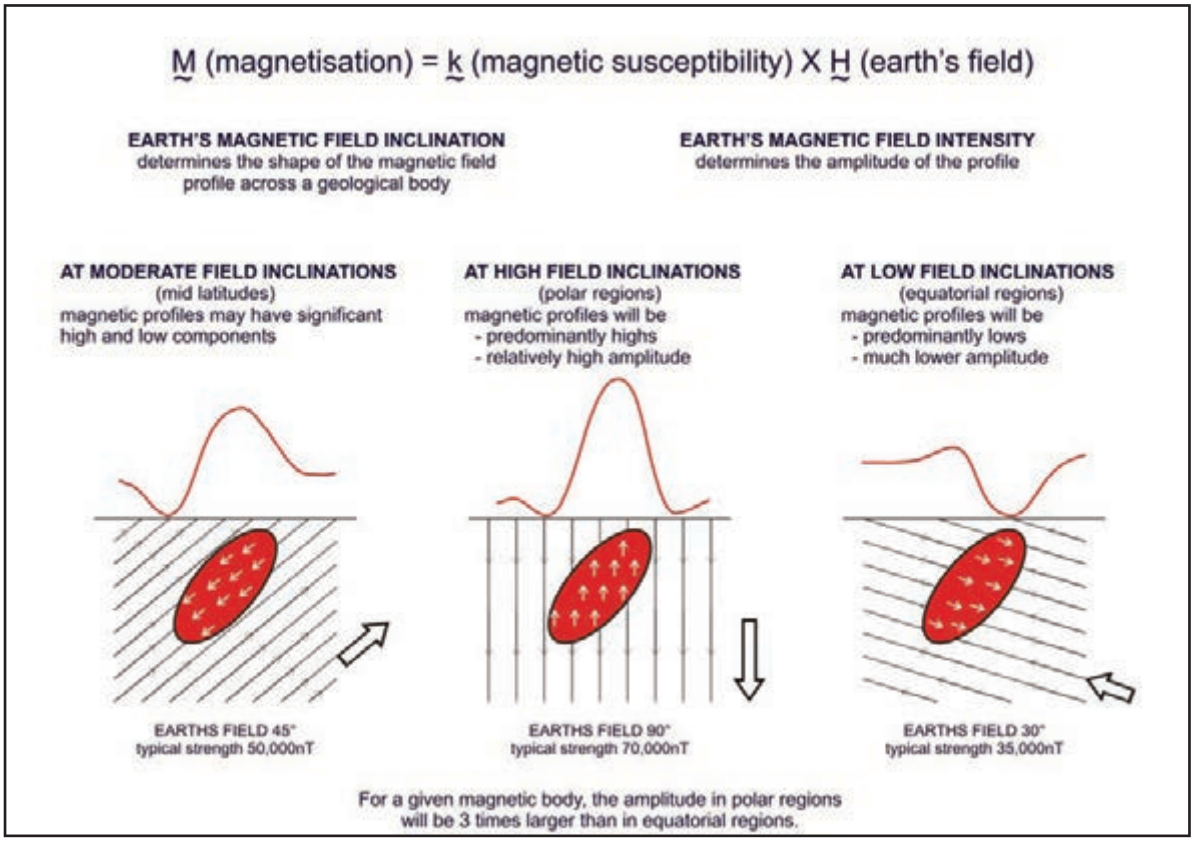

Figure 2.3: Illustration of rock magnetisation by magnetic induction.

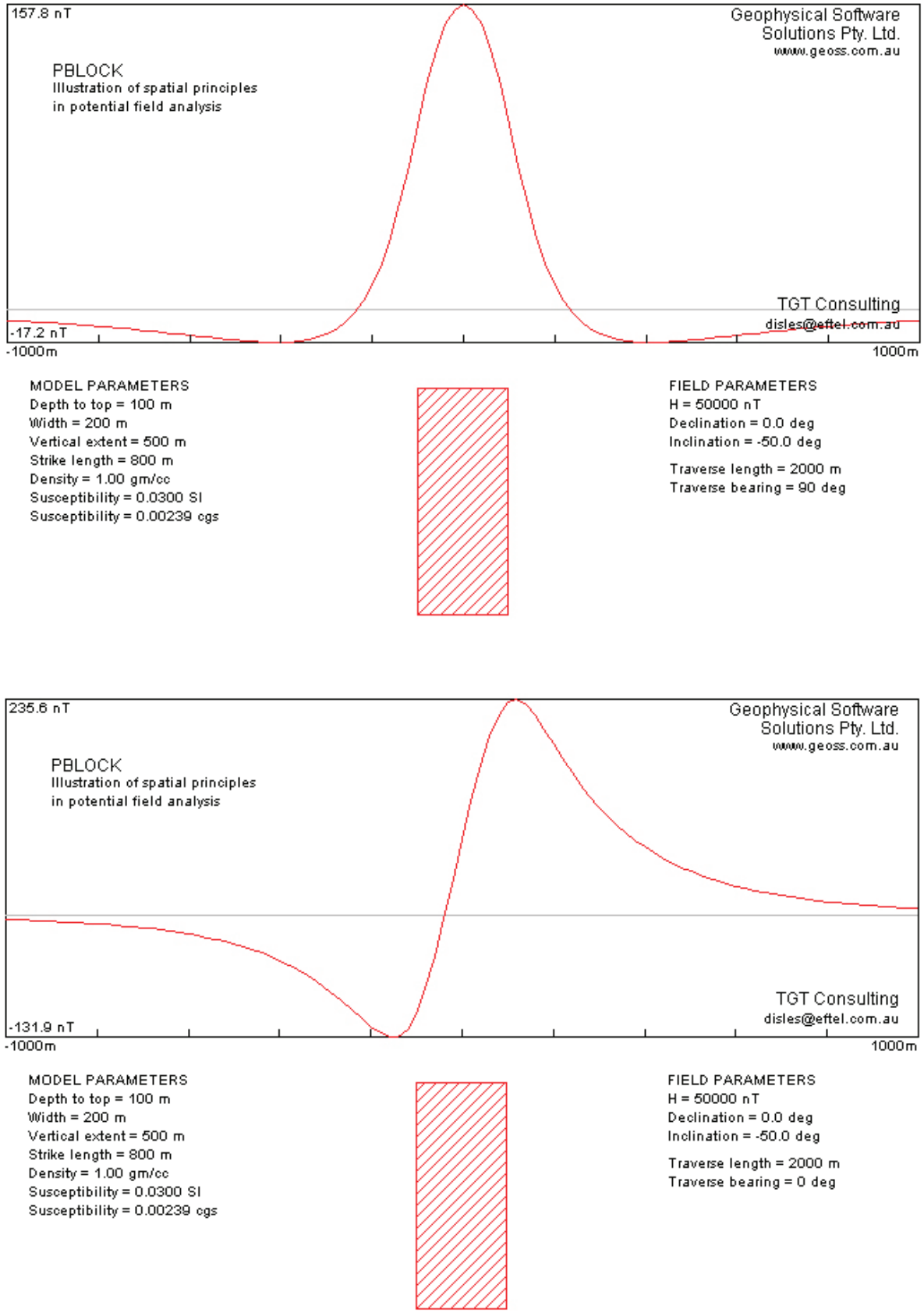

Figure 2.4: Pblock model with different strike orientations at Earth's field inclination of –50° (southern hemisphere). Note the symmetry when strike is N–S and the strong asymmetry when strike is E–W.

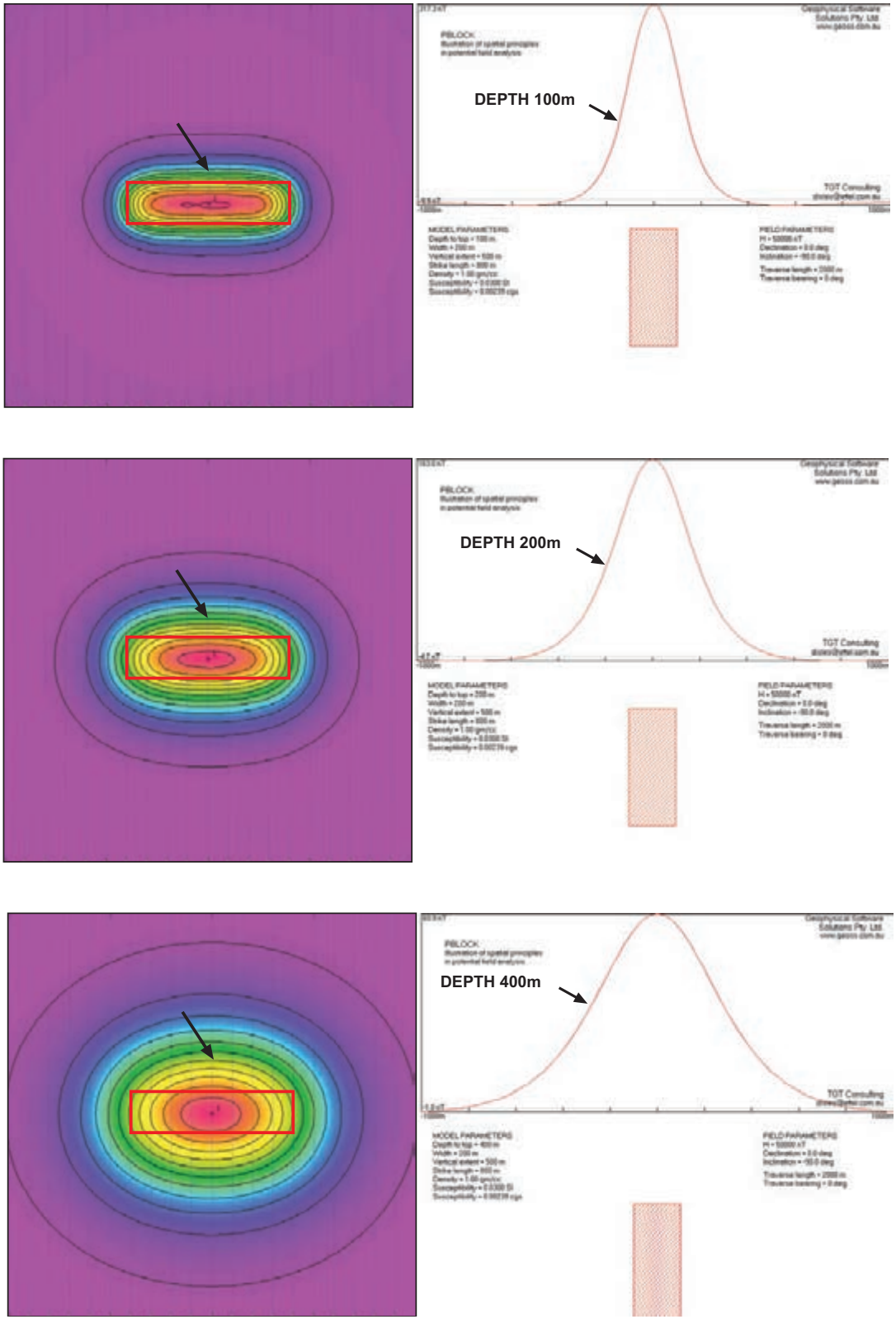

Figure 2.5: Pblock model at Earth's field inclination of 90° (polar regions) showing the link between body location and maximum gradient position (arrowed) for varying depths. The profiles cross the centre of the body.

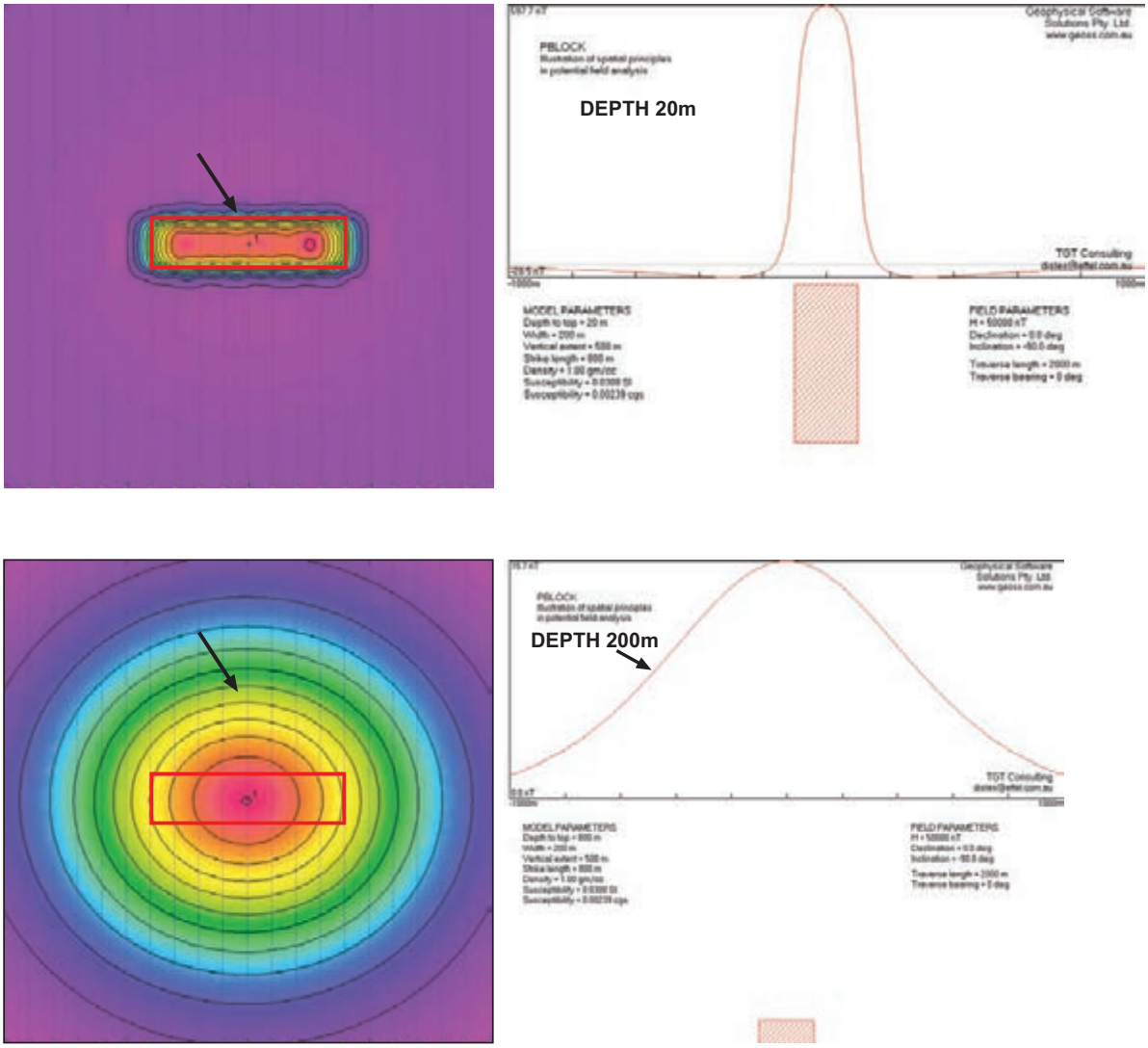

Figure 2.6: Pblock model at Earth's field inclination of 90° (polar regions) showing the link between body location and maximum gradient position for extreme depths. Note how the shape of the body is 'lost' when depth becomes greater than the lateral dimensions, and the maximum gradient position (black arrow) becomes a poorer indication of body edge location.

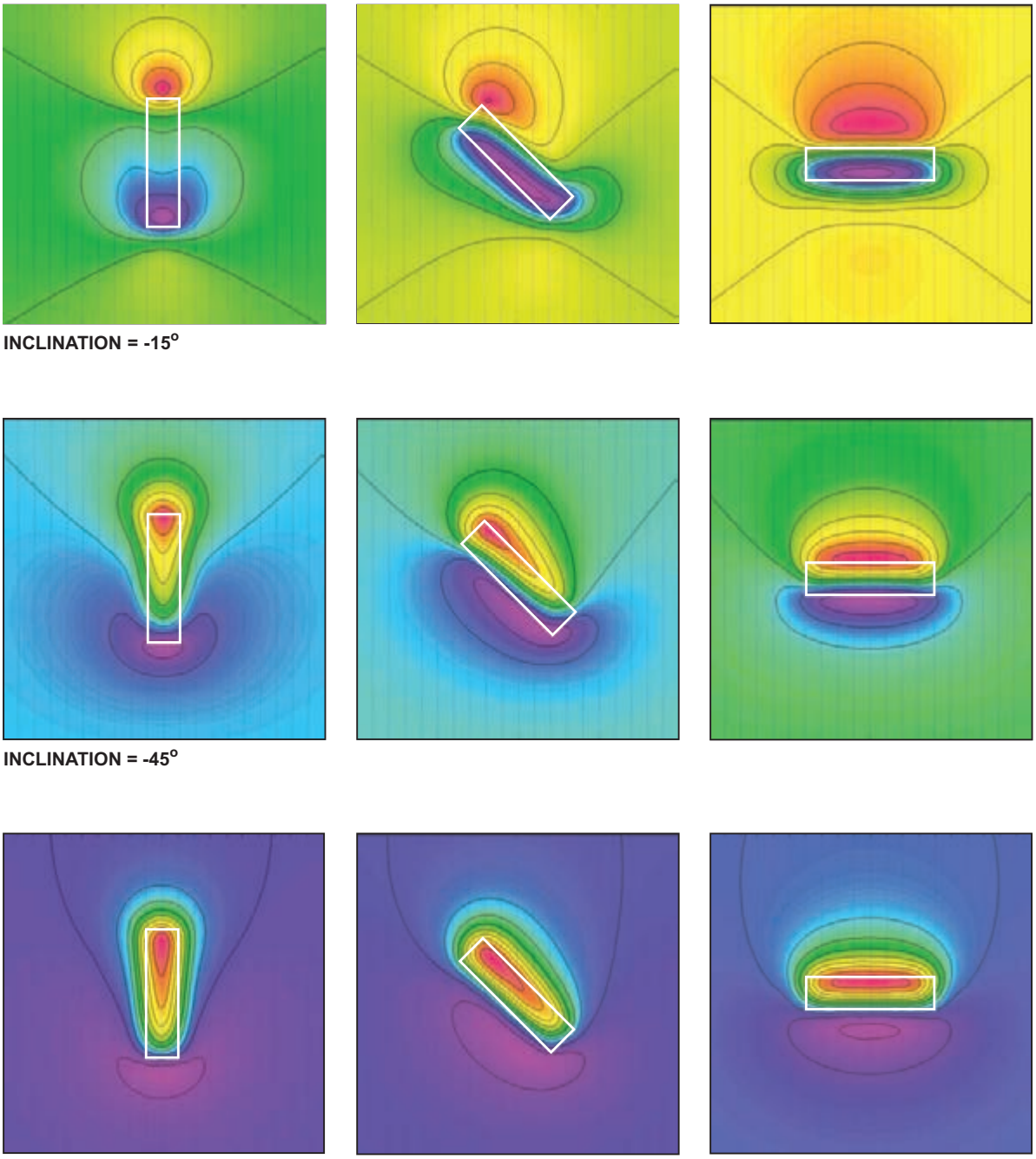

Figure 2.7: Pblock model (depth 100 m) showing the effect of varying Earth's field inclination and strike direction. Calculations are for southern magnetic hemisphere. The equivalent northern magnetic hemisphere models can be observed by rotating the diagram 180°.

Drawing the straight slope distance involes three simple steps:

1. Select an appropriate magnetic profile accross the centre of the anomaly (measured line profile data is preferable) and plot the profile at scale such that the anomaly is at least 3cm across.

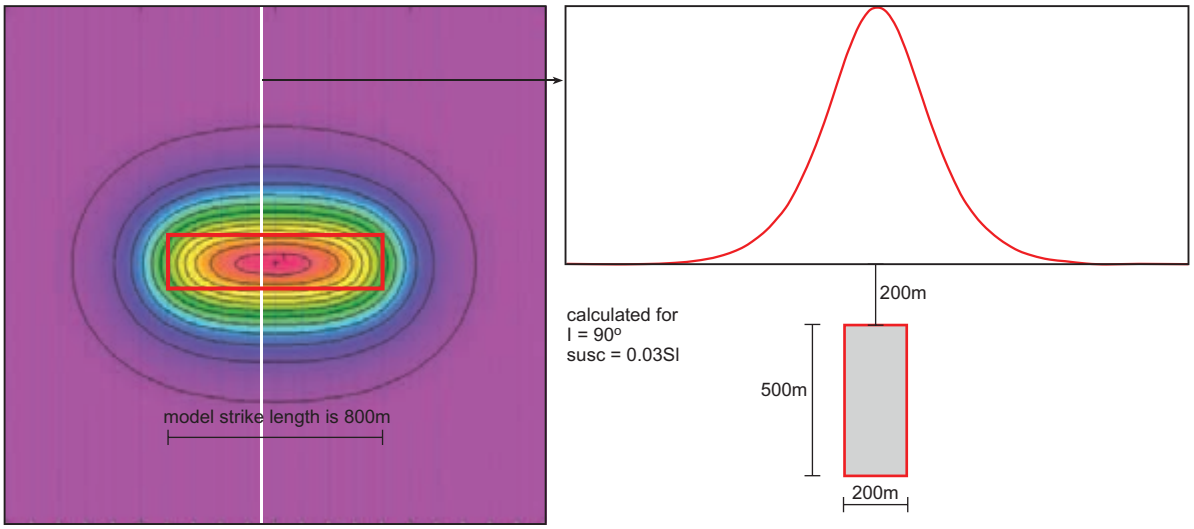

2. Draw in the section of the gradient that appears linear - the inflection points (circled) provide a guide for this line

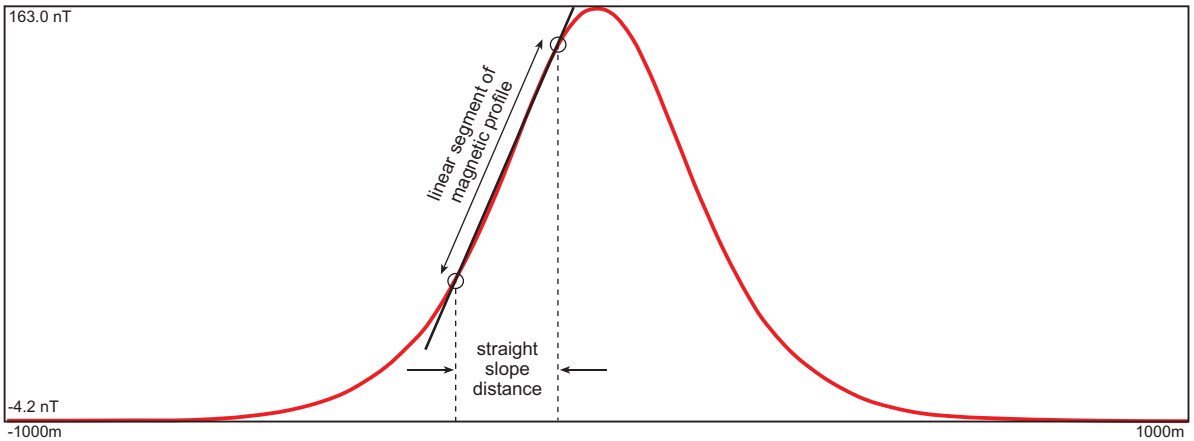

3. Project the points where the above straight line intersects the profile vertically down to the profile distance axis. The distance along this axis between the points is the straight slope distance.

Figure 2.8: Graphical construction of the straight slope distance.

Drawing the anomaly involves three simple steps:

1. Select an appropriate magnetic profile accross the centre of the anomaly (measured line profile data is preferable) and plot the profile at scale such that the anomaly is at least 5cm across.

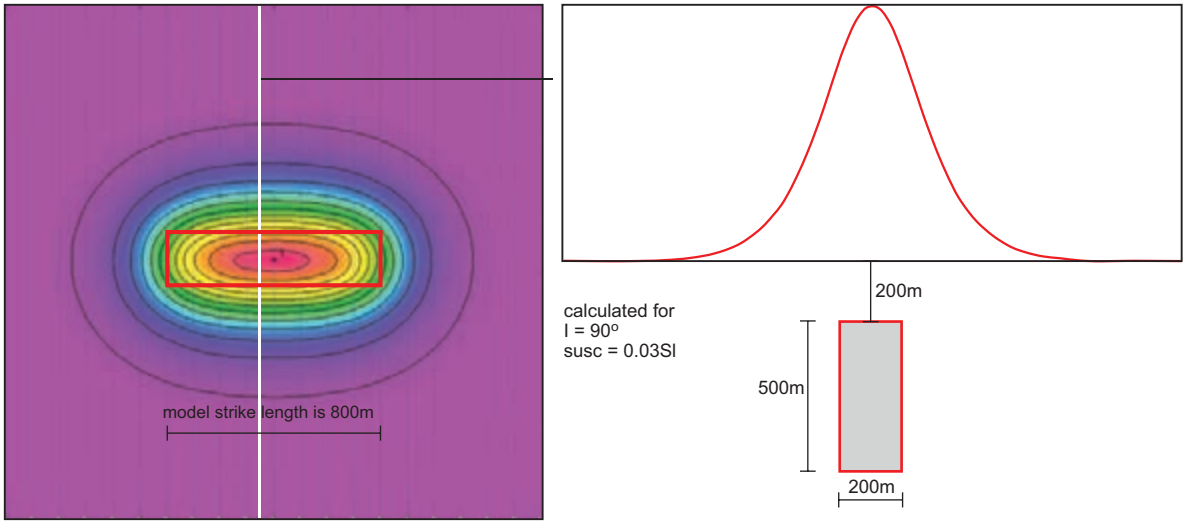

2. Determine the half anomaly amplitude line and mark the half anomaly points (circled) on the profile

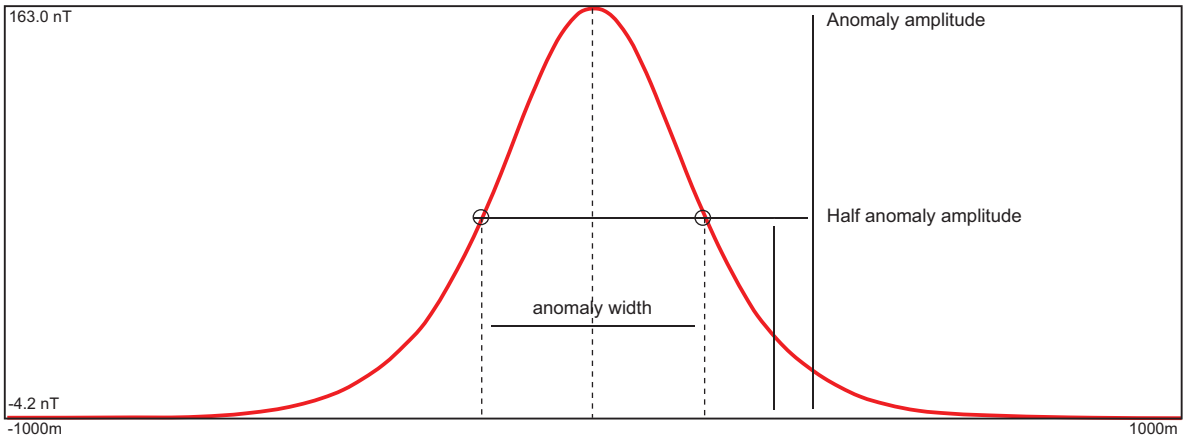

3. Project the half anomaly points vertically down to the profile distance axis. The distance is the anomaly width.

Figure 2.9: Graphical construction of '× 1/2', the width of the anomaly at half maximum amplitude.

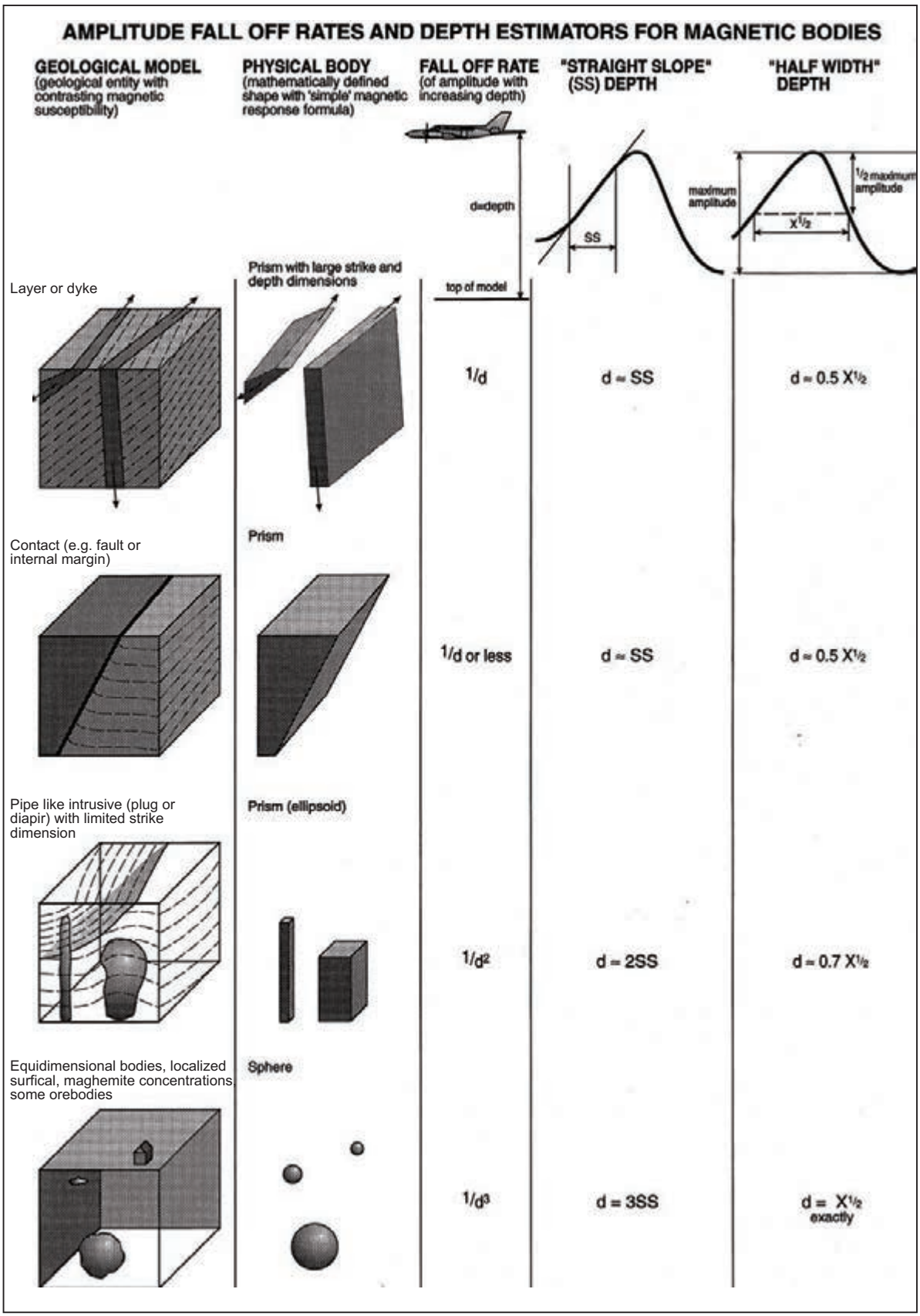

Figure 2.10: Amplitude fall-off rates and simple graphical depth estimators.

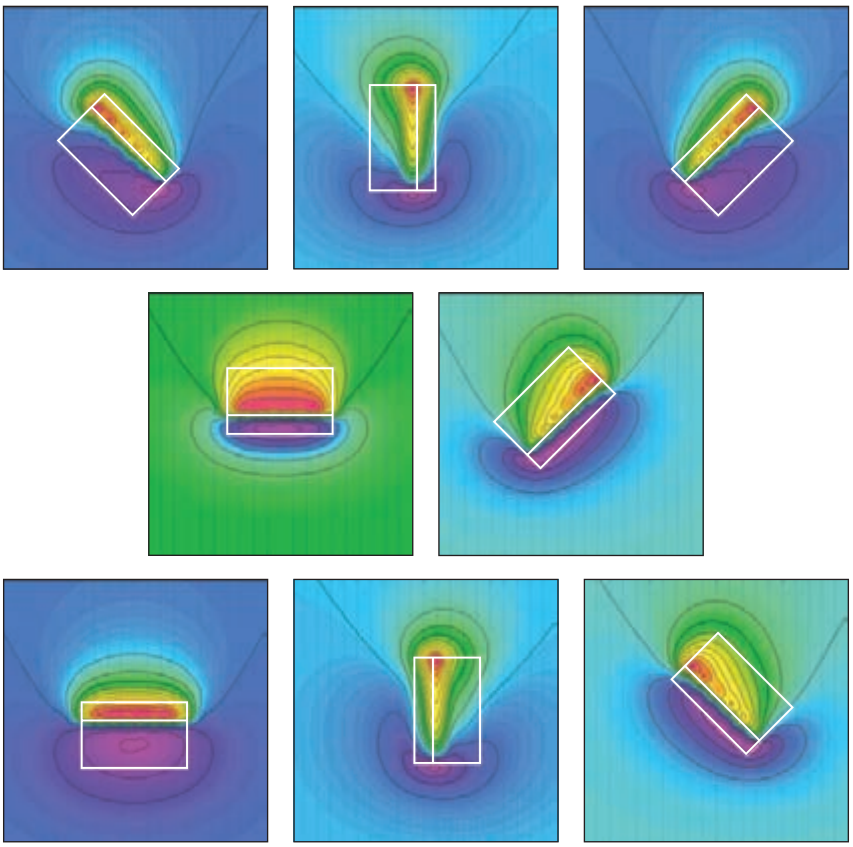

Figure 2.11: Pblock model (depth 100 m) dipping at 45° for a range of strike directions. Calculated at Earth's field inclination of –50°. Note in particular that when the dips are to the south, the asymmetry of the anomaly gives the impression of northerly dip. The equivalent northern magnetic hemisphere models can be observed by rotating the diagram 180°.

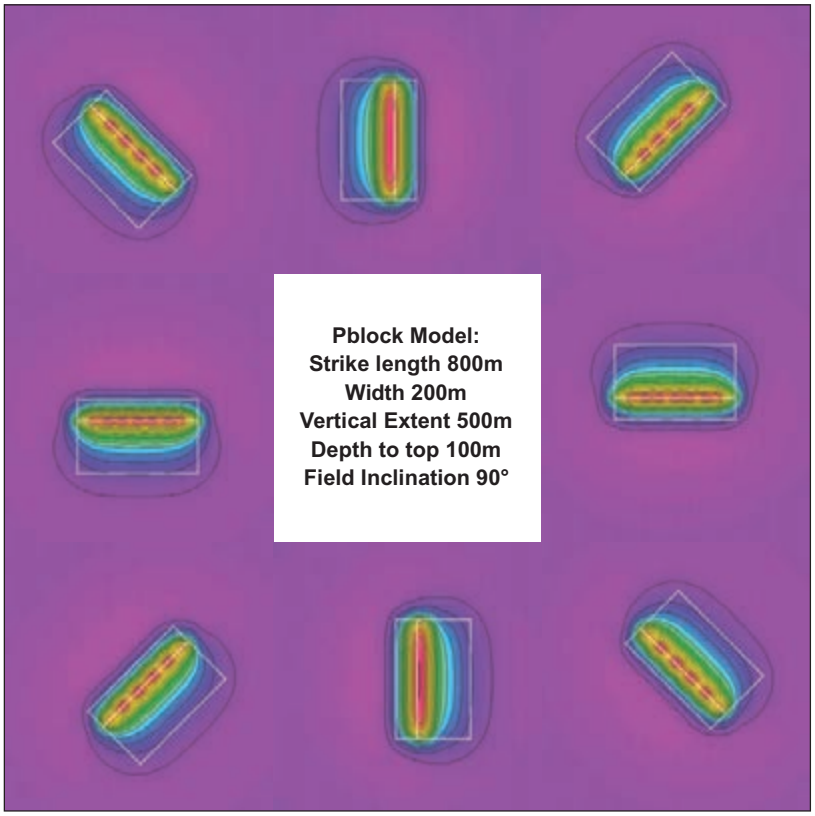

Figure 2.12: Pblock model (depth 100 m) dipping at 45° for a range of strike directions. Calculated at Earth's field inclination of 90°. Because the Earth's magnetising field is vertical in this example, the anomaly asymmetry closely reflects the geometry of the model body.

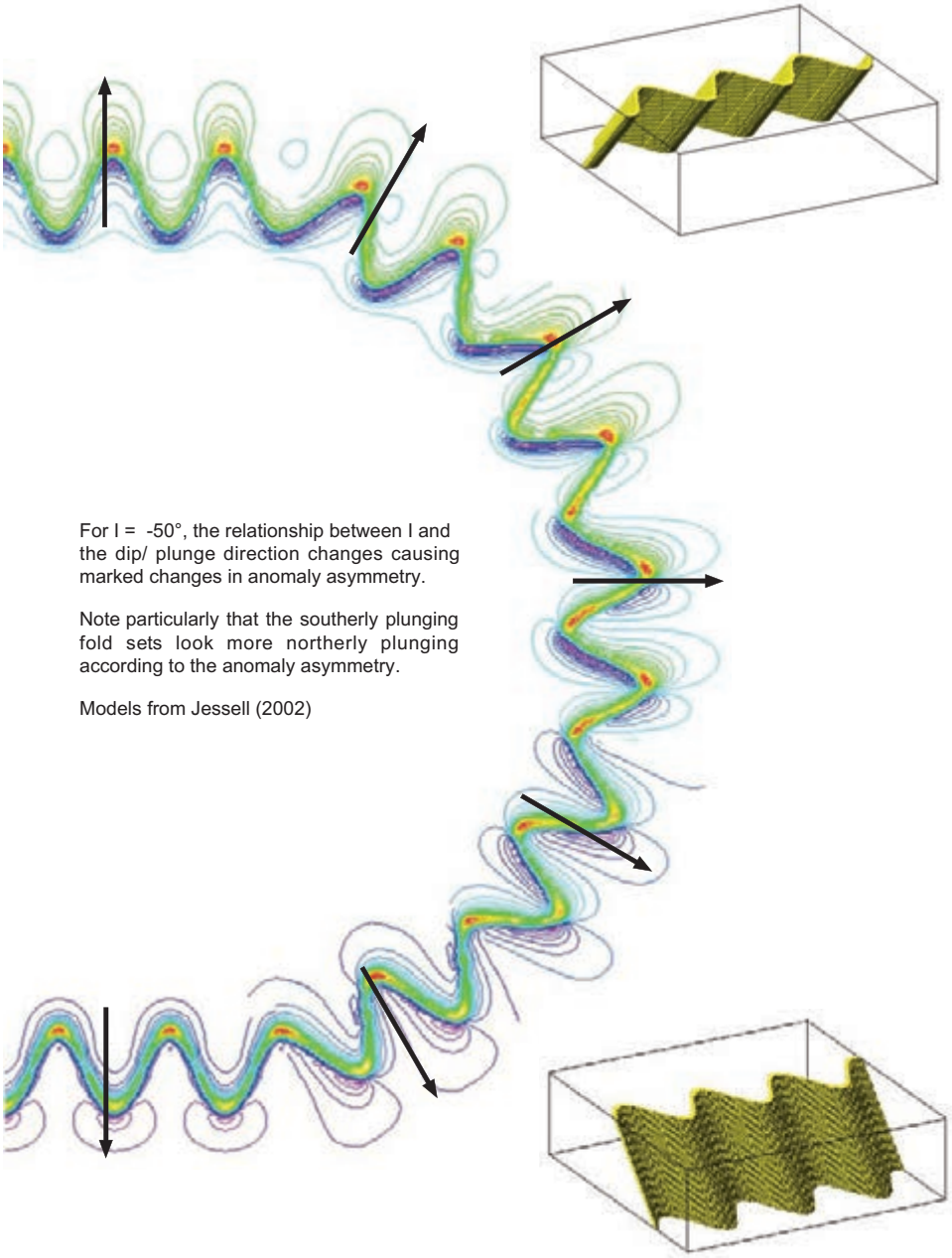

Figure 2.13: Dip and plunge effects illustrated by a single set of plunging folds, calculated for Earth's field inclination of –50° (southern magnetic hemisphere). Plunge is 60° and direction (arrowed) varies from north to south. The equivalent northern magnetic hemisphere models can be observed by rotating the diagram 180°.

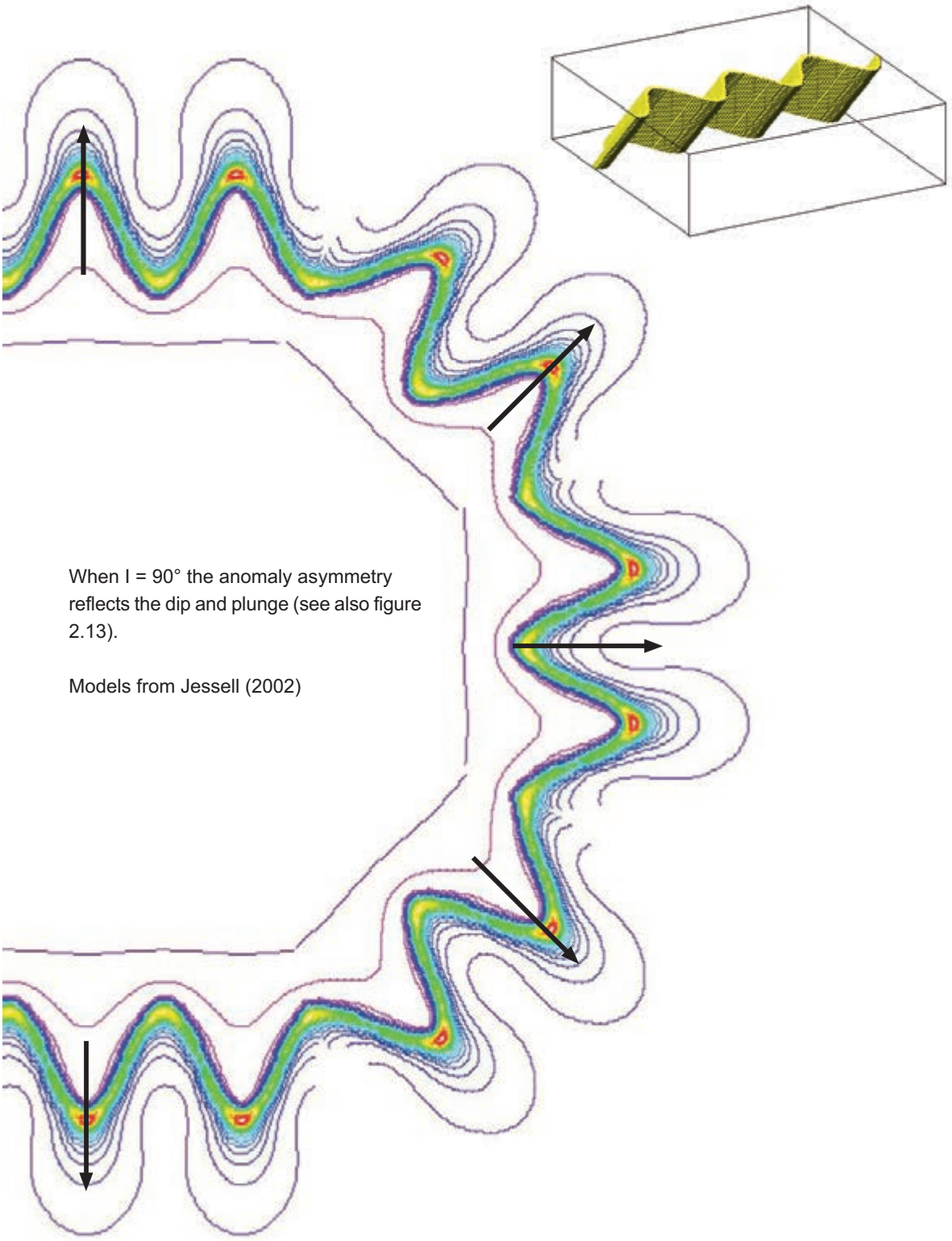

Figure 2.14: Dip and plunge effects illustrated by a single set of plunging folds for Earth's field inclination of 90° (polar regions). Plunge is 60° and direction (arrowed) varies from north to south.

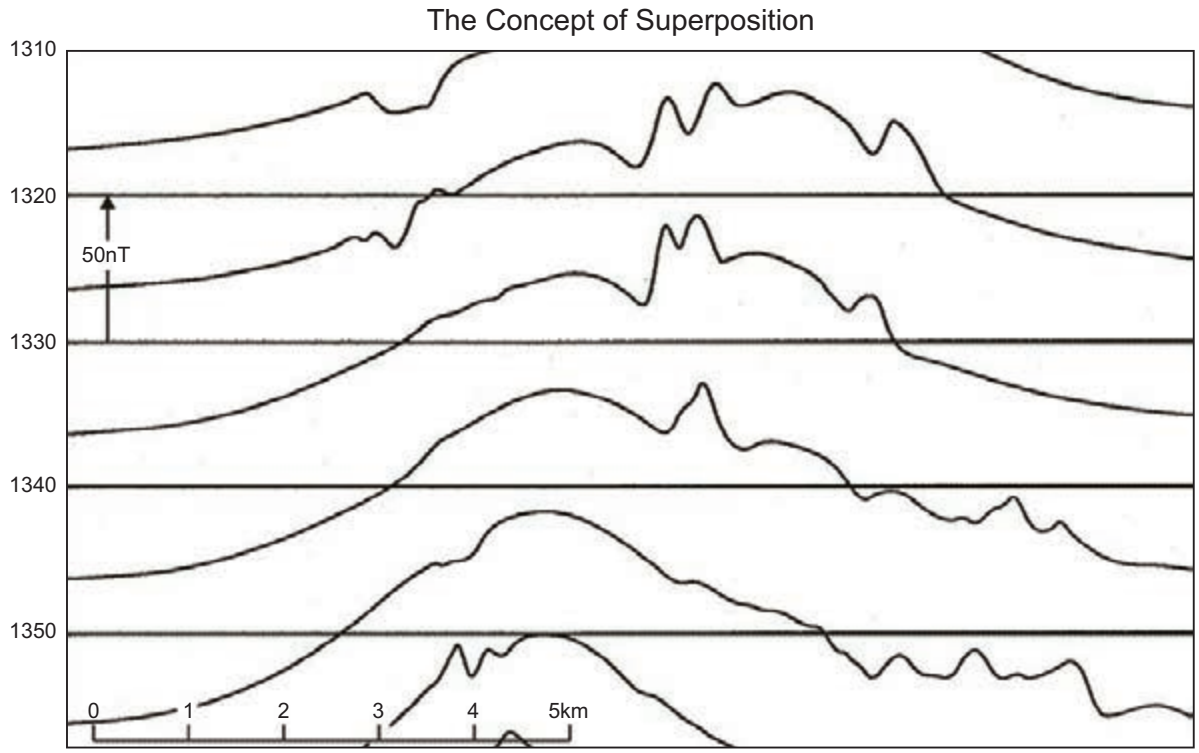

Figure 2.15: Stacked TMI profiles from northern Tasmania illustrating the effect of anomaly superposition. The broad anomaly is due to Proterozoic metasedimentary rocks at a depth of 1–2 km. The short-wavelength anomalies are caused by erratic, surficial basalt flows (100 m below magnetometer). There is a non-magnetic Mesozoic sequence overlying the Proterozoic basement. Data from Geoscience Australia National Database.

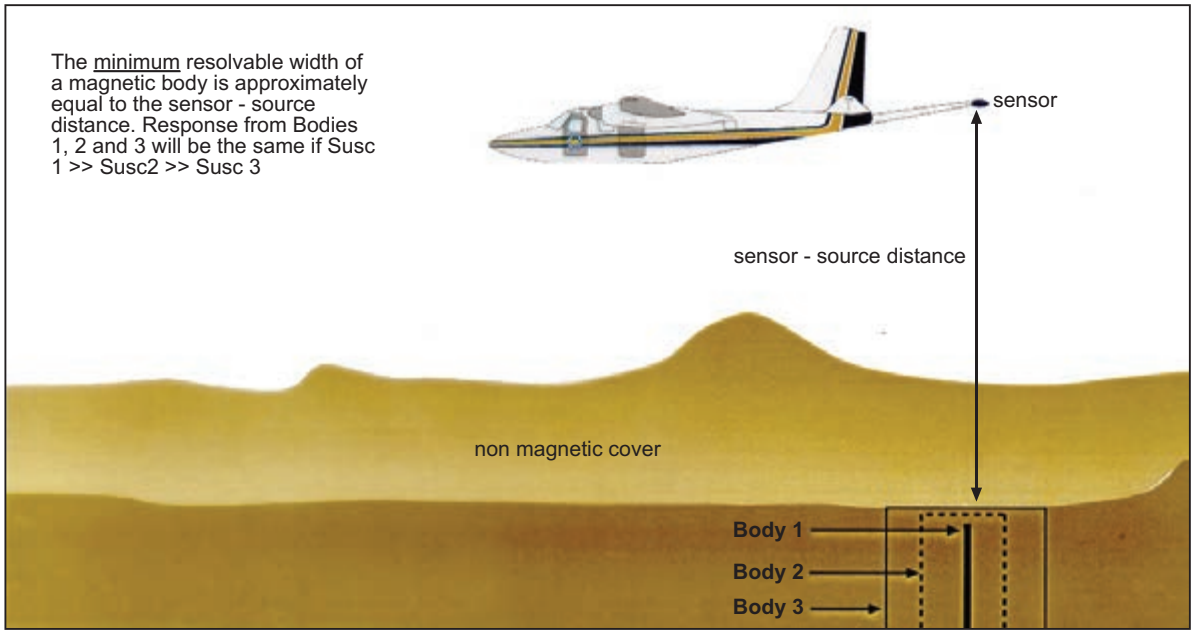

Figure 2.16: Resolution of magnetic body width. The sensor–source distance is the smallest resolvable magnetic body width. For widths smaller than this, many combinations of body width and magnetic susceptibility (at equal depths) will produce the same anomaly profile.

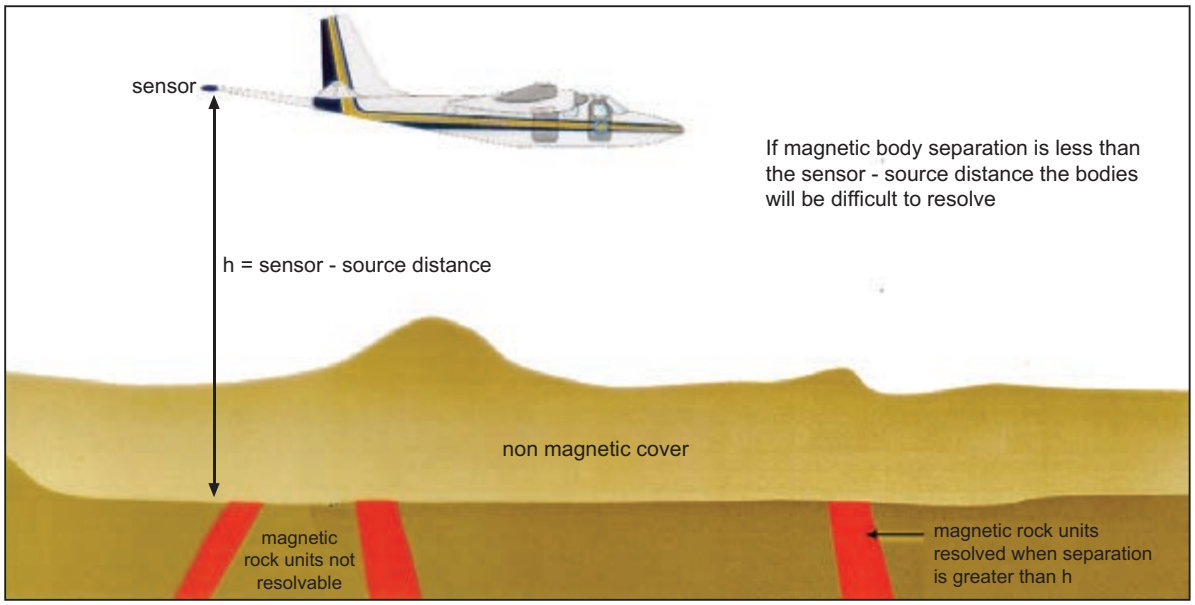

Figure 2.17: Resolution of individual magnetic bodies. If two bodies are closer together than the sensor–source distance, they will appear as one anomaly in the magnetic field profile. If they are further apart than the sensor–source distance, they will be resolved (see Fig. 2.18).

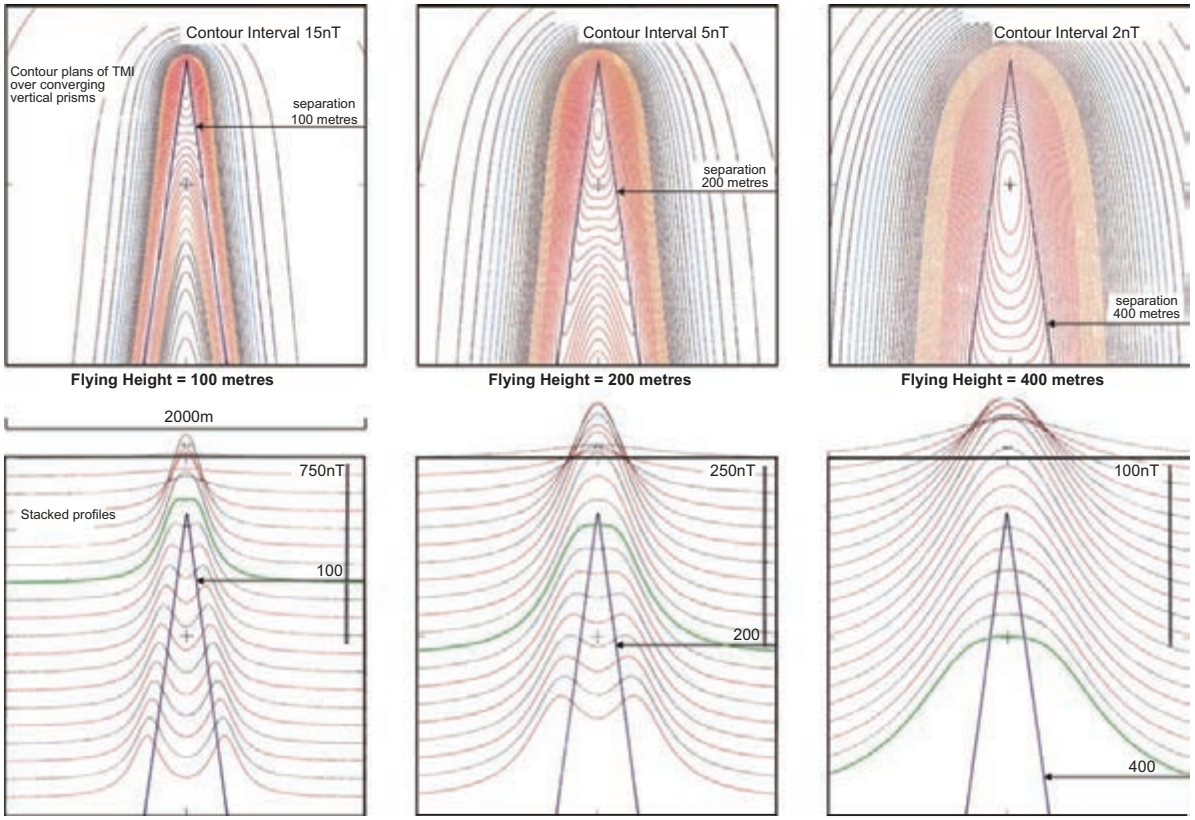

Figure 2.18: Resolution of individual magnetic bodies. The model study shows a pair of vertically dipping and converging thin magnetic units (perhaps simulating a vertically plunging fold), at depths of 100, 200 and 400 m below sensor. The green profile line cuts the model where the magnetic units are separated by exactly the sensor–source distance. Note that when the magnetic units are further apart than the sensor–source distance, they are clearly resolved, but when they are closer together than this distance they appear as a single anomaly. This is apparent in both contour and profile format.

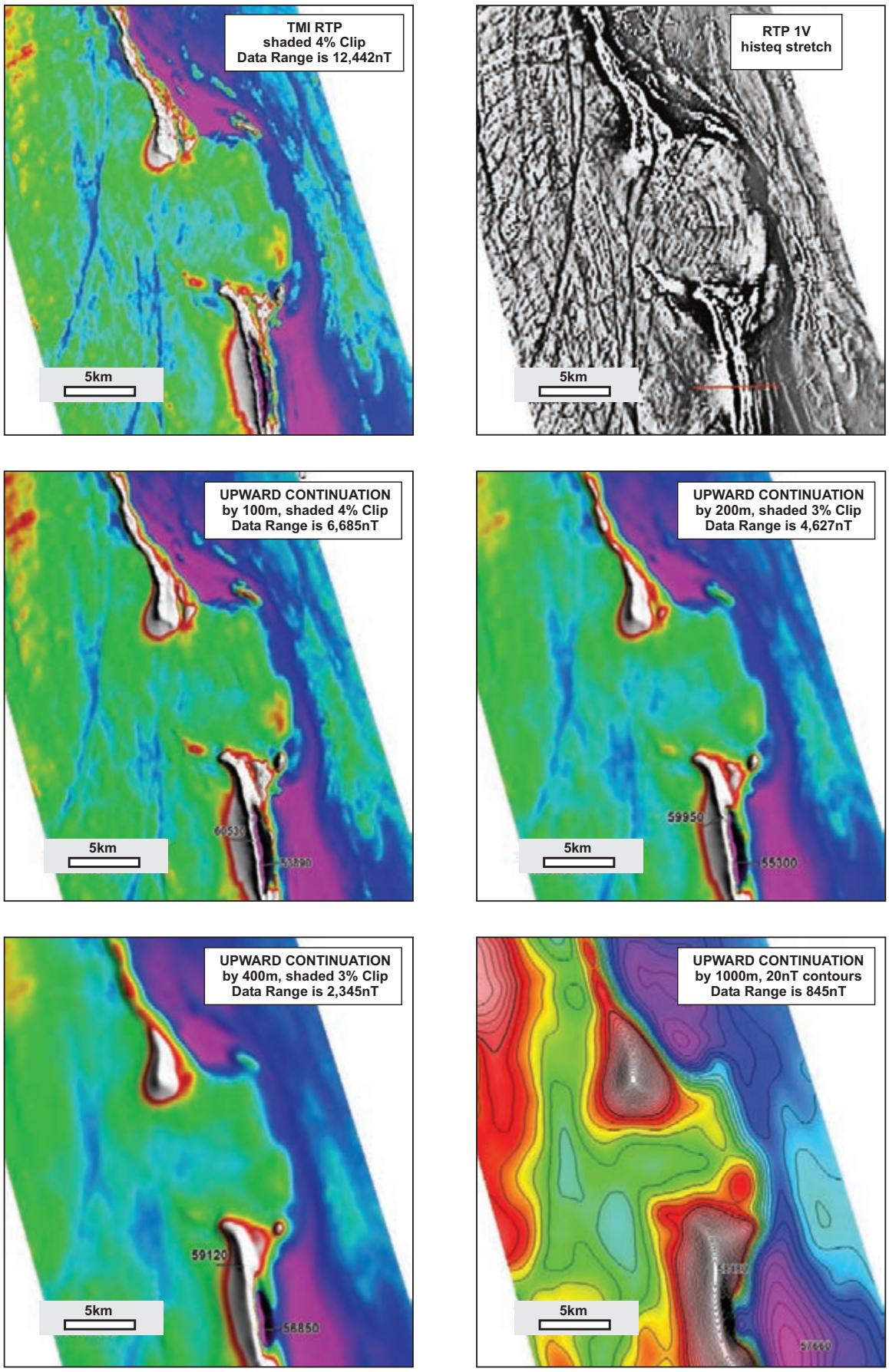

Figure 2.19: Illustration of the decrease in spatial resolution with increasing depth to source. Upward continuation (see Section 5.4.2) has been used to simulate increasing depth. Data from the Menzies district in WA (see Chapter 11) kindly provided by Fugro Airborne Surveys.

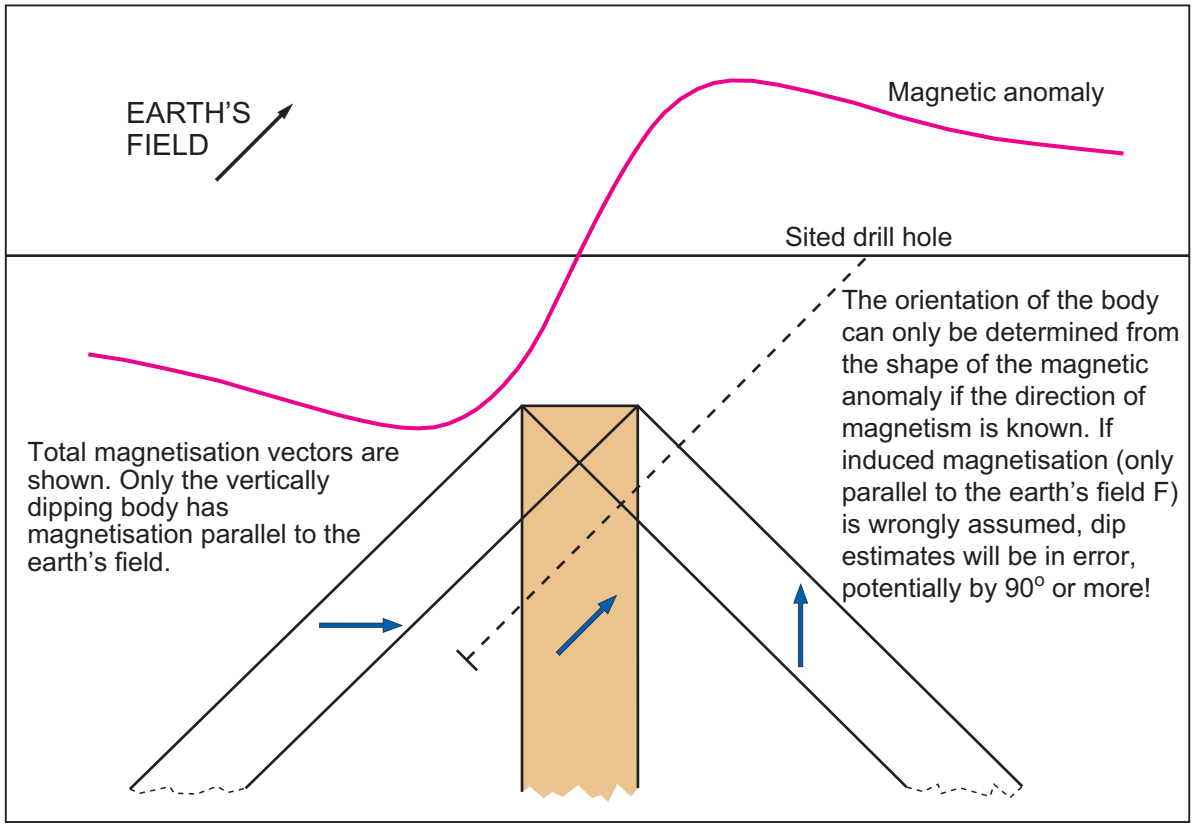

Figure 2.20: Ambiguity in dip determination. If the magnetisation direction of the rock body is unknown we cannot uniquely determine dip. Many combinations of magnetisation and dip (for a single strike direction) will produce the same magnetic profile. See Figure 3.31 for a case history.

3 Magnetisation of rocks

3.1 INTRODUCTION

Working with magnetic and non-magnetic rocks at the (various) scales of aeromagnetic surveys is, for the most part, relatively straightforward. Simple assumptions and approximations usually allow the aeromagnetic interpreter to integrate conventional geological mapping without needing to determine the complexities and intricacies of laboratory-scale behaviour of magnetisation in rocks. The key to effective integration of aeromagnetic data and geology is the understanding of these approximations and assumptions, combined with recognition of the situations where they may be inappropriate. In this book we emphasise the more common situations; in Section 3.4 we provide guidance in recognising and dealing with the unusual situations. We also emphasise the desirability, wherever possible, of observing and sampling the rocks in the field. Direct recognition of the source of aeromagnetic anomalies in hand specimen is undoubtedly the best way to link the remotely measured aeromagnetic data to the geology (Urquhart 1989).

The interested reader is referred to Clark (1997), Reynolds *et al.* (1990) and Reeves (2005) for more expansive discussions on the petrophysical aspects of magnetisation in rocks, and to Dunlop and Özdemir (1997) for a book devoted to the topic of rock magnetism.

The magnetic character of a rock is determined by several factors, most importantly:

a) the bulk geochemistry of the rock (i.e. how much Fe is present, and in what oxidation state);
b) the Fe-bearing mineral species present (i.e. how much of the Fe resides within magnetic mineral species), and the volume % of these species;
c) the different types of magnetisation displayed by the magnetic mineral species (induced, remanent, self-demagnetisation etc.);
d) the intensity and orientation of the external applied inducing field (i.e. the local intensity, inclination and declination of the Earth's field).

The first three factors are controlled by the geological processes that have influenced both the initial formation of the rock, and all subsequent processes affecting and overprinting it. The fourth factor depends solely on the present geographic locality of the rock (see Section 2.1).

We will first review the simplest and most common form of magnetisation (induced magnetisation) and the geological processes that control the magnetic susceptibility of minerals; then briefly examine the less common, (and more complex) forms of magnetisation, and their appearance in the data.

3.2 INDUCED MAGNETISATION AND MAGNETIC SUSCEPTIBILITY

3.2.1 Definition of magnetic susceptibility

Magnetic susceptibility is a measure of a rock's response to an applied magnetic field. In geological mapping applications, the Earth's magnetic field affects all crustal rocks and induces magnetic fields in magnetically susceptible rocks occurring at depths shallower than the Curie Point isotherm (see Section 2.1).

In a typical aeromagnetic survey, most of measured magnetic responses are associated with particular (ferromagnetic) iron-bearing minerals. However, in regions of subdued magnetic character (e.g. sedimentary basins), contrasts in magnetic susceptibility of both paramagnetic and diamagnetic minerals can be detected. Examples of these will be discussed in Section 3.2.2.

The equation relating strength of magnetisation in a rock to the local intensity of the Earth's field is:

$$M = \boldsymbol{k}H$$

where M is the magnetisation per unit volume, $\boldsymbol{k}$ is the magnetic susceptibility (for that volumetric unit) and H is the local intensity of the Earth's magnetic field. This simple equation can (and should) be expanded into much more complex vector (and sometimes tensor) equations when modelling anisotropic magnetic rock bodies. For routine mapping applications, however, the scalar version is entirely adequate and the following approximations and assumptions apply:

a) H can be considered a constant over areas <10 000 km^2 – its value worldwide can be readily sourced from government observatory data (e.g. NOAA, http://www.ngdc.noaa.gov/geomag);
b) $\boldsymbol{k}$ is related to the amount and type of magnetic mineral in the rock. In the majority of field-scale situations, the equation $\boldsymbol{k \simeq 0.035V}$ (where V is the volume % magnetite and k is expressed in SI units) is a valid approximation;
c) the Earth's magnetic field is a vector whose direction varies from vertical at the magnetic poles to horizontal at the magnetic equator. Since $\boldsymbol{k}$ can be treated as a scalar quantity in most broad-scale mapping applications, magnetisation will then be a vector with direction parallel to the Earth's field.

$\boldsymbol{k}$ can be easily measured from outcrop or hand specimen using a hand-held magnetic susceptibility meter (see Sections 3.5 and 9.9).

3.2.2 Magnetic susceptibility of minerals

All minerals have magnetic susceptibility, with each mineral exhibiting one or more of three classes of magnetic susceptibility.

a) *Diamagnetic minerals* – these have a very small negative magnetic susceptibility ($\boldsymbol{k}$) in an applied field. All materials exhibit diamagnetic behaviour, but its effects are almost always too small to be observed in aeromagnetic surveys. Where paramagnetism or ferromagnetism are present (see below), their effects far outweigh those of diamagnetism. The only common exception to this is halite, which (with sufficient volume) may exhibit a weak negative magnetic anomaly within magnetically quiet sedimentary basins. Magnetic lows associated with salt diapirs have been recorded from numerous sedimentary basins (see Gunn 1997b; Prieto 1998; Rowe 1998).
b) *Paramagnetic minerals* – these have a small positive magnetic susceptibility ($\boldsymbol{k}$) in an applied field. Paramagnetic minerals include pyroxenes, amphiboles and micas. The contribution of paramagnetic minerals to magnetic signatures in typical surveys is generally negligible. However, as for the example of halite, concentrations of paramagnetic minerals in sufficient volume in generally magnetically quiet sedimentary basins can be discriminated (see Mørk *et al.* 2002 for examples from Mesozoic sediments in the offshore Norway Basin). It should be noted that paramagnetic minerals are often used in laboratory-based studies of strain within deformed rocks (James 1975; Kligfield *et al.* 1977).
c) *Ferromagnetic minerals (s.l.)* – these exhibit substantial positive magnetic susceptibility values. Ferromagnetic minerals include magnetite, pyrrhotite (monoclinic variant), titanomagnetite, ilmenite, haematite, greigite, franklinite and maghemite. The broad definition of ferromagnetic used here (and for the rest of

the book) includes other forms of magnetic susceptibility, including ferrimagnetism, antiferromagnetism etc. (the differences between these forms are rarely important for the magnetic interpreter, and are beyond the scope of this manual).

The small family of iron-rich, ferromagnetic minerals accounts for almost all magnetisation observable in field geology and measurable using field magnetometers.

The 'magnetite family' (magnetite – ulvöspinel Fe_3O_4 – Fe_2TiO_4) has the highest range of ***k*** and is by far the greatest contributor to magnetisation in rocks.

Monoclinic pyrrhotite is the next most common mineral species responsible for measurable magnetic anomalies in rocks, accounting for probably less than 5% of measured field responses.

The much lower susceptibility ferromagnetic species such as ilmenite and haematite make a very minor contribution to the induced magnetic field responses and rarely play a large part in aeromagnetic survey interpretation. However, the remanent magnetisation occurring within these minerals can occasionally be significant.

Magnetic susceptibility generally decreases with increasing oxidation, hydration and/or sulphidation of the minerals. The trend from magnetite though ilmenite to haematite (increasing oxidation state) is accompanied by a rapid fall in ***k*** for these minerals. Similarly, monoclinic (low-T, low f_S) pyrrhotite is strongly magnetic, while pyrite and hexagonal (high-T) pyrrhotite are effectively non-magnetic. The observed magnetic susceptibility ranges of the magnetic minerals taken from Clark (1997) are presented in Figure 3.1.

3.2.3 Mineral grain-size, texture and magnetic susceptibility

The grain-size of ferromagnetic minerals such as magnetite also influences the ***k*** of the mineral. Figure 3.1 shows that both magnetite and pyrrhotite exhibit variations of greater than one order of magnitude between fine-grained (lower ***k***) and coarse-grained variants (higher ***k***).

The interconnectivity of grains also affects ***k*,** with massive magnetite having a higher ***k*** than dispersed grains with little or no interconnectivity.

Variations in ***k*** with grain-size can play a role in interpretation of mineralising processes, for example:

a) interpretation of localised strain variations in shear zones (possibly highlighting lower-strain mineralising fluid traps);
b) development of different phases of magnetite growth within complex hydrothermal and metasomatic alteration systems.

3.3 DISTRIBUTION OF MAGNETIC MINERALS

3.3.1 Magnetic susceptibility and rock type: the role of geological processes

While all minerals exhibit some form of induced magnetisation, the following discussion focuses on the most significant group – the ferromagnetic minerals.

A common misconception in the early days of aeromagnetic interpretation was that specific groups of rocks have characteristic values or ranges of ***k*** that would allow recognition of these lithologies within a magnetic survey.

It is now well established that all lithological groups may contain magnetic minerals in widely varying amounts and that the magnetic mineral assemblage in a rock is a function of both its primary composition and (perhaps more importantly) its geological history (i.e. all the geological processes that have contributed to its current state). The following summary discussion is drawn largely from Grant (1985a, b); these references are recommended reading for all those involved in aeromagnetic interpretation.

Separating geological processes into two general subdivisions, i.e. primary (the formation of igneous and sedimentary rocks) and secondary (the overprinting of these rocks by diagenesis, metamorphism, metasomatism, deformation and weathering), we find that the secondary processes can (and often do) have as great or greater impact on the prevailing ***k*** of a rock than the primary processes.

The amount of magnetic mineral in any rock is a function of:

a) chemical composition – low Fe content may correlate with low ***k*** (e.g. a quartz arkose with 0% Fe-bearing minerals), although high Fe content (e.g. a gabbro) does not necessarily correlate with high ***k***. The Fe content is dependent on both the mineral species in which the Fe occurs during the formation of the rock, *and* any subsequent geological processes that may add or remove Fe from the rock (metasomatism, alteration, weathering etc.);
b) chemical and the combined thermal and pressure history of the rock (crystallisation temperature, fO_2, f_S, $\%H_2O$, lithostatic pressure, hydraulic pressure, pH/eH). These factors, discussed in some detail later in this chapter, influence the partitioning of Fe into different mineral species.

Very small shifts in the oxidation and/or sulphidation states of any iron-bearing mineral assemblage in a rock can radically alter the percentage of magnetic mineral within the rock. As a consequence, subtle but important processes that may not be visually evident in hand specimen may be clearly expressed as marked changes in magnetic susceptibility. This can be dramatically expressed, such as magnetic zonation within geochemically similar intrusions, controlled principally by zonation of fO_2 (Fig. 3.2).

Hence, it may be that rock units mapped from outcrop as single bodies or entities may exhibit a wide range of ***k***, potentially giving insight into geological processes, some of which may have significant bearing on localisation of mineralisation.

The compilation by Clark (1997) of many thousands of measurements of ***k*** for a very wide range of lithologies (Fig. 3.3) illustrates three important features.

1. For any one lithology or lithological group, there is a possible range of ***k*** values of two to four orders of magnitude. This reflects not only variation in the bulk %Fe in the rock, but also the local conditions of oxidation/sulphidation, temperature of formation and other geological factors, both at time of formation and during subsequent overprinting processes.
2. There is a large degree of overlap in ranges of ***k*** between most lithologies, making identification of any particular lithology from its magnetic susceptibility (and consequently its measured magnetic intensity) virtually impossible.
3. Statistically, there are 'most common' ranges of ***k*** for most lithologies, reflecting the most common conditions of formation of that particular lithology. The extremes in ***k*** variation highlight the more unusual variants in conditions of formation and/or subsequent alteration of the rock type.

We can conclude from Clark's (1997) invaluable tabulation that magnetic susceptibility is never a reliable indicator of lithology and that the rocks we intuitively expect to be magnetic are very often non-magnetic, and vice versa.

We now explore the geological processes responsible for the above observations.

3.3.2 Geological processes: how they influence magnetic minerals

Primary processes – sedimentary rocks

Sediments show the widest variation in Fe content of all the common rock groups, with ~0% within an orthoquartzite to ~70% within outcrop-scale, massive magnetite-haematite layers of primary banded iron formation ('BIF'). It is therefore not surprising to find that the variations in ***k*** of sediments are extreme.

Magnetite and pyrrhotite, the minerals with highest ***k***, are both typically **metastable** in low T/low P, high fO_2 conditions, i.e. the conditions commonly prevailing in the post-early Palaeoproterozoic sedimentary rock-forming environment. Fe-bearing minerals initially formed in sediments are generally dominated by haematite (Fe_2O_3), siderite ($FeCO_3$), pyrite (FeS_2) and various hydrous oxides (goethite, limonite etc.). The local redox states of sediments (eH/pH, f_S and fO_2) are strongly controlled by the sulphur and carbonate content of the depositional environment (high %S sediments will be dominated by pyrite or pyrrhotite, while low %S sediments will be dominated by haematite, siderite etc.). However, magnetite was commonly stable in surficial conditions within the more reducing (low fO_2) global environment of the Archaean to early Palaeoproterozoic (with common development of magnetite BIFs).

Controls on the formation of Fe oxide, sulphide and carbonate species are therefore strongly dependent on both sedimentary facies and sediment provenance. For example, a reducing environment such as a barred basin is more likely to develop pyritic rather than Fe-oxide shales, while sabkha-related red-bed sedimentary environments are dominated by Fe oxides, particularly haematite. Weakly or non-magnetic Fe-bearing minerals are therefore the most common in sediment-forming environments. While this may initially suggest sedimentary environments are inappropriate for the application of aeromagnetic surveys, modern magnetometer sensitivities and surveying techniques allow us to map the tiny signals caused by the weakly to non-magnetic rocks which dominate these environments. We discuss this in detail in Chapter 10.

Three main processes can, however, facilitate the presence of substantial amounts of magnetite or pyrrhotite within sediments. Figures 3.4 to 3.7 illustrate the manifestations of these processes in aeromagnetic survey data. These are as follows.

1. The incorporation of detrital magnetite grains sourced from pre-existing basement rocks (hence the importance of sediment provenance as well as depositional environment). Magnetite grains will survive significant transport and hydrous activity because magnetite is metastable (rather than unstable) in near-surface conditions. Simple examples of this would be heavy-mineral sands and sandstones. The recognition of ancient long-shore strand lines associated with magnetic mineral accumulations in aeromagnetic surveys is a significant tool in exploration of heavy-mineral sand deposits (Fig. 3.4a). Detrital magnetite is also common in glacial till (Gay 2004) and in high-energy erosional environments such as the Rio Grande Rift (Hudson *et al*. 2008). Grauch and Hudson (2011) contains a compilation of the magnetic susceptibilities of clastic sediments and sedimentary rocks from various places, and Hudson *et al.* (2008) contains a compilation of the magnetic susceptibilities of clastic sediments and sedimentary rocks from a variety of locations. An example showing both modern and ancient drainages is presented in Figure 3.4b.
2. The chemical precipitation of Fe-bearing oxides, carbonates and sulphides from solution, with subsequent development of magnetite-haematite or pyrrhotite by early diagenesis through to low-grade metamorphism. Some obvious examples of this are:

   a) BIFs – Barley (2009) gives a good description of the diagenetic to low-grade metamorphic conversion of greenalite to haematite and magnetite within Precambrian BIFs, and Schmidt and Clark (1994) note the formation of late diagenetic magnetite from primary haematite within the BIFs of the Hamersley Basin, WA (Fig. 3.5);
   b) pyritic black shale basin sediments, e.g. Pine Creek Geosyncline pyritic shales, with localised thermal metamorphic conversion of primary or diagenetic pyrite to pyrrhotite (Fig. 3.6a; also see Chapter 12). A related example is shown in Fig. 3.6b from the Adelaide Geosyncline where Fe-rich siltstones have developed pyrrhotitic horizons through diagenesis.

   A less obvious example can be seen in Figure 3.7a, which shows low-order magnetisation in an impure Carboniferous limestone sequence. Very small concentrations of Fe-rich minerals dispersed throughout the sequence have formed magnetic minerals (probably pyrrhotite) during diagenesis. This area is analysed in detail in Section 10.5.
3. Diagenetic growth (and/or destruction) of magnetite and/or pyrrhotite in sediments associated with hydrocarbon traps and migration of hydrocarbons. The mechanisms that produce magnetite in hydrocarbon basin environments are not well understood at this stage, but are most likely a combination of the following factors:

   a) bacterial action (the most common agent). The production of magnetite by bacteria is well documented (e.g. Arato *et al*. 2001). In particular, production of magnetite by sulphate-reducing bacteria within anhydrite caps to major salt domes in the West Texas Gulf and in the Paqualin salt diapir of the Timor Sea (Smith and Whitehead 1989; Gunn 1997b) has been noted as the cause of anomalous magnetic caps and haloes to several domes. Reynolds *et al*. (1991) studied the Simpson Oil Field (North Slope, Alaska), where ferrimagnetic greigite (Fe_3S_4) is concentrated locally in Upper Cretaceous beds. They reported

the likelihood that early diagenetic chemical and mineralogical changes are variably overprinted by later epigenetic alterations, possibly related to hydrocarbon seepage. The greigite probably formed at different times from sulphate reduction by bacteria that used either organic compounds derived from hydrocarbons or detrital organic matter, or both, as food sources. Magnetic-property studies suggest the natural remanent magnetisation of greigite-bearing rocks may contribute to the magnetic anomalies;

b) conversion of haematite or other high fO_2 Fe-oxide species within the sediments to magnetite by introduction of a reducing fluid (migrating hydrocarbons). This effect is noted but poorly documented, and (we suspect) not well understood at present.

A further primary magnetic effect in sedimentary basins is the observation of magnetic lows due to halite concentrations in salt domes and salt walls. This is due to halite being diamagnetic, and therefore having a small negative magnetic susceptibility. The example in Figure 3.7b is from the Genesis Oil Field in the Gulf of Mexico (Rowe 1998).

An expanded discussion of the magnetic character of sedimentary basins is presented in Chapter 10, and readers particularly interested in magnetisation of sediments are referred to the overview in Reynolds *et al.* (1990).

Primary processes – igneous rocks

Primary fractionation

The partitioning of Fe into various silicate and oxide mineral species during the formation of igneous rocks (both intrusive and extrusive) is primarily controlled by:

a) bulk chemistry (%Fe);
b) temperature of crystallisation (Tx);
c) oxygen fugacity (fO_2).

The Fe-bearing silicate minerals which can form in igneous rocks are too numerous to list, but commonly include the olivine, pyroxene, amphibole and mica groups. All of the silicates are non-magnetic at the scale of field-based measurements (i.e. they are not ferromagnetic).

The Fe oxide minerals commonly found in igneous rocks form three significant solid-solution series:

a) titanomagnetites, with end members magnetite – ulvöspinel (Fe3O4 – Fe2TiO3)
b) titanohaematites, with end members haematite – ilmenite (Fe2O3 – FeTiO3)
c) the magnetite – ilmenite solid solution series (Fe3O4 – FeTiO3)

Mafic and ultramafic rocks contain more Fe (and more Fe-bearing minerals) than felsic rocks. However, the distribution of the stability fields of crystallisation of Fe-bearing mineral species (Fig. 3.8) highlights the trend of crystallisation towards increasingly oxidised Fe minerals from the mafic to felsic rocks (i.e. with increasing SiO_2). Figure 3.8 also indicates that Fe within mafic and ultramafic rocks is typically partitioned into non-magnetic silicate minerals (olivines, pyroxenes and amphiboles) before formation of oxides, while Fe within intermediate to felsic rocks is increasingly partitioned into more oxidised minerals (trending from titanomagnetite – magnetite – ilmenite – haematite).

Felsic to intermediate igneous rocks therefore commonly have higher $\boldsymbol{k}$ values than mafic and ultramafic rocks. Empirical data from Grant (1985a) indicate that dacitic (extrusive) and quartz-dioritic (intrusive) compositions in particular may exhibit very high $\boldsymbol{k}$ values in their primary state. This represents a balance between two competing trends:

a) with increasing SiO_2, the Fe/Ti ratio increases ($\boldsymbol{k}$ increases);
b) with increasing SiO_2, Tx decreases, with corresponding decreasing %Fe ($\boldsymbol{k}$ decreases).

The $\%SiO_2$ will also control the partitioning of Fe between silicate and oxide species, with silica-saturated melts producing silicate-dominated rocks, and silica-undersaturated melts producing more oxide- (probably magnetite-) dominated rocks.

The role of orogenic environment of emplacement

The fO_2 of an igneous system is also strongly controlled by the orogenic setting of the magmas. Grant (1985a) reviewed the oxidation state implications of two major styles of intrusive fractionation trends from Osborne (1962):

a) 'orogenic' environments (including arc-related calc-alkaline systems);
b) 'anorogenic' environments (dominated by Fe-rich gabbro to felsic intracratonic intrusions).

The orogenic magmas trend towards silica-rich residual liquids during fractionation, with early crystallisation of high-Ti titanomagnetite in mafic and ultramafic rocks. Combined with an increasing fO_2 environment (a combination of increasing silica, plus input of crustal H_2O – possibly principally from sea water), the felsic and intermediate rocks tend to crystallise higher Fe:Ti ratio oxides (with increased ***k***). This is illustrated by trend line A in Figure 3.8.

In contrast, the anorogenic magmas tend to have a lower fO_2, with little or no external introduction of H_2O. The residual liquid in this fractionation trend has a high FeO content, with progressively lower fO_2. Fe is commonly partitioned into Fe-Mg silicates in the mafic to ultramafic members of the fractionation trend, and Fe-Ti oxides form in the felsic to intermediate phases; this can produce an overall low ***k*** series of intrusions (trend line B in Fig. 3.8). Grant (1985a) does, however, note that many of the major layered mafic-ultramafic complexes formed in anorogenic environments (e.g. Skaergaard and Bushveld Complexes) are, for the most part, strongly magnetic, and suggests this may be due to both early crystallisation of Ti-silicates (leaving the oxide phases relatively magnetite-rich) and a slow cooling history (see next section).

The role of H_2O is not restricted to crustal input into the magmatic system during fractionation, but is also linked to the composition of the basement. Magmas derived from 'older' (H_2O-depleted) basement tend to produce low-***k*** granites, whereas those derived from 'younger' (H_2O-bearing) basement tend to produce relatively higher-***k*** granites.

These two trends were noted by Ishihara (1977, 1981), with the division of granitoid suites in Japan into 'magnetite' and 'ilmenite' series granitoids. The magnetite series fractionates along the orogenic trend, while the ilmenite series fractionates along the anorogenic trend.

Cooling history of igneous rocks

As previously stated, the species of Fe-Ti oxide that will crystallise from a melt is highly dependent on both T and fO_2. The ternary phase diagram for the Fe-Ti-O system is shown in Figure 3.9. Note that a miscibility gap occurs within each series, within which a solid solution mineral composition is metastable. The miscibility gap is temperature-dependent, and widens with decreasing T. Above a critical T for each series, the miscibility gap closes. Typically, the first oxide to crystallise will have an intermediate composition along one of the solid solution series. With cooling, the miscibility gap in the solid solution widens and the Fe-Ti-oxide species tends to spontaneously exsolve into intergrowths of its end members. Grant (1985a) highlights the example of the titanomagnetite solid solution, which exsolves into magnetite and ulvöspinel-rich intergrowths as the system drops below 600°C. This has the overall effect of increasing ***k*** for the igneous rock. The tendency for ulvöspinel to oxidise towards magnetite and ilmenite (Buddington and Lindsay 1964) further increases ***k*** for the same rock during cooling.

Oxidation of titanomagnetites to titanohaematites during cooling, with spontaneous exsolution into intergrowths of ilmenite and haematite, is a common reaction. While the ***k*** of this system is typically low, it can develop a strong remanent magnetisation (see Section 3.4).

Grant (1985a) and Haggerty (1976) also highlight that the rate of cooling of the igneous rock is important. With rapid cooling, and loss of the majority of volatiles from the system, the Fe and Ti tend to stay in solid

solution; this is one reason why many basalts have low ***k***. Deeper-seated mafic intrusions, with slower cooling and greater retention of volatile phases, commonly develop more magnetite-rich oxides (and therefore higher ***k***).

Examples of intrusive crystallisation environments are presented in Figures 3.10, 3.11 and 3.12. The Devonian granite complexes that were illustrated in Figure 3.2 formed in an oxidised orogenic environment as described by Moore (2004), and Figure 3.10 shows one particular pluton in detail. The range of intrusive lithologies (and hence % Fe content) is not as wide as the magnetic signatures would suggest (White and Chappell 1988) and exemplifies how subtle changes in oxidation state can have marked effects on magnetic character. The magnetite zonation suggests that this poly-phase pluton has intruded over a prolonged period.

Figure 3.11 shows the TMI variations over the Black Hill Gabbroic Complex (Adelaide Fold Belt, South Australia), which is an example of mafic intrusion in an anorogenic environment. It is an Ordovician, undeformed, post-tectonic intrusion and has been interpreted as a suite of alkali or A-type mafic intrusions of continental tholeiitic association (Turner 1991). Lithologies include gabbro, olivine gabbro, gabbro-norite, anorthosite, norite, troctolite, peridotite, diorite and quartz diorite. The magnetic characteristics, which include strong remanent magnetisation, have been studied by Rajagopalan *et al*. (1993) and Foss and McKenzie (2009).

The Archaean Ora Banda Sill (Fig. 3.12) is an example of a largely non-magnetic mafic-ultramafic intrusion. The more voluminous upper differentiates are largely non-magnetic whereas the basal units are moderately to strongly magnetic. It is likely that the basal units, including the massive olivine cumulate (dunite), were originally non-magnetic but have attained magnetisation through subsequent metamorphic and tectonic processes.

3.3.3 Secondary processes – metamorphism

Magnetite is a common product of the breakdown of Mg-Fe silicates during metamorphism. In general, the volume % magnetite content (and hence ***k***) of a rock increases with increasing metamorphic grade.

The two primary controls on how much secondary magnetite can be formed during metamorphism are:

a) the bulk %Fe within the rock;
b) the oxidation state of the system.

Clearly, without mass chemical transfer into or out of the system, sediments and igneous rocks with very low percentages of Fe cannot produce significant volumes of magnetite. Therefore sediments such as carbonates, sandstones and quartzites with very low Fe content will retain low ***k*** values during progressive metamorphism. Semi-pelitic to pelitic shales, mudstones etc. have a greater Fe content than most sandstones and will therefore show increasing magnetite content during metamorphism. Apart from heavy-mineral sand(stones) and BIFs, the Fe content of sediments tends to be greater in finer-grained sediments (due to a higher % of Fe-bearing clays etc.).

The oxidation state of the primary rock appears to strongly control the partitioning of Fe (see Chinner 1960; McIntyre 1980; Grant 1985a), with:

a) low fO_2 favouring Fe silicate formation;
b) medium fO_2 favouring magnetite formation;
c) high fO_2 favouring haematite formation.

Relatively simple metamorphism without mass chemical transfer in or out of the system generally does not change the overall oxidation state of the system. The final metamorphic assemblage in this case tends to reflect the oxidation state of the original (pre-metamorphic) rock. The fO_2 of a metamorphic system does change during particular mineral reactions, particularly with release of H_2O during silicate dehydration reactions. However, these reactions (which tend to favour the production of magnetite) are buffered by complementary reactions which preferentially form Fe- silicates.

Grant (1985a) summarised some common mineral reaction series which develop magnetite with prograde metamorphism. These are:

a) lower greenschist facies (chlorite – biotite zone: T~250° – 350°C)
$$\text{chlorite + haematite} \leftrightarrow \text{chloritoid + magnetite + quartz + } H_2O$$
b) upper greenschist facies (biotite – muscovite zone: T~350° – 450°C)
$$\text{chlorite} \pm \text{biotite + haematite} \leftrightarrow \text{muscovite} \pm \text{K-feldspar + magnetite + quartz + } H_2O$$
c) epidote amphibolite facies (almandine-staurolite-kyanite zone: T~450° – 550°C)
$$\text{chloritoid} \pm \text{quartz} \pm O_2 \leftrightarrow \text{staurolite} \pm \text{almandine} \pm \text{kyanite} \pm \text{magnetite} \pm H_2O$$
d) amphibolite facies (sillimanite zone: T~550° – 650°C)
$$\text{biotite} \pm \text{quartz} \pm O_2 \leftrightarrow \text{K-feldspar + (Fe, Mg) silicates} \pm \text{magnetite} + H_2O$$
e) granulite facies (cordierite zone): T~650° – 750°C)
$$\text{(Fe, Mg) Al-silicates.}H_2O \pm \text{quartz} \pm O_2 \leftrightarrow \text{K-feldspar + (Fe, Mg) silicates} \pm \text{magnetite} + H_2O$$

Hence the tendency is for significant magnetite formation at low metamorphic grade from haematite-bearing rocks, and at high grade from biotite – amphibole-rich rocks. An example from the high-grade Broken Hill Block in New South Wales is shown in Figure 3.13. McIntyre (1980) more fully discusses the magnetisation in metasediments in this area.

This trend of increasing ***k*** with increasing metamorphic grade reaches a limit with the initiation of partial melting. With anatexis and the development of migmatites in high-grade metamorphism, the amount of magnetite within the system is generally diminished, with Fe and Ti oxides combining to form low-***k*** magnetite – ilmenite solid solution minerals. This is because:

a) at high T, the magnetite – ulvospinel solid solution miscibility gap closes;
b) the fO_2 of the more mafic restite portion of the anatectic system decreases.

This is often observed in aeromagnetic data as a weakening or complete disappearance of magnetically defined gneissic layering within a zone of migmatisation, to be replaced by irregular patches of 'flat' or 'fuzzy' magnetic texture. At the same time, the lithologically defined gneissic layering may be relatively well preserved in the field. An example of this is shown in Figure 3.14.

The increase and decrease in temperature during prograde and retrograde metamorphism may also directly influence ***k*** by influencing the stability of existing Fe-Ti oxide solid solution minerals, particularly in pre-existing igneous rocks (see Section 3.3.2).

3.3.4 Secondary processes – metasomatic alteration

The introduction of alteration fluids within a system can have a profound effect on the magnetic susceptibility of the rocks. It is generally difficult to predict the detailed reactions within any single metasomatic system due to:

a) the fluids involved varying widely in temperature, pressure, eH, pH and overall chemistry (with H_2O, NH, CO_2, CO_3, S, Fe and Cl – rich fluids common from various sources);
b) local variations in pressure and temperature during fluid migration;
c) variable host-rock bulk chemistry;
d) potential for major chemical/mass migration into or out of the host rocks.

However, some of the more common effects of different metasomatic/alteration processes are listed below.

a) Increasing magnetite (or pyrrhotite) content.
   i) Serpentinisation of mafic-ultramafic rocks (H_2O-alteration of olivine and/or pyroxene to magnetite + serpentine minerals (see Fig. 3.15).
   ii) Potassic alteration as core or margin to zoned porphyry systems. Examples include the magnetite alteration core of Bajo de Alumbrera, Argentina (Fig. 3.16) and annular magnetite alteration haloes around pencil porphyries of North Parkes, New South Wales (Fig. 3.17).

iii) Potassic and biotite-magnetite alteration associated with the Mt Leyshon hydrothermal breccia pipe of north Queensland (Fig. 3.18).
iv) Iron-oxide-copper-gold (IOCG) magnetite – fluid phase; e.g. extremely intense magnetic anomalies associated with both Ernest Henry (Webb and Rowston 1995) and Prominent Hill (Hart and Freeman 2003) (Fig. 3.19).
v) Magnetite skarn development; e.g. carbonate-hosted magnetite-skarns associated with the Ok Tedi porphyry, PNG (Fig. 3.20).
vi) Pyrrhotite and magnetite alteration haloes to VMS deposits; e.g. Golden Grove/Scuddles (Robinson and Belford 1991) (Fig. 3.21).
vii) Magnetite growth associated with CO_2 fluid-driven charnockite development along major deep-seated shear zones such as that reported in Rajaram and Anand (2003).

b) Decreasing magnetite content.
i) Low-T hydrothermal porphyry-related argillic and propyllitic alteration; e.g. magnetite-destructive zones associated with the majority of Andean Cu porphyry deposits as seen in Figure 3.16.
ii) IOCG-related haematite alteration; e.g. magnetically subdued zonation associated with Olympic Dam mineralisation (Rutter and Esdale 1985) (Fig. 3.22).
iii) Epithermal alteration (low- to high-sulphidation); localised (vein) to pervasive alteration of primary magnetite to hydrous oxides and/or sulphides. Commonly seen as linear to irregular magnetic low zones within variably magnetic volcano-sedimentary sequences (Figs 3.23, 3.24, 3.25 and 3.26). An expanded account of the alteration styles and aeromagnetic signatures in the very young Waihi-Waitekauri epithermal Au-Ag mineralised region in New Zealand can be found in Morrell *et al.* (2011) and Irvine and Smith (1990).
iv) Haematite and/or hydrous Fe-oxide development in fractured rock with low-T meteoric H_2O circulation. Commonly seen as linear magnetic lows along faults/fractures within magnetic rocks (Fig. 3.15).

It should be noted that, while metasomatic alteration of magnetite to haematite decreases the magnetic susceptibility of the host rock, magnetisation of the rock may increase in some cases due to the development of remanent magnetisation within the haematite (see Section 3.4). It is also worth emphasising that a single mineralised environment may have both magnetic mineral 'creative' and magnetic mineral 'destructive' processes associated with it. Porphyry and epithermal precious metal systems are good examples of this (Corbett 2009).

3.3.5 Secondary processes – deformation

Mechanical deformation may also influence both the magnetic susceptibility and remanent magnetisation of rocks.

Folding or shearing of rocks at moderate to high T/P (plastic deformation) conditions can concentrate both magnetite and pyrrhotite into low-strain zones, thereby forming mechanically thickened zones (e.g. fold hinges or pressure shadow zones), having increased $\boldsymbol{k}$ with respect to the surrounding rocks. Thermal annealing of the grains after mechanical flow may increase grain-size and grain interconnectivity, further increasing $\boldsymbol{k}$.

The dynamic recrystallisation of magnetite during shearing can produce significant changes in grain-size. This may vary from a coarser grain-size with combined shear and annealing of the grains, to development of fine to ultra-fine grains in mylonite and ultramylonite zones. As previously mentioned, rocks with coarse magnetite grains usually have higher $\boldsymbol{k}$ than those with fine to medium grains. However, ultrafine grains may also show a significant increase in $\boldsymbol{k}$. Variations in strain along large-scale shear zones due purely to grain-size variations may therefore be evident in aeromagnetic data.

As previously discussed, the development of permeability and porosity within rock masses due to faulting and fracturing can also significantly alter the $\boldsymbol{k}$ of a rock by providing mechanical conduits for metasomatic and/or low T meteoric fluids.

Another effect of deformation on the magnetic signature seen in aeromagnetic data is the reorientation of blocks of remanently magnetised rock by folding and faulting (producing a simple mechanical tilt to the remanent magnetic vector). While this is not a change in magnetic mineral content or $\boldsymbol{k}$, it can be significant for interpretation (see Jessell 2002).

3.3.6 Secondary processes – weathering

Weathering of rocks typically diminishes their ***k*** values due to the metastable nature of both magnetite and pyrrhotite at the Earth's surface. Conversion of magnetite and pyrrhotite to hydrous Fe oxide species such as limonite and goethite is very common during the weathering process.

However, a common weathering product, often associated with lateritic profiles, is maghemite – a strongly magnetic mineral comprising a dimorphous mix of magnetite and haematite at the microscopic scale. The considerable magnetic signature associated with surficial maghemite presents a significant problem for the magnetic interpreter as it tends to mask the signal from the underlying bedrock. Mapping the maghemite distribution, however, may assist the resolution of palaeo-surface and palaeo-drainage patterns associated with development and erosion of a laterite surface; this can provide useful clues to the location of palaeo-placer mineralisation. Figure 3.27 illustrates a lateritic, maghemite environment developed on mafic and ultramafic rocks in the arid Kalgoorlie region in Western Australia and Figure 3.4b shows magnetic weathering products sourced from granites in modern and palaeo-drainage systems.

3.4 THE LESS COMMON AND MORE COMPLEX FORMS OF MAGNETISATION

3.4.1 Introduction

Apart from the prevalent induced magnetisation, there are several other relatively common but less pervasive types of magnetisation that can occur within natural geological systems. These produce components of magnetisation whose intensity and orientation are difficult to predict from aeromagnetic survey data and are often recognisable only from the unusual magnetic anomaly patterns they produce. These effects may not be readily recognisable in aeromagnetic data, as they are usually small compared to the induced component of magnetisation and may also be oriented parallel to it. Their impact on the interpretation of magnetic data can, however, be quite significant (see examples at the end of this chapter). Recent research has addressed the difficulties in recognising and accounting for magnetisation in rock bodies that is not parallel to the Earth's field, and the reader is referred to Foss and McKenzie (2009) and Pratt *et al*. (2012) for details of this work.

These less common modifying influences on magnetisation are:

a) natural remanent magnetisation (NRM) – this includes thermomagnetic remanence (TRM), chemical remanence, detrital remanence, isothermal remanence and viscous remanence;
b) self-demagnetisation;
c) anisotropy of magnetic susceptibility.

3.4.2 Natural remanent magnetisation (NRM)

NRM arises as the result of competing forces within magnetic crystals. One force aligns atomic moments in parallel fashion while the other reverses atomic moments in anti-parallel fashion. The latter reduces the overall magnetostatic energy of the grain to as close to zero as possible. Which force dominates is strongly dependent on grain-size. For magnetite, grains smaller than 1 μm are single domain (s.d.) with atomic moments close to parallel and are said to be magnetically saturated. For magnetite grains larger than 10 μm the magnetostatic energy would be huge if the grain was saturated so the grain becomes subdivided into domains, and the grain is said to be multi-domain (MD). While each domain may be close to saturation they are arranged in such a way that the overall magnetostatic energy is reduced close to zero, with many domains anti-parallel, and the net remanence is very small. For grains between 1 μm and 10 μm, net remanence may be largely carried by walls between domains, or domains possibly grossly different in size for irregularly shaped grains, so that one domain is dominant and the grain, while not being saturated, is left with a significant remanence. These grains are said to be pseudo-single domain (PSD).

Whether a rock carries a remanent magnetisation is therefore strongly dependent on the average grain-size of the magnetic particles. Fine-grained basalts often carry a strong remanence while coarse-grained granites carry a weak and unstable remanence. The magnetisation is aligned closely with the prevailing magnetic field and is effectively 'blocked' during a physical and/or chemical process, remaining in the same orientation and

amplitude with respect to the crystal after the removal or alteration of the external field that was originally applied to the crystal. The magnetisation of each crystal will be different, but overall the net magnetisation is usually close to the direction of the prevailing field when the magnetisation is blocked.

Both magnetite and pyrrhotite can (and often do) carry a strong remanent magnetisation. Pyrrhotite associated with VMS deposits and massive NiS mineralisation frequently has a significant remanent magnetisation component.

Haematite and ilmenite also form a solid-solution series. While pure end-member haematite carries a weak remanence, about two orders of magnitude less than that of magnetite (for similar volume %), certain compositions can display remanence almost as strong as magnetite (Dunlop and Özdemir 1997). For the rare occurrence of 50:50 intergrowths of the end-members haematite and ilmenite, the remanence can acquire the reverse direction to the prevailing field (Grant 1985a), creating unusual magnetic signatures. Figure 3.28 shows an example from South Australia (Earth's field inclination –60°) where this remanence results in unusual negative anomalies. The remanent magnetisation is controlled by the original oxidation state of the rocks, the variation in oxidation state associated with superimposed metamorphism and meteoric H_2O alteration, the Fe:Ti ratio of the rock and the grain-size of the haematite-ilmenite solid solution grains.

There are several variants of NRM; these are discussed below.

Thermoremanent magnetisation (TRM)

TRM is acquired when a magnetic mineral species (most commonly magnetite) cools below the critical Curie Point isotherm. Above this temperature, magnetic minerals cannot produce a significant magnetic field (either ferromagnetic-induced or remanent). When a rock cools below the Curie Point, the magnetic minerals produce an induced field, and on further cooling below the 'blocking temperature' may acquire a remanent component, usually parallel to the prevailing Earth's field. TRM is therefore very common in igneous rocks, but unless the remanent vector is stronger than that from induction and has a significantly different orientation to it, the presence of remanence will be difficult to recognise in aeromagnetic imagery and may go unnoticed. Similarly, high-grade metamorphic rocks may acquire a TRM during post-metamorphic cooling (e.g. Schmidt *et al*. 2007).

Unlike magnetic susceptibility, which requires an external field to produce an induced field, TRM remains after removal of the external field.

The classic and widespread manifestation of TRM is in the sea-floor basalts, erupting from mid-oceanic ridges and spreading away from these ridges. The cooling lavas acquire a remanent magnetisation parallel to the prevailing Earth's field. This relatively continuous eruption process, combined with the periodic reversals in Earth's field orientation, gives rise to the familiar 'sea-floor stripes' evident in magnetic data over all the spreading oceans (Fig. 3.29). Terrestrial basalts also frequently attain TRM, as seen in the example from the Colac district in western Victoria (Fig. 3.30). The sea-floor stripes provided the key data for recognising the occurrence of polar reversals and this was confirmed by land-based geochronology and palaeomagnetic studies of basalt flows, leading to the acceptance of the science of palaeomagnetism. Palaeomagnetic studies combine remanence direction measurements with local geochronological control (from isotopic data and the fossil record) to provide an additional arm to geological age-dating and, through the compilation of polar wander curves, key information on historic global tectonics. This fascinating topic rarely has a major impact on day-to-day geological interpretation of aeromagnetic data, but can provide key information in local, detailed structural studies. Butler (2004) and Tauxe (2009) are two excellent texts, available free on-line, that cover this topic and expand on the physics of remanent magnetisation.

We outlined the chemistry of magnetic mineral development in intrusive environments in Section 3.3.2. Figure 3.11 provides a good example of a mafic magma that has cooled slowly, enhancing not only the development of magnetite but also that of remanent magnetisation (Rajagopalan *et al*. 1993, 1995; Foss and McKenzie 2011). In this case, more than one remanent magnetisation direction occurs in the intrusive complex and, because of movement of the Australian plate, these directions are quite different from that of the prevailing Earth's field.

TRM is widespread in igneous rocks, particularly in younger geological environments, but situations where it manifestly dominates over induced magnetisation on a large scale, are encountered infrequently. Section 3.4.4 discusses how to deal with the complications caused by TRM, and the other less common forms of magnetisation.

Chemical remanent magnetisation (CRM)

CRM occurs during formation (or changes to grain-size) of Fe oxide or pyrrhotite occurring at temperatures lower than the Curie Point.

CRM may occur with the formation of Fe-oxides and/or pyrrhotite by:

a) primary deposition (e.g. haematite) from solution in primary BIF formation;
b) diagenetic growth within sediments;
c) metamorphic growth at low to moderate metamorphic grades;
d) metasomatic development. An excellent example is the strong negative magnetic anomaly (–2000 nT) associated with a magnetite-bearing, potassic-alteration hydrothermal breccia pipe related to the Mt Leyshon Au mineralised system, north Queensland (Fig. 3.18).

Detrital remanence

This type of remanence occurs by the slow settling of fine-grained Fe oxides from aqueous suspension. It is not commonly observed directly in aeromagnetic surveys, but may be found in glacigene varved clays and some layers of turbidite sequences. The expansion of interest in palaeomagnetic studies has led to more and finer sensitivity measurements of detrital remanence.

Isothermal remanence

This is a localised remanent field produced by instantaneous 'remagnetisation' by a very strong applied field. The most common cause of isothermal remanence is lightning strike, which produces remanence over a very small (outcrop-scale) area.

Although the effect is too small to be noticeable in aeromagnetic surveys, it is a source of 'noise' in detailed petrophysical measurements and palaeomagnetic (polar-wander) studies. Rocks that are subjected to magnetisation testing with a geologist's pencil magnet may acquire a small isothermal remanence and often be rendered unsuitable for subsequent laboratory magnetisation tests.

3.4.3 Self-demagnetisation

Self-demagnetisation is due to a (usually small) back-field which opposes the direction of rock magnetisation from either (or both) induction or remanence. The size of this back-field depends on the shape of the body and the orientation (and strength) of the induced plus remanent magnetisation of the rock. It will be zero where the magnetisation is parallel to the long axis of a needle-like body and maximum where the magnetisation is oriented parallel to the shortest axis of a disc-like body. Clark and Emerson (1999) advise, from extensive experience in laboratory and modelling studies, that self-demagnetisation becomes significant where $\boldsymbol{k}$ exceeds 0.1SI (roughly 3% magnetite equivalent). In this situation, corrections can and should be applied in quantitative modelling (Hillan and Foss 2012).

The Trough Tank case history (Gidley 1988) provides an excellent summary of the practicalities of dealing with self-demagnetisation, and Clark and Schmidt (1994) give a comprehensive overview of the range of unusual magnetic effects common to thinly bedded iron formations. Figure 3.31 (adapted from the two papers above) illustrates the interpretation limitations which prevail when the assumption of induced magnetisation is not valid.

3.4.4 Anisotropy of magnetisation

Anisotropy of magnetisation (Bhathal 1971) typically occurs within thin sheet-like bodies with relatively high percentages of Fe oxides (>5%). Although the effect may be quite widespread and observable at laboratory and outcrop scale, it is rarely evident in aeromagnetic data.

Within these thinly bedded units, an anisotropic, triaxial magnetisation field occurs, with the vector of maximum magnetisation occurring (typically) within the plane of bedding. The orientation of this maximum vector is not predictable and must be established by petrophysical measurements on oriented samples. This anisotropy is in part related to self-demagnetisation effects (Clark 1997).

Other manifestations of anisotropy related to mineral fabric, deformation and metamorphism occur but their effects are very rarely observable in magnetic anomalies. In essence, the interpreter should be aware of the likelihood of anisotropy in magnetite BIFs and pyrrhotitic ores, but apart from this, the phenomenon does not affect our general geological interpretation. The reader is referred to Guo *et al*. (2011) and Clark and Schmidt (1994) for enlightening summaries of the range of unusual magnetisation effects occurring in BIF environments. Figure 3.32 provides an illustration of this.

3.4.5 The effect of complex magnetisation on interpretation

We refer to the above 'less common' or modified forms of magnetisation as being complex or 'unusual' because their existence is generally recognised by the unusual magnetic anomaly forms they produce. Unusual magnetisation is likely to occur within any large-scale aeromagnetic survey. In many instances it is either:

a) sub-parallel to the current Earth's field and/or very weak compared to the induced field – in these cases we are unlikely to recognise its presence in aeromagnetic imagery, or;
b) broadly anti-parallel to the Earth's field and thereby producing readily recognisable unusual or anomalous patterns in magnetic imagery, alerting the interpreter to its presence. The Mt Leyshon breccia pipe (Fig. 3.18) is an excellent example. At the magnetic field inclination prevailing at Mt Leyshon, there is no plausible rock body shape that could produce a negative magnetic feature under the influence of induced magnetisation alone. We can therefore conclude that the magnetisation of the rock body causing this negative anomaly is non-induced. However, we must be wary of readily linking negative magnetic anomalies to unusual magnetisation. In equatorial regions, negative magnetic responses (from induced magnetisation) are far more common than positive ones. Hence the interpreter must become familiar with the normal and unusual magnetic responses within each new project area.
   Where the remanence is strong and askew to the prevailing Earth's field, it once again should produce unusual-looking anomalies (e.g. the Black Hill Norite – see Fig. 3.11), but the combination of the strike, dip and plunge directions of magnetic bodies has the potential to make these anomalies look quite normal. The danger zone is where strong remanence is close to the Earth's field direction (e.g. within 30°). This may not be recognised, with induced magnetisation assumed in subsequent modelling. Typically, the error in the direction to source is half of the angular departure (e.g. 15°), which is serious when siting deep drill targets.

Successful strategies for recognising and dealing with the presence or potential presence of these unusual forms of magnetisation are advancing rapidly in current research projects. The reader is referred to Foss and McKenzie (2009), Pratt *et al*. (2012) and Hillan and Foss (2012) for recent developments on this front and we discuss these in Chapter 8. We emphasise that specialist tools and experience are essential when the detailed investigation of rock units with complex magnetisation is required during an interpretation campaign. We list below some of the observations which should make the interpreter suspect the presence of such complex magnetisation:

a) rocks with significant (e.g. >3%) visible magnetite (and/or haematite or pyrrhotite);
b) rocks with very high magnetic susceptibilities (>0.1 SI);
c) rocks showing low susceptibilities but strong attraction to a swinging magnet (strong haematite remanence?);
d) magnetic anomalies with amplitudes of 1000s nT;
e) magnetic anomalies which look odd in the context of an entire magnetic image.

The Trough Tank example (Gidley 1988) highlights the potential interpretation difficulties presented by unusual magnetisation. In Chapters 2, 5 and 8 we discuss the techniques available and the methods by which we can infer the position and shape of the magnetic rock unit causing a magnetic anomaly. In concluding this section, we emphasise that the delineation of the depth and position of the top surface of a magnetic rock body can be done with some confidence, irrespective of the form of magnetisation. However, uncertainty in magnetisation translates directly to uncertainty in dip and plunge, so where drill holes are planned to intersect blind bodies at considerable depth, we emphasise that specialist analysis must be undertaken to reduce the risk of the holes missing their target.

As the Trough Tank example illustrates, once intersected, the magnetic rocks can be subjected to laboratory-scale petrophysical analysis to determine the magnetisation; this can then constrain future modelling and provide robust guidance in siting drill holes.

Another telling example of the impact of remanence in interpretation is the pyrrhotite-bearing, Kewell gold prospect in the Stawell district of western Victoria (Musgrave *et al.* 2006); this case study is recommended to the reader. In this case remanent magnetisation in pyrrhotite is found in association with a gold mineralised system.

3.5 MEASURING MAGNETISATION IN OUTCROP OR DRILL CORE

The magnetic susceptibility of a rock is readily measured in the field using a hand-held magnetic susceptibility meter. These devices are based on the principle of a strong alternating magnetic field produced by an electric coil in the measuring head of the meter, which generates an alternating induced field in the rock. The degree to which this field alters the reluctance circuit in the meter gives a measure of susceptibility.

We emphasise that the magnetic susceptibility meter will not respond to remanent magnetisation within a rock sample because the remanence is constant. Therefore, it is possible to get a very low or even zero magnetic susceptibility reading from an outcrop or drill core even when the rock is associated with a significant magnetic anomaly in the aeromagnetic survey. For this reason, it is advisable to combine the use of the susceptibility meter in the field with a small magnet (e.g. the commonly used swinging pencil magnet), which will detect significant magnetisation caused by remanence. We should add that rock samples exposed to the geologist's pencil magnet will be rendered unsuitable for laboratory remanence measurements because the magnet has a remagnetising effect similar to that of a lightning strike.

Where remanence is as strong as, or stronger than, the induced magnetisation in a rock body, a workable estimate of strength and direction can be obtained using a portable ground magnetometer. This involves some careful but relatively straightforward measurements on a fist-sized sample (core preferable but not essential) and some equally straightforward calculations. The method is outlined in Breiner (1999). We discuss the field follow-up of magnetic anomalies and the observation methodologies for magnetic susceptibility meters more fully in Section 9.9.

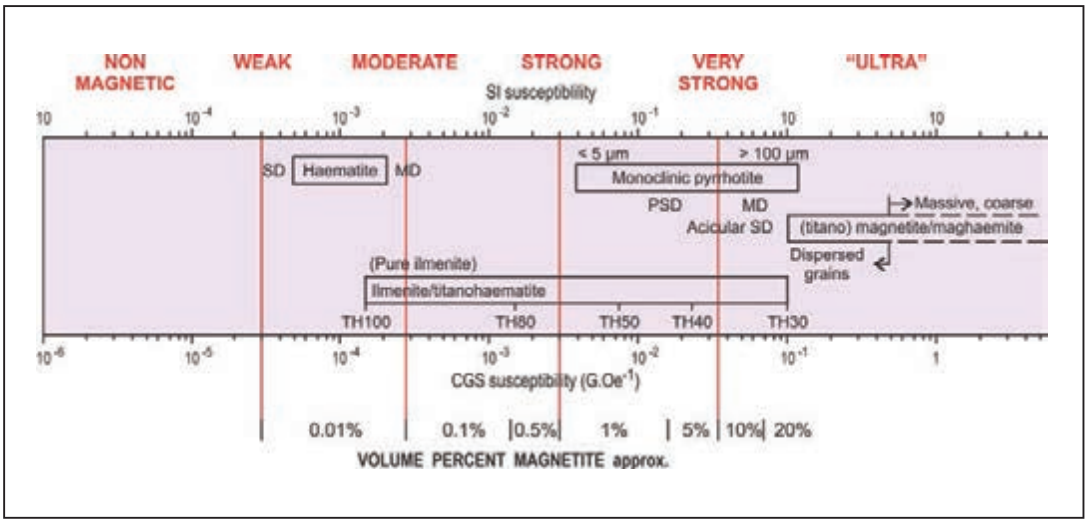

Figure 3.1: Observed magnetic susceptibility ranges of the magnetic minerals (after Clark 1997). The approximate equivalent volume % magnetite is indicated for each mineral as well as a rating of the strength of the associated magnetisation.

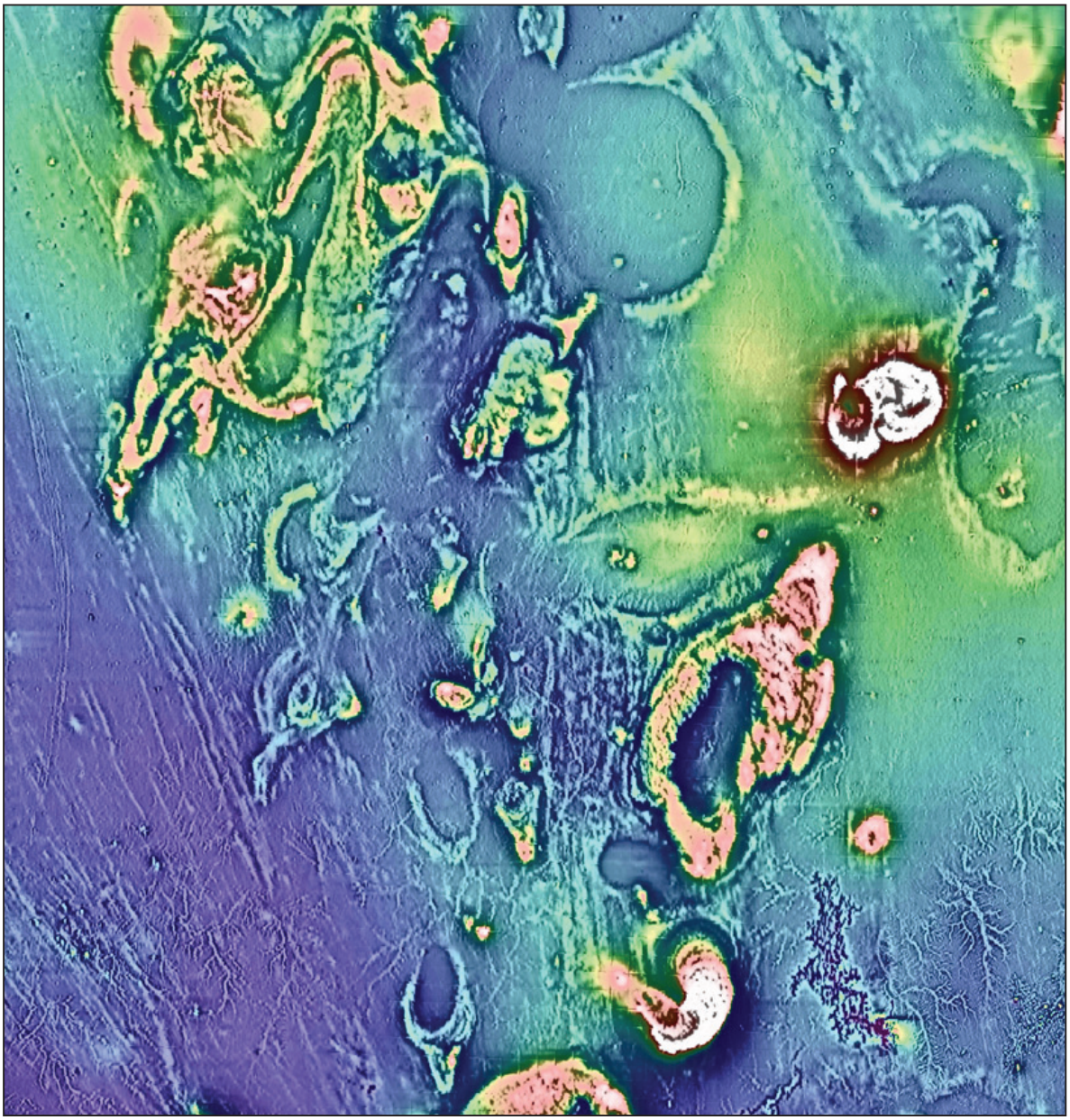

Figure 3.2: Magnetic zonation in granites, western Victoria. Data courtesy of Geoscience Australia and the Geological Survey of Victoria. The image is ~140 km E–W.

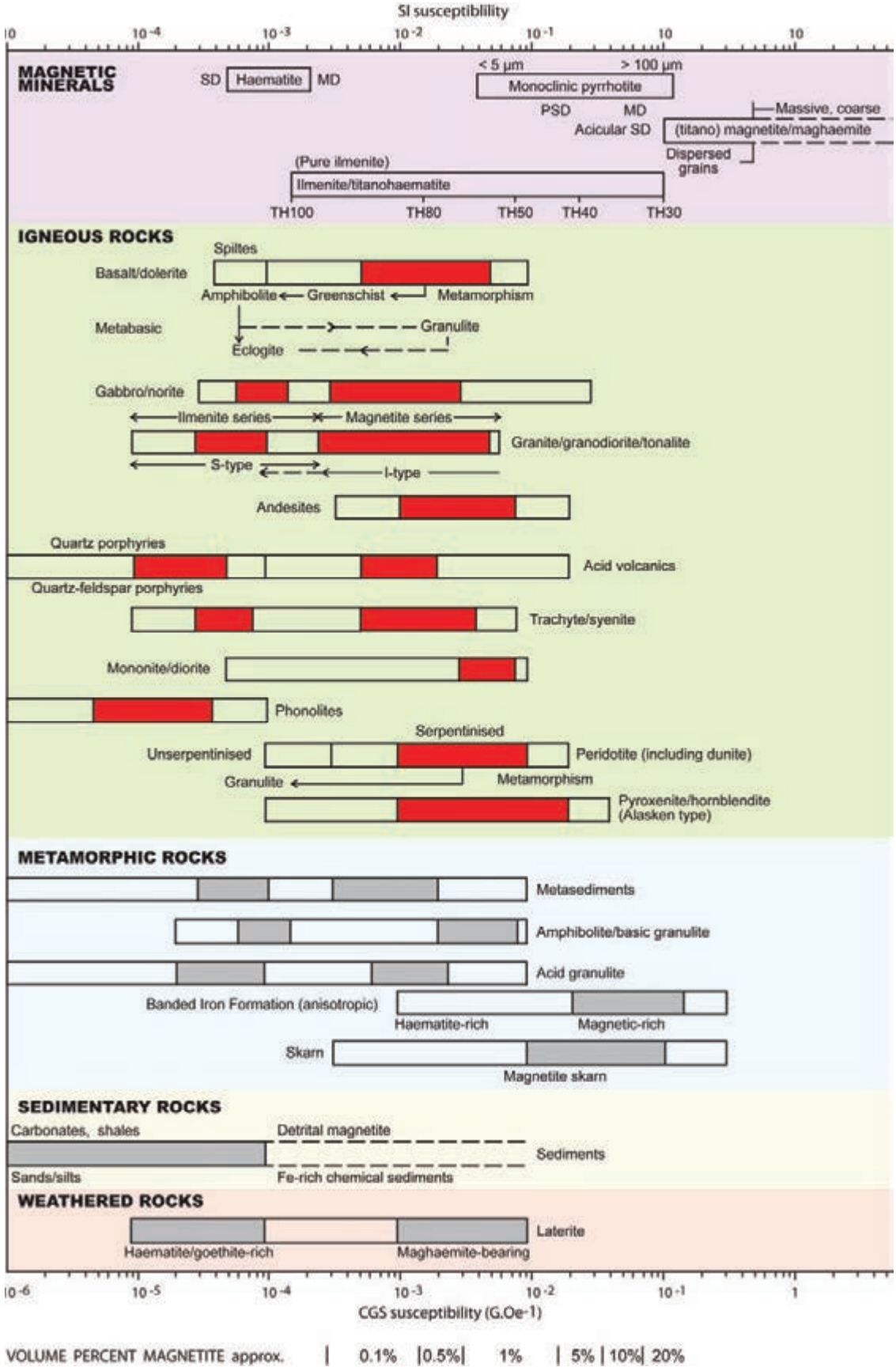

Figure 3.3: Observed and common magnetic susceptibility ranges for various rock types (after Clark 1997). The solid areas represent the main clusters of observations.

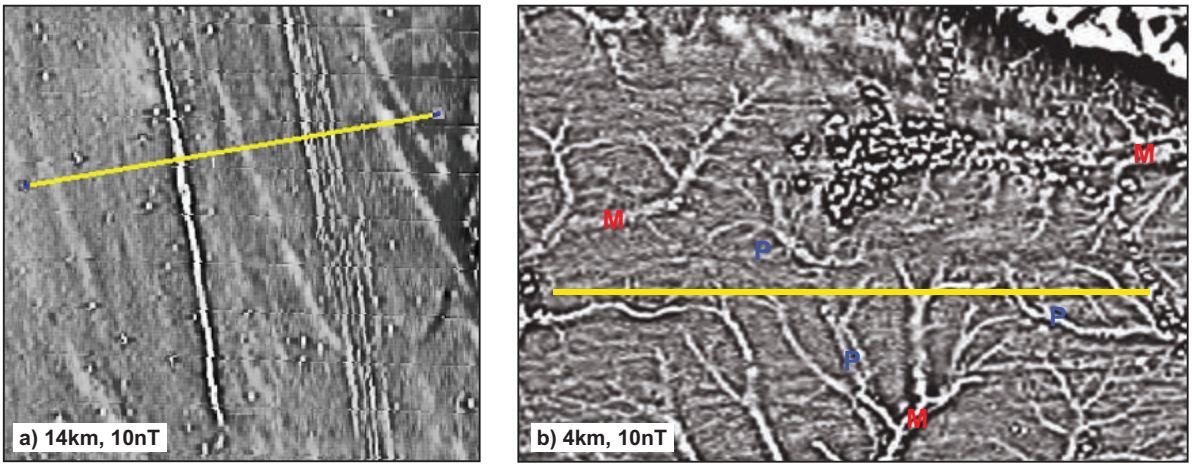

Figure 3.4: Aeromagnetic expressions in superficial sedimentary environments.
a) heavy mineral strand lines (western Victoria).
b) modern (M) and palaeo drainages (P) (western Victoria; see also Moore 2004, Fig. 14).
The length of the yellow line is indicated in the key as is the common amplitude of the sedimentary magnetic units.
Data from Geoscience Australia and the Geological Survey of Victoria.

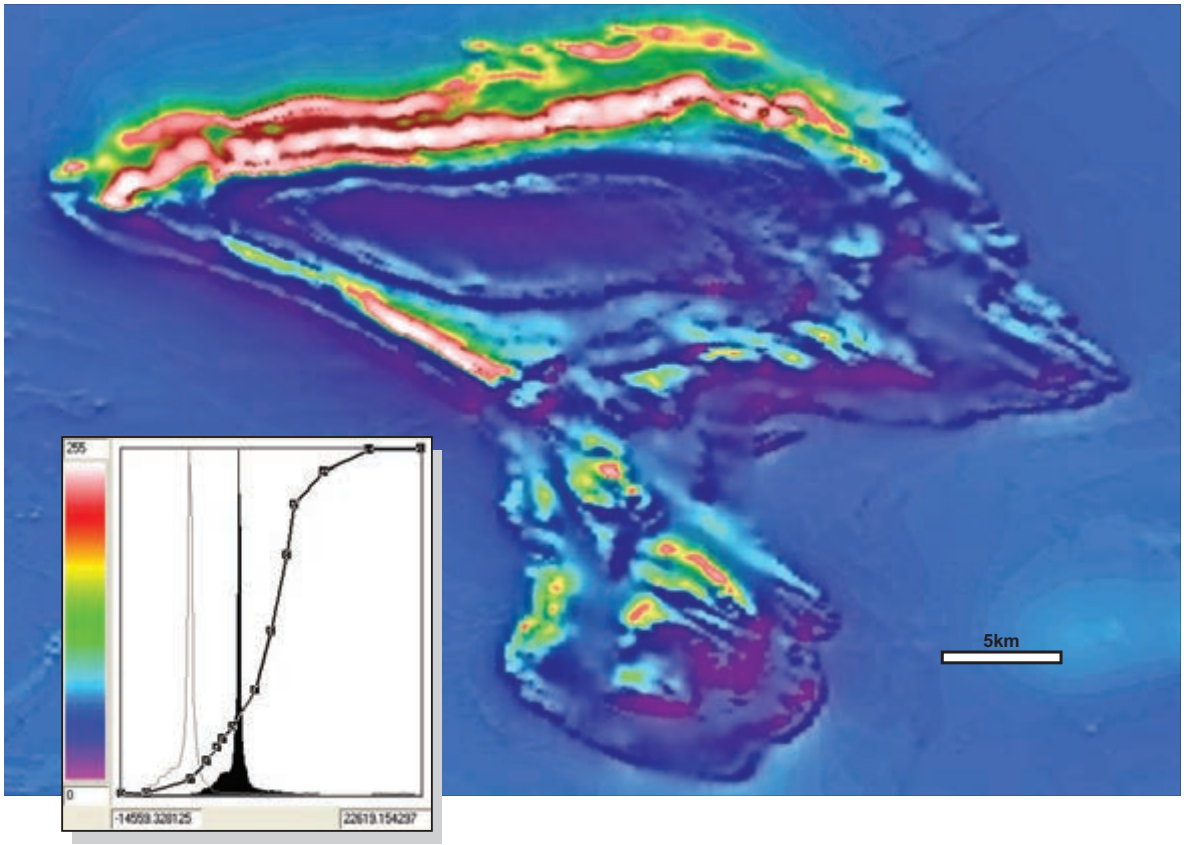

Figure 3.5: Composite aeromagnetic image over the Turner Syncline in the Hamersley Basin, WA. Note the enormous range in residual magnetic intensity (–14 500 nT to 22 600 nT) due to the magnetite BIFs. Data from Geological Survey of WA open file records.

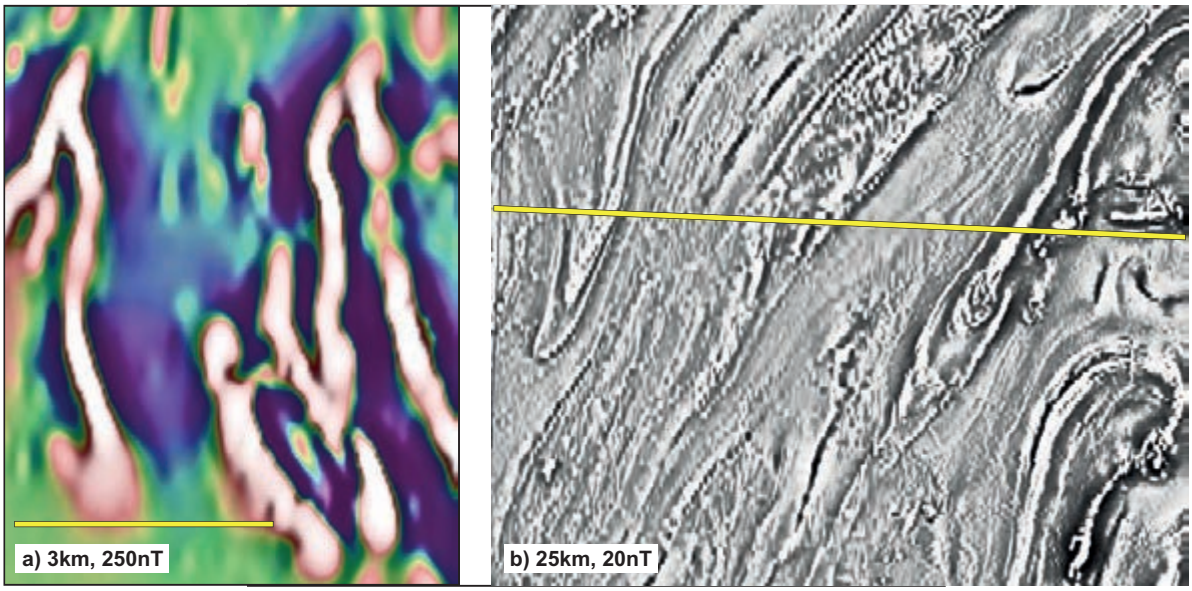

Figure 3.6: Aeromagnetic expressions in geosynclinal sedimentary environments.
a) Pyrrhotite-bearing black shales from the Pine Creek Inlier, NT.
b) Pyrrhotite-bearing siltstone sequence from the Adelaide Geosyncline, SA.
The length of the yellow line is indicated in the key is the common amplitude of the sedimentary magnetic units. Data from Geoscience Australia, NT Geological Survey and DMITRE.

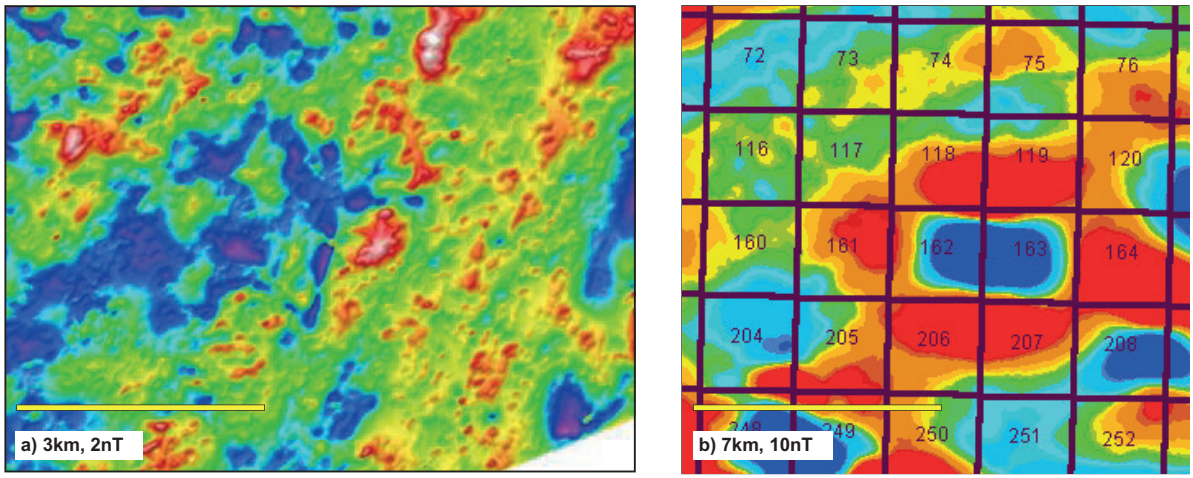

Figure 3.7: Very low-order magnetic variations in sedimentary environments.
a) Mesozoic limestone package (Galmoy, Ireland). Data courtesy Lundin Mining.
b) magnetic low over a salt dome (Gulf of Mexico, from Rowe 1998). Data courtesy Fugro Airborne Surveys.

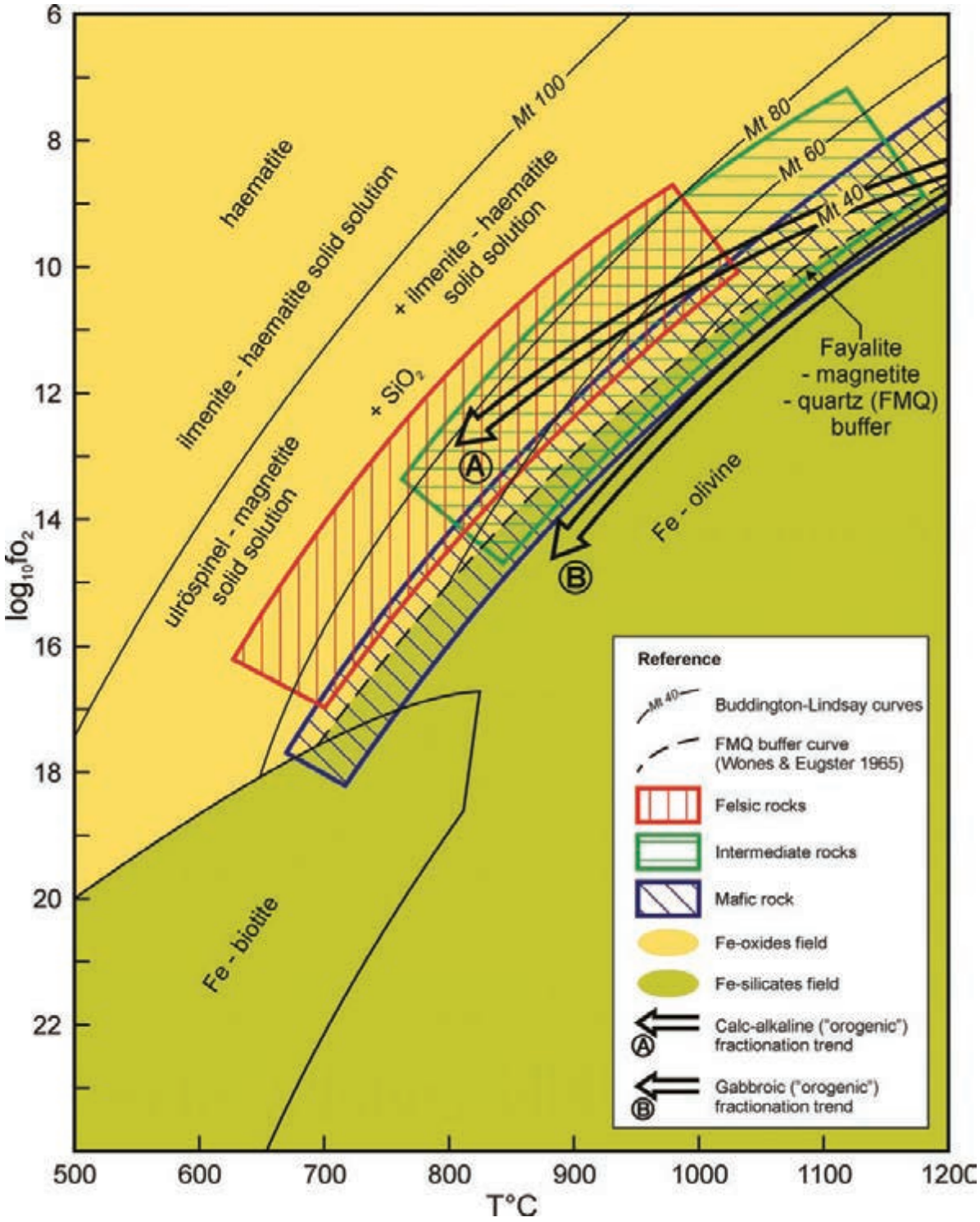

Figure 3.8: Buddington–Lindsay oxygen fugacy *v.* temperature curves for magnetite–titanomagnetite and haematite–ilmenite solid solution series, plus the FMQ curve (from Wones and Eugester 1965). Arrow A marks the general trend of fractionation of orogenic series magmas. Arrow B marks the general trend of fractionation of anorogenic magmas. Diagram adapted from Grant (1985a).

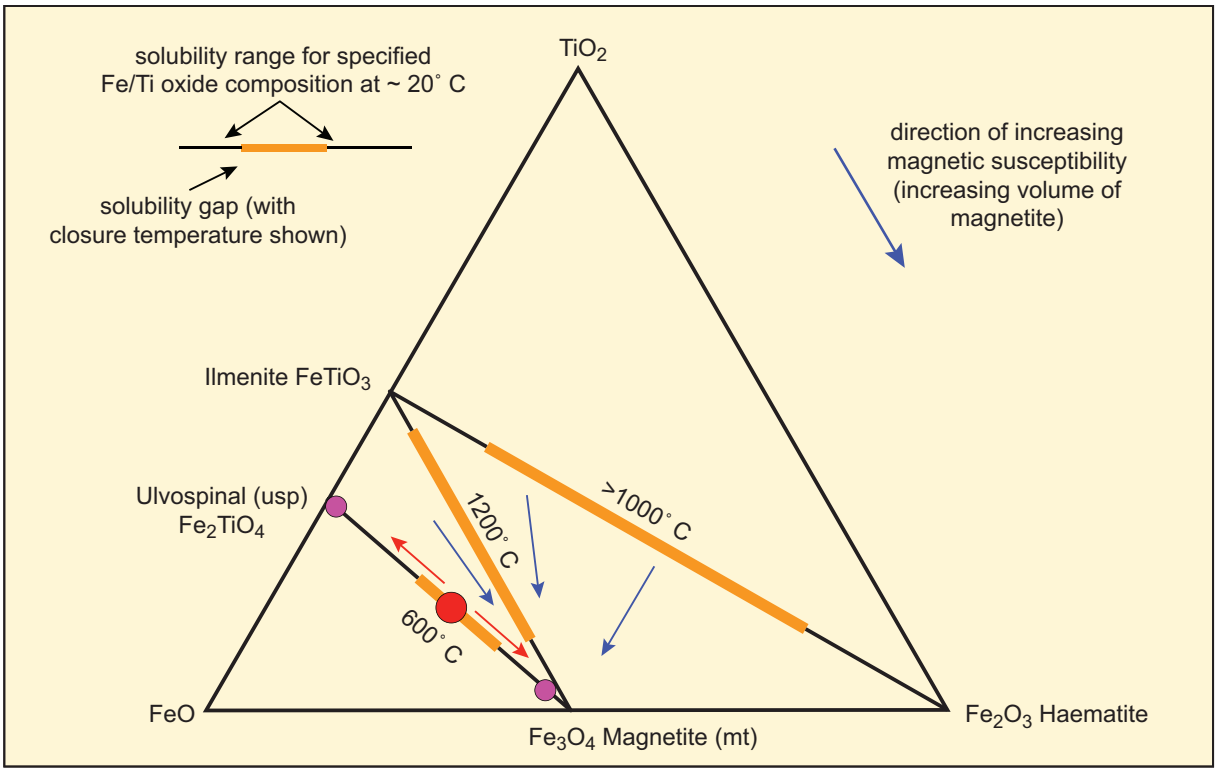

Figure 3.9: Fe–Ti–O ternary phase diagram (after Grant 1985a). A mineral species may initially crystallise as some intermediate composition at a temperature T along one of the solid solution series. As T decreases, the miscibility gap along the solid solution series widens and the mineral may become metastable, spontaneously exsolving into intergrowths of the end member mineral species. The example shown (red dot) represents a mineral phase within the mt-usp series, crystallised at T>600° (above the miscibility gap closure). With cooling, the phase exsolves into intergrowths of mt-rich and usp-rich phases, with a consequent increase in ***k*** for the rock.

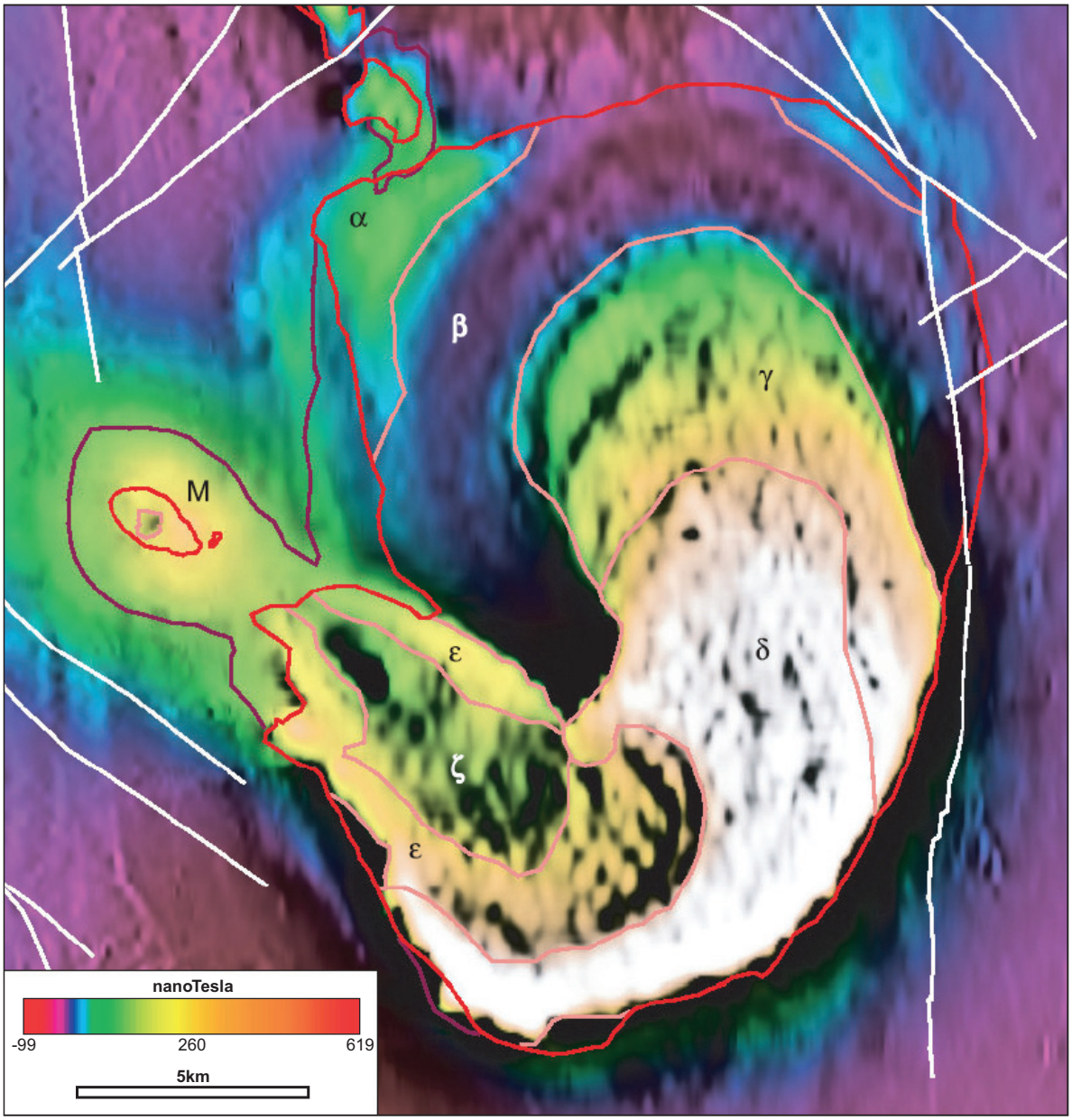

Figure 3.10: Composite RTP 1st VD image over the Tarnagulla Granite in NW Victoria (after Moore 2004). The magnetic zonation (labelled by Greek symbols) and structural form indicate prolonged intrusion in an oxidised orogenic environment.

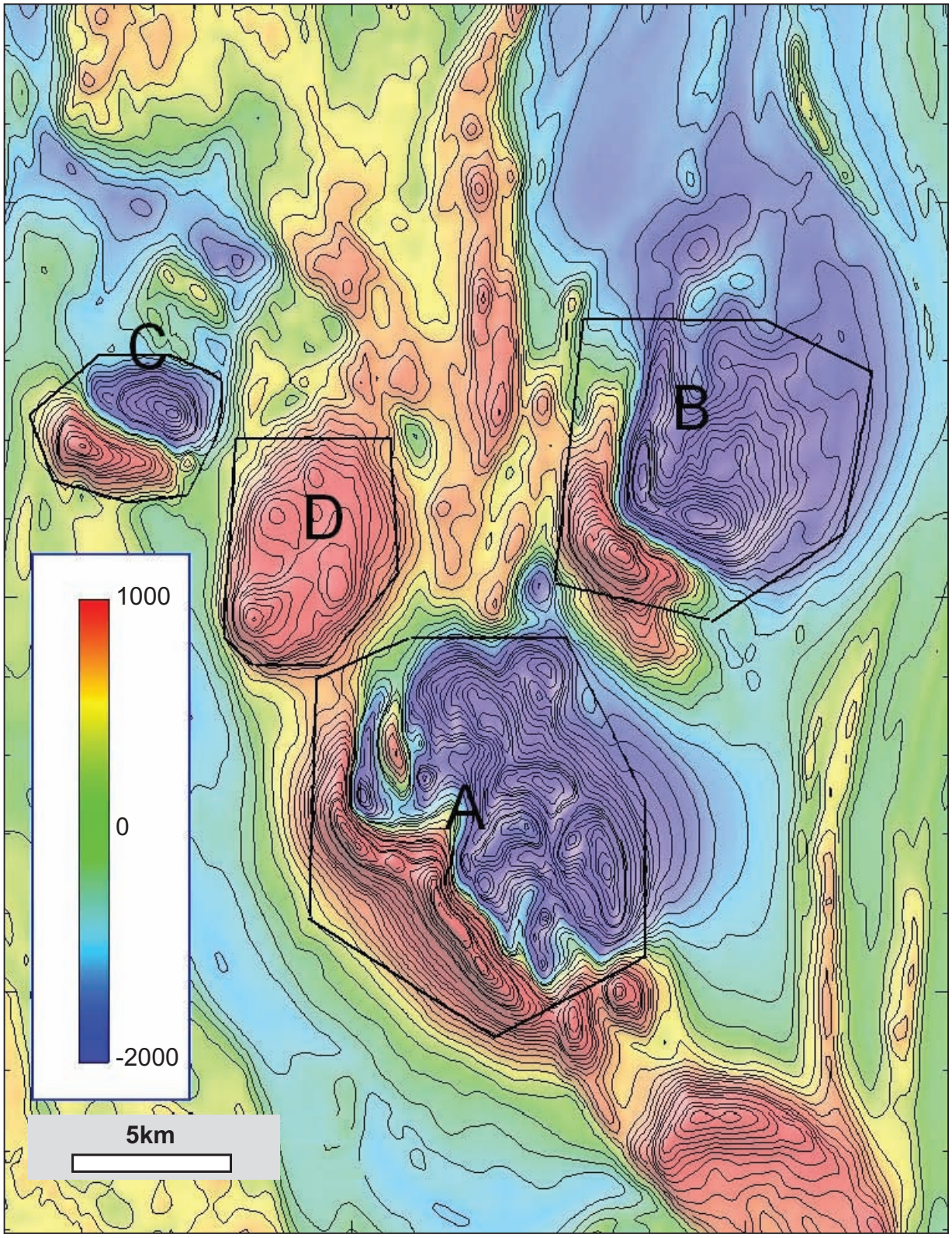

Figure 3.11: TMI image over the Black Hill Gabbroic Complex (after Foss and McKenzie 2011). This exemplifies strong primary magnetisation in a mafic complex that has crystallised slowly (at considerable depth) in an anorogenic environment, allowing exsolution to magnetite and also preservation of remanent magnetisation.

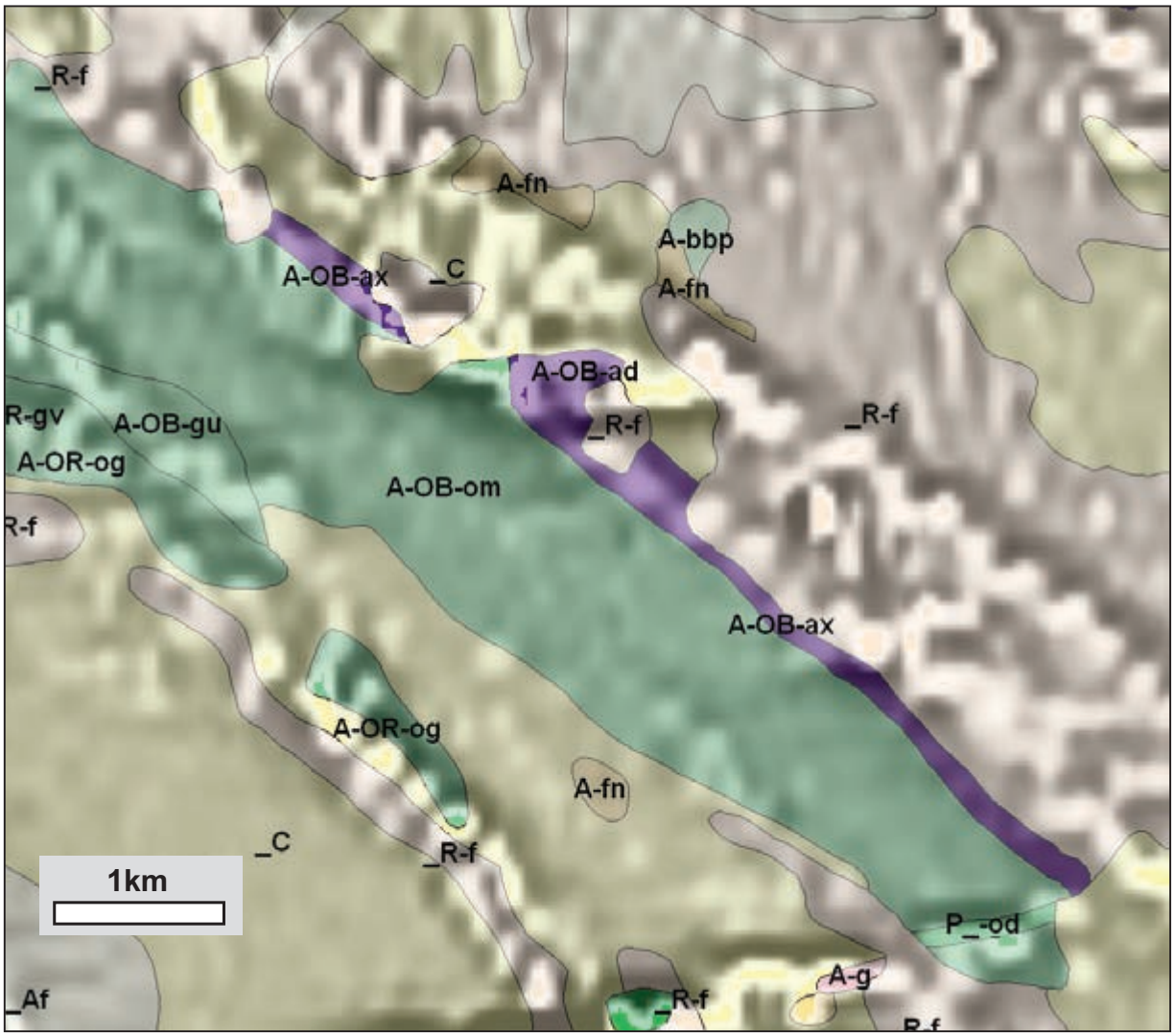

Figure 3.12: RTP 1st VD image superimposed on outcrop geology over the Archaean Ora Banda Sill (A-OB), WA. The sill faces SW and the upper differentiates, gu (quartz-gabbro/granophyre) and om (gabbronorite) are very weakly or non-magnetic. Only the basal differentiates, ax (bronzite/norite) and ad (dunite) are magnetic. Data from GSWA open file digital databases.

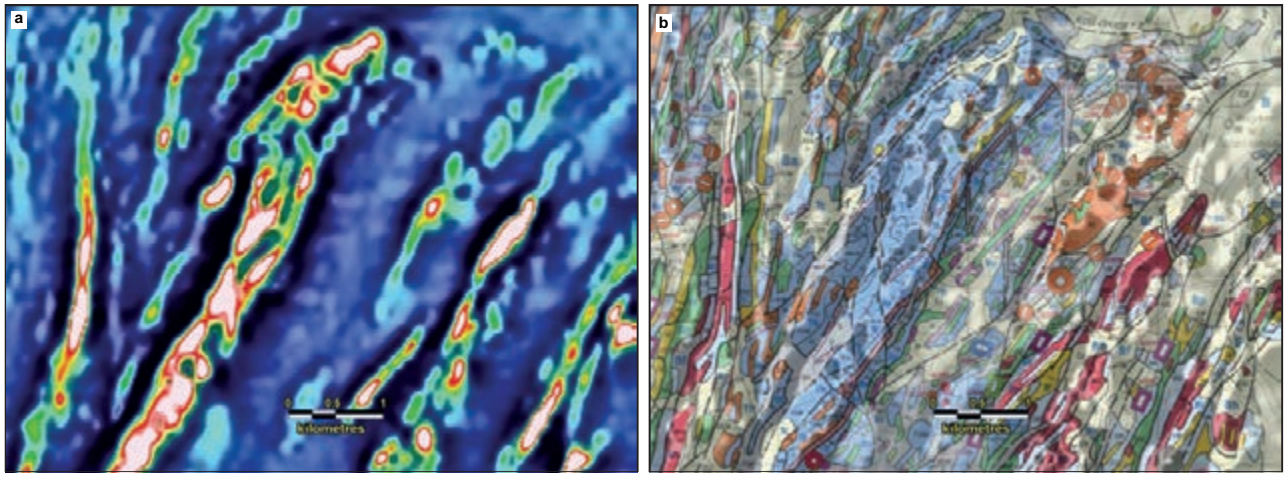

Figure 3.13: Aeromagnetic and geological images over the Maybell area, 20 km NW of Broken Hill in NSW. a) Composite RTP 1st VD/2nd VD image: the higher-intensity horizons have TMI amplitudes of 500 nT or more. b) Lithological map with RTP 2nd VD greyscale image superimposed: the pale blue geological unit comprises psammo-pelitic metasediments and the magnetite-rich horizons within these have developed during metamorphism. This area has been studied in detail by McIntyre (1980) and Isles (1983). Data from Geoscience Australia and Geological Survey of NSW.

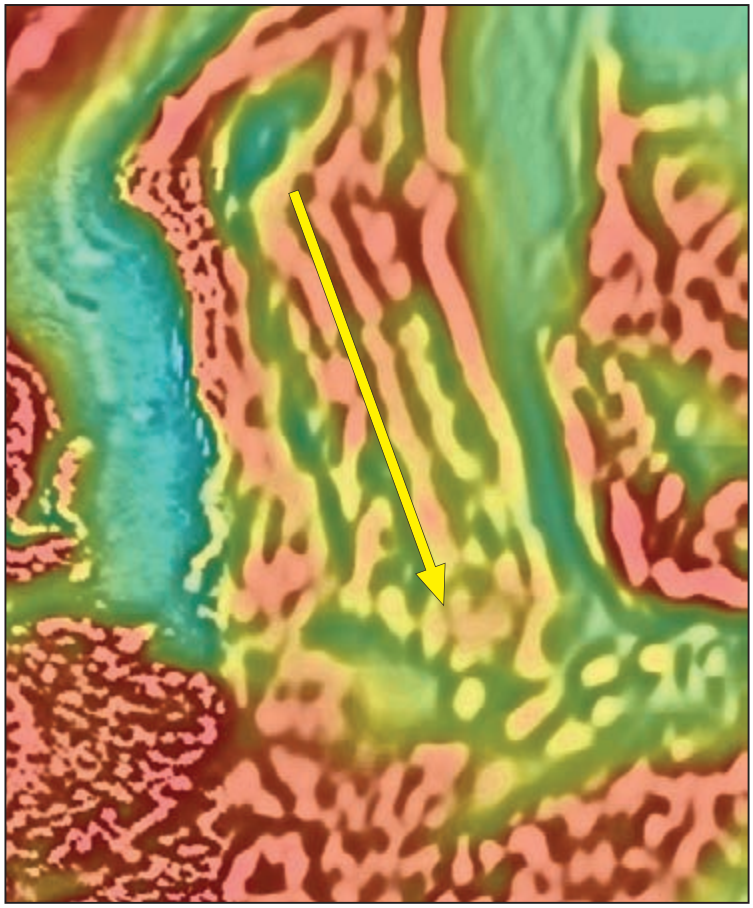

Figure 3.14: Diminution/destruction of magnetite caused by increasing migmatisation (arrow) of high-grade metamorphic rocks in the Olary region, SA. The image is a composite RTP 2nd VD and is 10 km E–W. Data courtesy of DMITRE.

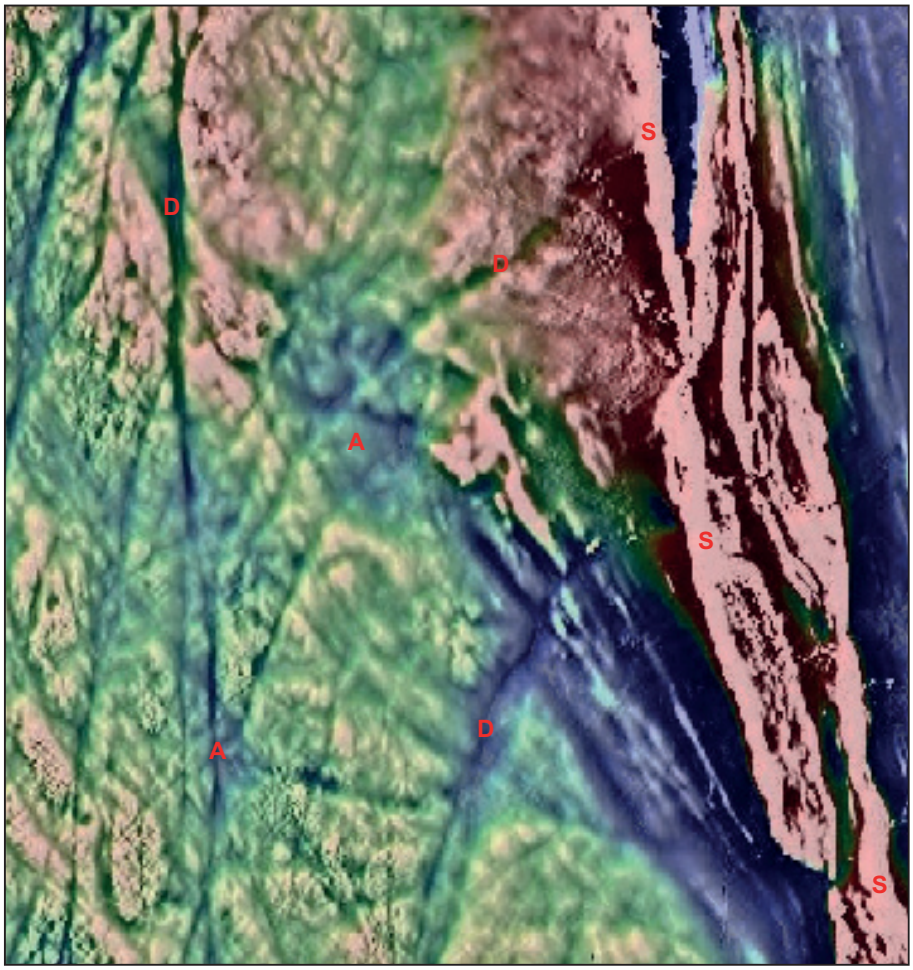

Figure 3.15: Magnetic alteration effects in the Goongarrie district, WA. Data courtesy UTS-Geophysics. S = indicates zones of serpentinisation, D = magnetite destruction/haematite development in fault zones, A = alteration/ magnetite destruction zone at junction of faults and intrusive contact. The image is 15 km E–W.

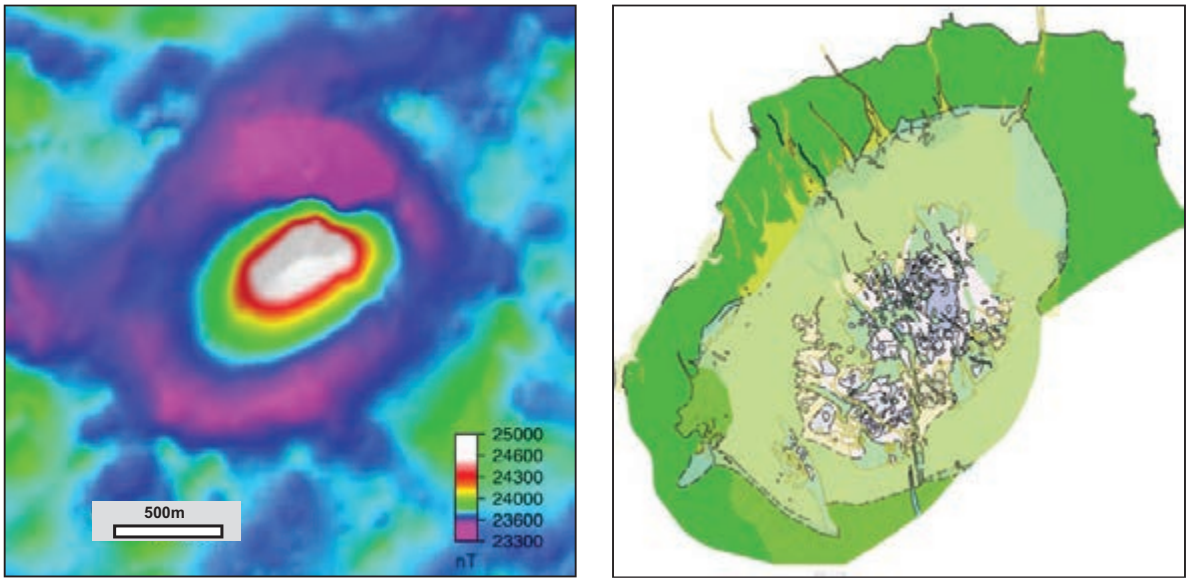

Figure 3.16: Aeromagnetic image and alteration map over the Bajo de la Alumbrera porphyry copper-gold deposit, Argentina (after Hoschke 2011). Note the magnetic core associated with magnetitie-biotite in the potassic alteration zone, and the surrounding flat magnetic area due to magnetite destruction in the phyllic (pale green) and propyllitic (dark green) alteration zones. The moderately magnetic host rocks are andesitic volcanics.

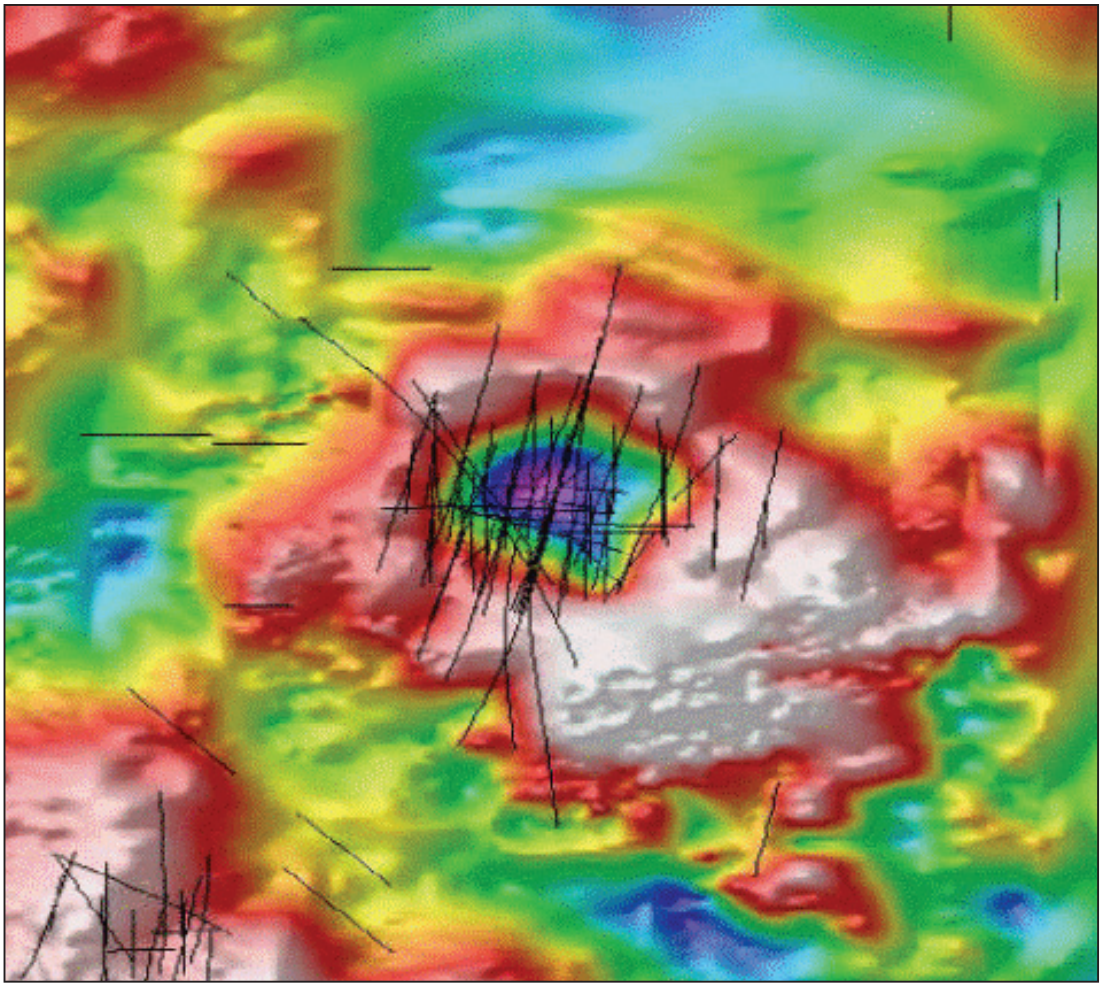

Figure 3.17: Magnetite alteration effects around one of the pencil porphyries, North Parkes district, NSW. The black lines are drill-hole traces, the image is ~1 × 1 km. Data Courtesy Rio Tinto Exploration.

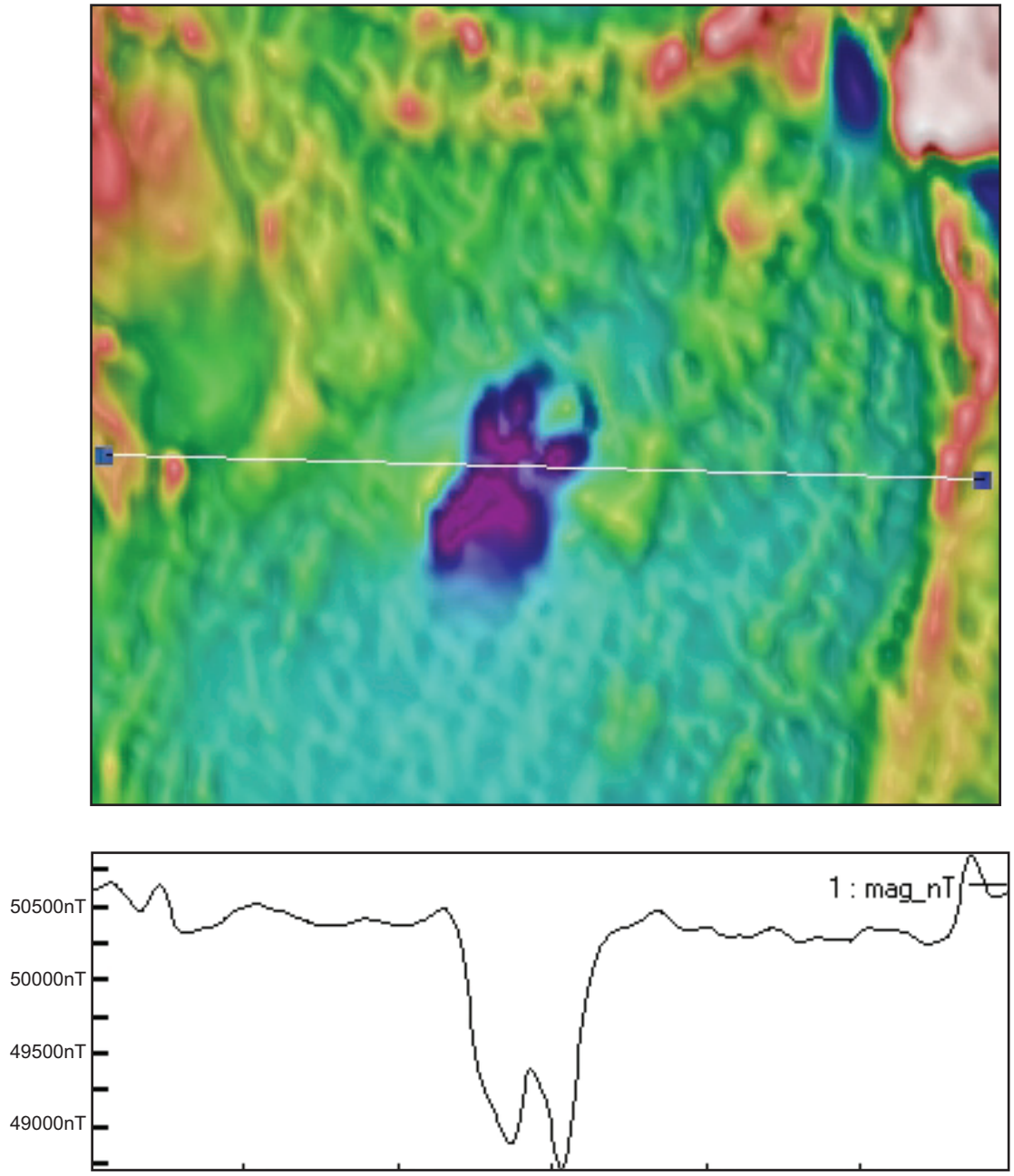

Figure 3.18: Biotite-magnetite alteration anomaly associated with the Mt Leyshon hydrothermal breccia pipe (Sexton *et al.* 1995). Note that in this case the magnetic response is anomalously negative indicating (chemical) remanent magnetisation. The profile is ~6 km long. Data courtesy Fugro Airborne Surveys.

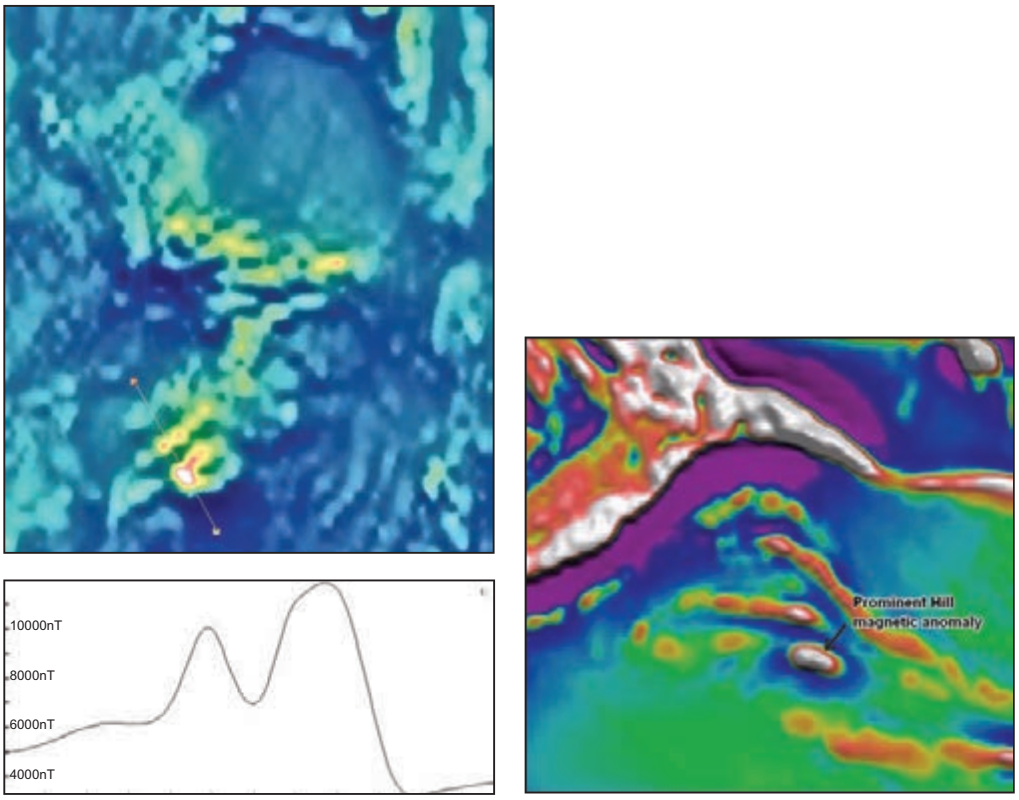

Figure 3.19: Magnetite alteration in and around the Ernest Henry (Qld) and Prominent Hill (SA) IOCG deposits. Ernest Henry is the peak in the southern part of the left-side image. Profile distance is 5.5 km. The right-side image is 15 km E–W and the Prominent Hill magnetic anomaly is ~1000 nT. Data courtesy Geoscience Australia, Geological Survey of Queensland and DMITRE.

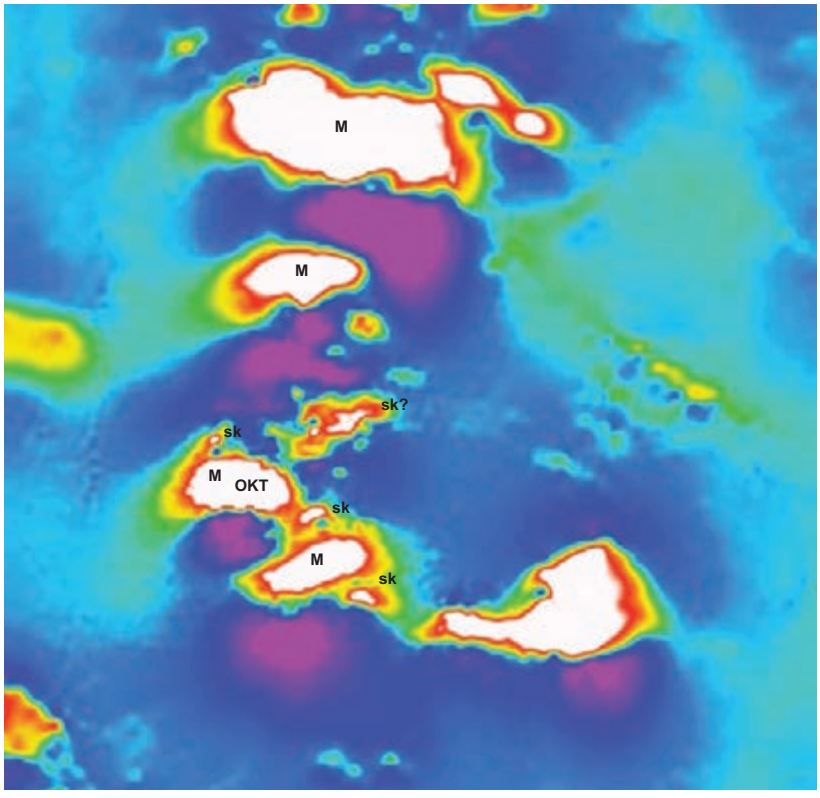

Figure 3.20: RTP aeromagnetic image illustrating magnetite skarns at OK Tedi (modified after Irvine and Robertson 1987). Magnetic bodies 'M' = monzonite intrusive bodies, sk = magnetite skarns, OKT = mine area. The image is ~15 km E–W.

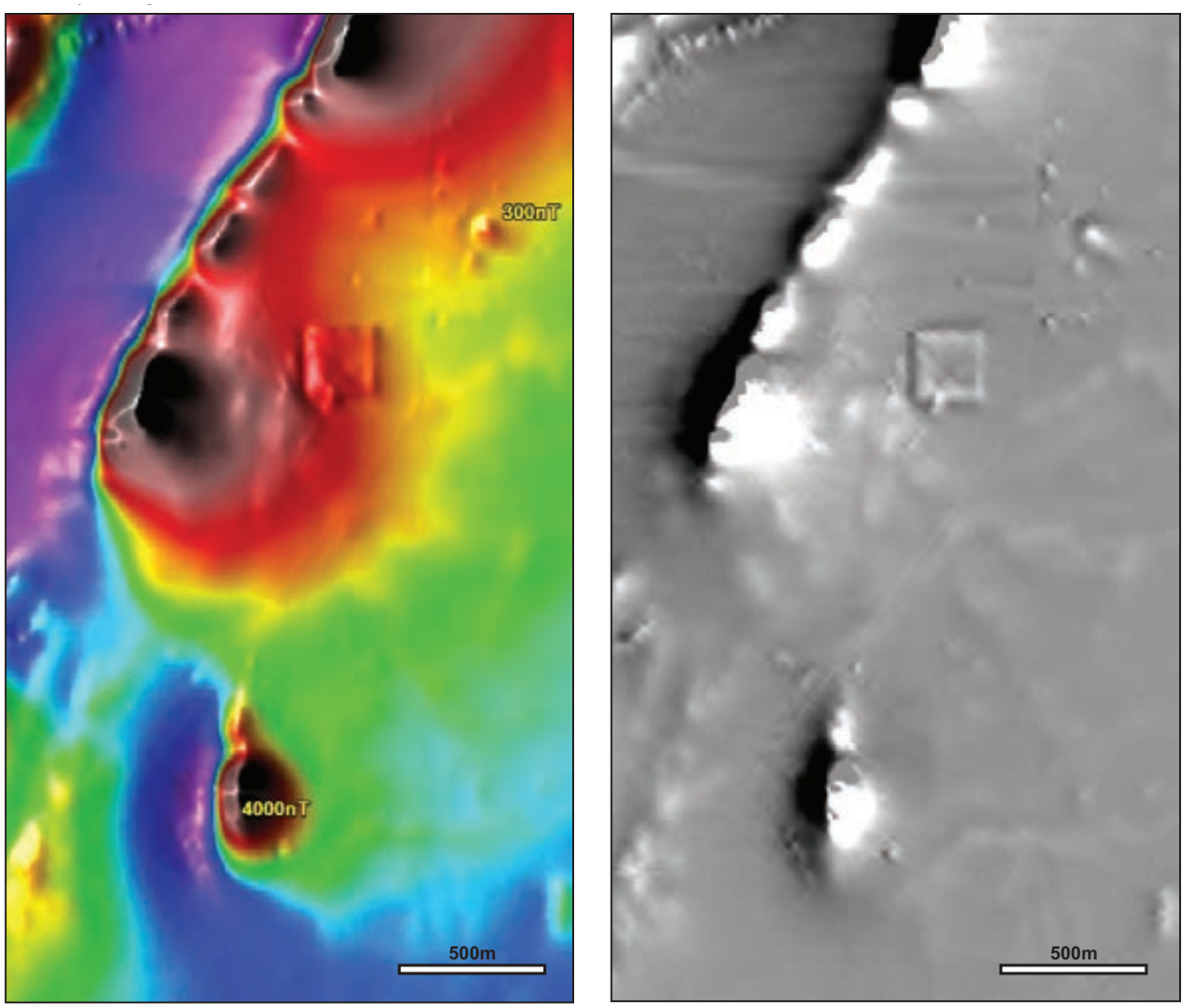

Figure 3.21: Aeromagnetic imagery from the Golden Grove/Scuddles mine district in WA. The magnetic anomalies at Gossan Hill (4000 nT) and Scuddles (300 nT) have a complex relationship with the VMS mineralised systems, but the relatively small anomaly at Scuddles was a key clue in the discovery of that orebody. See Robinson and Belford (1991). Helimag data kindly provided by Normandy Mining.

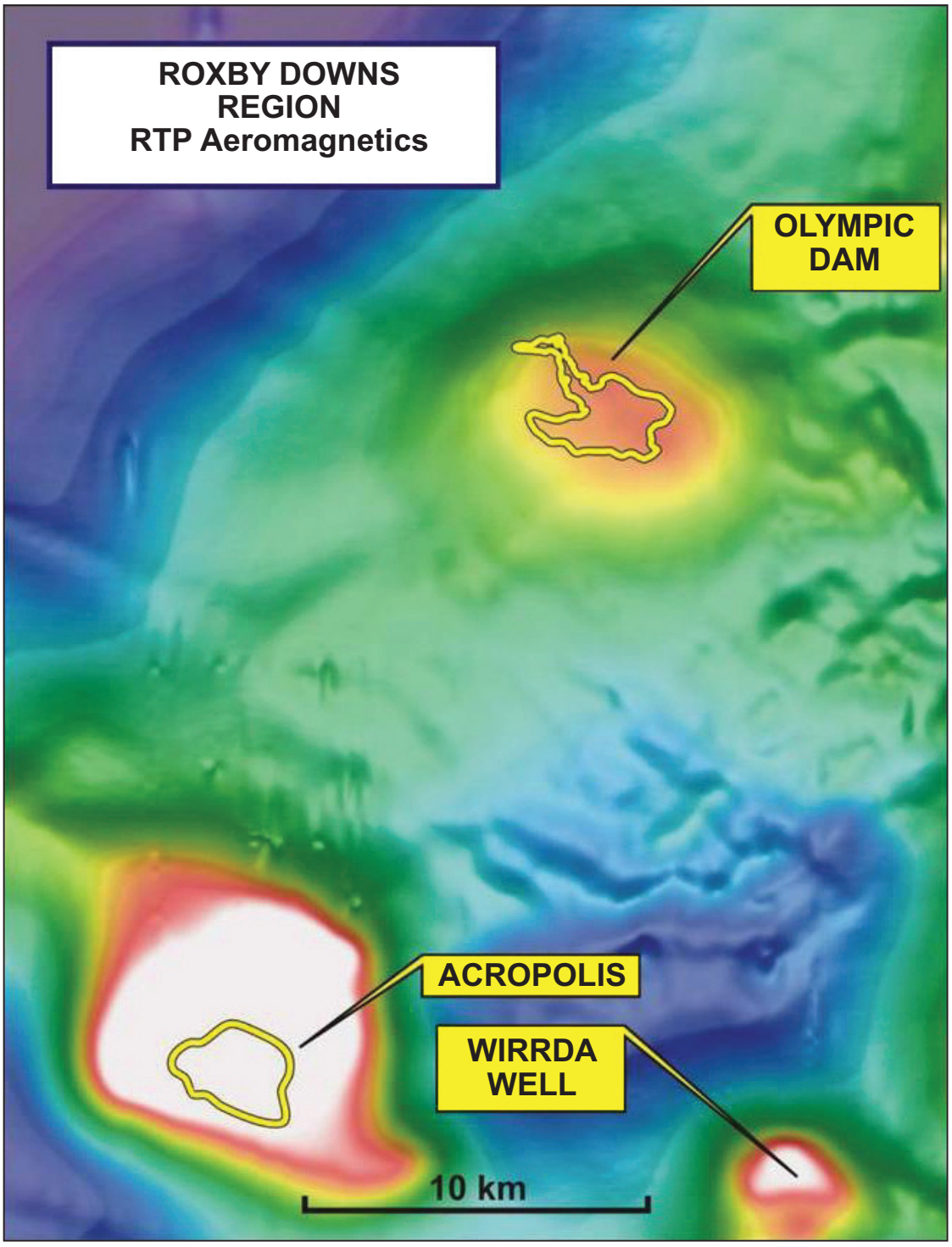

Figure 3.22: Aeromagnetic image over the Roxby Downs region including the Olympic Dam IOCG deposit, SA. Note the large depth (~2 km) of the magnetic source beneath Olympic Dam. This is thought to be magnetite alteration underlying the very thick, massive and essentially non-magnetic haematite zone associated with the deposit. Acropolis and Wirrda Well are magnetite-associated IOCG systems with subeconomic mineralisation. Data courtesy Geoscience Australia and DMITRE.

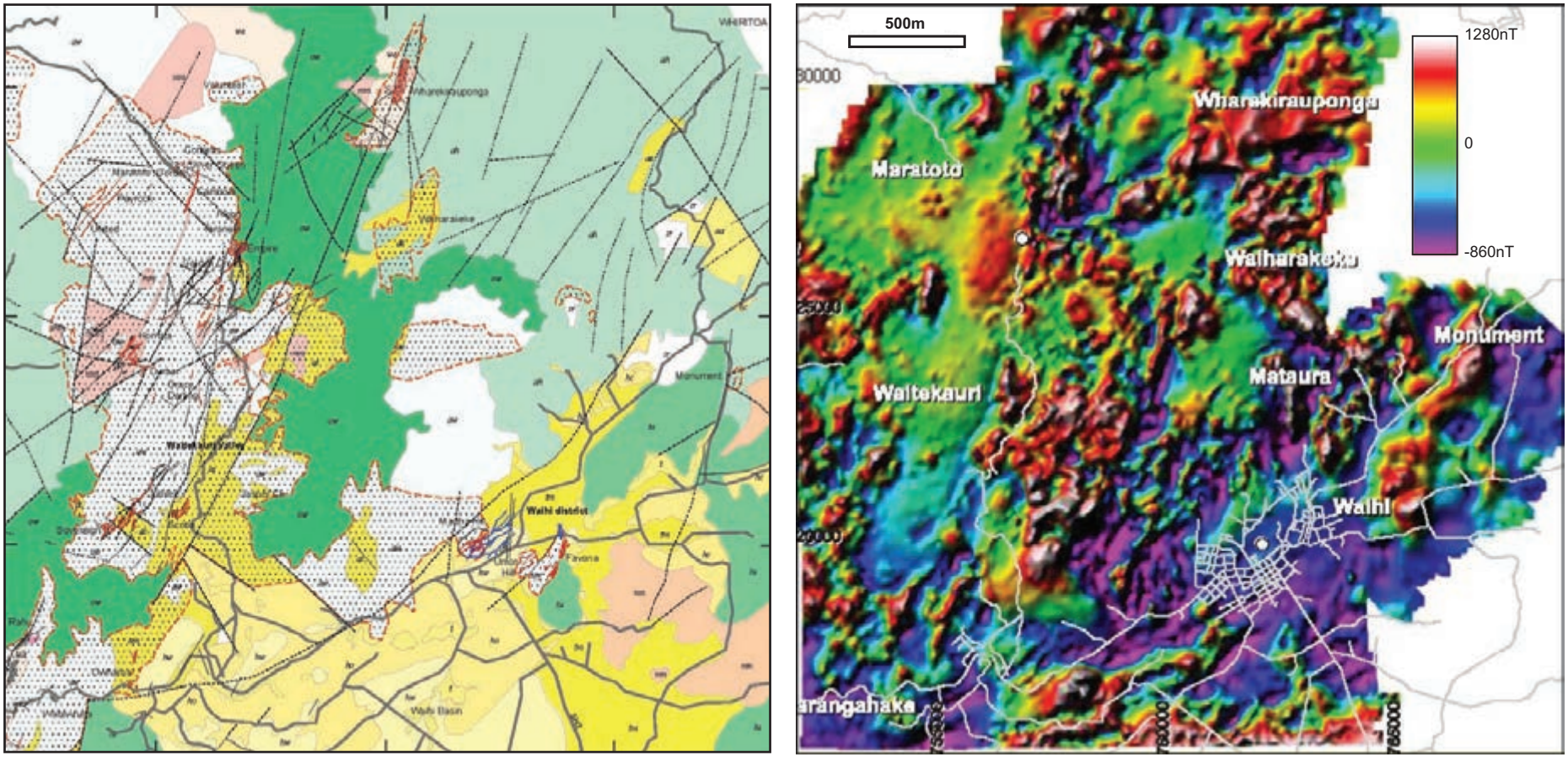

Figure 3.23: Geological map and RTP aeromagnetic image over the low-sulphidation epithermal Au-Ag systems in the Waihi Region, New Zealand (Morrell 2004). The stippled areas on the geology map indicate hydrothermal alteration and the red and blue lines show the vein systems. Lithology codes: andesite (aw,ak,ah,ow,iu), dacite (ae,ai,am), rhyolite (mn,mm,we), ignimbrite (ir,hc,ho,hw), superficial cover (tm,t). The low/flat magnetic zones clearly relate to the hydrothermal alteration.

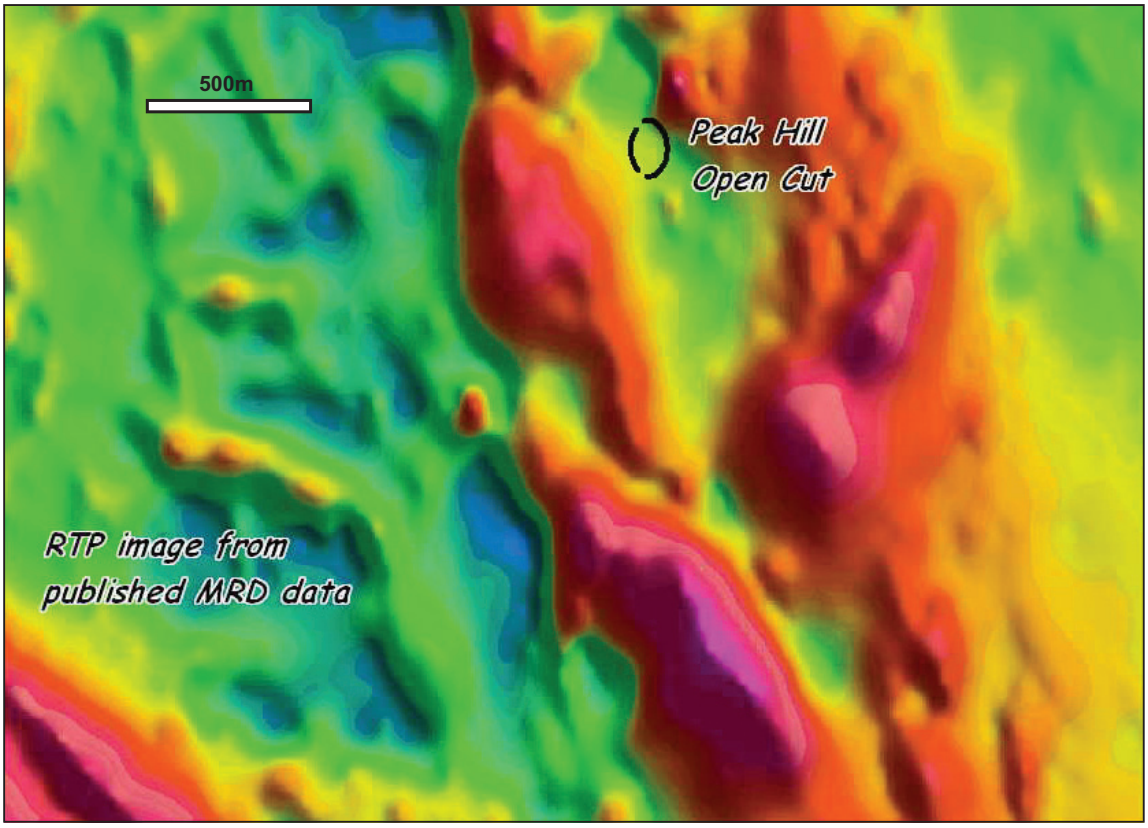

Figure 3.24: RTP aeromagnetic mage showing magnetite – destructive alteration associated with the Peak Hill (NSW) high sulphidation epithermal system. Data courtesy Geological Survey of NSW, images courtesy Steve Webster.

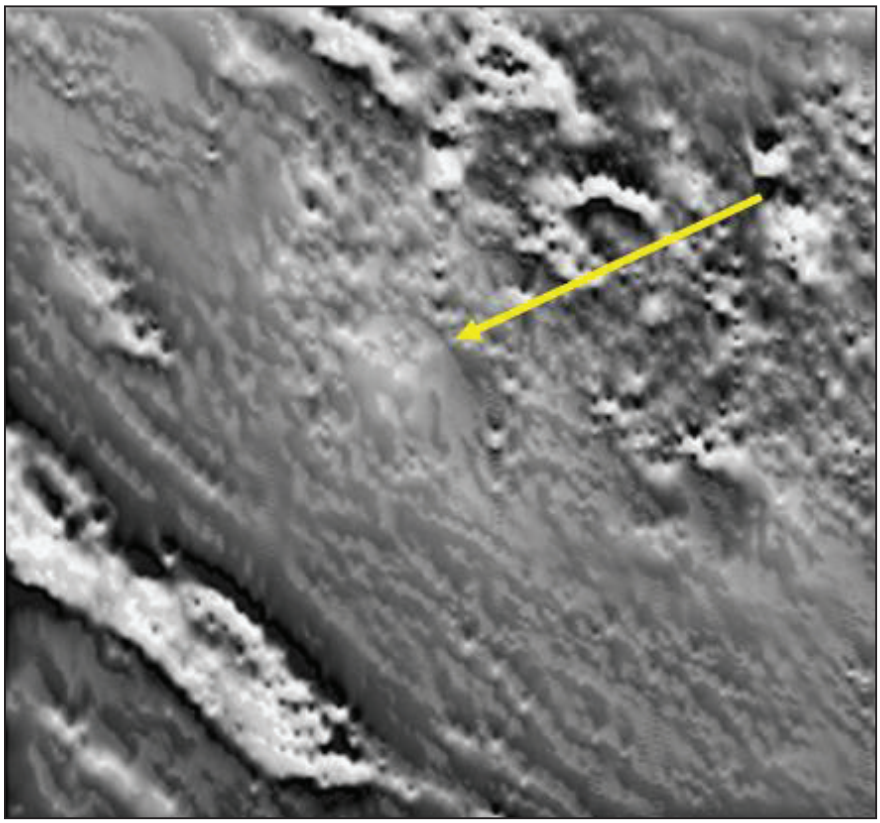

Figure 3.25: Greyscale RTP 1st VD image showing magnetite – destructive alteration associated with the PuebloViejo high sulphidation epithermal gold system (arrowed), Dominican Republic (García-Lobón and Rey-Moral 2004). The moderately magnetic host rocks are andesitic volcanics. The image is 30 km E–W.

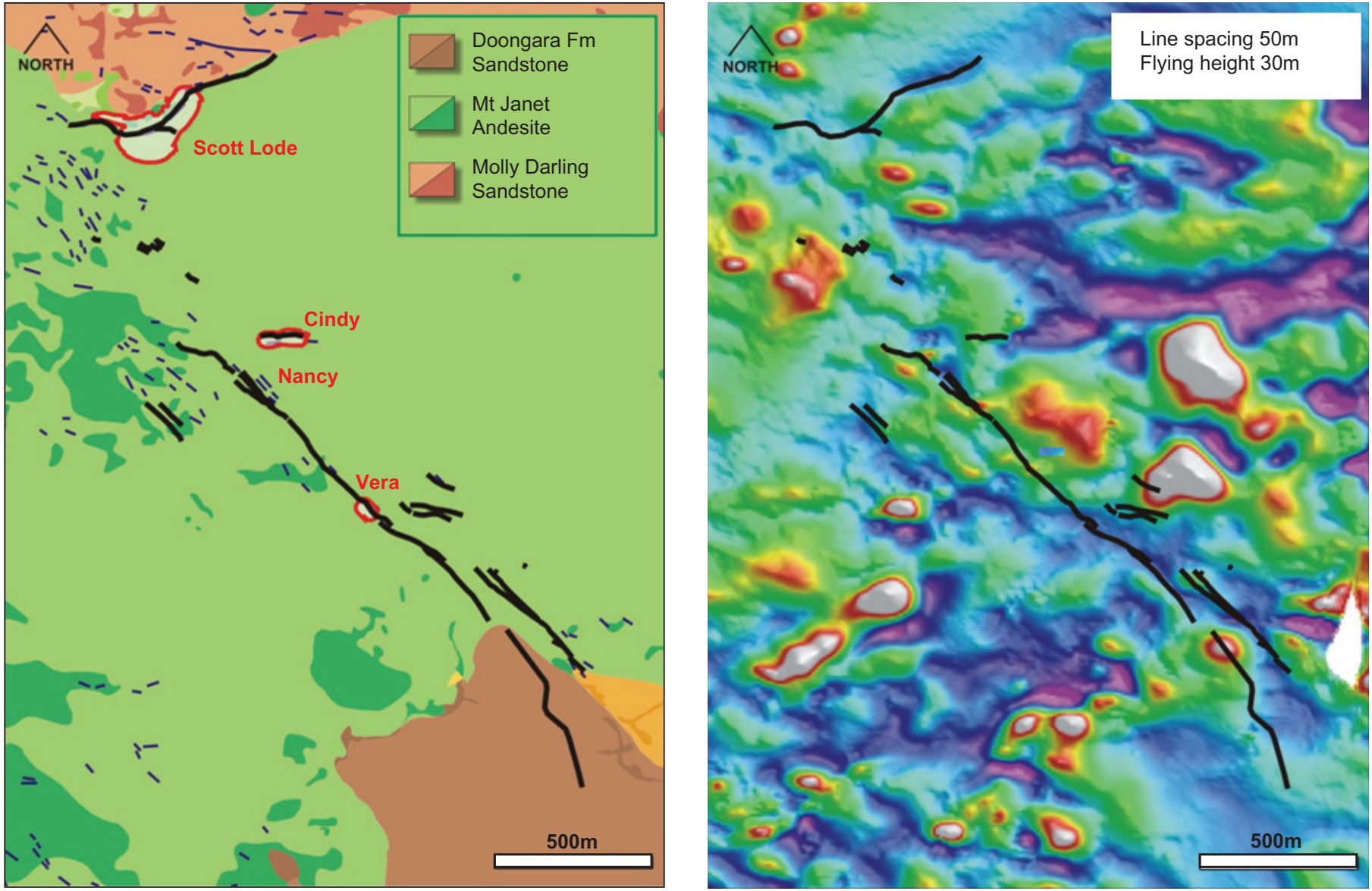

Figure 3.26: Detailed aeromagnetics and geology (showing Au-mineralised vein systems, black lines) from the low-sulphidation Pajingo, Vera-Nancy epithermal gold district in north Qld (after Hoschke 2011). Note that the vein systems follow the general pattern of fractures (evident as zones of magnetite destruction in the moderately magnetic intermediate volcanic host rocks) and show evidence of magnetite destructive alteration, but they are not uniquely targeted by the magnetics.

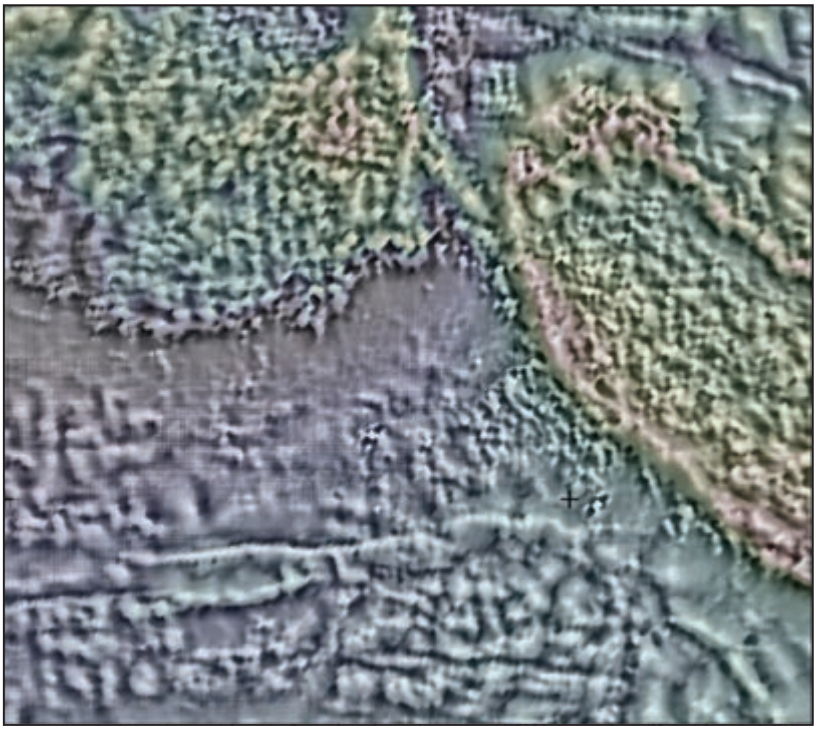

Figure 3.27: Ultra-detailed aeromagnetic image illustrating the development of surficial maghemite on a weathered laterite profile, Yilgarn Block, WA. Note the longer-wavelength features from the outcropping and subcropping bedrock. Image is 3.5 km E–W. Data courtesy Barrick Gold.

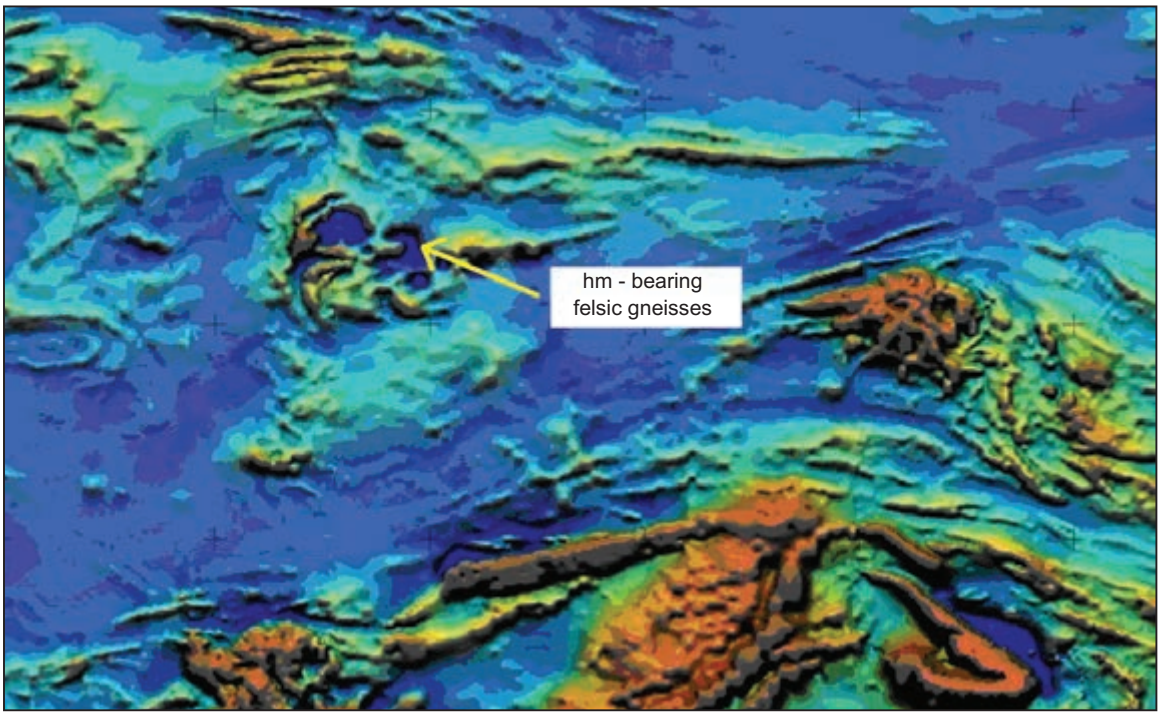

Figure 3.28: Moderately strong negative magnetic anomalies within the high-grade gneisses of the Coober Pedy Ridge area, SA. The magnetic anomalies are caused by anti-parallel haematite TRM within Fe-bearing felsic gneisses. Data courtesy of Geoscience Australia and DMITRE.

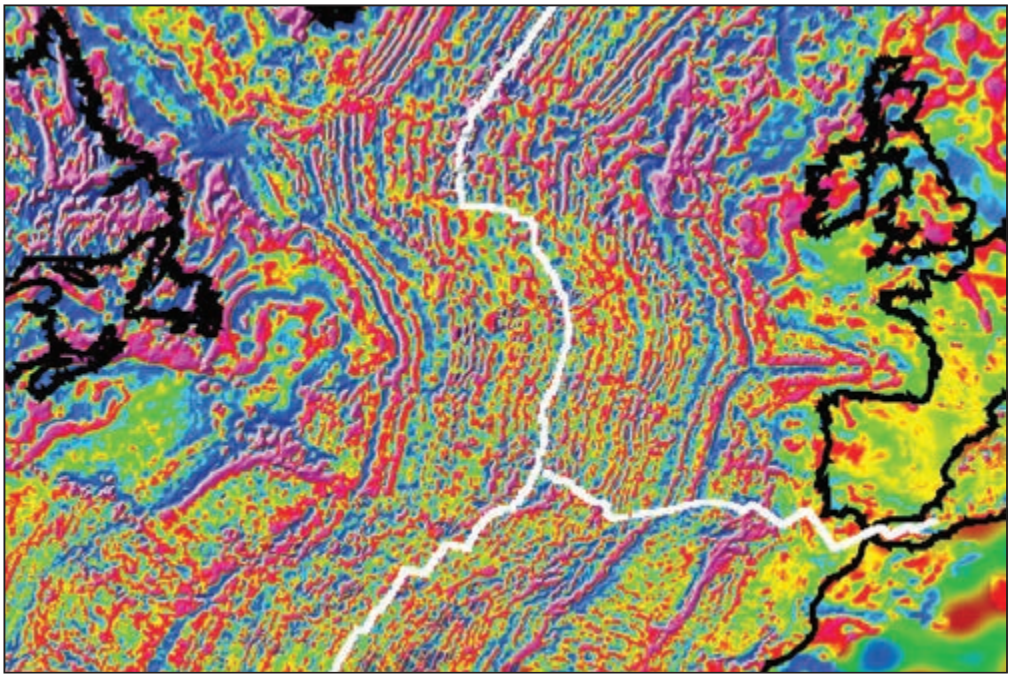

Figure 3.29: Section of the magnetic anomaly map of the world covering the north Atlantic and illustrating sea-floor stripes caused by progressive extrusion of basalt with alternating remanent magnetisation polarity (Korhonen et al. 2007).

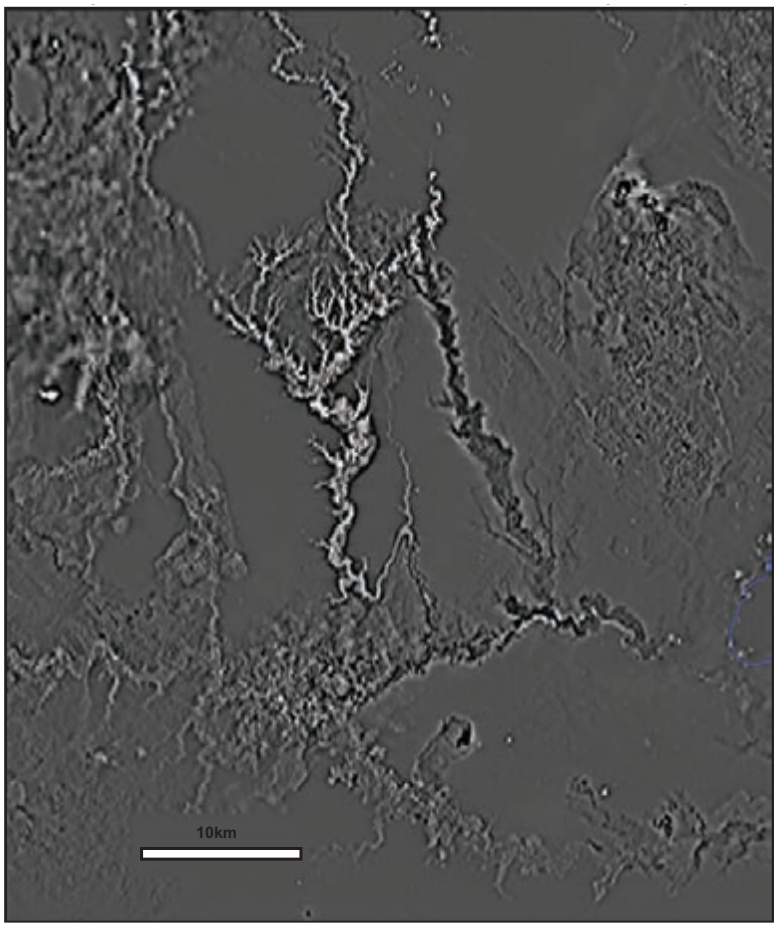

Figure 3.30: Greyscale 1st VD image of the Colac area in western Victoria showing terrestrial Tertiary basalt flows and vents. Note the positive and negative anomalous zones corresponding to normal and reversed polarity in remanent magnetisation in the basalts. Data from Geoscience Australia and the Geological Survey of Victoria.

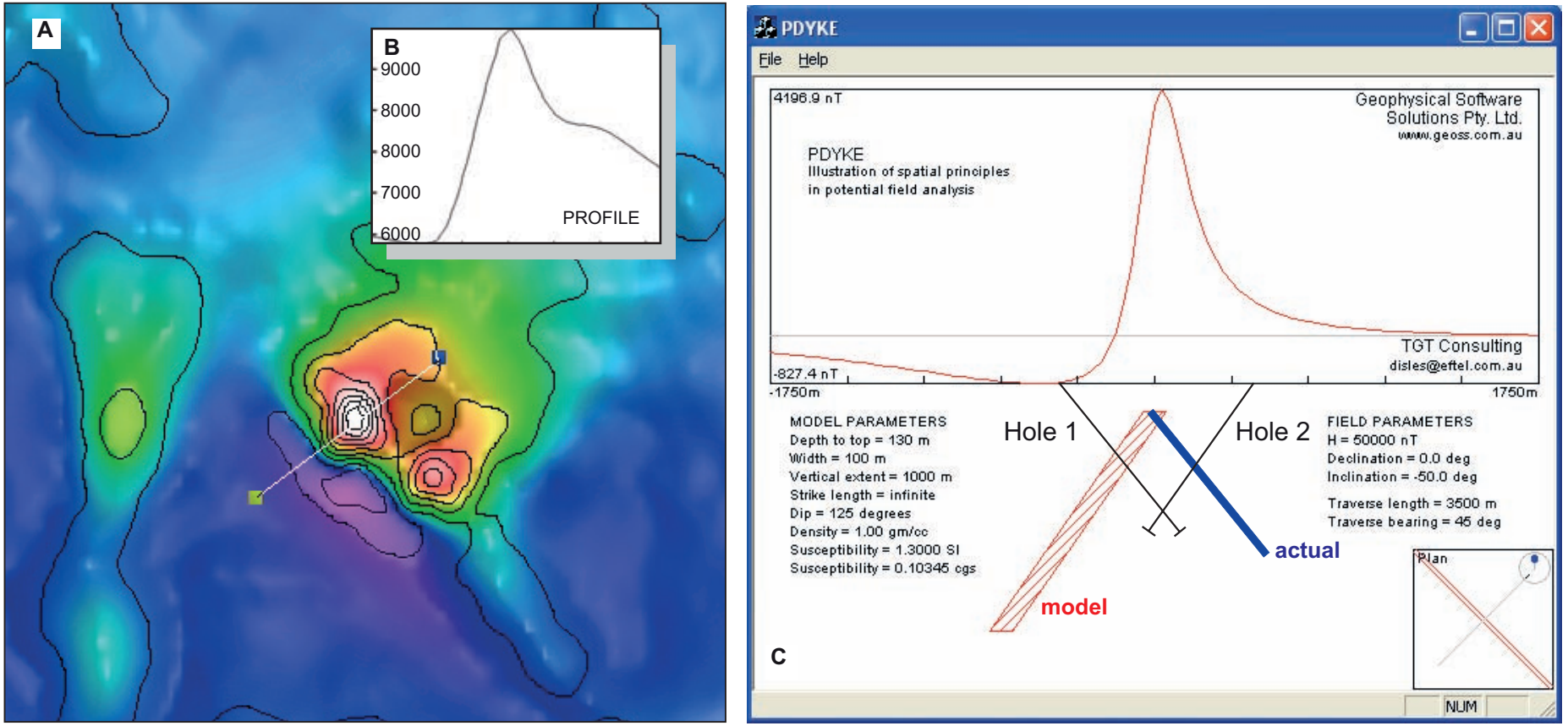

Figure 3.31: Self-demagnetisation effects at Trough Tank (Osborne) (adapted from Gidley 1988).
A) Aeromagnetic image, profile is 3.5 km long.
B) Airborne profile.
C) Model/schematic section showing initial hole (1) drilled assuming induced magnetisation, and subsequent hole (2) drilled with self-demagnetisation taken into account.

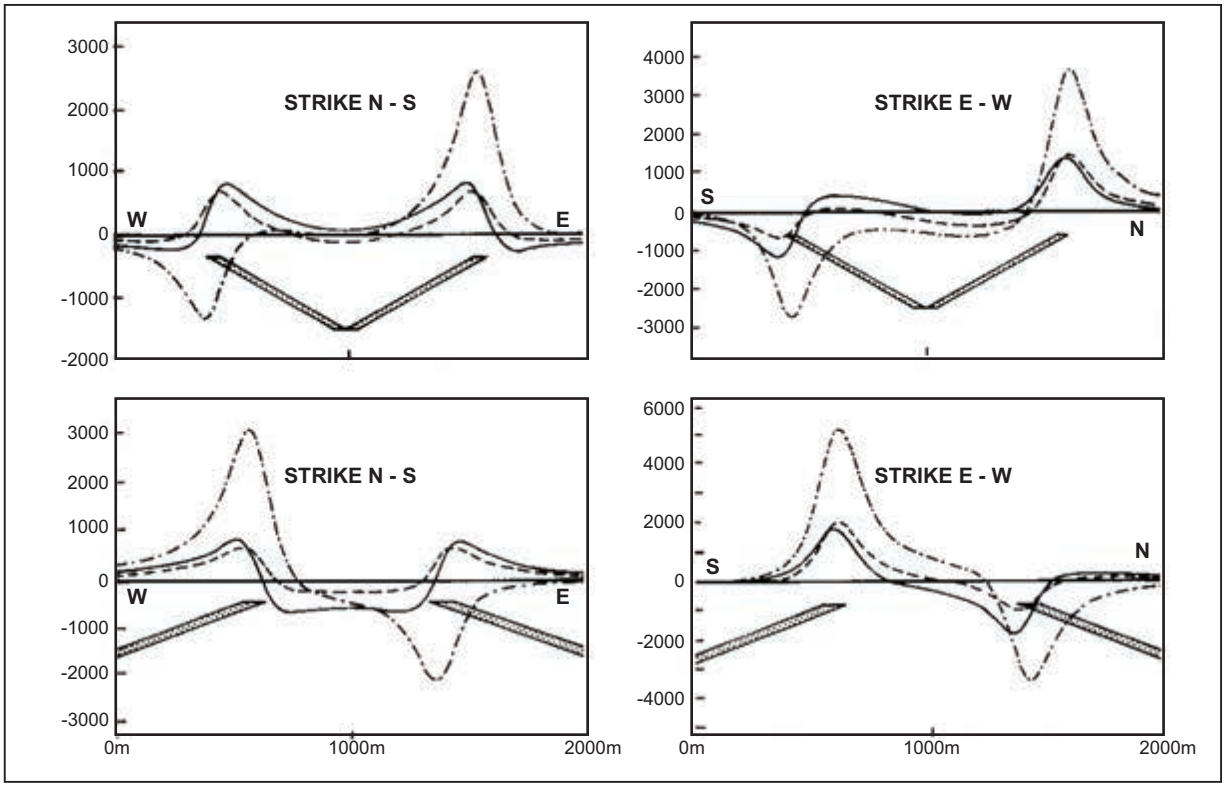

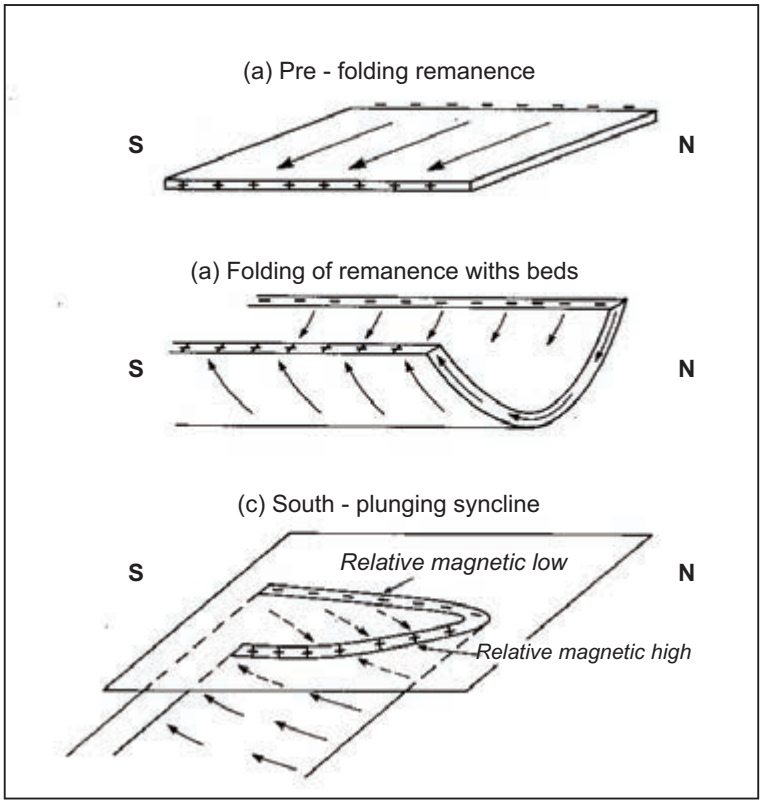

Figure 3.32: Illustration of magnetisation in BIFs in the Hamersley Basin, WA (after Clark and Schmidt 1994). The profiles are calculated over idealised fold structures and show the vast difference between the expected responses from purely induced magnetisation with isotropic susceptibility (solid line), induced magnetisation incorporating anisotropy (dashed line) and the summation of the effects of induction, anisotropy and (prefolding) remanence (dot-dash line). The sketch shows the effect of prefolding remanence on a typical Hamersley Basin fold structure. The arrows represent the remanence vectors, and the '+' and '–' signs represent magnetic poles produced at the edges of the unit by remanence.

4 Structural analysis from aeromagnetic data

4.1 INTRODUCTION

Structural geology, to quote Hobbs *et al*. (1976), 'deals with the ways in which rocks respond to the application of deforming forces, and with the structures that result from deformation'. In the broader sense, 'structure' in geology relates to all of the 3-D geometry of all rock units in a region, and the processes through time that have produced that geometry. Aeromagnetic data, with its inherent ability to 'see' magnetic rock bodies in 3-D, provides an excellent tool in the understanding of structure in our area of interest.

Structural analysis plays a key role in resource exploration. Almost all styles of mineral deposits and hydrocarbon accumulations are controlled either directly or indirectly by some form of structural focus. This may be at a local or regional scale, and at the crustal level of the deposit or at greater crustal depths.

A thorough understanding of the structural settings and key structures lying within or outside our area of interest allows us to:

a) compare and contrast our area to settings of known or modelled deposit styles;
b) apply predictive models for targeting.

Along with other geoscientific data, aeromagnetic data can be used for assessment of structural problems at all scales down to mine and prospect scale. The degree to which aeromagnetic data can contribute to (or even drive) structural analysis is governed by the magnetic character of the geology, the survey line spacing and flying height, and the degree to which structural information can be gained from other geoscientific datasets.

This chapter is not a review of structural geology and deformational processes, but is designed to provide the reader with a feel for the types of magnetic signatures simple structural patterns may produce and to outline a series of points that should be addressed when reviewing the interpretation.

The 3-D geometry of an area can be interpreted using the magnetic data by a combination of:

a) qualitative interpretation in 2-D plan view (integrating the aeromagnetic observations and any available geological data);
b) construction of cross-sections using the plan view interpretation;
c) quantitative interpretation by modelling of 2-D profile and/or 3-D grid data using a range of software tools (see Chapter 8) constrained by geological 'fact mapping'.

Compilation of our magnetic observations is usually a straightforward task, but expanding on these observations to develop a comprehensive structural interpretation requires considerable effort and geological insight.

Detailing styles and geometries of geological contacts, faults and folds etc., plus possible timing relationships, is rarely a simple process. It usually involves multiple, iterative attempts to produce an internally consistent geological story.

Some of the main points to remember when tackling an interpretation of structure are outlined below.

4.2 NON-UNIQUE INTERPRETATION

A single magnetic image can usually be explained by a range of different magnetic rock body configurations. For example, Figure 4.1 outlines three often-encountered simple geometries:

a) a single linear magnetic anomaly;
b) two parallel magnetic anomalies;
c) a Y-shaped junction between two linear anomalies.

As illustrated, each of these has more than one possible geological explanation. Which of the possible structures is the most probable for our survey area will depend on:

a) our knowledge of the area, the types of structures most likely to occur and the internal consistency of each structure within the overall interpretation;
b) the geological resolution of the data available (both the magnetic data and any other geological data!).

Our ability to recognise or interpret the most appropriate structural patterns (particularly in structurally complex terrains) rapidly diminishes with widening of flight line spacing and/or increasing flying height and, of course, increasing depth to magnetic source. This is particularly evident in areas with multiple fold generations producing complex interference patterns dominated by shallow to moderate dipping form surfaces (Fig. 4.2).

The scale of our interpretation (in relation to the geological resolution of the aeromagnetic data) is also important: if we are zoomed-in too close, the geological resolution breaks down and we may not recognise the interrelationships of units etc., but if we are zoomed-out to an excessively regional scale we may not be able to discriminate key geometric relationships among the overwhelming volume of detail.

4.3 STEP-WISE INTERPRETATION AND ITERATION

As mentioned above, the interpretation of structure from the aeromagnetic data is seldom straightforward and it should therefore be an extension of our observations rather than a distinct, separate and subsequent exercise. We should begin our work with some geological theme in mind and should be thinking about the underlying geology, even when we are making the most basic observations from the aeromagnetic imagery.

However, as we will see in Chapters 6 and 7, there is a logical and necessary sequence from more objective observations to quite subjective interpretation as we progress the integration of the aeromagnetic data with geology and related data. We will emphasise the need to document the stages of work on separate layers which effectively quarantine the different levels of fact, objective observation and interpretation.

This separation allows us to iteratively build and revise our work. The extremely interpretative aspects are very often subject to revision as our ideas and understanding of a project area evolve, whereas the basic observations made from the imagery rarely change. A simple but appropriate analogy is that our layer of observations forms the foundation of our work, the solid geology compilation is the bricks and mortar and the structural interpretation is the paintwork. The latter items are more subject to wear and tear and we expect to periodically renovate them, while (if constructed well) the foundations should stand the test of time.

Our layers of observation and interpretation develop into a plan view 2-D compilation that is essentially a solid geology map. Once this 2-D map reaches an advanced stage, the 3-D geometry of the interpretation should be investigated by compilation of cross-sections and/or block models. These will greatly improve the understanding of the geology and point to potential inconsistencies in our solid geology and structural interpretation layers.

4.4 INTERPRETED STRUCTURES

Aeromagnetic interpretations will typically include a range of styles of structures, such as conformable sedimentary contacts, concordant to discordant intrusive and extrusive contacts, erosional contacts, metamorphic layering, faults, shears, fractures, veins and folds etc.

4.4.1 Geological contacts

The nature of geological contacts evident in the aeromagnetic data is frequently ambiguous, and consequently these are usually lumped into a general classification 'geological contacts' in the early stages of our interpretation. While this term is principally designed to indicate (unmodified) sedimentary and igneous contacts, many simple-looking contacts may in fact be modified structures (layer-parallel faults and shears etc.).

Therefore, several alternatives should be considered when interpreting (apparently) simple geological contacts. For example, if we have parallel sedimentary or volcanic magnetic rock units evident in the data:

a) are these conformable, non-conformable, unconformable? The discordant nature may not be evident at the scale of interpretation or the discordance may only be seen in cross-section);
b) is the contact continuous at the scale of the interpretation?;
c) is the contact transitional (particularly if the magnetic character of the units varies along strike)?;
d) is the contact delineating a local unit, formation, group or supergroup contact?

Figure 4.3 illustrates a sequence of parallel magnetic layers with predominantly conformable contacts. Note, however, that layer-parallel faults and/or conformable intrusions (sills) might exist within this sequence but not be readily recognised in the aeromagnetic imagery.

For metamorphic sequences, other questions must be asked about the style of contact interpreted:

a) is the contact original layering (S_0) or is it a later tectonothermal fabric ($S_{0/1}$, S_1, S_2 *etc.*)?;
b) is the contact a layer-parallel shear zone or fault?

Figure 4.4 shows high-grade metamorphic rocks from the Broken Hill area, New South Wales. The central belt of disrupted linear magnetic horizons comprises predominantly metamorphic layering (which may also include early layer-parallel faults). Note the significant shear zone contact between the central metamorphic belt and a slightly discordant, layered metamorphic sequence in the north-west corner of the image.

4.4.2 Deformational structures

The two families of deformational structures typically evident in aeromagnetic data are folds and faults.

Folds

The forms folding may take in magnetic data include:

a) repetition of magnetic rock units;
b) direct observation of fold hinges.

Repetition of units may be created by several geological processes, including faulting (thrusting) and simple stratigraphic repetition of magnetically similar units. A mirror-image symmetry of several units of different magnetic character would give the interpreter increased confidence in the presence of a fold in this instance.

Direct observation of fold hinges within the aeromagnetic data is often unambiguous, particularly when the fold limbs are well separated (relative to the height of the magnetic sensor above the magnetic rock units) and steeply dipping. The critical relationship between separation of magnetic bodies and geological resolution has been dealt with in Chapter 2 (see Fig. 2.18). Where fold limbs are generally shallow-dipping (low-strain, very broad upright folds or high-strain recumbent folds) the resolution of layering within the magnetic data may be diminished to the point where recognition of folds may be difficult. This is particularly evident where the magnetic survey has a relatively wide line-spacing.

Figure 4.5 highlights the difference in appearance in magnetic data for an upright fold with steeply dipping limbs, and a reclined fold with asymmetrically dipping limbs. In the latter example, there is a significant

difference in amplitudes of the magnetic signatures of the two-fold limbs; it would be relatively easy to misinterpret the magnetic image as a north-west shear zone displacing a NE-trending linear unit.

A similar example from 400 m line-spaced magnetic data over the northern Musgrave Block (central Australia) is highlighted in Figure 4.6. In this example, two major structural subdomains are highlighted.

a) Subdomain 1 – a ~25 km wide, NW-trending belt of moderate to steeply dipping well foliated and folded granite gneiss associated with the Wankari Detachment Zone; in this belt, the steep fold limbs and some fold hinges are well resolved in the regional magnetic data.
b) Subdomain 2 – a ~75 km-wide belt of regional-scale, basement-cored recumbent folds and nappes, dominated by the same granite gneiss as that exposed in Subdomain 1. Within the majority of the area covered by the folds and nappes, the folded layering is relatively shallow-dipping and expression of magnetic layering is diminished in comparison to Subdomain 1; the recognition of major folding within the granite gneiss is now more difficult.

Where folding is more open and limbs are not steeply dipping, the patterns are usually easier to resolve. Figure 4.7 from the north-west coastal area of Tasmania (coastline shown in blue) features a folded mafic volcanic unit clearly defining anticlines (A) and synclines between the coast and the prominent (granitic) intrusion. The small amount of exposure onshore and on small islands to the north, when integrated with the aeromagnetic data, allows a quite detailed geological picture to be developed.

Hinge morphology

The development of increased magnetic intensity in the hinge of a tight fold is seen in Figure 4.5 and, as illustrated in Figure 2.18, this is due to the effective merging of the magnetic responses of the two limbs. It should be noted, however, that such higher amplitude hinge anomalies may also be developed by both:

a) a localised increase in the amount of magnetic mineral due to structural focusing of fluids into hinge zones during deformation;
b) limb attenuation and hinge thickening during strong fold deformation.

Decreasing spatial and therefore structural resolution with increasing depth of burial becomes increasingly important in the interpretation of folds within thick sedimentary basin sequences. With increasing depth, fold hinges within magnetic units will increasingly appear as single linear magnetic anomalies (see Fig. 4.8).

Faults and shears

The magnetic signatures of faults and shear zones can vary significantly, depending on factors such as magnetic character of the affected rocks, dip of the structure, metamorphic grade of formation, associated (or subsequent) metasomatic and/or weathering alteration effects, or magmatic activity etc. The more common styles of magnetic signature are described below.

a) The simple faulted contact.
   Where a sub-horizontal magnetic layer is in faulted contact with lesser or non-magnetic material, the faulted edge will produce an (often characteristic) signature. This is particularly common in younger and relatively undeformed geological terrains where layers are more likely to be horizontal, and faulting simpler in nature. A model representation of this situation is shown in Figure 4.9 and an excellent illustration of how this manifests in aeromagnetic imagery is given in Figure 4.10. These figures are taken from a comprehensive study of the Rio Grande Rift (Grauch and Hudson 2007), and the same authors provide a general overview of such structures in Grauch and Hudson (2011).
b) Faults with no magnetic anomaly signature.
   The majority of faults and shears do not have a direct magnetic signature. That is, they are not associated with observable magnetic highs or lows contrasting with the surrounding rocks.
   In these instances, the recognition of a fault is simply defined by displacement, dislocation or termination of identifiable magnetic units. Examples of such faults are shown in Figures 4.11 and 4.12.

Of course, a fault without a magnetic signature that transects a magnetically homogeneous unit is unlikely to be visible in the aeromagnetic data within that unit.

Where there is significant *vertical* displacement of magnetic units across a fault, we expect an abrupt change in the width (or wavelength) of the magnetic anomalies across the fault. This is clearly seen when the overlying material on the downthrown side of the fault is non-magnetic (see examples in Figs 4.13 and 4.14).

c) Faults with a magnetic anomaly signature.

Faults may have a contrasting magnetic signature to the surrounding rock, caused by either:

i) addition of magnetic mineral or;
ii) destruction of magnetic mineral within the structure.

Both may occur during or subsequent to deformation and may be caused by:

i) emplacement of intrusive material along the structure (e.g. a mafic dyke or sill) (Fig. 4.15);
ii) metasomatic alteration with introduction of magnetic minerals.
Migration of fluids along faults or shears can introduce significant magnetic mineral within the fault or shear. Magnetite-bearing faults are common in high-grade metamorphic terranes (e.g. the shear-hosted magnetite-quartz mylonites in the Karari Shear Zone shown in Fig. 4.14) and in IOCG-related systems.
iii) metasomatic or weathering-related destruction of magnetic minerals.
This commonly appears as linear, low-magnetic intensity zones in faulted or sheared magnetic host rock. It is caused by a decrease in magnetic susceptibility (and/or remanence) with conversion of magnetic minerals to haematite or hydrous Fe-oxides as fluids are channelled through the fault zone (see Figs 3.15, 4.12 and 4.16).
iv) variation in magnetic susceptibility and/or remanence due to grain-size variations during recrystallisation (e.g. within mylonite zones). This is occasionally recognised in very detailed aeromagnetic surveys.

The recognition of faults in magnetic data can be very obvious, particularly where several magnetic units or contacts are cut and displaced. Nevertheless, difficulties in recognition can occur when:

a) the structures are (sub) parallel to magnetic layering (e.g. flat sections of thrusts).
b) The structures are oblique to layering but their offsets are too small to be clearly recognised in the aeromagnetic imagery. This is likely to occur when the survey flight line spacing or the depth to the faulted magnetic rock units is larger than the fault offset.

Figure 4.17 shows two major strike-slip faults that are very largely parallel to stratigraphic layering. The westernmost of the two faults is relatively obvious, with a slight angular discordance between layering on either side of the fault observable in several localities along its strike length. The easternmost fault is far less obvious in the magnetic data. Its presence is only recognisable at one or two locations where angular discordance between individual layers can be observed.

Recognition and interpretation of deep-seated faults and shears

Aeromagnetic data captures information on rocks and structures at depths from 'zero' (the Earth's surface) to the Curie Point isotherm (typically 10–20 km). Where there is sufficient volume and concentration of magnetic minerals, the location and nature of deep-seated faults can be recognised in the data (see Fig. 4.18).

Deep-seated structures may also be evident from the presence of subtle trends of anomalous structures in the overlying sequences. For example, lateral movement along a deep-seated block fault within a sedimentary basin is likely to develop a broader zone of more strike-limited faults, folds and veins in the overlying sediments. These 'structural corridors' typically have a broad but subtle expression which can be difficult to delineate precisely. The Menzies Shear Zone discussed in Section 11.1 and illustrated in Fig. 11.3 is one such example.

As shown in Figure 11.3, we portray these as broad zones rather than discrete structures in our interpretation, and this is often best done on a separate summary layer. These structural corridors commonly form families of structures with a quasi-regular spacing (e.g. the common regularity of major block faults within sedimentary basins). The spacing of these structures is related in a complex manner to crustal thickness, rheological contrast, strain rates and thermal gradients etc. Recognition of deep-seated faults can be very important for exploration targeting, as these structures are widely regarded as the primary plumbing systems for migration of magmas and/or mineralising fluids from the deep crust or mantle into upper-crustal level traps; examples of the emplacement of major mineralised porphyries along significant deep-seated structures are well described in Camus *et al*. (1996) and Corbett and Leach (1998).

4.4.3 Analysis of structural data

The analysis of structures interpreted from magnetic data is essentially the same as the way we treat structural data from other sources such as field mapping.

There are several key points to remember.

a) Movement of faults or shear zones.
   We should remind ourselves that displacements directly observed or inferred in aeromagnetic data during compilation of qualitative 2-D maps, are apparent displacements. The true vector of displacement along any of these structures can only be determined with additional information. This may be:
   i) stratigraphic information from mapping and/or drilling that allows relative vertical displacements to be determined;
   ii) kinematic indicators from field mapping and/or drilling (note that these will only provide information on the vector of movement for a single episode of movement on a structure);
   iii) sufficient structural data from the magnetic and/or field mapping to allow reconstruction of unique linear structures that are offset by the fault. Figure 12.15a shows an example of this.

b) Interaction and relative timing of different structures.
   One of the limitations of field mapping, especially in areas with scattered and limited outcrop, is the highly variable density of information, particularly detailed structural mapping. The interrelationships of structures seen only in scattered and widely separated outcrops may be difficult to unravel, particularly between 1st-, 2nd- and 3rd-order structures, and/or structures formed in different deformation phases etc. In contrast, aeromagnetic data frequently provides continuity of key information (e.g. contacts and magnetic marker units) over a broad range of scales, allowing a more consistent analysis of the relative timings and interactions of different structures. This is well illustrated in the case studies of Chapters 11, 12 and 13.

c) Identification of 1st-/2nd-order structures.
   Large-scale, 1st-order 'master-faults' usually control the development of smaller-scale (2nd- and 3rd-order) structures which are often the most clearly recognisable features in our interpretation area. The large-scale and sometimes deep or laterally remote location of the 1st-order structures often make them difficult to recognise in a local study area. Examples of such 1st-order structures that are not clearly evident in the early stages of interpretation are shown in Figures 11.3 and 12.3. These examples highlight the need to review the data surrounding our area of interest and to *always* consider the structures identified with the study area in the broader regional context.

d) Grouping of structures and areas into structural subdomains.
   An important part of structural analysis is to subdivide the study area into subdomains which have similar structures, lithologies and/or strain histories. The identification of particular subdomains can assist in recognition of similar or related zones that may be mineralised. An example is the interrelationship between zones of transpression and transtension during deformation; if a transpressive (e.g. 'pop-up') subdomain is recognised within an area, it is highly likely that a complementary zone of transtensile behaviour (possibly favourable for dilational mineralisation traps) will be nearby (see Fig. 12.23).

e) Cross-cutting relationships.
It is often possible to group both lithologies and structures into relative age relationships based on cross-cutting relationships evident in aeromagnetic data.
However, caution should be exercised when interpreting age relationships based on apparent offsets of some types of structures. For example:
   i) Dykes and veins. If these were emplaced as tensile fractures they will commonly step or 'jump' across a pre-existing fault or contact, giving the (false) appearance that the dyke or vein is older, and offset. The ENE–EW-trending dyke in the north-eastern corner of Figure 11.6 is a good example.
   ii) Fault–fault intersections. Both extensional listric faults within sedimentary basins and low-angle thrusts in compressive environments will develop with step-wise offsets across pre-existing or contemporaneous transfer and/or transform faults, again giving the false appearance of being older structures. This is illustrated in the sandbox model in Figure 4.19. This highlights the need to be aware of the sets or families of structures that will develop under the influence of a single stress field. This is illustrated in the commonly used strain-ellipse diagram that highlights the orientations of the different structures associated with wrench fault or shear zone development (Fig. 4.20).

f) Grouping of structures of similar morphology.
The detailed morphology of faults and shear zones is dictated by various conditions at the crustal level of formation, including temperature, lithostatic pressure, hydraulic pressure and strain rate.
Narrow, linear faults or fractures with angular kinks and/or bends typically develop within shallow crustal levels, while broad, anastomosing and curvilinear shear zones are developed in mid- to deep-crustal levels. These differences are readily mapped in detailed aeromagnetic data (see Fig. 4.21).

g) Recognition and reconstruction of early structures.
The continuity of coverage and the 3-D representation of geology in aeromagnetic data can allow us to infer the presence of early major structures or trends that have been significantly modified by later (offsetting?) faults or shears. An example is shown in Figure 4.22. In this example, a late N–S dextral fault with an apparent 3.5 km displacement can be confidently inferred by simple, graphical cut-and-paste. Removal of this displacement reveals several subtle but significant earlier structures, including a more continuous view of the NW regional shear zone (red arrow), and a corridor of E–W oblique, probably tensile faults (blue arrow).
Rankin and Newton (2002) describe a more province-scale example of this concept in the Mesoproterozoic Musgrave Block of central Australia. In this area, the matching of broad geophysical domains across a province-scale E–W crustal shear zone often suggests an overall dextral displacement of roughly 120 km. With simple, graphical removal of this inferred displacement (and related displacements), a NE-trending series of early lithotectonic belts becomes apparent. These early belts could not have been recognised by recourse to the exposed geology alone.

h) Recognition of progressive versus multiple-phase deformation.
Often, the majority of structural elements seen in an area have been developed during a major (commonly early) phase of prolonged, progressive deformation. Any such deformation will produce a series of structures with different orientations and movement vectors that preserve the overall volume constraints of the area of deforming crust. An excellent example is the series of crustal-scale structures developed across the Eurasian plate to accommodate the N-trending collision of the Indian plate; Figure 4.23 shows the development of N-verging thrusts, conjugate transpressive and transtensile wrench faults, N–S-trending grabens and N–S wrench/transfer faults marginal to the Indian plate – all caused by the single N–S plate collision.
This example highlights the need to consider whether the structures interpreted in our area may be related to a single (and possibly prolonged) episode of deformation, or whether we are dealing with multiple events forming separate structures (and perhaps reactivating older structures). This is also emphasised by the development of multiple intersecting faults with varying displacement vectors during a single compressive deformation in the sandbox model in Figure 4.19.

Kinematic analysis

As previously mentioned, the vectors of displacement inferred from both faults and folds during compilation of a qualitative aeromagnetic interpretation are usually *apparent* movements (2-D projections of 3-D displacement vectors).

True movement vectors can often be determined from our interpretation by reviewing the interrelationships of different structural elements within the interpretation, and comparing these with other known structural settings or with analogue models.

An example would be the difference between a zone of dominantly compressive deformation (with development of folds parallel to a main thrust or reverse fault), versus a zone of strike-slip deformation, with development of folds oblique (and typically en-echelon) to the main fault or shear zone (Fig. 4.23).

The greater the number of individual structural elements of different morphology and orientation indicating the same deformation pattern, the higher will be the confidence in our interpretation. In Figure 4.24 the interpretation of dextral strike-slip movement along the E–W section of the Karari Fault Zone is supported by:

a) the clockwise rotation of earlier structures (layering, folding etc.) into the shear zone;
b) development of en-echelon NE-trending asymmetric folds;
c) development of dextral wrench basins along subparallel shear zones further to the south (Fig. 4.16).

Cross-sections

The final, very simple and often overlooked method of extending 2-D mapping to the third dimension is the construction of cross-sections. While the uncertainties surrounding aeromagnetic interpretation in poorly exposed areas may require considerable interpretive judgement in the construction of cross-sections, this task forces you to consider the 3-D implications of your 2-D work. Examples are presented in the case studies of Chapters 11, 12 and 13 (see Figs 11.11, 12.24 and 13.34).

4.5 CONSOLIDATION/PRESENTATION

To aid structural analysis in aeromagnetic interpretation, we recommend recording of different 'layers' of structural information at different structural levels and/or structural complexity. The two main structural interpretation layers used by the authors are as follows.

a) Structural framework.
   This comprises the structures inferred on our 'solid geology' layer, based on the constraints provided by the initial 'observation layer'. The structural framework layer captures all the detailed structures that are observable from magnetic rock units, plus discontinuities and trends interpretable in our geophysical imagery (see Chapter 6). It typically includes shallow structural detail as well as deep-crustal, inferred structural trends and includes all major geological contacts, faults, folds, fractures and shears etc.

   The structural framework should be separated into two or more layers if two or more crustal levels of structure are evident. For example, structures evident within a sedimentary basin sequence are best separated from interpreted structures and geometric variations evident in an underlying basement. This process is illustrated in Chapter 13.
b) Principal tectonic elements ('structural summary').
   This subsequent layer omits much of the fine-scale structural detail presented in the structural framework, and focuses on 1st-order and key 2nd-order structures. The structural summary will include subdomain boundaries, broad trends of intrusions and subtle structural corridors (such as deep-seated faults expressed by overlying anomalous structural trends).

   The sometimes subjective interpretations of stress and strain conditions, and the highlighting of inferred key structural zones or patterns (e.g. strain-release bends along key faults etc.) should be annotated on this layer.

As for the structural framework, the principal tectonic elements map can be separated into two or more layers to highlight different deformation phases and/or structural levels within the study area.

These more speculative layers of interpretation are an important part of our interpretation because they provide a platform for expressing the ideas that underpin our exploration targeting. We illustrate this structural interpretation and targeting process in each of the case studies in Chapters 12, 13 and 14.

In summary, aeromagnetic data can greatly expand our ability to recognise and interpret structure. We will see in later chapters that careful observation is the key to capturing structural detail from aeromagnetic imagery, and that the interpretation and presentation of these observations needs to be done in a step-wise fashion, progressing from quite objective 'observation' to more subjective 'interpretation'.

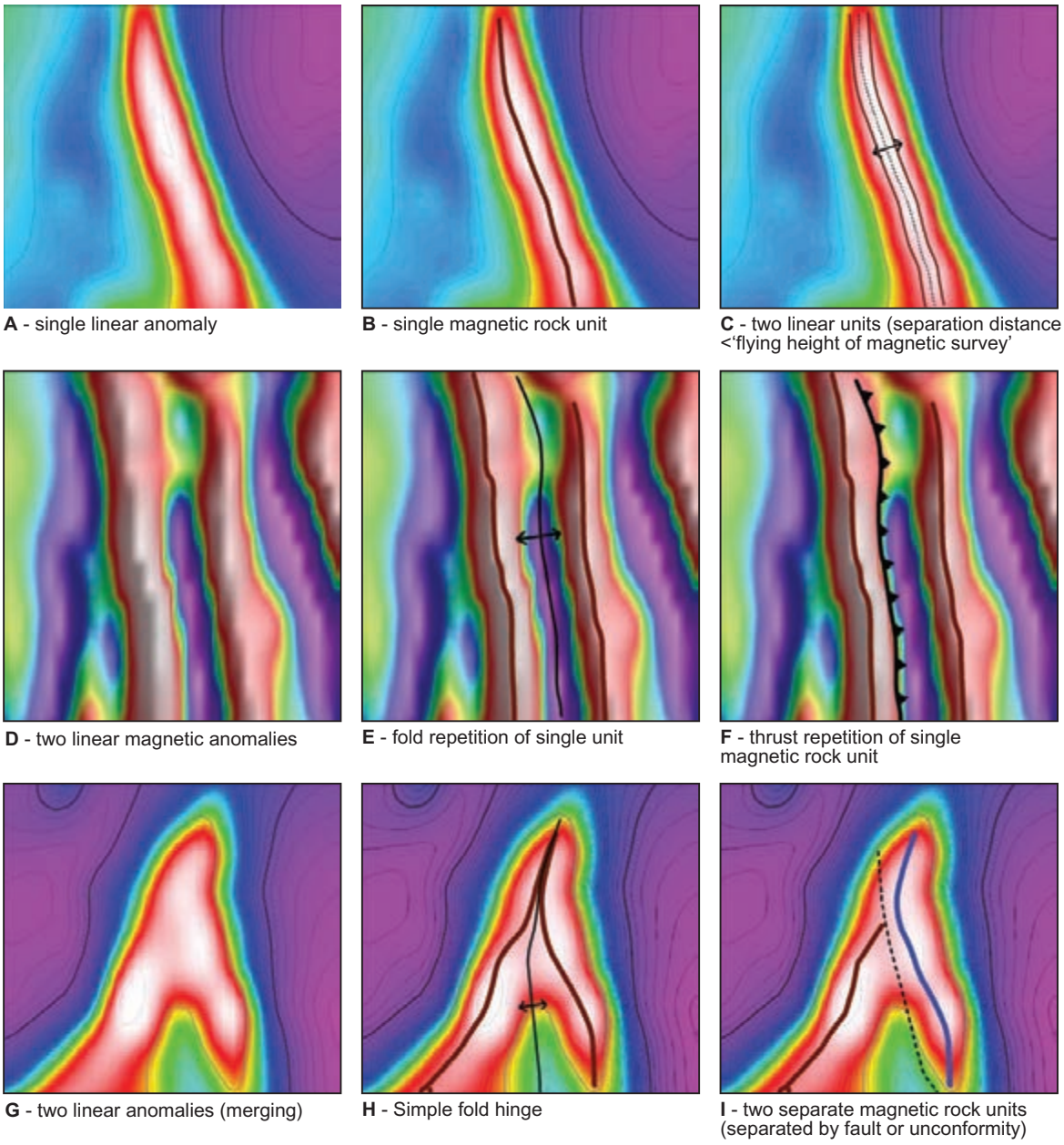

Figure 4.1: Illustration of alternatives in structural interpretation of aeromagnetics.

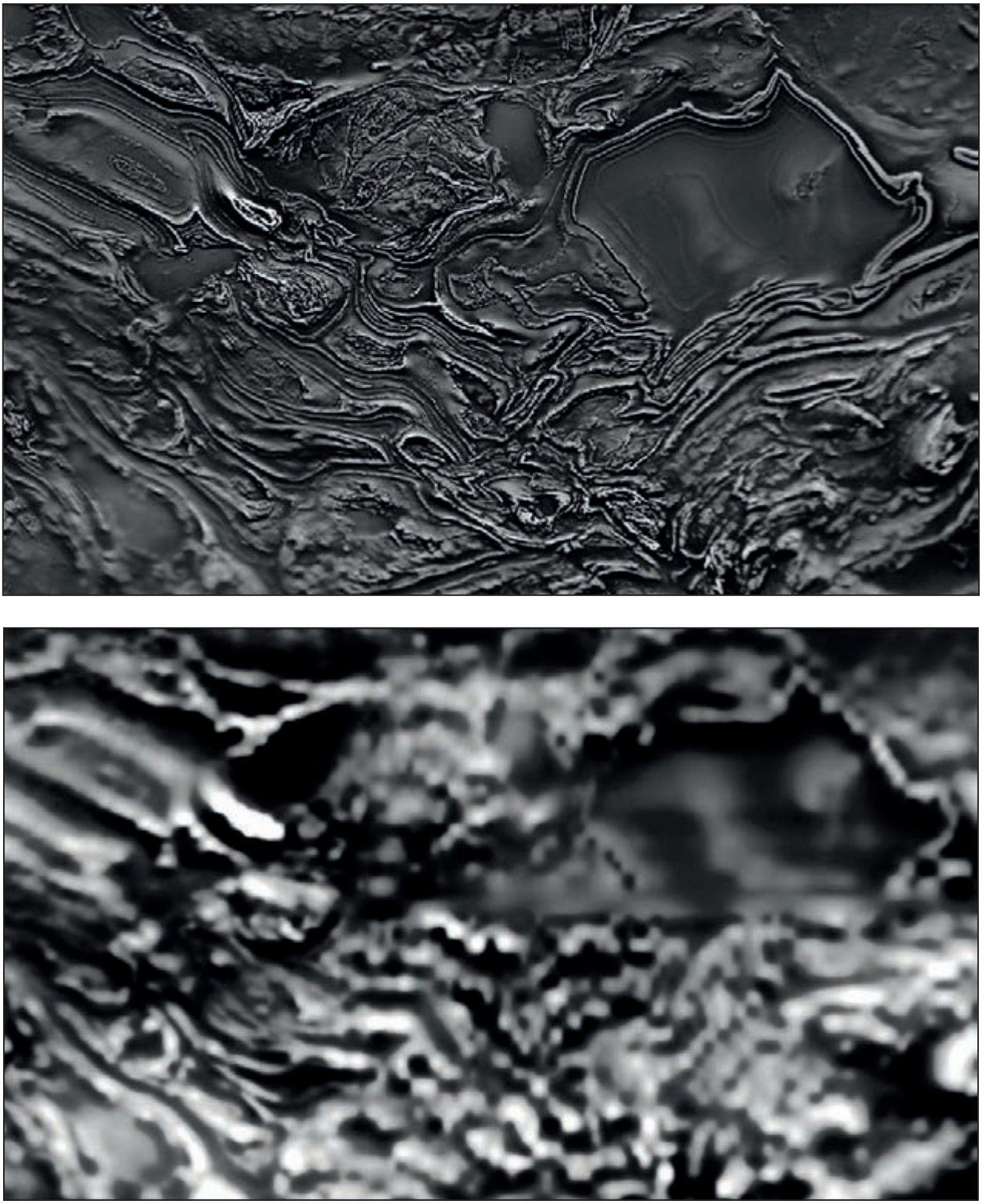

Figure 4.2: Composite TMI 1st VD aeromagnetic image of the Bonney Well region, NT, illustrating complex folding in Palaeoproterozoic sedimentary rocks. The area is 220 km E–W. The upper image is predominantly from 400 m spaced survey data (80 m flying height) and the lower is older 1600 m data (100 m flying height), illustrating the limitations encountered when the complexity of the geology is not matched by the sampling density of the data. Data courtesy of Geoscience Australia and NT Geological Survey.

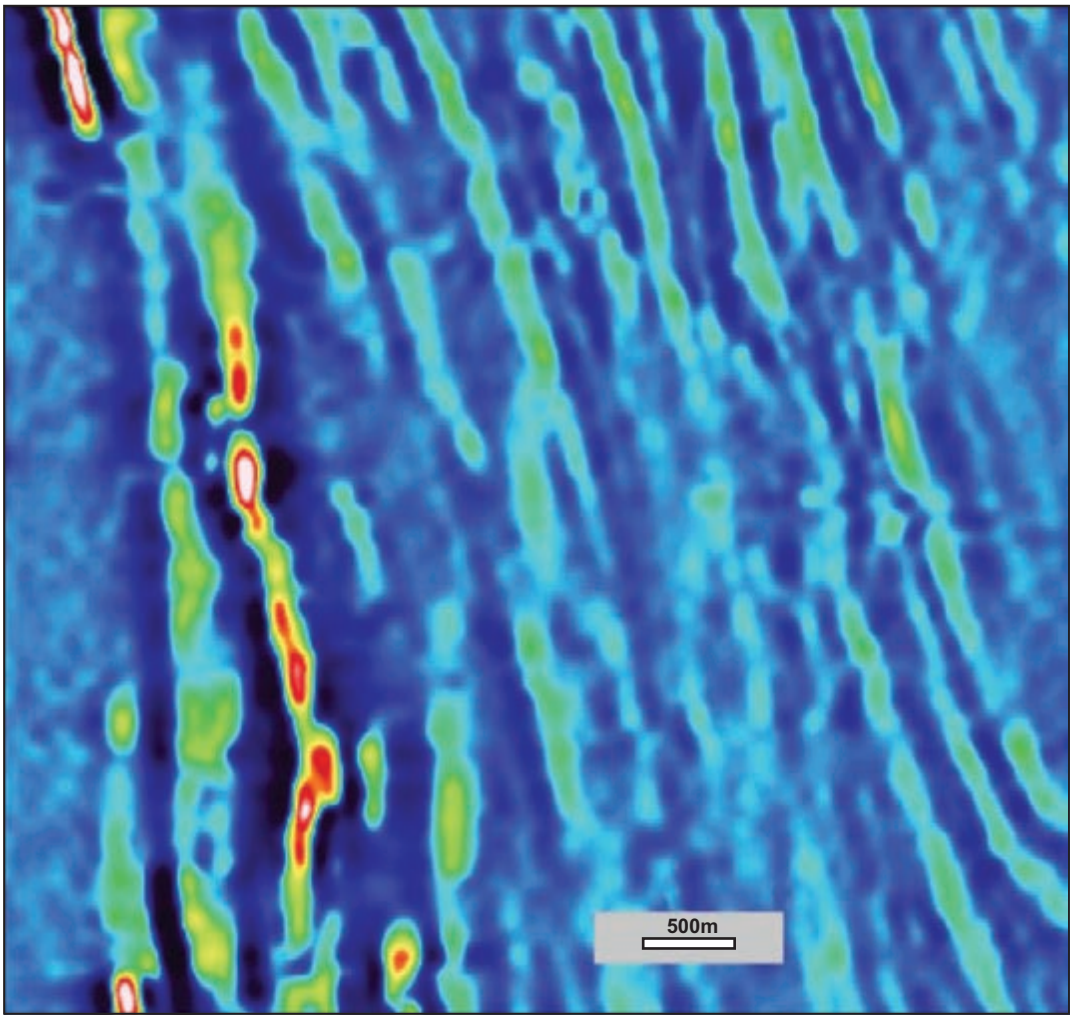

Figure 4.3: Image of a layered Neoproterozoic sedimentary sequence near Broken Hill, NSW. While the layering appears simple and conformable in the magnetic data, there may be significant shear/fault zones parallel to the magnetic layering in this high-grade terrane. Data courtesy Geoscience Australia and Geological Survey of NSW.

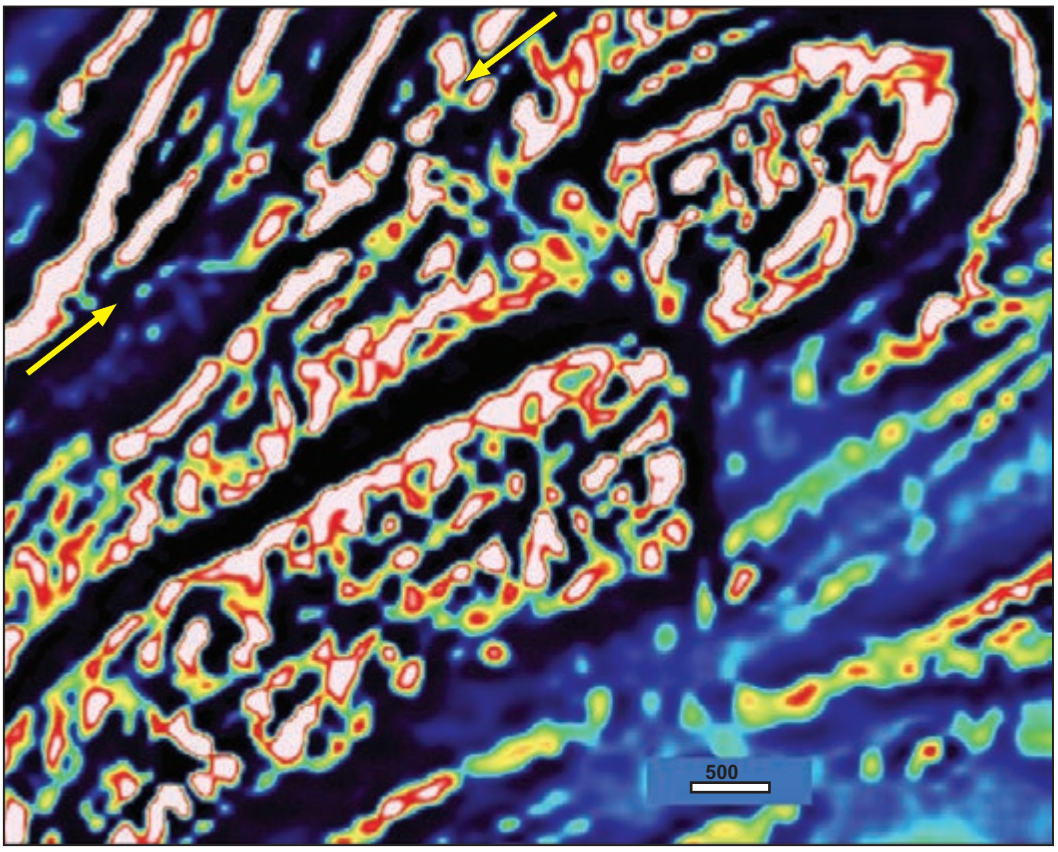

Figure 4.4: Image of high-grade (granulite facies and migmatites) metamorphic rocks near Broken Hill, NSW. Yellow arrows indicate discordant relationship between central belt of metamorphic layering, and discrete metasedimentary layers in the NW of the image. This is a locally significant shear zone contact between two metamorphic belts. Data courtesy Geoscience Australia and Geological Survey of NSW.

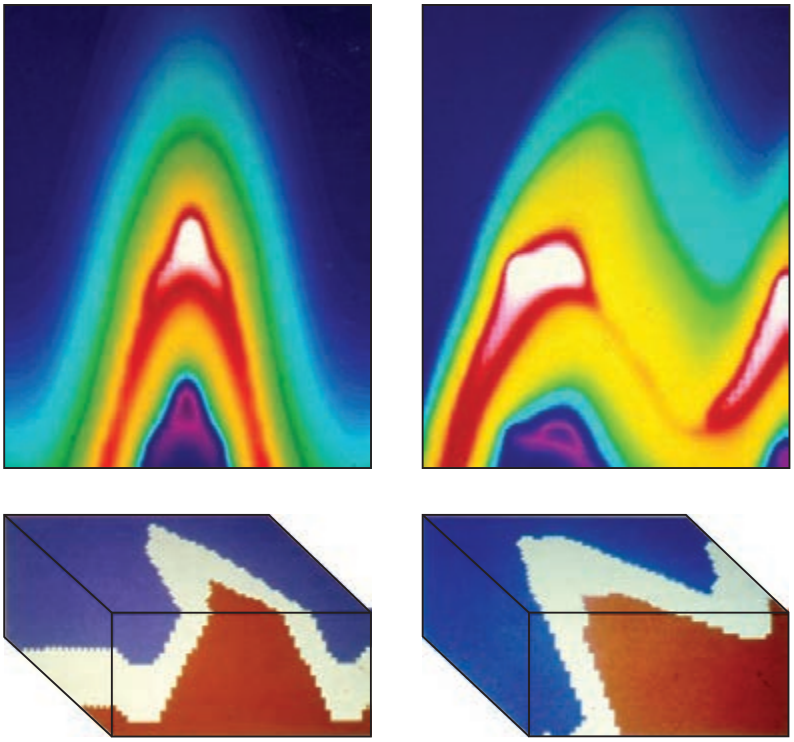

Figure 4.5: Model aeromagnetic data over a steep, upright anticline and shallow dipping reclined fold. Models calculated for Earth's field inclination –50°. Images courtesy Rick Valenta, see also (Jessell 2002).

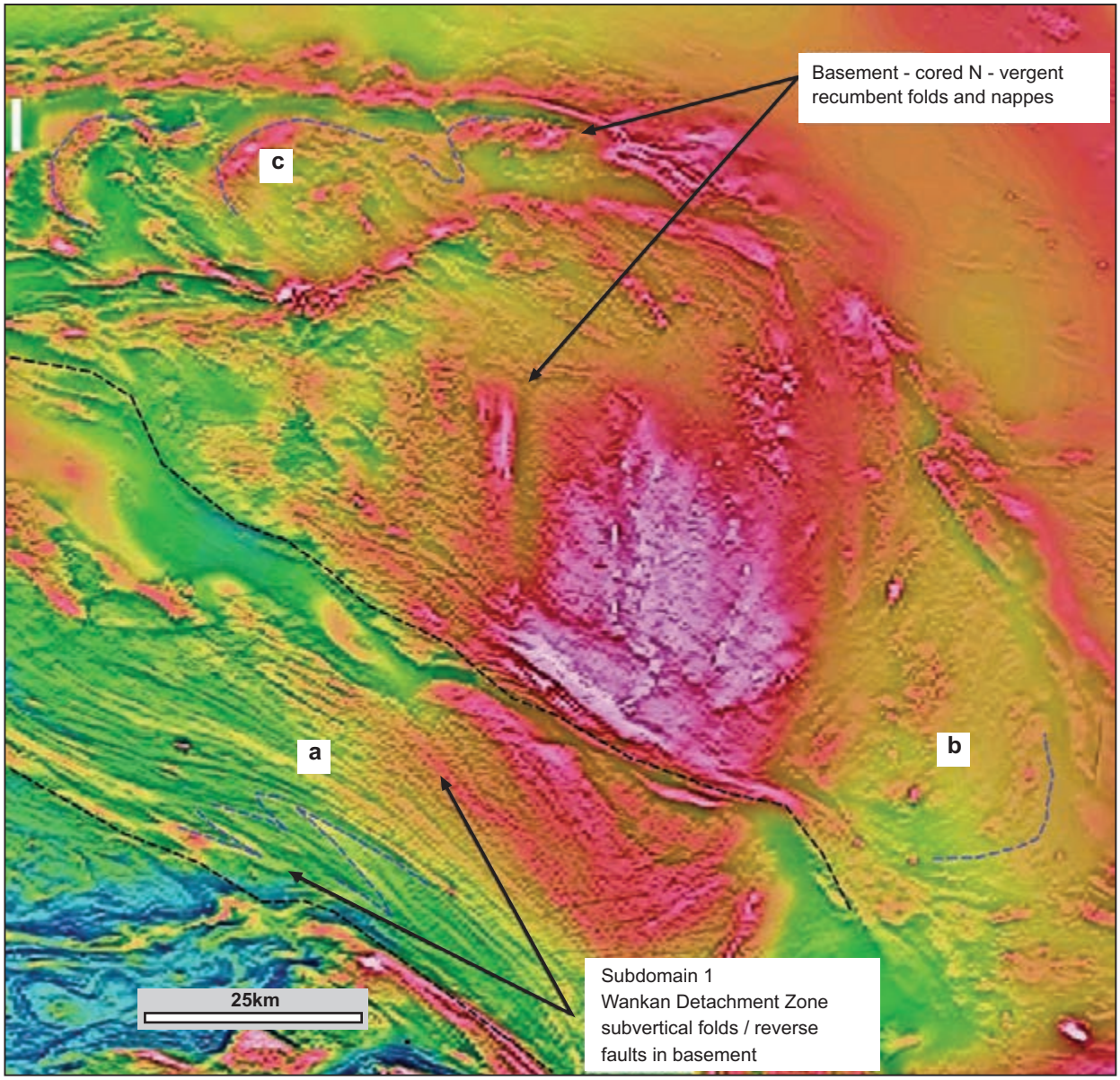

Figure 4.6: Aeromagnetic image over the northern Musgrave Block, Central Australia, highlighting the variations in appearance of folds with steeply dipping limbs (Subdomain 1) and folds (+/– nappes) dominated by shallow-dipping limbs (Subdomain 2). Zone a has well-defined magnetic layering and local fold hinges in granite gneiss. The same granite gneiss in Zone b has shallowly dipping fold limbs, so recognition of local- and regional-scale folding is more difficult. Zone c includes recumbently folded basalts – the fold hinges are expressed by a magnetic marker unit within the basalt. Data courtesy of DMITRE.

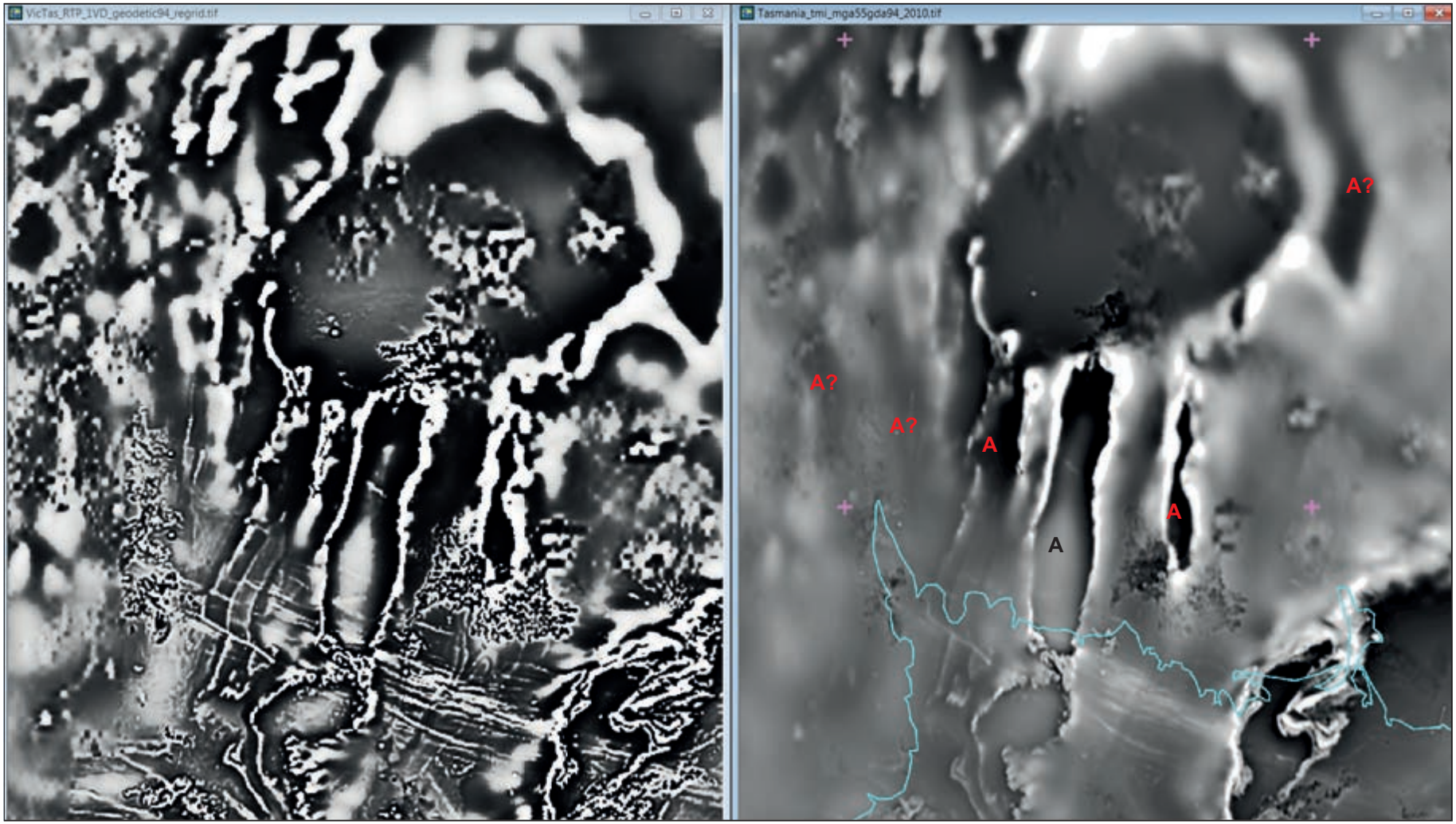

Figure 4.7: RTP 1st VD (left) and TMI (right) aeromagnetic images from NW and offshore Tasmania (coast line in blue, ticks are 50 km apart). The folded magnetic unit is the Neoproterozoic, mafic Spinks Creek volcanics. Inferred anticlines are marked 'A'. The ovoid low is a Palaeozoic granite (exposed on islands) and the patches of noisy response are Cenozoic basalt flows. Despite the increase in both water depth and thickness of younger cover, the fold patterns continue to be traceable north of the granite, especially in the RTP 1st VD image. Image and commentary courtesy DH Moore. Data from the Geoscience Australia national database.

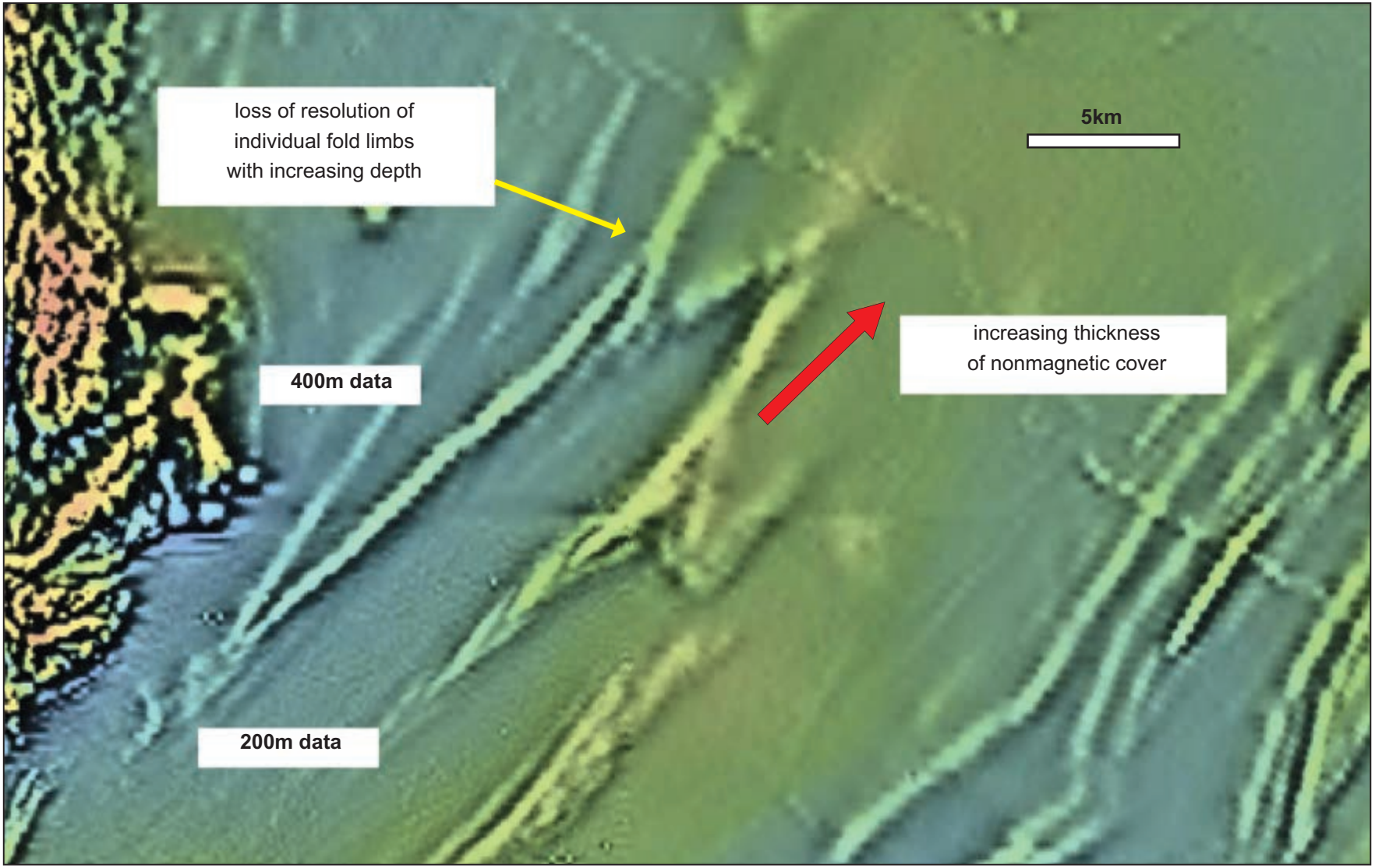

Figure 4.8: Aeromagnetic image from the Cloncurry region of the Mt Isa Inlier (Qld) illustrating the decrease in spatial and structural resolution (red arrow) with increasing depth (in direction of red arrow). Cover over the folded Proterozoic metasedimentary sequence thickens to the NE. Note also the change in resolution due to change in survey line spacing. The more detailed data in the SW corner has 200 m line spacing compared to 400 m spacing over the rest of the area. Data courtesy of Geoscience Australia and Geological Survey of Queensland.

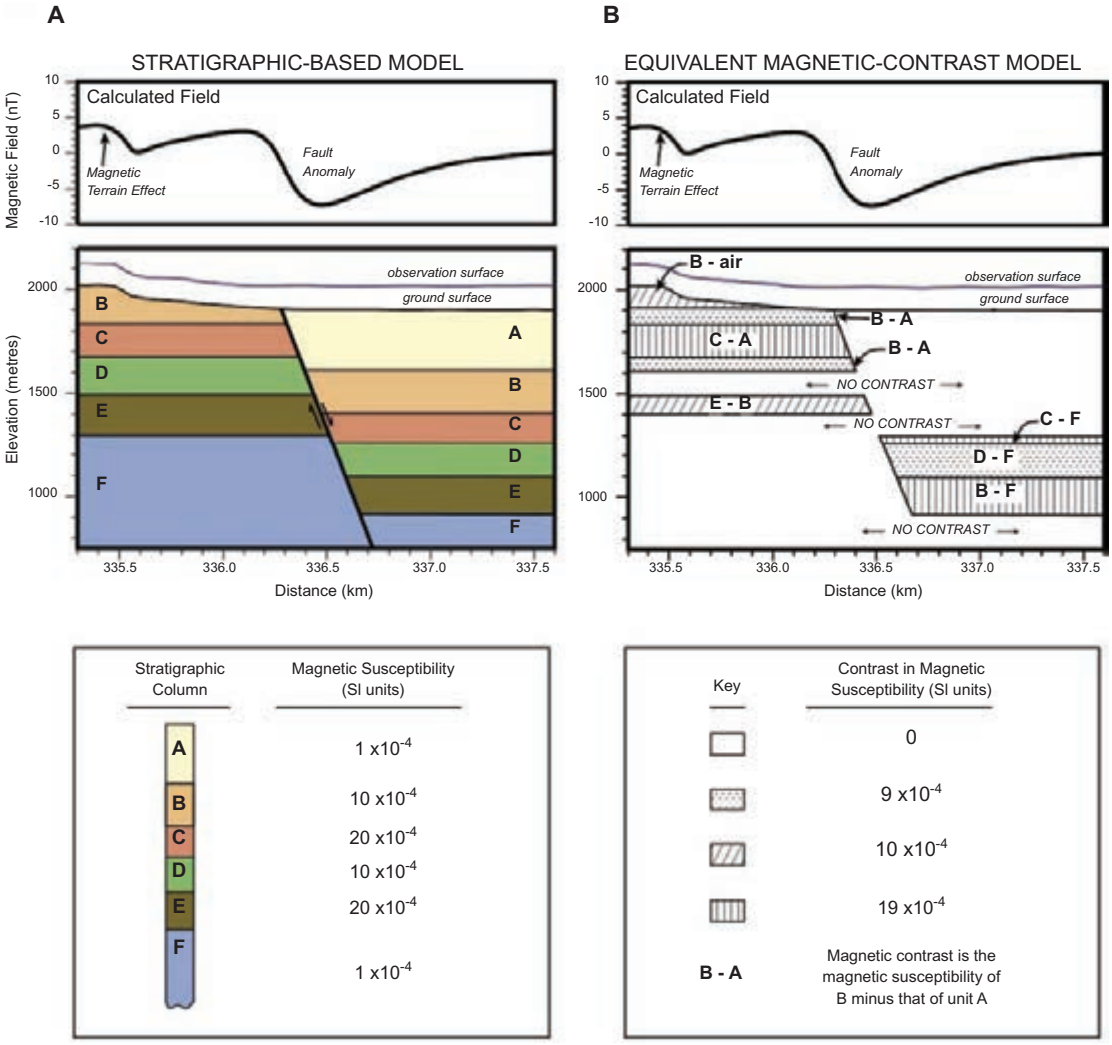

Figure 4.9: Hypothetical geologic model for a normal fault affecting multiple horizontal magnetic layers (A). B shows the equivalent geophysical model demonstrating the concept of lateral magnetic contrast. Where two juxtaposed strata have different susceptibilities, the magnetic-contrast layer is assigned to the side of the fault having greater susceptibility in B. Its thickness is determined by the vertical extent of the juxtaposition between the two strata. Note also the contribution of magnetic terrain effects from the hill composed of strata B, which has a magnetic susceptibility contrasting with adjacent non-magnetic air (Grauch and Hudson 2007).

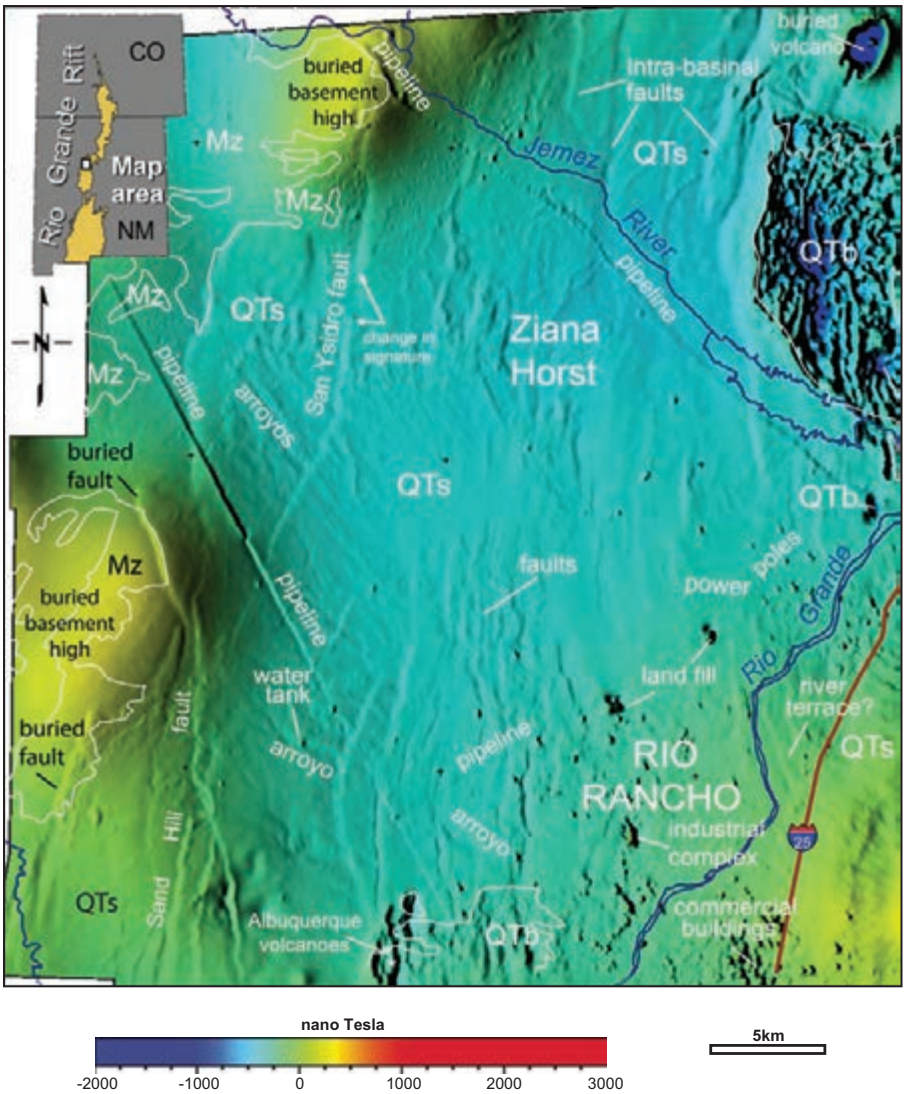

Figure 4.10: Colour shaded-relief image of reduced-to-pole (RTP) aeromagnetic data for the Rio Rancho area in the Rio Grande Rift (Grauch and Hudson 2007). The colours primarily reflect the broad variations in the data, whereas the illumination (from the west) emphasises smaller-scale variations, especially linear features associated with (mainly normal) faults.
Superimposed geological contacts from Geologic Map of New Mexico, scale 1:500 000.
QTs – Quaternary and Tertiary sediments (Santa Fe Group and alluvial cover).
QTb – Quaternary and Tertiary basaltic and andesitic rocks, undifferentiated.
Mz – Mesozoic sedimentary rocks.

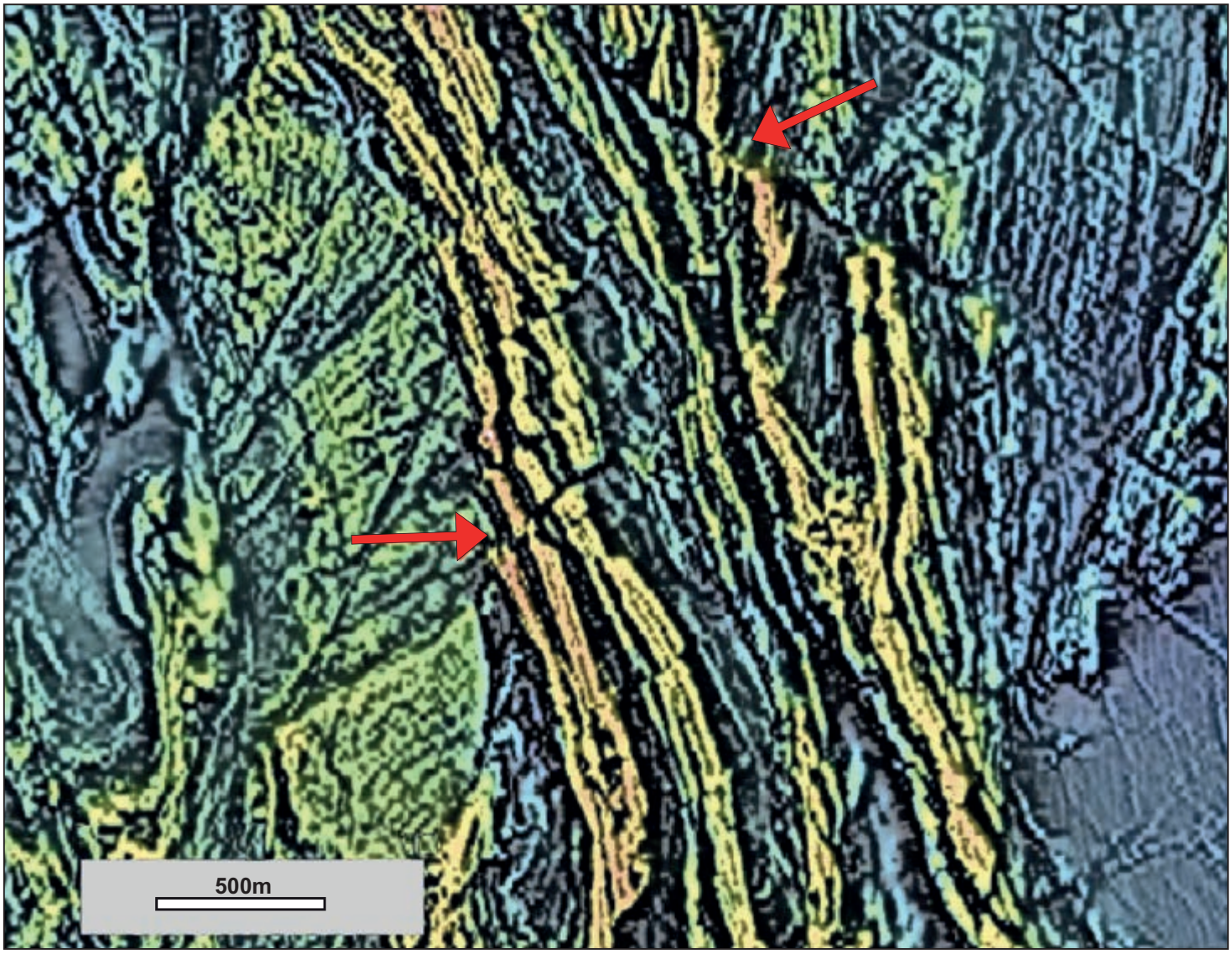

Figure 4.11: Aeromagnetic image from the Duchess area of the Mt Isa Inlier (Qld) illustrating the recognition of faults from lateral displacement of magnetic rock units. Note the conjugate NE dextral and NW sinistral apparent displacement (red arrows). Data courtesy Geological Survey of Queensland and Geoscience Australia.

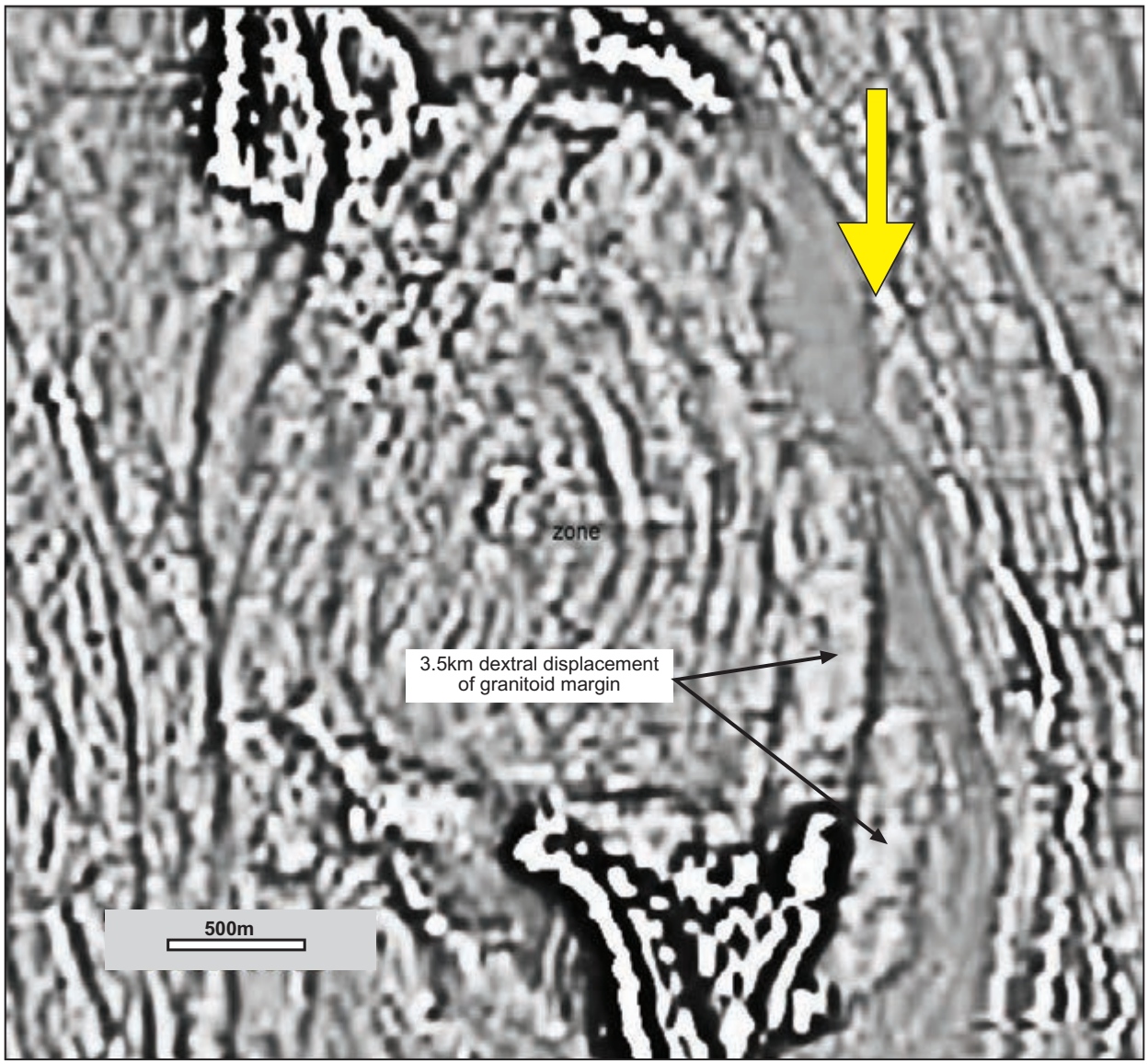

Figure 4.12: Aeromagnetic image from the Comet Vale area of the Yilgarn Block (WA), illustrating the recognition of faults from lateral offsets on magnetic rock units. Note in particular the ~3 km apparent dextral N–S displacement on the (yellow) arrowed fault. Data courtesy Fugro Airborne Surveys.

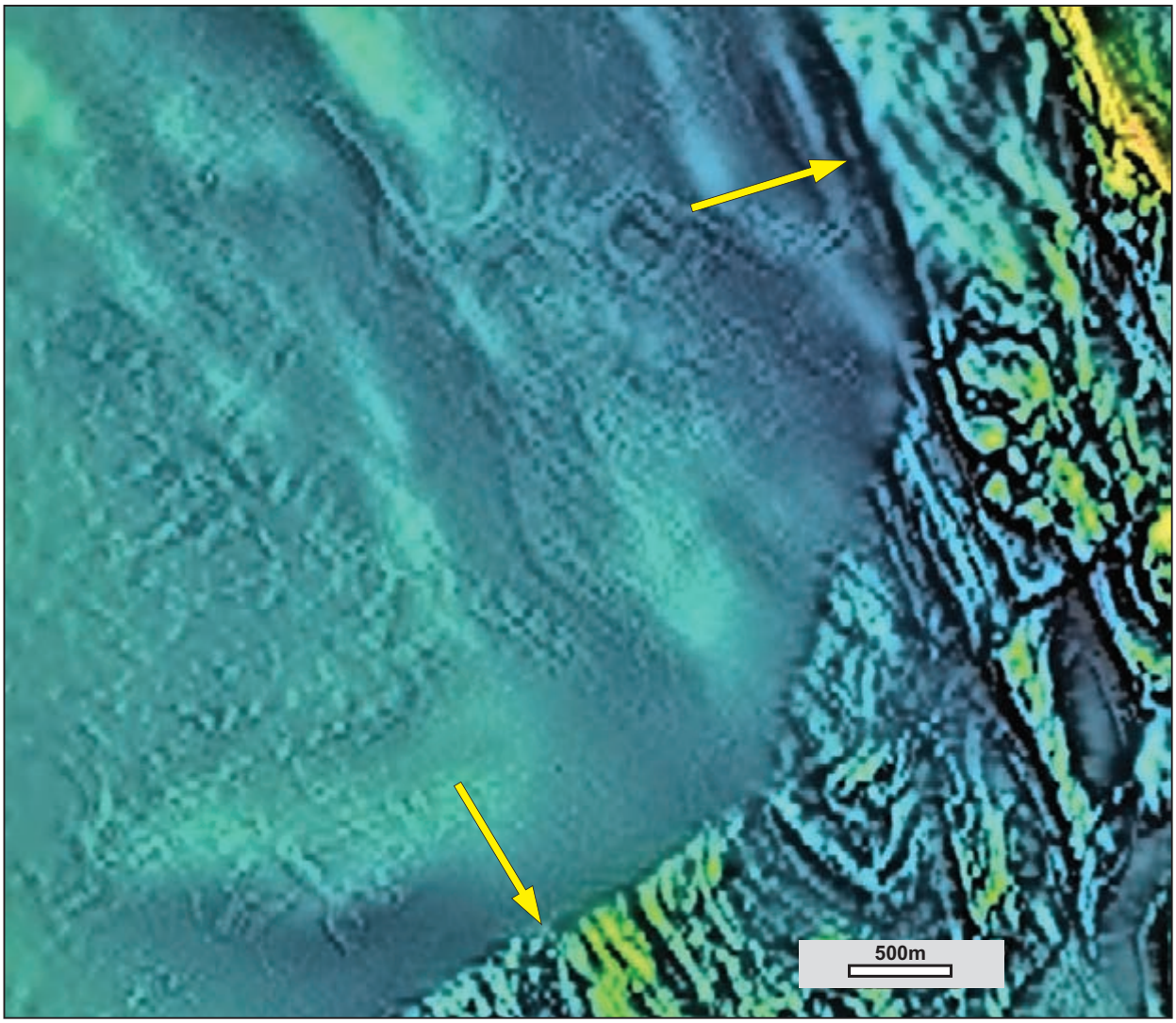

Figure 4.13: Aeromagnetic image showing normal faults (yellow arrows) in the Duchess region of the Mt Isa Inlier (Qld). The vertical displacement is around 1 km: the downthrown blocks have significant non- to weakly magnetic sediments overlying the variably magnetic metamorphic basement. Data courtesy Geological Survey of Queensland and Geoscience Australia.

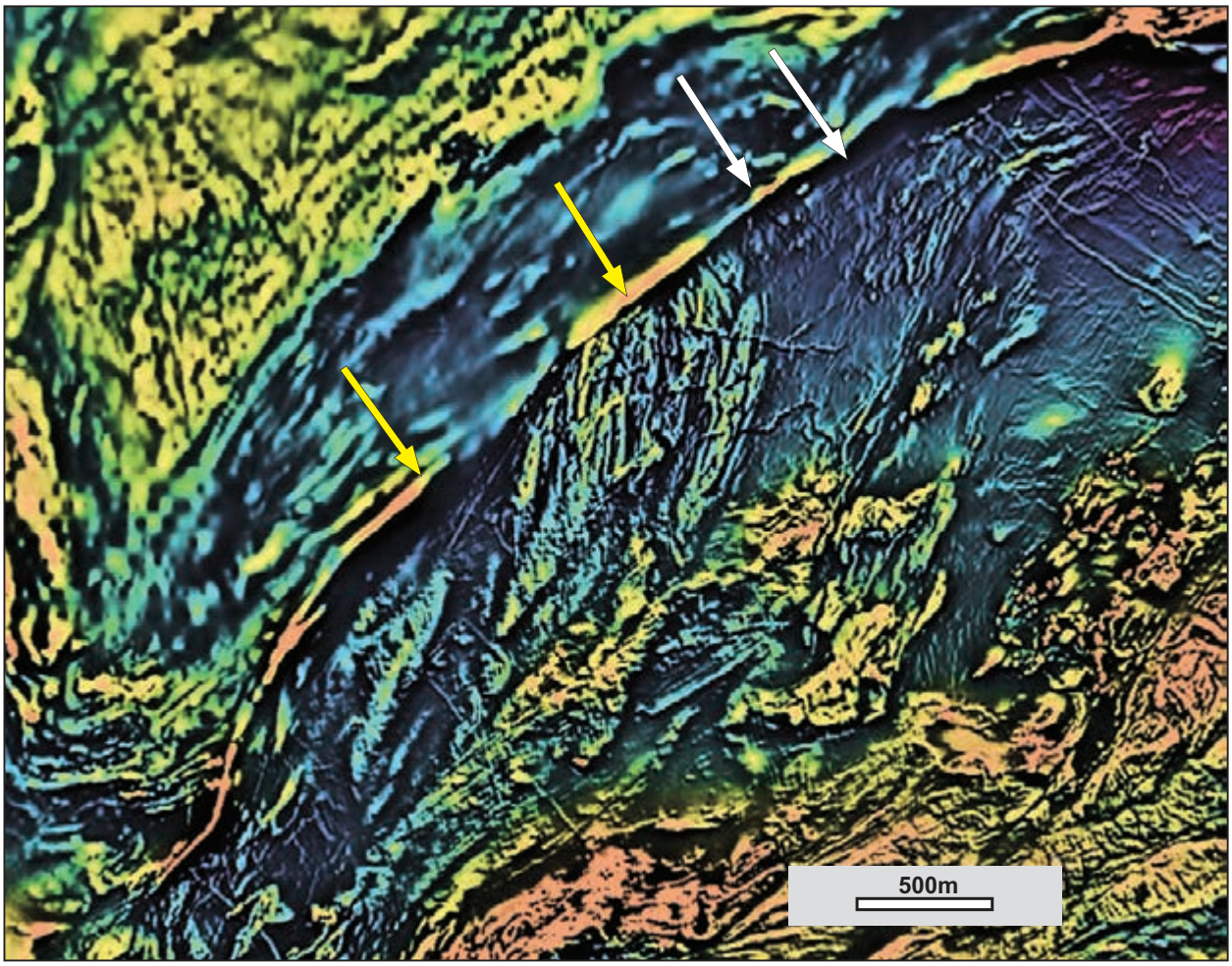

Figure 4.14: Aeromagnetic image over the NE-trending Karari Fault complex (white arrows) in NW SA. Note the change from shallow high-frequency (short-wavelength) magnetic character SW of the fault to deeper low-frequency (longwavelength) magnetic character NE of the fault (white arrows). This defines the Palaeozoic trace of the fault complex – the vertical displacement is ~1–2 km (NW block down). The fault zone includes a major Proterozoic shear zone (yellow arrows) where magnetite has been emplaced by both metasomatic fluid flow during deformation and possible shearing of pre-existing BIF. Data courtesy of DMITRE and Geoscience Australia.

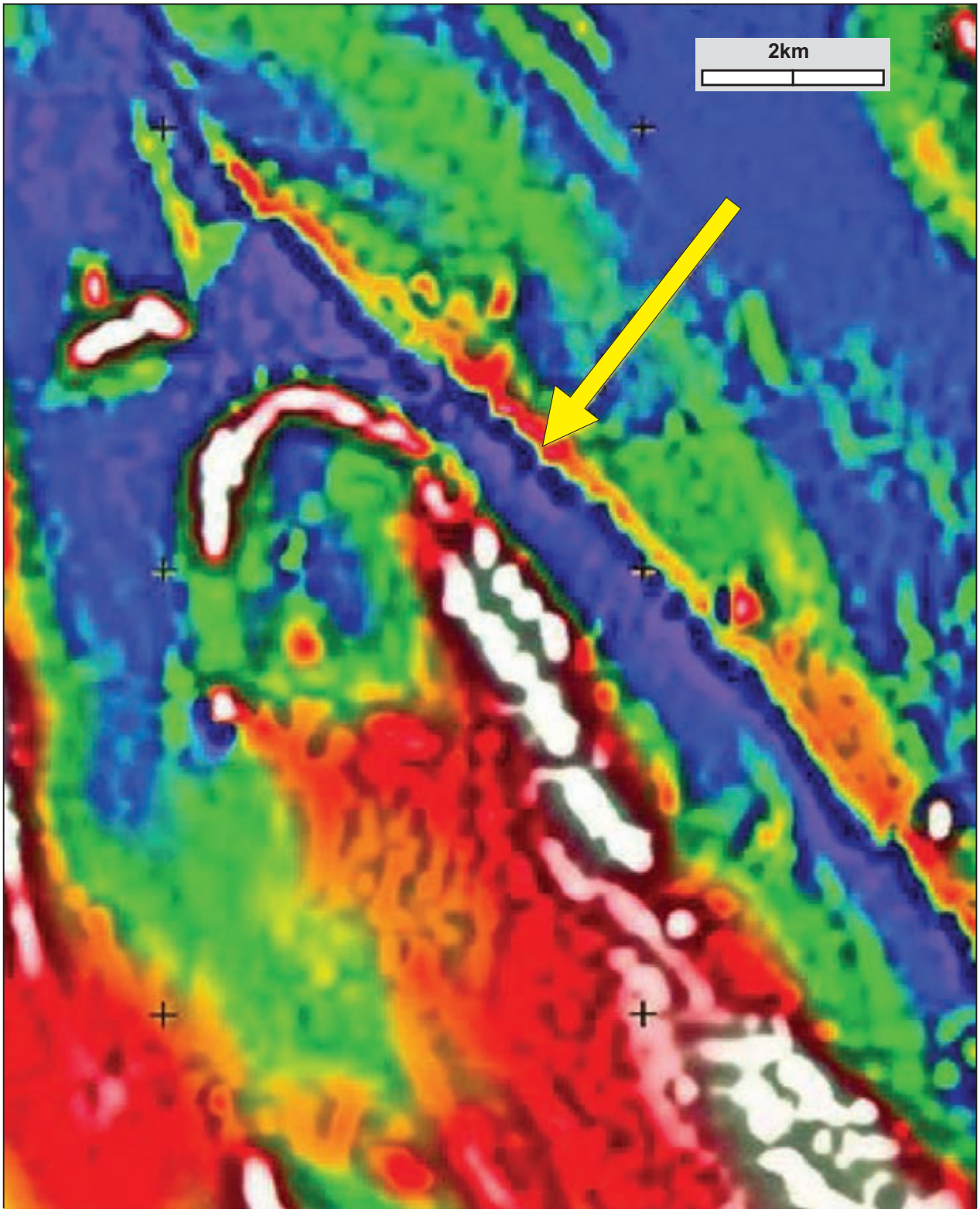

Figure 4.15: Example of a mafic dyke (NW-trending linear magnetic high – arrowed) intruded into a pre-existing fault zone, Kalgoorlie district, WA. Image from Boyd and Isles (2007), data courtesy Fugro Airborne Surveys.

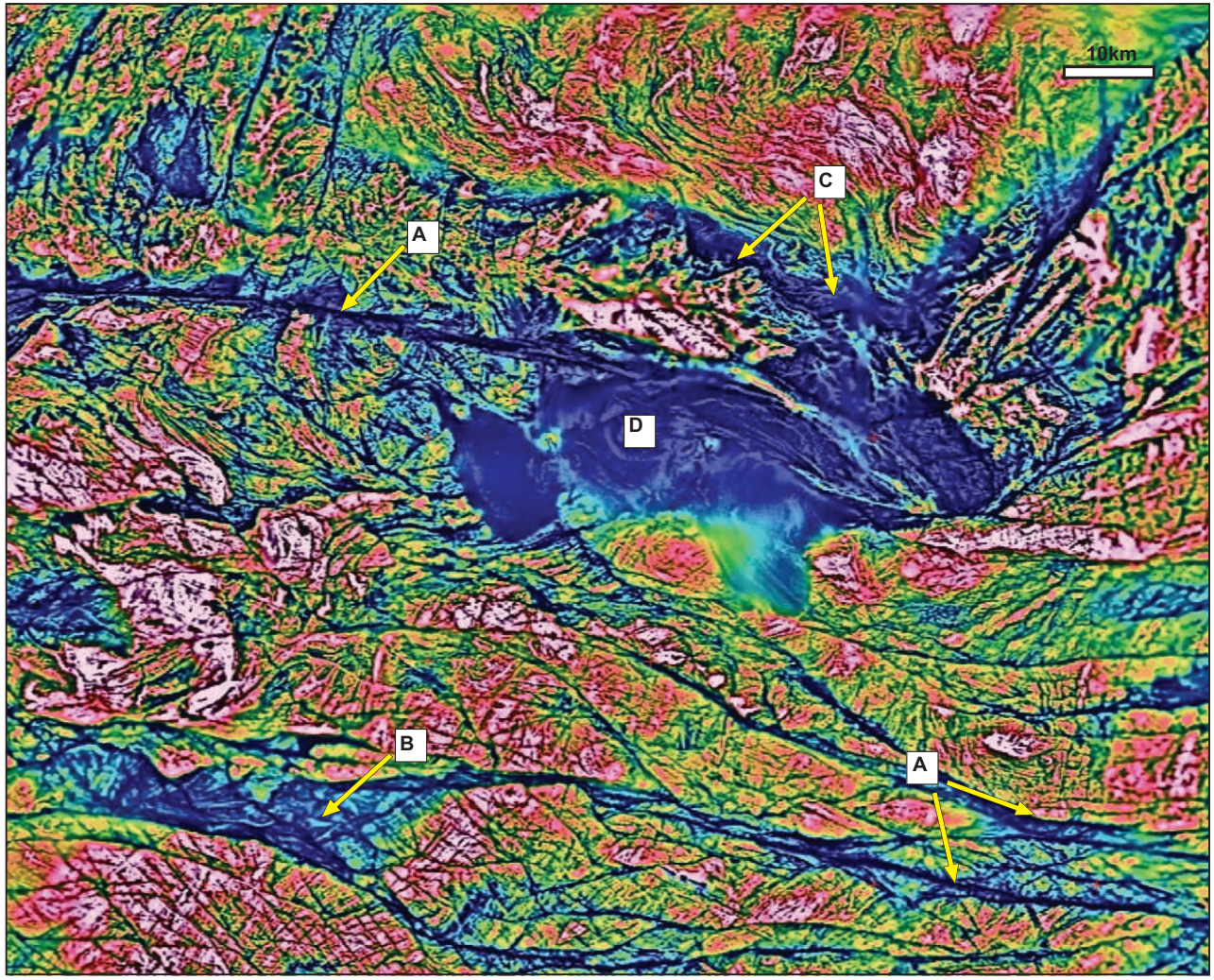

Figure 4.16: Aeromagnetic image from the Musgrave Block, SA showing magnetite destruction in fault zones (linear magnetic low zones). Data courtesy of DMITRE.
A) Narrow magnetite – destructive alteration within steeply dipping shear zones.
B) More regional magnetite – destructive alteration extending from first-order shear zone into subdomain of strongly faulted/fractured granulites.
C) Broad zone of magnetite destructive alteration within south-dipping Woodroffe Thrust.
D) Magnetic-low subdomain associated with thick non-magnetic sediments within the dextral – wrench Levenger Graben – overlying magnetic granulites.

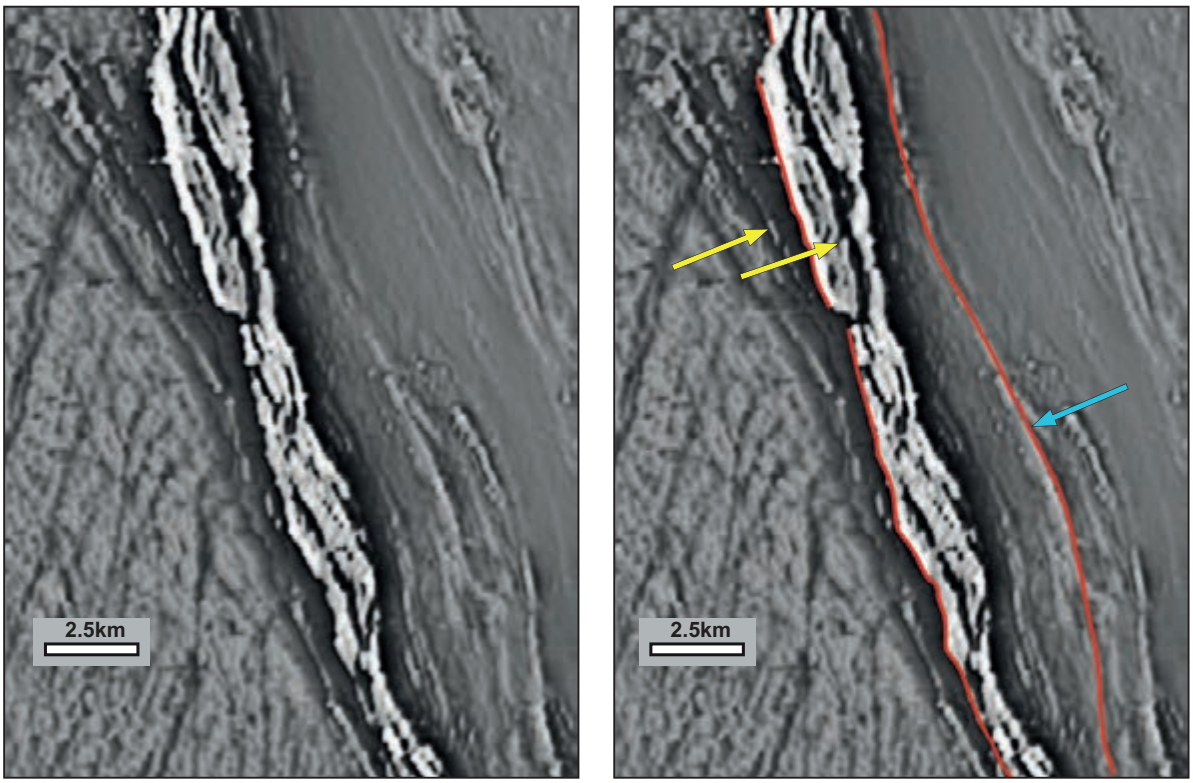

Figure 4.17: Major layer-parallel shear zones (red lines) in the Goongarrie district of the Yilgarn Inlier, WA. The westernmost shear zone is defined by yellow arrows. The easternmost shear zone is less obvious, with only one or two localities showing discordance between footwall and hanging-wall layering (blue arrow). See Chapter 11 for a full analysis of this area. Data courtesy Fugro Airborne Surveys.

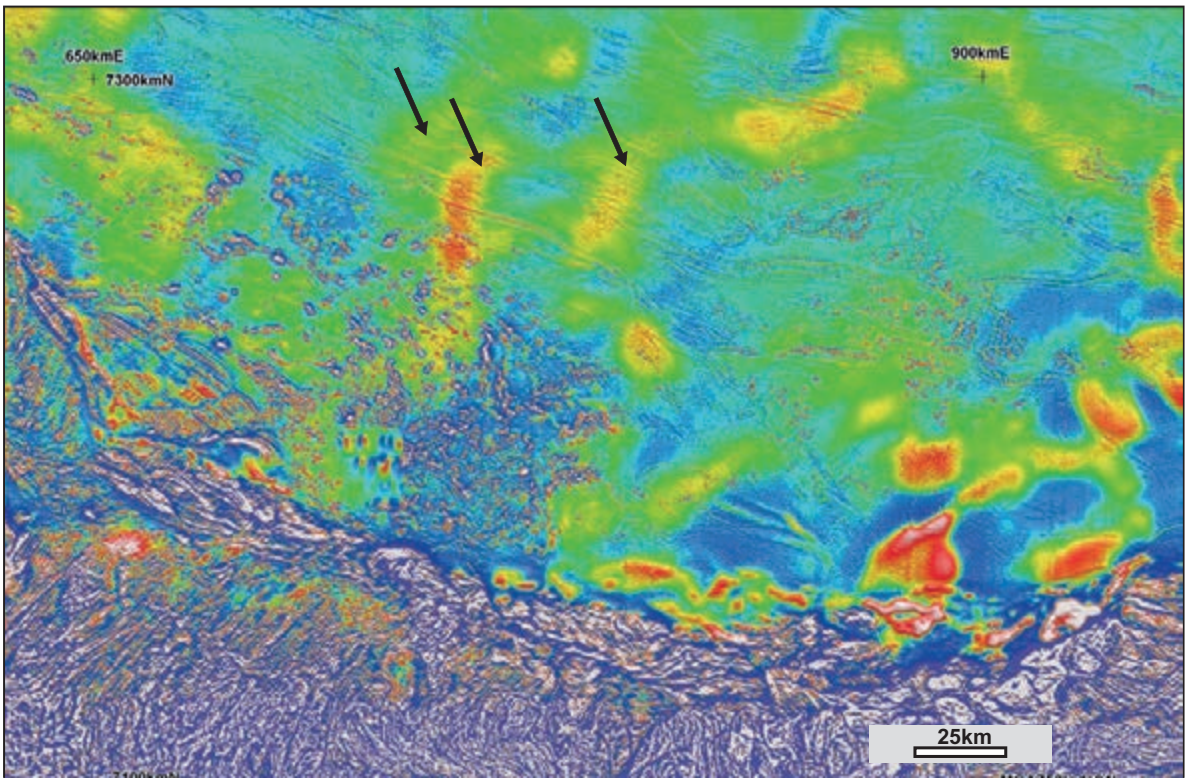

Figure 4.18: Deep (6–12 km) magnetic basement structures (highlighted by broad, low-frequency NNE- to NE-trending magnetic anomalies) seen beneath shallow sedimentary sequences, Amadeus Basin, NT. See Chapter 13 for analysis. Data courtesy Geoscience Australia.

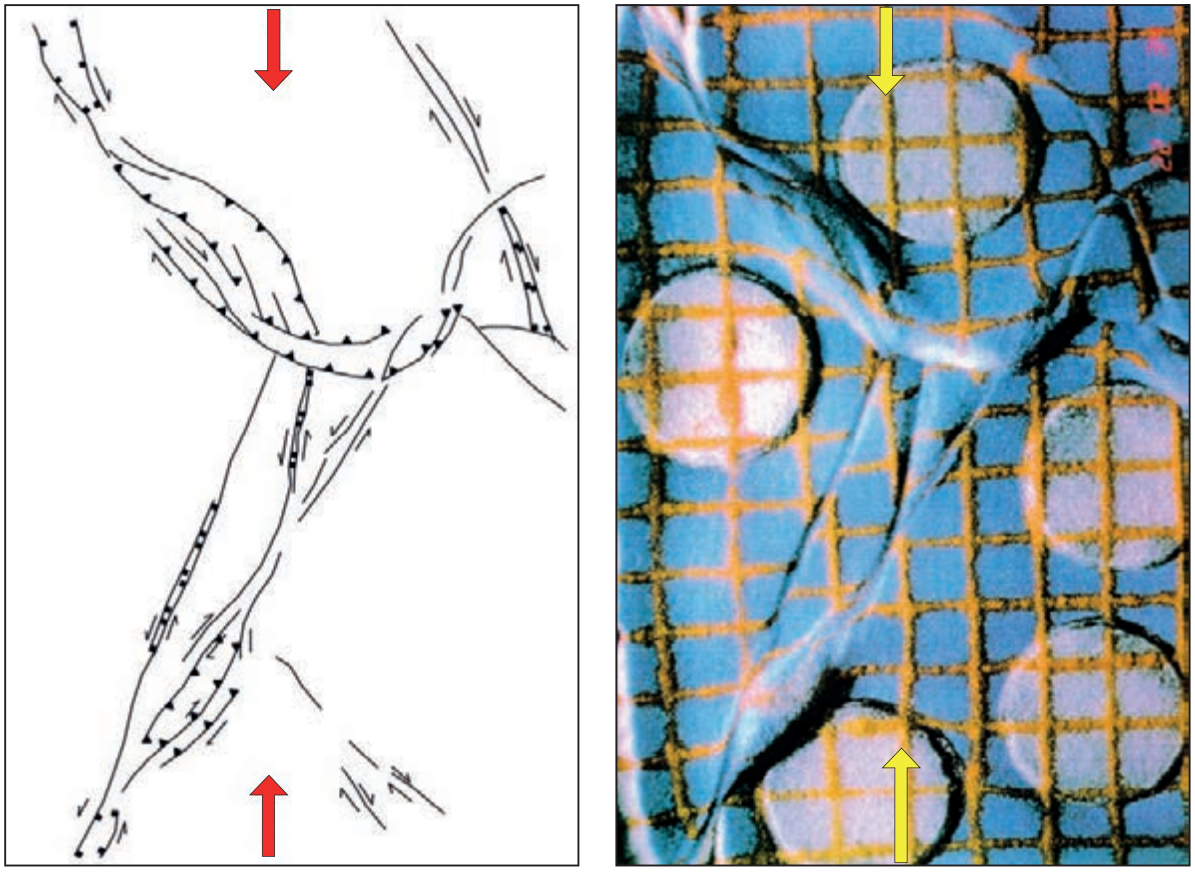

Figure 4.19: Experimental deformation model showing multiple, apparently cross-cutting structures derived from a single compressive event. Sandbox image courtesy of Lyall Harris.

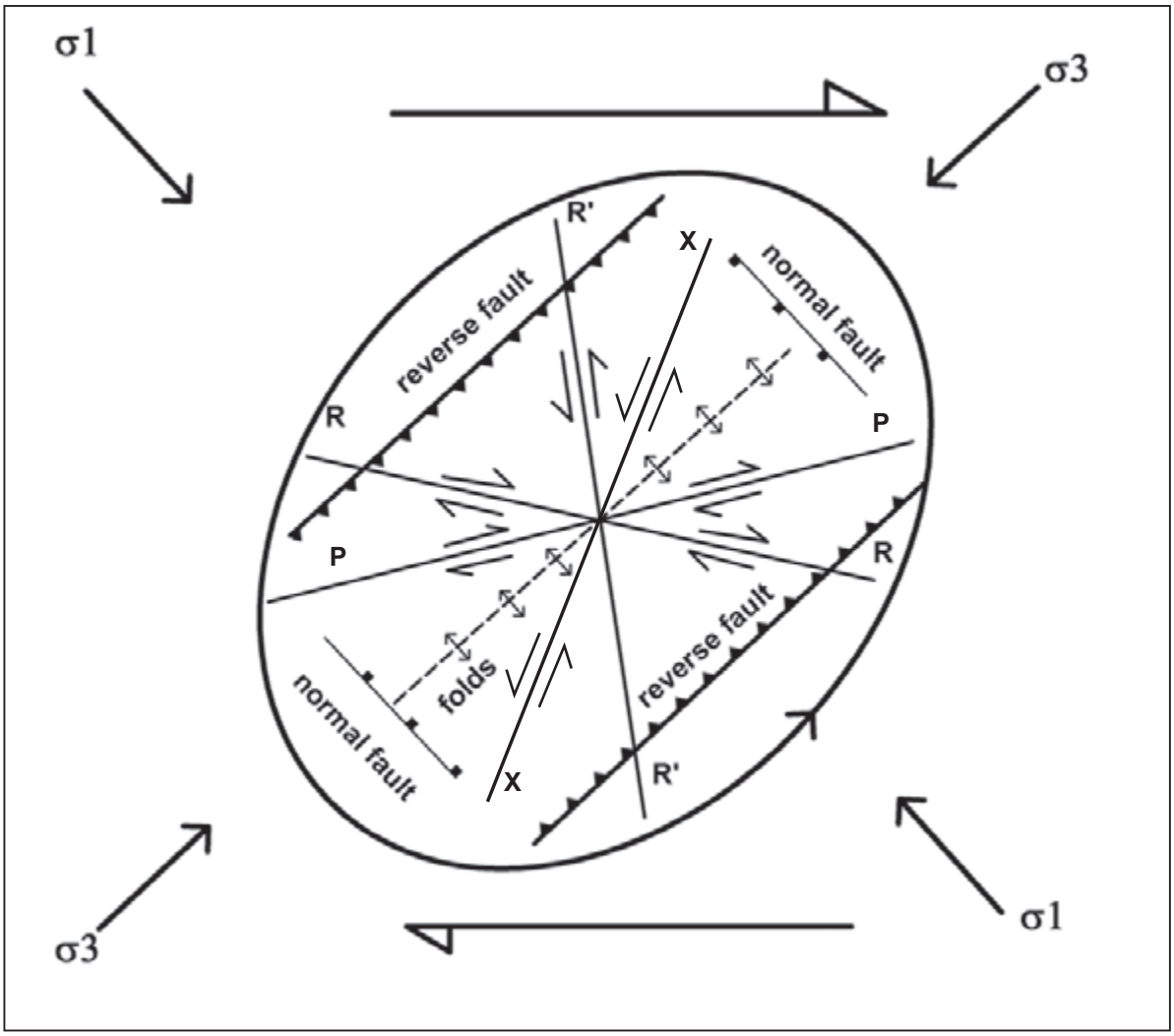

Figure 4.20: Regional strain-ellipse associated with a wrench/strike-slip fault system. The Reidel shear faults are the synthetic R and antithetic R' systems. In some systems synthetic P and antithetic X shears may also develop. Folds and compressive (thrust or high-angle reverse) faults are developed at 90° to ó1, whereas extensional (normal) faults are developed at 90° to ó3. Note that a set of structures with different orientations and movement vectors will be developed during one simple deformation.

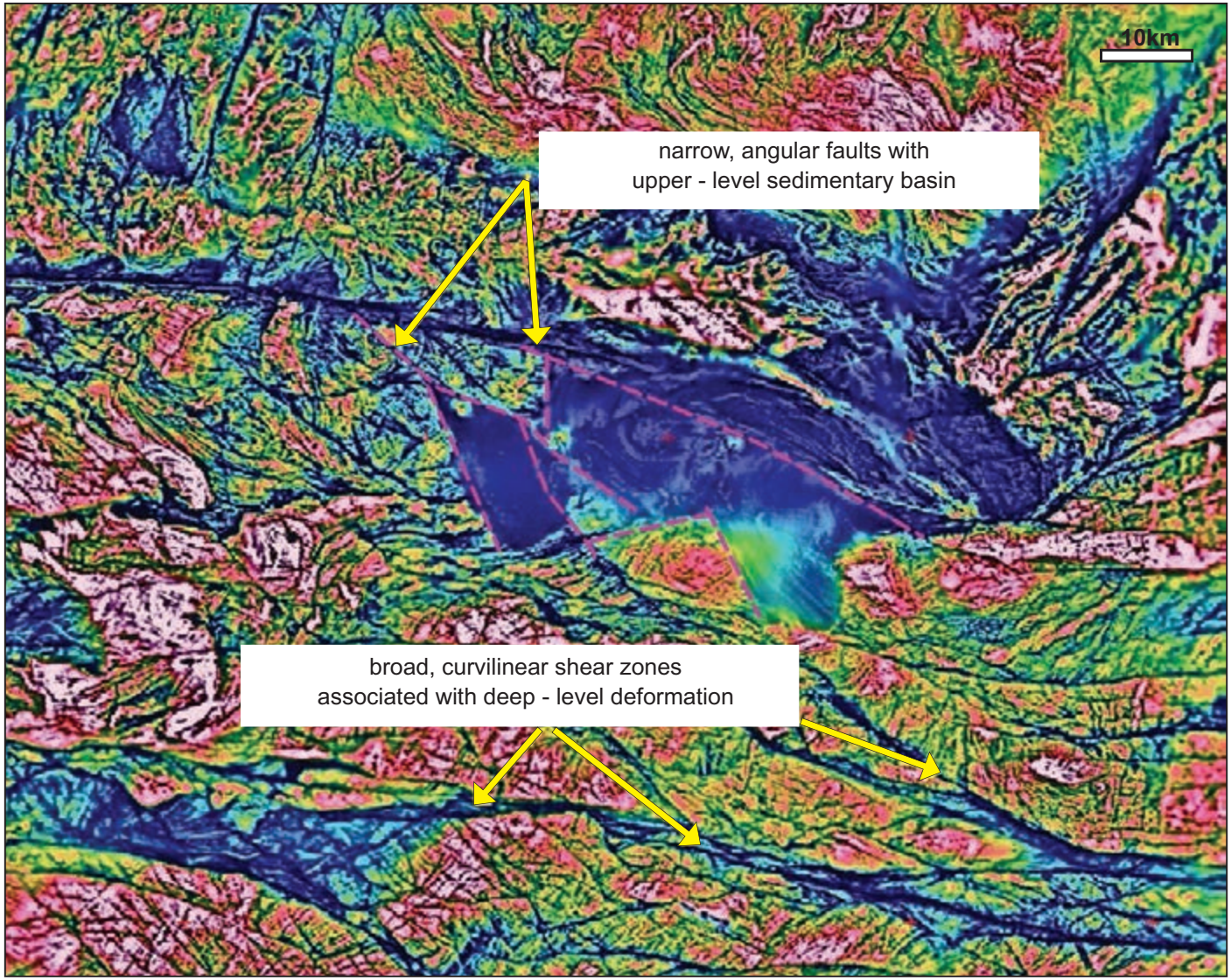

Figure 4.21: Aeromagnetic image over part of the Musgrave Block, Central Australia. Deep-crustal (high T, high P) deformation within the granulites is associated with development of broad, curvilinear, anastomosing shear zones. Shallow (low T, low P) deformation is associated with development of narrow, brittle faults with angular bends (pink dashed lines – faults associated with wrench basin opening of Levenger Graben). Data courtesy of DMITRE, NT Geological Survey and Geoscience Australia.

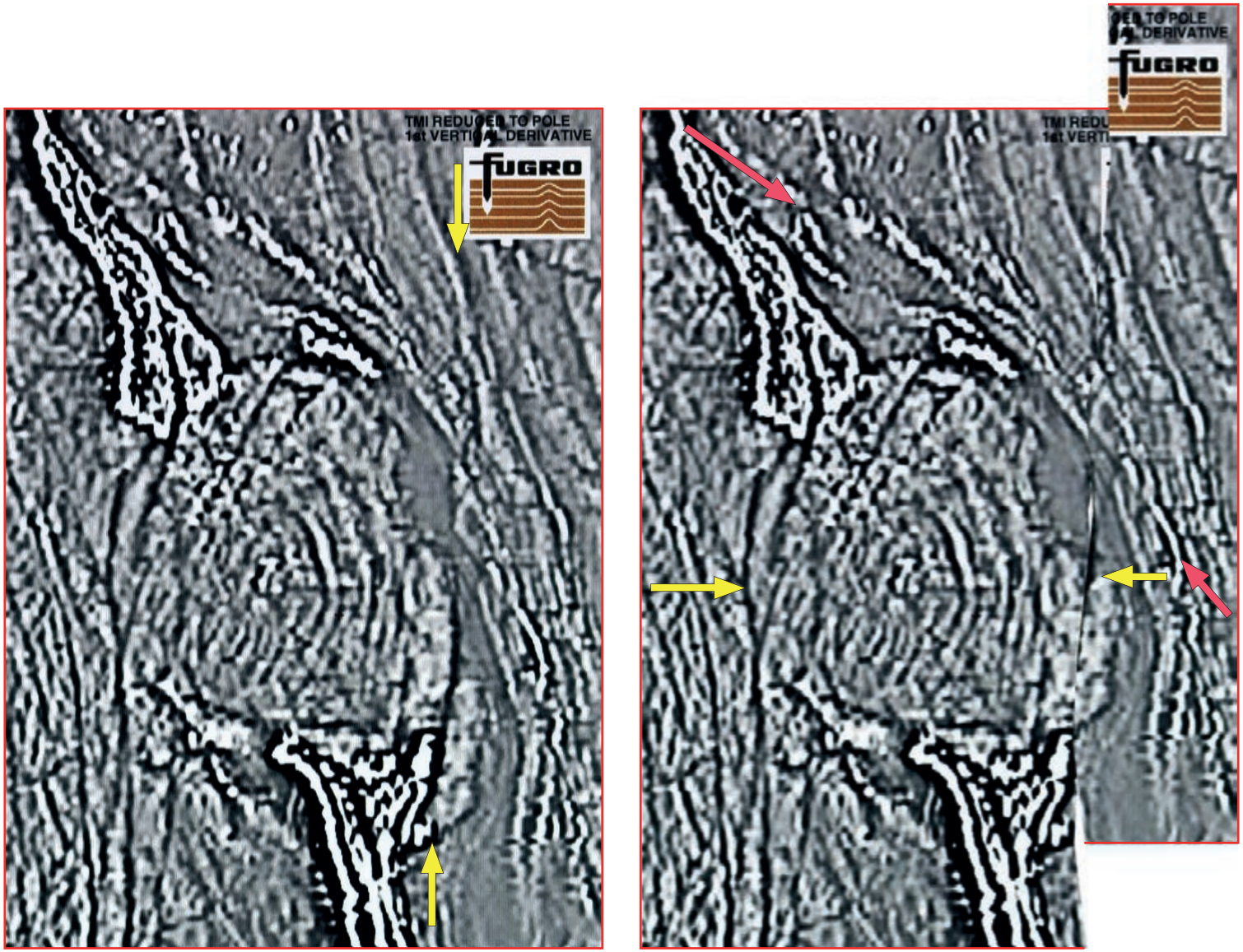

Figure 4.22: Reconstruction of approximate pre-faulting geometry by simple cut-and-paste of the appropriate image. Note how this not only reinforces the interpretation of the N–S fault (yellow arrows), but allows clearer recognition of earlier NW- and E–W-trending contacts and structures (red and orange arrows). Data from the Comet Vale area of the Yilgarn Block, WA, courtesy Fugro Airborne Surveys. See Chapter 11 for an analysis of this area.

Figure 4.23: The extensive family of structures caused by the single progressive N–S deformation due to the impact of the Indian and Eurasian Plates (after Tapponnier *et al.* 1982). Compare this to the experimental deformation model in Figure 4.19.

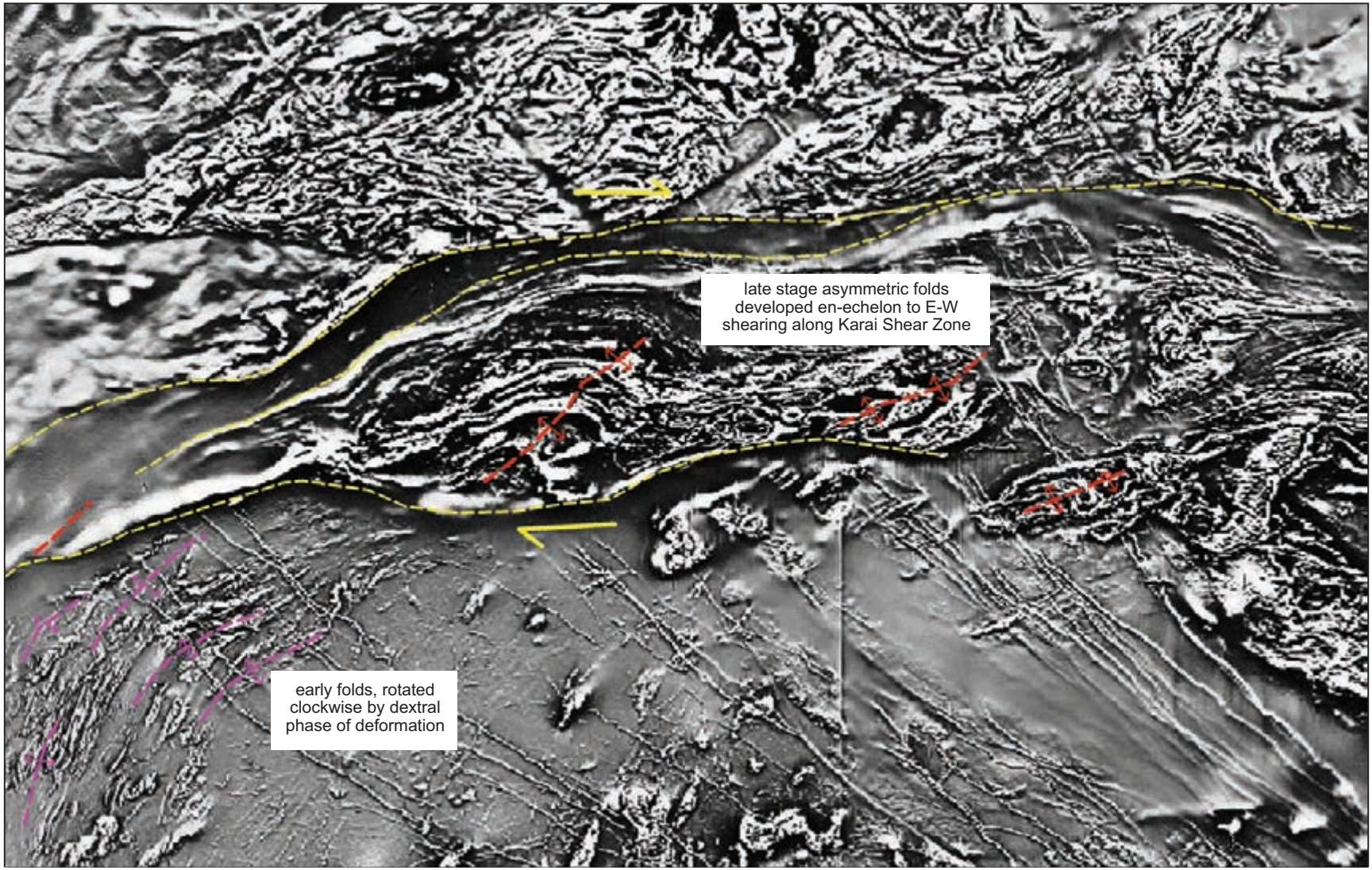

Figure 4.24: Aeromagnetic image over the Coober Pedy Ridge are of the NW Gawler Carton, SA. The traces of the Karari Fault Zone (plus associated structures) are shown (yellow dashed lines). An episode of dextral shear along this sector of the fault zone is interpreted from:
a) significant clockwise rotation of early folds into the shear zone (SW corner of image – pink dashed lines);
b) development of late-stage en-echelon, NE-trending asymmetric folds (central sector of image – red dashed lines). Data courtesy DMITRE.

5 Data acquisition and processing

5.1 SURVEY PLANNING – SURVEY SHAPES, SIZES, LINE ORIENTATIONS, SPACING, FLYING HEIGHT AND SAFETY

5.1.1 Overview

Care and attention to planning is essential to the outcome and success of any project. In aeromagnetic surveys there are many local issues such as seasonal climate and atmospheric conditions, topography and even politics which need to be addressed well ahead of the flying. Safety of flight crew and well-being of occupants of the survey area are of primary concern and these must be satisfactorily dealt with before any survey design is finalised. Matters of instrumentation and measurement technology are also important, but they are not dealt with in this book. Reeves (2005) covers these topics well; we assume here that the basic quality control function for the aeromagnetic survey data has been conducted well in advance of the interpretation. From the interpreter's viewpoint the key issue is having a dataset that enables the purpose of the survey to be fulfilled. The critical parameters that determine the interpretability of a dataset are line spacing and flying height and, to a lesser degree, line orientation and survey outline shape.

5.1.2 Survey shape and flight line orientation

Dealing with the less critical parameters first, in these days of high-precision satellite navigation any flight line direction and any survey shape can be achieved. In some cases the survey outline is constrained by aviation restrictions or by political or tenure boundaries. In most surveys, however, the planners are free to choose the outline and the line orientation. Some very practical considerations from the interpreter's viewpoint are listed below.

a) Odd-shaped surveys with many vertices and small segments make life difficult for the interpreter.
   It is hard to make geometric/geological sense of magnetic features which are only partly covered and/or appear in oddly shaped survey segments.
b) Simple, preferably rectangular shaped surveys aid recognition of geological structures.
   It also good practice to add ~10% additional area around the perimeter of the core survey area to provide adequate definition of magnetic features near the survey boundaries. We will deal with issues of survey costing and budgets below, when the topic of line spacing is addressed.
c) Odd line orientations have disadvantages.
   The conventional practice of flying perpendicular to 'strike' can be seriously questioned in these days of generally large-scale surveys and sophisticated structural analysis. Very often, the direction perpendicular to strike is an important structural direction, and focusing the airborne survey on this direction may diminish the interpreter's ability to recognise these strike-perpendicular structures. It is not uncommon

for such structures to be misinterpreted as data acquisition defects (see Fig. 11.6). The notion that flying perpendicular to strike allows us to use a wider line spacing and retain good correlation across lines is incorrect. Subtle geometric/structural variations which are often the key to robust structural interpretation may not be recognisable if this approach is adopted. Figure 5.2 shows how data with wide line spacing flown perpendicular to strike can give the appearance of strike continuity when it does not exist.

Another issue common in mineral exploration surveys with lines flown at odd (neither N–S nor E–W) orientations is that their grids are usually rotated in the process of producing standardised 'north up' images. An important factor here is the very common practice of merging new survey data with old to produce 'stitched' imagery. Merging and stitching requires all grids to have the same orientation, and rotation of grids to achieve this causes a degree of degradation of the rotated data. Where data has very close line spacing this degradation may be barely perceptible, but it is present.

In the authors' experience, is preferable to fly N–S or E–W oriented lines, although local factors such as terrain constraints or project/tenure boundaries can often override this.

d) Line orientation at low field inclinations.
Because of the (magnetic) N–S orientation of the magnetising field and the strongly extended nature of the measured responses over simple magnetic bodies at low field inclinations (see Fig. 5.10), it has been preferred practice to fly N–S oriented lines in these areas irrespective of predominant strike (e.g. Reeves 2005). We do not concur entirely with this practice and present our perspective in Section 5.1.5.

e) Line length.
The final issue relating to survey shape and line orientation is line length. Because of the large manoeuvre required for an aircraft (fixed-wing or helicopter) to change direction by 180°, very short flight lines will be more costly to the operator than longer lines. Most contractors stipulate a shortest line length (commonly 5 km for fixed-wing and 3 km for helicopter), but for the survey planners the big issue is that surveys with many short lines (particularly where lines are very closely spaced) will cost significantly more per-line-kilometre than if lines are longer. A typical survey flight path plot for a relatively small area is shown in Figure 5.1.

5.1.3 Line spacing – you get what you pay for

The survey line spacing dictates both the level of geological resolution achievable from the survey and the survey cost. A very common tendency is to expand the line spacing to enable a limited budget to cover a desired area. This is usually counter-productive because the diminished geological resolution compromises the quality of the interpretation. Planners need to start with an understanding of the degree of geological resolution required from the survey. This then firmly sets an upper limit to the line spacing.

Two fundamental rules have been established from extensive and hard-won experience in the airborne industry.

a) Maximum zoom scale: 1cm = 1 flight line spacing.
The scale to which aeromagnetic survey data can be validly and usefully zoomed is where 1 cm represents one flight line spacing (Boyd 1969; Boyd and Isles 2007). This means that a survey flown with 250 m line spacing can provide geological detail down to a scale of 1:25 000 but cannot be effectively interpreted at more detailed scales, such as 1:10 000. 'Zooming in' further is numerically simple, but the patterns observed will never confidently reflect the true underlying variations in the geology. While the choice of flying height will have a significant effect on geological resolution, post-acquisition numerical techniques usually allow us to improve resolution where the flying height is slightly larger than we desire. This is not the case with our choice of line spacing. Aeromagnetic survey data cannot be displayed sensibly in grid form at any scale where the line spacing is greater than 1 cm. We will discuss the numerical basis for this 'rule' in the data processing section. For now, the survey data examples in Figure 5.2 illustrate the point.

b) Halving the line spacing yields twice the geological resolution.
The second 'rule' is that halving the line spacing does indeed double the geological resolution (Isles *et al.* 1992). Most importantly, this assumes appropriate choice of flying height (discussed in the next section).

Once again, this 'rule' is based more on (sometimes bitter) experience rather than potential field theory and numerical analysis. In this regard, Figures 5.3a, 5.3b and 5.4 largely speak for themselves.

Tie lines

Tie lines are flown perpendicular to the main body of flight lines in order to provide a cross-check on magnetic field base levels and to facilitate matching of these levels from line to line. Base-level intensities vary continually due to the magnetic field generated in the ionosphere from the reaction to solar winds. These diurnal variations in field intensity are usually small and gradual. The combination of a continuous recording at a base-station in or near the survey area, and the duplicate field measurements at flight line–tie line intersection points, allows the removal of the diurnal variations from the field due to magnetisation in rocks.

Tie lines are most commonly spaced at around 10 times the nominal flight line spacing, but tighter tie line spacing may be warranted where maximum sensitivity is required (e.g. in sedimentary basins).

How closely can we effectively fly?

Fixed-wing surveys at line spacings of 25 m and sometimes 20 m have been commonly (and safely) flown, principally in gold exploration applications in Australia. These have used crop-duster type aircraft and have proved highly effective in defining the fine-scale geological structure that is not only crucial to gold exploration, but can also be extremely valuable in groundwater exploration. The typical flying height for these surveys has been 25 m although heights of 8 m have been flown over salt lake areas which cover extensive parts of the Western Australian gold and nickel provinces. Such data can be usefully analysed at 1:2000 and has proved beneficial in structural studies in mine environments.

As we have seen in Chapter 2, the flying height has a major influence on the achievable level of geological resolution in aeromagnetic surveys and hence the 'rules' we have tabled concerning flight line spacing must be considered in the context of flying height.

5.1.4 Survey flying height

The survey flying height is the major safety concern in aeromagnetic surveying and modern aviation practice places many obligations and constraints on all field survey operators. A good general rule for the planner and the potential interpreter is to ensure that all regulations relating to the safety of air-crew and the inhabitants of the survey area have been adhered to, and to trust the judgement and wisdom of experienced survey pilots and crew.

The illustrations in Chapter 2 (particularly Figs 2.5, 2.6, 2.18 and 2.19) clearly reinforce the intuitively obvious notion, common to all physical measurement, that the closer we are to the target, the clearer it will appear. Hence we would expect that in aeromagnetic surveying, the lower the flying height the better the geological resolution. This is true in general and Figures 2.16 and 2.17 highlight the role played by the source–sensor distance in quantifying this resolution. However, there is a range of situations where flying at the lowest safe height may not yield the best possible survey data.

Rugged terrain

Rugged terrain causes large variations in ground clearance because aircraft are not able to exactly 'drape' over the topographic surface. Very tight valleys will cause significant increases above the nominated ground clearance and very high hills will show different ground clearance profiles in different flight directions. Another factor is that severe aircraft manoeuvres may be needed in order to maintain the nominated lowest safe ground clearance. Such manoeuvres may result in excess wear and tear on instrumentation installations and on flight personnel. An increase in flying height of 10–30% may provide for a much smoother ride without significantly compromising the resolution of the data. In general, the flying contractors have wide experience in these matters and their judgement on lowest safe flying height and optimal height for high-quality, low-noise data is astute.

With availability of digital elevation data such as SRTM, it is possible to pre-plan the flight (drape) surface to minimise the problems encountered in rugged terrain. This is extremely helpful to the air-crew in attempting to match the flying height at the intersection of traverse lines and tie lines. A poor match to the heights at this intersection point can impact adversely on the quality of the final data grid.

Helicopters lessen but do not eliminate the above problems with rugged terrain and there are many situations where the substantial extra cost for a helicopter survey is not reflected in increased quality of data. For large-scale surveys in particular, it is advisable to explore the capabilities of fixed-wing platforms before electing to fly with helicopters. Large fixed-wing surveys with small areas of helicopter in-fill in difficult terrain are a feasible solution.

In spite of the physical reality that lower flying should yield sharper geological resolution, the very high sensitivity of modern magnetometers and the fact that amplitude fall-off rates for the great majority of magnetic rock bodies are modest (see Fig. 2.10) means that *slightly higher, smoother flying in rugged terrains is very often the best approach*.

Another issue with rugged terrain, particularly where strongly magnetic rocks occur near surface, is that strange magnetic field patterns will occur when the sensor is located near to, but at a lower altitude than, a magnetic rock body. This can occur in precipitous terrain, usually with helicopter surveys when the aircraft descends below a topographic high composed of magnetic material. In this case, flying slightly higher to achieve a smoother drape may again be desirable.

Rugged terrain is likely to generate topographic anomalies in the aeromagnetic data, even in the most astutely acquired surveys. While there are data processing schemes which attempt to minimise these topographic effects, they cannot be eliminated and the recognition and understanding of these features effectively becomes part of the interpretation process. That is, it is usually better for the interpreter to confront and deal with the terrain effects than to expect them to be removed at the data processing stage. Modern surveys are accompanied by good-quality digital terrain models (DTMs) derived from the difference between the GPS height (which gives absolute altitude) and the radar altimeter (which measures ground clearance). These DTMs are not only important in the interpretation process in rugged terrains, but nearly always aid the interpretation.

Near-surface magnetic material

There are many forms of near-surface magnetic material which constitute unwanted noise in aeromagnetic surveys. Cultural features such as farm sheds and machinery, mine-site infrastructure, road and rail ballast, electrified railways, ocean swell and even wire fences in remote areas are readily seen in modern, low-level detailed surveys. Towns and cities present even greater problems for low-level surveys and are usually excluded from surveys or flown at a considerably increased height. Geological features which fall into the noise category (depending on the geological focus of the interpretation) include sheet-wash and weathering products derived from lateritic surfaces in arid terrains, glacial debris in cold climatic areas, magnetic detritus in modern and palaeo-drainage systems and surficial lava flows. Examples of these features can be seen in Figures 3.4 and 3.27.

A common feature of these sources of noise is that they have much lower volumes and usually smaller dimensions than the underlying geological formations. Referring once again to Figure 2.10, we see that such sources have a much greater amplitude fall-off rate than typical bedrock geological sources (often $1/d^3$ compared to $1/d$). Hence there may be potential to choose a flying height which discriminates strongly against the near-surface sources without unduly compromising the signal from the underlying geology.

There are opposing views on this topic. Some prefer to fly a little higher to suppress the effect of superficial sources, others prefer to fly as low as practicable in order to clearly define these unwanted sources in the expectation that they may then be removed from the final data. We will see later that there are numerical techniques which allow us to separate magnetic sources from different depths and our ability to do this well is enhanced if the source–sensor distances from the deeper and shallower geological features are widely different. Flying lower will always increase this difference and flying higher, as proposed above, will always increase the tendency for the anomalies from different source depths to blend together. It is also relatively straightforward to 'upward continue' aeromagnetic data (i.e. re-compute the TMI for a higher survey altitude after the survey has been flown) but effective 'downward continuation' is much less achievable (see Section 5.4.1).

In the authors' experiences, some prior knowledge of the nature of the near-surface noise sources can greatly assist in survey design, and specialist assistance with model studies and processing alternatives is usually advisable.

5.1.5 Flying height relative to line spacing

Reid's (1980) definitive work relating flying height and survey traverse line spacing tells us that if our line spacing is equal to the flying height, all magnetic sources will be adequately sampled in a spatial sense. This effectively means that the frequency content of the data across line will be compatible with the frequency content along line (dictated by the flying height). We have seen the degree to which flying height affects geological resolution and our general desire would be to fly as low as practicable. Also, for maximum geological resolution, we would normally prefer to fly closely spaced lines. A typical safe flying height for fixed-wing surveys in undulating terrain is 80 m, so in terrains such as this a line spacing of around 80 m would yield adequate sampling. Budgets rarely permit us to match line spacing with lowest, safe flying height, so we need to be aware of the consequences of having a line spacing that is larger than the flying height.

It is worth mentioning what happens if we fly lines that are more closely spaced than the flying height. Sampling theory tells us that this will yield a degree of redundancy in the data, which should result in a cleaner (less noisy) dataset. However, the benefit of this improvement in signal/noise ratio would rarely be worth the considerable extra flying cost. One important possible exception is in sedimentary basin environments where signal levels may be tiny (<0.2 nT) and data coherency is critical to the study of the often discontinuous low-amplitude magnetic patterns (see Chapter 10).

As we increase the line spacing relative to the flying height we become progressively more undersampled (aliased). In hard rock aeromagnetic surveys, where magnetic rocks usually occur near surface, undersampling will result in the creation of artefacts in the data grid. The array of point measurements of magnetic field along flight lines must be interpolated onto a square grid in order to make plan view images and contour maps. The artefacts created when the line spacing is greater than the flying height usually take the form of a line-perpendicular bias in the gridded data. This is caused by the tendency for the numerical schemes that interpolate the line data onto the grid to give higher weighting to nearest neighbour data points which will, of course, be perpendicular to the lines. We will discuss the gridding process in more detail later in this chapter. For the current discussion on survey planning, we can state that the usual and preferred course of action is to fly as low as practicable (in the context of project economics and safety) and to choose a line spacing that suits the desired scale of geological analysis. While this strategy usually results in a degree of undersampling and the commensurate line-perpendicular artefacts, there are numerical schemes which enable these to be addressed at the data processing stage. It is rarely desirable to fly at a higher ground clearance in order to more closely match the chosen line spacing. This is illustrated in Figure 5.5, where we see the progression from 50 m line spacing to 400 m line spacing, all with 50 m flying height. The 200 m, and particularly the 400 m, data show the line-perpendicular artefacts. These observations are consistent with the conclusions of Reid (1980), who recommended that, to avoid intolerable aliasing, survey height should not be smaller than half of the survey traverse line spacing. If we had elected to avoid these artefacts by making the flying height half of the line spacing we sense that we would lose a significant amount of geological resolution. Our conclusion is that it is usually better to tolerate a degree of undersampling in order to preserve local geological detail. Figure 5.5 would suggest that a line spacing to flying height ration of 4:1 is acceptable, but 8:1 (as in the 400 m at 50 m height example) is not. In this case a flying height of 80 m (giving a ratio of 5:1) would have produced a better balance of geological resolution and artefacts. In fact, this configuration (400 m spaced lines at 80 m height) has been adopted in a great deal of government-sponsored flying in Australia (see Chapter 13). As Reid (1980) points out, the severity of the aliasing, usually manifest as line-perpendicular artefacts in our grid, will increase rapidly as we exceed the 2:1 ratio, so we need to be prepared to deal with these artefacts if we choose to fly lower and or wider lines than the ideal.

In this context we revisit the topic of flying orientation at low field inclinations. As mentioned in Section 5.1.2, N–S traverse lines are conventionally preferred at low field inclinations, irrespective of predominant strike. Where the line spacing and flying height are well matched (i.e. not greater than 2:1), the magnetic field is sufficiently well sampled to avoid artefacts and the choice of line orientation has limited influence on that nature of the data grid (see Section 5.2.1). Where we elect to fly at a lower height to gain spatial resolution, as we often do in mineral exploration surveys, we create artefacts perpendicular to the line direction. In this situation, at low

field inclinations, our problems are exacerbated by extension of magnetic anomalies in the N–S direction relative to their causative bodies, as shown in Figure 5.10. Where the predominant geological strike is N–S the conflict between low field inclination magnetic effects and the artefacts caused by undersampling is maximised, and because of this we make a case for flying E–W lines in this situation. We acknowledge that this contradicts conventional practice and agree that where dominant geological strike is not N–S, then N–S lines are preferable. The example shown in Figure 5.15 illustrates the successful use of E–W lines in eastern Senegal at a field inclination of 4° with flight lines 100 m apart at a height of 40 m. The predominant strike in the survey area is NNE and we have chosen a section of the survey where a fold structure provides a range of strike orientations. Interpretation work by both authors, including field verification, has concluded that the veracity of the magnetic grid is exceptional, enabling direct and quite accurate tracing of magnetic rock units in the subsurface.

We emphasise that we are nearly always faced with compromises when faced with the crucial choices of line spacing and flying height. Prior discussion and debate with experienced industry specialists is always advisable when planning an aeromagnetic survey.

5.1.6 Single-sensor versus multi-sensor surveys

There is a growing tendency for acquisition systems to include multiple magnetic sensors in order to directly measure transverse magnetic gradients. The purported benefits of the additional information relate mainly to improved across-line interpolation, effectively reducing the undersampling artefacts caused by flying lines much more widely spaced than the flying height (discussed above). In the extreme, some operators have claimed that line spacing can be increased with transverse gradient surveys to achieve the 'same quality' data as more closely spaced, single-sensor data. This notion has great appeal to budget-conscious exploration managers and government funding agencies but there are flaws in the arguments which need to be considered.

The usual multi-sensor configuration is to have magnetometers on each wing tip, often (and preferably) in addition to the tail-stinger installation. The transverse gradient information is most commonly introduced to enhance the gridding process and there are numerous examples (e.g. Fig. 5.6) illustrating the success of this approach. The cautionary note is that, while the gradient information should produce a smoother grid with diminished undersampling artefacts, the actual improvement in geological resolution will not exceed the ratio of the sensor separation to the flight line spacing. Hence a survey flown at 400 m spacing (e.g. at 80 m above ground level) with a conventional fixed-wing system having a wingspan of around 15 m, will still have 385 m between sensors on adjacent lines so an improvement in geological resolution of around 5% would be anticipated. On the other hand, where the wingspan is a larger fraction of the line spacing (e.g. 15 m for a 50 m spaced survey) we could expect the gradient information to very significantly improve geological resolution. While beneficial in theory, the practicalities of compensation (for aircraft manoeuvre) and the increased complexities with magnetic gradient data processing make magnetic gradiometer surveys much more involved than single-sensor surveys. In the authors' experience, achievement of the very low noise levels (~0.05 nT) required for surveys in sedimentary basins is more readily achievable with single-sensor surveys than with multi-sensor surveys.

5.1.7 Summary points for survey planning

a) Safety first. Each planning step needs to consider the safety of both flight crew and inhabitants of the survey area.
b) Heed the advice of experienced contractors.
c) Line spacing dictates the scale at which a dataset can be usefully analysed.
d) The rule of thumb scale is one line spacing = 1 cm.
e) Geological resolution improves in proportion to reduction of line spacing.
f) Flying lower will nearly always yield higher geological resolution.
g) Occasionally, flying a little higher will reduce noise.
h) Surveys with line spacing greater than around five times the flying height will usually produce excessive undersampling artefacts.
i) E–W and N–S line orientations are usually preferable.
j) Fine-tuning the line direction to suit structural directions is rarely advisable.

k) If line spacing is small, line orientation has limited influence on the final grid.
l) Multi-sensor surveys do not guarantee higher geological resolution.

5.2 DATA ACQUISITION AND ROUTINE PROCESSING

Readers are referred to Reeves (2005) for a commentary on the intricacies of field acquisition and the basic corrections applied to achieve final TMI data. The task of quality-controlling an aeromagnetic survey requires specialist geophysical experience and it is rarely undertaken by the person responsible for the data interpretation. The key issues for the interpreter are that the noise levels in the data are acceptably low and that the noise suppression schemes adopted during the basic processing stage do not adversely affect the geological signal. It is essential that quality-control personnel are fully aware of the final sensitivity required to achieve the objectives of the survey. For instance, the requirements in sedimentary basin environments (see Chapter 10) are considerably stricter than, say, in an environment dominated by igneous and metamorphic rocks (see Chapter 11).

5.2.1 Data processing – gridding

Once the appropriate basic corrections have been applied to the TMI measurements along line, the data must be interpolated onto a square grid. As illustrated in Figure 5.7 the grid cell size is ideally around 1/4 of the line spacing. It is instructive to examine this requirement in view of the parameters commonly employed in modern aeromagnetic surveys. The TMI sampling interval along flight lines rarely exceeds 10 m (commonly ~7 m). Considering a typical high-resolution survey with a line spacing of 100 m and a mean terrain clearance of 50 m, the recommended grid cell size would be 25 m. If it is much smaller than this (e.g. 10 m) the line-perpendicular undersampling artefacts are unacceptably exacerbated. If it is much larger (e.g. 50 m) we will lose detail recorded in along the flight lines. After many years of experimentation and fine-tuning of the various grid interpolation algorithms, the established constraint is that grid cell size should be between 1/5 and 1/3 of the line spacing. The choice will be partly dictated by the flying height and partly by the depths to magnetic sources in the survey: where depths are large, the need for fine-scale detail in the grid is reduced and the broader 1/3 line spacing may be appropriate.

We have encountered the fact that most surveys are undersampled (due to economic realities); this results in artefacts in the gridded data principally in the form of false, line-perpendicular magnetic data trends. Transverse gradient measurements can reduce these effects but at additional cost and usually with limited real increase in geological resolution. There are several numerical methods which can be applied to single-sensor data to suppress the false line-perpendicular trends and these offer improved aesthetic appearance of gridded data which can assist the interpreter. Some of these introduce user-defined directional trending to the gridding process to produce smoother and cleaner-looking grids, but run the risk of overriding real and important geological trends and breaks. The key issue for the interpreter is the integrity of the gridded data; an essential part of gauging this integrity is an appreciation of the limitations of the measured data. Numerical schemes which make the gridded data 'look better' but in doing so obscure the interpreter's ability to discriminate real trends from artefacts are not helpful for interpretation.

5.2.2 Data processing – levelling and micro-levelling

Small 'step changes' in TMI base level are commonly observed between flight lines and these only become apparent when the data is gridded. In raw data, these will be mainly due to the diurnal, which is the daily time variation in the measured field due mainly to currents flowing on the ionosphere (Campbell 1997). These time-varying fields can be largely eliminated from the final line data with routine field procedures and data processing (Reeves 2005). This removal of the diurnal field variations is not perfect and when the imperfections are larger than the inherent noise level in the final data grid we see line-to-line base-level changes. Often described as 'busts' and regarded as shortcomings in the data, these should more appropriately be thought of as indications of the ultimate noise level in the data.

Another source of these line-to-line busts is small differences in terrain clearance. It is not feasible to maintain a constant survey ground clearance (drape) so we expect (hopefully small) differences in the ground clearance profile from line to line. In areas of shallow, strongly magnetic rocks where vertical magnetic gradients will be high, these differences can translate into significant shifts in TMI levels. In this regard, rugged, strongly magnetic terrain presents the worst-case scenario. A common situation is where flight lines cross an ironstone ridge. The aircraft ground clearance profile on approach to the ridge will invariably be different from that on departure. The outcropping magnetic ironstone will have associated strong vertical magnetic gradients and the resulting TMI patterns close to the ridge will vary with line direction. There are numerical height correction schemes in use, but these are not simple to apply effectively. Hence it is not uncommon to have terrain clearance as well as diurnal bustsremaining in our data after standard corrections have been applied.

Removal of the busts is done via a process called 'micro-levelling'(e.g. Minty 1991). This process seeks to identify local and abrupt flight line parallel gradients and adjust the local base levels of the adjacent lines to match each other. There are several different numerical approaches to this, including one known as 'decorrugation' which discriminates against all short-wavelength, line-parallel magnetic gradients. While these processes invariably make the final TMI grid 'look better', they have the potential to obscure real and important line-parallel magnetic features and should be used with care and caution. Applied well, micro-levelling can reveal coherent structural variations in areas which would otherwise appear as incoherent noise-level variations (Fig. 5.8). Applied indiscriminately, micro-levelling can cause the interpreter to overlook critical structures. It should not be used as a means of disguising poor-quality data.

Good practice in assessing the usefulness and effectiveness of micro-levelling is to conduct early-stage processing (gridding, basic filtering and imaging) on the pre-micro-levelled (also called 'tie-line levelled') data. Contractors routinely supply raw data and the key information enabling subsequent users to reprocess the data with alternative gridding and levelling techniques.

5.2.3 TMI data as a reference point

In Sections 5.3 and 5.4 we discuss the wide range of numerical transformations and filters available to enhance aeromagnetic data. While the basic TMI grid may not be the form of data most used in the interpretation, it should always be imaged as the initial step in interpretation. The TMI grid is the interpreter's main display of the corrected survey measurements and it is an essential reference point when working with filtered and transformed versions of the data. We make the distinction between transformations and filters in this processing. Transformations are numerical processes that produce new 'versions' of the measured field intensity data. Filters are processes which seek to emphasise particular components of the data while suppressing others.

5.3 TRANSFORMATIONS

5.3.1 Reduction to the Pole (RTP)

RTP is a fundamental process which, in most situations, yields imagery representing the geometry of magnetic rock units much better than TMI data. Its physical basis is sourced in potential field theory (Baranov and Naudy 1957), and where it can be successfully applied numerically it is a 'must' for the interpreter. Campbell *et al*. (1992) present examples illustrating that RTP can be practically applied in most situations. As illustrated in Figure 5.9, RTP transforms TMI data measured at any Earth's field inclination to that which would be observed if the survey were conducted at the magnetic poles (I = 90°). In essence, the dipolar nature of magnetic anomalies is removed. Peak RTP magnetic values relate more closely to the centre of magnetic rock bodies and asymmetries in the RTP imagery more closely reflect true dips and plunges. The model examples shown in Figure 5.10 show how difficult the interpreter's task of delineating the true geometry of magnetic rock bodies from TMI data becomes, as the field inclination decreases. Even at relatively high field inclinations the dipolar nature of the TMI makes recognition of the true magnetic rock unit geometry challenging. At –60° inclination (Fig. 5.11) the differences between TMI and RTP data appear superficial, but the

subtle pattern changes have a significant impact on structural interpretation. At –45° inclination (Fig. 5.12) the differences become clearly apparent. At very low inclinations (<30°) the task of deciphering the true geometry from TMI imagery becomes impossible. The model studies in Figure 5.10 indicate that conducting this task using the RTP (I = 90°) data is straightforward.

The real world and the limitations of real datasets combine to create difficulties for the numerical application of RTP. Two situations arise where RTP may yield erroneous and/or misleading results.

RTP and remanence

Where rock bodies retain a strong component of remanent magnetisation (or other non-induced forms of magnetisation), the application of RTP to the anomalies over these bodies is theoretically invalid. This is because the technique assumes that the magnetisation direction for the entire area to be transformed is known and equal to that of the local Earth's field. For rock bodies dominated by non-induced magnetisation we very rarely know the magnetisation direction. Much discussion and debate on this subtopic could be presented, but for the purposes of this book the authors will simply put their viewpoint based on experience from numerous survey areas.

Remanently magnetised bodies are rarely the dominant sources of magnetic anomalies in a survey area. In these cases the majority of the magnetic rock bodies will be depicted more clearly in the RTP data than the TMI. The challenge for the interpreter is to recognise those features which are affected by remanence. There are strategies for achieving this (see Section 3.4.4) and methods to deal with the interpretation (see Section 8.3). In the authors' experience, the benefits of applying RTP far outweigh the potential pitfalls and the known or suspected presence of remanence should not deter interpreters from making use of RTP. This is illustrated by the successful use of RTP in the (dominantly) remanently magnetised Semail Ophiolite in the Sultanate of Oman (Al Azry *et al*. 1993). Figure 5.13 compares TMI and RTP data over the remanently magnetised alteration pipe at Mt Leyshon in north Queensland (Sexton *et al*. 1995). The interpreter's ability to delineate the outline of the top surface of the pipe is unaffected by the RTP and the geological trends of the surrounding country rock are enhanced by the RTP.

Where remanence does dominate the survey area, it can be argued that RTP should create a less complex picture than the TMI owing to its effect on the induced component of magnetisation in the survey area. While this has not been demonstrated in theory, the authors are aware of unpublished examples where RTP has made an important contribution in most challenging magnetic environments.

Environments dominated by thick BIFs may render RTP unsuitable for detailed structural interpretation, because the magnetisation will probably include remanence, anisotropic susceptibility and self-demagnetisation effects (see Section 3.4). Once again, however, computation of the RTP is likely to be of assistance along with the TMI and other transformations such as Analytic Signal, which is discussed below.

RTP at low Earth's magnetic field inclinations

The other situation where the use of RTP is challenging is in areas of low magnetic field inclination. This arises because the computation involves division by increasingly small numbers as the field inclination decreases. The resulting numerical instability is typically manifest as false trends in the data parallel to the Earth's field declination (i.e. magnetic north). Where datasets are undersampled (i.e. line spacing is much greater than flying height) and the gridded data contains interpolation artefacts (as discussed above), this effect will be more pronounced. However, where line spacing and flying height are reasonably matched, there are several numerical remedies which allow RTP to be successfully performed at low field inclinations.

It is important to emphasise that RTP is a critical tool for structural interpretation at low field inclinations. Once again, Figure 5.10 shows the difficulty faced by the interpreter if constrained to the use of TMI. If we imagine what this model data would look like if the line spacing was wide, we realise how wide line spacings at low field inclinations produce data with serious limitations in the context of fine-scale structural interpretation.

We present two excellent examples of RTP at low field inclinations. Both were flown with 100 m line spacing. The survey in southern Sumatra (Fig. 5.14) had N–S flight lines and covered a Tertiary Au-Ag epithermal-vein province. The Earth's field inclination is –28°. The importance of effective RTP and the ability to apply

high-pass filters such as 1st VD (see Section 5.4) is paramount in exploration in this area because mapping and targeting require accurate definition of fault and fracture patterns, and recognition of often-subtle magnetic mineral alteration effects. Similarly, the data from eastern Senegal (Fig. 5.15, I = 4°) cover a gold exploration play in a Neoproterozoic volcano-sedimentary sequence. The detailed definition of structural features required for gold exploration can only be confidently determined from the RTP and its derivatives. The robust nature of the RTP at this near-equatorial field inclination results from astute numerical implementation of the RTP equations and the fact that the line spacing is tight. A further feature of note is that the flight line orientation is E–W, dispelling the often-quoted notion that N–S oriented lines should always be used at very low field inclinations.

In summary, in the great majority of situations RTP enables the interpreter to more clearly decipher the geometry of the underlying geology and, subject to certain limitations, it should be considered a routine part of any aeromagnetic survey.

5.3.2 Analytic Signal (AnSig)

This 2-D transformation, devised by Nabighian (1972), cleverly separates the 'angle terms' from the 'space terms' in the equations that describe the anomalous field over a magnetic rock body. Nabighian's (1972) concept has since been approximately extended to 3-D in the calculation of the Total Gradient Amplitude and somewhat unfortunately this parameter has retained the name '3-D Analytic Signal', frequently and colloquially abbreviated to 'AnSig'. To avoid confusing readers who already have many maps and images labelled 'Analytic Signal', we persist with this now established usage, but refer readers to Li (2006) and Haney *et al.* (2003) to gain an appreciation of the differences between 2-D Analytic Signal and Total Gradient Amplitude. Henceforth in the book the term 'AnSig' will refer to the Total Gradient Amplitude – but we do acknowledge that 'TGA' would be a more appropriate abbreviation. Mathematically, AnSig is the magnitude of the vector sum of the three component directional derivatives and it broadly tracks the loci of the shallowest edges of a magnetic body irrespective of the orientation of the body's magnetisation. That is, the AnSig will effectively map these edge locations at low field inclinations and in the presence of remanent magnetisation (and the other non-induced forms of magnetisation).

This makes AnSig a most powerful tool.

The limitations of AnSig are illustrated in Figures 5.15 and 5.19. The AnSig response over a magnetic body is more complex than both the TMI and the RTP, as is to be expected given that it produces an anomaly over each body edge. This means that AnSig is unsuitable for defining subtle, fine-scale structural variations. AnSig, like TMI and RTP, also loses its effectiveness when the depth to the magnetic rock body begins to approach its lateral dimensions.

Computation of AnSig is simple and robust and, like RTP, it should be considered as a routine transformation, appropriate in most if not all aeromagnetic surveys.

The situations where AnSig is a critical tool are:

a) where the interpreter suspects the presence of non-induced magnetisation. Detailed observation of the AnSig, TMI and RTP over bodies suspected to have remanence, self-demagnetisation or anisotropic susceptibility effects should enable the interpreter to resolve the body location and determine whether or not unusual magnetisation is present;
b) at low field inclinations where the robustness of RTP may be in question. Again, detailed comparison of AnSig, TMI and RTP should allow the interpreter to gauge the degree to which the RTP can be trusted and utilised.

Rajagopalan (2003) presents a succinct discussion of the pros and cons of AnSig and RTP and their relationships to TMI imagery.

In summary, AnSig, (the Total Gradient Amplitude) is a key tool enabling the interpreter to identify and deal with some of the more complex and difficult interpretation situations.

5.4 FILTERS

The concept of filtering in any form of data processing involves retention and/or enhancement of the desired portion of the signal, and elimination or suppression of the unwanted part. In aeromagnetic surveys, filtering is usually aimed at separating the deeper and shallower components in the data and sharpening the clarity with which these components can be observed by the interpreter. Figure 5.16 illustrates the process of filtering. The two main classes of filters noted are high-pass and low-pass filters. High-pass filters are so named because they retain the higher-frequency content in the data. Higher frequencies have shorter wavelengths; these in simple terms will have shorter straight slope distances (see Fig. 2.8). Hence we expect that the high-pass filters will emphasise shallower sources in aeromagnetic data. Conversely, low-pass filters retain low frequencies which have long wavelengths and therefore long straight slope distances which will relate to deeper sources. In this book we keep the realm of filtering to a basic minimum, acknowledging that beyond the numerical schemes mentioned, there are many more potentially useful products, and individual practitioners will invariably have favourite combinations of filters and images. For the aspiring magnetic interpreter, the filters covered in this book will cater adequately for all situations. For those wishing to explore an expanded range of filters, Cowan and Dentith (2003) provide an excellent and succinct summary.

5.4.1 High-pass filters

Surveys in hard rock terrains typically use high-pass filters to provide a sharper picture of the near-surface geological structure. The numerous high-pass filters designed for aeromagnetic surveys can be a source of confusion to interpreters, particularly when individual specialist geophysical advisors commonly have strong leanings to particular and often esoteric filters. We do not attempt to present or categorise all the available filters. Rather we present the main, established, conventional filters and give some guidance on the benefits and pitfalls of venturing into the domain of the more complex and extreme filters. Our strong preference is to use filters that can be directly related to the location of magnetic rock bodies and have a simple and sound basis in potential field theory. Our cornerstone high-pass filter is the First Vertical Derivative (1st VD). Illustrated in Figure 5.17, and discussed in detail below, the 1st VD provides a very reliable starting point for the process of extracting structural detail from aeromagnetic data. Figure 5.18 illustrates a basic set of high-pass filters and Figure 5.19 shows some of the more complex ones. We will refer to these figures as we briefly describe the various filters.

First Vertical Derivative (1st VD)

The 1st VD is the most widely used high-pass filter for aeromagnetic survey data because it is robust in computation, reliable in outcome and readily interpretable in the context of magnetic rock bodies. The simplest way to envisage 1st VD is as the vertical magnetic gradient we would observe from two magnetometer sensors mounted one above the other. The 1st VD is the difference in magnetic field measurements at the two sensors. In fact, during the 1970s such vertical gradient measurements were conducted by mounting magnetometer sensors at the top of the aircraft tail as well as on the stinger at the base of the tail. This practice was only discontinued when it was discovered that the 1st VD could be quite reliably determined from (good-quality) single-sensor data (Paine 1986).

The 1st VD has no directional bias and this is a key characteristic in improving the spatial and structural resolution in the imagery. Peak positions from the TMI (or RTP) are retained in the 1st VD but, as seen in Figures 5.17 and 5.18, the 1st VD anomaly is considerably narrower and more closely reflects the width of the magnetic rock body causing it.

Second Vertical Derivative (2nd VD)

The 2nd VD is effectively the first vertical derivative of the 1st VD. As expected, it further reduces the width of the anomaly and theoretically should much more closely reflect the width of the causative magnetic rock body. Although the theory and computation of 2nd VD is based on sound potential field physics, in practice 2nd VD tends to be 'noisy'. The simplest explanation is that 2nd VD is a more extreme high-pass filter than 1st VD. It seeks to provide much more detail and it emphasises and enhances the higher-frequency parts of the measured TMI (or RTP) signal. In so doing, it also enhances the inherent noise in the data that will consist of

the fundamental noise level (see Reeves 2005) in the measured line data plus any artefacts introduced during the gridding process. For very high-quality data with close line spacing, the 2nd VD should be clear and interpretable. For datasets with wider line spacing and perhaps higher inherent noise levels, it may appear very noisy and complex, to the extent that the resolution of geological structure is hindered rather than enhanced.

Signal versus noise

It is a fundamental of signal processing (and of physical measurement) that there is no distinct level which differentiates signal from noise. In aeromagnetic survey data the major noise sources are predominantly high-frequency and (hopefully) very low amplitude. The high-pass filters used to enhance aeromagnetic data emphasise these characteristics in both signal and noise. In essence, the harder we try to enhance fine-scale detail in the signal, the closer we will get to enhancing the noise. Hence the more extreme high-pass filters will be unavoidably more noisy. This does not mean they have lesser value in the interpretation than the more moderate high-pass filters, but they do produce imagery which is more complex and unquestionably less aesthetically pleasing.

A useful rule in this quest to visualise the fine-scale detail in aeromagnetic data is that if no noise is visible in the data, and the dataset looks clean and smooth, then it follows that we are not seeing the smallest level of signal. Put another way, if we wish to see the smallest signals in a dataset we must expect to also see and deal with a certain degree of noise. While the smallest signals may be of little interest in the interpretation, it is prudent to be prepared to use imagery which looks somewhat noisy and complex. It is also prudent to be wary of imagery of high-pass-filtered aeromagnetic data that looks exceptionally smooth. For the interpreter, the rough edges often hold the key to recognising subtle but important structures.

Downward continuation

Potential field theory tells us that once the field is defined by measurements on one surface it can be calculated on surfaces above and below that measurement surface. The mathematical definition of this continuation is straightforward (Reeves 2005) and the numerical application is limited only by the quality of the data (theoretically data can be downward-continued to the top of the magnetic source).

Downward continuation, whereby the field below the measurement surface is calculated, provides us with another high-pass filtering option. In the context of sharpening the magnetic responses and providing the interpreter with a clearer view of the geological structure, downward continuation has no distinct advantages over 1st VD and 2nd VD. For data of reasonable quality, downward continuation to around half of the flying height is readily achievable. Beyond this, the limitations of noise in the data result in effects similar to those encountered with 2nd VD.

Conversely, continuation to surfaces above the measurement surface presents no numerical difficulties and its veracity is limited only by the lateral dimensions of the dataset. This upward continuation will be discussed further in the section below which covers low-pass filters, but it is noteworthy here that continuation has a unique place in the data processing armoury, because it allows us to adjust the measurement surfaces of adjacent surveys to a single height. For example, a localised low-level survey may be upward-continued to facilitate direct merging with a broader-scale survey flown at a higher level. Hence continuation plays a major role in the stitching and merging of aeromagnetic surveys, the prime example being the aeromagnetic map of the world (Korhonen *et al*. 2007).

Automatic gain control (AGC)

AGC is another extremely useful item in the filtering toolbox which allows us to deal with the frequently encountered problem of dynamic range. Most aeromagnetic surveys include signals of many hundreds if not thousands of nT, while at the same time having real geological signal at levels of 0.25 nT or less. The challenge of portraying both the huge and the tiny signals in a single presentation (either profiles or images) has been addressed in radio signal processing and subsequently in seismic data processing, where very large amplitude signal from shallow reflectors needs to be referenced on the same section as tiny signals from reflectors at

many kilometres depth. Rajagopalan (1987) and Rajagopalan and Milligan (1994) adapted AGC for aeromagnetic data processing, allowing a variable degree of amplitude modification and achieving a remarkable enhancement of the shallow structural aspects of most datasets.

AGC is an extreme high-pass filter and the example in Figure 5.19b illustrates its typically noisy appearance in image format. The profile example shown in Figure 5.17, however, highlights the ability of AGC to resolve subtle low-order variations in the presence of much larger signal. The profile example also illustrates how AGC, like other extreme high-pass filters, amplifies the noise as well as the low-order signal. This reinforces the notion that in order to clearly view the lowest-order signals in aeromagnetic data, we are invariably obliged to tolerate a degree of the noise in the data.

Tilt derivative

Potential field 'tilt' is the arctan of the ratio of the 1st VD and the modulus of the total horizontal derivative (Miller and Singh 1994). Because it is derived from a ratio, it has a normalised data intensity range. It produces patterns similar to the 1st VD, but portrays responses from deeper and shallower sources in similar ways and hence may be confusing to the interpreter aiming to isolate and trace individual magnetic rock units. Figure 5.19 illustrates the comparison of tilt with other filter types.

Directional filters

The most common directional filters are the so called shaded-relief operators (also known as 'illuminations' and 'sun angles') and horizontal gradients. These are used in association with raster imaging systems to digitally illuminate datasets from a chosen direction (horizontally and vertically), creating lighter shades on the data gradients facing the illumination direction and darker shades on the gradients facing away from the illumination direction.

While these shaded images typically have excellent visual impact and can enhance selected structural trends in the data, it is important to be aware of the bias that they introduce to the images. In simple terms, these directional filters discriminate against features parallel to the illumination direction and have the potential to introduce false trends in the direction perpendicular to the illumination. They also move the peak responses (mostly towards the illumination direction), so they cannot be used to accurately locate anomalies. Figure 5.20a shows the (minor and benign) effects of shading when the line spacing is small. Figure 5.20b shows the same area but with 400 m spaced data and the associated undersampling artefacts. The shading can potentially mislead and hinder the interpretation process but may also be used to suppress undesirable or distracting features in the data. We emphasise that, while shading certainly enhances the aesthetics of aeromagnetic data, it should be used with caution and shading should be subtle (i.e. low-contrast) so that intensity variations can still be recognised.

Directional filters need not be in the form of image shading. Operators such as decorrugation and trending, both discussed in Section 5.2.1 on gridding, are directional filters and, while beneficial to the interpreter in some circumstances, should be used with caution because (like shading) they may obscure or even eliminate real and important geological features.

In summary, directional filters can be used to advantage to enhance particular structural features or suppress unwanted features, but the interpreter must be aware of their potential to falsely portray structure in aeromagnetic imagery.

5.4.2 Low-pass filters

Most low-pass filters are inherently simpler in application than the high-pass filters because they effectively suppress detail rather than attempt to enhance it. As discussed above, low-pass filters aim to emphasise deeper sources and suppress shallower sources. Situations where low-pass filters are applied include the study of deep basement geometry which may be obscured by shallow magnetic cover (e.g. younger volcanic flows) and the suppression of surficial magnetic sources such as laterite and glacial till covering relatively shallow bedrock.

Upward continuation

Upward continuation is often chosen in these situations because the signal from the shallower material, having smaller volume and/or linear dimensions, should diminish more rapidly than that from the deeper, larger-volume sources. While this generally achieves satisfactory results it must be remembered that the shallow sources are suppressed but never removed in the filtered data. Where the shallow signal has high intensity and/or substantial linear dimensions its presence is likely to remain, even when upward continuation is taken to large heights. Examples of the application of upward continuation are given in Figure 2.19.

Wavelength filtering

Another low-pass filtering strategy is to separate longer wavelengths in the signal from shorter wavelengths. Although relatively simple in numerical application and intuitively logical, wavelength filtering does not result in a clean separation of sources from different depths. This is because the total signal from deep sources contains short as well as long wavelengths and, conversely, signals from shallow sources include both long- and short-wavelength components. Although not strictly applicable in theory, filters which retain long wavelengths and remove short wavelengths frequently yield useful results in the study of deep magnetic sources. Wavelength filters are used and illustrated in Chapter 13 (see Figs 13.10 and 13.11).

Separation filtering ('matched filtering','depth slicing')

Separation filtering is essentially a more sophisticated approach to wavelength filtering. Studies of the Fourier spectra of individual magnetic sources and, in particular, ensembles of magnetic sources have shown that the depths to sources can be determined from these spectra. Sources from very different depths show characteristic patterns in the spectra, to the extent that, in favourable circumstances, a clean separation of the signals from differing depths can be achieved. Spector and Grant (1970) pioneered the application of this methodology and it has enormous potential to assist interpretation in sedimentary basins. Recent publications illustrating the application include Morgan (1998) and Cowan and Cowan (1993), and case history examples are presented in Chapter 13.

Filtering of aeromagnetic data is an essential part of the preparation of data for interpretation. The wide choice of filters gives the interpreter scope to focus attention on specific aspects of the data and this invariably brings clearer insights into the underlying geology. An astute and selective choice of filters is very important. Applying a blanket approach and generating too many filtered versions of the data usually does more to confuse than enlighten the interpreter.

5.5 DATA PRESENTATION

Our choices in presentation of aeromagnetic data include pixel images in many forms and the 'pen line' displays – contours and profiles. Image processing has greatly advanced the visualisation of aeromagnetic data; the older styles of data presentation, which have much less visual impact, have become less used. It is important, however, to recognise that the pen line displays have an important role to play, particularly when we work with smaller volumes of data and at detailed (i.e. zoomed-in) scales.

Milligan and Gunn (1997) present an overview of imaging processing applied to aeromagnetic survey data. The techniques of combining greyscale intensities with colour variation provide the processor with scope to portray multiple aspects of data in a single image (Spencer *et al.* 1989). The fundamental strength of pixel imagery is its capacity to present very large volumes of data in a small viewing space. The space may be either a graphics screen or hardcopy. For the interpreter the choices are many and inappropriate choice may adversely affect the observation of key information in the data. We present below some simple guidelines which should be of assistance.

5.5.1 Image stretching

This refers to the portrayal of data ranges as varying shades of grey or varying colours. An important first step in assessing an aeromagnetic dataset is to identify the extreme values and the range of the most commonly occurring values. This is usually done via a simple histogram. Figure 5.21 illustrates the range of stretches that

we would normally view to assess a new dataset. The right-hand side panels show the histograms that map the magnetic intensities onto colours on the image. The top row shows a stretch that highlights only the areas of very high intensity. This is an essential exercise in every dataset because it allows us to identify the location of any very strong anomalies. A similar stretch can be applied to locate extreme magnetic lows, if they exist. The second panel column shows a simple linear stretch. This is usually desirable in some selected images because it gives a clear view of the intensity relativities in our survey area. The fourth column is an example of an extreme non-linear stretch. It assigns an equal number of intensity pixels to each colour interval. This is called 'histogram equalisation', and it can be very beneficial in portraying very small and very large amplitude variations in the one image (in a similar way to AGC). It does, however, often hide the extreme values and distort the amplitude relativities and should always be used in conjunction with images that have linear type stretches. The third column is described as 'optimal'. It has been created manually by the interpreter to maximise that definition of the different magnetic rock units. This optimal, manual customised approach to stretching is desirable and advisable in almost all imaging situations. Applying 'recipe-standard' stretches will very rarely bring out the full range of information in the data. It is common to apply more than one transform to a single grid of the data, in order to capture both the low-level variations and the extremes, and with most imaging software it is possible to manually optimise the transform to tailor the image to suit the interpreter's requirements.

5.5.2 Colour versus greyscale imagery

A general rule is that greyscale presentation allows the human eye to more easily perceive high-frequency detail in imagery, while colour presentations are better suited to visualising low-frequency variations. Another way of stating this is that colour has a simplifying effect on our perception of an image, while greyscales allow us to absorb larger amounts of fine-scale detail. As a consequence, when we are zoomed-out and displaying large volumes of data in a small viewing space, greyscale imagery will usually be more effective than colour, whereas when we are zoomed-in the reverse may be true.

With aeromagnetic data, there are no hard and fast rules and personal preference plays a large part in the interpreter's choice of imagery. The two most important issues are that the images are appropriately stretched, as discussed above, and that they are appealing to the interpreter's eye.

Common selections of imagery are presented in Figures 5.4, 5.18 and 5.19 (see also the worked examples of Chapters 11, 12 and 13). The recurring theme is to have the total field imagery (TMI, RTP and AnSig) presented as colour images, with or without contours, and the high-pass-filtered imagery (1st VD, 2nd VD and AGC) presented in greyscales, but mixing and matching presentation styles can add greatly to the interpretability of images.

5.5.3 Scale of analysis – pixel images versus contours

A much more critical issue of presentation relates to scale of analysis. Aeromagnetic surveys typically cover areas of hundreds of square kilometres and line spacing is commonly in the range 50 m to 400 m. Recalling the rules that govern the selection of grid cell size (~4 cells per line spacing) and the maximum zoom scale (1 cm ~1 line spacing) we see that, when analysing the data at maximum zoom scale, our basic pixel size will be 0.25 cm. Figure 5.22 illustrates this situation. Using the Menzies-Comet Vale dataset analysed in Chapter 11 (see Section 11.5) we have zoomed-into a particular area of interest (the MRW target) at maximum scale, and see that the image format ceases to look appealing. The 'pixelly' nature of the images, evident in both greyscale and colour formats, can be overcome using smoothing or reinterpolation (Panel d), but when we consider the images in the context of the line spacing it is apparent that, at this scale, variations in colour or greytones are not an effective method of portraying the finest-scale variations in the data. The introduction of contour lines in both the RTP and RTP 1st VD imagery shown in Figure 5.22 allows us to do this well.

When working at zoomed-in scales, contour lines are a better medium for presenting aeromagnetic data than images. The same principle applies when we are working with data which is dominated by long-wavelength, low-frequency variations.

The general rule on presentation format is that pixel imagery will be the most effective means of portraying data when large volumes of detailed variations need to be presented in a small space. Contour format will be better when the data is sparse or the wavelengths of the data are long in the context of the viewing space.

5.5.4 Profiles

The measured TMI data and certain filter types lend themselves to presentation in profile format. While working with profile data gives the interpreter comfort that they are not exposed to potential artefacts caused by the gridding process, profile analysis is (at best) a tedious and time-consuming process, which offers limited additional information over and above that gained from optimal use of gridded data.

The place of profile analysis in the interpreter's toolbox is restricted to quite specific and localised features where the maximum amount of local spatial detail is sought. Once constrained to a small area, the use of profiles can resolve specific problems and provide critical pieces of extra spatial information. This may also have application where we are seeking to trace distinct but small-amplitude anomalies in the presence of higher-amplitude host rock, such as mineral sand exploration. The example of Figure 5.23 illustrates how reverting to profile analysis can overcome specific ambiguities. It also illustrates how well-prepared images provide a much more user-friendly medium for deciphering the often complex patterns in aeromagnetic data.

5.6 SUMMARY

Although there are many and varied matters to consider in planning, acquisition and processing of aeromagnetic surveys, there are simple rules that will invariably guide us to a satisfactory set of imagery for interpretation. The authors' advice is to pay close attention to the filtering and imaging stage and to carefully select a small set of 'telling' maps and images on which to base the interpretation. The scattergun approach, where many possibly useful versions of the data are produced, will tend to confuse and slow down the interpretation process.

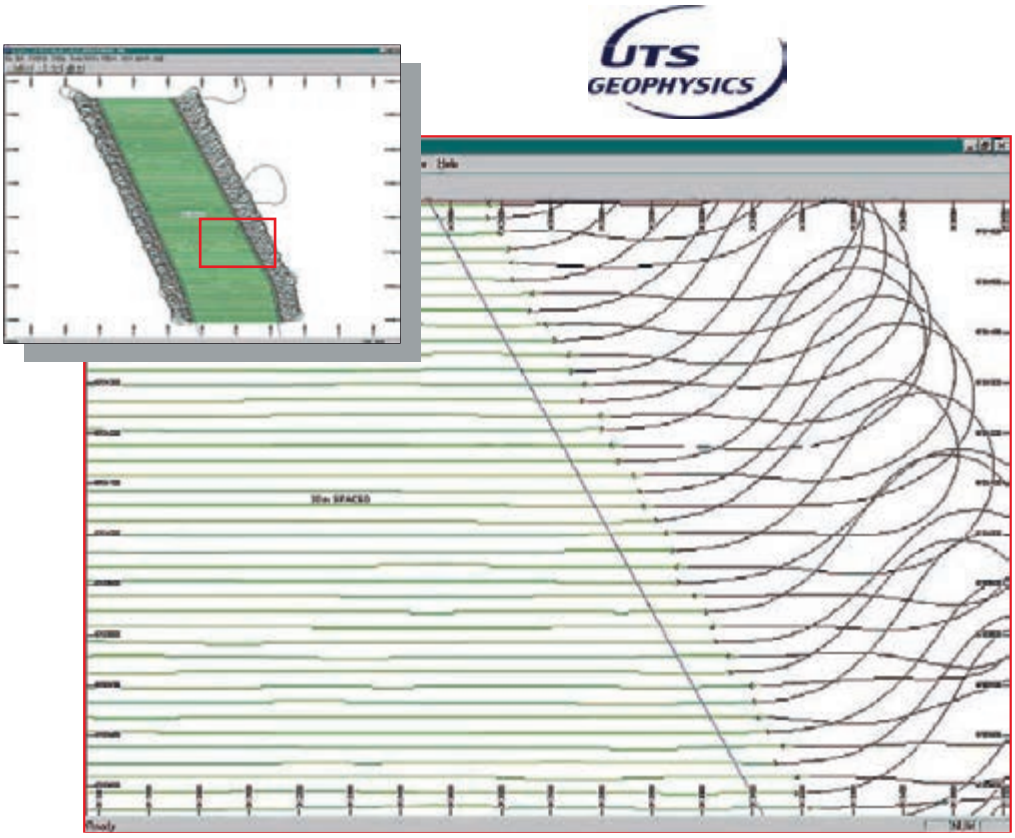

Figure 5.1: Example of a detailed (20 m) airborne survey flight line path map. Note the preferred choice of E–W lines, rather than strike-perpendicular lines, and the large amount of flying consumed on the turn. The latter underlines the desirability of longer lines, wherever practicable. Graphic courtesy of UTS Geophysics.

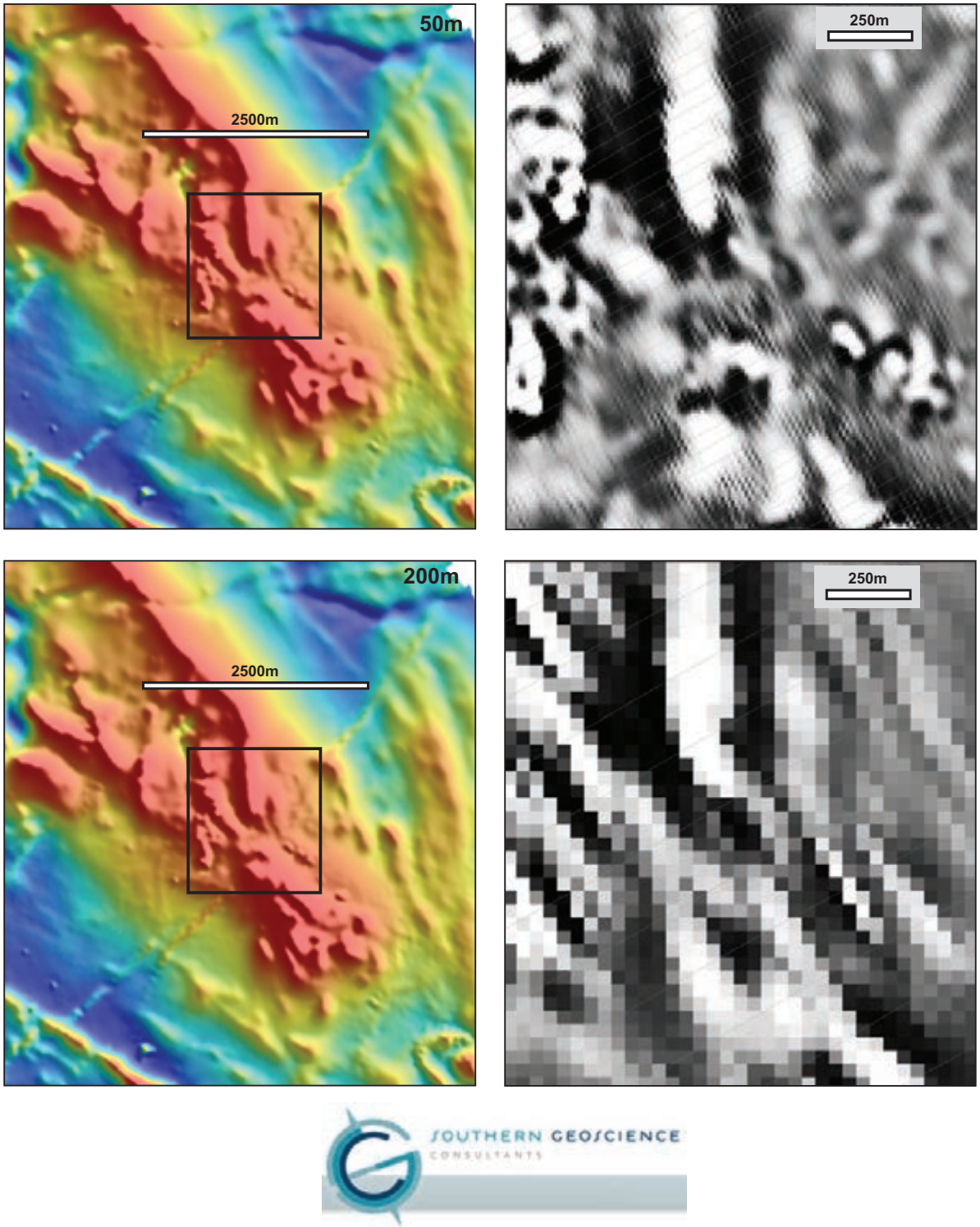

Figure 5.2: Line spacing and geological resolution. The left-side panels show TMI shaded from the NE at 1:100 000 scale, the right-side panels show a subsection (black outline in TMI panels) of this data high-pass filtered (RTP 2nd VD) at 1:10 000 scale. Line spacings – 50 m (top), 200 m (bottom), flying height 50 m in both cases. The 50 m data can be readily zoomed to 1:10 000, but the 200 m data is not acceptable at 1:10 000. This illustrates the maximum zoom-in scale to 1 cm = 1 flight line spacing. Note the similarities of the two datasets when displayed at zoomed-out scales. See Figure 5.4 for expanded illustrations of line spacing *v.* resolution and Figure 5.5 for an illustration of changing survey height. Survey data from the St Ives area in the Kambalda region of WA, from Geological Survey of WA open file records. Processing and imaging courtesy Southern Geoscience Consultants.

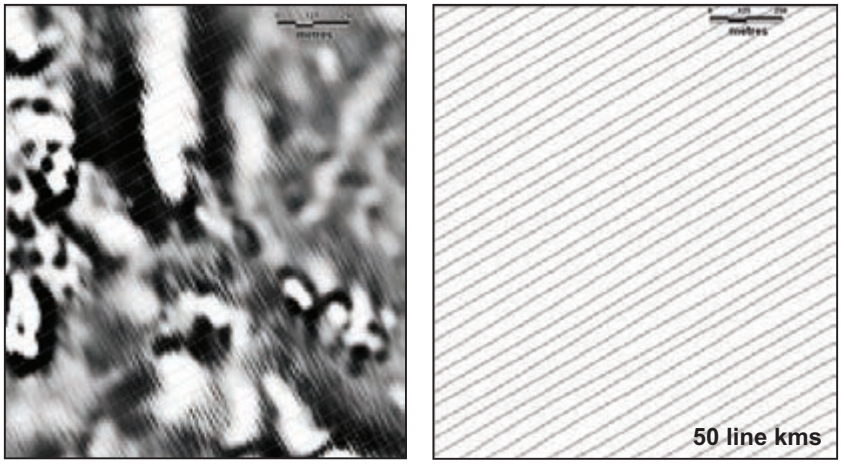

50m line spacing. 10m pixel and native cell size. Note the line-perpendicular 'noise' inherited from noisey measured data and exacerbated by the gridding. Modern data should be better than this, but in this case, it is worth tolerating the noise in order to see the sharpest view of the magnetic rock units.

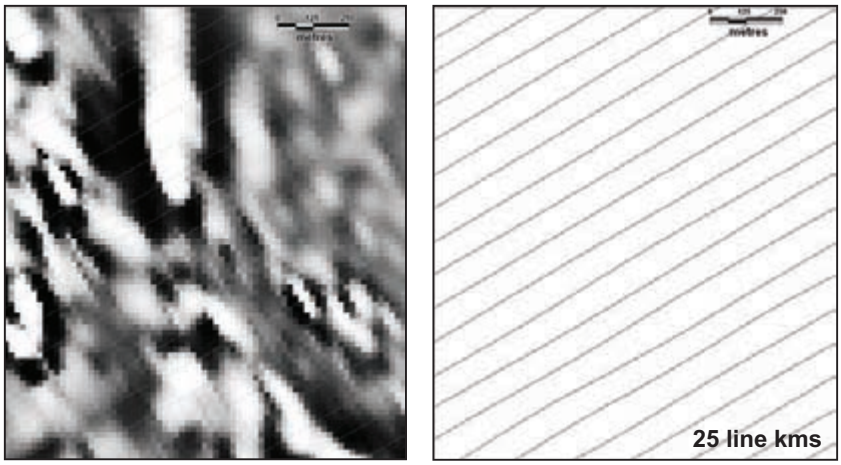

100m line spacing. 20m pixel and native cell size. It is important to view this at native cell size because we remain aware of the limitations in the data. 'Smoothing' with resampling and reinterpolation might have us 'believe' some of the line perpendicular features.

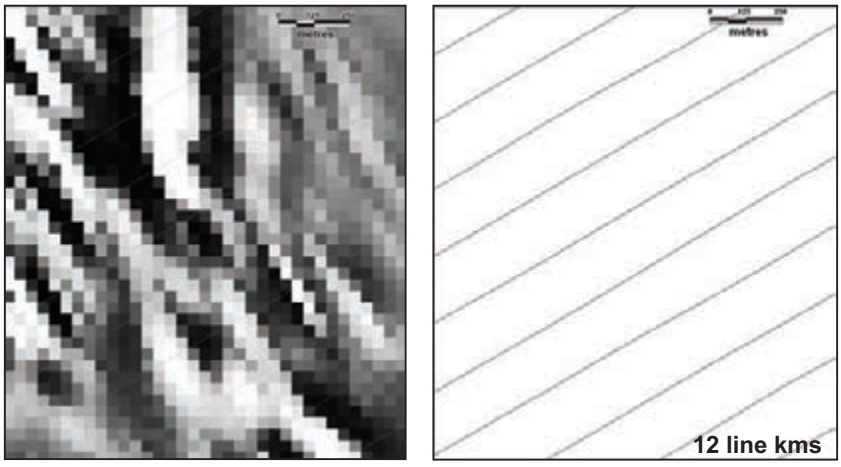

200m line spacing. 40m pixel and native cell size. The line-perpendicular gridding artefacts are exacerbated by the 2nd VD filter to the point where this presentation of the data is very misleading. Compare the RTP 1st VD image in figure 5.3b.

Figure 5.3a: Comparison of geological resolution for line spacings of 50 m, 100 m and 200 m. Images compiled at 1:10 000 scale (mine-scale) show RTP 2nd VD filtered data presented in greyscale format to accentuate shallow structural detail. This presentation gives the best measure of resolution. The right-side panels show the flight path annotated with the total line kilometres. Note the increasing line-perpendicular bias with wider line spacing.

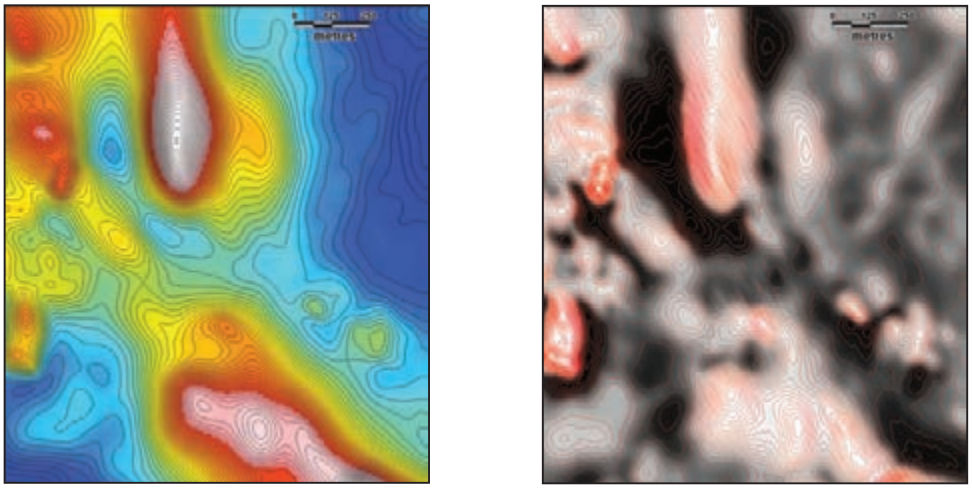

50m line spacing. The pixel size is 10m, same as the native cell size. Because the line spacing and flying height are the same, there are no gridding artifacts. The 1st VD filter sharpens the view of magnetic rock units. Note the benefit of the contours. Without them the 1st VD images looks 'fuzzy'.

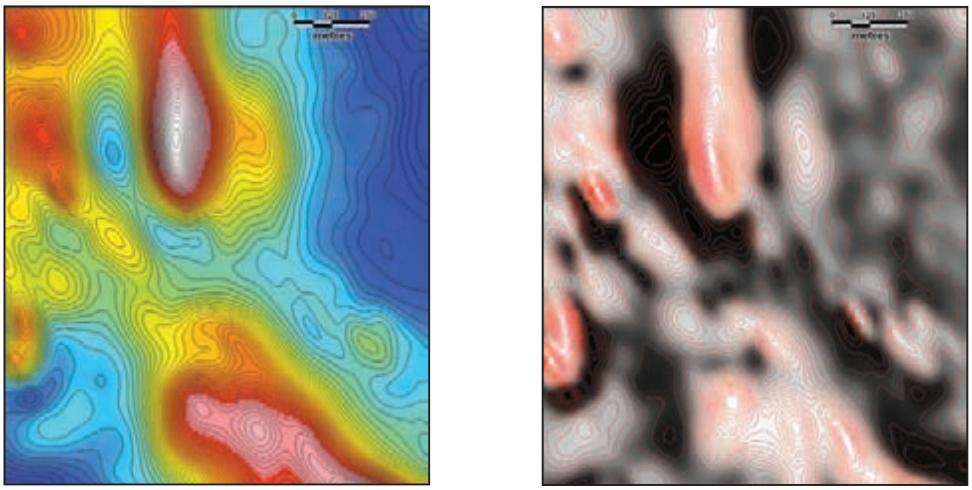

100m line spacing. Image pixel size is 10m, resampled and reinterpolated from 20 native cell size. The line spacing is 2 x the flying height but gridding artifacts are not apparent. Note the 'disappearance' of the NNE trending dyke,seen in the 50m data. This is an important 'pit-scale' geological structure.

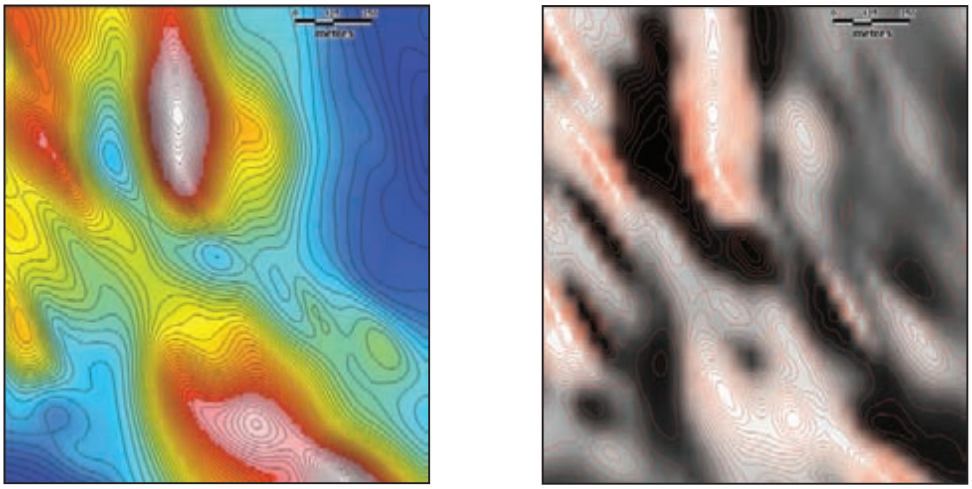

200m line spacing. Image pixel size is 10m, resampled and reinterpolated from 40 native cell size. The line spacing is 4 x the flying height and line perpendicular gridding artifacts begin to appear. The bias is now dominant in the RTP 1st VD image. The RTP is 'useable', but the RTP 1st VD, although 'presentable', is misleading.

Figure 5.3b: Comparison of geological resolution for line spacings of 50 m, 100 m and 200 m. Images compiled at 1:10 000 scale (mine-scale), RTP intensity presented as colour image with contour overlay, RTP 1st VD images (below) presented as greyscale images with contour overlay. Note the strong similarity of the RTP images and the better resolution evident in the RTP 1st VD images. Compare these with the RTP 2nd VD images in Figure 5.3a.

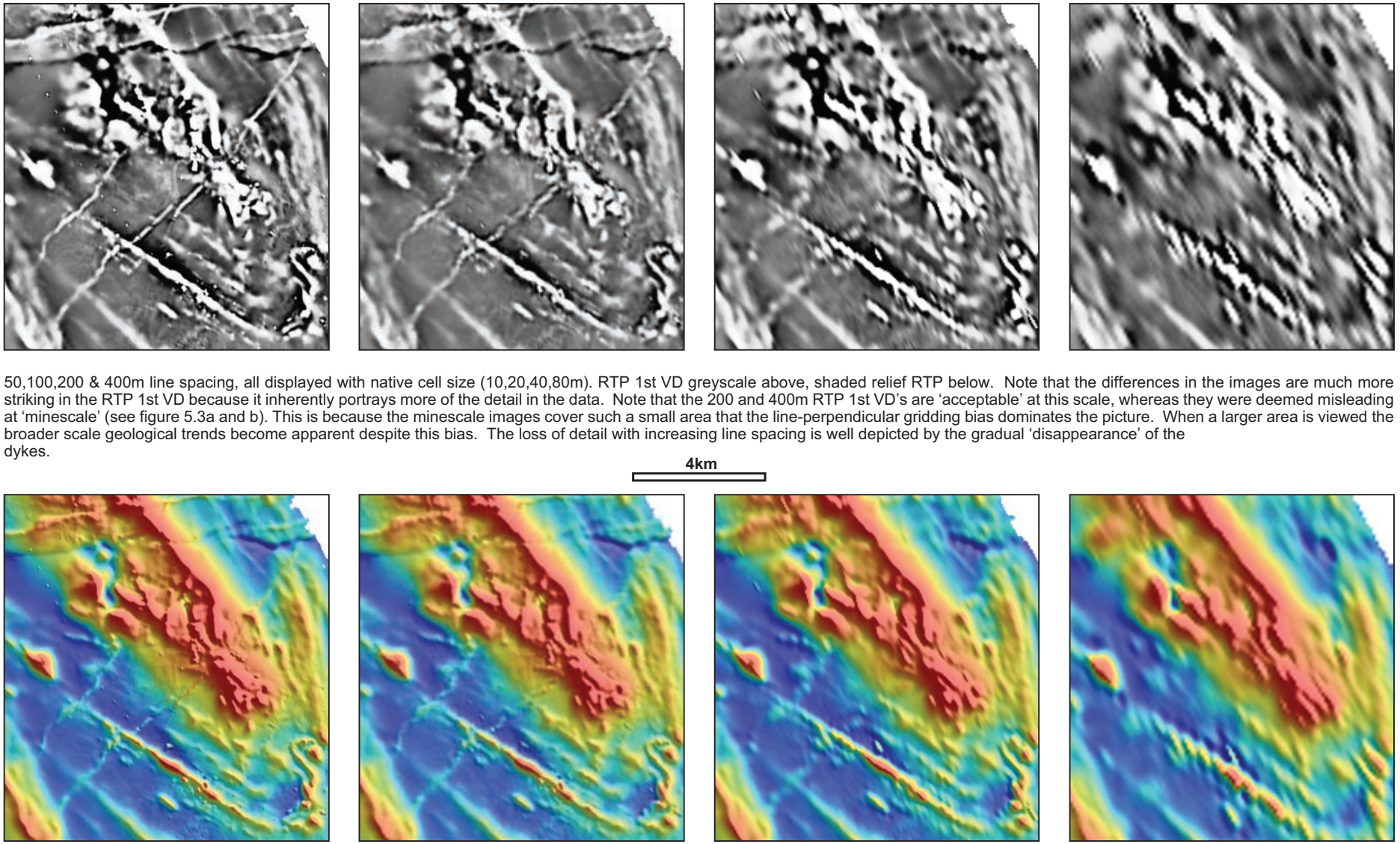

50,100,200 & 400m line spacing, all displayed with native cell size (10,20,40,80m). RTP 1st VD greyscale above, shaded relief RTP below. Note that the differences in the images are much more striking in the RTP 1st VD because it inherently portrays more of the detail in the data. Note that the 200 and 400m RTP 1st VD's are 'acceptable' at this scale, whereas they were deemed misleading at 'minescale' (see figure 5.3a and b). This is because the minescale images cover such a small area that the line-perpendicular gridding bias dominates the picture. When a larger area is viewed the broader scale geological trends become apparent despite this bias. The loss of detail with increasing line spacing is well depicted by the gradual 'disappearance' of the dykes.

Figure 5.4: Line spacing comparison at zoomed-out scales. St Ives area (WA) survey data from Geological Survey of WA open file records. Processing and imaging courtesy Southern Geoscience Consultants.

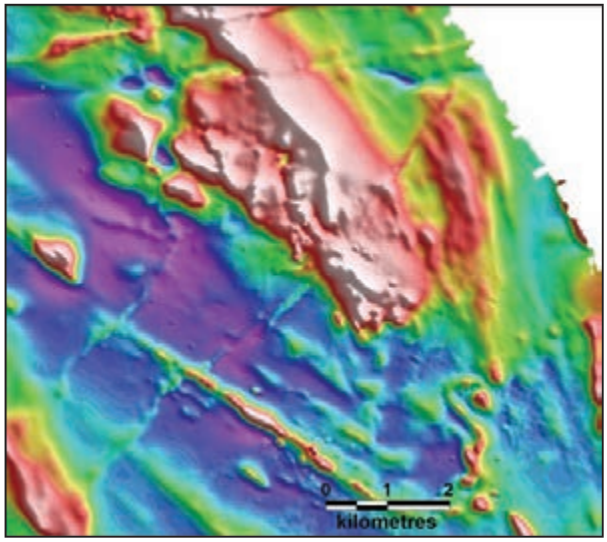

50m height, 50m line spacing

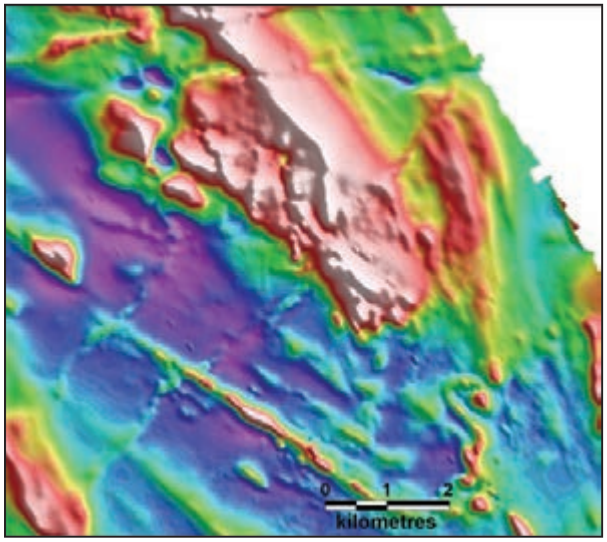

50m height, 100m line spacing

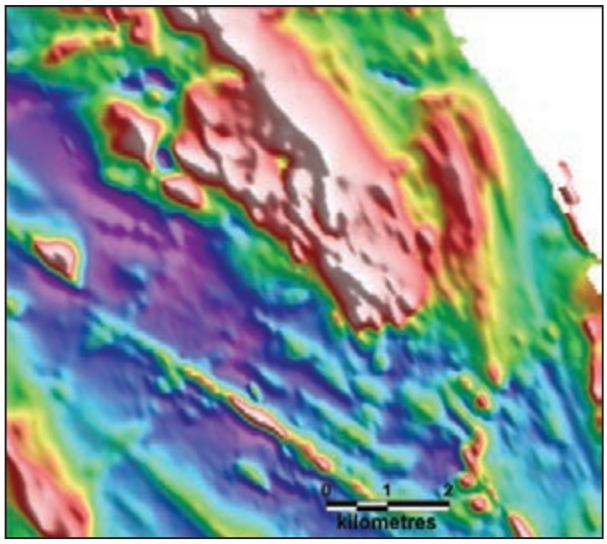

50m height, 200m line spacing

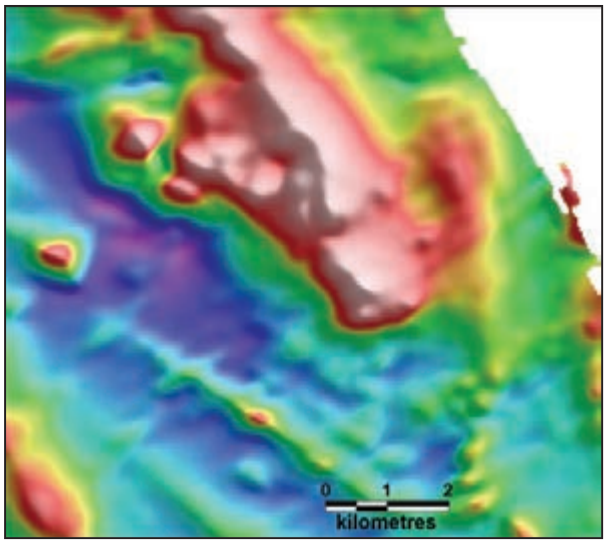

200m height, 200m line spacing

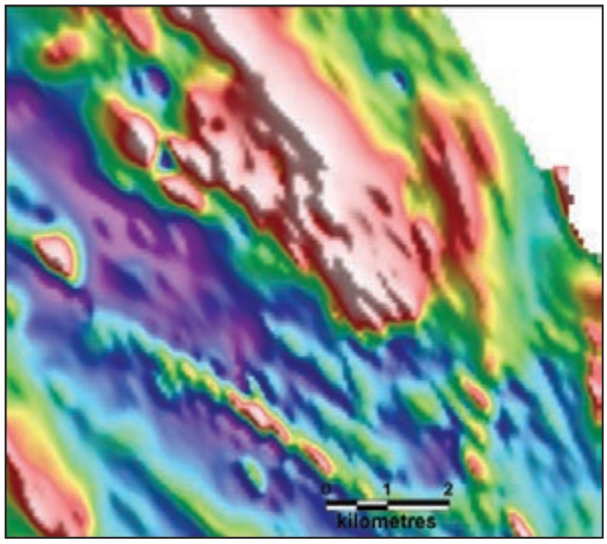

50m height, 400m line spacing

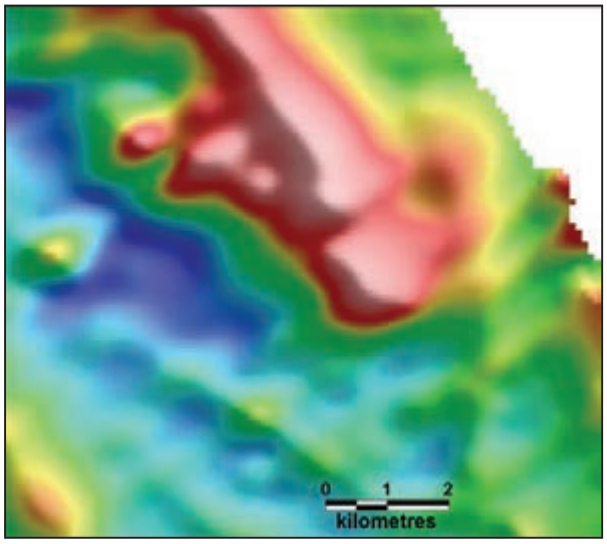

400m height, 400m line spacing

Figure 5.5: The effect of increasing flying height. The loss of spatial detail with height is significant. The gridding artefacts seen where line spacing greatly exceeds flying height are tolerable in light of the retained spatial detail. Data processing and imaging courtesy Southern Geoscience Consultants.

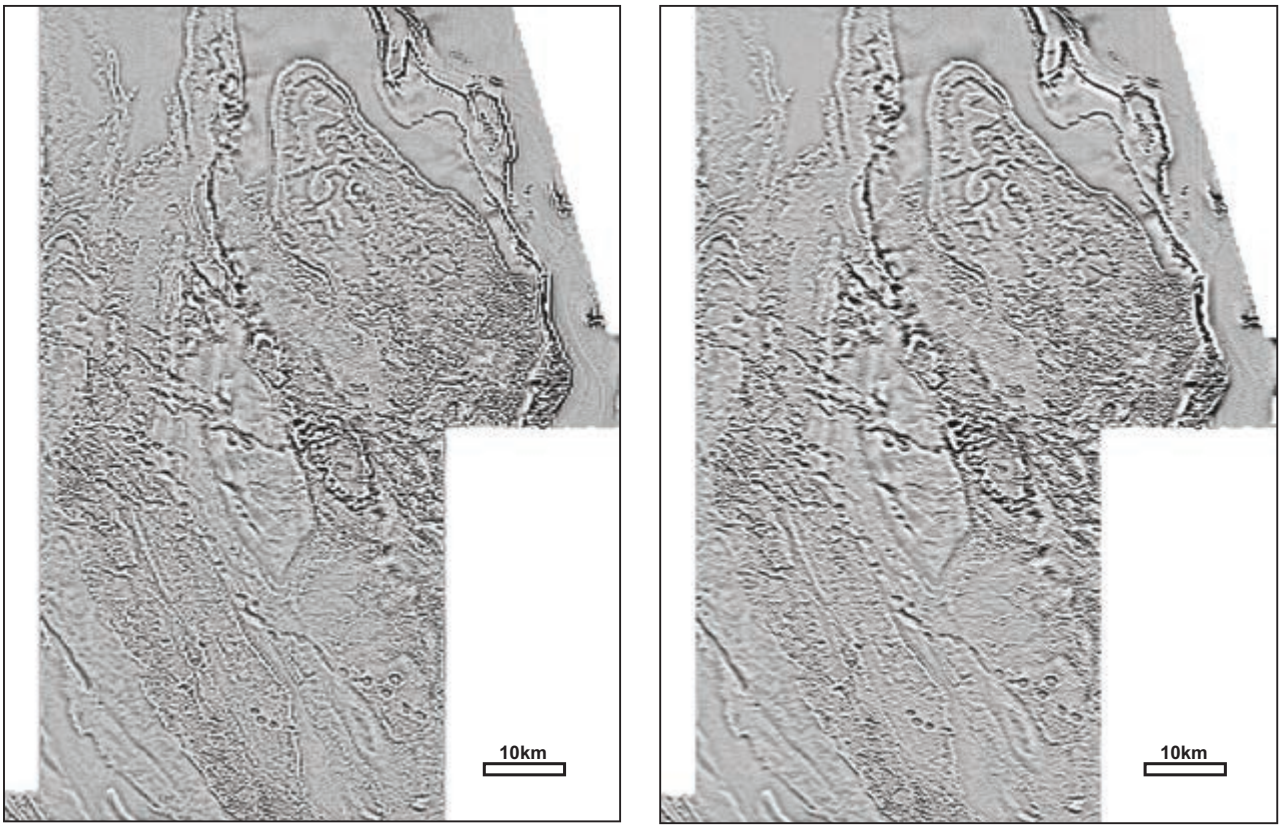

Figure 5.6: An example of gradient-enhanced gridding. The survey has 400 m spaced, N–S-oriented lines and was flown at 80 m. The left-side image is single sensor data gridded using a minimum curvature algorithm, the right side is gridded using the transverse gradients. In both cases the grid cell size is 80. Images courtesy Cowan Geodata Services. Data from Newcastle Waters region (NT) courtesy NT Geological Survey and Geoscience Australia.

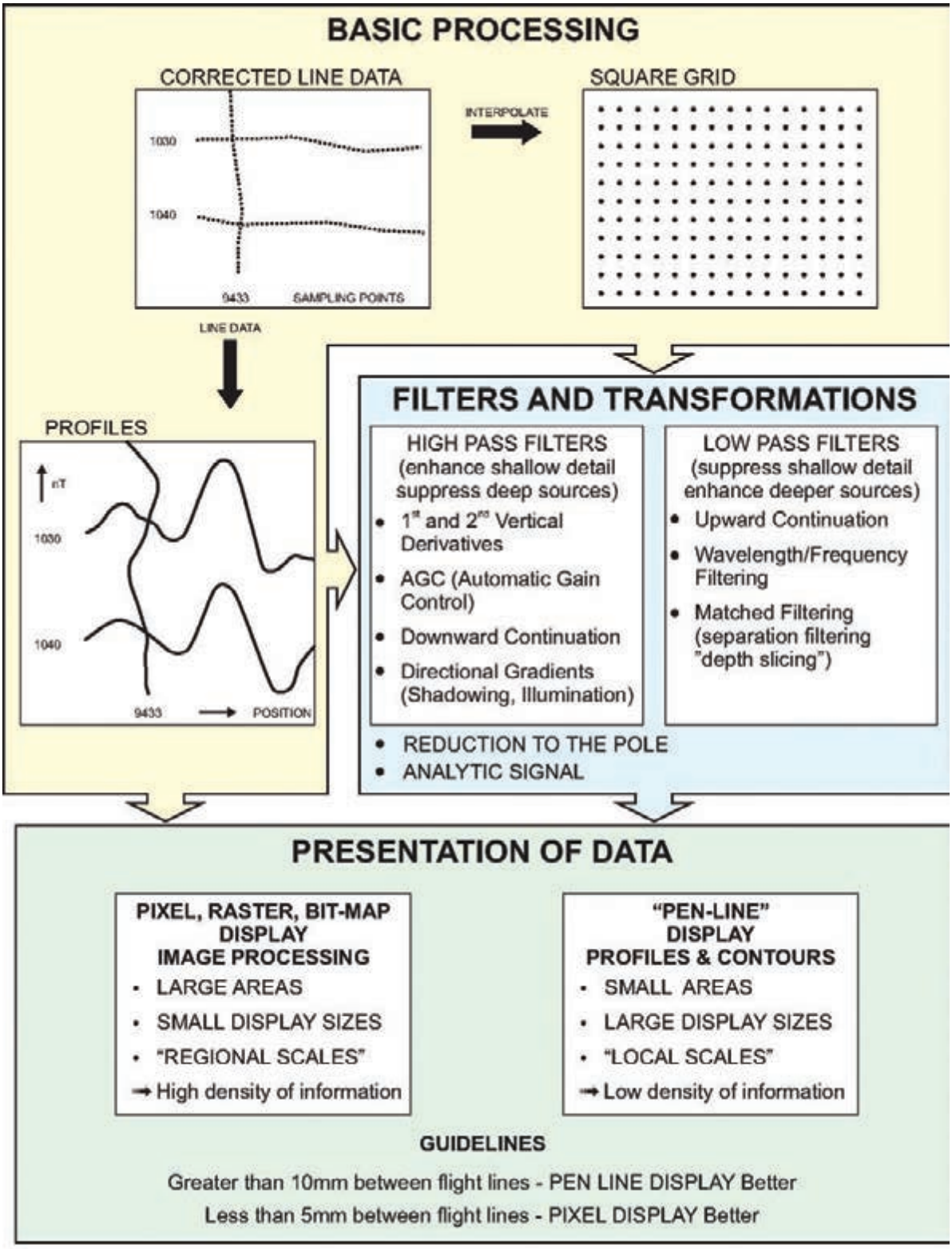

Figure 5.7: Aeromagnetic data processing and presentation flow diagram.

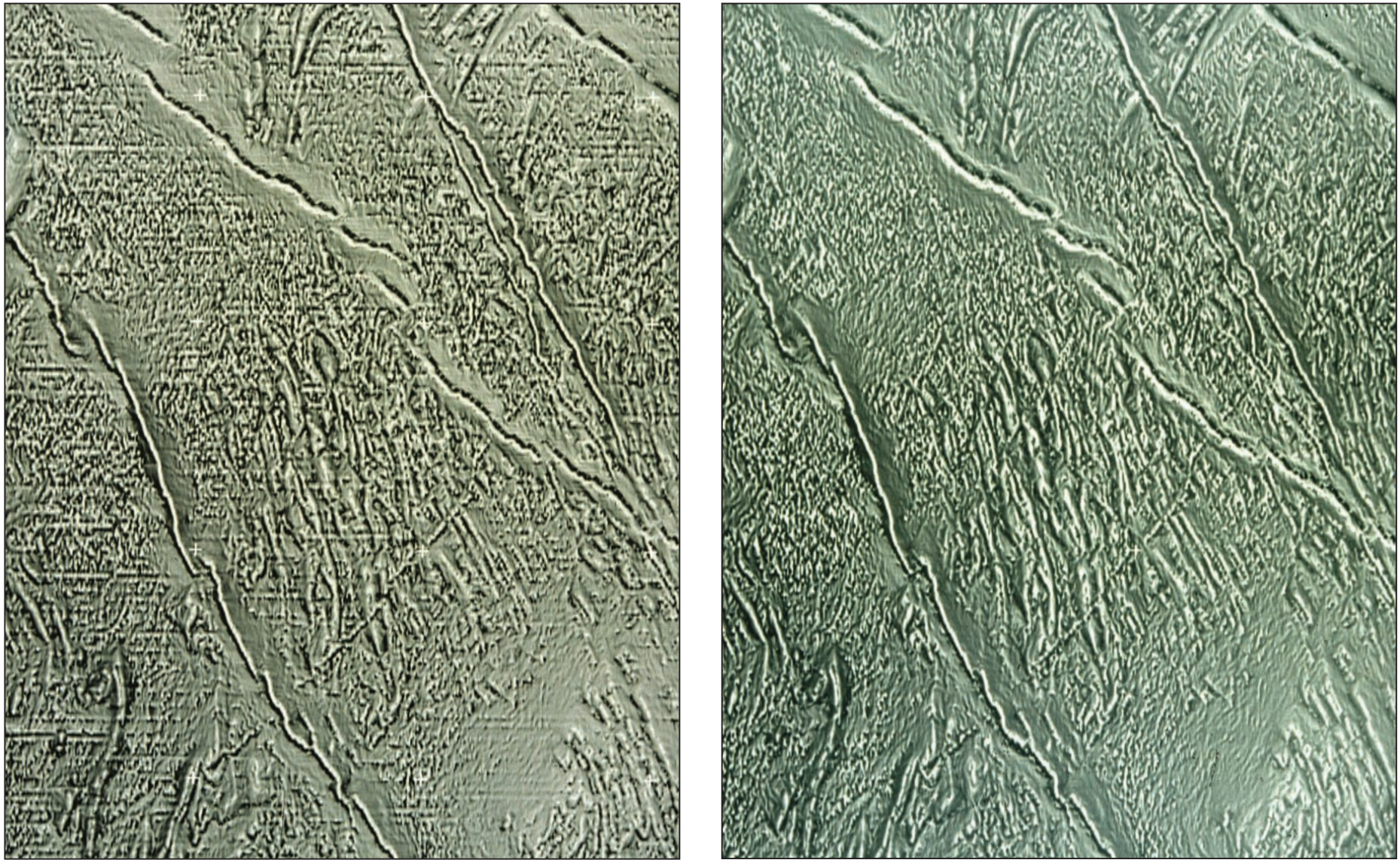

Figure 5.8: Example of micro-levelling, Pine Creek region, NT. The panel on the left is tie-line levelled and enhanced with an AGC filter (see Section 5.4.1). The panel on the right has had the same enhancement filter applied after micro-levelling. The line busts are ~0.25 nT and the small signal levels in the data are ~0.1 nT. Data courtesy NT Geological Survey and Geoscience Australia. Filtering by Ian Campbell, Austerra.

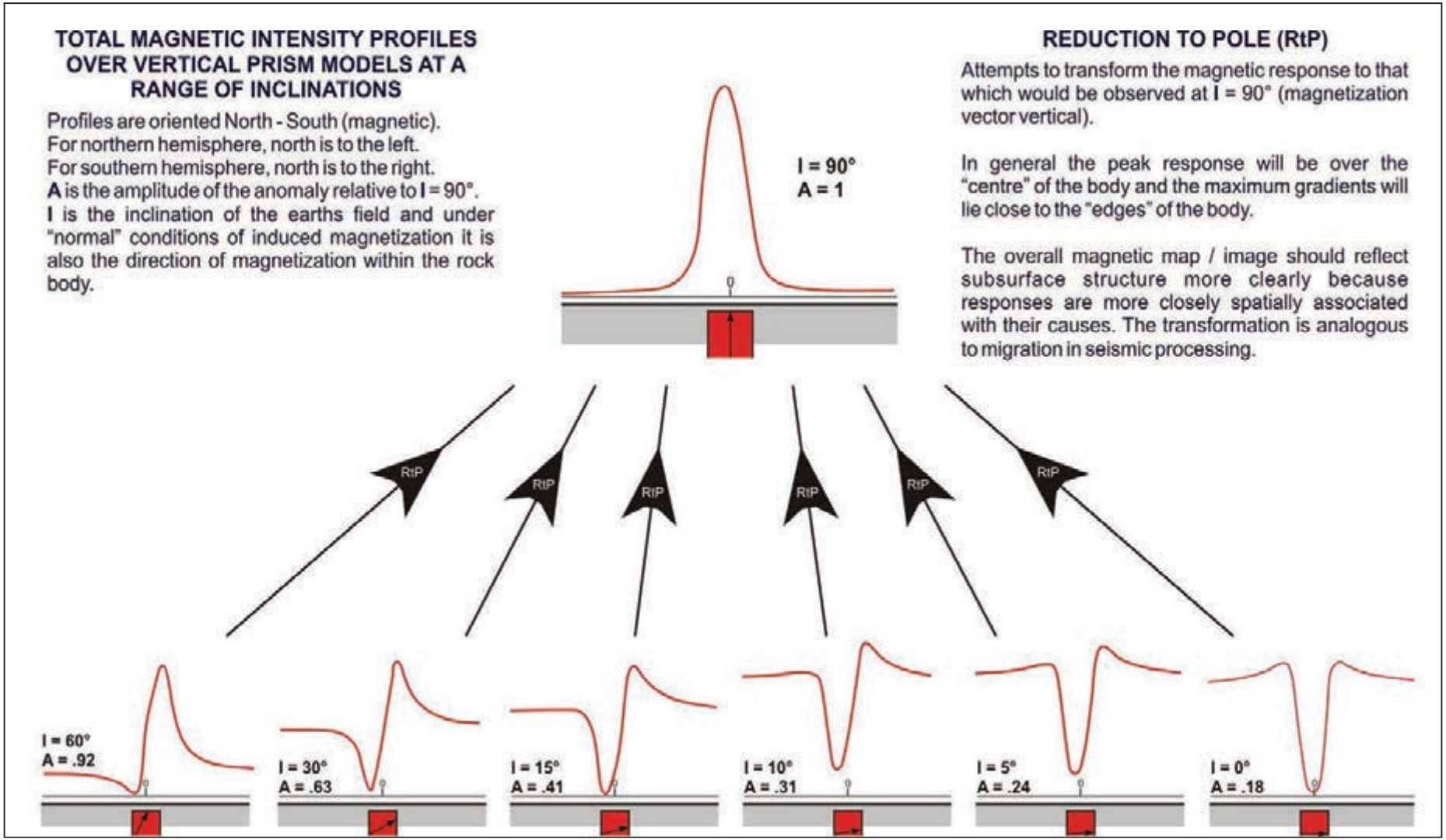

Figure 5.9: Illustration of the RTP process.

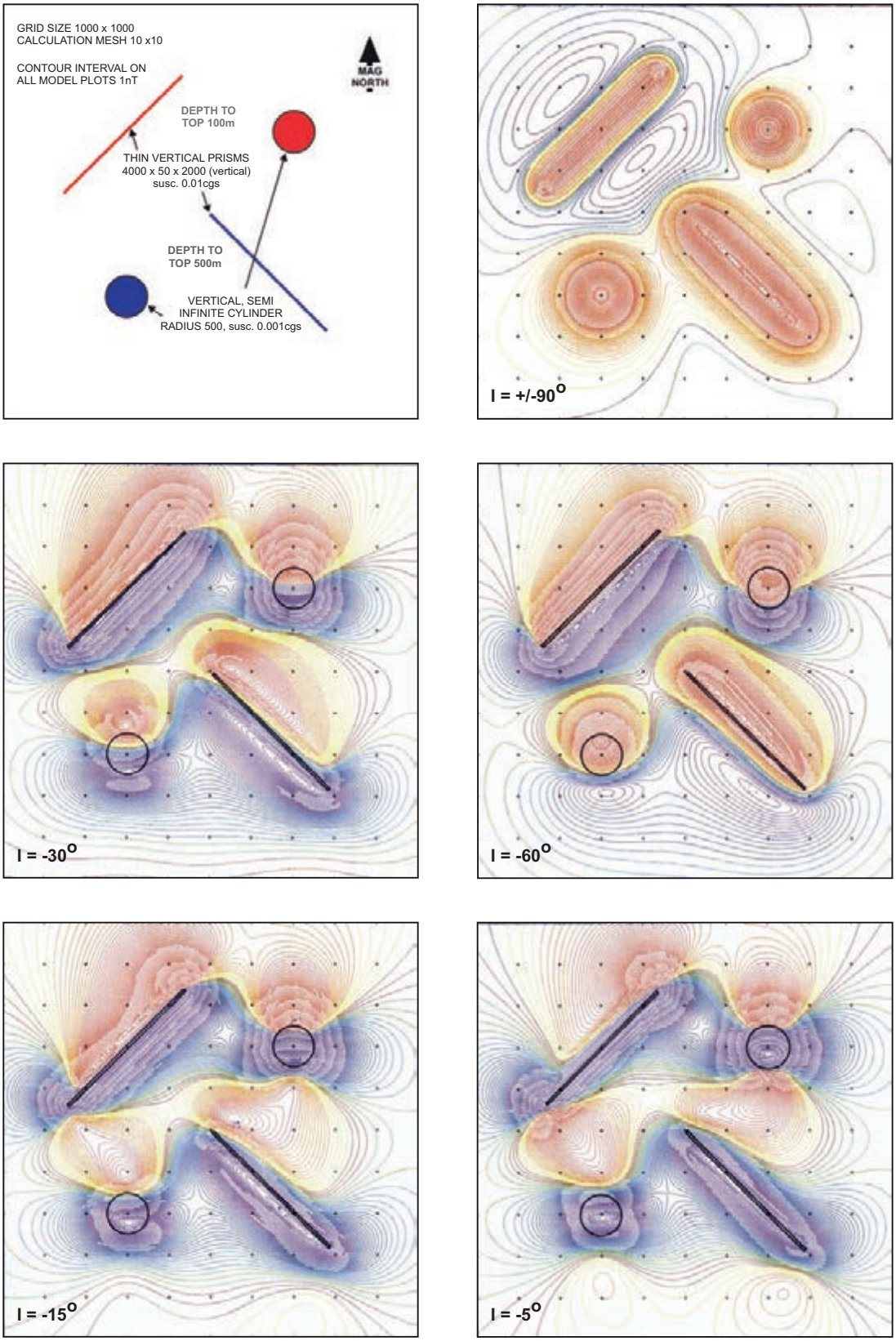

Figure 5.10: Model study showing the impact of Earth's field inclination on the recognition of magnetic rock unit geometry from TMI data. The I = ±90°case represents the expected result when RTP is applied to the TMI data from any field inclination. Models calculated for southern hemisphere. Viewing this page upside down will simulate the northern hemisphere case. Models computed by Steve Saul.

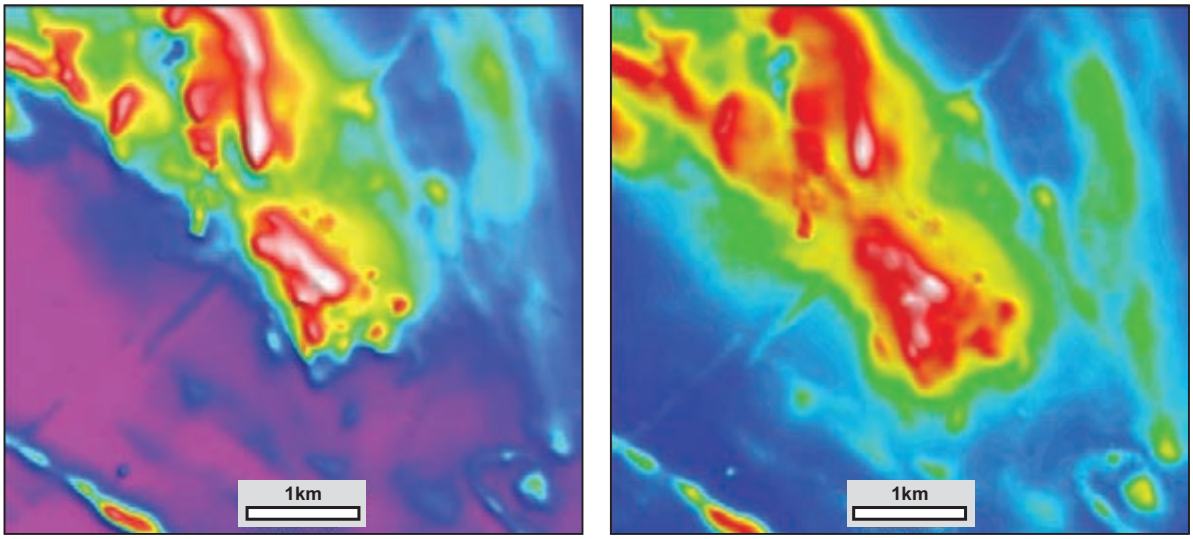

Figure 5.11: Comparison of TMI (left) and RTP (right) in the St Ives area, WA. Despite the high Earth's field inclination (–60°) the RTP data clearly portray the SE-plunging antiformal structure better than the TMI. Data from Geological Survey of WA open file records.

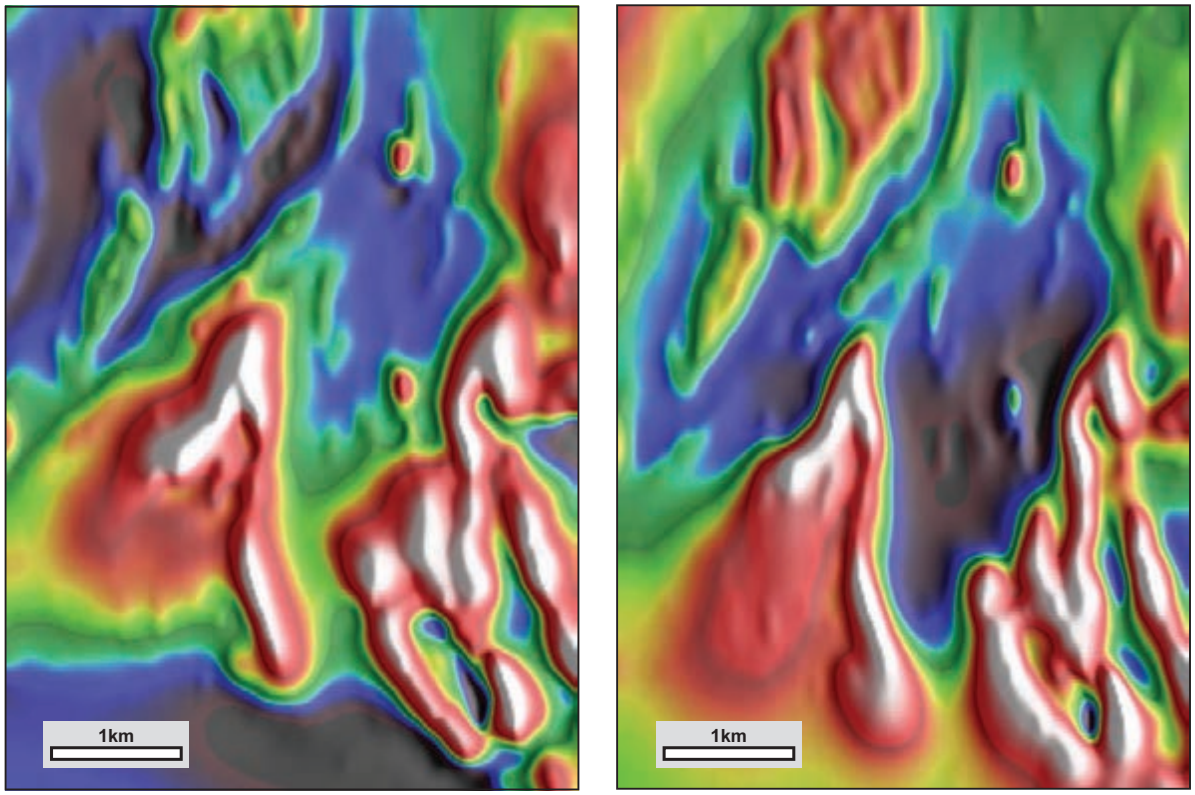

Figure 5.12: Comparison of TMI (left) and RTP (right) in the Golden Dyke area, NT. The Earth's field inclination is –45°. The geometry of the folded metasediments is much clearer in the RTP data. Data from NT Geological Survey and Geoscience Australia. Imaging by Southern Geoscience Consultants.

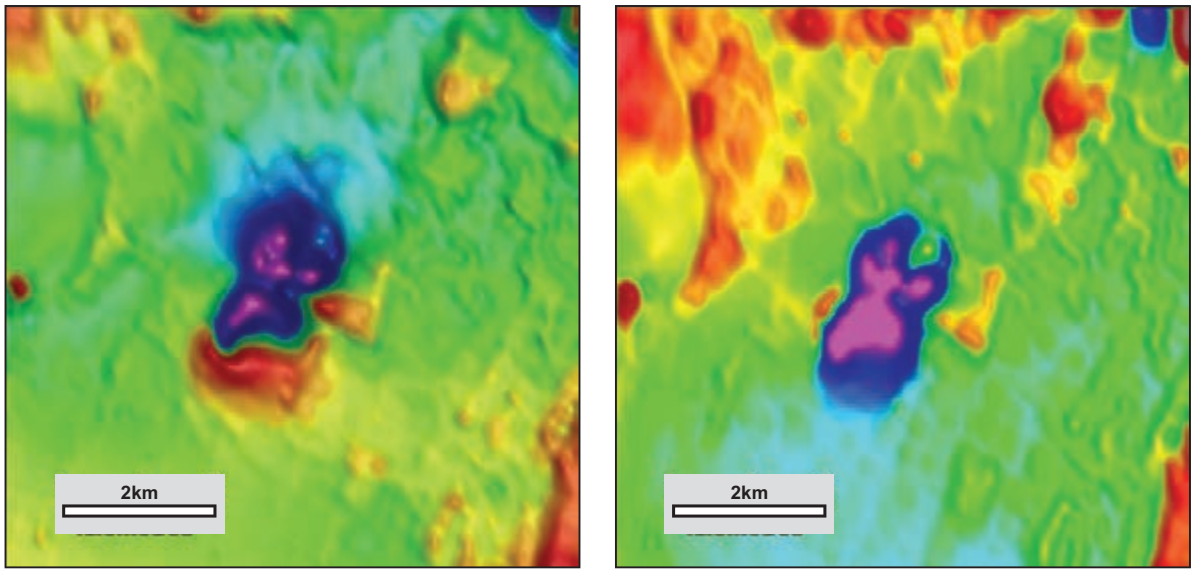

Figure 5.13: Comparison of TMI (left) and RTP (right) in the Mt Leyshon area, Qld. The Earth's field inclination is –50°. The very intense negative anomaly is a steeply dipping, remanently magnetised alteration pipe. Note that the application of RTP has no adverse effect on the recognition or location of the pipe. Data courtesy Fugro Airborne Surveys.

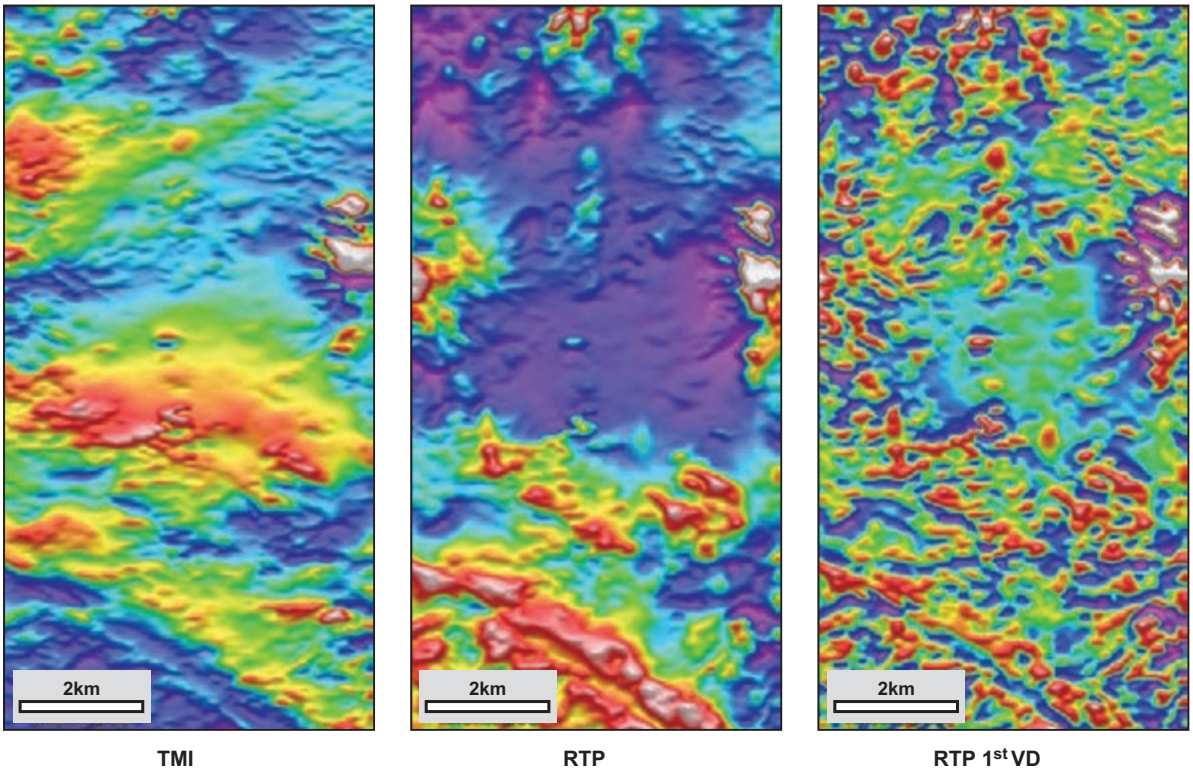

Figure 5.14: TMI, RTP and RTP1st VD images from the WayLinggo region, southern Sumatra. The Earth's field inclination is –28° and the differences between the TMI and RTP are profound. Significant gold prospects in the area are marked by magnetic alteration effects and controlled by broad-scale fracture systems. Neither of these can be delineated without using the RTP data; the TMI data alone are misleading. Data courtesy Kingsrose Mining. Survey by GPX Airborne Surveys.

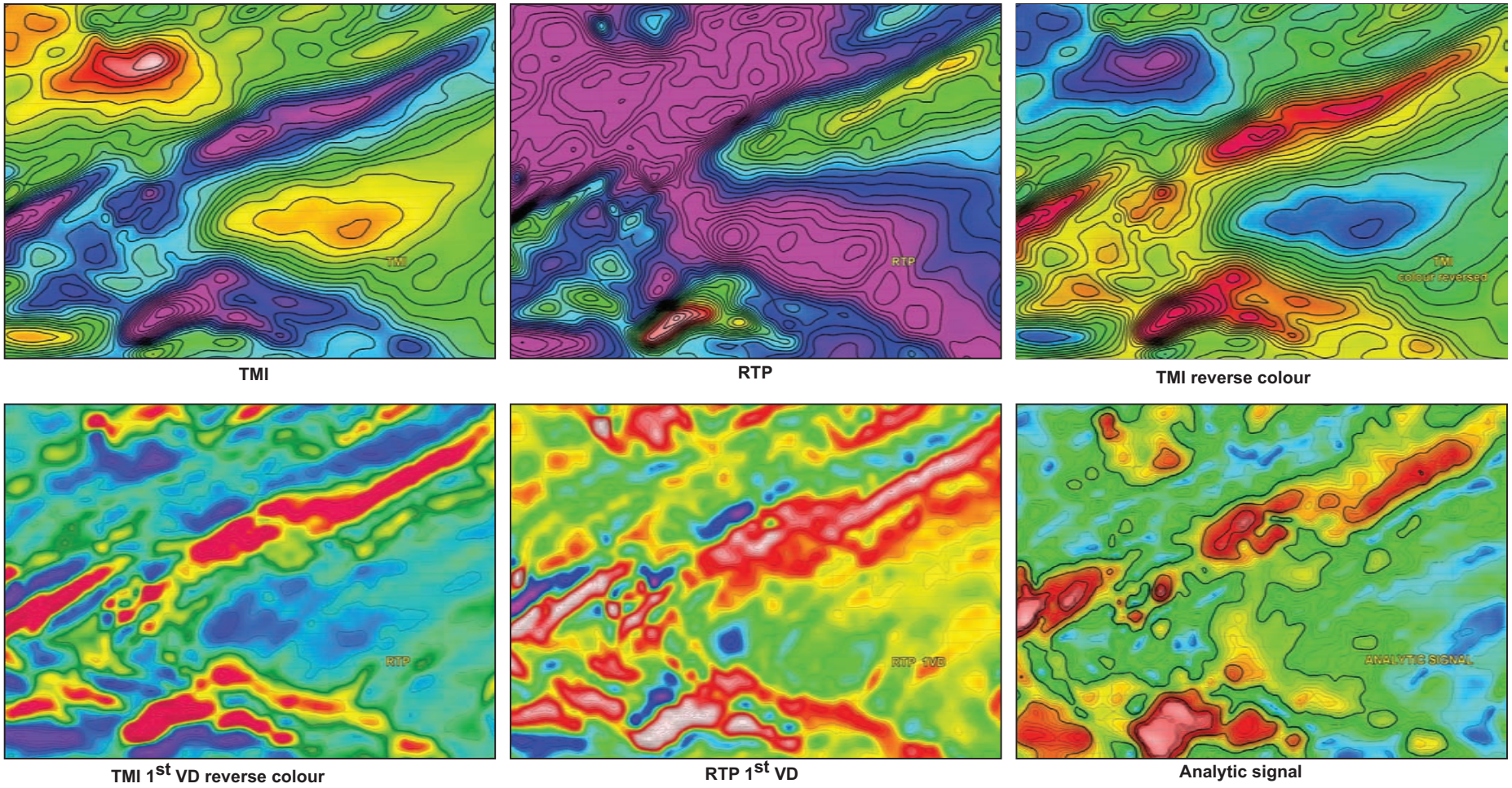

Figure 5.15: 100 m spaced E–W-oriented survey data from the Sabodala region in eastern Senegal. The Earth's field inclination is 4°. A robust RTP is achieved largely because of the close line spacing. The RTP 1st VD accurately delineates magnetic rock units that define a fold structure. The TMI 1st VD yields similar patterns when displayed with a reversed colour (lows red, highs blue) but it does not accurately reflect the location or geometry of magnetic rock units in detail. The analytic signal faithfully records magnetic rock unit outlines but lacks the fine-scale spatial resolution of the RTP 1st VD. The E–W line orientation challenges the conventional view that magnetic surveys at low field inclinations should be flown with N–S lines irrespective of geological strike. Data courtesy Mineral Deposits Ltd and Sabodala Mining Co. Survey by GPX Airborne Surveys. Processing by Austerra.

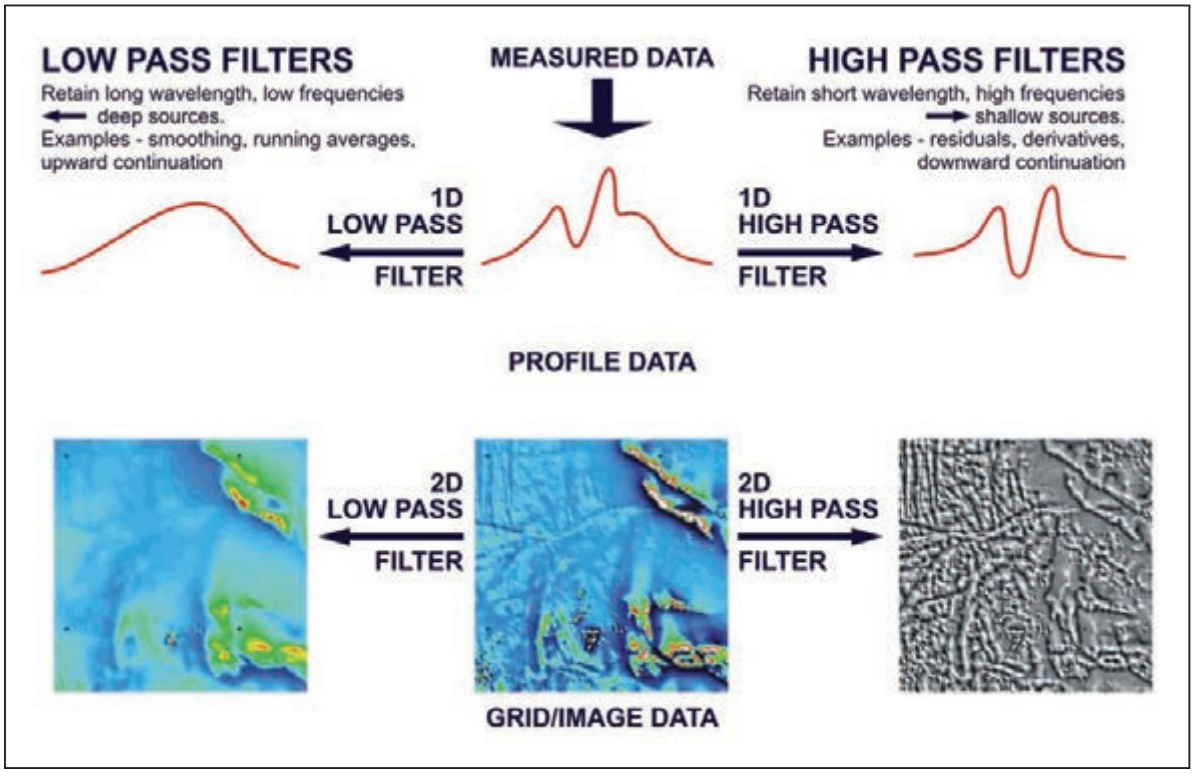

Figure 5.16: Summary of the mechanics of filtering.

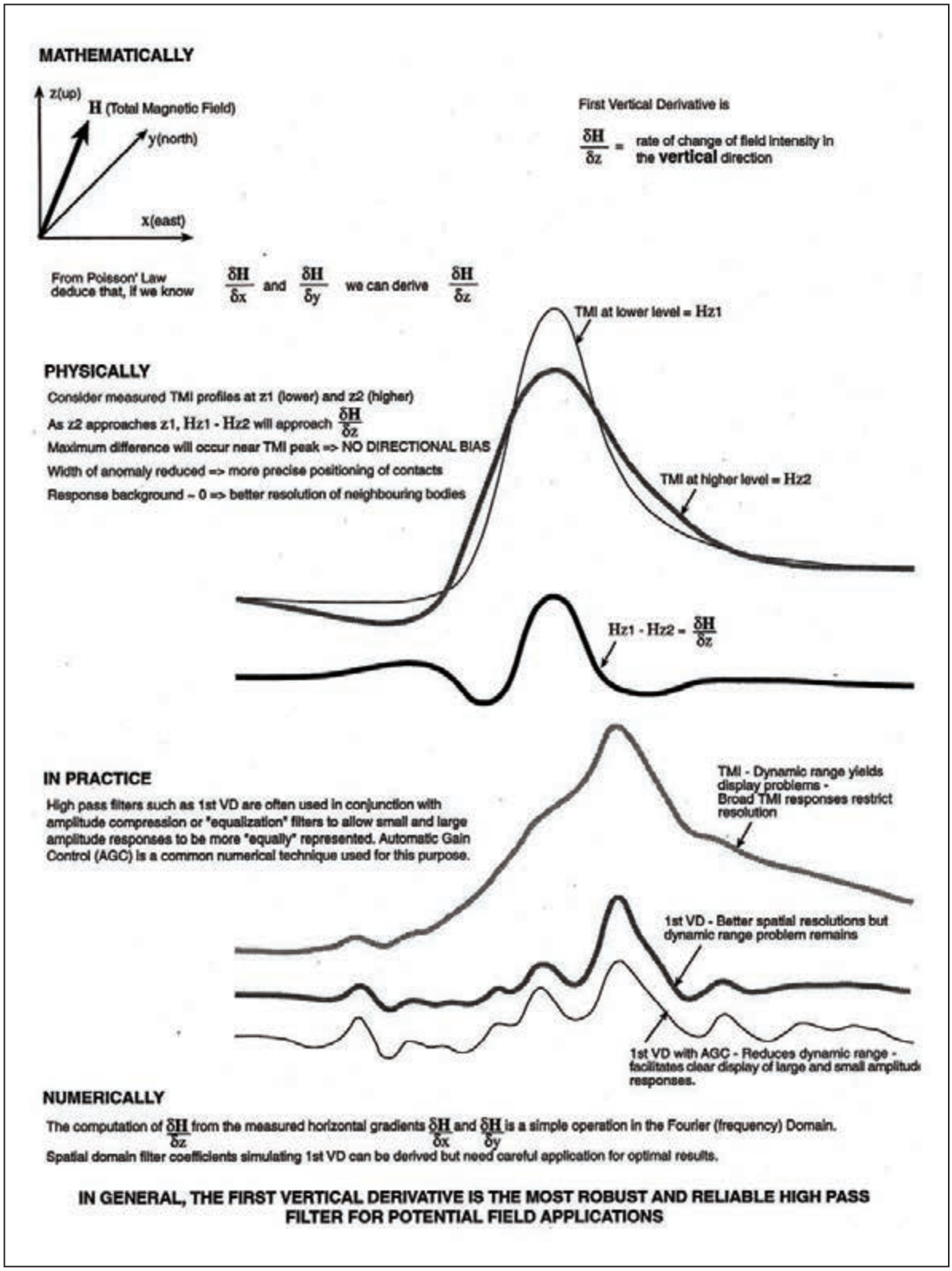

Figure 5.17: Explanation of the 1st VD.

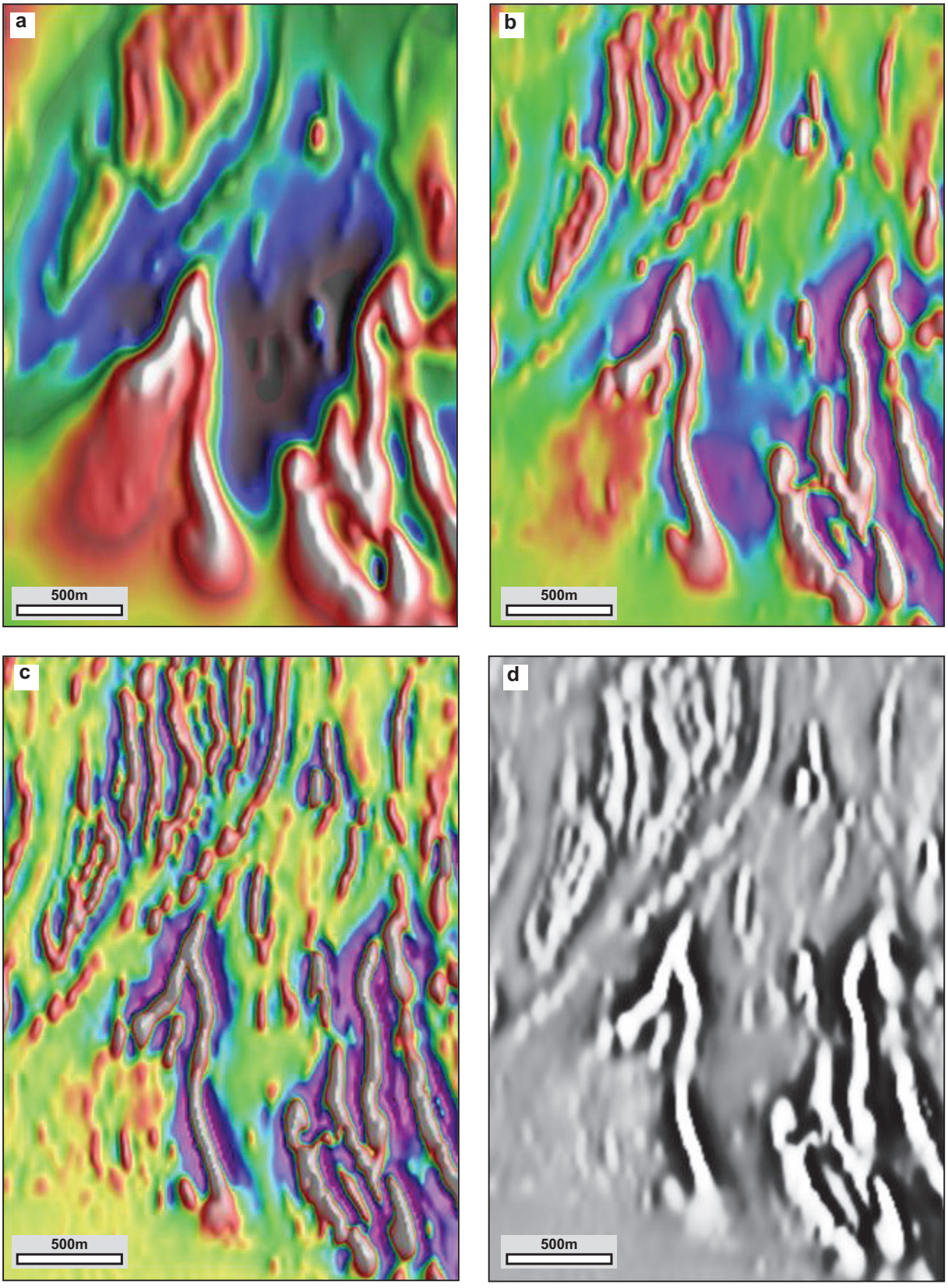

Figure 5.18: Common high-pass filters applied to the Golden Dyke area, NT.
a) RTP with (subdued) illumination from the east.
b) RTP 1st VD with (subdued) illumination from the east.
c) RTP 2nd VD with (subdued) illumination from the east.
d) RTP 2nd VD presented in greyscale (no illumination).
Data courtesy NT Geological Survey and Geoscience Australia. Imaging by Southern Geoscience.

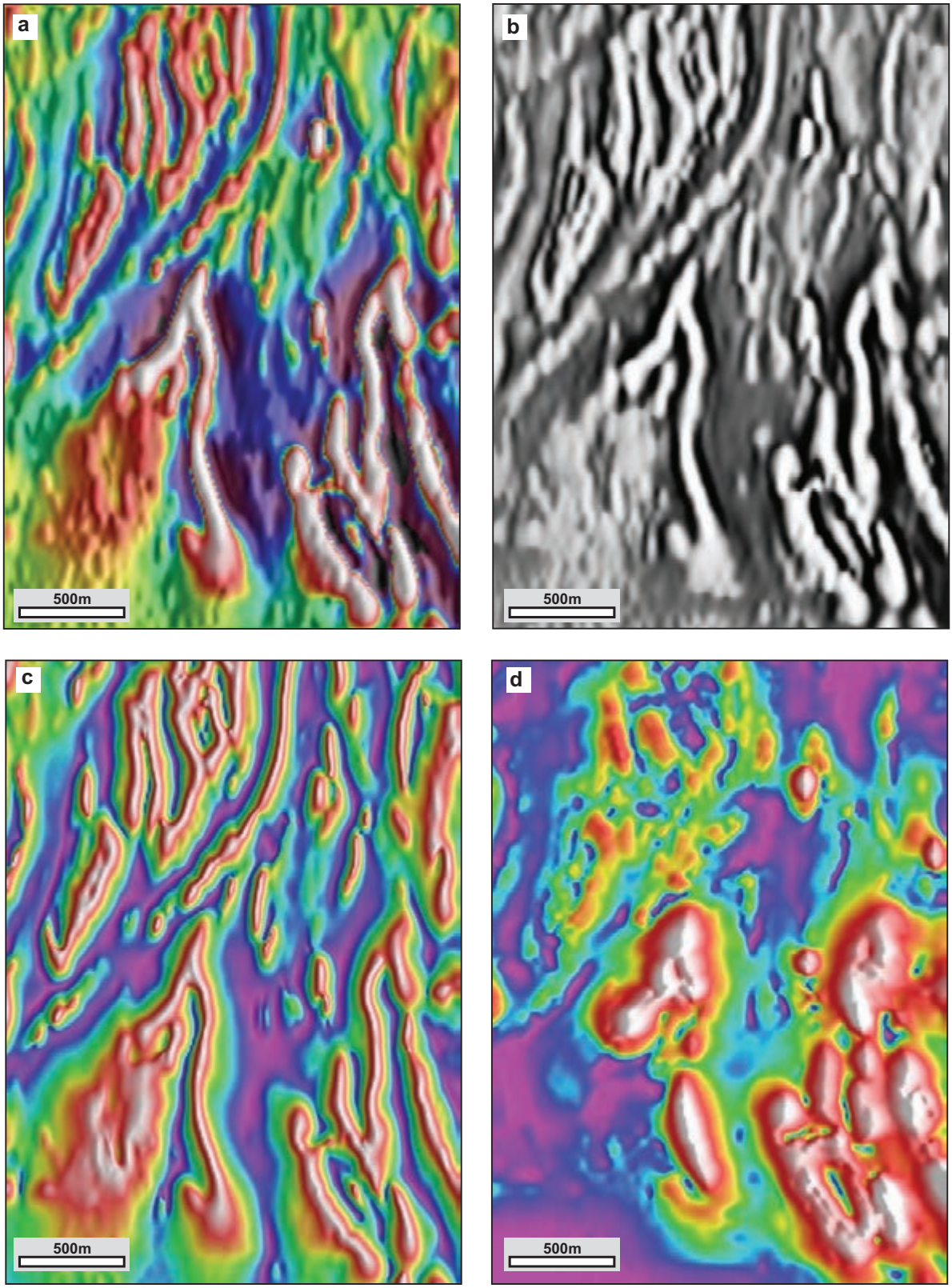

Figure 5.19: Composite/complex high-pass filters applied to the Golden Dyke area, NT.
a) RTP 1st VD with (subdued) AGC-shading from the east.
b) RTP 2nd VD with AGC filter applied.
c) RTP tilt with (subdued) illumination from the east.
d) ANSIG with (subdued) illumination from the east.
Data from NT Geological Survey and Geoscience Australia. Imaging by Southern Geoscience.

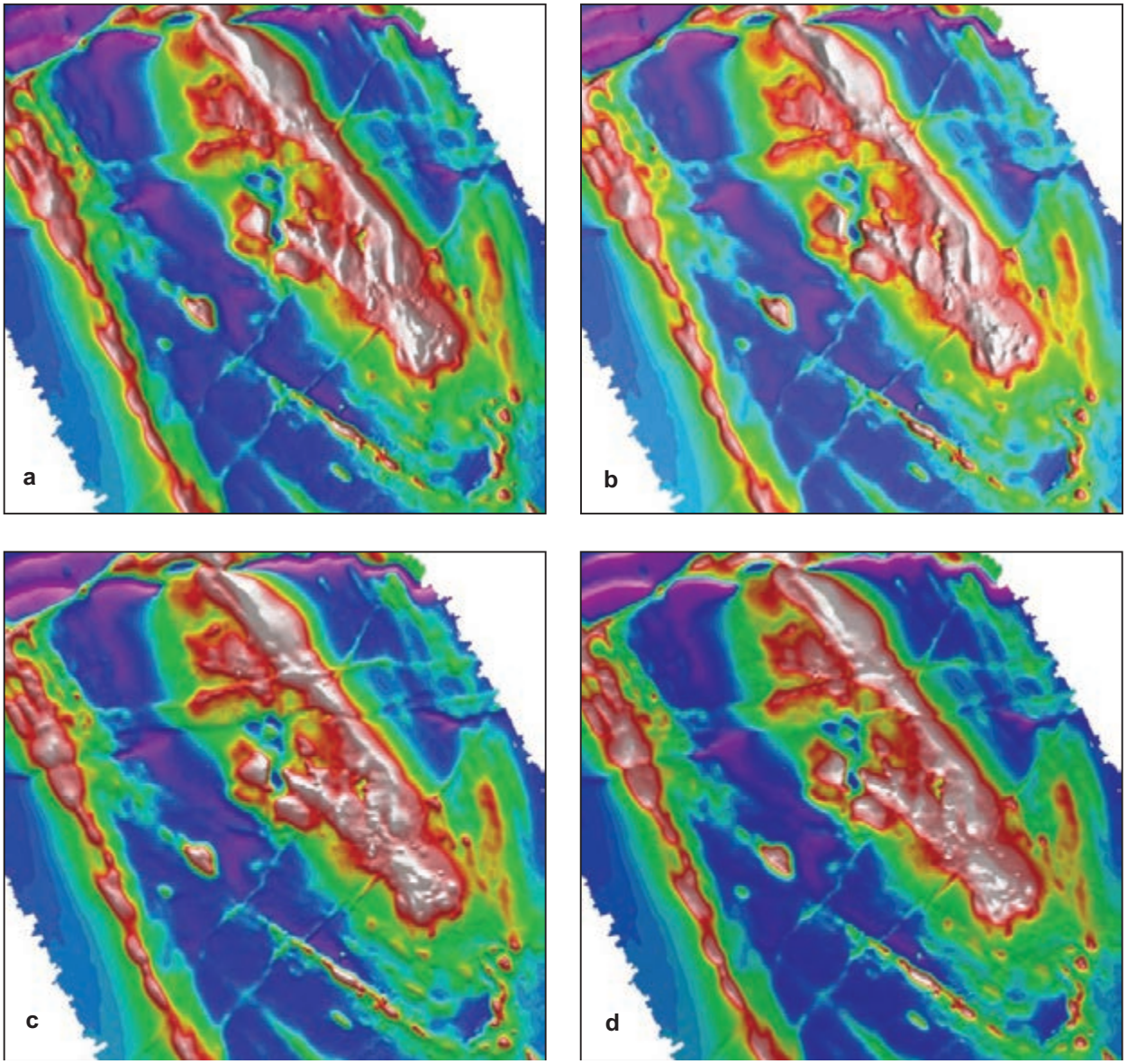

Figure 5.20a: Shaded RTP images from the St Ives area, WA. 50 m line spacing data.
a) Illumination from the west.
b) Illumination from the east.
c) Illumination from the north.
d) Illumination from the south.
Data from GSWA open file records, Processing by Southern Geoscience Consultants.

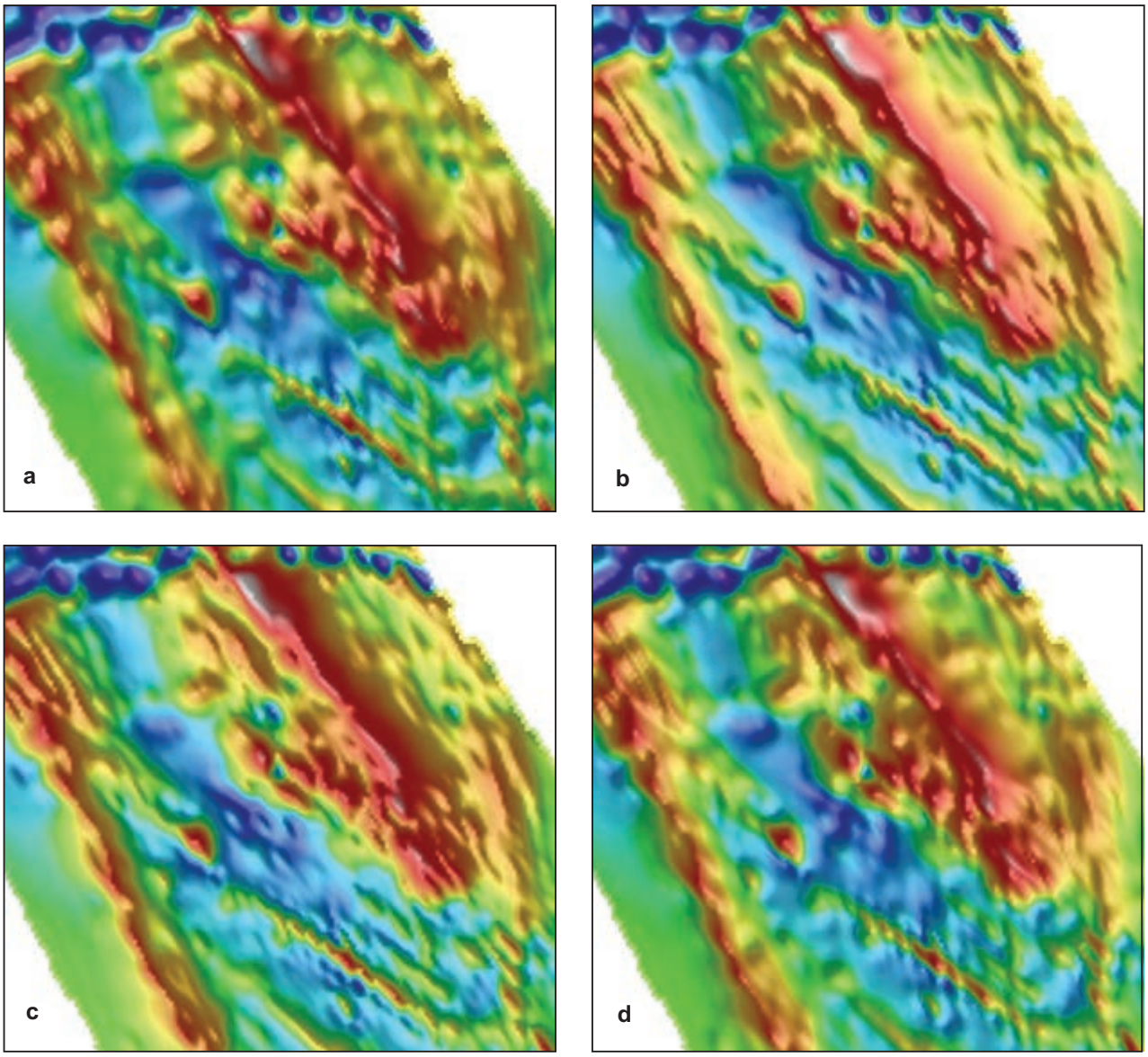

Figure 5.20b: Shaded RTP images from the St Ives area, WA. 400 m line spacing data subset.
a) Illumination from the NW.
b) Illumination from the NE.
c) Illumination from the SW.
d) Illumination from the SE.
Data from Geological Survey of WA open file records. Processing by Southern Geoscience Consultants.

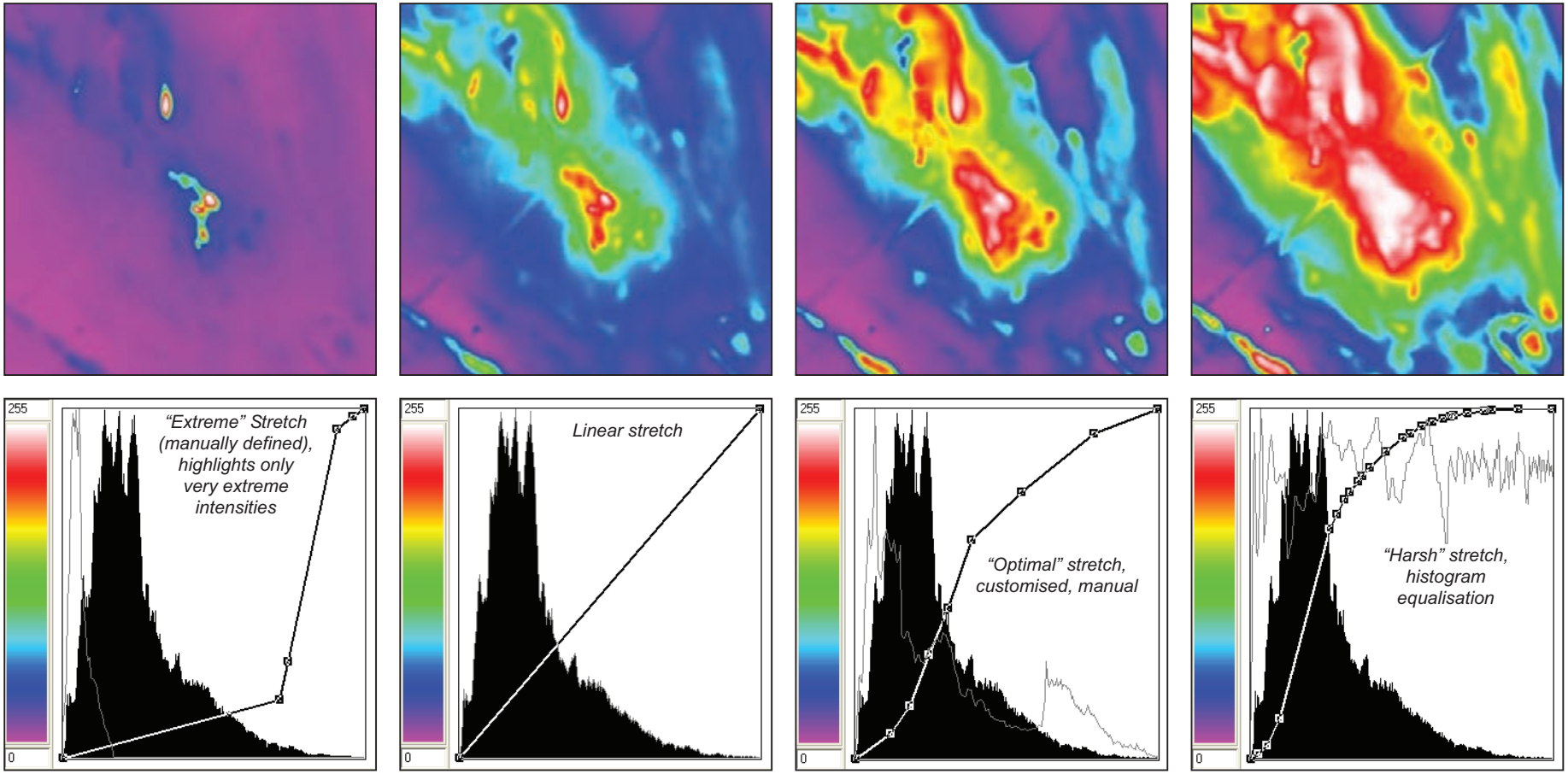

Figure 5.21: Illustration of image stretching. The histogram on the right-side panels shows the relative number of pixels (cells) in each magnetic intensity interval. The graph line on these panels shows how these intensity intervals are mapped onto the colour range. The range of data in the area is 1140 nT. Data from the St Ives area (same area as Fig. 5.11).

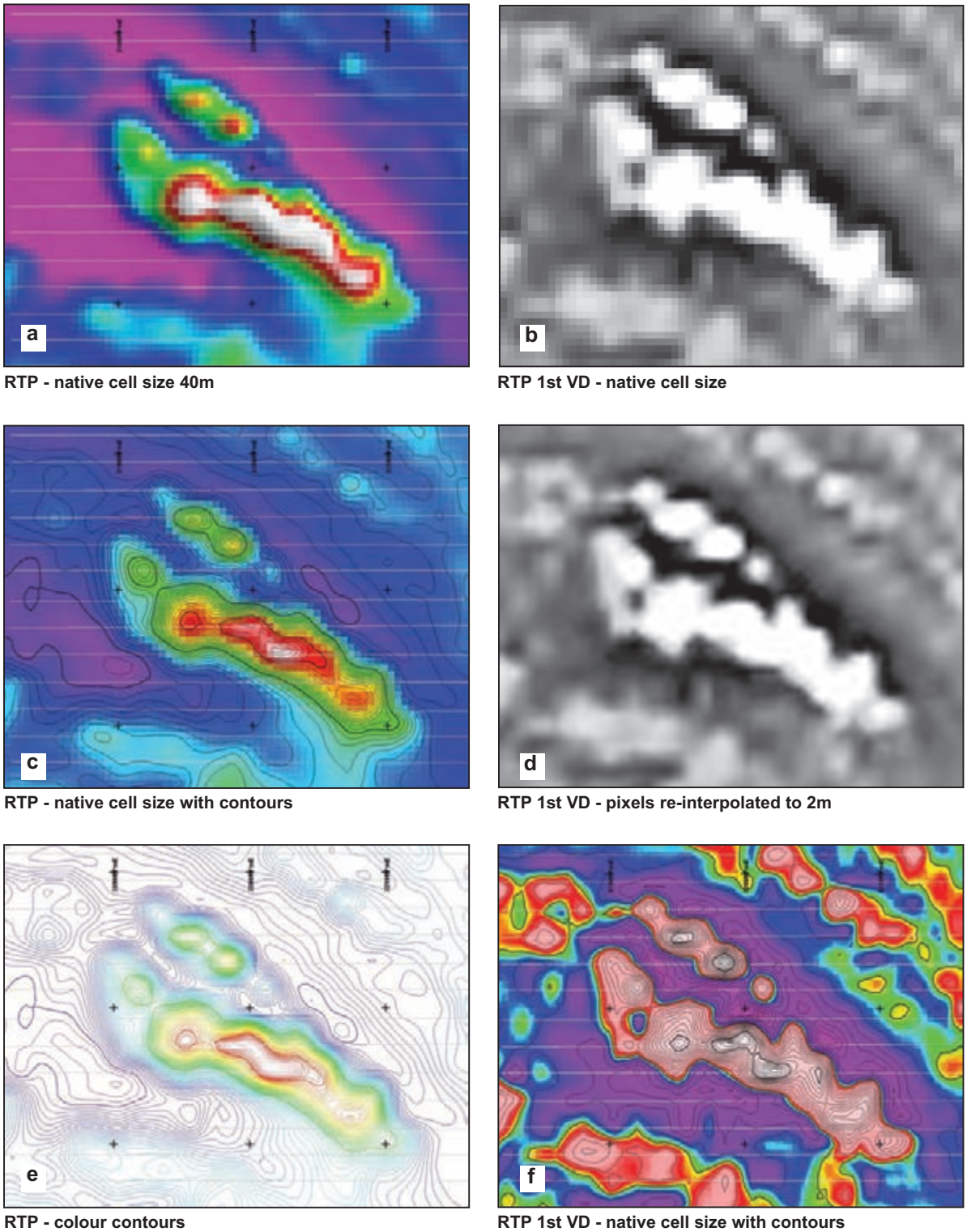

Figure 5.22: The effect of zooming in to maximum scale (1 cm ~ 1 flight line spacing). The native grid cell size (constrained to 1/3rd–1/5th of the line spacing, in this case 40 m = 1/4 of the line spacing) is clearly apparent and the image formats (a and b) have an unattractive, pixelly appearance. This can be improved by introducing contours (c) and/or by reinterpolating the grid cells to a smaller size (d). Ultimately, in order to capture maximum structural detail, contours are essential (compare panels d and f) and the conventional colour contours arguably give the best representation of the RTP.

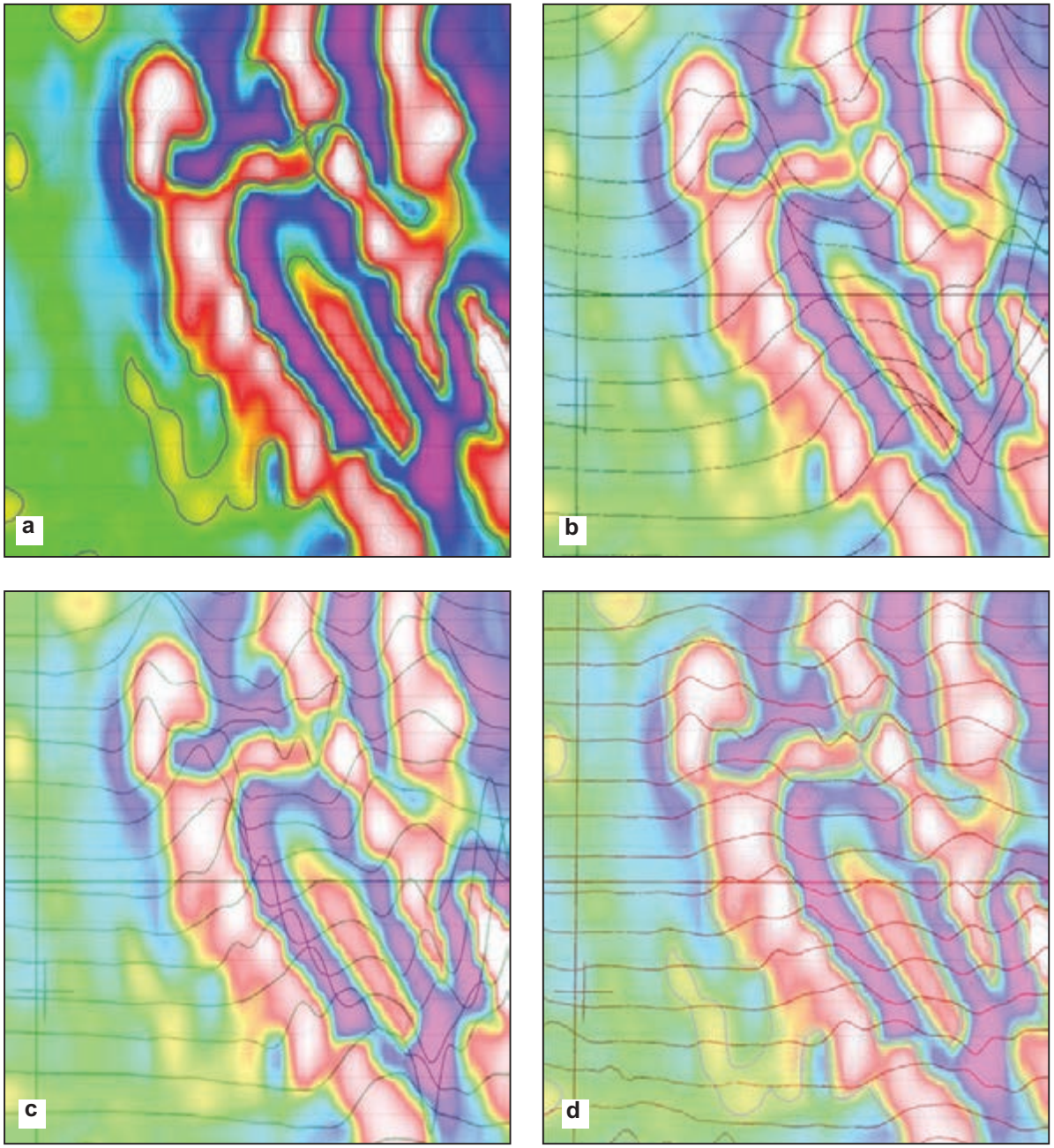

Figure 5.23: The role of profiles in analysis of aeromagnetics. The underlying image is RTP 1st VD. Survey line spacing is 200 m, flying height 60 m. Panel a shows evidence of undersampling artefacts on the SW side of the main continuous magnetic unit. These are geologically questionable N–S (flight line perpendicular) trends. Panel b shows the TMI profiles, panel c shows profiles of 1st VD (calculated along line from the measured TMI). Panel d shows 1st VD profiles with an AGC filter applied. The 1st VD-AGC clearly resolves a small, parallel magnetic subunit on the SW flank of the main anomaly. Manual correlation of this subunit from line to line, made possible by the use of profiles, makes better geological sense than the N–S, en-echelon trends produced from the gridding of the (undersampled) data. See also Section 12.4.3. Data from NT Geological Survey and Geoscience Australia.

6 Observation methodology

Careful, considered and comprehensive observations, duly recorded, are the essence of high-quality interpretation. Having selected an appropriate set of imagery from a well-planned and executed aeromagnetic survey, we embark on this task of interpretation. In much the same manner as geological mapping, we start by making and recording simple and repeatable observations and use these observations to build the interpretation. We will expand on and illustrate the interpretation methodology as we progress to the worked examples in Chapters 11–13. This chapter focuses on the nature of the observations that we make to form the foundation of our interpretation.

6.1 CLASSES OF OBSERVATION

There are two quite distinct and separate classes of features observable from an aeromagnetic image. The first of these is magnetic rock units and the second is pattern trends and discontinuities. Magnetic rock units will become the basic building blocks of our interpretation while the pattern trends will guide our thinking on how these building blocks are linked. During the observation stage it is advisable initially to focus on the magnetic rock units before drawing too many discontinuities and trends.

6.1.1 Magnetic rock units

The observer's objective in delineating magnetic rock units is to estimate the location and shape of the 'top' of the magnetic rock body causing a particular magnetic anomaly. The analogy in geological mapping is the tracing of an exposed contact. The task is to read through the magnetic field patterns and focus on the bodies that are causing them, rather than to simply record the magnetic field patterns themselves.

When recording magnetic rock units the interpreter should consider the following questions.

a) Is this body shallow or deep?
b) Is this a narrow or broad magnetic body?
c) Is this a single magnetic unit or a group of related units?
d) Is this body complex or simple in its magnetisation?

While recording these magnetic rock units, we must be aware that other datasets such as mapped geology, radiometric, digital terrain and gravity data, plus imagery such as Google Earth® (where available), will contribute to our final interpretation. No one dataset contains all the geological information in an area. Each reflects a particular characteristic of a rock package and can lead to a better interpretation. We expand

on the integration of other data with aeromagnetic surveys in Chapters 7 and 8, and emphasise that, in this book, we focus on the methodology of working with, and extracting maximum (geological) value from, aeromagnetic data.

There are many matters of judgement which will influence the way that the interpreter records magnetic rock units. This judgement requires some level of understanding of the local geology. Without some degree of geological control or theme, our observations may be poorly focused and somewhat mechanical. For example, if we consider the array of magnetic rocks in the Comet Vale area of Western Australia (Fig. 6.1) we readily see that there are logical groupings of magnetic units. The two most strongly magnetic groups illustrate the above matters of judgement well. The NNW-striking belts comprising narrow linear magnetic anomalies could easily be outlined as a unit. The consistency of magnetic intensity and orientation of the linear features suggests that the group of linear magnetic features forms a single geological unit or sequence. We will find in Chapter 11 that this is indeed the case, but at this early stage in the interpretation we may be unsure of the source of the magnetic rock units. When we carefully trace the individual linear units within this group we discover a range of spatial associations which provide excellent structural indicators. Had we simply outlined an envelope of linear units and classified it as a single entity, those structural details could have been easily overlooked. By contrast, the central and western magnetic zones shows linear variations in magnetisation but the individual magnetic highs and lows appear to define a linear texture rather than a series of linear magnetic rock bodies. While mapping this texture is useful and valuable to the end result, the meticulous tracing of individual highs and considering them as discrete magnetic rock units is unnecessarily time-consuming and portrays this area incorrectly. Limited outcrop and some local experience tell us that the latter area is a foliated and magnetically zoned granitoid, while the former is an interval comprising mainly ultramafic volcanic flows. Delineation of the individual magnetic ultramafic units clearly adds significantly to the geological picture whereas mapping the magnetic zonation in the granitoid in intricate detail, in this case, does not.

6.1.2 Delineating magnetic rock units

When delineating magnetic rock units we should remember that it should be possible to confirm their sources by mapping or drilling and directly measuring the magnetic properties of a rock sample; the magnetic rock units are physical, tangible entities. The challenge for the interpreter is to read through the magnetic field patterns to trace the location and shape of the magnetic rock unit. We have illustrated this in Figure 6.2. Note the different styles of observation. The 'splitter' style in Figure 6.2a is typical of an observer focused on the very fine detail. The 'lumper' style in Figure 6.2c exemplifies observation by someone more interested in the broad subdivisions. The level of detail, continuity and generalisation shown in Figure 6.2b is a more balanced representation of the magnetic rock units within this ultramafic package.

The lessons learned in Chapter 2 on resolution, ambiguity and superposition are important when observing magnetic rock units. For deep features we must recognise the resolution limitations and not expect to see or delineate individual rock body shapes in detail (Fig. 6.3).

The convention adopted by the authors is to depict magnetic rock units as outlines that approximate the top surface of the magnetic rock body. In some cases, this can be done with a closed polygon, but we often find that body edges can only be traced locally, leaving 'open' body outlines. This is especially the case when the data resolution is limited (see Fig. 6.3). When resolution is good and magnetic bodies are narrow, a single line will often be a suitable representation of the magnetic rock unit. The mechanisms for recording these observations are discussed in Chapter 9. At this stage we note that the authors (and many experienced colleagues) prefer to record observations from hardcopy maps onto transparent film overlays using pens and pencils. Currently available hardware and software are capable of doing this but they can be cumbersome and inflexible. It is anticipated that this situation will soon improve such that freehand recording of observations on screen will enhance the observation and interpretation process, whereas currently it provides many impediments.

It is essential to differentiate magnetic rock units from discontinuities and trends in the observation process. This is most effectively done by using different colours and line types (Figs 6.1 and 6.2).

Most importantly, the observation process should stand as a record of the interpreter's work. The interpreter must be able to review their observations at a later date and understand them. It is also highly desirable that these observations can be reviewed and reused by other colleagues. As such, it is essential that the observation layer remains separate from the much more subjective and interpretive line work that is created on the subsequent layers of the interpretation.

6.2 DISCONTINUITIES AND PATTERN TRENDS (BREAKS)

These observations are typically more subjective and often require personal judgement. However, they are just as important as the magnetic rock units in documenting what the interpreter sees in the aeromagnetic data, as opposed to what they interpret geologically. The degree of subjectivity dictates that these observations should be treated as subsidiary to the magnetic rock units and in some cases it is preferable to draw them on a separate layer. We reiterate that initial focus on the magnetic rock units is advisable, and emphasise that experience will improve our judgement of which 'breaks' are reasonable and which may be problematic.

What are these 'breaks'? Faults, fractures, shear zones and unconformable contacts are the most common sources of geological discontinuities and we expect that these will be frequently well expressed in aeromagnetic data. However, there is a broad range of perceivable linear features in an aeromagnetic image, some of which may not relate directly or simply to faults and contacts affecting the magnetic rock units we delineate. We should remember that the aeromagnetic data reflect magnetisation variations occurring at range of depths, raising the possibility that we will see trends from shallower and deeper features superimposed in the data. It is hence unrealistic to expect that all discontinuities observed will be readily interpretable as faults or contacts, and often inappropriate to expect that they will have expression in outcrop.

Trends observed in magnetic gradients may be tenuous and magnetic zonation boundaries can often be transitional, so we should not expect their definition to be razor-sharp.

A representative set of such observations is illustrated in Figures 6.1 and 6.4. More extensive examples are shown in the case studies in Chapters 12–14.

Because of the subjective nature of this class of observations, it is advisable to exercise restraint. The old-fashioned 'lineament-style' map is rarely a useful or geologically realistic base from which to build a solid interpretation. Our general guidelines for drawing discontinuities and trends are as follows.

a) Record them where you can definitely *see* them. Don't extrapolate or interpolate them (if desired, this can be done during the second, more interpretative stage of the interpretation process).
b) Record detail. Many 'straight lines' in geology (and hence in aeromagnetic images) are assemblages of small segments and the geometry of these segments often provides critical information on structural style. Long, straight, thick lines are rarely appropriate as observations.
c) Consider a range of possible orientations when marking breaks that have dimensions similar to the aeromagnetic flight line spacing. If there is considerable doubt, leave these breaks off the observation layer and perhaps consider them for inclusion in subsequent more interpretive layers (see Fig. 6.4).
d) In most situations, 'less is more'. Save the more subjective, interpretive line work for the second stage of the interpretation process.

6.3 THE WHITE PAPER TEST

No single style of observation will suit all types of aeromagnetic imagery. Different geological settings can yield vastly different magnetic patterns and different scales of observation frequently require adjustments to the way we approach the observation stage. Even experienced interpreters usually need to feel their way carefully when confronted with a new dataset in an unfamiliar terrain. We therefore need a procedure for progressively checking and validating our observations. The white paper test is a straightforward and reliable way to do this. It simply consists of considering our observations in isolation from the imagery and asking ourselves three questions.

1. Are the lines drawn a reasonable record of what I am seeing in the imagery?
2. Do they look 'geological'?
3. If I revisit these observations after a long time interval, will I understand them? (And would colleagues understand them?)

If the answer to any of these questions is no, some adjustment to the style of observations is required.

The name 'white paper test' relates to the method of placing a blank white page beneath the observation overlay to view the observations in isolation. This can be done equally well with observations on hardcopy overlays or on a graphic screen (Fig. 6.5).

6.4 SOME SPECIFIC ISSUES

Having established the need to differentiate between magnetic rock units and discontinuities, and to periodically check the progress of our observations with the white paper test, we now consider some of the more specific issues affecting the integrity and usefulness of the final observation layer. We reiterate that the observation layer forms the foundation of our interpretation and it should be compiled as separate document. It also needs to be preserved for potential reuse; our observations should be largely repeatable and somewhat static, but our interpretation of these observations is always likely to evolve, improve and change with time. A single set of observations may give rise to several generations of interpretations.

6.4.1 Geological control

There is a school of thought that recommends aeromagnetic interpretation should be done totally objectively without being influenced by existing geological data. This has resulted in development of software packages for automating the observation stage and, while these undeniably eliminate the subjectivity of human observation, they focus on the physics of the data and make no allowance for the underlying geology. The vagaries of data quality and geological processes affecting magnetisation make human experience and judgement a key factor in linking magnetic features to geology.

In the authors' experiences, the time spent by the interpreter making the observations effectively lays the foundations for effective integration of the two datasets. Moreover, having and using the available geological data (both fact and interpretation) greatly assists the observation process because we have some appreciation of what we are observing.

Hence our unequivocal recommendation is that all available, pertinent geology be both assembled and largely absorbed before the observations on aeromagnetic data commence.

6.4.2 Objectivity

While we have just strongly advised of the need to have some prior geological knowledge before commencing observations, we do need to approach the observations objectively. Tying and bending our observations to fit pre-existing mapping, models or interpretation can be tempting but it is completely counterproductive.

The purpose of the aeromagnetic survey is to discover new aspects of the geology. We should expect the integration of the aeromagnetic data with the geology to change (and hopefully improve) our understanding of the geology. In fact we should be disappointed if the aeromagnetic data totally agrees with and simply reinforces what we already knew about the geology!

Having a clear understanding of the limitations of both the aeromagnetic and geological data is essential. Compiling the aeromagnetic observations with a preconceived geological theme is valuable but we must avoid letting this theme dictate our observations.

The balance between conservative and clinical objectivity, and creative, semi-interpretive observations can sometimes be hard to achieve, but adopting one or other of the extremes will almost certainly be detrimental to the final interpretation.

When confronted by conflicts, complexities or ambiguities at the observation stage, remember that we will progress to a second layer where we have greater freedom to exercise a large degree of interpretation. Furthermore, we expect this second layer to be a dynamic and evolving document; it will change as we gather more

hard information (e.g. by drilling) and as our ideas on the geology evolve. Hence it is wise to err on the side of caution and objectivity at the observation stage, knowing that our interpretive urges will be satisfied as we progress to the second and subsequent layers of our work.

6.4.3 Varying depths

Most aeromagnetic surveys will show features sourced from a range of depths. We demonstrated in Chapter 2 that rock bodies with substantial volume and strong magnetisation can be seen in aeromagnetic data to depths of many kilometres and so we need to be prepared to differentiate deeper magnetic rock units from shallower ones.

There are two very common situations where shallower magnetic features directly overlie deeper and largely unrelated features. The first is in sedimentary basins where inter- and intra-sedimentary magnetic units overlie magnetic basement (Fig. 6.6). The second is where superficial sources such as drainages, sand dunes, laterite, younger volcanic flows, scree deposits, till and eskers overlie magnetic bedrock (see Figs 3.4 and 3.19). In situations like these it is highly desirable to compile separate observation layers for each depth range. An example, presented in Chapter 13, illustrates the use of matched filtering to image the shallower and deeper sources separately. While the geology of the shallower and deeper sections may or may not be related, it is generally useful to visualise the geometry of the different depth sections in isolation, often leading to compilation of separate interpretation layers for the different depths. This can be extremely helpful in identifying timing relationships of the magnetic rock units.

We commonly observe a single magnetic unit which varies in depth through a study area. We expect that its geometry will be more clearly defined where it is shallower and more fuzzy where it is deeper, so our method of delineating and depicting such units will change with depth. A simple example is presented in Figures 6.7 and 6.8 where outcropping Archaean mafic-ultramafic units cross a Proterozoic unconformity and are seen deepening beneath non-magnetic sandstone cover. Note that detailed observations of these apparent depth changes may allow us to identify structures and timing relationships, and the qualitative observations we make at this stage should point to the need for quantitative depth determinations as part of the observation process. This is dealt with more fully in Chapters 10 and 13.

6.5 GEOLOGICAL ANOMALIES

The term ‘Magnetic Anomaly Map’ is used particularly in continental-scale maps to describe the difference between the measured field and the IGRF (see Section 2.1.1). This is established usage, which arguably should extend to the description of TMI maps at all scales. We also usually refer to specific magnetic highs and lows in images or on profiles as magnetic anomalies, regardless of whether their shapes, amplitudes or even locations are unusual or ‘anomalous’.

In this section, we use the term ‘anomaly’ in its literal sense to describe features that are truly unusual and/or unexpected in the context of the local geology. These can take many different forms.

Extremely high or extremely low field intensity values are obvious anomalies when they occur out of geological context, but they may be quite normal and expected in magnetite-BIF environments or some igneous environments. Local and sometimes subtle increases or decreases in intensity may equally reflect unusual geological processes, and care is required in the imaging and observation of aeromagnetic data to allow recognition of these.

In addition to variations in field intensity, unusual changes in the geometry of magnetic rock units may constitute geological anomalies.

There are no clear formulae for defining anomalies. The key to recognising and defining anomalies is an appreciation of what is commonplace and what is unusual, not only in the magnetic field variations but in the underlying geology. For this reason the most appropriate times to consider what is anomalous are the latter stages of both the observation and interpretation phases, when we can expressly review the data to identify anomalies. It is clearly important to record all such features ***boldly*** to differentiate them from the more routine features; the use of bold colours and/or symbols is an effective means to achieve this.

As emphasised in Chapter 5, it is essential to use a range of imagery, particularly image stretches, at the observation stage to fully appreciate the extremes as well as the subtleties in the aeromagnetic data. Figure 6.9 illustrates a range of anomaly types.

The final word on anomalies and unusual features concerns mineral deposits. Mineral deposits, be they metallic, hydrocarbon or even groundwater, invariably result from combinations of unusual and often extreme geological processes and they frequently display unusual or extreme physical properties. Hence the detailed scrutiny of aeromagnetic (and other geoscientific) datasets for anomalies is an essential part of the exploration and discovery process. It is wise to cast a relatively broad net when identifying and recording anomalies. Narrow criteria and fixed recipes for defining anomalies frequently result in important features being overlooked. While it is important to have a degree of focus and firm guidelines when undertaking the exploration targeting process, expecting the unexpected is always a prudent approach, as is being cognisant of the potential for commodities other than the main focus.

6.6 SCALES OF OBSERVATION

The style of our observations on aeromagnetic imagery will change considerably with both varying flight line spacing and the scale at which we make the observations. Where we have a large volume of data compressed into a small viewing space we experience 'information overload' and it becomes difficult to digest and record all the visible information. In this case we are forced into some form of generalisation and simplification of observations, usually accompanied by a degree of subjectivity. In the other extreme, where the data in our viewing space are sparse, our observations are often poorly controlled. The subjectivity in the process relates more to inferred interpolations and poor control on the orientation and nature of discontinuities.

Each of the worked examples in Chapters 11, 12 and 13 illustrates the varying observation styles as we progress from more regional scales to detailed scales.

We normally conduct our interpretation at (at least) two scales:

a) a coarser scale which allows easier recognition of broader variations and serves as an overview. As noted, the observations we record at this scale tend to be somewhat generalised;
b) a finer scale which readily facilitates the extraction of the desired level of detail in the data. Time, care and attention to detail are required for these observations.

Defining a regional setting of a study area is an established part of the geological mapping process. This need applies equally to the analysis of aeromagnetic data. Ideally, in both geological mapping and aeromagnetic interpretation, we should have data covering an area of 10–20 times the study area to provide regional context and allow recognition of large-scale features which may not be readily recognised within the local study area. This means that for a study area of 10 × 20 km, the regional data should cover at least 30 × 60 km. While the obtainable data surrounding our study area may be of lower quality, viewing this with the data from our study area at coarse scales invariably improves our understanding of the area as a whole. Assessing the interrelationships between the regional and detailed features is an integral part of geoscientific mapping. It is particularly applicable in aeromagnetic surveys where datasets of different ages and with different survey specifications may be much more readily merged than different geological mapping campaigns. We will pursue this topic more fully in the next chapter.

Having acquired data surrounding our study area to provide the regional context, we need to choose an appropriate scale at which to observe and record these broader-scale features. The rule of thumb, established mainly from experience in geological mapping, is that the scale of regional assessment and the scale of more detailed analysis should ideally differ by a factor of 4 or 5. If they differ by less we experience a degree of duplication of effort and if they differ by much more, the links between information at the two scales become difficult to visualise.

For example, studies at 1:250 000 scale are usually supported with regional data at 1:1 000 000 scale and prospect-scale mapping at, e.g., 1:5000 will generally have a backdrop of coarser mapping at 1:25 000 scale. The worked examples in Chapters 11–13 illustrate this process.

6.7 WHERE TO START?

The observation stage of the interpretation process will take days on an average survey and sometimes weeks on a very large survey program. The guidelines for approaching the observation process are very similar to those used by geologists when planning surface mapping.

a) Start in an area where the magnetic features are relatively well defined and (where possible) where their causes are understood. Ideally, this will be an area where there is some rock exposure to assist the process. It is best not to start in a very complex area.
b) Starting somewhere near the centre of the survey area is usually better than starting at the edge.
c) Select an area relevant to the main purpose of the survey. This may be a specific area of interest.
d) It is best to avoid starting by marking in the *very* obvious features. This may inhibit our ability to recognise more subtle but equally important features (see Fig. 6.10).

It may take some time to become familiar with the patterns in a new aeromagnetic survey, so being prepared to review, erase and revise observations is an important part of the process, particularly in the early stages of the work.

6.8 KEY POINTS – OBSERVATION METHODOLOGY

a) Become familiar with the regional and local geology before commencing observations on the aeromagnetic imagery.
    i) Record the geological features that have magnetic expressions, not their magnetic responses. Read through the magnetic field patterns to delineate the geological features causing them.
    ii) Where available, use other datasets to help understand the geology as reflected by the magnetic data, and to assist with your observations on the aeromagnetic imagery.
    iii) Record magnetic rock units and pattern discontinuities with distinctly different line types.
b) Regularly conduct the white paper test.
    i) *Be objective*. Expect your observations to challenge and extend existing geological knowledge.
c) Actively look for geological anomalies, ideally in the latter stages of observation.
d) Address the regional context of both aeromagnetic data and geology.
e) Be prepared to revise your observations as you become more familiar with the data.
f) Start simple, but not too simple!

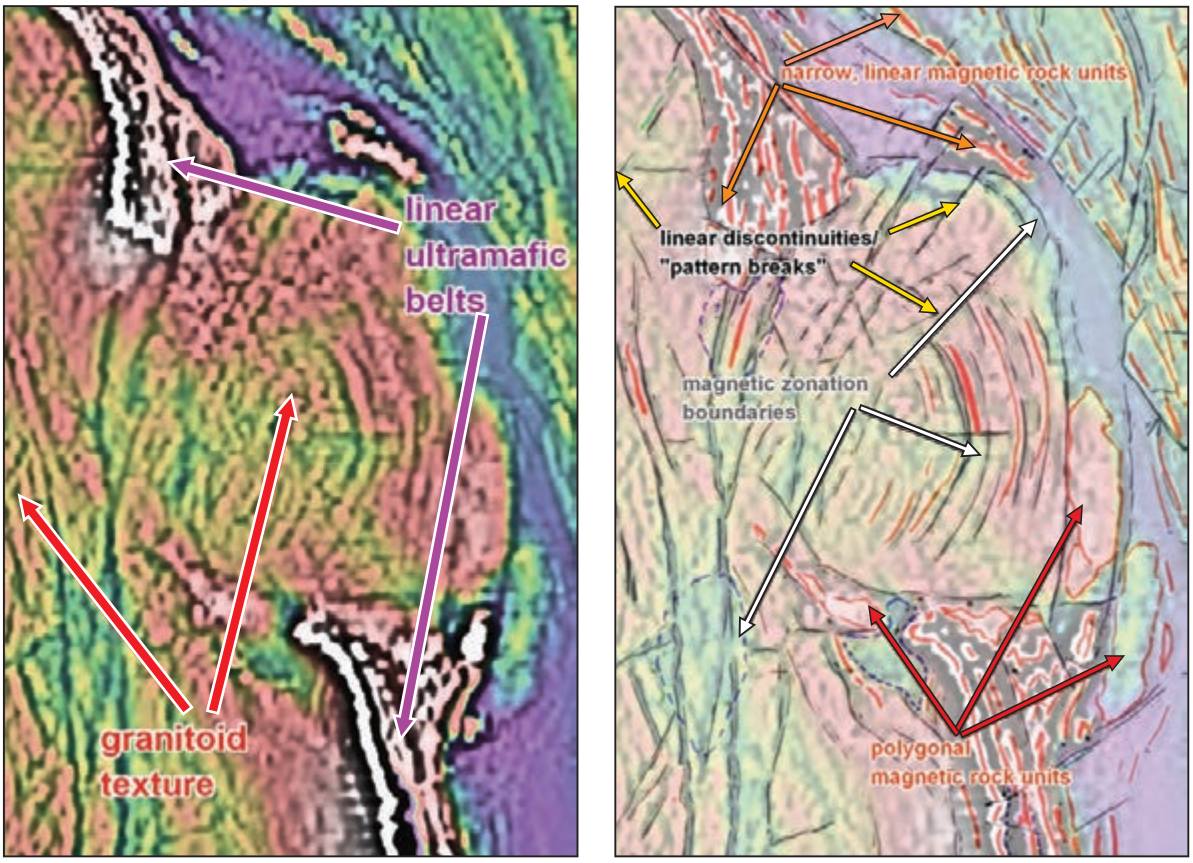

Figure 6.1: Aeromagnetic image illustrating a belt with individual linear magnetic rock units and broad magnetic zones showing linear texture. Note the different observation styles in these areas.

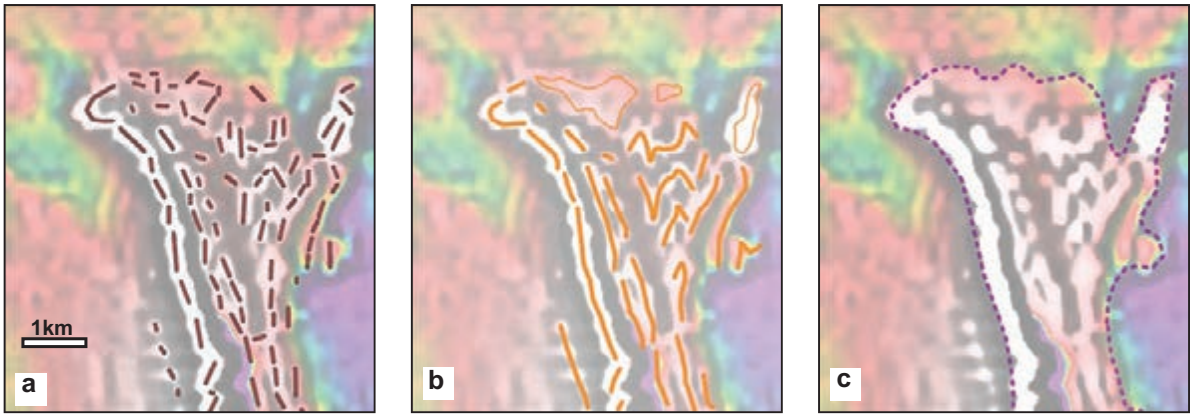

Figure 6.2: Observation styles – magnetic rock units. Comet Vale area. The image is RTP field in colour draped on RTP 1st VD greyscale intensity.
a) Too detailed – geological continuity and discontinuity not well represented (splitter-style).
b) Ideal – structural detail is preserved with a good balance of geological continuity.
c) Too generalised – no structural subtleties preserved (lumper-style).

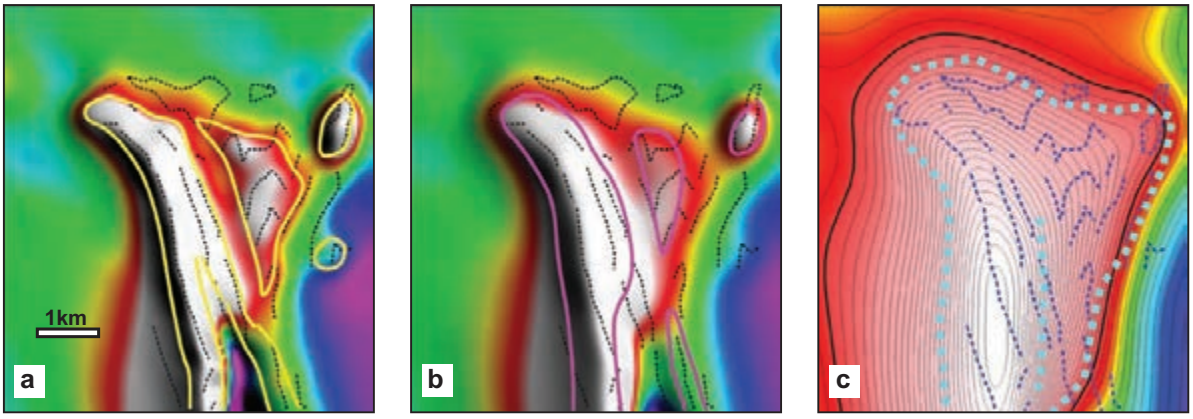

Figure 6.3: Observations – deep magnetic rock units. Comet Vale area. The image is RTP field colour, shaded from the NE. Contours added for the deepest image to elucidate local trends. The magnetic rock units mapped from the original data (60 m mtc) are shown for reference (thin dotted lines).
a) 250 m depth (yellow lines).
b) 500 m depth(magenta lines).
c) 1000 m depth (dotted pale blue lines).

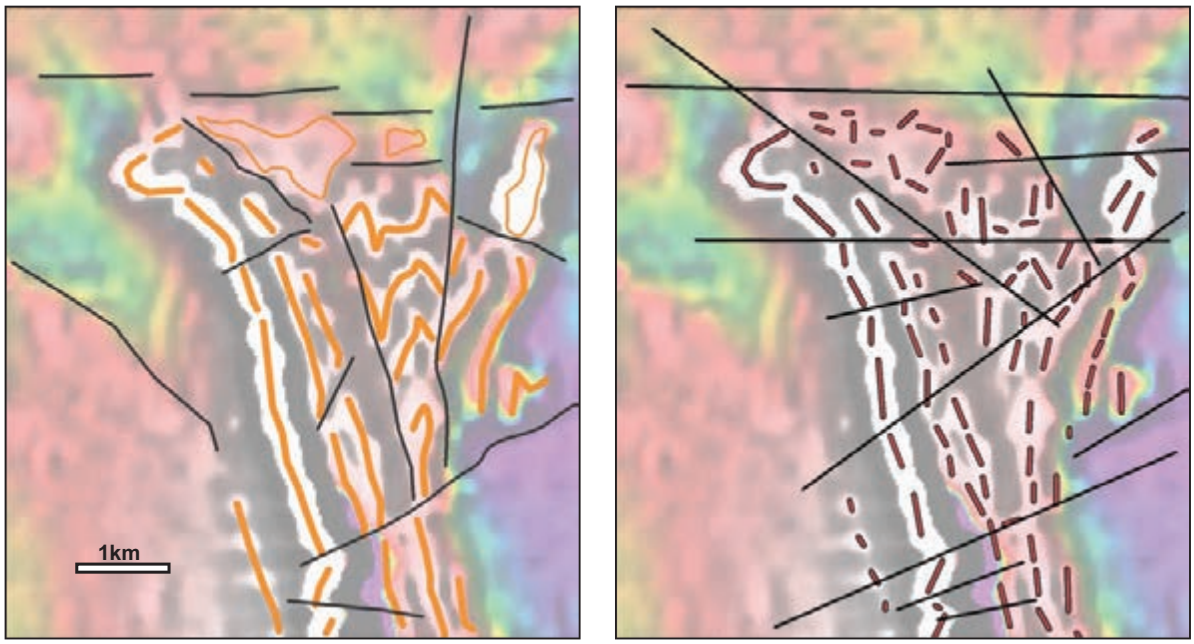

Figure 6.4: Aeromagnetic data discontinuities and trends in the Comet Vale area. Left side is appropriate. Right side (lineament map) has too many extrapolated straight lines and the orientation of some lines is questionable. The right-side observations lack geological sensibility. Note that the flight line orientation is E–W, so that E–W breaks and trends in the imagery may relate to acquisition or processing artefacts. In this image, minor artefacts of this type are observable on the SW side of the main belt of linear magnetic rock units. See Chapter 5.

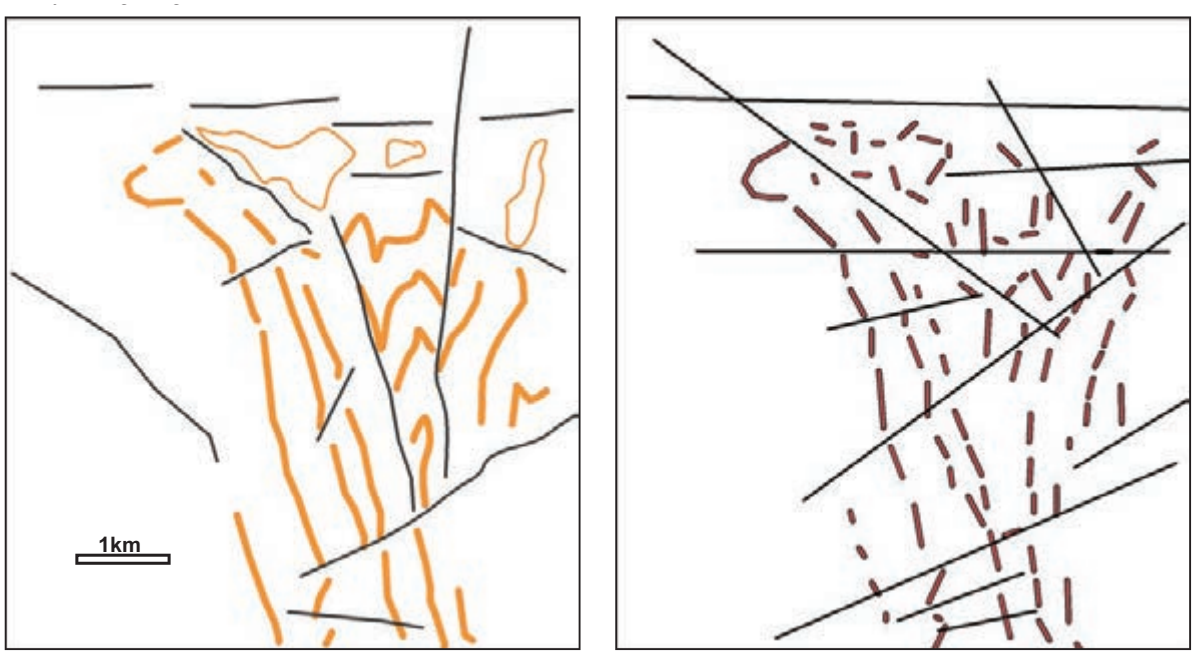

Figure 6.5: The white paper test.
Do I understand my observations?
Do they look 'geological'?

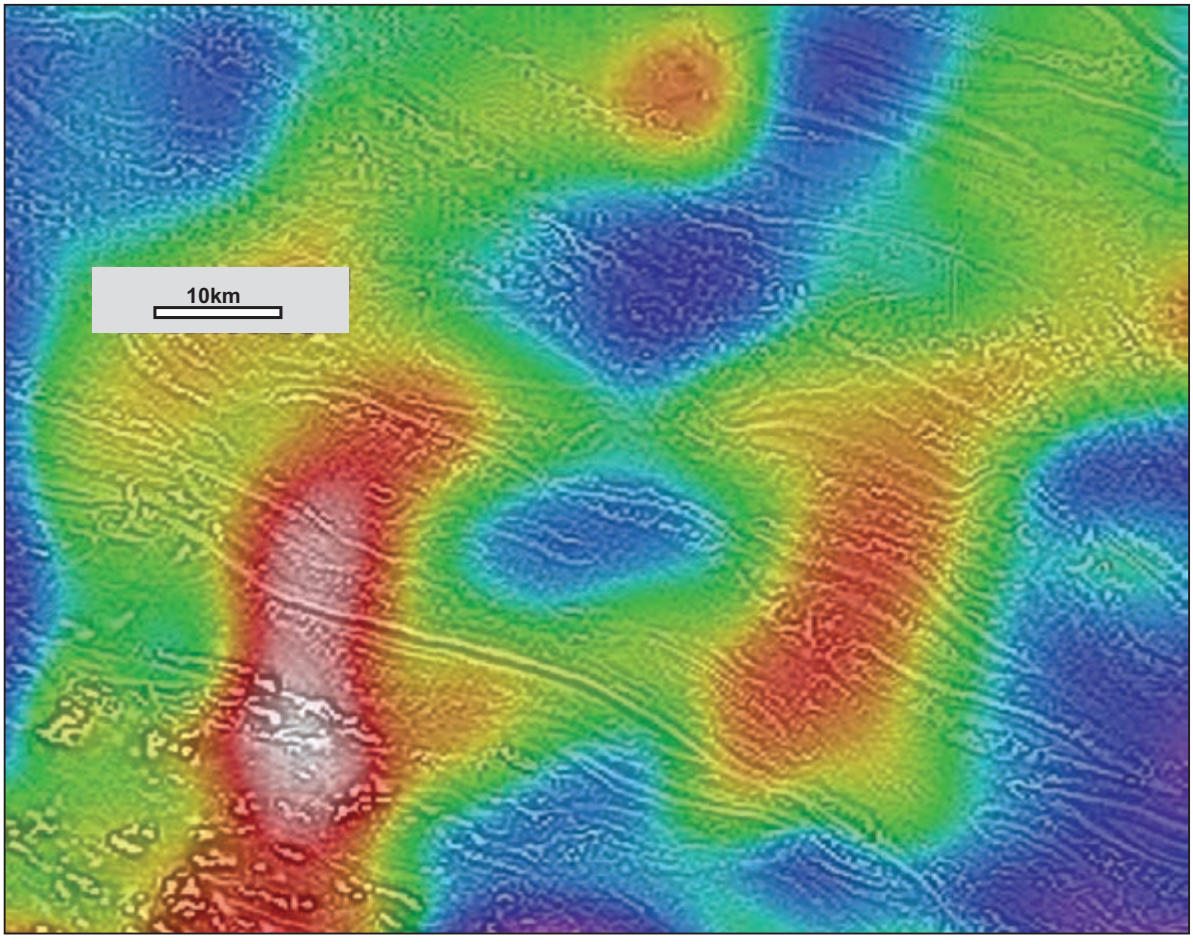

Figure 6.6: Composite aeromagnetic image from the Amadeus Basin, NT, showing the coincidence of shallow (Cambrian) sediments overlying Proterozoic basement. See Chapter 14. Data from Geoscience Australia and NT Geological Survey.

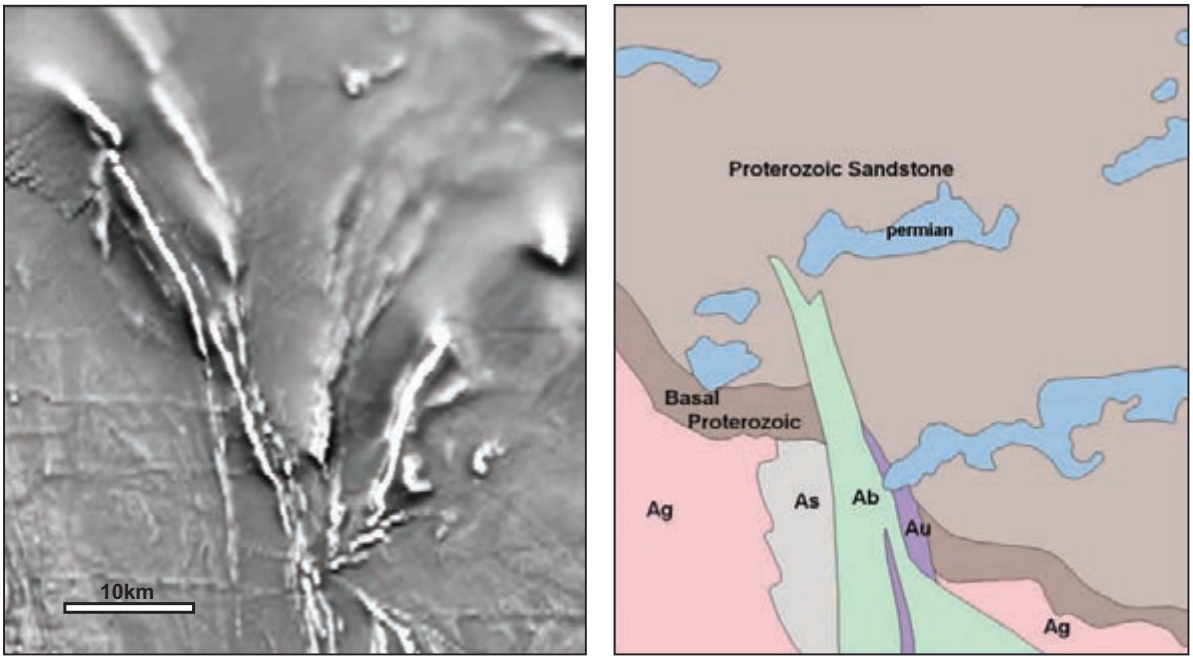

Figure 6.7: Solid geology and aeromagnetic data from the Kingston area, WA, showing the major unconformable contact between Archaean rocks and Proterozoic sediments. Note the increasing fuzziness of the Archaean magnetic rock units as they become more deeply buried under the Proterozoic basin. Data from Geoscience Australia and Geological Survey of WA.

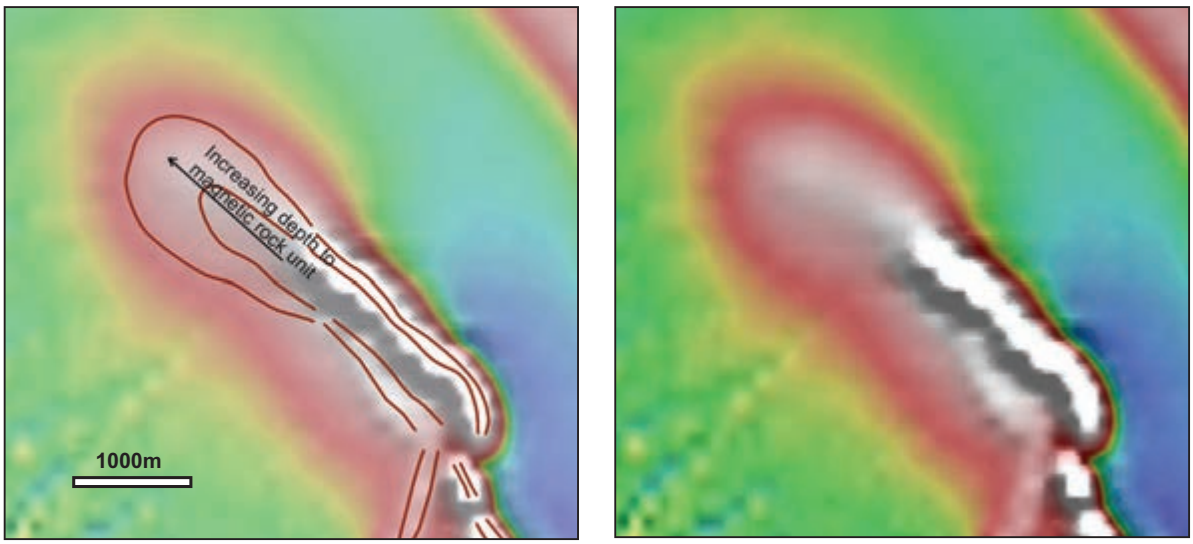

Figure 6.8: Detailed view of the NW corner of the data in Figure 6.7 showing the delineation of deepening magnetic rock units beneath an unconformity surface. Note that the magnetic rock units do not necessarily become wider as they get deeper, but their anomaly shapes widen as definition becomes poorer and we are less able to trace their contacts. The rapid change in width of the main magnetic anomaly may suggest a fault at or below the unconformity. Annotation of the increase in depth is a useful addition to the observation layer line-work.

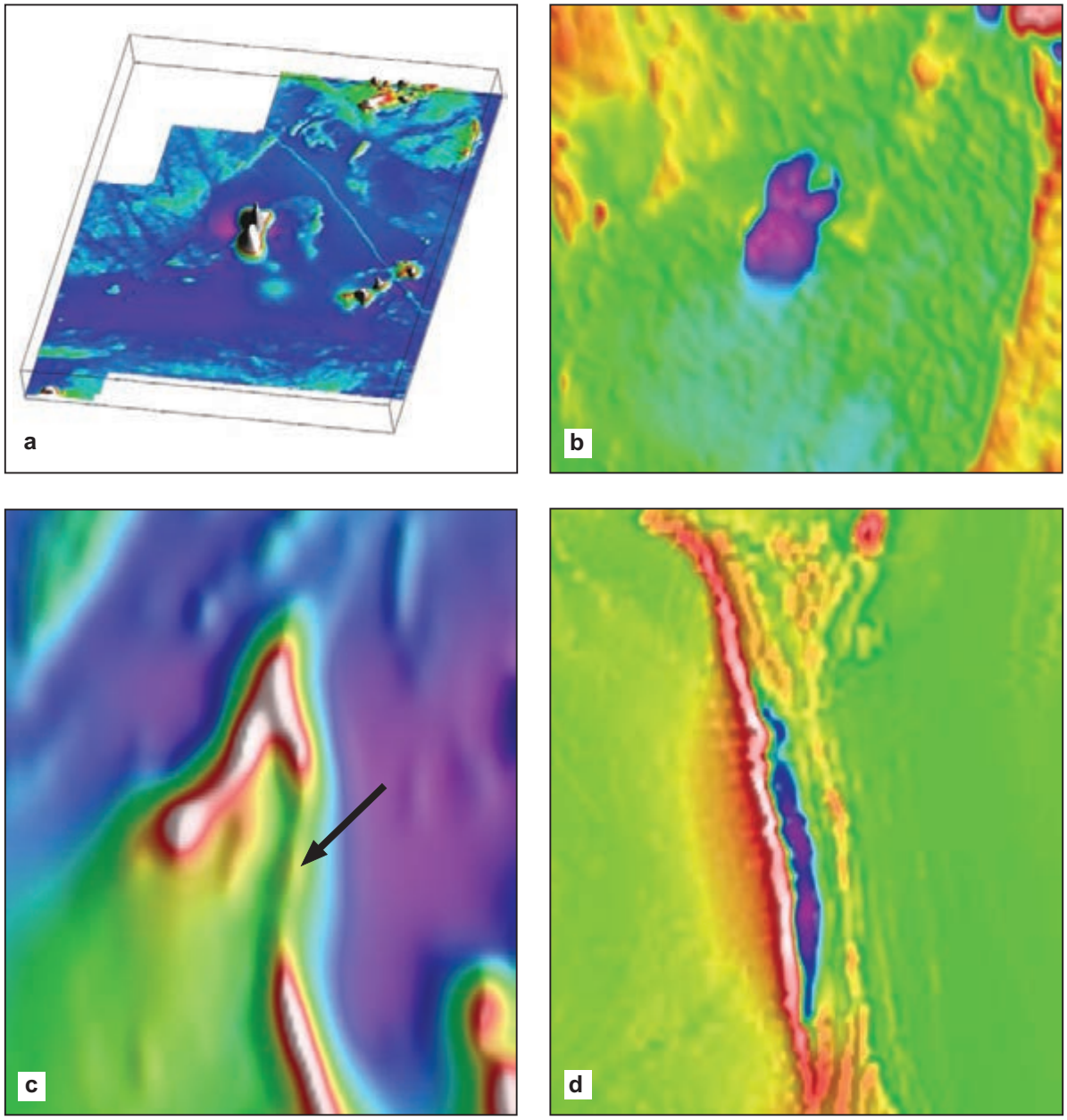

Figure 6.9: Anomalies.
a) Magnetite BIFs from the Tarcoola region, SA. Intensities >5000 nT, image 40 × 40 km. PIRSA data. Image courtesy Chris Anderson.
b) The alteration pipe at Mt Leyshon, Qld. Intensity –2000 nT, image 10 × 10 km. See Section 3.3.4. Data courtesy Fugro Airborne Surveys.
c) Subtle lower-intensity zone on pyrrhotite-rich marker horizon, Pine Creek region, NT. Higher intensities ~900 nT, lower intensities ~450 nT, image 3 × 3 km. Data from NT Geological Survey.
d) Remanently magnetised ultramafic sill, Goongarrie district, WA (negative anomaly, purple colour). Intensity –4500 nT, image 10 × 10 km, Data courtesy Fugro Airborne Surveys.

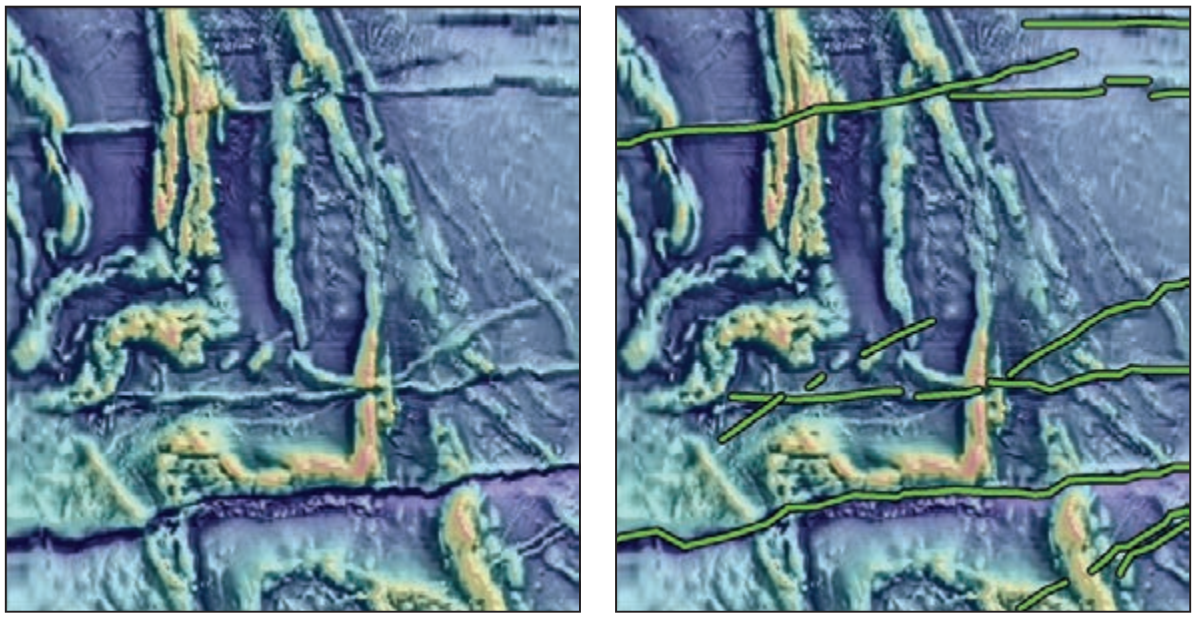

Figure 6.10: Illustration of very obvious magnetic features which may mask subtle but more important features. These obvious features are best recorded late in the observation stage. Data courtesy Fugro Airborne Surveys.

7 Integration methodology

7.1 INTRODUCTION

The integration of observations from aeromagnetic survey data and observations from surface geological mapping is a crucial step in getting optimum value from the survey. While it can be a slow and painstaking process, allowing adequate time and being prepared to face the challenges that it invariably presents will reap rewards for the interpreter.

The integration process is subject to the limitations of both the geological and aeromagnetic data:

a) aeromagnetic data shows only magnetisation variations in rocks (see Chapter 3) and our observations are subject to limitations of data quality and observer experience;
b) geological mapping is also strongly influenced by observer experience and is often limited by the extent or accessibility of observation locations. Time and cost factors frequently cause geological maps to be based heavily on aerial photo interpretation with minimal ground traversing and limited hard observations on outcrop and hand specimen.

In the past there was a strong tendency to take the geological mapping as the 'ground truth' and treat the aeromagnetic observations as 'just geophysics'. Where conflicts occurred between the two, the aeromagnetic information was often dismissed as being subsidiary and less reliable (and less important) than the geological mapping.

Before commencing the integration of the two data sources it is essential to give due consideration to the following.

a) How much information is contained in the aeromagnetic data?
    i) Line spacing, flying height, quality and scale of presentations.
    ii) Magnetic characteristics of the survey terrain.
b) How much information is contained in the geological maps?
    i) Extent and quality of exposure.
    ii) The number and extent of field observation points.
    iii) The quality and scope of the observations.
    iv) The number of (and time differences between) mapping campaigns.

We emphasis here that while the information extractable from aeromagnetic data clearly has limitations, its overwhelming strength lies in its uniformity, continuity and repeatability, irrespective of cover and irrespective of the vintage of the data.

Furthermore, having understood Chapter 3, geologists should be aware of the extraordinary range of geological information potentially contained in aeromagnetic survey data. The notion that some features observed in well-compiled aeromagnetic maps can be dismissed as spurious, has no place in the effective integration of geology and aeromagnetic data.

7.2 RADIOMETRIC, GRAVITY, SEISMIC, ELECTROMAGNETIC AND REFLECTANCE DATA

At this point, we expand on the need to use and integrate other relevant data where available. Modern geological maps frequently make use of satellite data and sometimes of airborne and ground geophysical data, in addition to the traditional aerial photography. The role that these other remotely sensed datasets might play in our interpretation depends on many and varied factors. The purpose of this book is to provide users with the means to become proficient in the use of aeromagnetic survey data. Similar texts would be required on radiometric, gravity, electromagnetic and satellite–airborne 'reflectance' data to adequately prepare interpreters for the challenges of their integration with geological mapping. We briefly describe each of these methods, their capabilities and limitations, and our approach to integrate the data they generate with geology. This is not to deny the effectiveness of other datasets. An interpreter should use all the data at hand. Rather, we feel that the philosophy and much of the methodology detailed here can be transposed to gravity, radiometric and other datasets. As well, magnetic data are generally the most detailed data available in an area. Anderson and Nash (1997) present an excellent example of the integration of aeromagnetic data with a wide range of other datasets in the Rossing area of Namibia.

7.2.1 Multi-spectral scanners – reflectance data

A wide range of satellite and airborne remote-sensing radiometers can provide useful information on near-surface geology. The common characteristic of these devices is that they measure reflected electromagnetic (EM) radiation. This may be done over a wide range of EM frequencies and with spatial resolution ranging from 1 m to 100 m.

The 'radar' band of wavelengths (1 cm to 1 m) is particularly suited to mapping topographic variations (Tapley 2002) and the Shuttle Radar Topography Mission (SRTM) yielded digital elevation models (DEMs) at a resolution of a few tens of metres, for much of the Earth's surface (Farr *et al*. 2007). Australian digital elevation data can be downloaded from Geoscience Australia's GADDS portal.

Since the inception of the publicly available ERTS and Landsat satellite data in the 1970s, there has been a huge expansion of purpose-built satellite-borne radiometers, monitoring weather, agricultural, cultural and of course geological variations at and near the Earth's surface. Campbell (2002) describes the various devices and their applications. Following the successful implementation of these devices in satellites, airborne versions (which provided higher spectral and spatial resolution) appeared in the 1980s.

For geological applications, multi-spectral scanner data such as Landsat 7, Aster and HyMap (Cudahy *et al*. 2008; Laukamp *et al*. 2010) can provide detailed information on surface geochemistry. A variety of alteration styles, regolith types and lithologies can be mapped via their reflectance spectra. The main limitations are variations in vegetation, water content and weathering. In areas of reasonable outcrop and/or subcrop these often high-resolution and commonly low-cost data sources can be of enormous value to mapping and exploration.

Interpretation and integration of these data with geological and geophysical data follows the methodology of aerial photo interpretation and is similar to the observation layer–solid geology layer approach outlined in this book. For integration with aeromagnetic data, we must remember that reflectance data portrays only surface variations. Hence it is best suited to enhancing the surface geology (including regolith and cover rocks). This is best done before the integration of geology and aeromagnetic data. Figure 7.1 illustrates high-resolution HyMap data, along with geological mapping, airborne magnetic and radiometric data, and airborne gravity gradiometer data, from the Broken Hill (NSW) area. Integrating the 'true colour' HyMap enhancement with the digital elevation data can be particularly revealing (Fig. 7.1, top left panel).

7.2.2 Gamma ray spectrometer data – radiometric data

Gamma ray spectrometry, commonly (colloquially) referred to in field geoscience applications as 'radiometrics', has accompanied aeromagnetic surveys since the 1950s. It is logistically very suited to incorporation with aeromagnetic surveying and can add a wealth of additional information to that survey at a generally small additional cost. Natural gamma ray energy sourced from radioactive isotopes of potassium, thorium and uranium is recorded, resulting (in modern surveys) in maps and images of the apparent surface concentration of these elements.

The source of the recorded gamma ray energy is restricted to the top few centimetres of the ground and the radioelement concentrations are inferred from gamma ray counts striking a large crystal detector mounted in the aircraft. The recorded signal strength is strongly affected by ground moisture and topographic variations, and is also subject to atmospheric conditions. The footprint of each airborne radiometric measurement point is approximately twice the survey height and recording intervals are longer than those for aeromagnetic data in order to obtain meaningful signal (i.e. meaningful numbers of counts). Hence, imagery of radiometric data is inherently more fuzzy (lower resolution) than aeromagnetic imagery. Hansen (1980) presents an excellent summary of the radiometric survey method, and Thomson *et al*. (2007) provide a recent guide to its applications.

Radiometric surveys yield surface geochemical maps in much the same way as multi-spectral scanners. Since the radio-elements mapped are not well discriminated by reflectance devices, radiometric surveys add another dimension to surface mapping. The application and interpretation of radiometric data is very similar to multi-spectral scanner data, and the two datasets are conducive to co-processing using techniques such as principal component analysis.

The interpretation methodologies for radiometric and multi-spectral scanner data are very similar, but the spatial resolution of radiometric data is usually inferior. The value of the resulting radio-element maps should not be underestimated and their use in geological mapping and exploration is very well established. Commodities such as uranium, phosphate, bauxite and zircon present direct targeting opportunities, as do potassic alteration systems associated with deposits such as copper porphyries. As with multi-spectral scanner data, the integration of radiometric data with surface geology, including identification of anomalies, should normally precede integration with aeromagnetic data. Figure 7.1 lower central panel shows the potassium variations from a detailed aeromagnetic–radiometric survey in the Broken Hill area. In Section 12.4.4 we show an example of the integration of radiometric data with geological and aeromagnetic data.

7.2.3 Airborne electromagnetic data (AEM)

AEM surveys are most commonly used to search for conductive ore bodies and/or to map near-surface conductivity variations for regolith or groundwater studies. Many different fixed-wing and helicopter-borne measurement configurations are in use, each with its own special features. AEM systems with reasonable depth penetration require powerful and heavy transmitters, and hence they require larger (and more costly) aircraft than those used for aeromagnetic (and radiometric) surveys. These transmitters interfere with magnetometer measurements, so that magnetic data gathered on the same platform as AEM are invariably noisier than typical aeromagnetic data. The multi-channel output from AEM surveys can be compiled into maps and images of conductivity variations, each of which can be loosely linked to a different depth. In ideal circumstances the depth of investigation for AEM surveys may be many hundreds of metres, but more commonly (particularly for the smaller and less costly systems) it is in the 100–200 m range. Thomson *et al*. (2007) review modern usage of AEM systems and provide an extensive reference list on this and other topics in airborne geophysics.

It is common practice for aeromagnetic data to be gathered during AEM surveys, so interpretation and integration of the two datasets is a required outcome. AEM data often provide useful (albeit shallow) bedrock mapping information and this can be quite compatible with the integration of geology and aeromagnetic data. The depth discrimination capability of AEM means that several layers of observation may be necessary in the interpretation process, or it may be done using 3-D visualisation methods. The integration of these layers or 3-D compilation with aeromagnetic observations and surface geology requires careful thought,

particularly regarding the depths of magnetic rock units. Figure 7.2 illustrates images of multiple AEM channels showing conductivity variations at increasing depths.

In summary, AEM provides a large amount of data on relatively shallow conductivity variations and suits a narrower range of applications than aeromagnetic surveys. Its particular strengths are the detection of conductive mineralisation and detailed mapping of the regolith, but to do these confidently at depths greater than 200 m, large and costly systems must be employed.

7.2.4 Gravity data

Gravity data are very similar to but much simpler than magnetic data. Both are potential field methods but, in simple terms, whereas the magnetic field is dipolar, the gravity field is monopolar. While the gravity field equations and the consequent modelling schemes are far less complex than those for magnetic data, the ambiguities in gravity data are extreme. Standard geophysical textbooks such as Dobrin and Savit (1988) emphasise and illustrate this ambiguity. Furthermore, the density changes which cause the gravity field variations range from 1 g/cm^3 (= 1 t/m^3) for water to around 4 g/cm^3 in very dense ultramafic rocks, such that the contrasts are moderate compared to magnetic susceptibility contrasts which span many orders of magnitude. Hence, the gravity signal has an inherently lower dynamic range than that for magnetic data. Furthermore, the gravity field is mathematically equivalent to the integral of the magnetic field, which means that the gravity field is inherently composed of broader wavelengths as well.

Measurement of the gravity field has, until recently, been land- or ship-based because of the need for a stationary instrument. The utility of gravity data has been widely acknowledged in sedimentary and regional mapping applications since the 1950s and countries such as Canada, the US, China and Australia have extensive coverage of ground gravity at (very roughly) one station per 100 sq km. The measured gravity field facilitates the mapping of density variations through and even below the Earth's crust as well as in the near surface. Powerful as the gravity method may seem, it is limited by the time and cost required to acquire data in sufficient detail to map at anything other than regional scales. Ground gravity surveys are commonly sampled at between one station per 20 km^2 and one station per 200 m^2. This roughly corresponds to investigations at scales of 1:250 000 and 1:25 000. The slow rate of acquisition and the high cost compared to aeromagnetic surveys dictate that detailed survey coverage is usually of limited areal extent.

Where close spaced sampling is practicable, however, the data can provide a remarkable range of information for exploration and geological mapping. This information is highly complementary to aeromagnetic data.

Airborne gravity surveying became a practical and useful reality in the 1980s and has advanced greatly in the last decade (Thomson *et al*. 2007). There are two distinctly different types of airborne gravity systems. Airborne gravimeters aim to measure the Earth's total gravitational acceleration '**g**' and typically have a spatial resolution measured in kilometres. Airborne gravity gradiometers measure the directional rate of change of **g** and have spatial resolution of hundreds of metres.

Gabell *et al*. (2004) describe the modern application of airborne gravimeter surveys. Their spatial resolution dictates that they can only be usefully flown with line spacing of several kilometres, and this constrains their use to broad-scale exploration and mapping. They are particularly useful in the evaluation of extensive sedimentary basins where ground gravity coverage is poor. Similarly, for general geological mapping at scales of 1:250 000 or more, airborne gravimeter surveys have much to offer.

The advent of the airborne gravity gradiometer (AGG) in the late 1990s (Dransfield 2007) enabled rapid data acquisition with similar resolution to ground gravity surveys at reasonable cost. With line spacing of 100–300 m, AGG data have shown their capacity to map quite subtle features of those dimensions (Isles and Moody 2004). AGG surveys typically include aeromagnetic and radiometric data acquisition with little or no reduction in the quality of these data. While the value of AGG data in mapping and exploration is very high, the cost of surveys is typically around 10 times that of combined aeromagnetic–radiometric surveys, so their application is less widespread. Figure 7.1 lower right panel illustrates output from an AGG survey in the Broken Hill area of New South Wales. This survey was flown with 200 m spaced lines oriented along strike and produced a remarkable match with pre-existing detailed ground gravity data (Lane 2004).

The integration of gravity data with other datasets is best done in the mid to late stages of the interpretation. Gravity datasets are nearly always more coarsely sampled than aeromagnetic surveys, and show variations from a wide range of depths. Integrating the gravity data after considering the other, more detailed datasets is generally the most effective approach.

The multiple datasets illustrated in Figures 7.1 and 7.2 sourced from different locations by different sensors and based on different physical rock property variations illustrate the challenges of integration. It is important to develop a firm appreciation of each individual dataset before proceeding too far with integration. Nevertheless, the basic approach of compiling an observation layer for each and correlating this with hard geological data wherever possible is common to all the data sources.

7.2.5 Seismic reflection data

The integration of seismic reflection and aeromagnetic data in the past involved the recognition and delineation of magnetic basement and intra-sedimentary magnetic rocks such as volcanic and intrusive rocks. Very often this took the form of profile modelling of strongly magnetic rock units along seismic lines, but in more recent times the subtle expressions of faults and sedimentary layers have been directly correlated with seismic sections. Examples in the Vulcan Sub-Basin of north-west Western Australia (Norman 1993) and the Otway Basin in south-eastern Australia (Gunn 1998) illustrate this integration. We expand on the increasingly important role that aeromagnetic surveys play in sedimentary basins, in Chapter 10 of this book.

7.3 POSITIONING

The correct coordination of our datasets is crucial to interpretation. The methodology used to position each dataset and the projection and datum system chosen to convey this positioning must be fully investigated before we start to correlate aeromagnetic (or other) observations with mapped geology. In some cases assistance from specialist GIS or survey personnel may be necessary to clarify coordination in either dataset, as it is not uncommon for this information to be poorly described on maps and in digital data metafiles.

Double-check this. Unrecognised mismatches in coordinate and positioning systems will invalidate much if not all of our integration work, and potentially cause large amounts of wasted time. In particular, be aware of the age of the data. For example, much Australian data collected before 2000 were acquired and presented using an AGD66 datum. Most current surveys are collected using a GDA94 or WGS84 datum, which are ~200 m north-east of the old datum. Since the difference between the two at 1:250 000 scale is less than 1 mm, you may not notice it until you move to more detailed scales, which may mean redoing days of work.

7.4 PREPARATION

The preparatory steps for the aeromagnetic interpretation have been covered in Chapter 5. The scales selected for observation will nearly always be the same as those we use for the integration process. Our preparation of the geological data will require, as a minimum, the geological mapping, drill hole and mineral occurrence locations, topographic data and any prior interpretation maps presented at the same scales as our aeromagnetic images. We should also ensure at this stage that the geographic projection and datum information of our various datasets are well understood and can be presented in a uniform geographic framework. Where we have access to digital data and GIS software, our options in co-displaying the datasets become broader and this greatly enhances the integration process. For many interpreters, however, the use of hardcopy imagery, transparent overlays and light-tables remain the most practical approach to building an integrated interpretation.

In addition to the geological data and the aeromagnetic imagery, it is essential to have our aeromagnetic observation layer usable in the same formats. Where GIS software can be used, hand-drawn hardcopy observation maps can be scanned and co-registered with the geological information and our imagery. A key point is that the integration process is an amalgamation of observations from rocks, aerial photos and aeromagnetic images. The observation maps are the foundations or framework on which the interpretation will be built.

Hence, we will refer more to our aeromagnetic observation layer than to the individual data images during the integration process.

Having prepared our data and assembled our tools – be they GIS systems, hardcopy overlays and pens or both – we can commence the task of bringing the aeromagnetic data and geology together into one map.

7.5 DEALING WITH CONFLICTS

We have assessed the relative merits and limitations of the aeromagnetic and geological data, double-checked their geographical coordination and are now well prepared to integrate them. We should expect conflicts between the two data types to arise and be prepared to deal with these conflicts. Two common examples are:

a) a major contact between more magnetic and less magnetic rocks occurs in an area mapped as a single lithotype (Fig. 7.3). The likely explanation is that the lithology has a magnetic and non-magnetic phase and the difference is not obvious in hand specimen. Another possibility, of course, is that the magnetic contact is concealed by overlying non-magnetic rocks. Careful observations on hand specimen and/or thin section and magnetic susceptibility should resolve this;
b) a major geological contact is transgressed by a well-defined magnetic feature (Fig. 7.4). The likely explanation is that the magnetic feature occurs at some depth beneath the surface/near-surface geological contact. Another possibility is that the cause of the magnetic feature is very narrow or sporadic in its exposure and may not be easy to find at surface.

There are many other situations where the patterns observed in the two datasets do not agree. We make two important points here.

1. We should expect the aeromagnetic data to change, extend and improve our understanding of the geology. Hoping and expecting that it will fully agree with what we already 'know' is not a good way to approach the task of integration.
2. There is always an explanation for observed or perceived conflicts. An inability to readily find this explanation does not make either dataset 'right' or 'wrong'. The resolution of the conflict usually requires some field testing but may often simply lie in thinking harder and longer about both datasets.

In summary, it is necessary to have a sound appreciation of each dataset before commencing the integration. Using one dataset to simply supplement the other is not an appropriate way to achieve an effective integration. The resolution of conflicts between the two datasets is often the key to significantly enhancing the understanding of the geology.

7.6 TIME

One final aspect of planning should be mentioned – time. The compilation of our observation layer can be done rapidly, as it is a fairly direct and mechanical process. However, the time needed to digest and interpret the interrelationships between the aeromagnetic and geological data is usually substantially greater. There is no firm rule about the time required to interpret aeromagnetic data; clearly some datasets will be much simpler and more readily interpreted than others. As a guide from the experience of the authors, it is rare to be able to complete the preparation, observation and interpretation of any aeromagnetic survey inside a four- or five-day time frame. Taking five days as the minimum time required for a reasonably substantial interpretation, we should allow approximately one day of the interpreter's time for each 1000 line kilometres. In many cases, where in-depth structural analysis, computer modelling and field validation are part of the interpretation process, this time frame can expand markedly. It will rarely be done adequately in a shorter time frame.

Furthermore, the aeromagnetic data may have cost about $50 000–100 000 for a survey covering an area of around 1000 km^2. If you are the first person to interpret the data it makes no economic sense to spend only one or two days (equating to maybe 1–2% of the survey cost) interpreting it.

Like geological mapping and compilation, aeromagnetic interpretation should be conducted in solid blocks of time. The task is not suited to brief, part-time instalments.

7.7 WHERE TO START?

The starting point guidelines presented for the observation stage (Chapter 6) also broadly apply to the integration stage. Initially, address areas where the geology and the aeromagnetic data tend to reinforce one another. Work from these areas into areas of greater uncertainty or complexity. During the integration stage we will be more likely to skip from one small area to another to establish firm interpretations from which more speculative interpretations can be built. It is common to have a patchwork of 'solved' areas from which we must expand and extrapolate to complete our integration.

7.8 THE SOLID GEOLOGY LAYER – METHODOLOGY

Our first staging point in the integration/interpretation process is to compile a solid geology map. This will normally exclude superficial cover formations and may or may not include deeper, underlying geology such as concealed intrusive bodies. We aim to define lithological or stratigraphic polygons for our entire survey area and to delineate faults, fractures and trends on which a structural interpretation can be based. Although our ultimate aim is to develop an understanding of the 3-D geology and the nature and timing of geological history, we need to start by establishing one complete layer which includes rock type classifications as well as structures. Our solid geology layer will therefore define our interpretation of rock formation distribution in our survey area and the location and orientation of faults and fractures. In its initial stages, the solid geology layer will not normally show cross-sectional information or any interpretation of geological history.

Each area and each different aeromagnetic survey presents new challenges which require us to adapt our style of observation and interpretation. Hence, there is no set, rigid 'recipe' to guide the compilation of our solid geology layer. The following sequence of tasks will, in most cases, enable us to produce a suitable end product.

7.8.1 Resolve local areas

Map geological contacts and units that are clearly defined in the combined geological and aeromagnetic data. Figure 7.5 illustrates the delineation of the boundary of the strongly magnetic ultramafic package and the surrounding, more weakly magnetic (mainly mafic) units. There are other areas in Figure 7.5 where either the geology or the aeromagnetic observations provide a firm guide for the solid geology layer.

7.8.2 Interpolate between resolved areas

Figure 7.6 illustrates how our understanding of local areas expands into the lesser known areas.

7.8.3 Extrapolate into areas of sparse information or poor control

There will be areas which have little or no information and are not readily relatable to areas where some control is present. A strictly scientific approach may have us leave these areas blank, but in most cases it is preferable to extend our interpretation into the realm of educated guesswork using knowledge from neighbouring districts or similar terrains. The areas of no outcrop and minimal magnetic expression in the northern section of Figure 7.6 present this situation, and the educated guesswork needed to complete the solid geological picture is derived from data several kilometres along strike (see Chapter 12).

We may choose to highlight features which are particularly well defined and/or consistent. Portraying confidently interpreted features more boldly than those which are tenuous is an effective means of conveying the robustness of the interpretation to subsequent users of your interpretation.

7.8.4 Add faults and fractures

We sometimes leave the definition of faults and fractures until we are well advanced in delineating the polygons defining our lithostratigraphic units. The inferences we make when deciding 'which rocks are where' will greatly influence our interpretation of faults (with inferred displacements) and fractures (which have no displacement). However, where the faults and fractures represent a significant proportion of the boundaries of our units, it is appropriate to define them as we progress. Many of the pattern trends and

breaks that we record on our observation layer will become faults, fractures and contacts on our solid geology layer, but some may be disregarded as observations which lack geological credence or are superfluous in the presentation of our interpretation. Figure 7.7 shows several trend lines recorded on the observation layer that are not considered sufficiently relevant to warrant inclusion in the solid geology. Similarly, we have not included the clear internal detail evident in the patterns of magnetic rock units within the ultramafic sequence. In an interpretation of this area at a more detailed scale we may well choose to include these features, to show the finer-scale geological variations. What is and is not included in the solid geology is a matter of judgement for the interpreter; it will rely on considerations of scale, clarity of presentation and purpose of the interpretation.

7.8.5 Review, revise and simplify where necessary

Taking time to review the entire study area, considering the geological implications of your compilation and streamlining your interpretation, will add considerable value to your final product. It is common to come across inconsistencies or to recognise previously missed correlations of units and/or structures when we review our first-pass interpretation. Immediate review and revision of the initial map is common and prudent practice.

7.8.6 Highlight anomalies

Having compiled the solid geology layer, we should reconsider the aeromagnetic features identified as anomalous at the observation stage and consider aspects of our geological layer which might seem unusual. It is important to remember that during the processes of forming a coherent solid geology we may have overlooked local oddities. After checking for any oversights, anomalies should be documented and presented, particularly where the final products will be used by exploration groups. Figure 7.7 depicts an inferred 'alteration overprint', probably due to a tongue of granite intruding and/or underlying the partly exposed mafic unit. Reviewing Section 6.5, we recall that anomalies may take many forms and a concerted effort is required in data processing and observation to identify them. The ways that we portray these in our consolidated integration of geological mapping and our aeromagnetic observations may vary, but it is essential to make our record of anomalous or unusual features an obvious and accessible component of our final compilation.

7.9 WHAT NEXT?

The worked examples in Chapters 12, 13 and 14 provide an extensive guide to the range of situations encountered in the integration of geology and aeromagnetic data. The reader is encouraged to study the methodology illustrated in those chapters as a matter of priority.

We now face the most interesting and challenging part of the interpretation process. Building on our integrated 2-D solid geology, we can extend our analysis to the third dimension to create cross-sections then address the geological history and structural development of our survey area. While this stage of our work can be highly interpretive and speculative, it is the stage which requires us to critically examine and extend our observations to form a working geological model. In the context of exploration, this process is critical to the definition of 'target areas'.

Having compiled the solid geology as the second layer of our interpretation, we now look at subsequent layers which will focus on particular aspects of the geology such as structural style, structural history and exploration target areas.

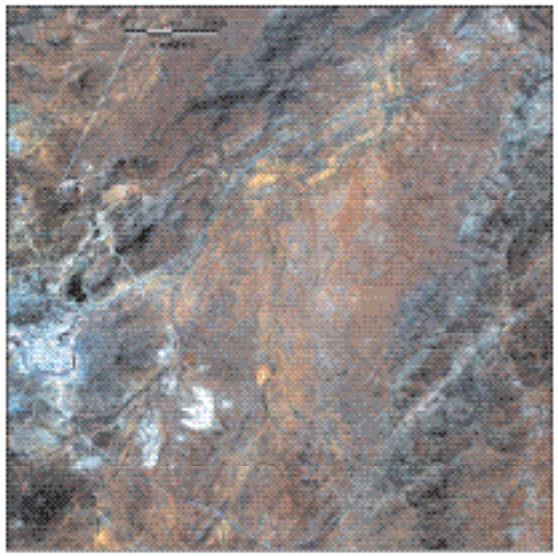

HyMap hyperspectral true colour ('pseudo aerial photo') image draped on a digital elevation model illuminated from the north-west, pixel resolution 6m.

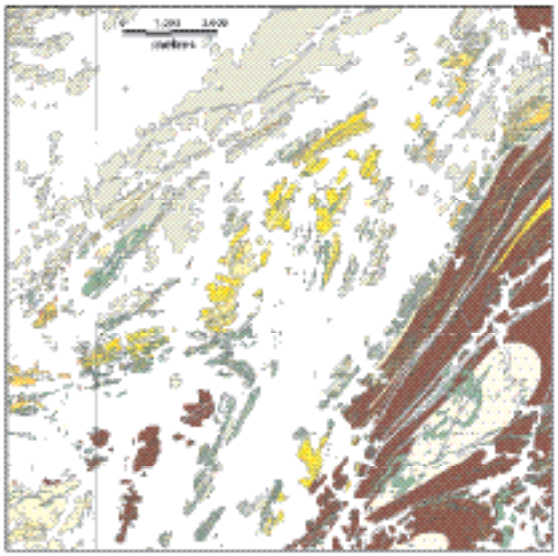

GSNSW 1:25,000 geological mapping, based on 1:12,500 aerial photography and field traverses.

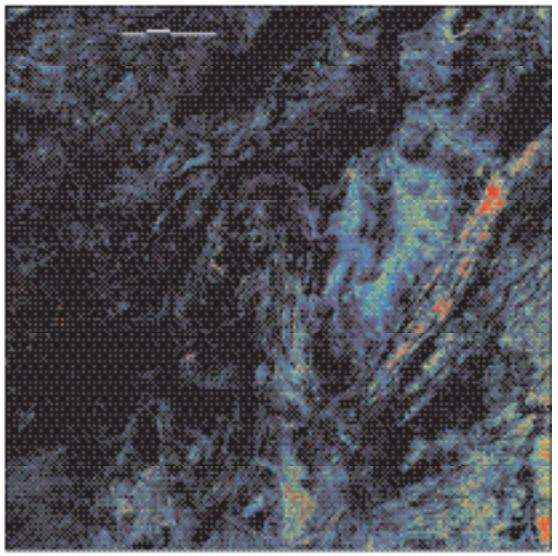

HyMap ferric iron content image.

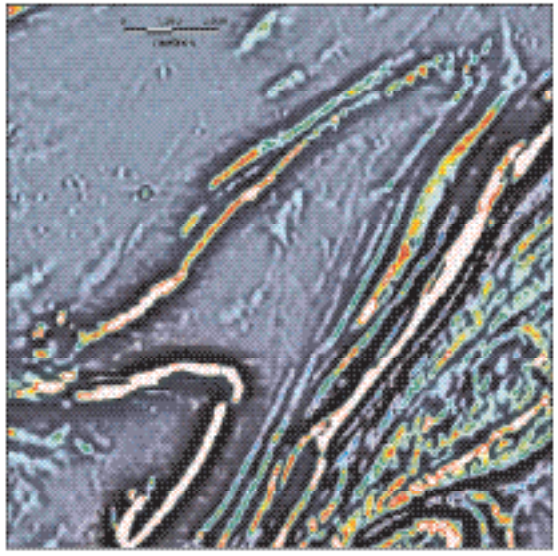

Composite aeromagnetic image from 100m (EW) line spacing survey, pixel resolution 25m.

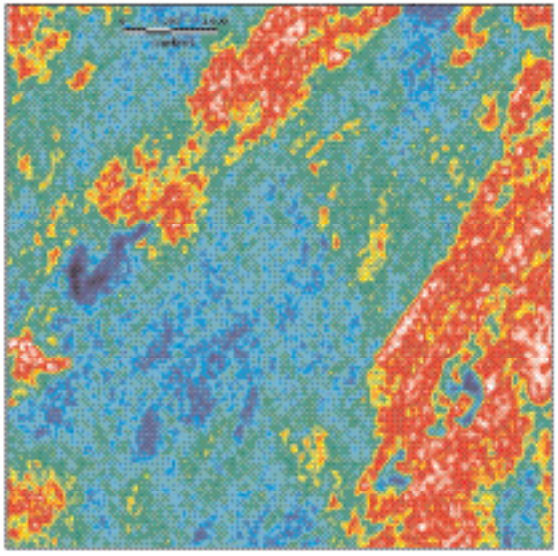

Potassium channel radiometric image from same survey as aeromagnetics.

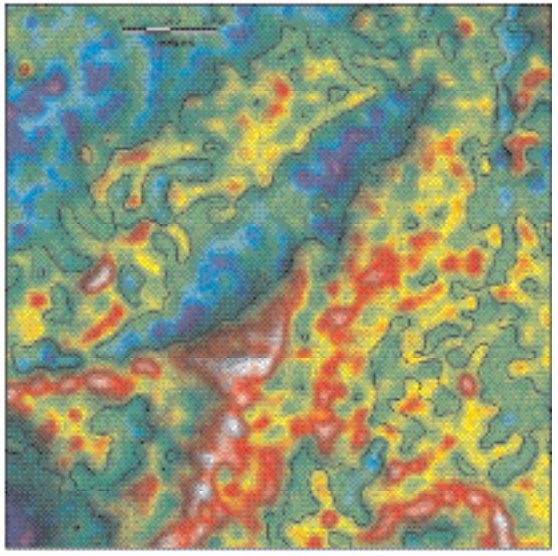

FALCON® AGG survey data, 200m line spacing, 60m pixel resolution

Figure 7.1: Remote sensing data from the Broken Hill district, NSW. All data sourced from Geological Survey of NSW.

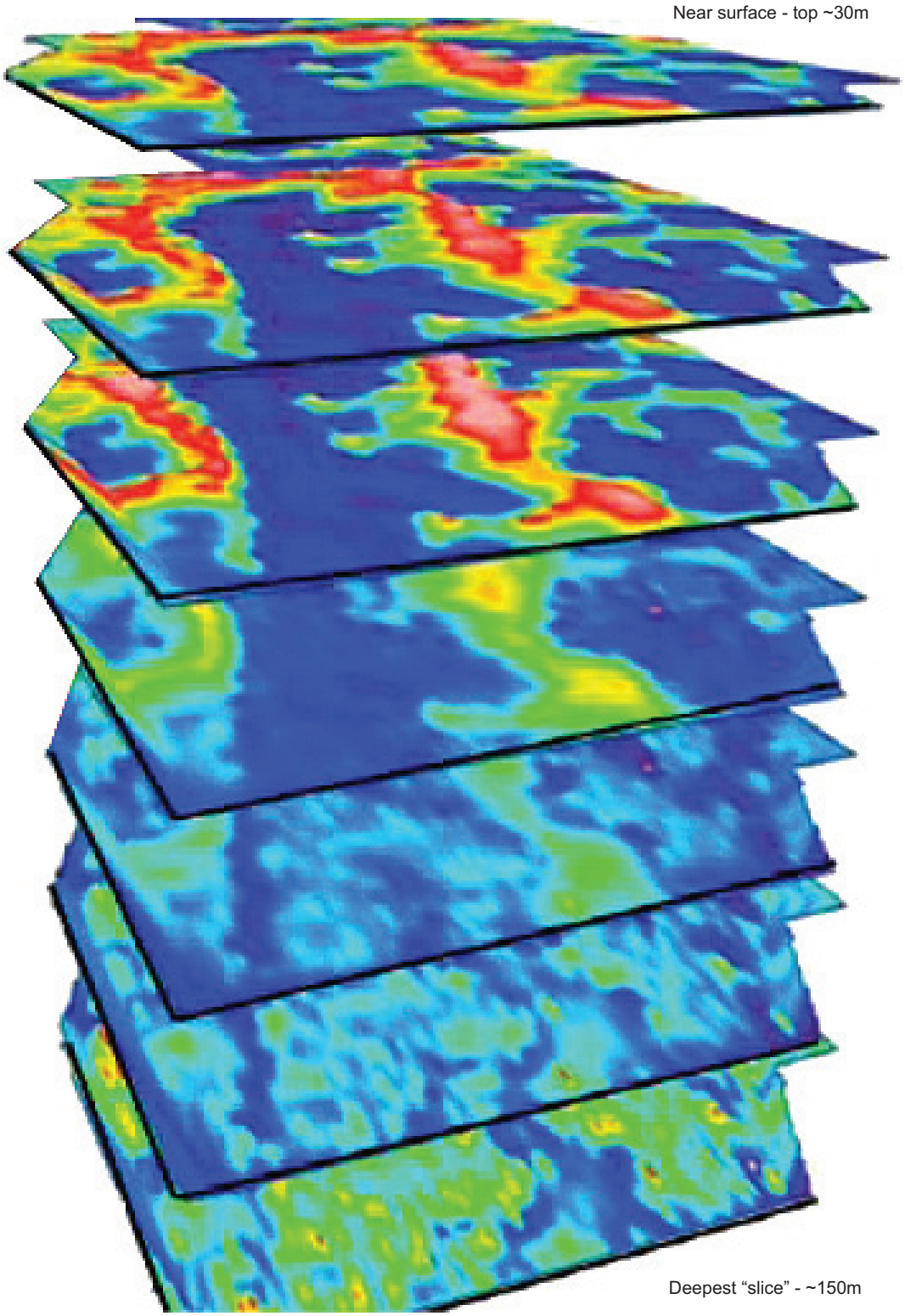

Figure 7.2: Stacked conductivity images corresponding to approximate depth increases (down). Image area is ~20 × 20 km. Hoistem helicopter-borne TEM data. From Boyd (2009).

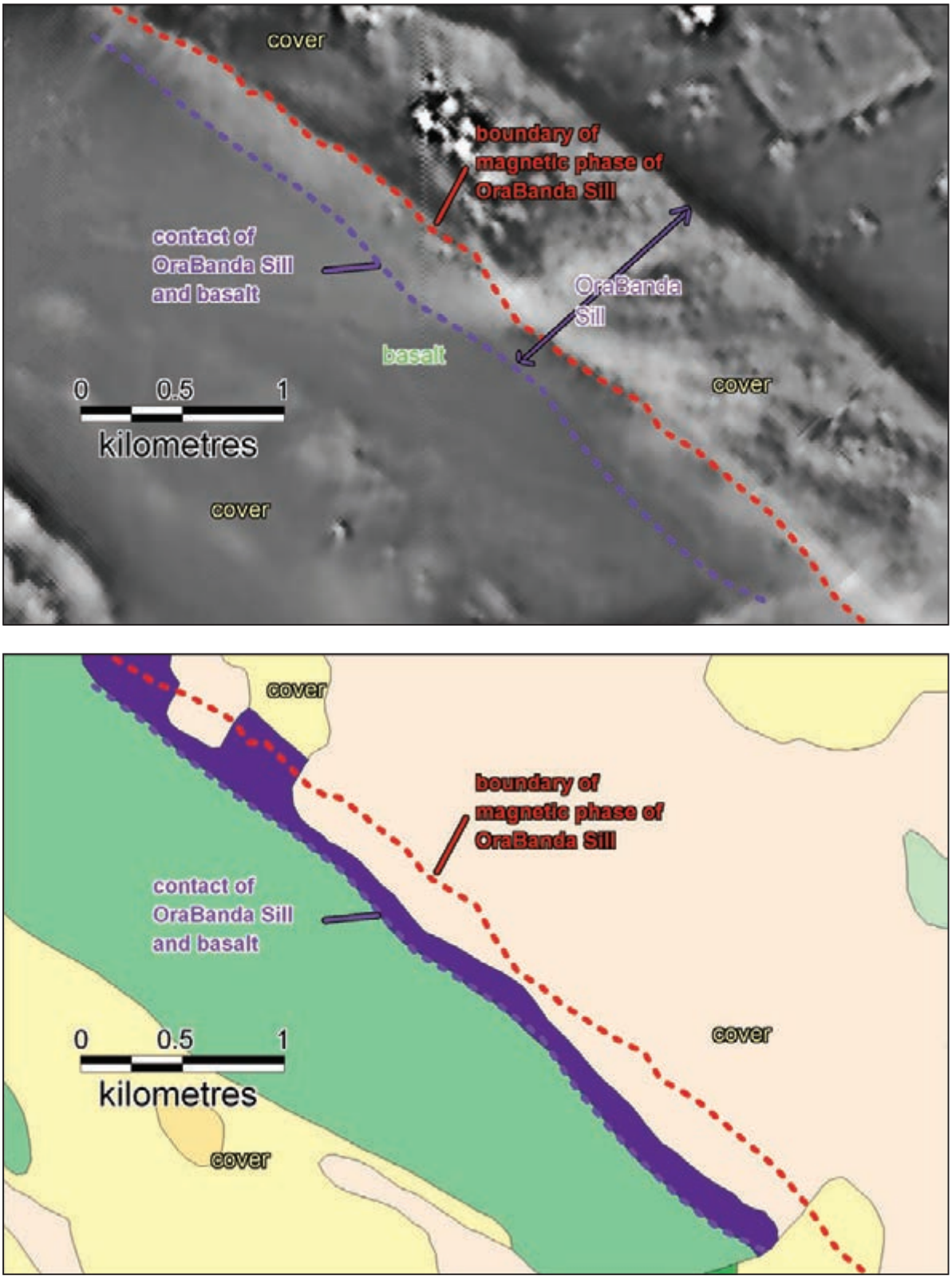

Figure 7.3: Aeromagnetic image and geology map from the Ora Banda area, WA. Note the non-magnetic phase of the Ora Banda Sill on its SW margin. Data from Geological Survey of WA open file records.

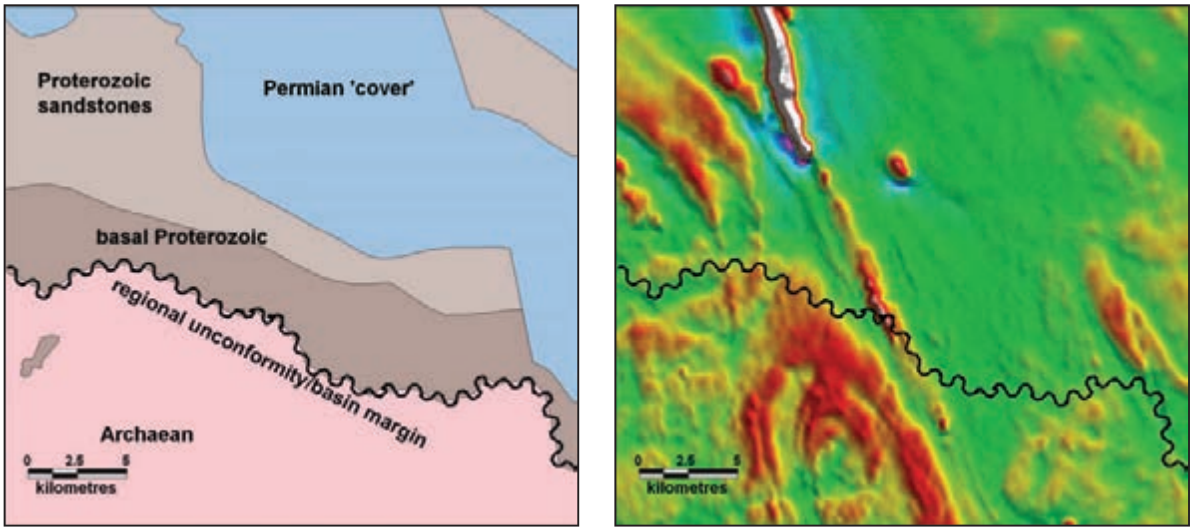

Figure 7.4: Aeromagnetic image and geology map from the Kingston area, WA. Note the magnetic unit transgressing the major stratigraphic boundary (and the way the Proterozoic and Permian outcrops seem to be controlled by an Archaean fault). Data from Geoscience Australia and Geological Survey of WA.

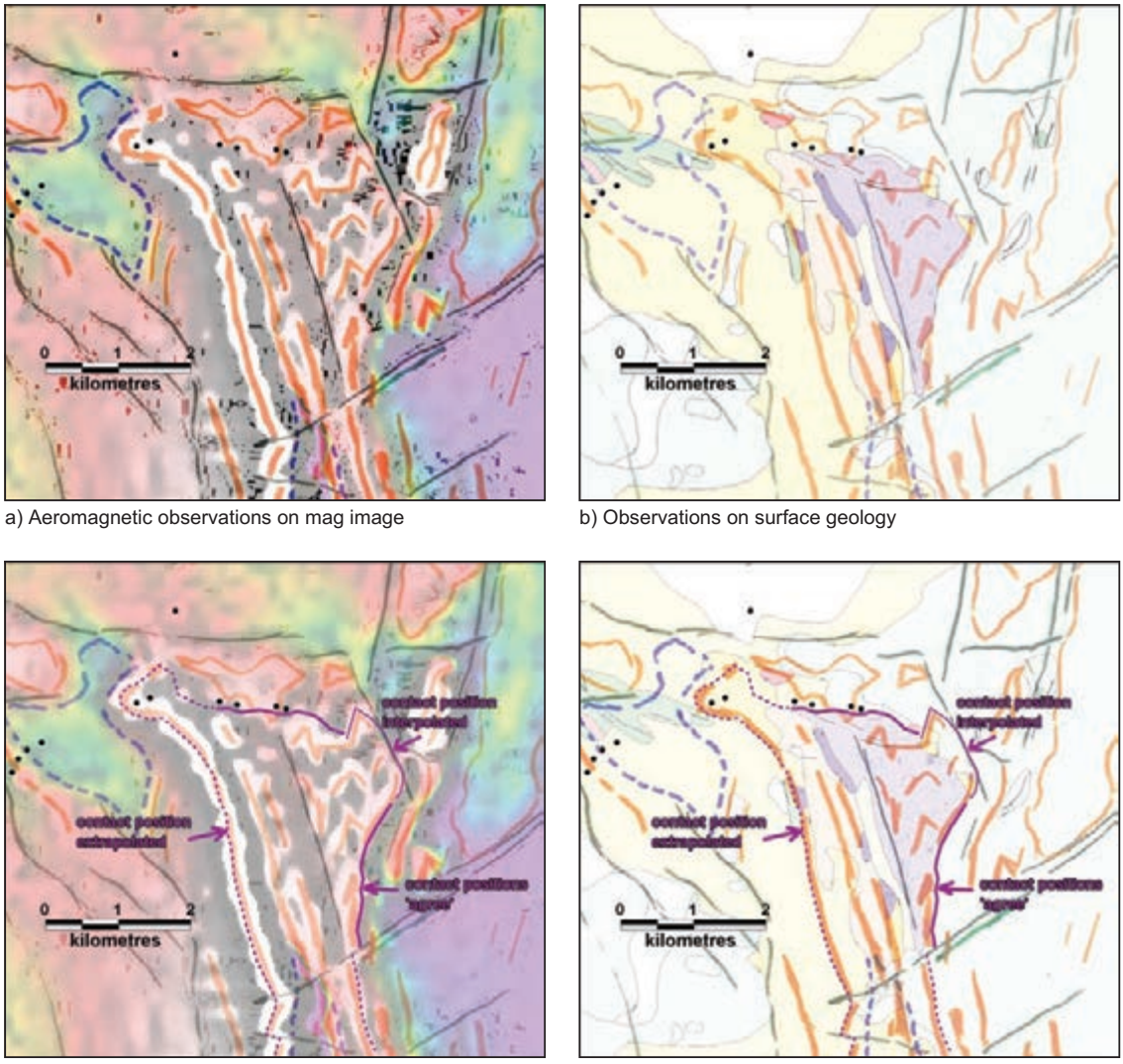

a) Aeromagnetic observations on mag image

b) Observations on surface geology

c) Boundary of ultramafic unit on aeromagnetic image

d) Boundary of ultramafic unit on surface geology

Figure 7.5: Illustration of the delineation of a lithological contact zone integrating mapped surface geology and aeromagnetics, Goongarrie District, WA. a) Aeromagnetic observations on mag image. b) Observations on surface geology. c) Boundary of ultramafic unit on mag image. d) Boundary of ultramafic unit on surface geology.

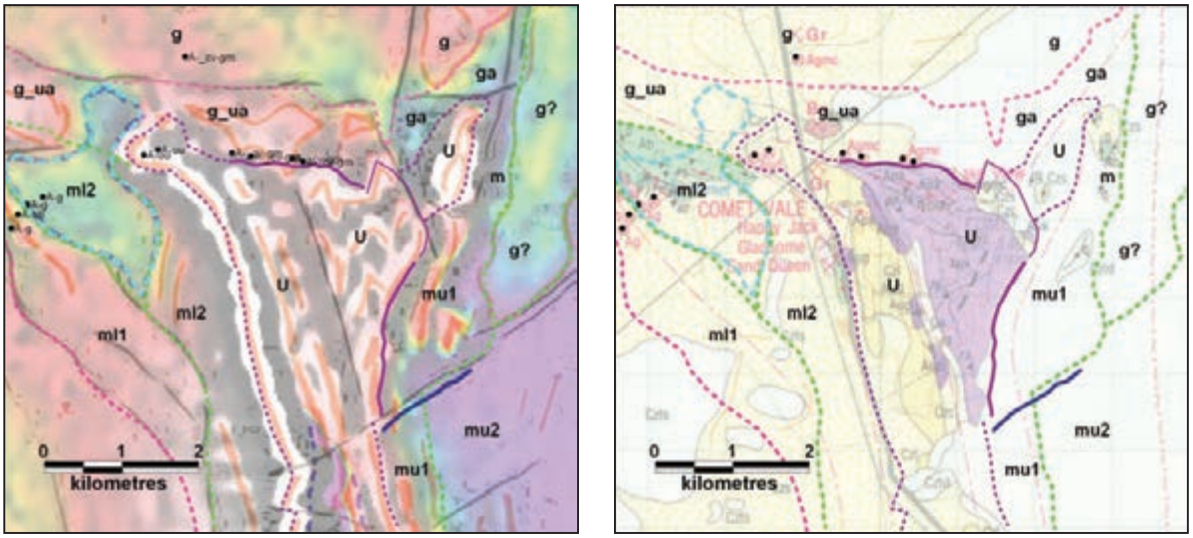

u-ultramafic sequence, ml-lower basalt sequence, mu-upper basalt sequence
g-granite, ga-altered/non magnetic granite, g_ua- mixed granite/ultramafic contact zone

Figure 7.6: Interpolation and extrapolation of surface mapping control using the aeromagnetics to define lithostratigraphic polygons. Note the use of the aeromag observation layer to pinpoint boundary locations. The pale blue outline defines a discordant magnetic low, overprinting the stratigraphic and structural trends.

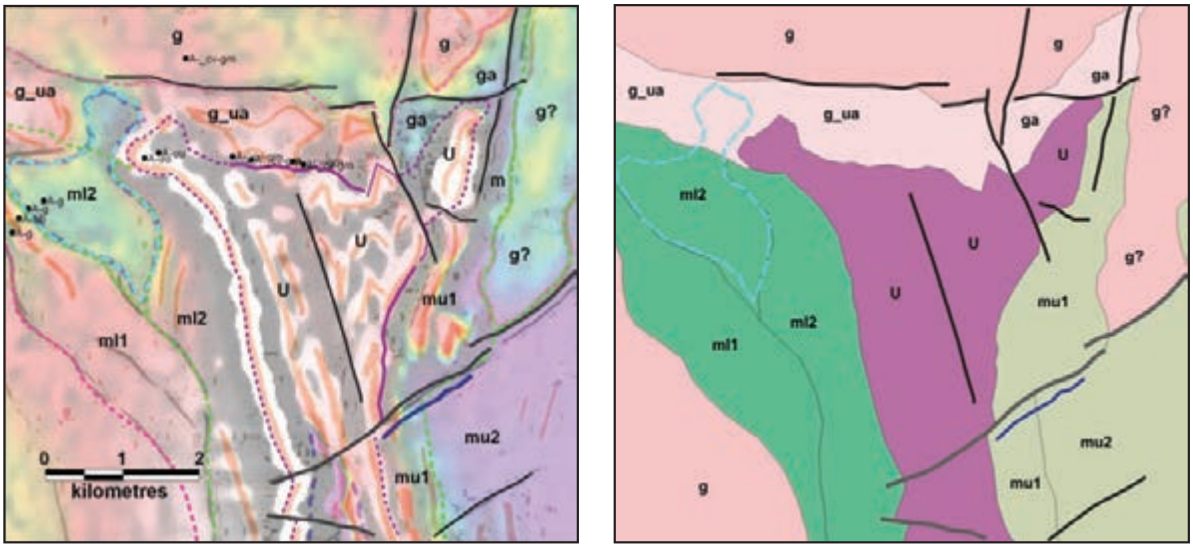

Figure 7.7: Final stages of basic solid geology map. Identified faults and fractures are added (thicker grey lines are faults with clear displacement) and the lithostratigraphic polygons are filled with appropriate colours. The pale blue alteration overprint is shown as an anomalous feature.

8 Quantitative techniques and their role in interpretation

8.1 INTRODUCTION

There are many numerical techniques which have the potential to greatly enhance our aeromagnetic interpretation by quantifying the depths, shapes, orientations and magnetic properties of rock units. These techniques are best applied to provide specific information on local areas of interest, the prime example being the location, depth and orientation of a magnetic rock unit which is to be drill tested. The exceptions are the 'depth-to-basement' schemes which are often applied to determine overburden cover thickness in mineral exploration, and in sedimentary basin studies to aid in the delineation of deep basin architecture. It is important to recognise that all these techniques are subject to the limitations of the survey data collection specifications and instrument resolution. Clever numerical schemes will not compensate for wide line spacing and will not enable us to resolve fine-scale geometric detail when our magnetic sources are deep. We normally apply these quantitative techniques during the mid stages of the interpretation process when we are seeking to answer specific questions raised by our qualitative analysis, and during compilation of the solid geology layer.

The reader is referred to Nabighian *et al*. (2005) for a comprehensive account of the progression of quantitative analysis of aeromagnetic data, to Oldenburg and Pratt (2007) for a summary of modern modelling and inversion techniques, and to Gunn (1997a) for a summary and critique of depth computation schemes.

8.2 FORWARD MODELLING

The simplest of the quantitative techniques is forward modelling, where we calculate the magnetic response of a rock body that has an idealised shape and generalised magnetic properties. Forward modelling has two forms. The simpler form involves computation of the magnetic response of an idealised geological situation in order to test a concept, explore resolution sensitivities or assist in survey planning. Almost all modelling software packages facilitate this option but one in particular, 'Noddy', is specifically designed to allow creation of both simple and highly complex geological configurations and exploration of their magnetic (and gravity) responses in some detail. A very instructive compilation of Noddy models can be found in Jessell (2002). The other form of forward modelling involves generating model data to fit measured survey data and thereby make inferences on the nature of the geological bodies causing these measured magnetic responses. This is a manual, iterative process whereby we progressively adjust the shape, depth, orientation and magnetic properties, based on comparison of measured and model data, until the model calculation matches the measured data over the feature of interest. Although it is a trial and error process, adept users of forward modelling

software can normally match the model to measured data for a single, simple anomaly profile in a matter of minutes. Models can be constructed using simple geometric shapes such as rectangular prisms and ellipsoids, or using irregular shapes which may be 2-D (i.e. irregular in section but unchanging along strike), 2 1/2-D (as for 2-D but with finite strike length) or 3-D (irregular in all dimensions). The time needed to define model parameters, compute models and compare with measured data increases significantly with the complexity of the model. This is particularly true where the modelling involves multiple bodies, and the matching of computed and measured data is to be achieved on multiple profiles or on a grid.

A good example of the application of simple and quick modelling is where a depth and dip is required for a narrow, linear magnetic rock unit (Fig. 8.1). The depth (to top) inferred from this model should be within 20% of the actual depth and the dip, subject to the assumption of induced magnetisation, should also be better than ±20%. These uncertainties increase when the depth to source is in the order of kilometres because our ability to recognise the likely shape of the magnetic rock unit becomes poorer. The principal criterion in proposing models is that their shapes be geologically reasonable. An important secondary consideration is that the *simplest* (geologically reasonable) shape which fits the data well, is likely to be the best starting point for understanding the source of the magnetic feature. At this point it is worthwhile reviewing the resolution and ambiguity matters discussed in Chapter 2. It is sobering to remember that even when we achieve a perfect match between the measured and calculated data, parameters such as width, dip and magnetisation cannot be uniquely determined. By contrast, in most cases, the depth to the top for a body of simple shape should be quite well constrained. Exceptions to this rule include rounded geological features that have not been truncated by an unconformity surface or fault, such as ellipsoidal ironstone bodies and granites. These features without sharp edges can produce excellent agreement between measured and model data with depths (to top surface) that are falsely shallow.

It is advisable to compute a range of models that fit the measured data. In simple terms, aiming to produce a 'shallowest possible', a 'deepest possible' and a 'preferred' model will keep the modelling in a sensible perspective. Wherever possible, we should apply constraints on model parameters. In some cases we may have direct observations from mapping or drill hole data that can be used in the forward model calculations, in other cases we can apply reasonable assumptions concerning the shape and the magnetic properties that allow us to narrow the range of acceptable models.

Magnetic properties of rocks are of particular concern. We saw in Chapter 2 that the less common forms of magnetisation can add much complication to the task of modelling and that, without control from direct measurements, our abilities to confidently determine dip and width are seriously compromised. Even when we do have direct measurements of magnetic rock properties, it is rare for these to provide a representative sample for the entire rock body. The volume of rock that we typically sample is minuscule compared to the volume of the entire magnetic body and very often our measurements are taken at or close to the surface where weathering processes are active and may affect the rock properties. In addition, the assumption that magnetic properties will be uniform throughout a rock body is often inappropriate. In particular, once the horizontal dimension of the magnetic rock body is less than its depth of burial, the impact of local variability in magnetic properties is virtually undetectable.

The process of magnetic modelling is rarely straightforward and robust. However, if we recognise the limitations and apply sensible constraints and assumptions, modelling can add significant value to our interpretation. The key to the effective use of modelling is to clearly define the information that is sought from the model and focus our attention on the smallest number of variables needed to deliver that information. The cautionary tone above will give the reader some insight into the hazards of embarking on the modelling of complex shapes and multiple bodies. This is by no means meant to discourage enthusiastic interpreters from extending and testing their qualitative work with computer modelling. The critical matter is the effective use of the interpreter's time. Complex modelling will consume significant amounts of time and brain activity. The interpreter should therefore have a clear view of the desired outcome before embarking on this task.

Figure 8.2 illustrates a typical, modern example of forward modelling and illustrates the level of complexity that can be resolved from careful and considered quantitative analysis. The Amadeus Basin interpretation case study in Chapter 13 gives a fuller illustration of the role of modelling and depth determination in aeromagnetic interpretation.

8.3 INVERSION

The numerical schemes used to calculate the magnetic response of rock bodies may be adapted to automate and optimise the trial and error approach used in forward modelling. Inversion schemes begin with some form of starting model and make adjustments to the model parameters based on the numerical comparison of computed and observed data. The inversion culminates when a desired match between observed and computed data is reached. This match is quantified as a minimum point in the sum of the point-to-point differences. This sum is normally the square root of the sum of the squares of the differences. As illustrated in Figure 8.3, there can be a wide field of numerically achievable solutions and those that best match the data may not adequately match the known or inferred geology. The most appropriate model is one which strikes a balance between the geological model style and the data. Once again, it is prudent to consider a range of solutions rather than attempt to fix on a single 'best' solution.

While these schemes can save the interpreter time, they are most effective when, as with forward modelling, we take the time to incorporate geological and petrophysical constraints. Without some degree of control and intervention by the interpreter, inversion results can be geologically meaningless.

As with forward modelling, focusing the inversion on a small, specific area to investigate a well-defined proposition will lead to the most useful outcomes. It is unwise to expect that an inversion will be able to provide realistic geometry over broad areas with complex assemblages of magnetic rock units. Inversion schemes are very well suited to modelling single magnetic anomalies or local anomaly complexes at depth to provide guidance for drill testing. It is important to remember, however, that the limitations of resolution and ambiguity apply equally to all forms of numerical magnetic modelling.

Figure 8.4 illustrates two typical magnetic inversions taken from Oldenburg and Pratt (2007) and this reference provides an excellent outline of current practice in numerical modelling and inversion.

8.4 MODELLING AND INVERSION IN THE PRESENCE OF COMPLEX MAGNETISATION

Chapter 3 introduced the difficulties encountered in quantitative interpretation when rocks have significant components of remanence, self-demagnetisation or anisotropy of magnetisation. We emphasised the ambiguity relating to the orientation of the rock body and the orientation of its magnetisation. In essence, without some knowledge of one of these parameters the other cannot be determined with confidence. As illustrated in the example of Figure 3.31, drill-hole location and orientation may be radically inappropriate if the potential effects of complex magnetisation are overlooked. This is an increasingly serious problem as exploration under cover, often seeking blind targets many hundreds of metres deep, becomes commonplace.

Recent (and not so recent) research into this problem has resulted in the development of strategies to resolve the total magnetisation vector and thereby reduce the above orientation ambiguity. The concept of magnetic moment analysis (e.g. as applied in Schmidt and Clark 1998) provides some control on the total magnetisation vector and allows the process of trial and error modelling or inversion to proceed within workable constraints. Pratt *et al*. (2012) demonstrate that the remanence direction can be determined on single, simple anomalies by judicious application of inversion and introduce the concept of a defining a departure angle of the resultant total magnetisation from that of the inducing field. Foss and McKenzie (2009) present an effective staged inversion approach that yields both magnetisation and body geometry. Figure 8.5 illustrates this approach where the target rock unit has both complex geometry and complex magnetisation. We paraphrase the narrative from Foss and McKenzie (2009) below:

> *Figure* [8.5] *shows the results of inversion of an isolated, complex anomaly … We digitised a starting model to the TMI and analytic signal images and inverted the TMI data to obtain estimates of depth and magnetisation. We subsequently freed the vertex locations so that the inversion could also reshape the body. The estimated magnetisation direction remained stable during these inversions. By monitoring the progress of the inversions we realised that the sheet body could not explain the sharp negative at the north, and added a steeply-dipping cylinder with identical resultant magnetisation direction. This model explains the anomaly closely as shown in figure* [8.5]. *The pipe component of the model consistently positioned at shallower depth than the sheet … and we interpret it as a flow or sill fed from the pipe body … We believe that this inversion recovered both an acceptable resultant magnetisation direction and a feasible geological source model.*

This gives excellent insight into the interaction of the interpreter with the software, and the integration of geological and geophysical inputs into the solution of a challenging modelling task.

The specific situation of self-demagnetisation (SDM) presents different problems from those caused by remanence, since the SDM effect is a function of magnetic susceptibility and body shape. Strong SDM effects can therefore occur where remanence is absent.

All magnetic bodies have some SDM but this rarely impacts on the approximations of magnetisation direction being parallel to the Earth's field, and magnetisation strength being $\boldsymbol{k}$H as presented in Chapter 2. For bodies with high magnetic mineral concentrations (> ~3%, $\boldsymbol{k}$ > ~0.1 SI), and particularly narrow bodies with sharp edges, the effect of SDM on the orientation of the total magnetisation can be significant. This will adversely affect the results of modelling and inversion, the most common problem being erroneous inference of body dips and plunges as illustrated in the Trough Tank example (see Section 3.4.2). Approximate correction schemes for SDM have been in place since the 1960s and are incorporated into most modern modelling software, but recent research by Hillan and Foss (2012) provides scope for a more rigorous approach to the problem, including the modelling of multiple bodies.

8.5 DEPTH DETERMINATIONS

Where the rocks of interest in our survey area are not exposed, depth estimation is an important component of our interpretation. We saw in Chapter 2 that simple graphical constructions applied to profile plots could provide useful ball-park depth estimates; where better precision is required, the forward modelling and inversion schemes discussed above should fulfil this role. Where large numbers of depth determinations are necessary, it becomes time-consuming to use modelling and inversion; a separate type of numerical analysis has been developed to deal with these situations. These are loosely called 'depth-to-basement' methods. Their common characteristics are that they yield depth solutions wherever significant magnetic field variations occur and they rely on simple assumptions of magnetic rock body geometry. Gunn (1997b) briefly describes and critiques the different approaches to automatic depth computation. Shi (1993) provides a more comprehensive review of depth-to-basement methods. All the depth-to-basement methods require interpreter input to define constraints on solutions and all have the ability to produce misleading or meaningless results if they are not appropriately constrained.

Naudy's profile-based curve matching technique (Naudy 1971) is one of the more robust automated depth-to-basement schemes. A refinement of Naudy's method, called 'AUTOMAG' (Shi and Boyd 1993), has been implemented by Encom Technology (now Pitney Bowes Software Inc.) in the ModelVision Pro™ software package. AUTOMAG operates on profile data and utilises interpreter interaction as well as inversion methodology. It bridges the gap between automated depth to magnetic source methods and pure interactive modelling, thereby facilitating a high degree of interpreter input and control on depth to magnetic source calculations. The end result is an ensemble of simple bodies with well-determined depths to top, and a match between measured and model data along each line (Fig. 8.6). An expanded example of the application of AUTOMAG is presented in the sedimentary basin case study in Chapter 13.

8.6 WORMING

Worming is a numerical technique which attempts to trace magnetic body edges as they increase in depth. It is frequently applied to gravity data as well as aeromagnetic data. It is based on the use of upward continuation (see Chapter 4) and the expectation that body edges with larger dimensions will retain a stronger expression than more localised sources when viewed from a distance. It is most commonly used in broad-scale structural analysis as illustrated in Figure 8.7 from Poudjom Djomani *et al.* (2007). Musgrave *et al.* (2007) further discuss the effective application of worming and illustrate the integration of the technique with conventional potential field modelling and 3-D geological analysis.

8.7 SUMMARY

Quantitative techniques allow us to introduce some rigour into the third dimension in our interpretation. There is a range of tools available and each has its strengths and weaknesses. In all cases, these techniques provide best value after we have given due consideration to the qualitative aspects of observation, solid geology and structural analysis. With clear definition of the desired quantitative outcome, combined with the application of appropriate constraints, robust and extremely enlightening results can be obtained. The key ingredient is informed interpreter input. If we take the time to incorporate our best available geological, geophysical and petrophysical knowledge, and constrain the exercise to focus on a specific problem or area, quantitative techniques will add substantial value to our interpretation.

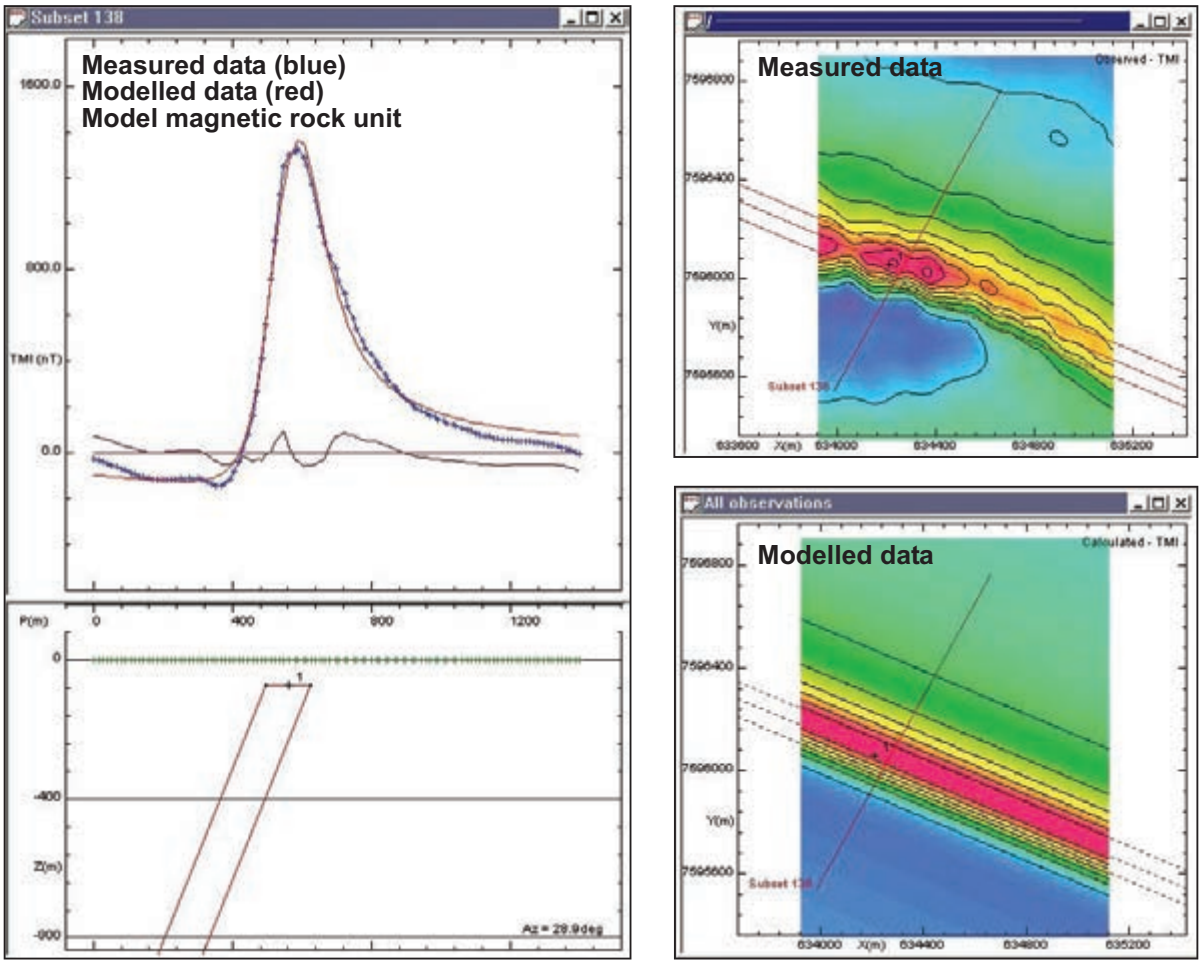

Figure 8.1: Simple but effective forward modelling of a single magnetic body. This type of modelling is appropriate for defining drill-hole locations to test isolated, single magnetic anomalies. Model courtesy Richard Almond, using Potent software, Geophysical Software Solutions.

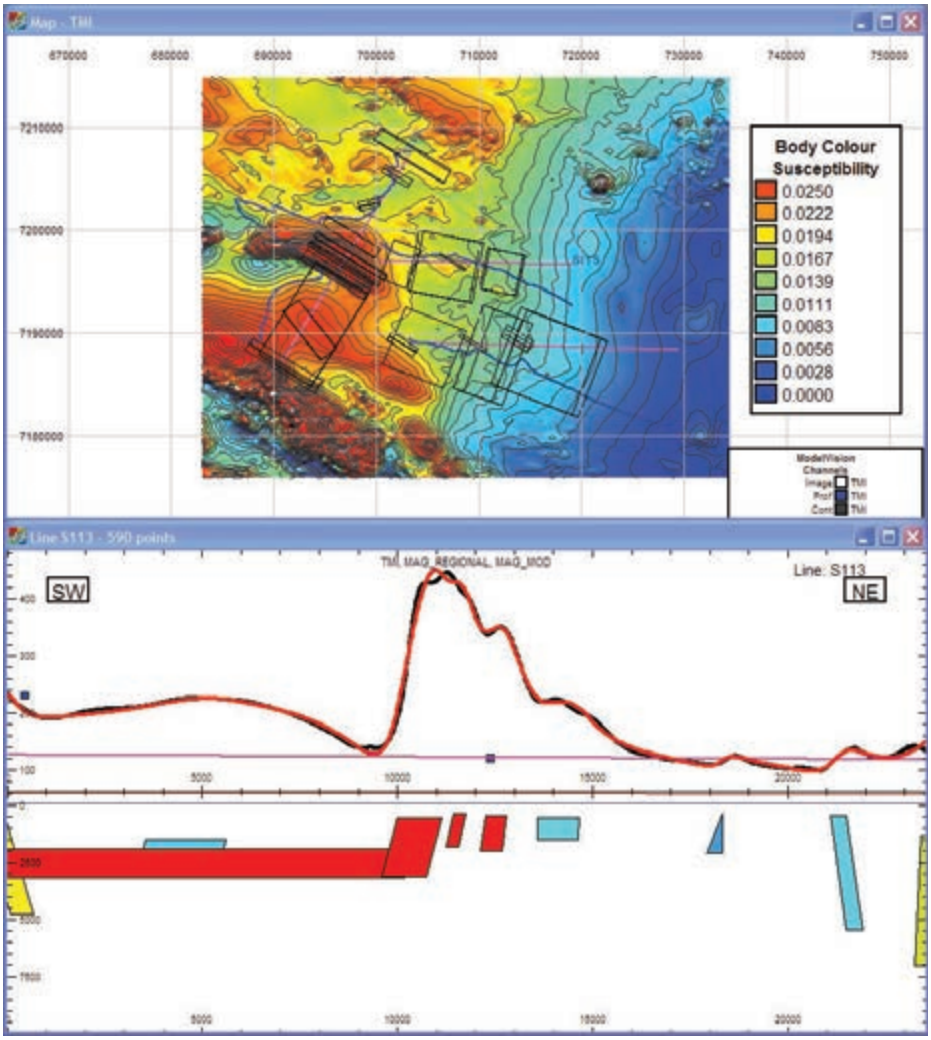

Figure 8.2: Multi-body forward model. Modelling by Zhiqun Shi using Model Vision Pro™ software. See Chapter 13 for an expanded account of this modelling.

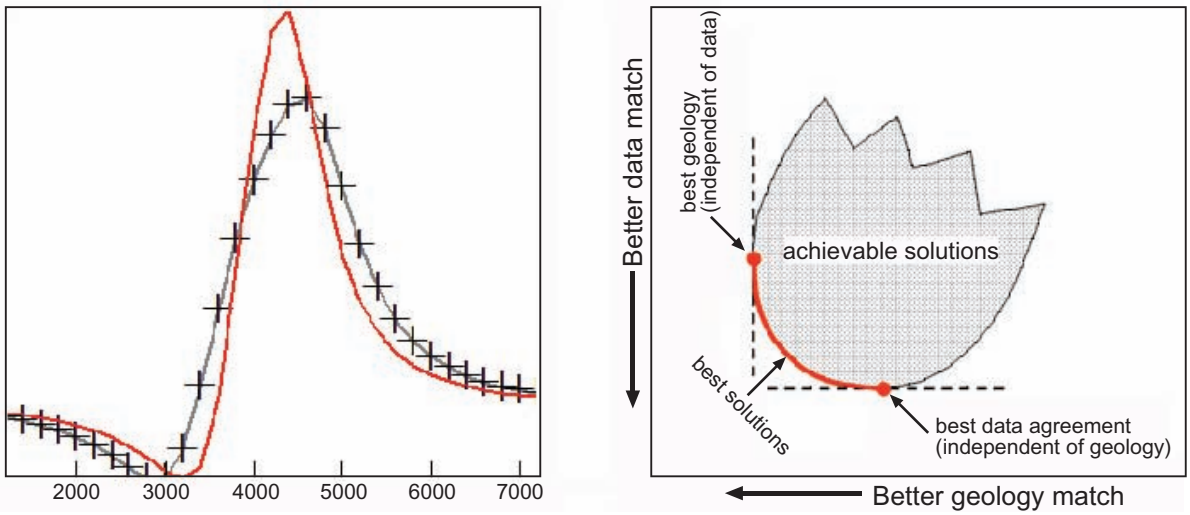

Figure 8.3: Illustration of inversion principles. At each iteration, parameter adjustments are made based on the mismatch between measured (crosses) and model data (red line). This proceeds until the sum of the squares of the differences reaches an acceptable minimum. The achievable solutions field in the right-hand graphic represents numerically acceptable minima in the sum of the squares of the differences. The 'best' solutions are where there is a balance between the closeness of the data match and adherence to geological constraints. Figure from Oldenburg and Pratt (2007).

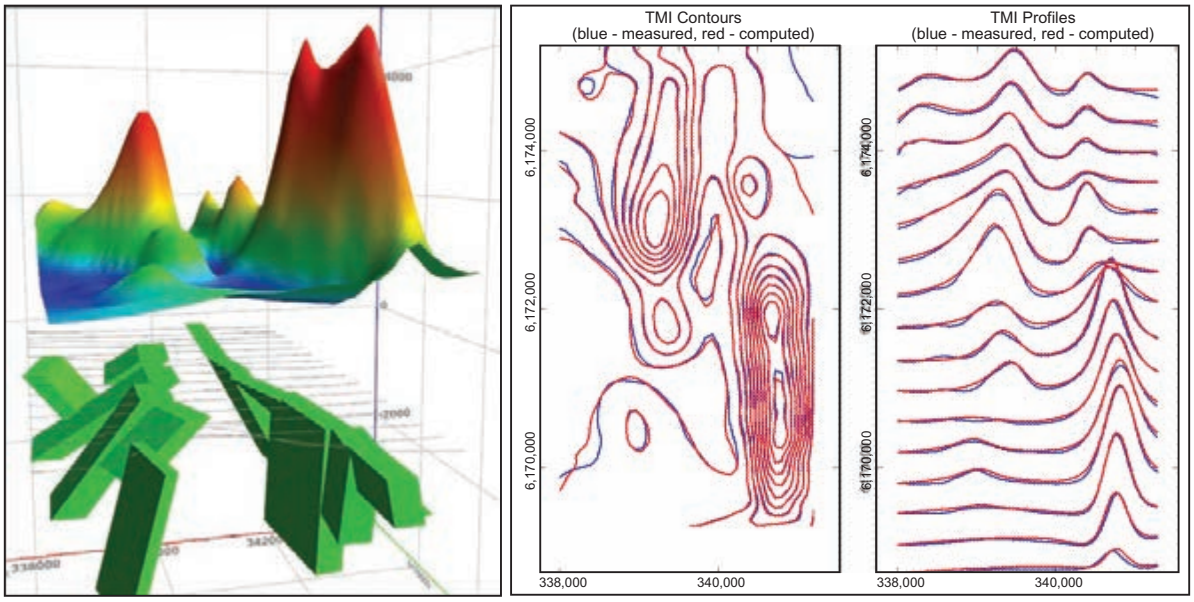

Multibody, multi-anomaly inversion using set body shapes. Each body has uniform (but not the same) magnetisation

Magnetic Image

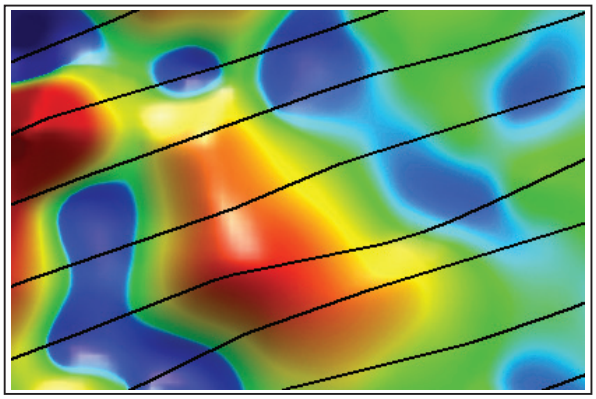

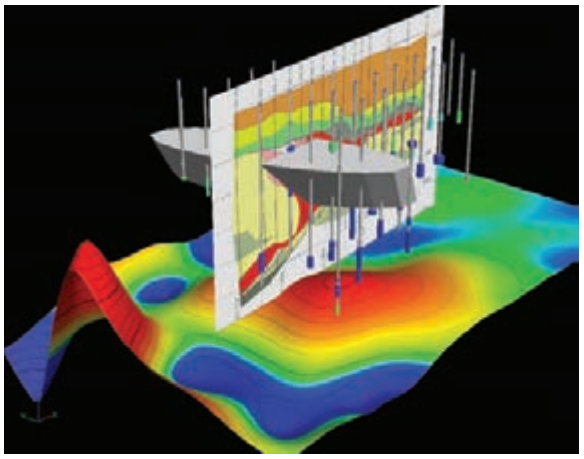

Single anomaly, 'expert system' inversion incorporating geological and petrophysical constraints and using a flexible body shape (frustum)

Figure 8.4: Inversion examples (Oldenburg and Pratt 2007).

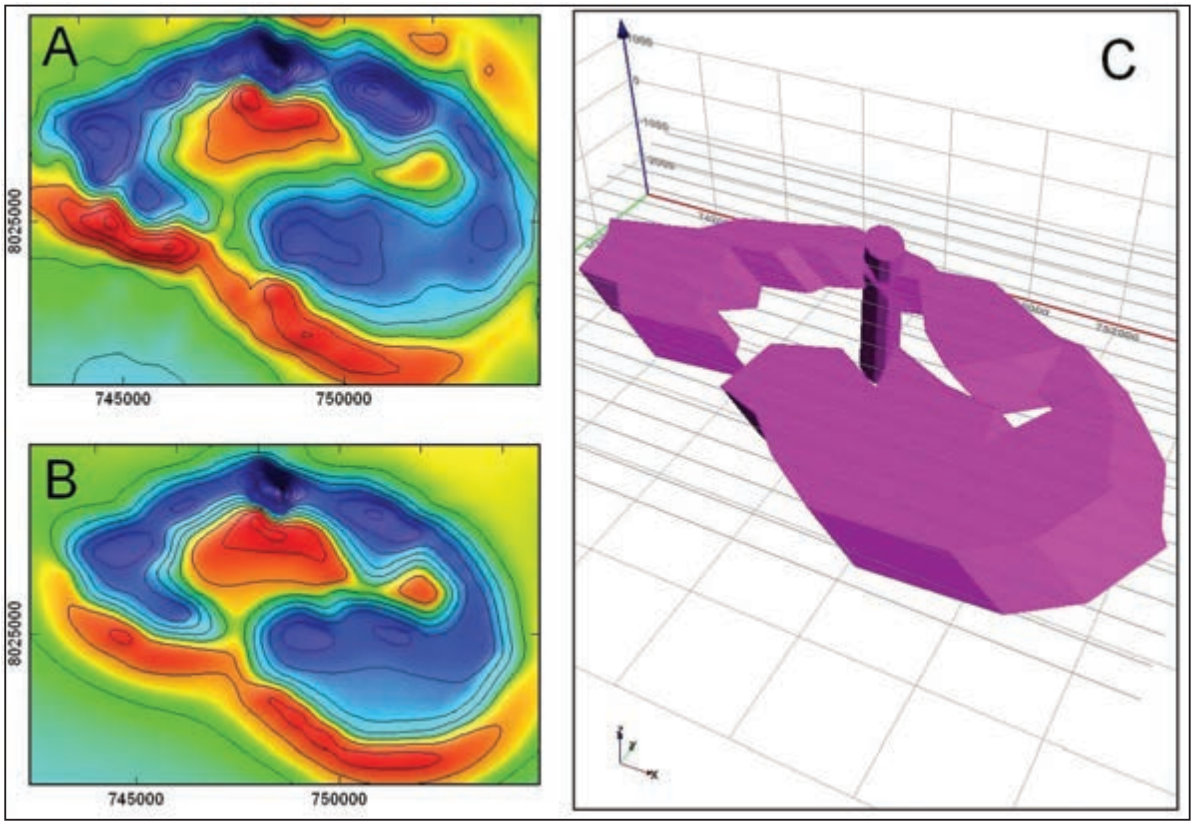

Figure 8.5: Inversion of a multi-component magnetic rock unit from the Newcastle Range volcanics in the Georgetown area, NW Qld (Foss and McKenzie 2009). A is the measured TMI, B is the model TMI and C shows the model. The inversion sequence is described in the text.

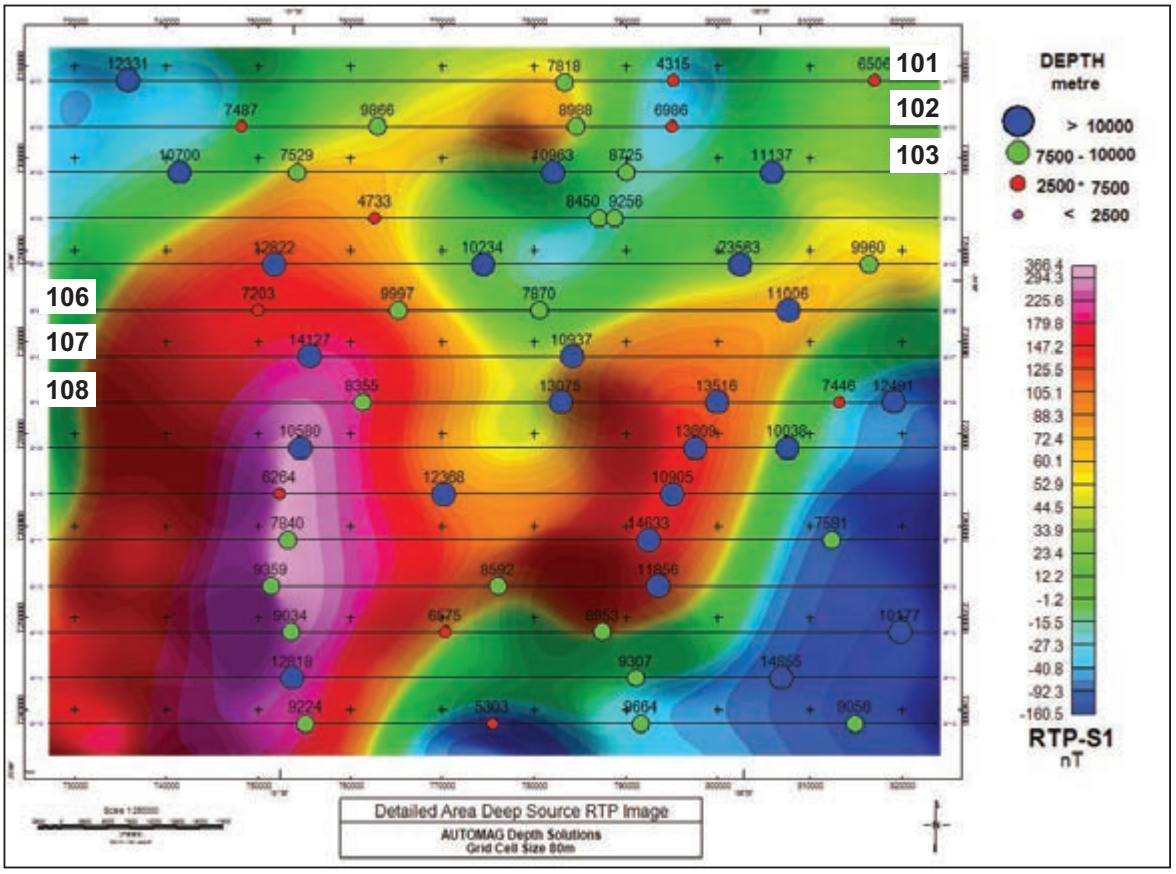

Solutions displayed on RTP data

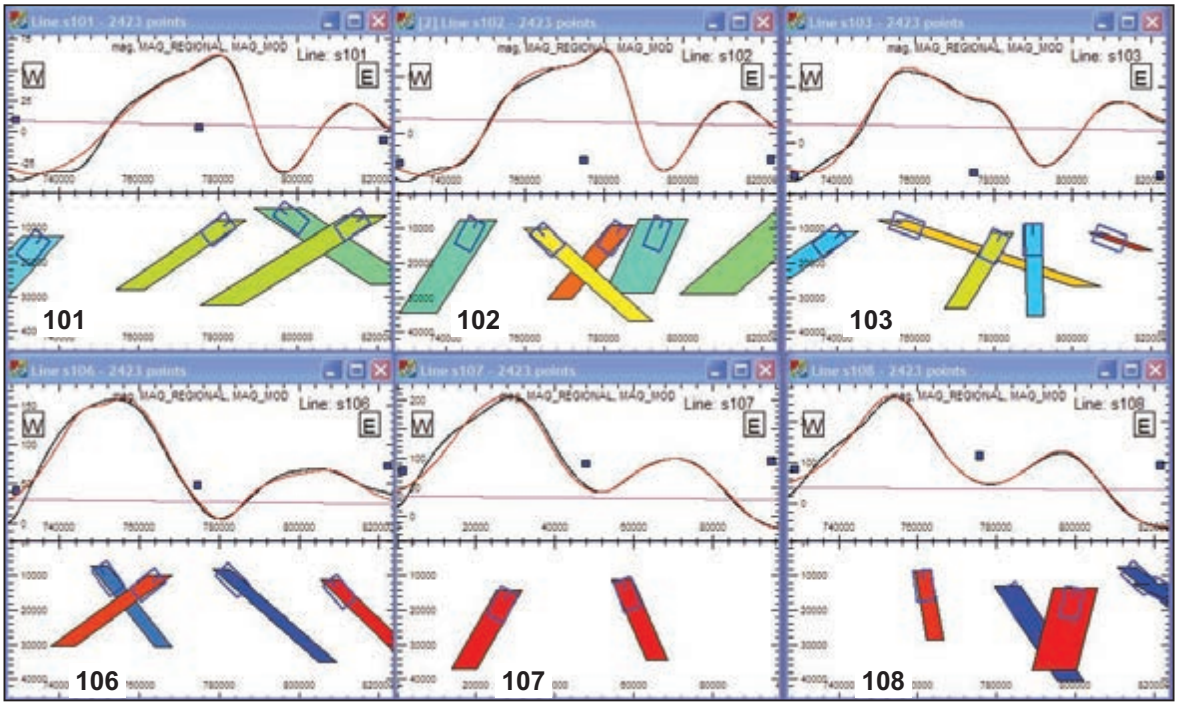

Line-by-line inversion results showing models and measured/model data comparisons.

Figure 8.6: Example of AUTOMAG application, Amadeus Basin, NT (see Chapter 13). AUTOMAG analysis by Zhiqun Shi using ModelVisionPro™.

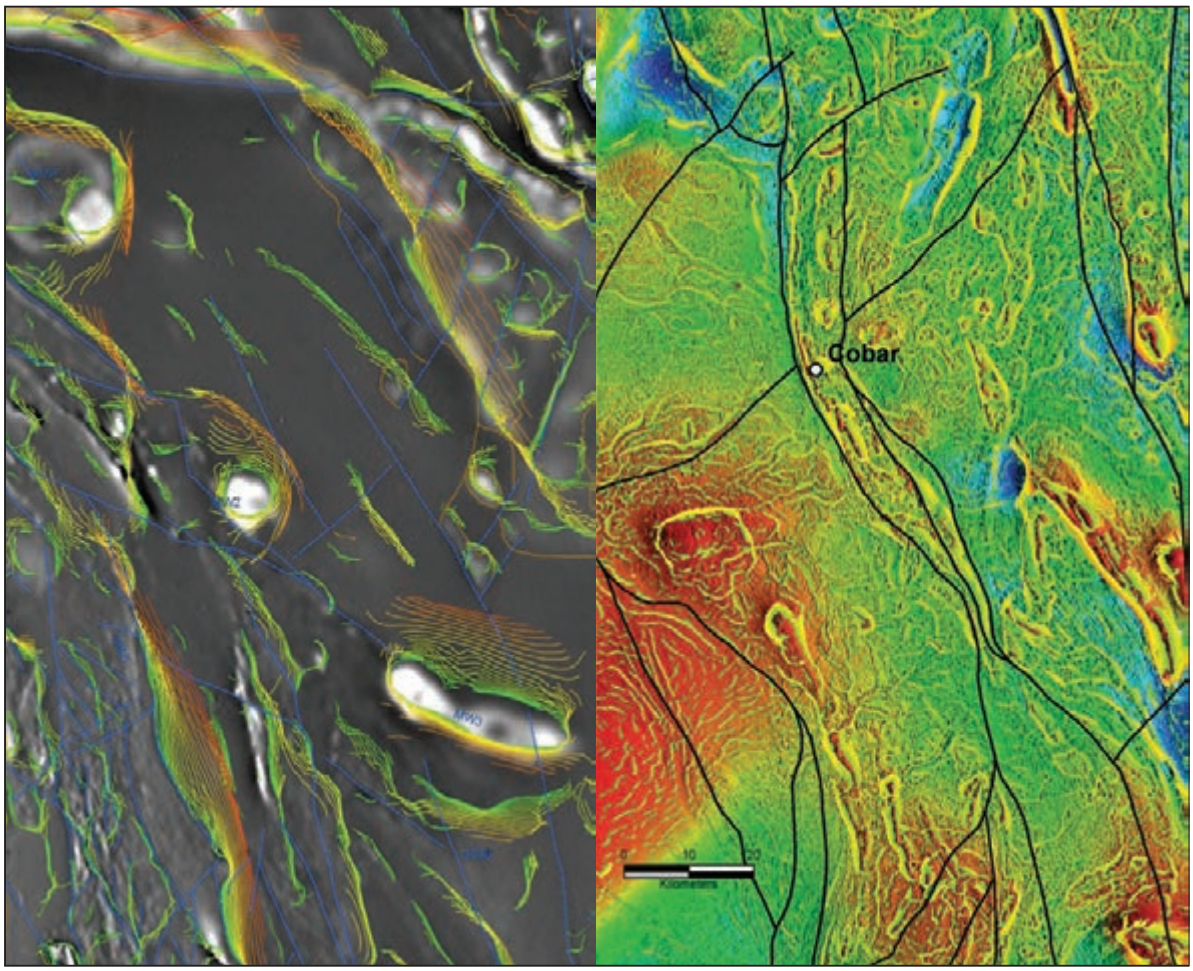

Figure 8.7: Illustrations of the worming technique applied to aeromagnetics in western NSW. The left-side panel from the Cobham Lake 1:250 000 sheet area is 60 km E–W and the right-side panel is from the Cobar region. Figures from Poudjom Djomani *et al.* (2007), reproduced courtesy of NSW Trade & Investment.

9 Interpretation strategies

9.1 OVERVIEW

Having compiled a solid geology layer integrating aeromagnetic data with all available relevant geology and other geophysical information, we are able to extend our interpretation to embrace the third dimension (depth variations), to build a structural model and to form views on the geological history and resource potential. There are many different interpretation paths which suit different objectives for different users of any one aeromagnetic survey. This chapter briefly describes several of the most common paths and provides guidance on the approaches to a variety of interpretation objectives. The worked examples in Chapters 11, 12 and 13 emphasise the need to extract the maximum amount of geological detail from the aeromagnetic surveys. Doing this will give the interpreter the best possible opportunity to realise their ultimate goals.

In practice, we are rarely able to allocate sufficient time to investigate *all* aspects of an aeromagnetic survey and must focus on the aspects that are most relevant to our particular purpose or application. For example, the case study in Chapter 11 shows interpretations at three scales from the same survey. The broad scale (1:250 000) shown in Section 11.3 would be sufficient for a general overview as part of a regional geological mapping campaign at the same scale, or as part of a project generation study for exploration. The 1:100 000 scale study (Section 11.4) requires more time and care and would be a necessary component in mapping at district scales, or as the pointer to exploration targets in that area. The 1:25 000 scale study (Section 11.5) concentrates on a much smaller area containing a defined target, and in Section 11.6 we focus solely on that single target area. The degree of time and effort needed for each study varies according to the size of the area, the scale and the end products required.

In the following sections we outline the topics that should be addressed as we plan our interpretation. To reinforce the key points, we repeat some of the guidelines mentioned in earlier chapters.

9.2 GEOLOGICAL AND STRUCTURAL THEMES – BEING PREPARED

Interpretation in geoscience is unavoidably subjective. Our understanding of the physical and chemical characteristics and behaviour of the Earth is limited and our data resources are patchy. Hence, our progress in improving our understanding relies heavily on working hypotheses. We have already emphasised the need to gather and consider as much of the pre-existing relevant data as possible, and to form our own view of the current level of geological understanding. This includes not only the geological and magnetic data considered in this book but also, where relevant, radiometric, gravity, satellite, electromagnetic and topographic data like Google Earth® and aerial photographs. Each dataset gives a different view of our area and so helps guide us to a better understanding of it.

There is a school of thought that prefers analysing aeromagnetic data totally objectively, using computer algorithms without recourse to existing geological interpretation or human judgement (e.g. Core *et al*. 2009). It has been the authors' experience that making use of earlier work, be it data or interpretation, and taking an open-minded approach to (human) observation lays a much sounder foundation for the integration of aeromagnetic data with geology.

Our methodology requires time to collect and digest existing information, to form a view of the quality and rigour of this information and then to approach the observation phase of interpretation expecting new and interesting features to appear. We expect this approach to result in a clearer picture of geology and structure and an interpretation which advances the understanding of the area. While this preparation has the potential to bias our observations, we are firmly of the view that it is an important factor in allowing the interpreter to read geological meaning into the aeromagnetic imagery.

9.3 THE IMPORTANCE OF REGIONAL SETTING

We are frequently focused on a specific project area and faced with a limited time frame in which to produce the best possible interpretation of our data. This often leads us to overlook some peripheral aspects of our project, including data which may be relevant but somewhat removed from our main purpose. Stepping back and looking at our project area at coarser scales using broader (and usually less detailed) datasets should never be regarded as peripheral. We will see in the worked examples in Chapters 11,12 and 13 that large-scale structures may not only have a major influence on a local project area, but may be very difficult to recognise if we look only at the project-scale data. Understanding the regional setting as best we can is a critical step in the interpretation process. We should view the regional data before our main (project-scale) phase of interpretation; conversely, we often find that regional data makes better sense once we have digested a good proportion of our project data. Hence, periodic review of the interplay between the regional and project-scale data during the interpretation process is the best approach.

9.4 TIME ALLOCATION

We have stressed the link between quality of interpretation and time spent on the process. We have also mentioned that it is rare to have the time to fully investigate all the intricacies of an aeromagnetic survey. In some cases a 'quick and dirty' interpretation is the pressing need, in others a thorough and rigorous analysis of the data is essential for the desired outcome. An example of the former is where the interpreter must nominate areas of principal interest in a short time frame, perhaps in a competitive land tenure bidding situation. A much more in-depth interpretation is required where the survey is flown over a defined area of interest and the project relies on thorough analysis to extract fine-scale detail to guide future mapping, exploration or resource-definition drilling.

Our *very general* rules of thumb for time allocation are:

a) allow at least one day for every 1000 line kilometres of data;
b) allow a minimum of four days (total) to prepare for and report on the interpretation;
c) consider the cost of interpretation in the context of the survey cost;
d) 5–10% of survey cost is a good initial budget to target.

While these provide a useful guide, each new survey and new application requires careful thought in planning the time and cost commitment for interpretation. Too often, high-quality datasets receive cursory or superficial interpretation because the users think that most of the work is done and the expenditure 'spent' when the final survey data and imagery are received. Interpreters will always want more time (and budget) to fine-tune their work, while managers will always need to adhere to budget limitations. The judgement of the best balance requires communication and mutual understanding.

The key point lies in the extraction of value from the survey. Allocation of too little time and budget to interpretation may well result in the survey expenditure being largely wasted.

9.5 BUILDING ON THE SOLID GEOLOGY

Chapters 6 and 7 have outlined the methodology for basic aeromagnetic interpretation. After compiling a solid geology layer we can build further layers of interpretation, extending the interpretation to include structural style and geological history and, of course, to define target areas consistent with the objectives of our project.

A good place to start this more advanced stage of our interpretation is with cross-sections, including a critical assessment of the nature of faults and contacts.

9.5.1 Cross-sections and fault/contact assessment

Extending our interpretation to the third dimension is always desirable and may be achieved with simple qualitative analysis of our 2-D solid geology. We can use stratigraphy, (pre-existing) field structural measurements and geological common sense to classify the nature of contacts and faults, and to infer structures such as folds. Identifying local timing relationships in our solid geology map is a further important and qualitative step which prepares us for the task of compiling cross-sections.

There is an interdependence of structural style and cross-sectional interpretation. Frequently we have insufficient hard observational data to infer contact dips and plunges, and we face significant ambiguity in constructing cross-sections. This is where computer modelling (and inversion) will often help answer key questions.

We emphasise that the qualitative assessment of our observational work (both geology and aeromagnetic data) using appropriate geological rationale can take our interpretation to an advanced stage, including the compilation of cross-sections. The examples presented in Chapters 11 and 12 (see Figs 11.11 and 12.24) have been compiled without recourse to modelling or other quantitative methods, whereas the cross-section shown in Figure 13.34 has utilised qualitative analysis, automated depth computations and forward modelling. This raises the question of when to introduce these quantitative methods to our interpretation.

9.5.2 The role of modelling and inversion

Aeromagnetic data can provide depth and location information for magnetic rock units with a consistently reliable level of precision. Dip and plunge information can be inferred subject to (sometimes unreliable) assumptions. Magnetic properties (susceptibility, remanence etc.) and body widths can be estimated but these usually require some hard control from geological mapping or drill-hole data if they are to be confidently inferred. The range of quantitative techniques available, and their strengths and weaknesses, are discussed in Chapter 8. For this chapter we simply emphasise that modelling etc. is no substitute for incisive geological reasoning based on careful observations.

Modelling is best used to solve particular local problems such as determining:

a) the depth to top of magnetic rock units;
b) the dip of magnetic contacts;
c) the best location and orientation for drill holes to intersect magnetic rock units.

The quantitative tools available allow us to build complex arrays of magnetic bodies which match the observed magnetic data. However, with each increase in the level of model complexity there is an increase in the time taken to achieve a satisfactory match, and an increase in the level of ambiguity. Our guiding principle is that time and effort spent on quantitative analysis needs to return sensible and robust answers to specific, relevant and important questions. Once the answers to these questions are known we can approach the final stages of our interpretation.

9.5.3 Geological history and structural style

We now try to unravel the sequence and nature of geological events responsible for the patterns we have produced in our solid geology interpretation. Our solid geology is supplemented with cross-sections and supported by modelling results, and has been interrogated to yield inferred timing relationships. The nature of contacts, faults and folds has been considered. The questions we try to answer are as follows.

a) What geological events have occurred in our study area?
b) In what sequence did they occur?
c) How do the different structures interact?
d) In what type of geological environment(s) did these events evolve?

By addressing these questions we build a picture of the geological history, particularly the structural evolution, of our study area. The effort that we apply to this stage of our interpretation is governed partly by the nature of the geology and partly by our interpretation objectives. The important point is that the work we compile to produce solid geology, cross-sections and local observations such as fault and fold styles,should allow us to put forward a geological 'story'. The value of this story to users of our interpretive work is very high. They not only have our observations and compilation, but also our opinions on what it means. Users may not agree with our conclusions and may choose to reinterpret our basic work, but having our views gives them a flying start in their use of the survey data. For this reason we encourage interpreters to do just that – interpret. Maintaining a cautious approach and limiting our work to observation and compilation without speculation is like leaving the icing off the cake! More importantly, we fail our management by not alerting them to new possibilities. These are so often the possibilities with the best chance of the biggest positive surprise.

9.6 TARGETING

The last and usually most important stage in our interpretation is targeting. What areas of interest have arisen from our work and with what activity (or activities) do we propose to investigate those areas?

Targeting may take very different forms within the confines of a single aeromagnetic survey. For example, the data analysed in Chapter 11 can be equally well used by government survey mappers, by gold, nickel and diamond explorers, and for groundwater exploration. Targets for the government mappers would primarily be areas which enhance the understanding of the general geology and can be readily field tested. The gold and nickel explorers would focus on favourable stratigraphy and give emphasis to particular structural situations. Diamond explorers would primarily seek specific magnetic anomalies potentially caused by kimberlite pipes. Groundwater explorers would focus on such things as palaeo-channels and fracture patterns in bedrock.

While each targeting style is different, all require the basic observation and integration steps outlined in Chapters 6 and 7. They all also benefit from some or all of the more advanced tasks discussed in this chapter.

The identification of targets is the primary purpose of most interpretation. We form our interpretation strategy based on the nature of our targets and, while the various interpretation steps involve a range of challenges and highlights, we should not lose sight of the fact that our work has been commissioned to assist the discovery of particular commodities and/or to enhance geological knowledge.

Targeting requires discipline. It is easy to define large areas as having some potential and requiring further investigation. It is much harder to prioritise areas of possible interest, present our informed choice of high-priority targets and recommend a course of action to test those targets. The balance of high-, medium- and low-priority target areas cannot be predicted or prescribed for any given project.

Our guiding principles here are:

a) **optimism** – approach interpretation expecting that suitable targets will be found;
b) **honesty** – if there are no suitable targets, say so;
c) **diligence** – clearly describe the nature of and rationale behind each target;
d) **judgement** – prioritise thoughtfully but succinctly. Large numbers of low-priority targets will inevitably distract attention and effort from your high-priority targets;
e) **commitment** – as interpreters, our appreciation of the target styles and the work that has gone into their definition makes us well placed to prescribe the methods of target testing. We should do this, even in situations where we will not have the opportunity to control or participate in the testing process.

With targets defined and prioritised, and our recommendations for follow-up presented, our interpretation work is done. Or is it?

9.7 TARGET TESTING

Interpreters often find themselves disconnected from the process of target testing. Specialist field personnel take the interpreter's recommendations and execute the plan agreed to (and funded) by management. This separation of responsibilities is very unfortunate, but a reality in many projects. As much as possible, the interpreter should stay engaged during the target testing stage. Ideally the interpreter should be responsible for execution of the testing. The next-best scenario is where those involved in the field testing are engaged to some degree in the interpretation and targeting process. The more engaged, the better the outcome is likely to be.

Most importantly, interpreters should follow the progress of any target testing, actively promoting and helping to advance it, and being prepared to absorb and digest the results.

9.8 REVIEW AND UPDATE

Results of target testing will rarely be exactly what interpreters predicted or hoped for. However, almost every new piece of information acquired in target testing will add value to the interpretation. This new data will usually cause some rethinking and require revision and refinement of the interpretation. We should anticipate and plan for this.

As with geological maps, the periodic updating of our interpretations should be factored in to the long-term plan to get full value from an aeromagnetic survey.

9.9 FIELD TESTING OUR INTERPRETATION

We have emphasised the need for interpreters to participate in the field testing of their ideas and target areas. This section discusses some of the practicalities of that field testing, and the frustrations often encountered when concerted effort is not successful in resolving key questions.

Field investigation is often a challenging and unrewarding task, especially in areas where exposure is limited or difficult to access. In most cases we have limited time and funding, and are forced to confine our field work to the more contentious aspects of our desktop interpretation. We are also usually forced to use surface material which may not be sufficiently fresh to be ideal for geological description or magnetisation determinations. Nevertheless, our best efforts in field follow-up of desktop interpretations are a critical part of making best use of our interpretation and, indeed, getting appropriate value from our aeromagnetic data.

9.9.1 Key points for field work

There is a checklist of factors to consider.

a) Check and double-check coordination of geology maps, aeromagnetic data and field location medium (GPS devices or aerial photos). Errors of a few hundred or even tens of metres can result in a lot of time spent observing and measuring the wrong rocks in the wrong place.
b) Be prepared to amend the desktop interpretation!

   The limitations of the aeromagnetic data and the generalisations we are usually forced to make in our initial interpretation make it highly likely that field observations will not exactly fit this interpretation. Expecting this to occur and treating the new information and our subsequent revisions of our work as a positive progression in our exploration or mapping, is an important state of mind. We should never consider field observations that are inconsistent with our interpretation as indications that the interpretation was erroneous or of limited value. Remember that our interpretive work is always designed to get us closer to our exploration or mapping objectives, and it achieves this by pointing us to field locations where ideas can be tested. We improve our understanding irrespective of whether these ideas turn out to be true or false.

   The new information we obtain from the field may indicate a need for further, perhaps more detailed, data processing which could lead to a review of the observations and even a fresh observation layer. Review and revision of our interpretive work should be factored in as a normal phase of the use of aeromagnetic data in exploration and mapping.
c) Expect more complexity in outcrop than that apparent from airborne data.

Aeromagnetic data will only give direct information on variations in magnetic mineral content and its resolution is limited by line spacing and survey height (see Chapter 2). We must give due consideration to these limitations when walking on outcrop and recording the local feast of information that outcrop provides. Remember that the airborne magnetometer senses bulk magnetisation contrasts over volumes far greater than a single outcrop and that it will see these magnetisation contrasts at considerable depth. This raises our next point.

d) Consider the likely depths to magnetic rock units before seeking their sources in outcrop.

Although there will always be some uncertainty in depth estimates, simple, rapid, graphical methods enable us to gauge the likelihood that the source of a magnetic feature is exposed. If these depth estimators indicate a likely buried source, our field observations will need to be modified accordingly. Drilling may be the only suitable test.

e) Spread field observations as widely as practicable.

Magnetic susceptibility variations may be extreme over very short distances, even in a single and seemingly uniform geological unit and even in hand specimen. Once again, remember that the airborne magnetometer sees the bulk or average susceptibility of a considerable volume of rock. Single, localised magnetic susceptibility measurements can be very misleading, so we should ensure measurement points are widely spread and numerous. The susceptibility of any rock unit should be quoted in statistical terms indicating variability as well as mean or median values. We should always indicate the number of measurements taken and, of course, their locations.

f) Make careful observations of geology and magnetic susceptibility.

In addition to multiple, statistically meaningful magnetic susceptibility measurements, we must have accompanying appropriate descriptions of the sampled rocks and their environment. The cost of field work in both time and money is often considerable, especially in remote or inaccessible areas. Hence we should always make the most of the time we spend on outcrops. These observations are crucial in obtaining answers from our field investigations because we are usually limited in the number of samples we can take from the field for laboratory or office analysis, and we often have only one opportunity to spend time at each field testing location.

g) Pay attention to surface conditions.

Weathering and near-surface processes such as limonite staining, silcrete or calcrete development often affect only a thin outer layer of exposed rock. As with geological observations, measurements of magnetic susceptibility should be done on fresh rock as far as is practicable. As magnetite and pyrrhotite are often casualties of the weathering process, it is very common for weathered variants of magnetic rocks to have diminished magnetic susceptibilities compared to their fresh counterparts. In the extreme case, it may be possible to recognise the original rock type in its weathered state but record its magnetic susceptibility as zero. The fresh, magnetic equivalent of this rock, that is the cause of our aeromagnetic feature, may lie just a few metres below us. In this situation we would expect to see weathering products of the magnetic minerals such as haematite, limonite and goethite providing clues to the nature of the fresh rock, but in some cases these too may have been removed by the weathering process.

9.9.2 Objectivity!

It is not uncommon to be standing, correctly located, on an outcrop that appears to bear no relationship to and perhaps strongly conflicts with our aeromagnetic interpretation. In this case close review, first of our observations and then of the aeromagnetic imagery itself, is required – as perhaps are expanded observations of geology in the field.

What we *must not* do is give up and dismiss the aeromagnetic data as being 'wrong'.

Remember that the aeromagnetic data is sourced from the geology, so apparent conflicts are resolvable. More hard work and/or lateral thinking may be needed to resolve these conflicts.

We must, of course, double-check that our coordination and positioning are correct and consistent with the other datasets integrated into the interpretation. This should be done at the very beginning of our work, as emphasised above.

Remember that mineralised environments will often show unusual magnetic and geological characteristics. These may not be obvious or direct indicators of mineralisation, and may yield puzzling observations in the field. Hence it is prudent to treat unusual or puzzling observations with heightened interest, rather than hide them in a dark corner.

9.9.3 Use of magnetic susceptibility meters

There are several types of magnetic susceptibility meter in common use. All are relatively straightforward to operate, but each has idiosyncrasies and it is essential to spend time becoming familiar with the instrument before embarking on a measurement campaign. One very useful habit to adopt when using a meter for the first time is to determine its maximum reading, its minimum reading and, most importantly, the meter reading that indicates the (approximate) 1% equivalent magnetite (see Section 3.1). This gives the user a guideline for estimating magnetic mineral content in hand specimen, and gauging whether or not these minerals should be visibly obvious. We make no recommendation on choice of magnetic susceptibility meter. We do, however, urge users to read instrument instruction books carefully and be confident of measurement procedures before using the instrument in the field. The cost of incorrect or ambiguous measurements in the field can be very substantial.

We emphasised earlier the need to take multiple readings and to spread readings widely across outcropping rock units. At each measurement point, ensure that readings are repeatable to better than ~3%. In particular, repeat any very high readings and estimate the equivalent % magnetic mineral content. At the same time, ensure that local variability (which can be common on a sub-metre scale) is recorded, not 'buried' by recording only averages. We may choose to use an average susceptibility value when describing or computer modelling a magnetic rock unit, but having knowledge of the real variability and the precise location of our measurement points can be important in understanding the relationships between outcrop and aeromagnetic features. A suitable table for recording magnetic susceptibility readings is shown below.

Traps for the unwary

Magnetic soils clinging to rock samples, and iron staining on rocks and sometimes in veins can register magnetic susceptibility that is unrelated to the primary rock. Clean, fresh samples are always better than ones that are hastily grabbed and measured.

Be wary of conductive rocks. The magnetic susceptibility meter senses high conductivity, so very sulphidic or even graphitic rocks may register susceptibility due to conductivity rather than magnetic mineral content. For this reason, the meter must also be kept away from metal core trays (remove core samples by at least 20 cm before measurement)!

Finally, be generous with sampling and take time to record geological information well. Collect *representative* samples as well as unusual samples for possible, subsequent laboratory measurements.

PROJECT

Location _____ **Date** _____ **Operator** _____

Coordinate Projection & Datum _____ **Susc Meter Type** _____

Sample No	Coordinates		Susc Max	Susc Min	Susc Mean	Comment
	X	Y	Units			

9.10 DOCUMENTATION, GIS CAPTURE AND PRESENTATION

In this section we discuss some of practicalities of recording, documenting and presenting our interpretation. At the time of preparation of this book, the state of hardware and software allowing interpreters to conduct their work on-screen was quite inflexible and cumbersome for most users. Most experienced interpreters (including the authors) still prefer to record observations on physical film overlay using conventional drawing implements, and the examples presented in Chapters 11, 12 and 13 have been compiled in this way. We acknowledge that on-screen observation and interpretation will be the way of the future and expect that the user-friendliness of the available tools will soon accommodate those who have spent a lifetime with light-tables, hardcopy imagery, overlay and pens. Despite the use of this ageing methodology for our observation and integration, we emphasise that effective digital compilation and presentation of interpretation is already an essential part of getting the message across to potential users of the work.

In previous chapters, we have given our views on choices relating to data enhancement and presentation, as well as the important choice of the principal scale for interpretation. We re-state that a set of around five aeromagnetic images, optimised for the selected interpretation scale, should be more than adequate for most projects. Geological data coordinated to match our aeromagnetic imagery is essential, and aerial photos, Google Earth® imagery, topographic and cadastral data are highly desirable. Other datasets that may form part of our integrated study include gravity, satellite reflectance imagery and airborne electromagnetic data. Chapter 7 describes how these datasets can be incorporated into our interpretation and emphasises the need to record observations from each dataset on a separate layer or overlay.

9.10.1 Preservation of observation layers

We should treat our desktop observations in the same way as geologists treat the observations in their field notebooks. This record is the basis of our interpretation and will often be revisited when our interpretation is reconsidered or reviewed. If observations are created digitally, they may be readily stored and/or appended to reports. Users of interpretation maps invariably find value in the accessibility of original observations. Where observation layers are drawn onto hardcopy overlays, they should be scanned and registered ready for use in GIS packages. This is best done during the interpretation process to allow the broadest possible correlation of our observations with other datasets and imagery that may not be in hardcopy form.

We should remember that the observation layers are the record of work aimed at deciphering often complex patterns in often complex data. Preservation of these for later re-use is very important.

9.10.2 Compilation of interpretation work as layers

The current state of the art in compilation of geoscience maps and databases is reflected in the (often freely) available GIS packages released by state and federal governments worldwide (e.g. Geological Survey of Queensland 2000). Once our observation stage is advanced, and we commence compilation of the interpretive layers, our practices follow those used in geological mapping almost exactly.

The layering will usually commence with the definition of **lithostratigraphic polygons**. If our interpretation relies more on the aeromagnetic data than ground geological control, we may attribute these polygons with descriptors that give the user insight into magnetic characteristics as well as interpreted lithology or stratigraphy. Any significant magnetic **marker units** or horizons should be part of the solid geology compilation, and these may be incorporated into the layer of lithostratigraphic polygons or, if they are numerous and widespread, they may be better placed on a separate layer. Delineation of **faults** that have visible or interpreted displacement will follow the above polygons, and these warrant isolation onto a single separate layer, showing displacement indicators. **Possible faults**, fractures with no discernible displacement and **trends/form lines** that do not relate to lithostratigraphic boundaries (and are therefore subsidiary to the previously defined faults and contacts) are also best placed on a separate layer. **Fold axes and inferred dips and plunges** are a logical next separate layer. It is important to qualify dip and plunge indicators if they are inferred from aeromagnetic gradient asymmetries, and to differentiate these from measurements made directly from field exposure. At this stage we may have formed an interpretation of the structural evolution of our project area and may wish to prepare an additional separate layer summarising only the main structural elements.

Anomalies that we have defined must be designated clearly and on a separate layer. These may be specific, unusual aeromagnetic highs or lows, or zones of characteristic texture suggestive of alteration or mineralisation processes. They will normally be portrayed as open polygons because they will be superimposed on the solid geology. Anomalies and **targets** should be placed on separate layers, even though many anomalies may also be considered as targets. In most cases our targeting will include geological/structural situations which are not specific magnetic anomalies. Anomalies are directly observable/perceivable entities but may not constitute targets in the context of our particular project. They may, however, be of significant interest to users of our interpretation who are exploring for different commodities or are seeking different leads on the geology. Hence we anticipate that the targets layer will be dynamic, varying according to purpose and changing as field work provides new information likely to give increased confidence and maturity to our interpretation. Targets, like anomalies, should be portrayed as open polygons.

Where we have **magnetic rock units at depth**, underlying the bedrock defined in our solid geology layer, we may choose to create a separate 'deep units' layer. The importance we give to this layer and the form it should take in our consolidated compilation will vary according to its relevance to project aims. Two examples, where such units should be portrayed on our final map, are:

a) where we have subsurface intrusive bodies which may have some influence on our bedrock geology or some bearing on our targeting strategy, they can be represented as transparent polygons with an appropriate pattern fill. Depth estimates to the top surface of these features should be included in the deep magnetic rock units layer;
b) in some situations, we can decipher from the aeromagnetic data a separate and distinct basement response underlying the nearer surface solid geology that we have defined. This may have considerable character, to the point where both structure and lithology can be mapped. Sedimentary basins are the obvious but not the only situation where this may occur. Where this basement geology is valuable to our project aims we should compile a separate **basement solid geology** in the same manner as our nearer surface solid geology. Although this will invariably contain less geological detail, it may be of considerable significance in understanding the geological evolution of our project area. Depth determinations are an essential ingredient in this basement solid geology and they should be prominently shown. Clearly this compilation will have its own set of layers and it will not lend itself to co-display with the nearer surface geology. Chapter 13 provides an illustration of a near-surface solid geology and corresponding basement geology interpretation.

The number and type of layers we create in an interpretation project will vary with scale and purpose but maintaining a layered approach to our analysis, compilation and presentation has many benefits, particularly for subsequent users of our work. This approach is illustrated in Figure 9.1, which illustrates the layering applied at both the interpretation stage and the final compilation of the detailed scale interpretation featured in Chapter 12.

This brings us to the topic of three-dimensionality in our interpretation, and the means at our disposal to deal with this.

9.10.3 Cross-sections

Cross-sections are an essential ingredient in any interpretation. Regardless of the purpose of our analysis and the depths of main interest to us, dips of faults and contacts, plunges and closures of fold axes are best visualised in section. The act of preparing cross-sections is often the best way to identify gaps and shortcomings in our 2-D interpretation. It may be a reminder that we need more depth and dip information from the aeromagnetic data and may cause us to conduct further modelling or inversion work to firm up our interpretation.

There are few, if any, situations where cross-sections are not highly beneficial to an interpretation. The cross-sections for the interpretation shown in Figures 12.21 and 12.27 are presented in Figure 12.23. Construction of these cross-sections has a major impact in the presentation of the interpretation and the user's ability to comprehend the structural styles portrayed.

9.10.4 3-D geological compilations

Modern software packages facilitate 3-D visualisation of geology, incorporating surface geology, topography, reflectance imagery, geophysical data, geochemistry and drill-hole data. At ore body and mine district scales, such compilations and visualisations have a profound effect on exploration and production planning, and are an established part of day-to-day mine and near-mine activities. At broader exploration scales, where the density and continuity of data become poorer, the application of these visualisation methodologies has less impact but they retain value in interpretation and particularly in local problem-solving. When combined with integrated 3-D geophysical modelling and inversion, these tools can be very powerful in planning exploration target drilling.

The application and implementation of 3-D geological compilations at regional scales is in its infancy but it is undoubtedly the way of the future. The implications for aeromagnetic interpretation are not profound, since the starting point for most 3-D compilations is a good 2-D solid geology. Our approach to observation and interpretation is unlikely to change significantly, but our abilities to extend our interpretation to the third dimension will be enhanced as we are more readily able to combine 3-D geophysical models with 3-D geological data (see Fig. 8.4).

9.10.5 Presentation and reporting

It is important for interpreters to present their work as presentably compiled maps. Digital databases with multiple, attributed layers will be a standard deliverable product, but interpreters must provide a basic range of graphic products which can be immediately accessed by users and which tell the story of the interpretation. There is no difference between the presentation of an aeromagnetic interpretation and that of a campaign of geological mapping. In both cases there will be basic observations that cannot be effectively or completely displayed on interpretation maps and must be confined to digital databases accompanying the interpretation. The challenge for the interpreter is to present the key results of the work in such a way that the users (frequently the sponsors of the work) can rapidly appreciate the new concepts and targets stemming from the work. Examples of final presentation maps can be found in the following case study chapters (Figs 11.28 and 12.28).

The extent to which written documentation of the observation, integration and interpretation process is required will vary greatly. Local exploration projects will rarely need fully referenced, formally structured scientific style reports, while government-sponsored projects do require full and formal documentation. Regardless of the degree of formality, it is important to convey your interpretation and follow-up recommendations with words as well as maps and data. Clear explanation of your interpretation and targeting rationale is critical to effective use of your work. Expansive descriptions of the data itself and your methodology are not. The authors' advice is to give strongest emphasis to explanatory text that assists the user to understand and hopefully get excited by your interpretation. Large, verbose reports rarely do this.

9.10.6 Some published examples

We list below some published examples of in-depth aeromagnetic interpretation that show a range of interpretation styles in a range of geological environments. Although many of the larger interpretation projects are sponsored by government organisations or private exploration companies and are not made public or readily accessible, all the ones we have selected are broad in scope, comprehensive in their analysis and available in the public domain.

Corner B, Wilsher WA (1989) Structure of the Witwatersrand Basin derived from interpretation of aeromagnetic and gravity data. In *Exploration '87. Proceedings*. (Ed. GD Garland) pp. 532–546.

Hegarty R (2011) Interpretation of aeromagnetic and gravity data from western New South Wales – identifying basin and basement geology. Australian Society of Exploration Geophysicists Conference, Brisbane. *Extended Abstracts*, pp. 1–4.

Isles DJ, Harman PG, Cunneen JP (1989) The contribution of high resolution aeromagnetics to Archaean gold exploration in the Kalgoorlie region, Western Australia. *Economic Geology Monographs* **6**, 389–397.

Moore DH (2004) 'St Arnaud 1:250 000 map: a geological interpretation of the geophysical data'. Department of Natural Resources and Environment. Victorian Initiative for Minerals and Petroleum. Report 82.

Rankin, LR, Newton CA (2002) *Musgrave Block, Central Australia: regional geology from interpretation of airborne magnetic data*. Primary Industries and Resources South Australia. Report Book 031.

Tucker DH (1983) The characteristics and interpretation of regional magnetic and gravity fi lds in the Broken Hill district. Australasian Institute of Mining and Metallurgy Conference, Broken Hill, NSW. *Extended Abstracts*, pp. 81–114.

Urquhart WES, Strangway DW (1985) Interpretation of an aeromagnetic survey of the Qian'an Archean metamorphic rock series in China. In *The Utility of Regional Gravity and Magnetic Anomaly Maps*. Society of Exploration Geophysicists, Tulsa Conference 1985. (Ed. WJ Hinze) pp. 439–449.

Whiting TH (1986) Aeromagnetics as an aid to geological mapping – case history from the Arunta Inlier, Northern Territory, Australia. *Australian Journal of Earth Sciences* **33**, 271–286 http://dx.doi.org/10.1080/08120098608729364.

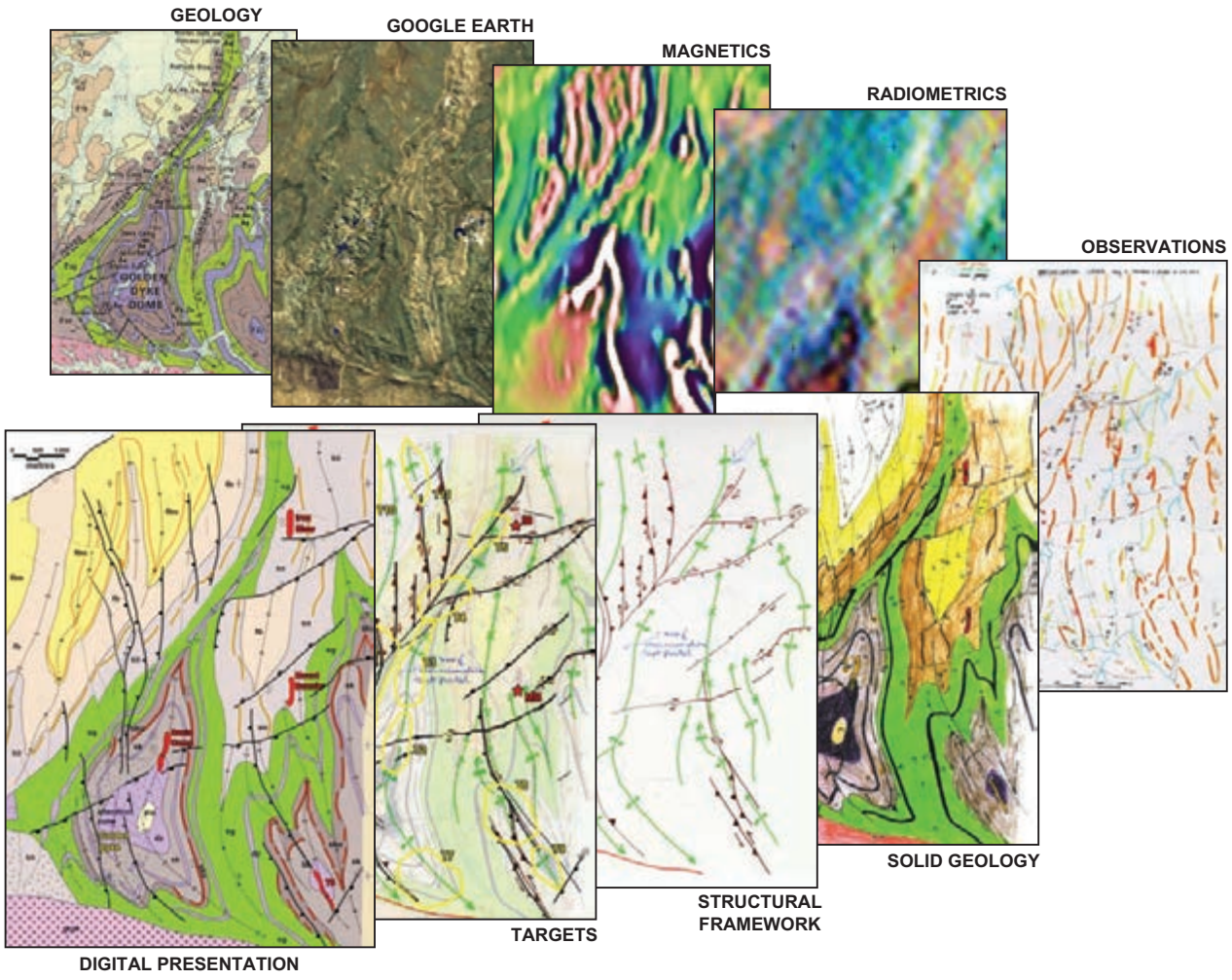

Figure 9.1: Illustration of layering in the data integration and interpretation process, Golden Dyke district, NT. See Chapter 12 for analysis of these datasets.

10 Aeromagnetic data in sedimentary basins

10.1 INTRODUCTION

The use of aeromagnetic surveys in sedimentary basins dates from the late 1940s when magnetometers that had been used in aircraft for hunting submarines were adapted to map magnetic basement in the petroleum exploration sector. Conventional use of aeromagnetic surveys, commonly in association with ground gravity surveys, has helped to delineate basin architecture via depth-to-basement studies. This has evolved to the point where such work is integral in the early stages of basin exploration, frequently preceding and guiding the acquisition of seismic data. The speed and uniformity of coverage, plus the relatively low cost of aeromagnetic surveys, have consolidated their role in this application.

Two quite comprehensive publications cover these conventional applications: Gunn (1997b) and Gibson and Millegan (1998). We touch on the major topics addressed in those volumes but refer the reader to the original references for a thorough account of the methodology. In this book we explore two avenues which extend the conventional applications of aeromagnetic surveys in sedimentary basins:

1. applying our hard rock style of observation and structural analysis in the interpretation process. This is done as a case study presented in Chapter 13;
2. mapping structure, sometimes also stratigraphy and occasionally also hydrocarbon alteration processes within sedimentary sequences via the tiny signals recorded from very weakly magnetic sediments.

Since the early 1990s, high-resolution aeromagnetic surveys (HRAM – see Norman 1993; Bird 1997; Berger *et al*. 2004; Anderson *et al*. 2006) have gained momentum due to the identification of these very small signals and the employment of closer line spacing. Final grid data noise levels of 0.5–1 nT were the standard until around 1990. Since then, the better application of Cesium vapour magnetometers, closer attention to aircraft motion compensation and the remarkable navigation improvement due to the advent of satellite Global Positioning Systems (GPS) has enabled noise levels of 0.05 nT to be achieved in final gridded data. Line spacing of 200–500 m (compared to the conventional 1000 m–10 000 m) is now routinely employed in sedimentary basins; this not only provides higher spatial resolution in the shallow subsurface but adds a valuable level of data redundancy to the commonly less coherent, deeper signal content of the aeromagnetic data. The concept of data redundancy is well established in the seismic industry (Dobrin and Savit 1988), where repeated readings are employed to increase the signal-to-noise ratio.

In this chapter we emphasise the range of geological information that modern, high-resolution aeromagnetic data can add to sedimentary basin studies. We fully acknowledge the leading role played by seismic surveys and the key contribution from gravity surveys, but we have not included full integration of these data into

the case studies in this chapter due to time and space limitations. We have instead chosen to focus on the integration of aeromagnetic features directly (as far as possible) with available geological data and interpretations. Incorporation of this work with seismic and gravity interpretations would normally be carried out at an early stage of the basin evaluation process.

10.2 SOURCES OF AEROMAGNETIC SIGNAL IN SEDIMENTARY BASINS

Gunn (1997b) provides a comprehensive outline of the range of geological sources of aeromagnetic signal in sedimentary basins. These are summarised below and illustrated in Figures 10.1 and 10.2, taken directly from Gunn's paper. Prieto (1996) gives an excellent range of model studies of the above sources, based on a variety of real-life case histories. The study of magnetisation in sediments has expanded substantially in recent times (e.g. Mørk *et al*. 2002) such that our understanding of the very subtle signals has advanced significantly.

10.2.1 Magnetic basement

Basement to a sedimentary basin will usually contain magnetic rock units. It should be emphasised, however, that much of what we understand to be 'basement' will be non-magnetic, or too weakly magnetic to be recognised in an aeromagnetic survey. Basement magnetic rock units may or may not occur at the basement/basin interface, so care is needed when using depths and geometries derived for these magnetic rock units to infer basin architecture. Where depth to magnetic basement is large, the resolution of magnetic rock units becomes poor, as does our knowledge of the geology. Taking these limitations into account, we usually start with the assumption that magnetic rocks in the basement do mainly occur at the basin interface, such that their depths provide a guide to basin thickness. Hence, assemblages of depth computations are frequently compiled into 'depth to magnetic basement' maps and the structural forms evident in these maps used to infer basin architecture (e.g. Gunn *et al*. 1995). During any basin study, it is important to be clear as to the definition of the basin sequence and the definition of basement.

10.2.2 Igneous rocks

Magnetic igneous rocks may occur anywhere within, beneath and above the basin sequence. They may be extrusive volcanic intervals within the basin sequence, younger sills, dykes or intrusive bodies, or they may be post-basin volcanic cover. Pre-basin igneous rocks may also be thrust over sedimentary basin sequences. The differentiation of these magnetic sources from those regarded as magnetic basement is rarely straightforward and usually requires support from independent data such as seismic or gravity data. Figure 10.3 illustrates a basin with magnetic basement, intra-sedimentary volcanic rocks, early and post-basin sills, and post-basin volcanic cover.

10.2.3 Magnetic sedimentary rock units

As described and illustrated in Chapter 3 (Section 3.3.2), low concentrations of magnetic minerals are very common in sedimentary rocks. Even relatively young (Mesozoic to Cainozoic) sedimentary basins may contain distinct magnetic sedimentary 'marker horizons' that can be extremely useful as stratigraphic and structural guides in the subsurface. Figures 10.4 to 10.7 show examples of such marker horizons in basins of various ages.

Within the commonly magnetically quiet sedimentary environment, the contribution from very weakly magnetic mineral species can sometimes be detected. For example, halite concentrated within significant salt structures (salt domes, salt walls) can be detected as weak but measurable magnetic lows. This is due to halite being diamagnetic, and therefore having a small negative magnetic susceptibility. Prieto *et al*. (1993) and Prieto (1996) show detailed models of the negative magnetic anomalies associated with salt diapirs from the West Texas Gulf. Negative magnetic anomalies associated with salt domes are also highlighted in magnetic data covering the Genesis Oil Field in the Gulf of Mexico (see Fig. 10.8 from Rowe 1998).

The contribution of paramagnetic minerals such as clays, micas and detrital amphiboles to weakly magnetic sedimentary basin sources has been described within the offshore Norway Basin sequences by Mørk *et al*. (2002).

While these diamagnetic and paramagnetic sources are real and measurable, direct recognition of their contribution in aeromagnetic imagery (with the exception of salt tectonic structures) is very difficult without significant petrological and petrophysical data from outcrop or drill core.

10.2.4 Diagenetic and alteration effects

The types of sediments that may have detectable magnetic signatures and the geological processes controlling their development have been briefly outlined in Section 3.3.2. Diagenesis grading to low-grade metamorphism can strongly influence the magnetisation in sediments.

A very important example of this is the diagenetic to low-grade metamorphic conversion of primary non-magnetic Fe species (e.g. greenalite and primary haematite) to magnetite within BIFs (Barley 2009; Schmidt and Clark 1998), thereby producing extensive, very high-intensity magnetic units.

Sedimentary basin sequences may also be exposed to local- and/or regional-scale thermal alteration associated with syn- to post-basin intrusions. This may increase the magnetite content of the sediments through increased conversion of Fe-bearing silicates to oxides (see Section 3.3.3) or it may cause conversion of pyrite to monoclinic pyrrhotite within sulphide-dominated sediments. This thermal alteration effect is clearly illustrated in Figures 12.2 and 12.5 from the Pine Creek Inlier study (Chapter 12), where the increase in magnetic intensity of the sedimentary sequences proximal to the exposed and concealed granite plutons is due to development of pyrrhotite in originally pyrite-bearing siltstones and shales.

Magnetite (and possibly pyrrhotite) may also be produced by diagenetic reactions associated with the interface between hydrocarbons and less-reduced sediments. These reactions may be due to:

a) redox reactions between the hydrocarbons and the surrounding sediments;
b) bacterial growth of magnetite, associated with either sulphate-reducing bacteria (producing appropriate redox conditions) or bacteria that directly grow and incorporate magnetite within their cells (e.g. Arato *et al*. 2001).

As mentioned in Section 3.3.2, several examples of magnetite haloes or caps to salt domes within sedimentary basins have been highlighted in the literature, including Smith and Whitehead (1989) and Gunn (1997b). These appear as relatively localised magnetic bodies within generally non-magnetic to very weakly magnetic sequences.

Similar diagenetic development of magnetite is associated with migrating hydrocarbons within fault zones within the West Shetlands Basin (Norman, pers. comm., 2011). In this example, faults evident in the aeromagnetic data correlated with seismically mapped faults and showed higher magnetic intensity in areas of known seepage (from the seismic and seep mapping data) than the faults crossing areas of no seepage.

In contrast, the magnetic mineral content of basin sediments may be diminished or totally obliterated by diagenesis and alteration.

The migration of more oxidising basin fluids during and post-deposition may involve oxidation of magnetite and/or pyrrhotite to haematite and/or other non-magnetic oxide species. This may occur as a regional alteration, with widespread decrease of the sedimentary magnetic signatures, or it may be localised, particularly along faults.

Destruction of magnetite, leading to decreasing magnetic signature within sediments, has also been attributed to interaction between sediments and hydrocarbons. In a detailed case study by Morgan (1998), weak magnetic lows caused by magnetite destruction were found to be associated with hydrocarbon accumulations in the Morecombe Fields sediments of the East Irish Sea.

In cases involving hydrocarbons, where the creation or destruction of magnetite or pyrrhotite occurs, the key agent for oxide/sulphide mineral reactions are bacteria and the actual resultant oxide-sulphide species developed are difficult to predict due to local complexities in eH/pH, f_S and fO_2 (Arato *et al*. 2001; Riedinger *et al*. 2005).

10.3 SURVEY PARAMETERS AND DATA PROCESSING

10.3.1 Line spacing and flying height

Sections 5.1.2 and 5.1.3 cover the issues of survey line spacing and flying height, with emphasis on the extraction of geological detail at scales appropriate to the objectives of the survey. Sedimentary basins are a particular case where we expect that interpretation will be carried out over a wide range of depths. In localities where

the emphasis changes to the deeper magnetic sources, our choice of survey parameters will require modification from those applicable to more near-surface studies.

In early basin studies, when magnetic basement was the main survey focus, wide line spacing and relatively high survey altitude were not only commonplace but deemed preferable. The rationale for the wide line spacing was that features at basement depths would yield signals with long wavelengths which could be readily defined by lines spaced at, for example, 1/3 to 1/5 of the target wavelength. This resulted in surveys with line spacing of multiple kilometres, deemed sufficient to define basement features at depths equal to or greater than the line spacing. Survey altitudes were also higher because it was argued that signals from nearer surface and lower-volume magnetic sources would be more strongly attenuated than those from deeper, larger-volume basement. While there remains some merit in these arguments, the advent of HRAM surveys has created the opportunity to map magnetic signals throughout the sedimentary section. By capturing all these signals, geophysicists have been able to apply Fourier and wavelet analysis to more accurately extract and differentiate the wavelengths or families of signals due to basement rocks from those within the sedimentary pile.

Close line spacing is required to define shallow structural relationships. For onshore surveys in particular, near-surface sources are often present and the delineation and interpretation of these is an important step towards understanding the signals from the deeper sedimentary section and the basement. Depending on the scale of analysis envisaged for the survey data, line spacing of 200–500 m is commonly employed in HRAM surveys, although there are some instances where even closer line spacing has been utilised.

Flying at the lowest safe survey height is normal practice for mineral exploration, but is rarely appropriate in sedimentary basin applications. A slightly higher altitude may facilitate smoother flying conditions and therefore likely lower magnetometer noise, and may also suppress the potentially masking magnetic signal from surficial magnetic soils (see Fig. 3.27). However, where larger-volume surface sources (e.g. flood basalts) are present, it is important to adequately define their signals. In such a case, adequate definition of the basalt signal will not only enable us to recognise and account for its presence, but provide the opportunity to separate this unwanted signal from the deeper and more important signals. It should also be recognised that structures affecting (and visible in) magnetic cover to our basin sequences may be related to structures within the basin. Detailed mapping of the near-surface structure from the detailed magnetics may therefore reflect important but more subtly expressed structures within the target sediments. In light of this, survey heights of 80–150 m are most common in HRAM surveys.

In offshore surveys, where water depth may be many hundreds to thousands of metres, the need for close line spacing is reduced. Planning the survey line spacing to match the water depth is a valid approach, but planning should take into account the value of data redundancy in defining tiny signals from large depths. Surveys with line spacing wider than 500 m will rarely produce HRAM-type resolution and there is anecdotal evidence (Norman, pers comm., 2011) suggesting that the high-frequency component in offshore fault aeromagnetic signals is strong enough to justify tighter line spacing. Ocean swell noise is sometimes an issue in offshore surveys: the movement of saline water through the Earth's magnetic field yields electric currents which themselves generate time-varying magnetic fields. Ocean swell therefore creates a magnetic signal that is readily measurable in airborne surveys. The ocean-swell noise will be reduced by an increase in flying height, but sometimes the preferred flying height (from geological considerations) is one where some degree of ocean-swell noise may be anticipated. Removal of ocean-swell noise is made easier with closer line spacing and may be minimised by judicious choice of flight line orientation, but close attention to understanding the contributions of normal diurnal variation and ocean-swell noise is essential in offshore surveys irrespective of line spacing.

10.3.2 Data noise levels and micro-levelling

The tiny signals sought in HRAM surveys require measured data noise levels to be <0.1 nT 'peak-to-peak'. Reeves (2005) outlines the different ways of defining noise levels and the range of potential sources of noise. Surveys with very low magnetometer noise will usually retain small, line-to-line level shifts caused by imperfect diurnal removal and/or small variations in survey altitude. These can be minimised, if not removed, by micro-levelling techniques (see Section 5.2.2).

For the interpreter unfamiliar with the intricacies of acquisition and data processing, a useful yardstick for HRAM noise levels is a TMI contour map of a representative, low-gradient section of a survey, using a contour interval between 0.05 nT and 0.1 nT. If the noise levels are greater than this, the map will show artefacts in the form of local, incoherent closures and/or abrupt line-to-line level shifts. We should be aware that there are numerical smoothing techniques that can enable noisy data to be portrayed as smooth data. The potential to conceal problems in the data in this way, underlines the need for detailed logs of data processing history in HRAM surveys and special expertise during the quality-control stages. In particular, attention should be paid to the specific application of micro-levelling, as this can be adapted to disguise unacceptably noisy data as HRAM. It is good practice to insist on viewing grids of data before the application of micro-levelling and in many cases it is valuable to use these grids, in addition to micro-levelled grids, in the interpretation. Micro-levelling has the potential to adversely modify real geological signal, regardless of the integrity of the measured data. While the pre-micro-levelling grids will usually appear noisy, they provide reassurance to interpreters that they are seeing the data in its unfiltered form.

10.3.3 The importance of Reduction to the Pole (RTP)

Section 5.3.1 outlines the application of RTP and Figures 5.9 and 5.10 illustrate the profound differences in RTP anomaly shapes compared to TMI anomalies. The key issue in sedimentary basin interpretation is the location of the edges of magnetic rock units at depth. We note from Section 5.3.1 that the RTP anomaly shape is a much better representation of the magnetic rock unit than the TMI, in particular, the degree of difference between RTP and TMI anomalies increases significantly with depth. A specific example is shown in Figure 10.9, where a very large shift in anomaly outlines is evident: consider the implications of basing qualitative observations on TMI rather than RTP data. Irrespective of low field inclinations or the suspected presence of remanence in basement magnetic sources, RTP grids should be the primary medium for interpretation in sedimentary basins.

10.3.4 Wavelength filtering and matched filtering

The range of magnetic source depths encountered in sedimentary basin studies makes it essential to apply some form of source separation filtering. Simple regional-residual separation numerical techniques are sometimes adequate, but more sophisticated approaches are usually desirable.

Wavelength filtering separates the signal into its wavelength components and works on the premise that increasing depth will be accompanied by increasingly longer dominant wavelengths in the aeromagnetic signal. While this premise is valid, we must be aware that the anomaly from any magnetic source will contain a wide range of wavelengths. As we have seen in Chapter2, anomaly width is only partly related to source depth, and there is no direct link between anomaly wavelength and depth. Separation of aeromagnetic survey data into wavelength ranges is, however, a very simple numerical process and produces a useful, if strictly empirical, visualisation of deeper and shallower magnetic sources. Examples of wavelength filtering are presented in the Amadeus Basin study in Chapter 13.

Matched filtering (see Section 5.4.2) utilises the observation that ensembles (or groups) of magnetic sources occurring at similar depths produce a characteristic pattern in the Fourier spectrum of the magnetic field. Where ensembles of sources exist at widely different depths, not only can these depths be identified in the spectrum but manipulation of the spectrum can be undertaken to separate the signals from the different depths. This methodology works well where source depths are both closely grouped and widely separated, but it is complex in application where magnetic sources are spread evenly over a range of depths. The ideal application is where near-surface magnetic sources obscure the patterns from much deeper sources. Although use of the spectrum to accurately quantify depths is not recommended, analysis of the spectrum to gauge the range of source depths present in an area and the application of matched filters to emphasise particular groups of source depths is worthwhile in most sedimentary basin applications. This technique is commonly and appropriately called ‘separation filtering’ (Cowan and Cowan 1993), but it should be emphasised that clear separation of different depth source ranges is achievable only in ideal situations. The term ‘depth-slicing’ is sometimes used to describe the technique; this is somewhat misleading because the ‘slices’ usually represent

signals from a range of depths, and it is not possible to produce a horizontal 'slice' at a nominated depth as we would do with a level plan in a mine or a time slice in a 3-D seismic survey. We apply and further describe matched filtering in the worked examples of Section 10.5 and in Chapter 13.

10.3.5 Depth-to-source computations

The range of techniques for determining depth to magnetic sources is discussed in Chapter 9, and an expanded but succinct description and assessment can be found in Gunn (1997a). Automated methods such as Werner Deconvolution, Naudy's curve-matching method and Euler's method have value, but they require astute, specialist application and preferably input from geological considerations. Shi and Boyd (1993) describe a Naudy-based method that is well suited to determining depth variations on a single surface such as an unconformity. Where wide depth variations and multiple source ensembles occur, Shi (1993) concludes that a combination of forward and inverse modelling is required to supplement and sometimes replace the application of the automated techniques.

In general, the successful determination of magnetic source depths requires geological input. A concerted effort in geological reasoning and qualitative interpretation, in conjunction with implementation of the quantitative methods, will greatly enhance the value of these methods (see Chapter 13).

10.4 OIL FIELD EXAMPLE – CLIFF HEAD, OFFSHORE WESTERN AUSTRALIA

Data and analysis courtesy of Roc Oil (WA) Pty Ltd (ROC) and Fugro Airborne Surveys.

This brief study highlights the ability of aeromagnetic data to supplement and extend seismic interpretation in the environment of established hydrocarbon fields.

The Cliff Head Oil Field was discovered ~15 km offshore in the North Perth Basin (Fig. 10.10) in December 2001 by ROC, as operator of the WA-286-P Joint Venture. The reservoir depth is a little less than 1300 m, within the NNW-trending Permian Play Fairway. The reservoir comprises a stacked series of Permian sands sealed by the early Triassic marine Kockatea Shale. The area is structurally complex, with the field defined by a fault and dip-closed structure.

Production from the Cliff Head Field commenced in 2006, with a total of 9 mmbl (1.43 × 106 kL) of oil produced as at 31 December 2009 (DMP 2010). Current production in 2011 was 3000–4000 barrels of oil per day, with ultimate recoverable reserves (2P) around 18 million barrels of oil (www.rocoil.com.au).

The area includes sublittoral reefs around the immediate field area and closer to shore. Seismic acquisition is difficult along the coastal transition zone and around the shallow offshore reef systems.

A HRAM survey was conducted over the Cliff Head Oil Field by Fugro Airborne Surveys in 2003. The data were acquired at 100 m line spacing at a flying height of 60 m. Comparison with an earlier (1992), 1 km line spacing survey shows a profound improvement in resolution, evidenced by the recognition of key structures in the coloured MagSlice images (Anderson *et al.* 2006) shown in Figure 10.11.

Figure 10.12 shows a greyscale MagSlice 2 (shallow) image of the aeromagnetic data. The inset map shows the Cliff Head Field Top Permian reservoir map. The bounding faults of the reservoir are clearly recognisable in the aeromagnetic data.

Seismic data provided by ROC on behalf of the Cliff Head Joint Venture were utilised in the interpretation procedure. Fault exposures of the top of basement, the base of Permian and the overlying Jurassic Cattamarra Coal Measures were projected to the surface and overlain on the magnetic images. This allowed direct comparison of the defined seismic horizons with the magnetic data in plan view and showed that the magnetic responses around the field predominantly reflect the fault geometries. It also enabled extrapolation of the seismic structures mapped from the 2-D seismic data into surrounding areas, including those where it was not possible to acquire seismic data (e.g. the littoral reef areas).

The faults with distinct magnetisation characteristics are likely to represent fluid migration pathways that have focused magnetic minerals into the fault zones. The relationship of this emplacement of magnetic mineral into fault zones to the hydrocarbon migration event is yet to be studied.

Several major normal N–S- and NW–SE-trending normal faults are recognised in the data. Some of these faults, such as the major, west-dipping Geraldton Fault to the west of the Cliff Head Field, can be imaged in the magnetic data at several depths along the fault zone, as highlighted in Figure 10.12 and evident in Figure 10.11. The N–S-trending magnetic high is sourced from the upper Geraldton Fault, while the more subtle, diffuse magnetic response to the west appears to be sourced at a depth where the Geraldton Fault intersects basement rocks. In this instance, modelling shows that the linear magnetic response appears due to a combination of increased magnetisation within the fault zone, and the magnetic susceptibility contrast between weakly magnetic horizons offset by or juxtaposed to faults.

Another intriguing outcome of the survey was the recognition of the area of subdued magnetic response broadly coincident with the Cliff Head Field (shown as a dotted outline in Figs 10.11 and 10.12). This subdued zone is fringed by the stronger linear magnetic features related largely to faults, and appears to relate at least partly to reduced magnetic response along the internal faults. The cause of this decrease in magnetisation along the faults within the field is not known. Magnetic susceptibility measurements on four wells (Cliff Head 3, Cliff Head 4, Mentelle 1 and Vindara 1) showed that both the primary and secondary reservoirs are weakly magnetic where intersected in the productive Cliff Head 3 and Cliff Head 4 wells. However, the same stratigraphic units have no measurable magnetic susceptibility in the Mentelle 1 and Vindara 1 wells, which are outside the field (and outside this study area). The magnitude of the susceptibilities in the reservoir rocks is very weak, and the corresponding magnetic response would be attenuated at the depth of the reservoir such that it would not be detectable by the airborne survey. The observation of subdued magnetic response along the faults within the field, but apparently enhanced magnetic susceptibility in the reservoir horizons in the Cliff Head 3 and Cliff Head 4 wells, raises questions concerning primary lithological or secondary alteration effects. The possibility that the magnetisation effects relate to alteration that is directly associated with the accumulation of hydrocarbons has yet to be studied. The observed variations, however, definitely warrant further investigation.

10.5 GALMOY EXAMPLE – SHALLOW CARBONATE SEQUENCE

Galmoy is a lead-zinc mining district located in central Ireland, some 110 km south-west of Dublin. The area comprises mainly Carboniferous carbonate sequences, largely covered by thin (5–20 m) overburden which includes extensive peat bogs. It is an established farming area with extensive infrastructure that is visible in detailed aeromagnetic data. The aeromagnetic survey was flown several years after the initial discovery to assist with structural and stratigraphic mapping. The authors thank Lundin Mining Corp (Dick West, Ciara Talbot and Andy Bowden) for generously providing the aeromagnetic data and geology for use in this example.

10.5.1 Geology

The study area lies within a NE-striking belt of Lower Carboniferous carbonates (mainly limestones) which generally young and dip gently to the SE (Fig. 10.13). The key sequences in the Galmoy mine area are the Waulsortian Limestone (WA) and the underlying Upper Ballysteen Limestone, the upper part of which is an argillaceous bioclastic limestone (ABL). The Galmoy mine and the nearby Lisheen mine, some 8 km along strike to the SW, are high-grade, Zn-Pb deposits which have formed at or near the contact between WA and ABL within an inferred NE-SW fault zone. Close to and NW of this fault zone there is a 4–5 km wide corridor where the WA is strongly dolomitised. The Zn-Pb deposits are hosted in the dolomitised Waulsortian. Doyle *et al.* (1992) and Lowther *et al.* (2003) describe the district geology and the ore body characteristics respectively. The simplified bedrock geology map shown in Figure 10.13 is derived from these references and form the Geological Survey of Ireland's country-wide, 1:100 000 digital compilation which is freely available online.

10.5.2 Aeromagnetic survey and data processing

The survey was flown in 1996 and comprised NW–SE-oriented lines spaced 100 m apart at an altitude of 60 m above ground level. The final micro-levelled TMI data is imaged in Figure 10.14. The range of TMI

values is 90 nT, with the top 30 nT due to cultural sources and the main body of variation caused by a very broad regional gradient. The TMI image shows no expression of the major NE fault and no indication of any shallow structural or stratigraphic variations.

The prevalence of cultural sources (mainly farm infrastructure) in the final data created a need for 'de-culturing'. This was successfully achieved using a semi-automatic approach. Suppression of the dominant regional gradient was also carried out using a low-order polynomial surface filter. These processes yielded a residual TMI grid with remarkable character and a full data range of 5 nT (Fig. 10.15). Subsequent application of RTP gave a clearer picture of geological contacts and faults, but the pattern of variations remained complex (Fig. 10.16). Given the extraordinarily small intensity range, the narrow variation in lithologies and relatively flat-lying stratigraphy, it is not surprising that clear definition of contacts is lacking. On this basis, application of separation filtering was considered worthwhile to better resolve the shallower and deeper magnetisation variations in the sedimentary sequence.

The separation filtering yielded three discernible depth segments at ~100 m, 250 m and 400 m, shown in Figures 10.17, 10.19 and 10.21 respectively. These segments are not very different in depth and almost certainly represent slightly different depth versions of the same, essentially shallow, geological configuration. The deeper windows do, however, present a simpler and more coherent picture which appears to reflect the main structural and stratigraphic elements of the study area. The shallow window shows the fine-scale variations in magnetisation of the near-surface stratigraphic units; while this also seems to highlight some quite well-defined, shallow faults, it tends to mask the broader, systematic geometry that becomes apparent in the deeper windows.

10.5.3 Observation layers

Observations were carried out on each individual window as shown in Figures 10.18, 10.20 and 10.22. Geological control is understood to be good close to the mines, but is otherwise severely limited by the extent of superficial cover. Bedrock mapping within the study area has relied largely on stratigraphic drilling, hence the loci and orientation of contacts are not well constrained. Consideration of the three observation layers, particularly the shallow layer in the context of the bedrock geology data, yields the following key points.

a) The Ballysteen Limestone has a consistent and relatively strong magnetisation. Simplistic modelling indicates a bulk susceptibility of this unit of around 0.0003 SI, which equates to ~0.01% magnetite (Fig. 10.26). There is a suggestion that the upper Ballysteen unit, the ABL, has the strongest magnetisation, but access to more detailed information, in particular drill-hole locations and logs, would be required to test this suggestion.
b) The dolomitised Waulsortian shows consistently low/weak magnetisation, suggesting that the magnetic minerals in the unaltered Waulsortian have been either been removed or (more likely) converted to non-magnetic iron-bearing minerals in the dolomitisation process.
c) Some parts of the supra-Waulsortian sequence appear to have consistent and traceable magnetic signatures.
d) There are clear ENE, E–W and NW fracture sets evident and these appear to have some bearing on the location of mineralisation at Galmoy and Lisheen.

10.5.4 Interpretation

No clear definition of stratigraphic unit boundaries is possible because of the extremely low orders of magnetisation and the erratic nature of the distribution of magnetic minerals through the sequences. In spite of this, systematic variations are observed and can be broadly related to mapped stratigraphy. Consideration of the three spectral depth windows highlights the need to observe and interpret at different levels. The shallow window shows fine-scale variations which, in places, define contacts sharply and give a good account of the variability of magnetisation through the sequences. Precise definition of fault locations is seen in places but the overall look of this window is fuzzy and essentially incoherent. The mid-depth and deep spectral windows show smoother and increasingly coherent variations. This facilitates the subdivision of the study area into zones of consistent magnetisation, although contacts, faults and fractures are rarely sharply defined. We have chosen to present the interpretation as two layers, one

shallow and one deeper; the deeper layer is based on both the mid-depth and deep spectral window observations.

We emphasise that the interpretation presented here has not had access to any drill-hole data or other hard geological information. It has relied on the published solid geology maps referenced above. Hence, it must be regarded as a working hypothesis requiring testing against and integration with the hard geological data.

Shallow layer

The shallow-layer solid geology is presented in a draft form superimposed on spectral depth window-1 (Fig. 10.23), and in a more professional and final form (Figs 10.24 and 10.25).

The key elements include:

a) the thickening supra-Waulsortian sequence in the SE of the study area commencing along a NE-trending line which probably relates to the basement structure referred to (but not shown) in Doyle *et al*. (1992);
b) the likely delineation of the dolomitised Waulsortian Limestone by an apparent zone of demagnetisation. The geochemical constraints and resultant Fe species formed during the dolomitisation event have yet to be studied;
c) the apparent NNE fault zone which transects the Galmoy mines area. This zone has some local expression at ore body scale (Lowther *et al*. 2003), but the aeromagnetic data suggest it may be regionally significant;
d) a very strong corridor of NW faults which impacts directly on the Galmoy ore bodies. Both the main ore zones are oriented NW and the K-ore-body lies directly on one of the fault segments identifiable in the aeromagnetic imagery;
e) the series of E–W to ENE fault segments which appear to separate the Ballysteen Limestone from the Waulsortian in the Galmoy and Lisheen areas. These appear as en-echelon segments in an ENE-trending corridor. The supra-Waulsortian sequences thicken to the SE of this corridor, reinforcing it as a structure of regional significance.

There are numerous uncertainties in the solid geology interpretation. Most of the stratigraphic contacts are based on subtle changes in the very weak patterns of magnetic mineral distribution, and the degree of control in the various bedrock geology maps is not known. However, the degree of consistency and coherence in the aeromagnetic trends provides confidence that the data are making a very useful contribution to the geological picture.

Deeper layer

The interpretation of the two deeper layers is presented in Figures 10.27 and 10.28. The NW fault corridor evident in the shallow interpretation is also strongly evident in the deeper layer, as are the E–W faults. However, the shallow NNE fault seen in the Galmoy area is not. A group of inferred N–S faults east of the Lisheen mine area, which was vaguely apparent in the shallow interpretation, is quite strongly evident in the deeper layer. Probably the most interesting feature of the deeper level interpretation is the apparent continuity of ENE- to NE-trending ridges of the upper Ballysteen Limestone. These may represent anticlinal hinge-zones and may place the mineralised Waulsortian area within a broad synclinal structure.

10.5.5 Conclusion

While the interpretation is somewhat speculative, the aeromagnetic data clearly raise important questions concerning the geology and the structural setting of the Zn-Pb mineralisation. The answers lie first in careful cross-referencing of the aeromagnetic features with drill-hole and any available outcrop data, and second in stepping back and considering the study in a broader geological (and hopefully aeromagnetic) context. The key conclusion from this study is that, despite the extremely weak aeromagnetic signal levels, there is enough magnetic mineral distributed through this limestone sequence to enable the data to add significantly to the geological understanding of the area. If we reconsider the initial 'final' TMI grid (Fig. 10.14), dominated by cultural anomalies and a very broad regional magnetic gradient, it would have been possible to dismiss the aeromagnetic survey as of no

value in mapping the limestone stratigraphy and key structures in the mineralised environment. In view of what has been achieved by persisting with sophisticated but conventional data processing, this would have been a bad decision. Clearly, the painstaking removal of the cultural anomalies and the attention to detail in performing the separation filtering have unveiled a wealth of information relevant to mapping and exploration.

10.6 HOW DEEP CAN WE DETECT WEAKLY MAGNETIC ROCKS?

The Galmoy example in Section 10.5 highlights the range of information extractable from even the weakest of magnetic signals. The intensity range of the residual TMI data which formed the basis of the processing and interpretation was 5 nT. The most strongly magnetic stratigraphic interval had an average equivalent magnetite content of ~0.01%. The variations studied in that example occurred from surface to ~400 m depth. In this section we examine the effect of making this geological package deeper and observing the depth at which the magnetic variations become too small to be recognised and used for geological interpretation. Upward continuation (see Section 5.3.2) has been applied to the Galmoy aeromagnetic data to simulate the deepening of the Galmoy sedimentary section.

500 m depth

Figure 10.29 shows the aeromagnetic patterns that would be observed if the Galmoy study area was covered with 500 m of non-magnetic sediment (or water). The data range is reduced to ~1.8 nT but the geological coherence of the image remains excellent and highly interpretable. An interesting aside is that the deeper spectral depth window (Fig. 10.21), which emphasised sources at ~400 m depth, shows very similar patterns to the upward-continued 500 m. This is not surprising in light of the similarities between the shallow and deeper geometries determined in the Galmoy interpretation.

1000 m depth

At 1000 m depth (Fig. 10.30) the data range is just over 1 nT. Despite considerable loss of resolution, the key geological elements are still represented. If we consider that a survey seeking information at this depth would normally cover a larger area, the degree of geological coherence makes the data very useful.

2000 m depth

The data range is now 0.6 nT (Fig. 10.31) and there is only mediocre representation of only the gross geological elements. As at the 1000 m depth, we would typically expect to have (and in this case need to have) coverage of a much larger area for the aeromagnetic patterns to make geological sense. However, we can recognise the main magnetic units and their broad geological form and would have to conclude that the data remain useful when the weakly magnetic limestone sequence is 2000 m deep.

4000 m depth

With a data range of ~0.3 nT (Fig. 10.32) and recalling our resolution rules from Chapter 2, it is not surprising that the picture at this depth is too fuzzy to be of any use. It could be argued that in a survey of much greater extent we should recognise the existence of the weakly magnetic limestone sequence at 4 km depth and if it maintained continuity over large distances we could map its broad form. However, it would be prudent to conclude that this package (ABL, see Fig. 10.26), with a bulk susceptibility of 0.0003 SI (0.01% mgt equivalent) and dimensions of 300–400 m vertical extent by 1–2 km width and 10–15 km strike length, would not be coherently mapped at 4 km depth.

We conclude from this simulation exercise that 4000 m is the approximate limit of detectability of this limestone sequence. However, we emphasise that in the context of the conventional use of aeromagnetic data, this sequence would be considered non-magnetic and it would be unlikely that an aeromagnetic survey would be considered as a tool to map and explore in such an environment. How wrong this decision would be! Not only is the near-surface aeromagnetic expression of structure and stratigraphy highly informative, but we see important features down to depths in excess of 2 km.

10.7 SUMMARY

Magnetic minerals are widely distributed in low but measurable concentrations through many, if not most, sedimentary sections. Modern aeromagnetic surveying has the ability to map real geological magnetic variations of the order 0.05 nT, which gives us the potential to recognise even very weakly magnetic sequences down to depths of several kilometres. Maintaining such low data noise levels requires special attention to field acquisition practices, and this usually means increased time in the field and the use of highly experienced field personnel. Hence, specification of these high standards in data will necessarily attract a premium in survey cost. The authors believe that the examples presented in this chapter and in Chapter 13 make a strong case for paying the premium and reaping the reward of the additional geological resolution.

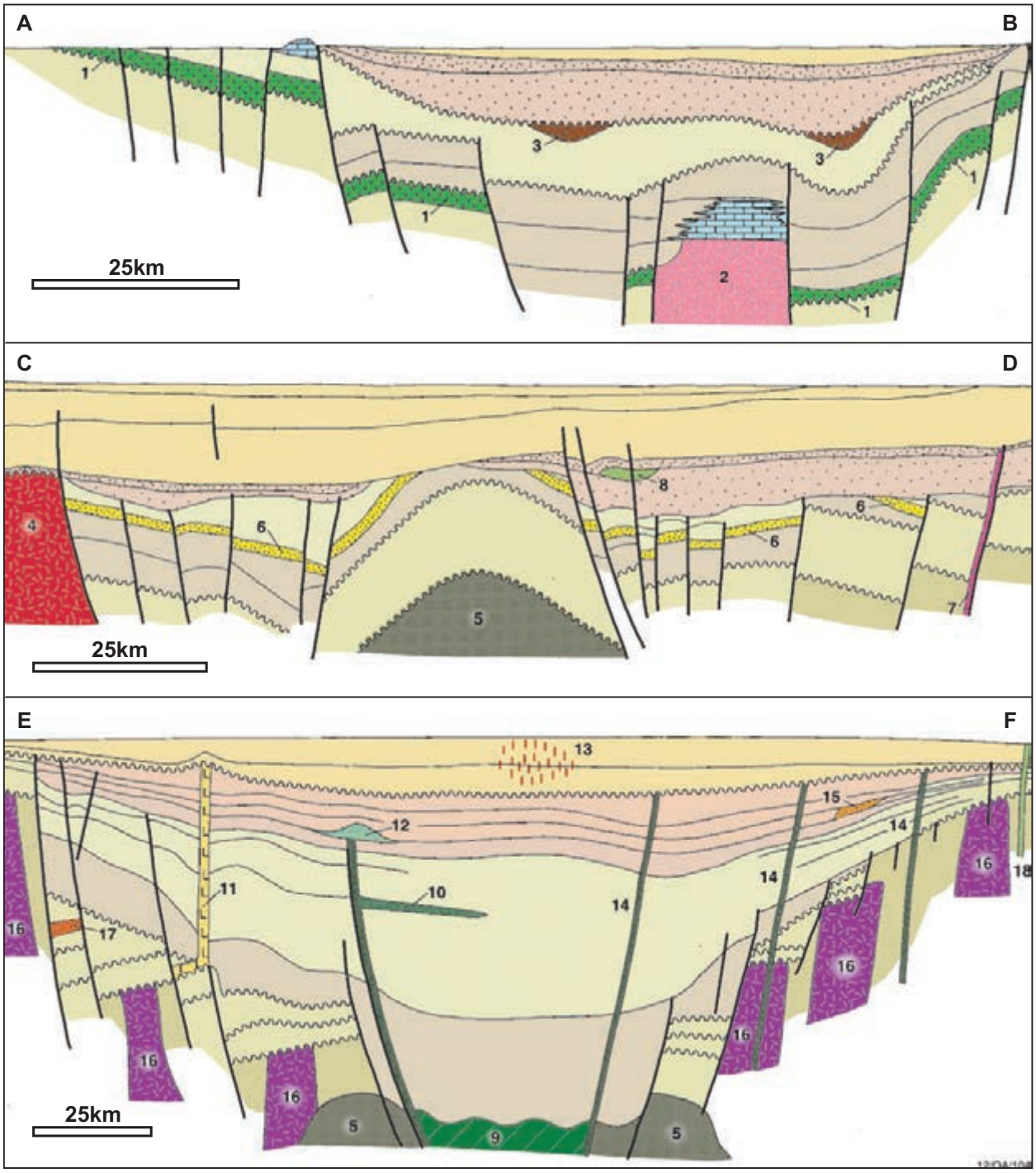

1) Pre-existing flood basalts.
2) Magnetic basement high resulting from intrusion, erosion or deformation.
3) Detrital or chemically precipitated magnetic minerals in palaeochannels.
4) Magnetic basement flanking the basin.
5) Mid-basin crustal intrusion.
6) Magnetic 'stratigraphic' sedimentary unit.
7) Magnetic minerals precipitated in fault plane.
8) Intrasedimentary volcanics.
9) Oceanic crust.
10) Igneous sill.
11) Salt diapir.
12) Buried volcanic centre.
13) Diagenetic magnetite or pyrrhotite formed by hydrocarbon plumes.
14) Igneous dykes.
15) Detrital magnetic minerals in bar and fan systems.
16) Intra basement magnetic bodies
17) Massive sulphide mineralisation, Cu-Pb-Zn-Au-Ag.
18) Kimberlite and lamprioite intrusions.

Figure 10.1: Idealised cross-sections illustrating units and structures that can cause magnetic responses in sedimentary basins (Gunn 1997b).

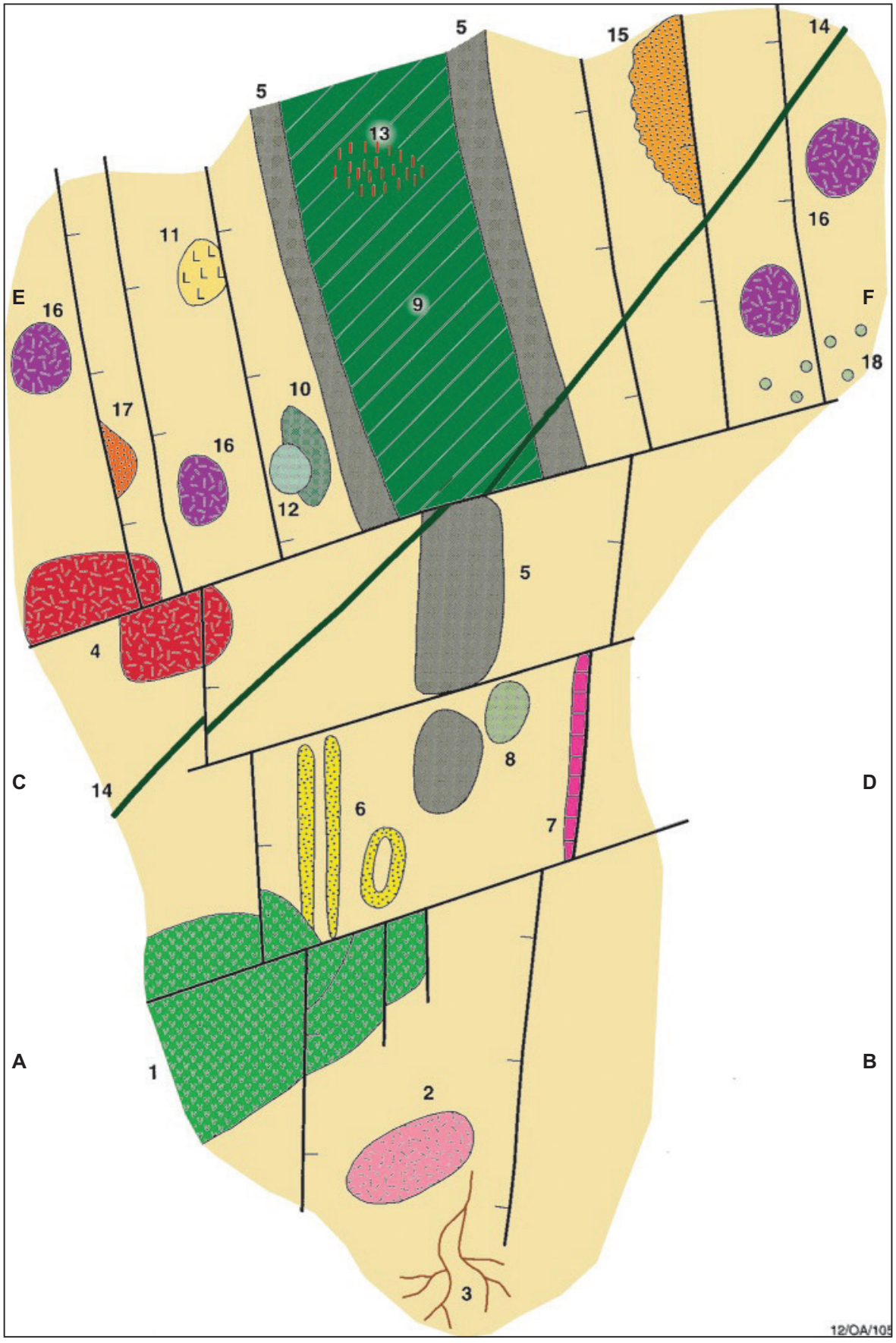

Figure 10.2: Plan showing idealised distribution of units and structures that can cause magnetic responses in sedimentary basins. The location of the representative sections shown in Figure 10.1 is included. Figure 10.1 explains each of the illustrated elements (Gunn 1997b).

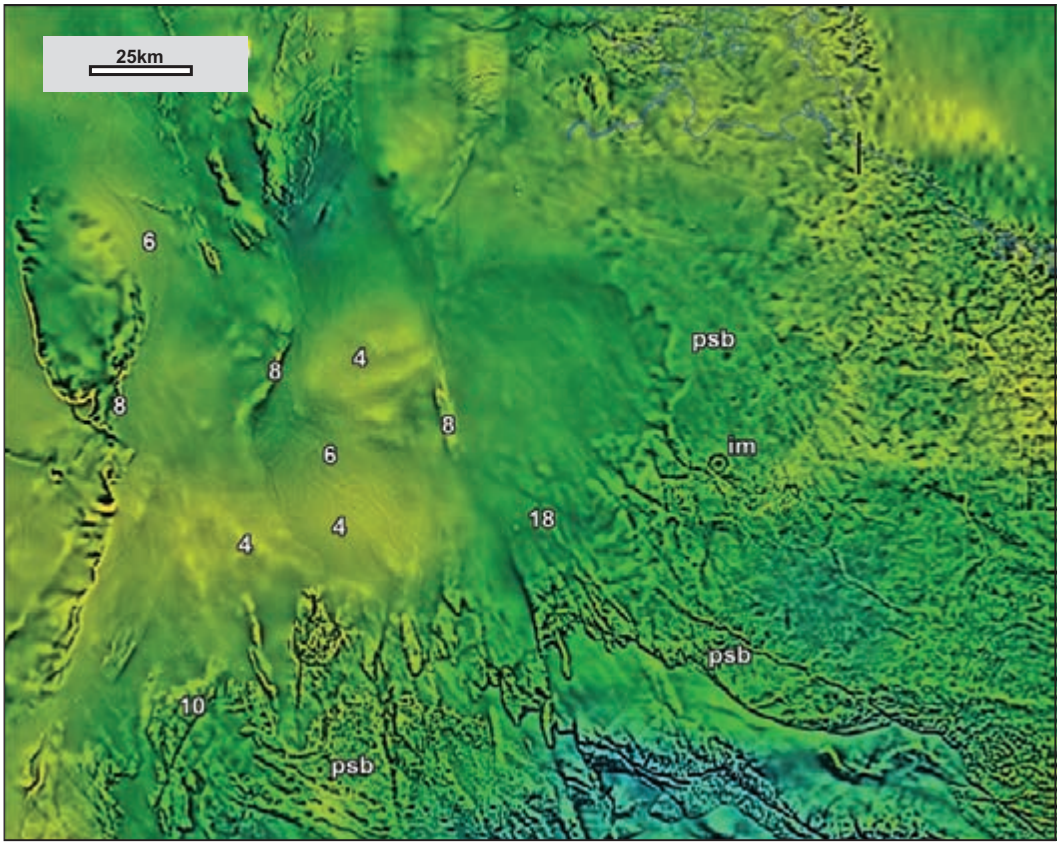

4 magnetic basement
6 magnetic sedimentary units
8 intra-sedimentary volcanics
10 intra-sedimentary sill
18 post basin intrusion

psb post basin flood basalts
im impact structure affecting psb.

Figure 10.3: Regional aeromagnetic image, McArthur Basin, NT. Numbers refer to features in Figure 10.1. Data from Geoscience Australia nation-wide grid.

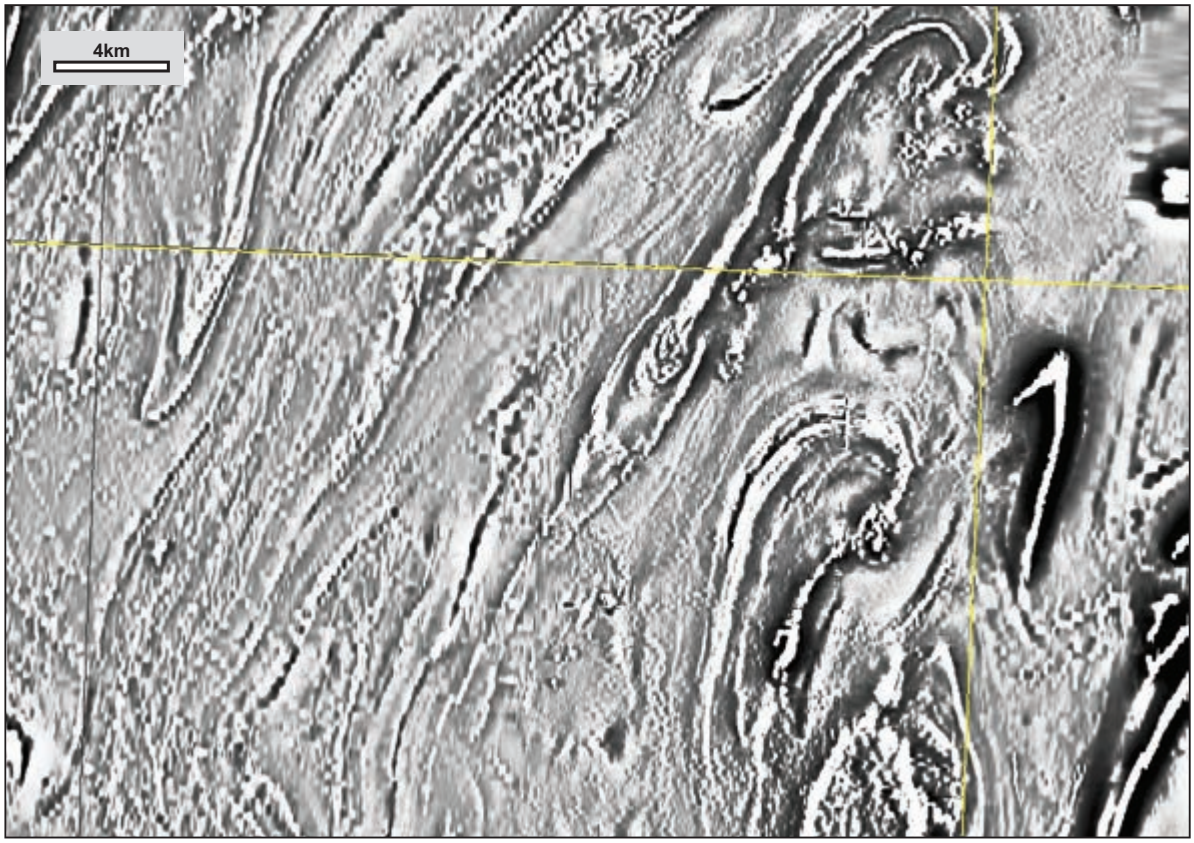

Figure 10.4: Neoproterozoic magnetic sedimentary units (predominantly siltstones) in the Adelaide Geosyncline, SA. Data from DMITRE.

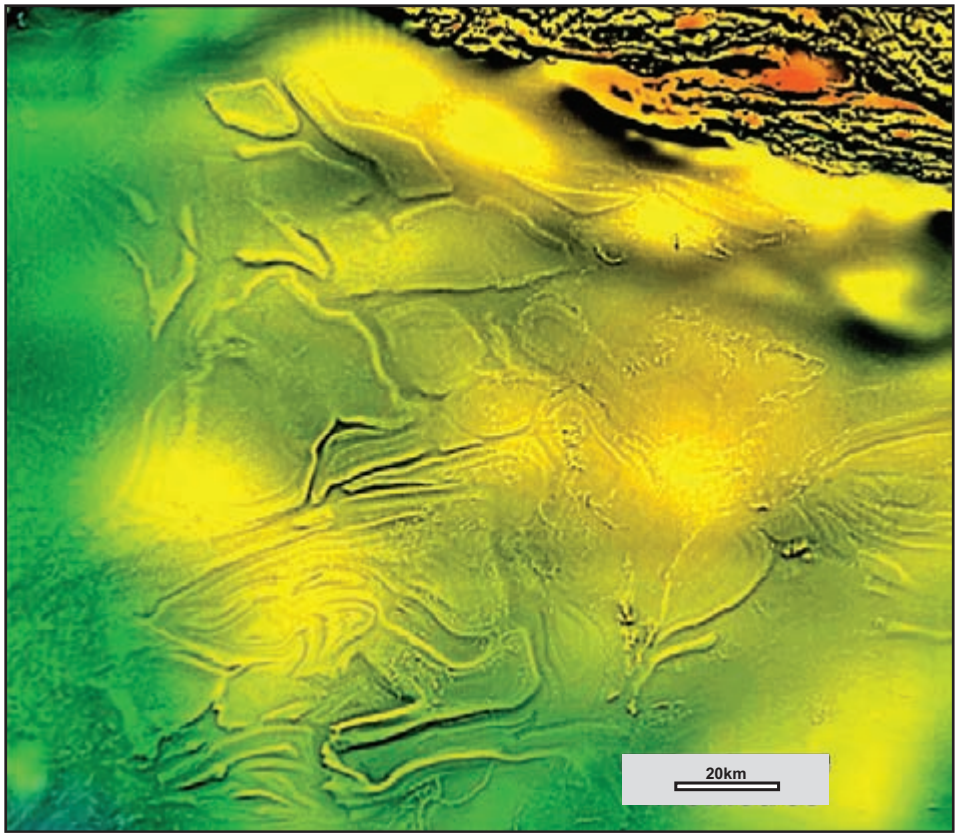

Figure 10.5: Folded Cambrian sediments, NW Amadeus Basin, NT. Data from Geoscience Australia nation-wide database. See Dentith and Cowan (2009) for discussion of this area.

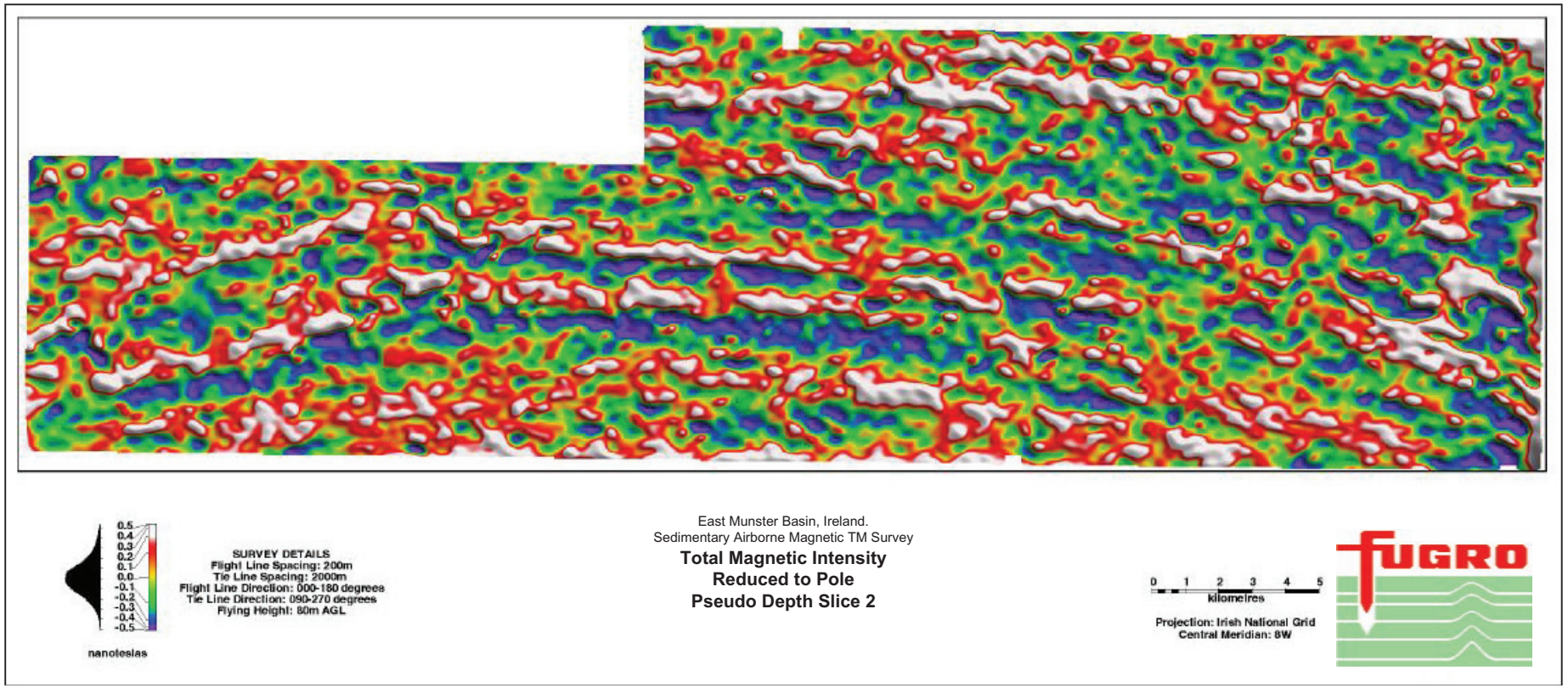

Figure 10.6: Upper Devonian Old Red Sandstone magnetic markers, East Munster Basin, Ireland. The overlying Lower Carboniferous carbonates also contain magnetic rock units. Example courtesy World Geoscience (now part of Fugro Airborne Surveys). Note the tiny signal levels which are the result of separation filtering. The full intensity range in this image is 1 nT. Pseudo Depth Slice2 is a shallow-source component emphasising magnetic rock units at depths of ~200–400 m.

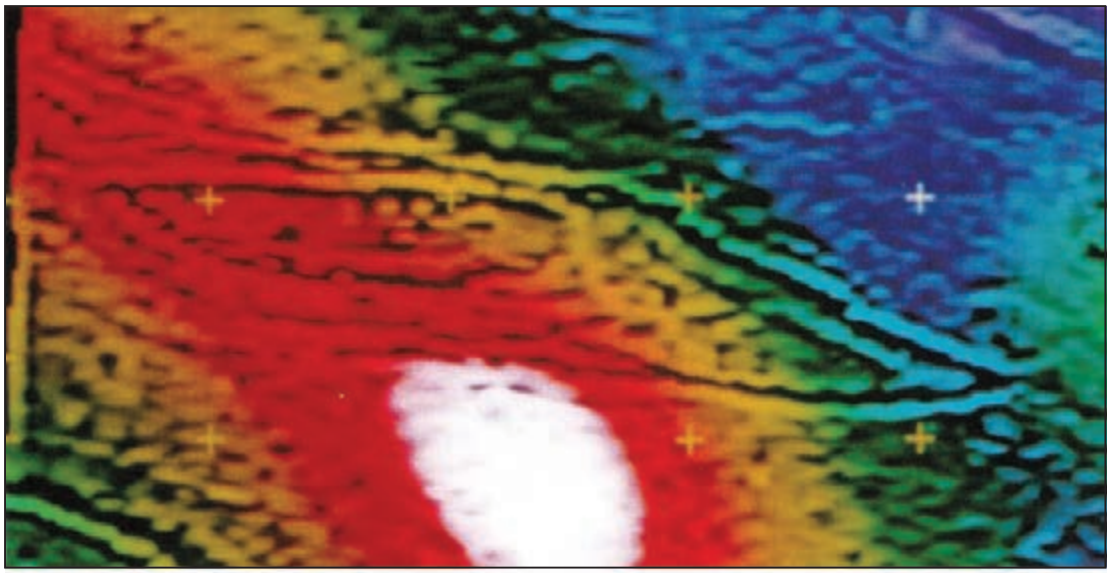

Grey scale AGC Enhancement of Magnetics with colour Total Magnetic Intensity

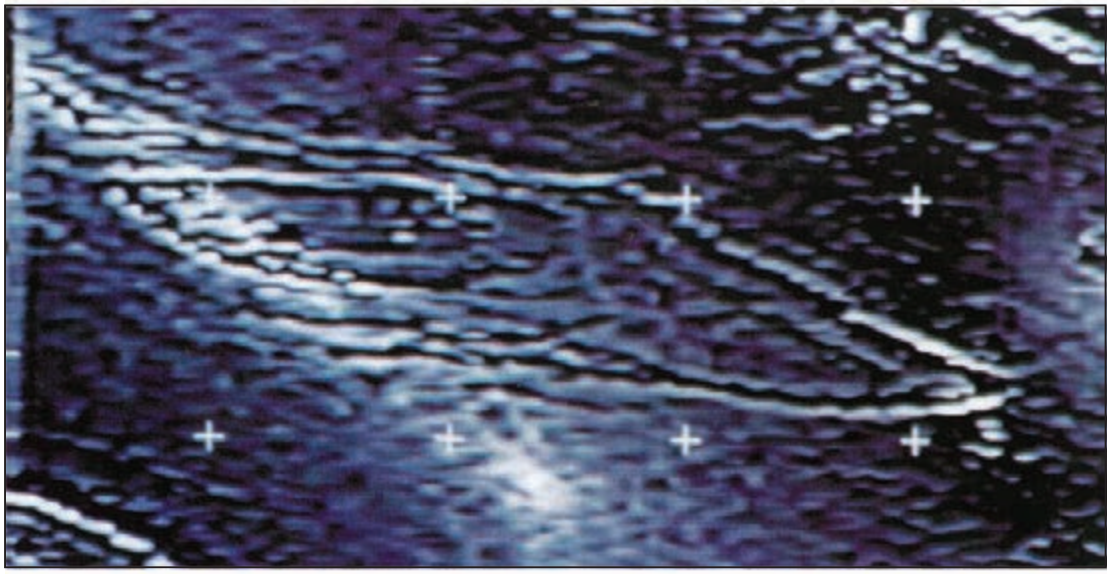

Grey scale AGC Enhancement of Magnetics

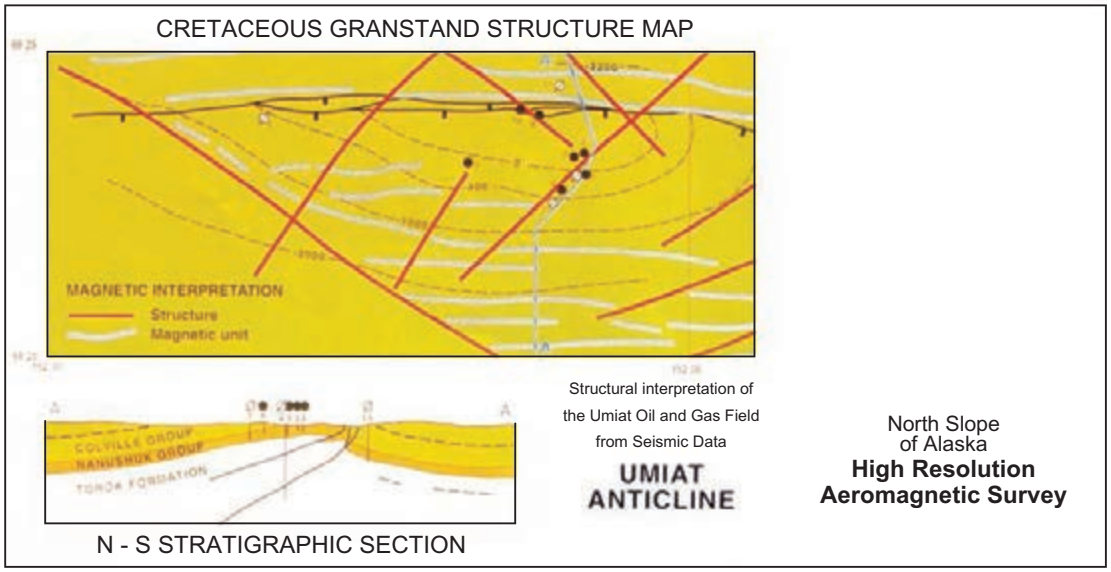

Figure 10.7: Aeromagnetic imagery over the Cretaceous Umiat oilfield in North Slope, Alaska (Norman 1993). The data highlight significant structural discordance and detachment between shallow-level folding and deeper basement structure.

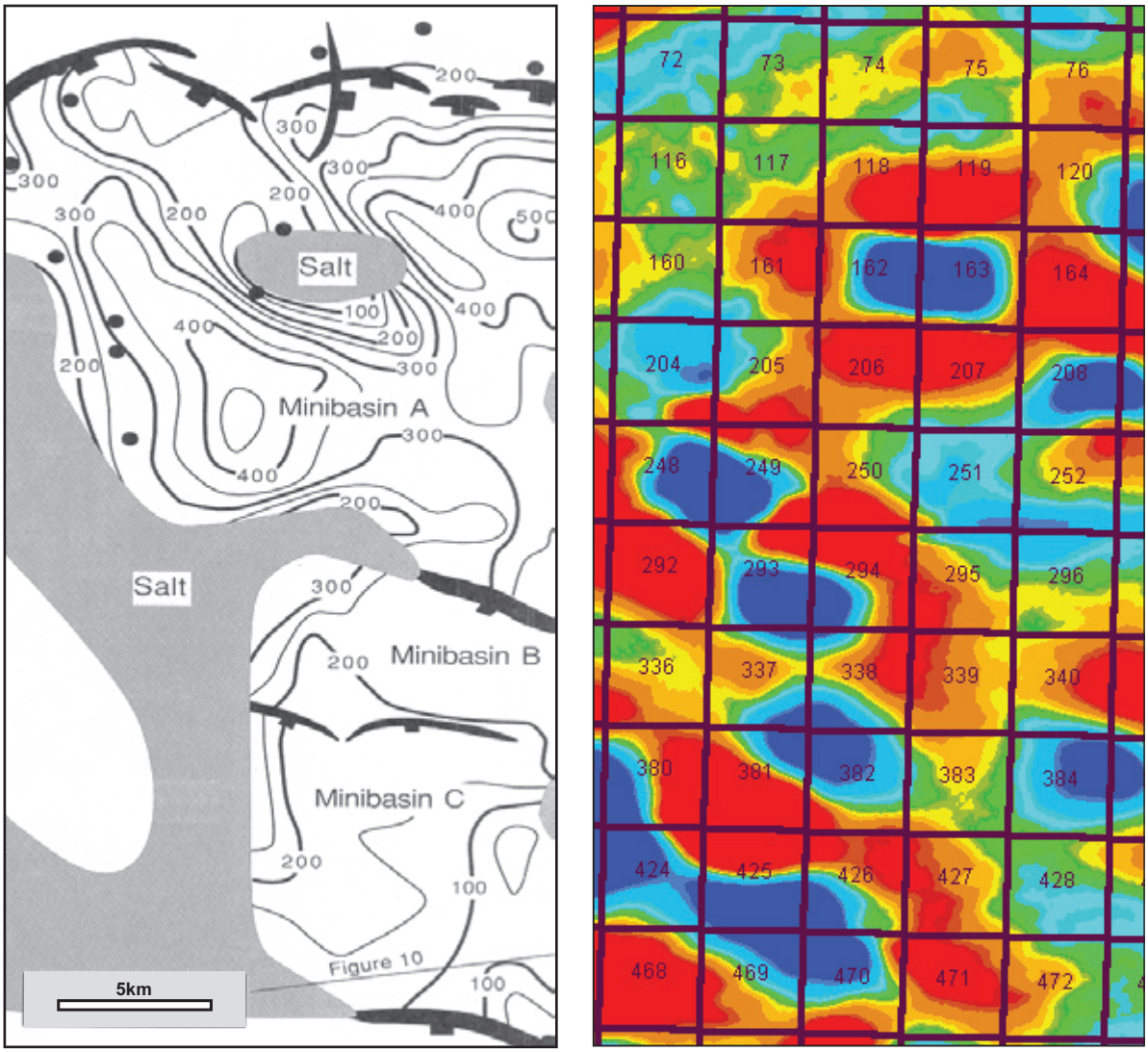

Figure 10.8: Magnetic low anomalies over intrusive salt structures, Genesis Field, Gulf of Mexico. The blue areas represent magnetic lows in the residual aeromagnetics. The seismic interpretation is shown for comparison. Graphics from Rowe (1998), courtesy of Fugro Gravity and Magnetic Services.

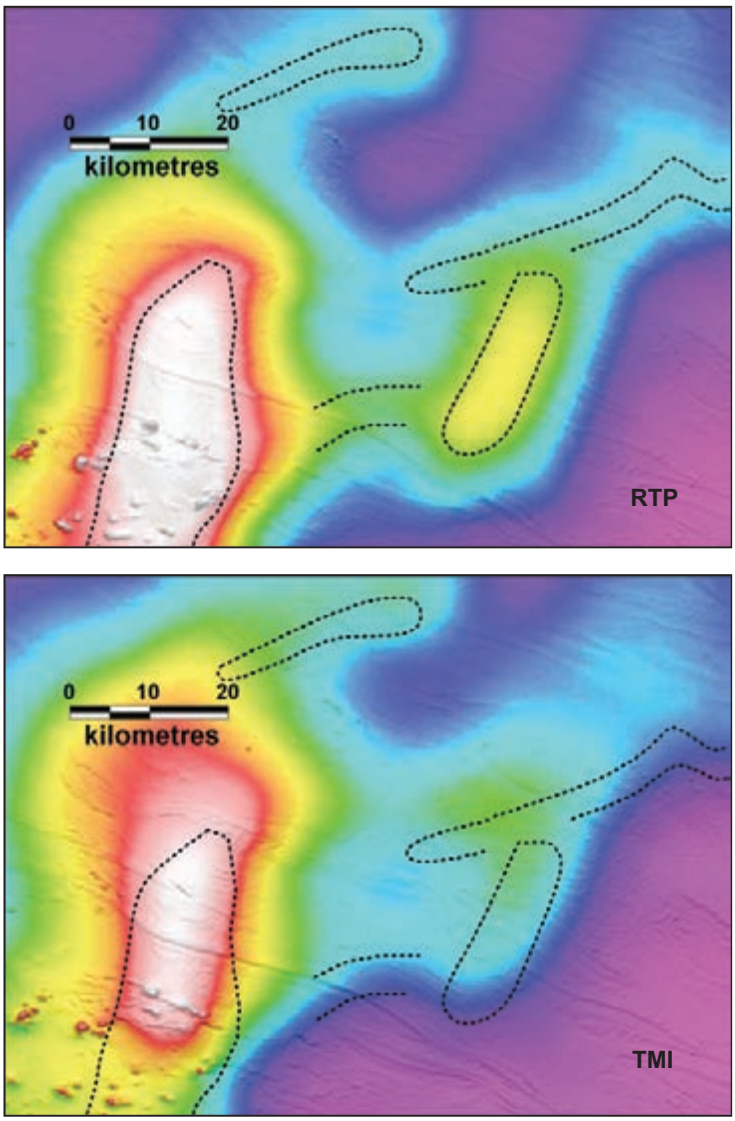

Figure 10.9: Comparison of RTP and TMI images for part of the Amadeus Basin study area. Note the large shift in anomaly outlines from the RTP (top) to the TMI (lower). The RTP outlines should better represent the shape and location of deep magnetic rock units.

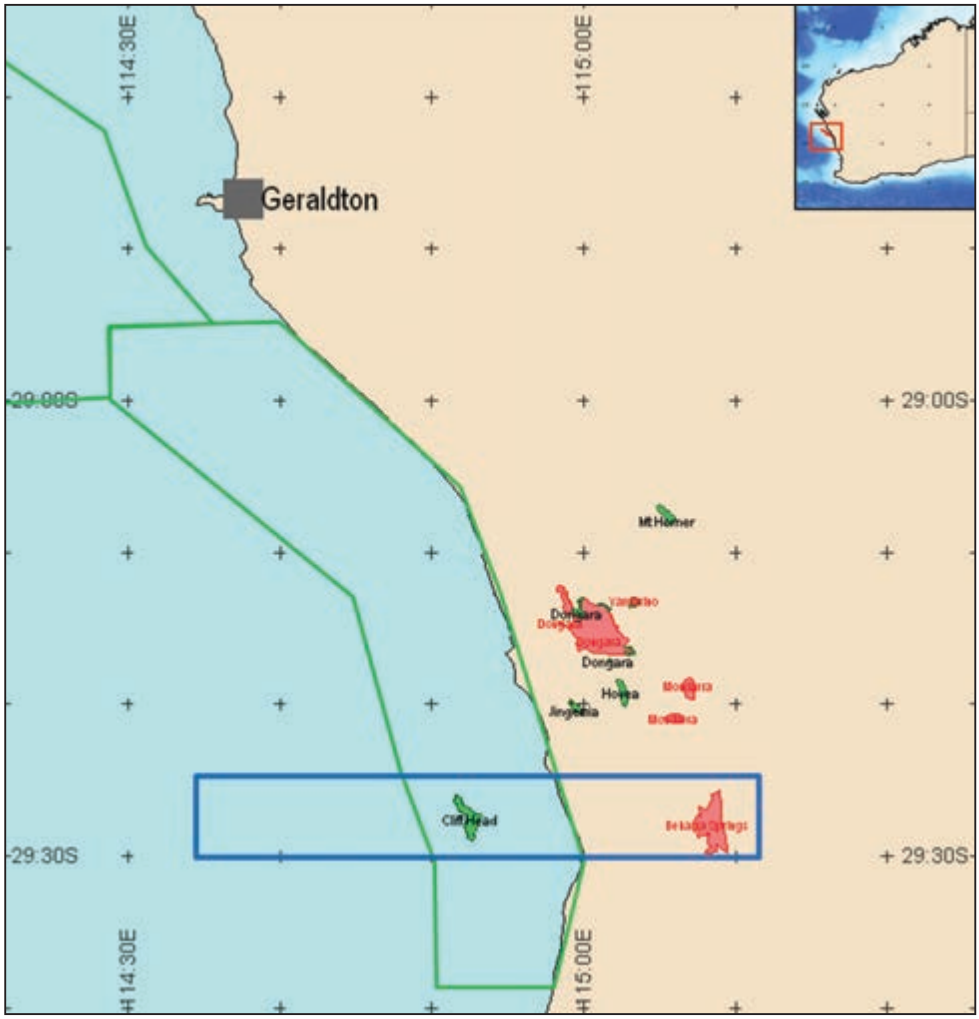

Figure 10.10: Location of Cliff Head Oil Field, ~15 km offshore and 80 km SSE of Geraldton. The blue box shows the outline of the aeromagnetic test strip acquired by Fugro Airborne Surveys in 2003 with a flight line spacing of 100 m. The green outlines show the more extensive aeromagnetic surveys subsequently acquired at 150 m line spacing by Roc Oil (WA) Pty Ltd as operators of the WA-286-P Joint Venture offshore WA.

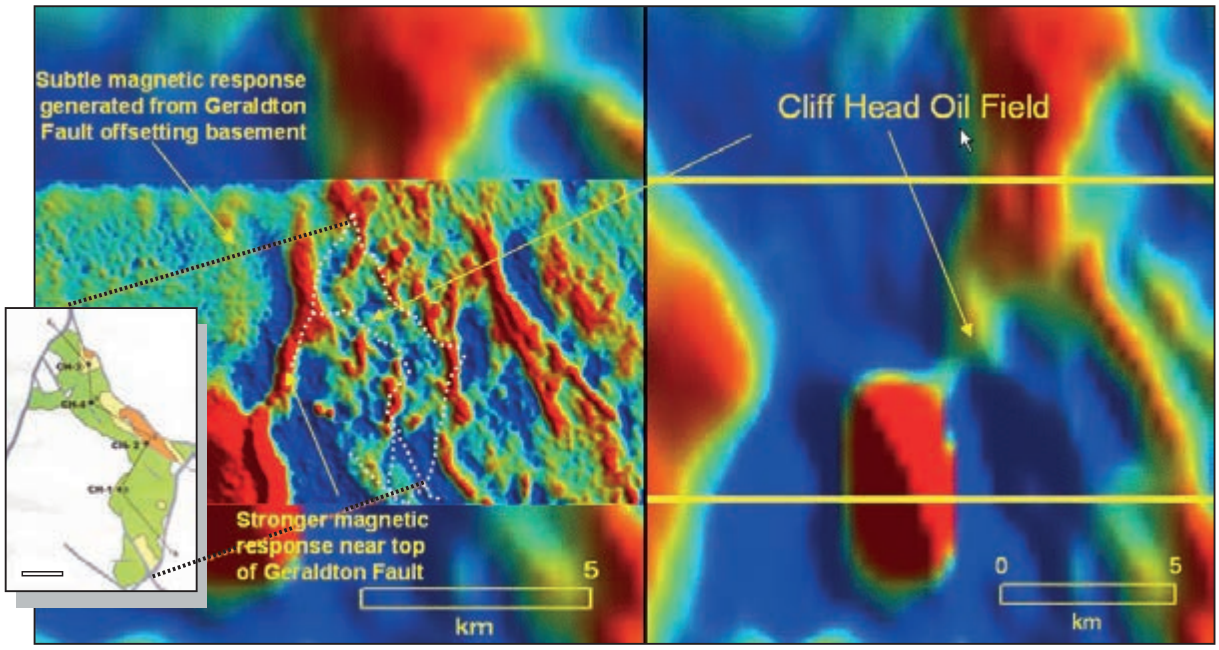

Figure 10.11: Comparison of 100 m and 1 km lines spaced aeromagnetic data acquired over the Cliff Head Oil Field. The increase in structural resolution is clear, including better definition of NNE–SSW-trending intrasedimentary faults. The inset map shows the Cliff Head Field Top Permian Reservoir Map – a strong correlation is evident between the bounding faults and the magnetic data. Data courtesy of Fugro Airborne Surveys.

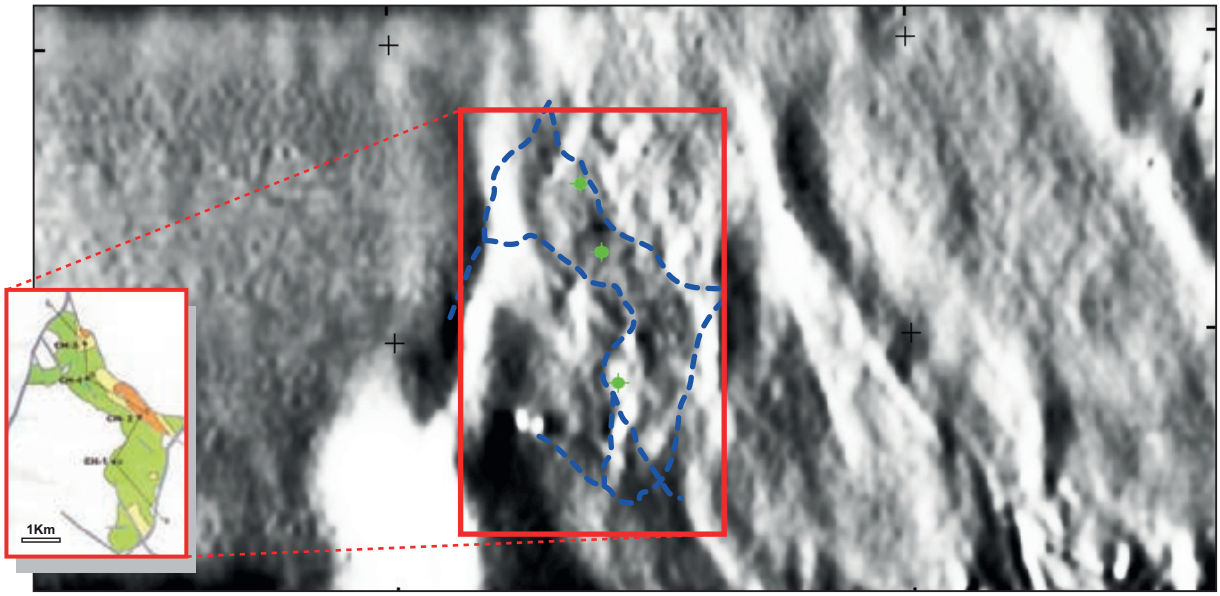

Figure 10.12: Aeromagnetic data over Cliff Head Oil Field acquired at 100 m line spacing. The greyscale MagSlice 2 image (shallow spectral depth window) highlights magnetic responses in faults at varying structural levels. For example, the west-dipping Geraldton Fault is imaged at several depths, resulting in parallel magnetic features. Note also the reduction in magnetic response coincident with the Cliff Head field. Data courtesy of Fugro Airborne Surveys.

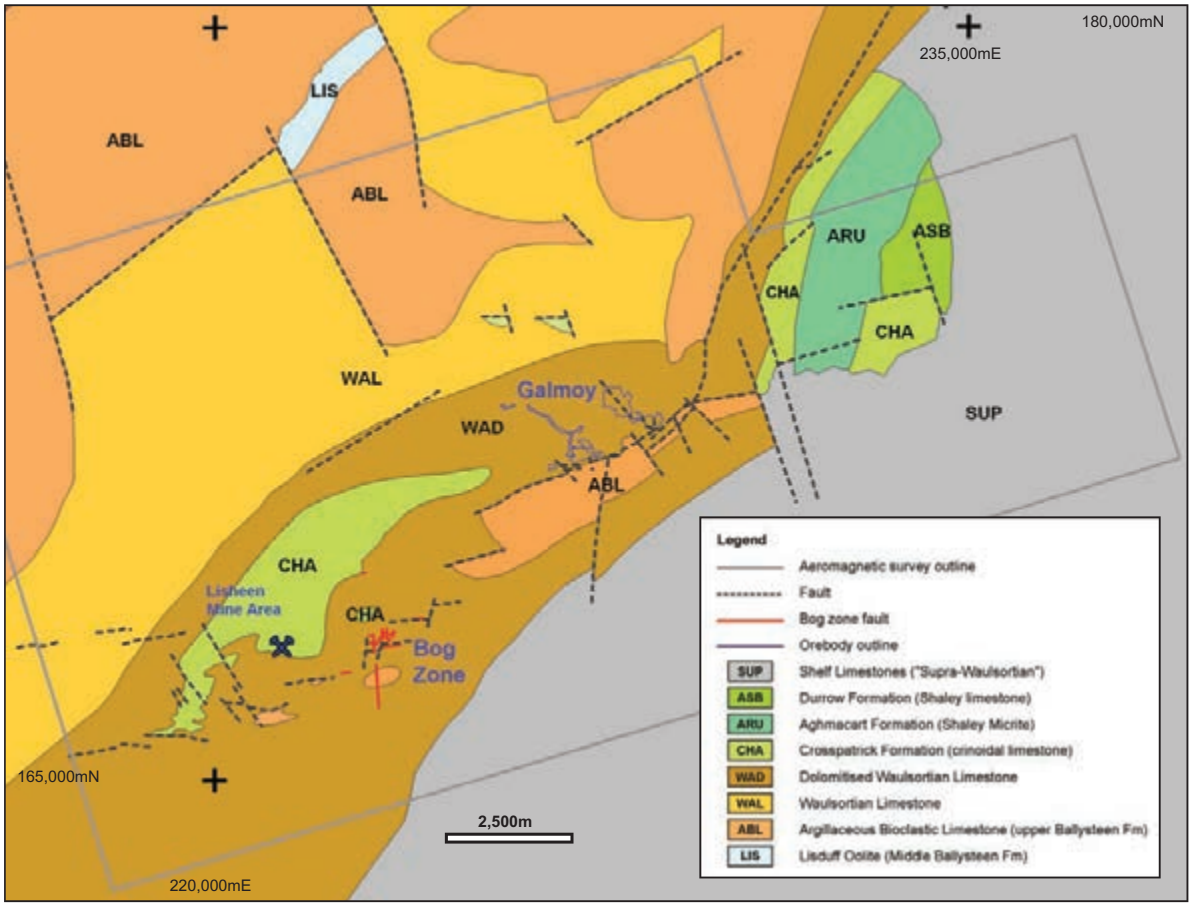

Figure 10.13: Bedrock geology map of the Galmoy area derived largely from drill-hole information. Data courtesy Lundin Mining.

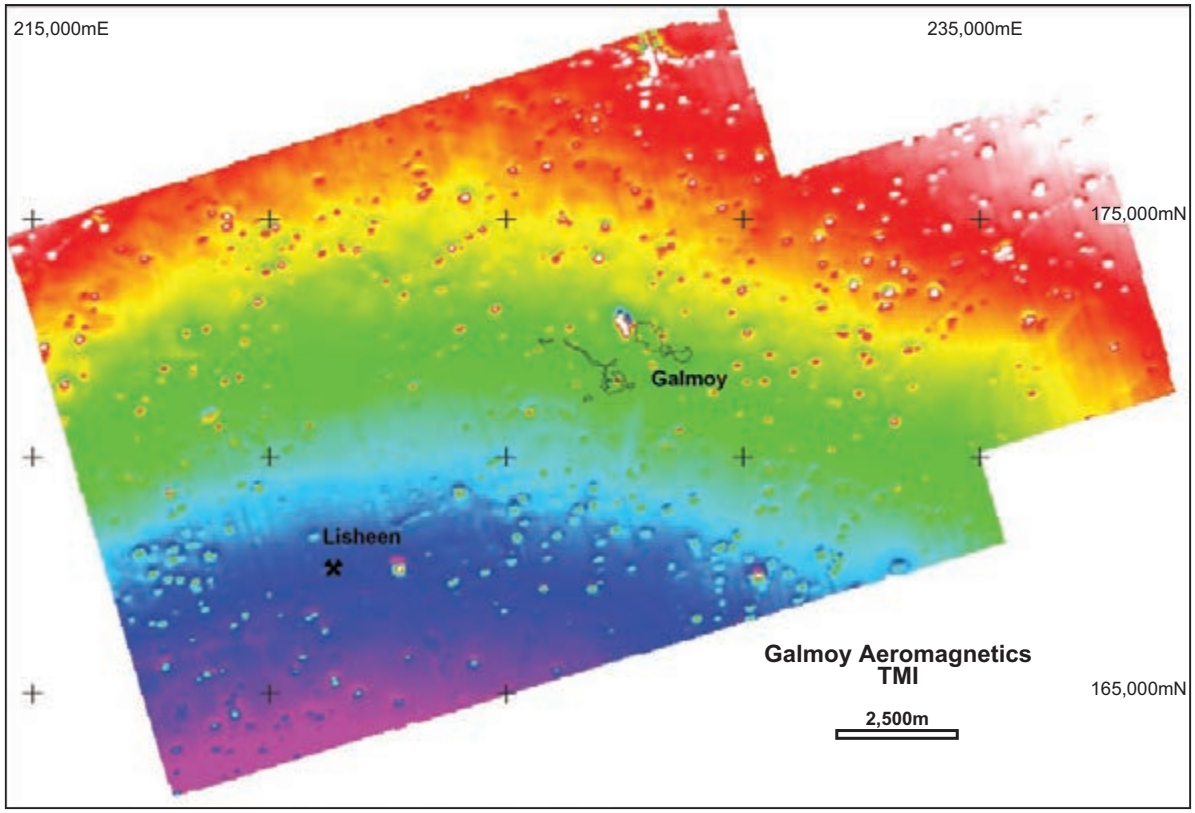

Figure 10.14: Final TMI image. The intensity range is 90 nT. The Galmoy ore bodies are outlined with a faint line and the crossed-picks symbol indicates the general Lisheen mining area. Data courtesy Lundin Mining.

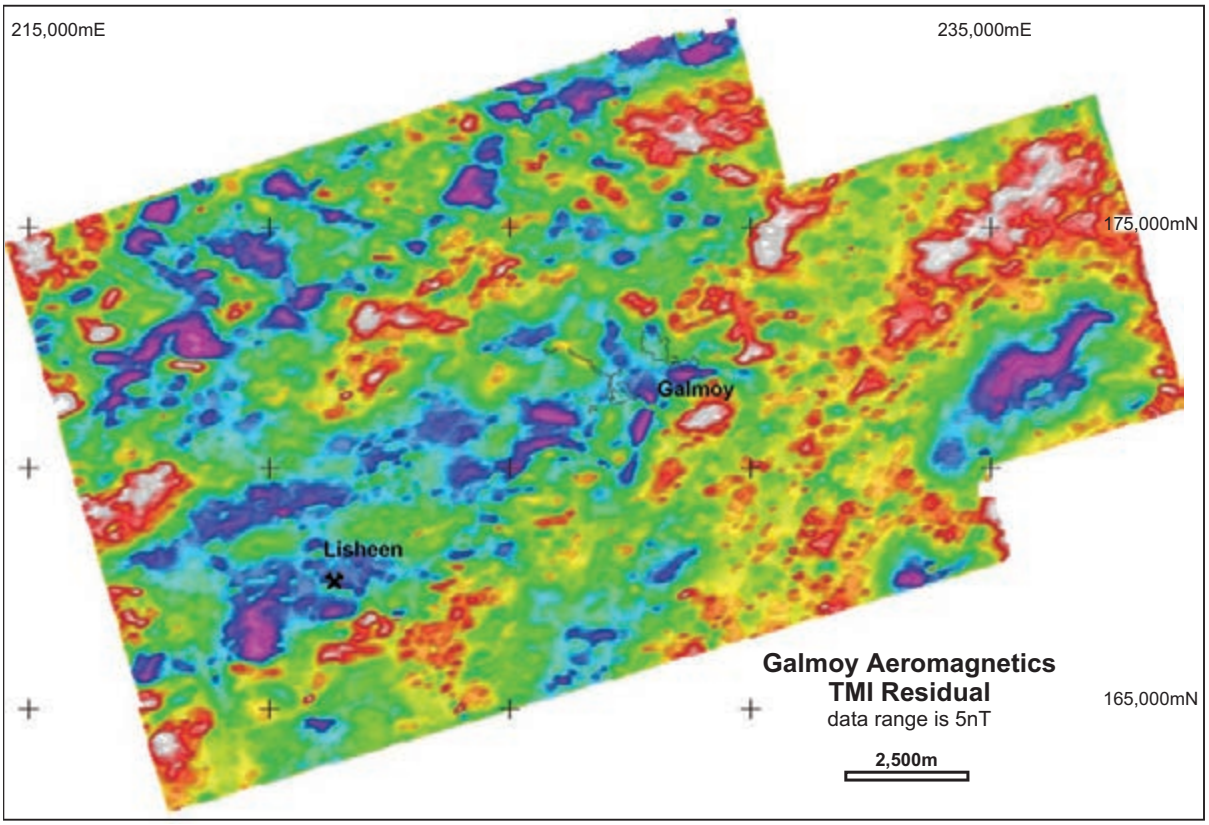

Figure 10.15: Residual TMI image. Cultural sources and regional gradient have been removed. The intensity range is 5 nT.

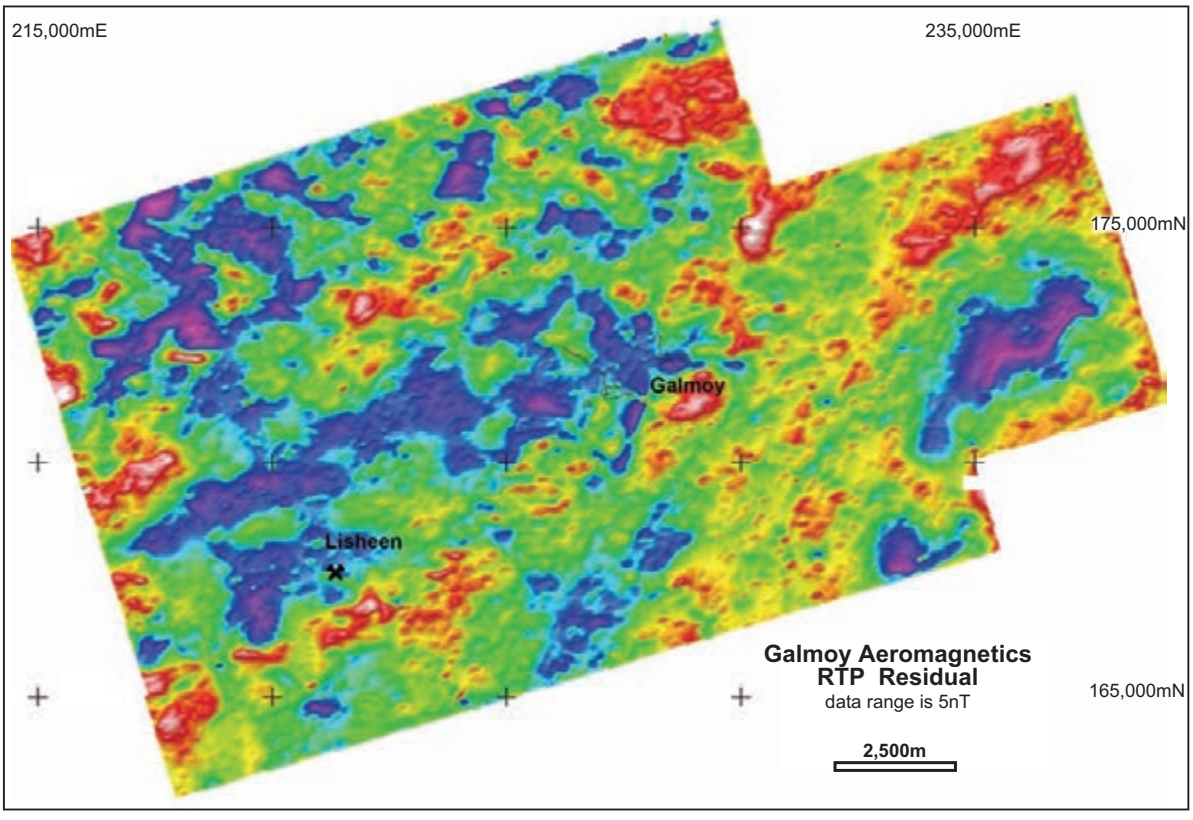

Figure 10.16: Residual RTP intensity image. The intensity range is 5 nT.

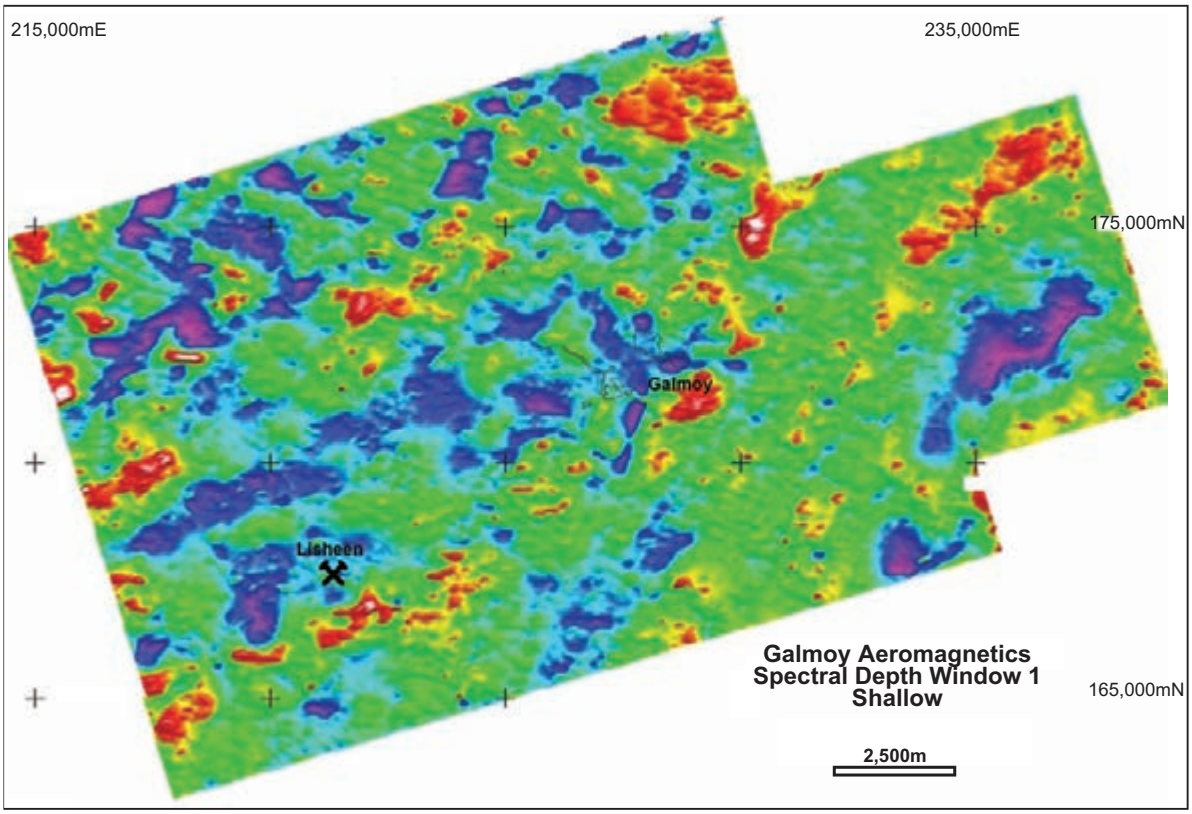

Figure 10.17: Residual RTP spectral depth window 1. This emphasises shallow magnetic sources (~0–150 m depth).

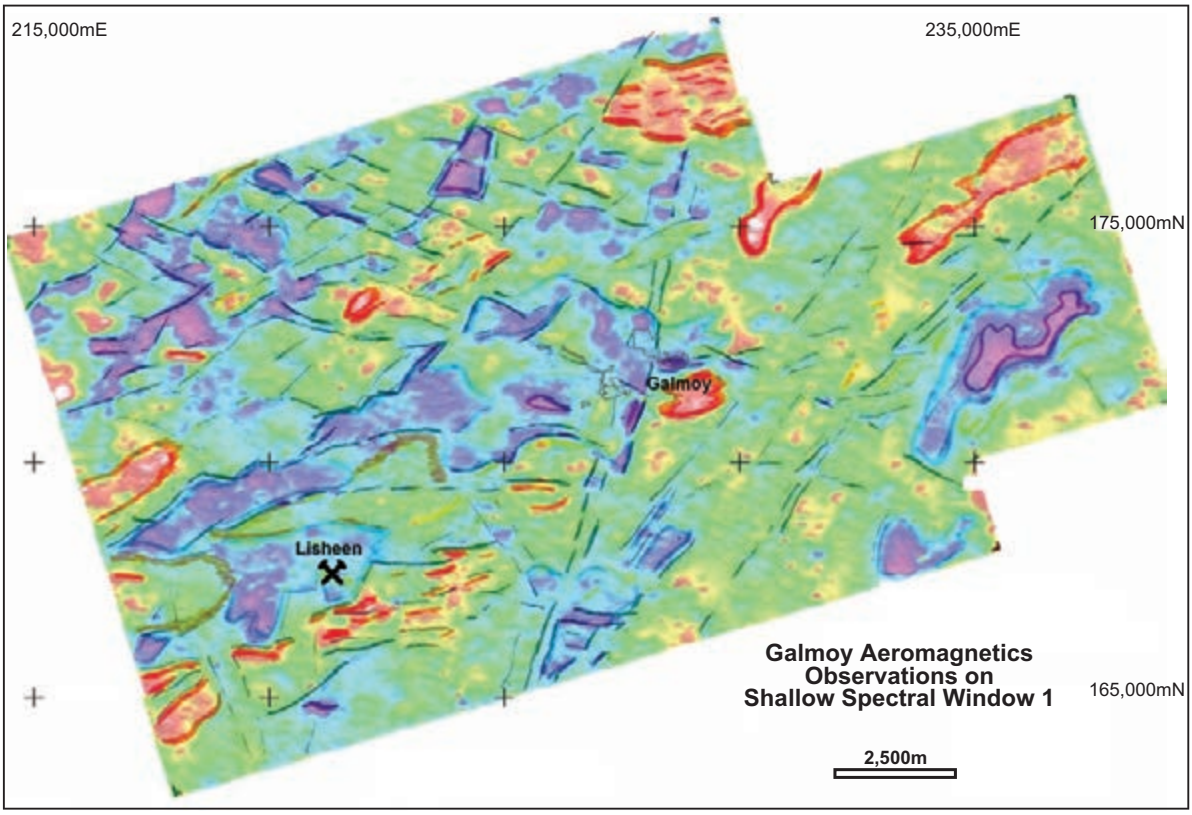

Figure 10.18: Observation layer on spectral depth window 1. The red/orange lines outline the stronger magnetic zones, the blue/purple lines very weak or non-magnetic zones and the black lines show contacts, fractures and faults.

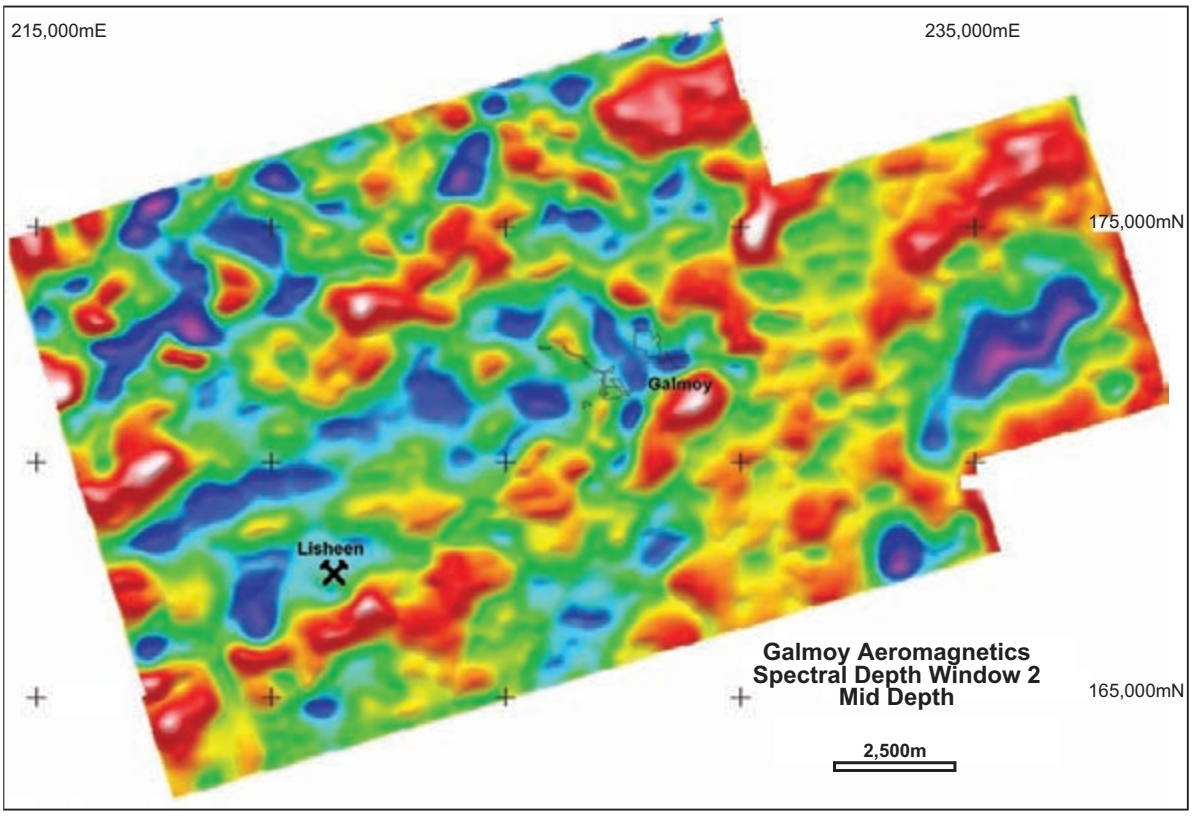

Figure 10.19: Residual RTP spectral depth window 2. This emphasises mid-depth magnetic sources (~100–250 m depth).

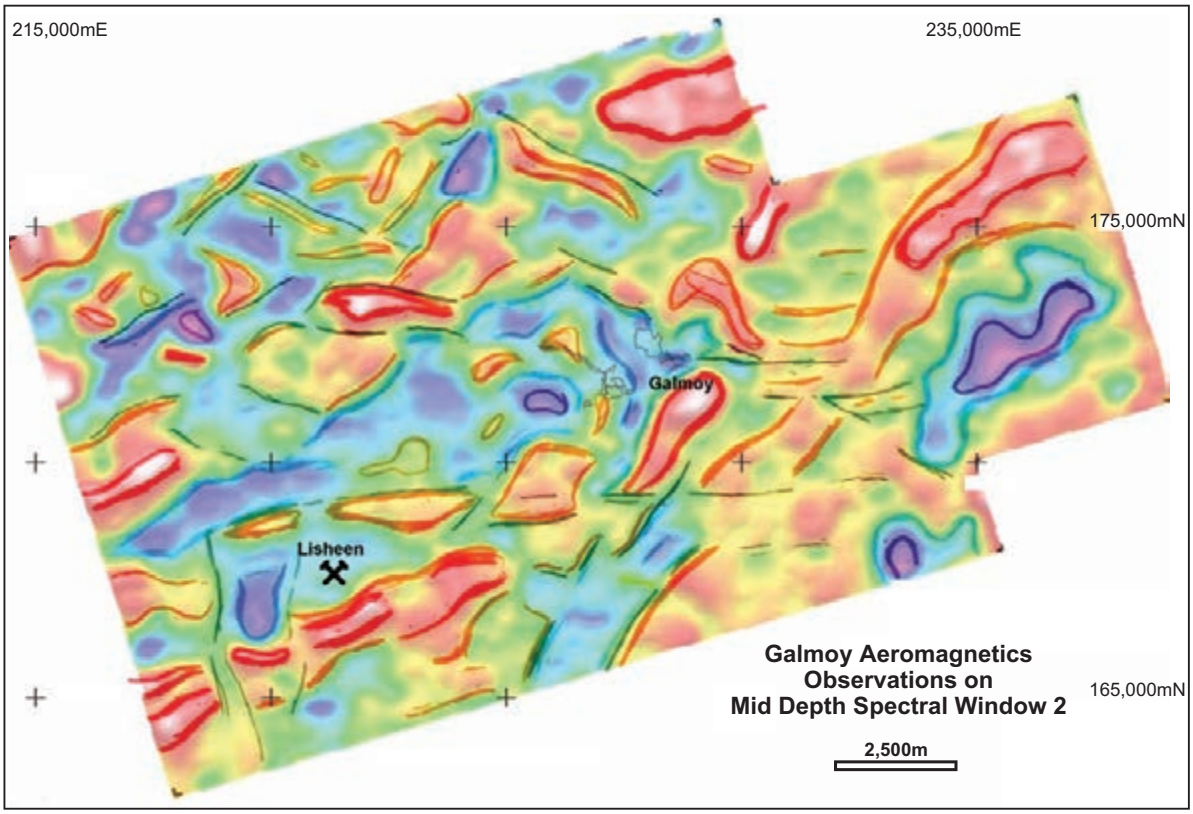

Figure 10.20: Observation layer on spectral depth window 2. The red/orange lines outline the stronger magnetic zones, the blue/purple lines very weak or non-magnetic zones and the black lines show fractures and faults.

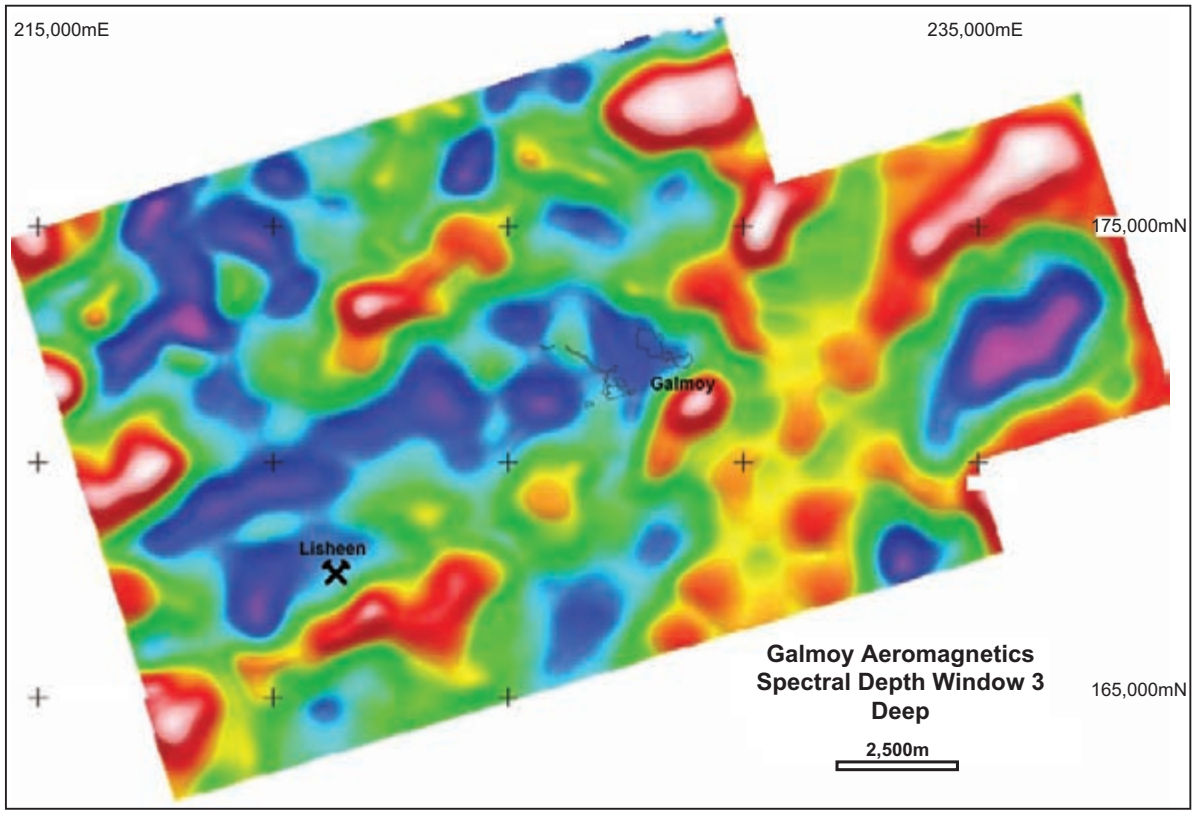

Figure 10.21: Residual RTP spectral depth window 3. This emphasises mid-depth magnetic sources (~300–450 m depth).

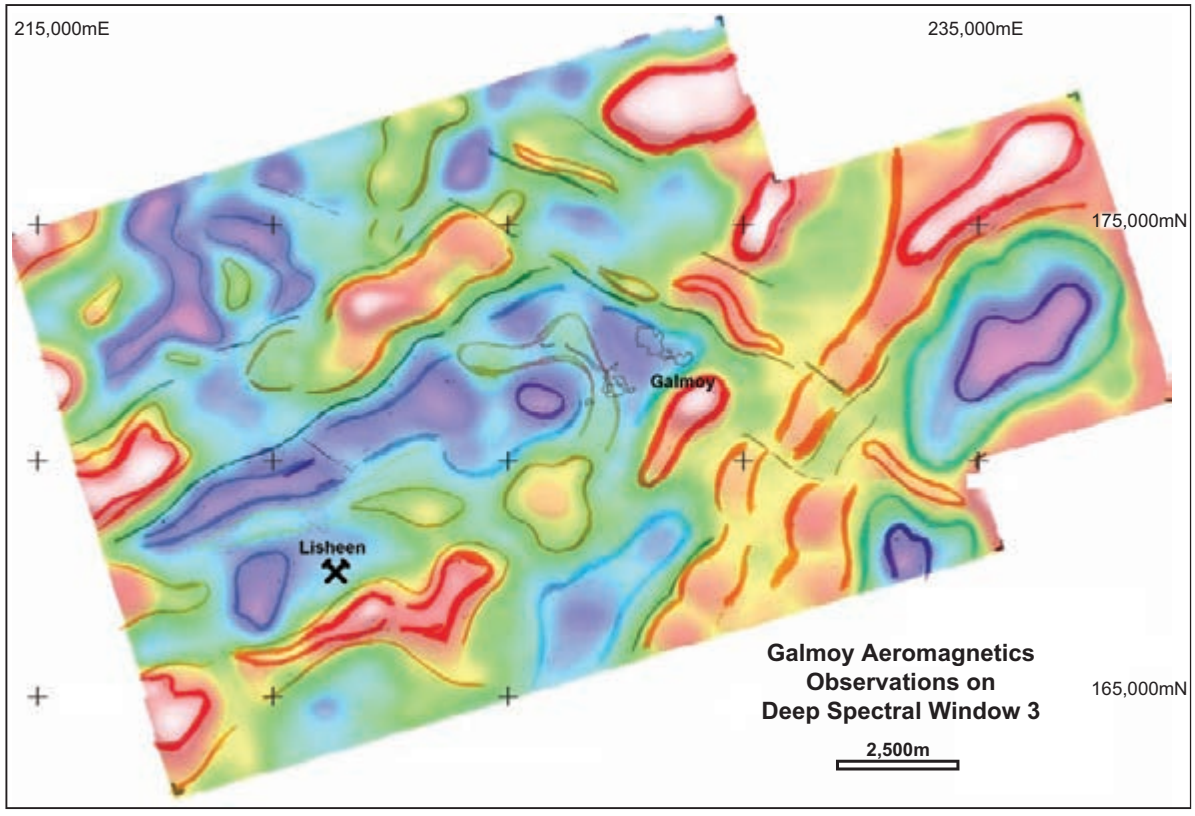

Figure 10.22: Observation layer on spectral depth window 3. The red/orange lines outline the stronger magnetic zones, the blue/purple lines very weak or non-magnetic zones and the black lines show fractures and faults.

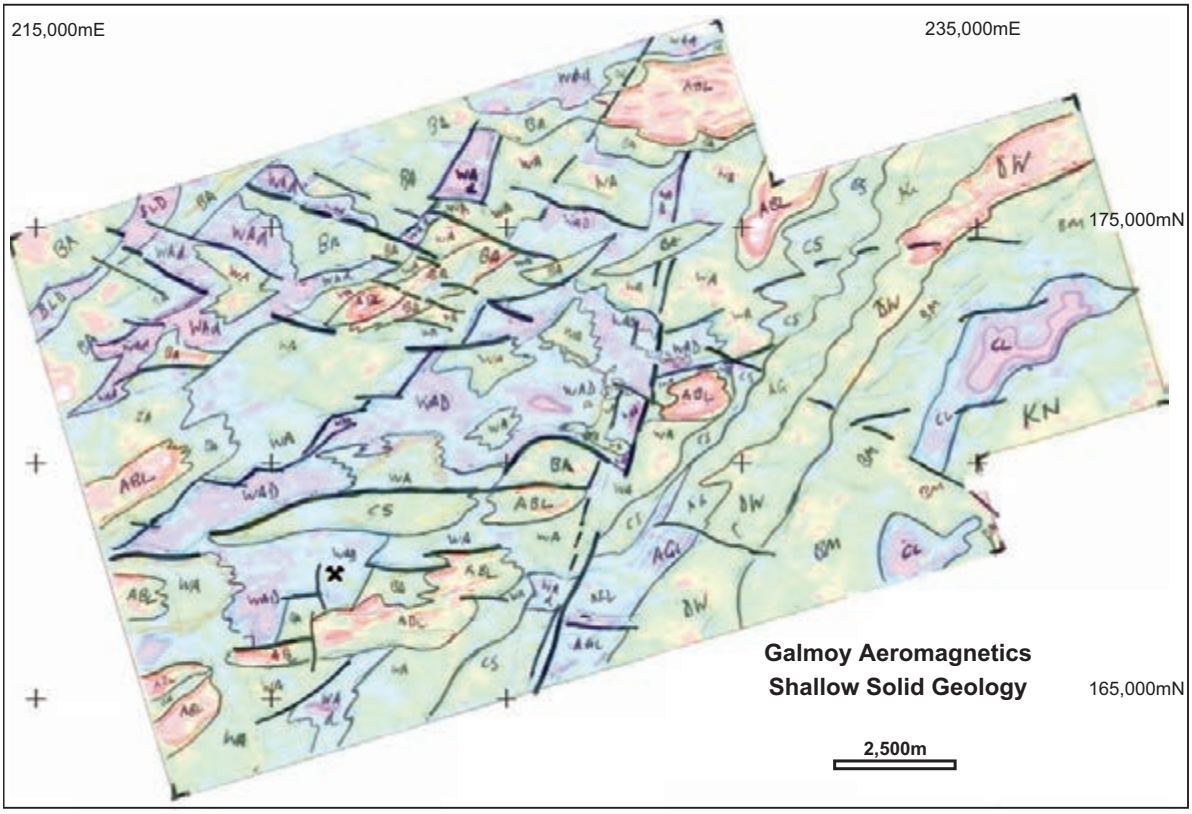

Figure 10.23: Draft shallow solid geology superimposed on spectral depth window 1.

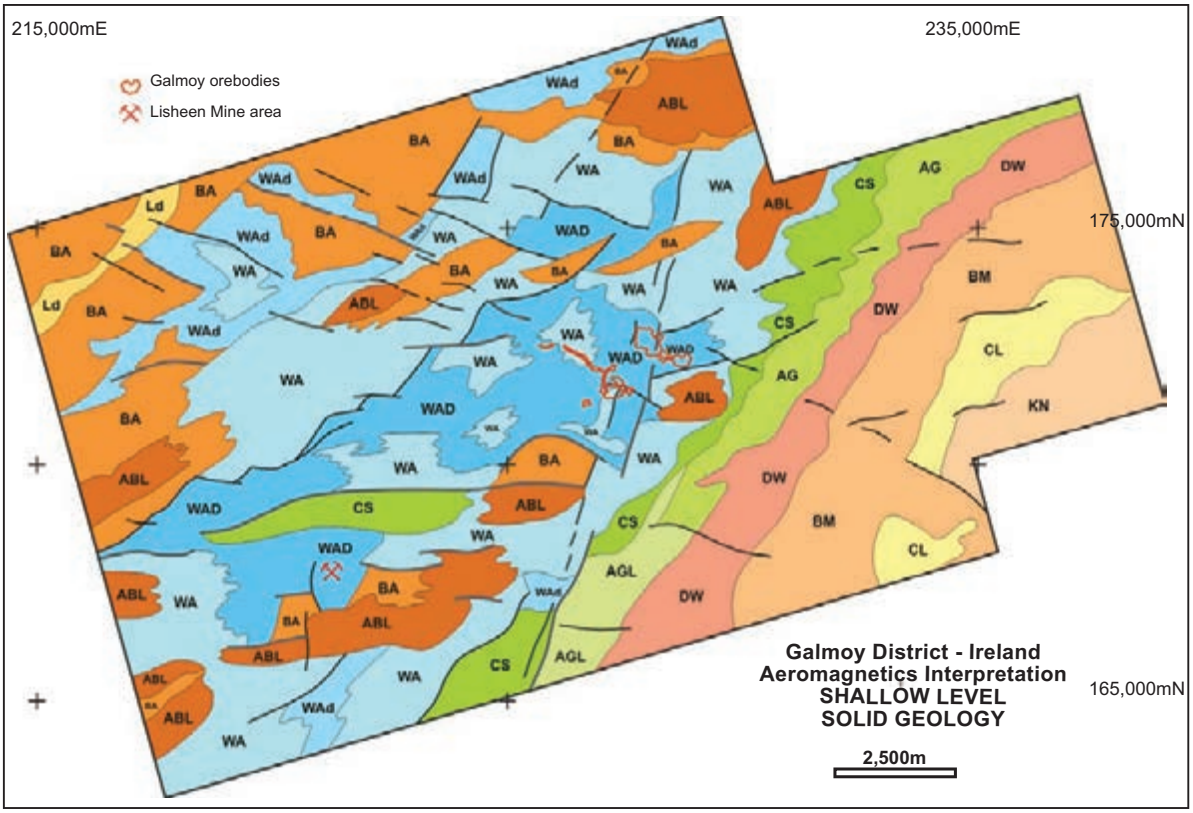

Figure 10.24: Shallow solid geology interpretation.

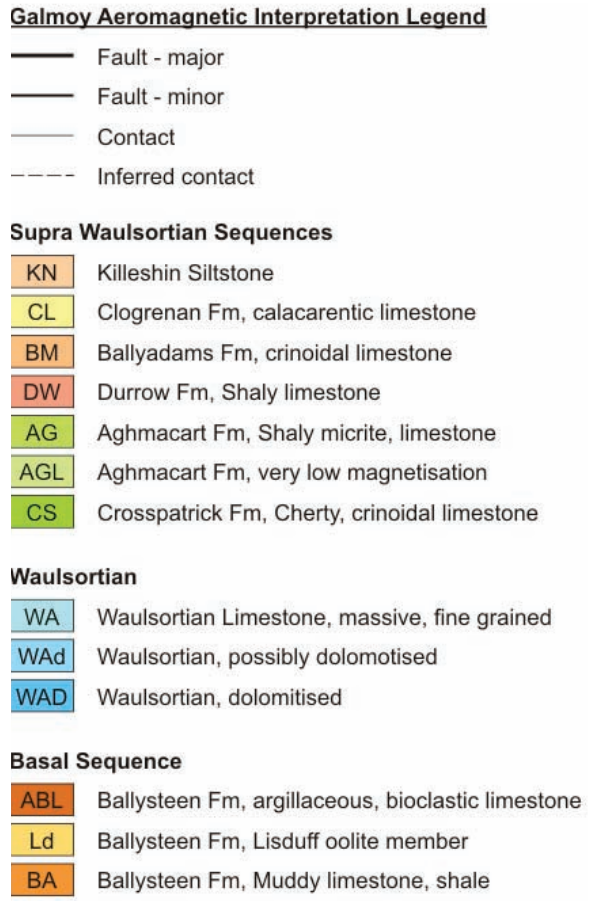

Figure 10.25: Legend for both shallow and deep solid geology interpretations (Figs 10.24 and 10.28).

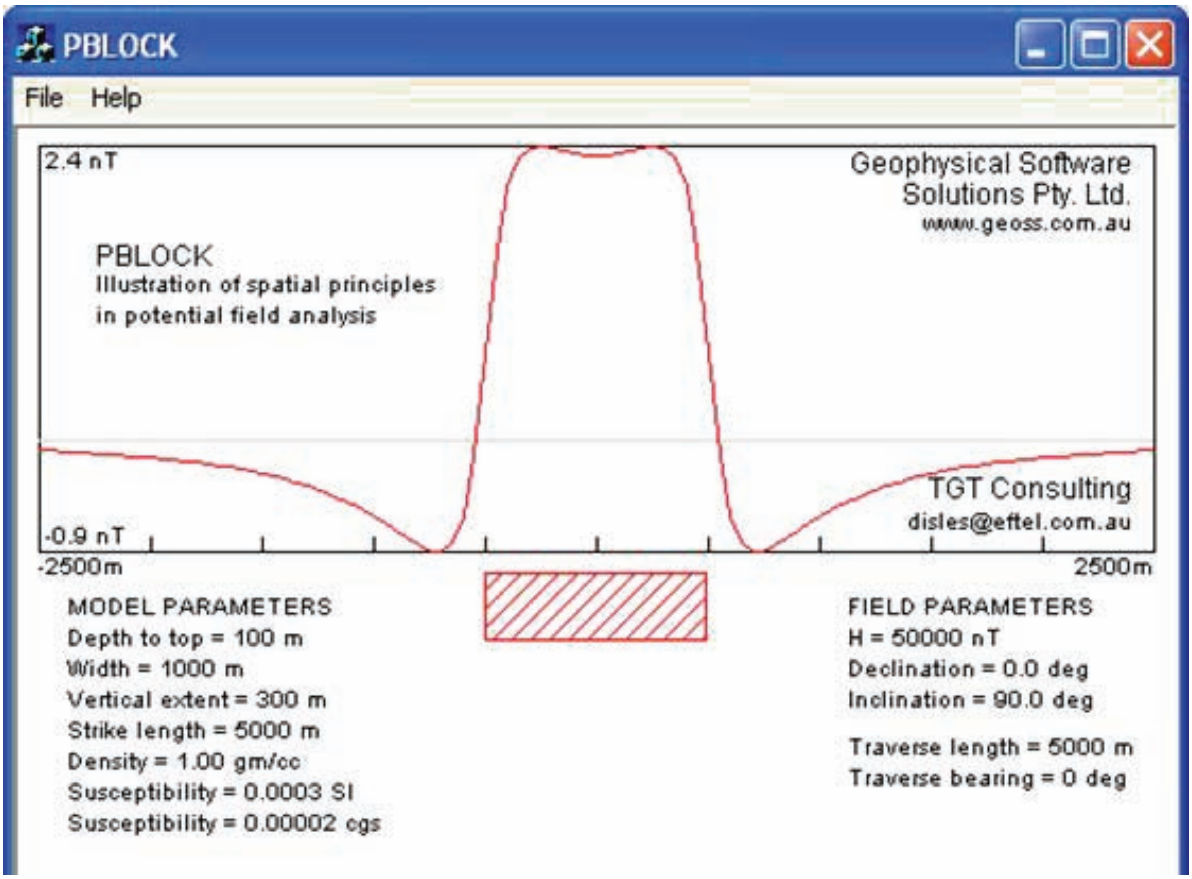

Figure 10.26: Simple model for the basal Ballysteen Formation limestone sequence.

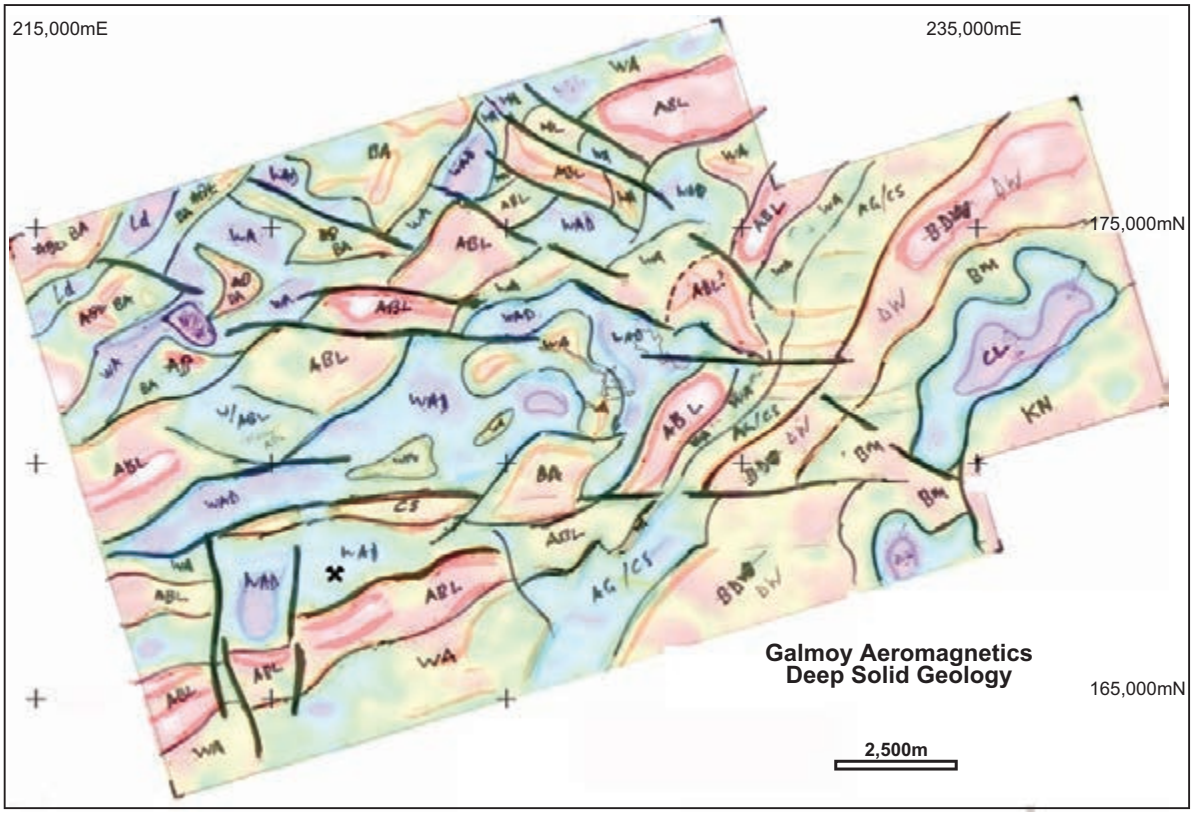

Figure 10.27: Draft deeper-level solid geology superimposed on spectral depth window 2.

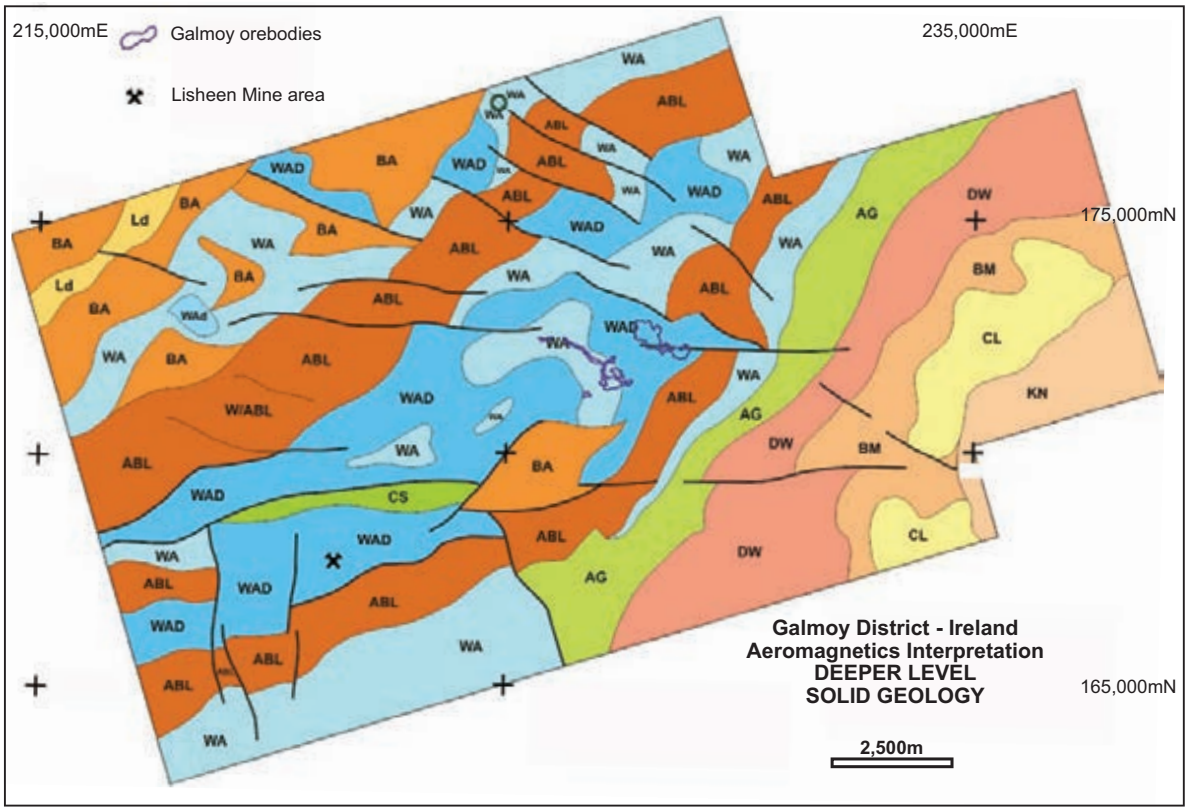

Figure 10.28: Deeper-level solid geology interpretation. See Figure 10.25 for legend.

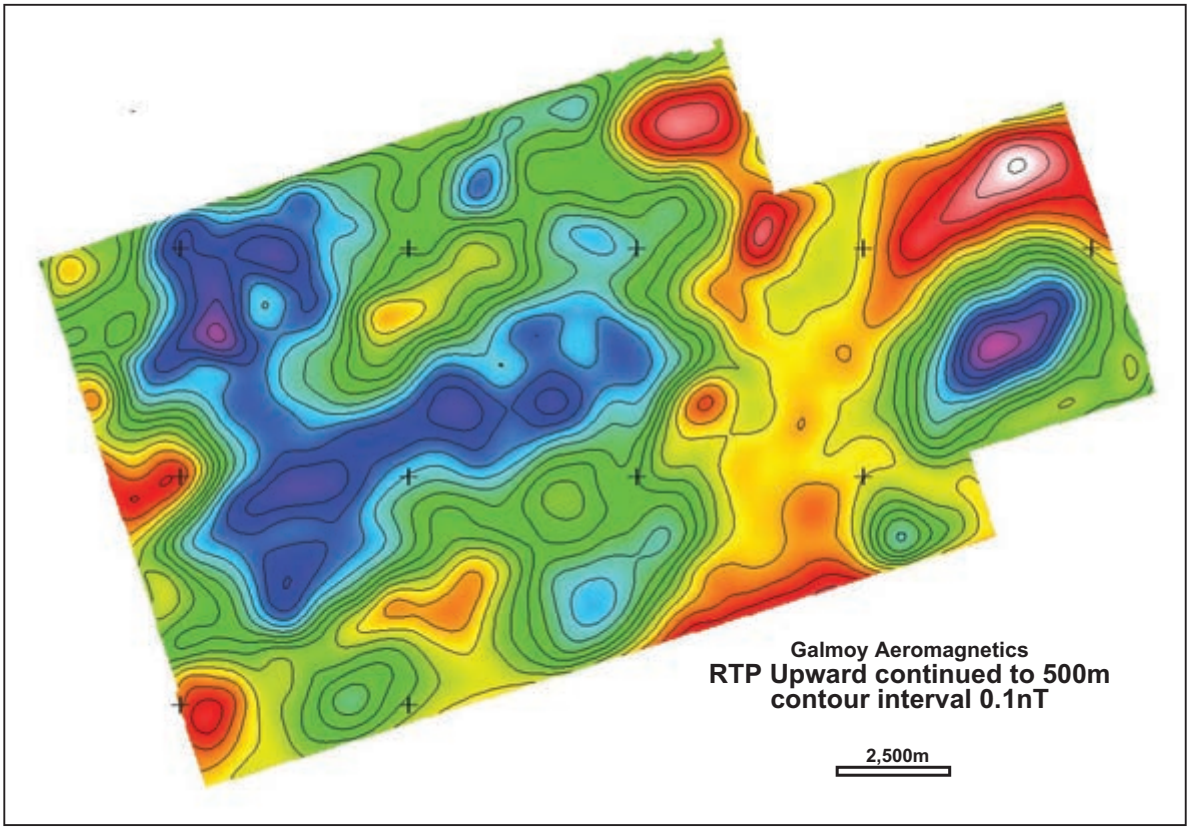

Figure 10.29: Galmoy residual RTP magnetic intensity upward-continued to 500 m agl.

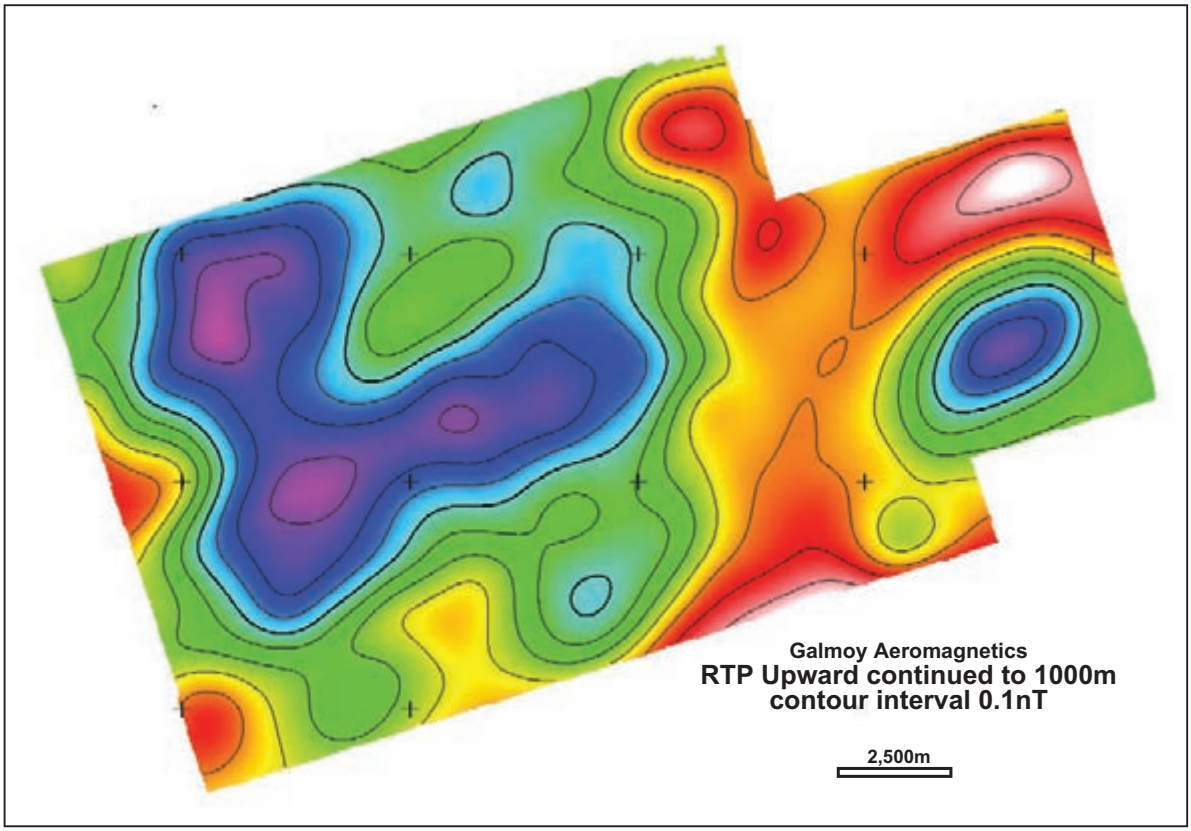

Figure 10.30: Galmoy residual RTP magnetic intensity upward-continued to 1000 m agl.

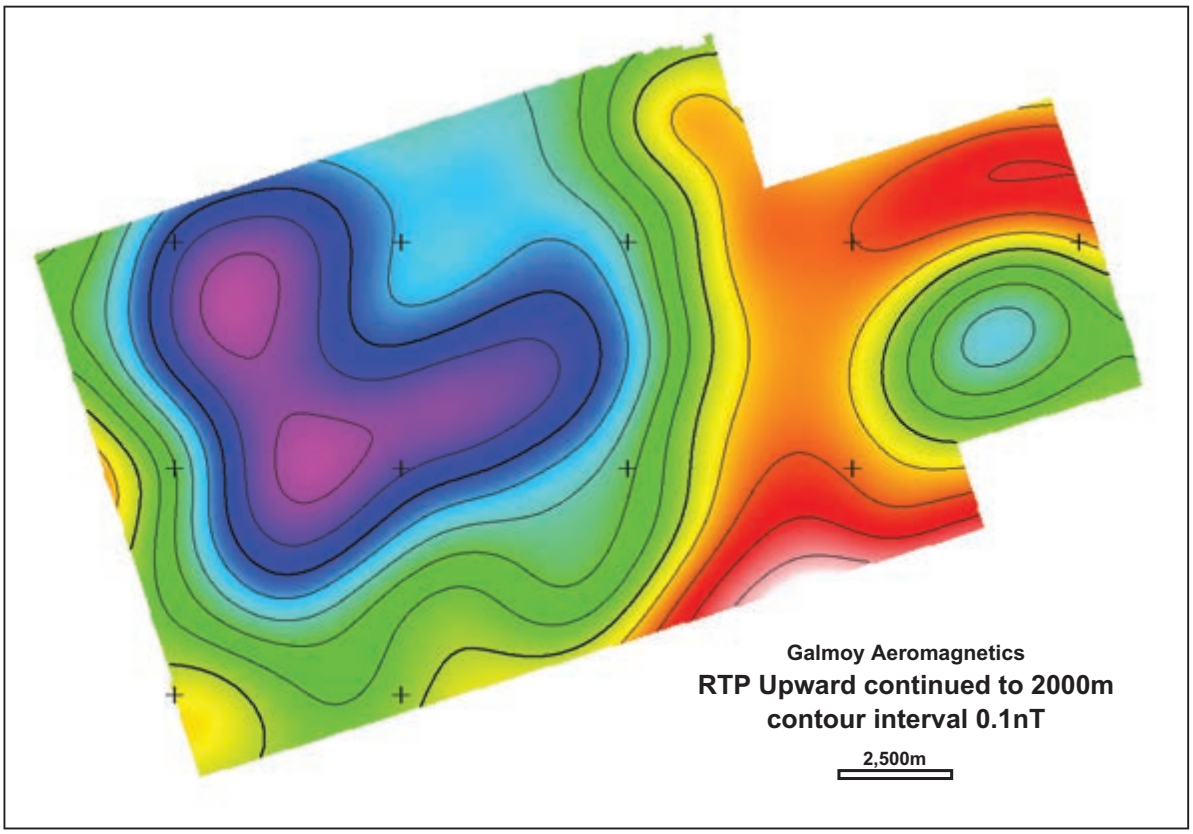

Figure 10.31: Galmoy residual RTP magnetic intensity upward-continued to 2000 m agl.

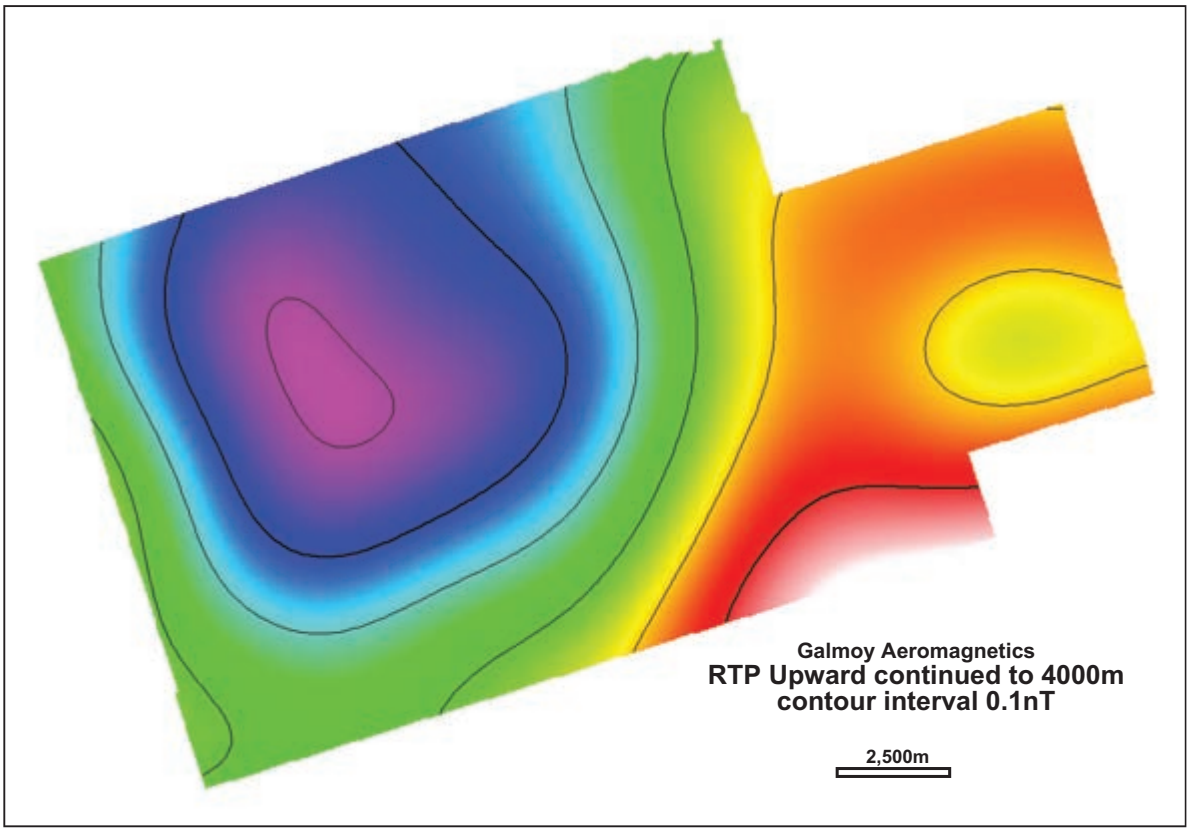

Figure 10.32: Galmoy residual RTP magnetic intensity upward-continued to 4000 m agl.

11 Menzies–Comet Vale–Goongarrie case study – Archaean granite-greenstone terrain

11.1 INTRODUCTION

This chapter is the first of three which present worked examples of real-life aeromagnetic interpretation projects. We use this gold and nickel exploration study to illustrate the methodology outlined in Chapters 6, 7 and 8, and to encourage readers to follow this general methodology. We emphasise, however, that each new project area presents new and different challenges. The worked examples relate to mineral exploration but the techniques are equally applicable to many other fields of geology, such as groundwater studies and routine mapping. The examples focus predominantly on magnetic data but the methodology is equally applicable to radiometric or gravity data. Indeed, integrating these data into the interpretation will almost always add value to the final outcome.

It is important to be prepared to adapt to different geological situations and to expect, over time, to develop your own style of interpretation. The interpretations in this book have been compiled by authors with considerable prior experience in the project areas. Hence, readers should not be surprised if observations and conclusions that are presented in a definitive manner appear somewhat subtle to the inexperienced eye. The key in every situation is to grasp the geological problem to be solved by the aeromagnetic data, and allow a generous time frame for the interpretation.

The Menzies–Comet Vale–Goongarrie study area is a poorly exposed Archaean granite–greenstone terrain with a well-developed regolith. Transported cover and *in situ* regolith are very extensive, with weathering profiles commonly around 100 m in thickness and the relics of a Tertiary laterite surface obscuring over 95% of the Archaean bedrock. The area is part of a major gold- and nickel-producing province known as the Norseman-Wiluna Belt (Groves *et al*. 1989), situated in Western Australia's Yilgarn Craton. Key references for the study area that outline the stratigraphy, structure and mineralisation in the region are Swager *et al.* (1990) and Witt (1993).

The objective of the study is to integrate semi-detailed (200 m spaced) aeromagnetic data with the published (1:100 000 scale) geology over a large project area (1500 km^2) to identify prime areas of exploration interest for gold and nickel. This will be done progressively from regional scales to prospect scales using the same datasets. We present the work, done by both authors (at times in isolation) as it progressed over time. Each new phase of work has yielded amendments to the interpretation. These changes in the interpretation at each new scale are an important lesson for interpreters; your understanding of a region will grow over time and result in (often significant) changes to the initial interpretation.

The end point of this interpretation will be the selection of a particular, high-ranking target area which will be the subject of on-ground investigation and field exploration planning.

11.2 ESTABLISHING THE REGIONAL CONTEXT

Our first task is to gain an appreciation of the regional-scale geological influences on the study area. Readily available government geology and aeromagnetic data covering an area of around 20 times our study area and presented at a scale of around five times our project-scale images will be used for this. This means collecting the data over a buffer zone of one to two times on each side of the area of interest.

We need not pay too much attention to detail in data processing and presentation for this precursor phase of our integration study, since we are just seeking to identify broad-scale geological features and will commit only a small amount of time to this regional overview. The need is to compile a simple observation layer and structural summary recording the gross geometries of the major geological features influencing our project area.

11.2.1 Data processing and presentation

High-quality regional geological and aeromagnetic data have been sourced from both the Geological Survey of Western Australia (GSWA) and from Australia's federal agency – Geoscience Australia. The published 1:500 000 scale interpretive solid geology map (Fig. 11.1) and a composite TMI–1st VD (first vertical derivative) aeromagnetic image (Fig. 11.2) have been chosen for our overview. These datasets extend well beyond our area of interest and can be effectively viewed at scales as broad as 1:2 500 000. Since our initial work on the project datasets will be at 1:250 000 scale, we chose a regional area which covers a manageable page size at ~1:1 000 000.

11.2.2 Observations

Our observations are typically brief and generalised at this scale. We will return to the regional-scale data during the main phase of interpretive work to clarify the nature of large-scale features, but at this point we are merely setting the scene.

Figure 11.3 illustrates our observations and structural summary. We note in particular:

a) the NNW structural grain in the greenstone belts;
b) the apparent folding of the strong magnetic rock units;
c) the broad areas of quite uniform magnetic texture;
d) major linear breaks interpreted as fault/fracture corridors.

11.2.3 Interpretation

The GSWA geology map (Fig. 11.1) includes a large degree of aeromagnetic interpretation and captures most of what we see in our aeromagnetic imagery. Our further integration of this geology with the aeromagnetic data highlights several features of particular interest.

a) The study area is focused on a greenstone belt which is bounded to the east and west by NNW-trending fold structures. Published mapping indicates that both these structures are granitoid-cored domes and the linear, strongly magnetic rock units flanking the domes are ultramafic volcanic rocks.
b) There is a recognisable NNW linear control on the greenstone belt geometry extending SSE from the study area. This NNW structural corridor includes the world-class Kalgoorlie goldfield. Regularly spaced, NNW-trending greenstone belts occur throughout the region.
c) A major NW break appears to terminate the greenstone belt to the north in our study area. This break separates the structural domain containing our area (characterised by thick greenstone belts) from a NE subdomain dominated by extensive areas of massive granitoids. It is clearly a feature of considerable regional tectonic significance traversing our study area through the Menzies gold district. We will refer to this as the Menzies Shear Zone in our subsequent study of the area. The Menzies Shear Zone appears to be one of a set of regularly spaced NW linear breaks. These appear to be overprinted by the NNW geometry of the greenstone belts and are regarded by the authors as deep basement faults.
d) The discordant 'circular' feature which occurs in the central northern part of our study area appears to be a late-stage intrusion and coincides with a subtle westerly change in strike to the north in the main greenstone belt.

e) NNE- and N–S-oriented linear magnetic lows (probable fault zones) are seen in the granitoid domain in the western part of the study area. There is strong evidence of apparent dextral offset along these linear structures, with some suggestion that their influence extends across the greenstone belt to the north.
f) Two sets of dykes oriented NE and ENE are clearly apparent on Figure 11.2. These cross-cut and therefore post-date the greenstone belt development. Notably, these are broadly at right angles to the greenstone and may be regarded as paralleling the predominant structural shortening direction. It is also notable that these are not shown on the published solid geology map (Fig. 11.1), despite having a regionally significant scale.

The published geology and the locations of gold and nickel mineral occurrences reinforce our choice of the area as one worthy of exploration. At this stage, our presentation of the regional study comprises a simple structural sketch (Fig. 11.3) to accompany the images with brief notes (as above) which highlight the features likely to impact on our study area.

11.3 DISTRICT-SCALE (1:250 000) ANALYSIS

11.3.1 Background and preparation

Over a few days, we aim to evaluate an area of ~65 × 25 km (1625 km^2), to identify the initial areas of exploration interest. This exercise requires us to identify the areas of most interest for gold and nickel exploration. We select a scale which allows us to capture a reasonable degree of detail, while maintaining a viewing space of manageable size. 1:250 000 is a suitable scale for the confines of this book, allowing the study area to be displayed on one page. In practice, expanding the viewing space by a factor of two or more would be highly preferable. An experienced interpreter would normally limit the time spent on this district-scale analysis to a few days, including time to become familiar with the geology, read and absorb the main references and compile the interpretation into presentable working formats. Rather than attempt an in-depth analysis at this scale, we will focus on developing a working solid geology and structural model from which subareas of particular interest can be identified. These subareas can then be assessed in more detail at finer scales.

11.3.2 Aeromagnetic data

The data that we have for evaluation comprises government geological mapping published at 1:100 000 scale (Swager and Witt 1990) and non-exclusive airborne geophysical data kindly provided for this study by Fugro Airborne Surveys. Background to the data is presented in Bullock and Isles (1994) and the impact of this aeromagnetic survey program on gold exploration in the region is outlined in Isles *et al.* (1989, 1990). The airborne survey was flown in 1986 with 200 m spaced, E–W flight lines at a mean terrain clearance of 70 m. Radiometric data were also acquired on this survey but due to the extensive cover and deep weathering profile it has limited value for our purposes in this study. It is worth noting that our study area comprises around 9000 line kilometres of data and, at 200 m line spacing, can be usefully analysed with geological coherence down to a scale of 1:20 000. At this scale, in this location with a magnetic field inclination of –60°, we have elected not to apply the Reduction to Pole (RTP) process. We will see the differences between the TMI and RTP data and the benefits of RTP when we progress to the more detailed scales. In this area, at 1:250 000 scale, for our initial analysis, the differences are relatively minor.

11.3.3 Geology

The geological map (Fig. 11.4a) highlights the extensive cover over the Archaean rocks of interest. This cover comprises both transported sediments and a thick weathering profile. The cover thickness in this region is commonly around 50 m and is rarely greater than 100 m. The 1:100 000 scale mapping loses clarity when presented at our current working scale of 1:250 000 and serves mainly to show the locations of outcrops. The broader lithostratigraphic packages are visible, but the detail on individual units and contacts is hard to decipher. Despite this, it is more appropriate to use the mapping as it is, in preference to recasting it in a more generalised fashion to suit the scale of analysis.

Briefly comparing the geology (Fig. 11.4a) and the aeromagnetic imagery (Fig. 11.5) confirms that the extensive areas of relatively uniform magnetic texture are due to granitic rocks. The areas with linear magnetic rock units are dominantly mafic and ultramafic greenstone belt sequences. The very strongly magnetic linear rock units appear to be exclusively associated with ultramafic rocks. These are not only an outstanding feature of the aeromagnetic images but are a key element in the geological evolution of the area, and are host to major nickel deposits. Hill *et al*. (1988) give a useful outline of these ultramafic rocks, which includes commentary on those occurring in our study area. An almost total absence of structures on the geology map is testimony to the sparse and discontinuous nature of the Archaean exposure. In contrast, the aeromagnetic imagery presents a wealth of structural information that will add significantly to the integrated geological picture.

11.3.4 Where to start?

The aeromagnetic imagery selected for the interpretation follows the guidelines outlined previously whereby we require a minimum of three images. The image chosen to emphasise the structural detail and texture is, in this case, the 1st VD (Fig. 11.6). Our other preferred image presents magnetic field intensity changes in colour, draped over the 1st VD (Fig. 11.7). As always, the TMI is selected as our basic record of the measured data (Fig. 11.5) but, as discussed in Chapter 5, we rarely rely on shaded images to commence our observations.

We choose to start the observation phase of our interpretation with the 1st VD image because it best portrays the structural detail that is lacking in the gross geological picture. In this image, the strongly magnetic linear units associated with the ultramafic rocks stand out as coherent layers and are potentially helpful in defining the structures. By beginning our observations on these units we will be better prepared to progress to adjacent areas with weaker, more subtle linear units in the greenstone belts. Textural and structural features within the granitoid areas can be outlined later, and these observations will benefit from us having worked through the more obvious features in the greenstone belts.

11.3.5 Observation layer

We emphasise the need to allow ample time to carefully observe and record the large quantity and range of information contained in the aeromagnetic imagery. Overly rapid and generalised observations on this dataset create the risk of overlooking subtle (but key) features which often become an important part of our final analysis. The observation layer, presented in Figure 11.8, is the result of several hours work by an experienced interpreter with some local knowledge of the study area. More time would be required for a less experienced interpreter, especially if they were unfamiliar with the regional geology.

Our approach has been to focus initially on the magnetic rock units (shown in colour) then progress to recording observations of geological discontinuities or breaks. We reach a stage where we have recorded the most clearly defined observations and our rate of progress declines. The more subtle features in the image will take longer to recognise, but they are equally important to our analysis. Be prepared to patiently absorb the information in the images, as this will greatly enhance the end result.

We will increasingly see breaks which largely relate to faults and fractures. Discipline must be applied to record these only where we can clearly recognise them. It is often tempting to unduly interpolate and extrapolate these straight-line trends to produce long and continuous lineaments. Remember that we are at the early observation stage of our interpretation and, as we progress to the more interpretive layers, we will have ample opportunity to infer continuity and simplicity from observations that may at first appear fragmented and somewhat incoherent. Another important tip in recording breaks is to look for subtle features, not unduly focus on the more obvious ones (see Chapter 8). As a general rule, the most obvious breaks will probably relate to the more recent structures. Earlier structures will be equally important but commonly have a much more subtle expression. Some excellent examples (labelled ‘a’) are highlighted in Figures 11.6 and 11.8. The minor and subtle discordances between linear magnetic rock units in two greenstone packages probably represent belt-parallel fault zones. Another example is the subtle line of terminations (labelled ‘b’) which is possibly part of the previously identified Menzies Shear Zone.

At this stage we also see flight line-parallel features which potentially relate to difficulties or shortcomings in data acquisition, processing or enhancing the images. Our awareness of the flight line spacing allows us to identify single-line features, which will always raise our suspicion. However, we must always consider the possibility of geological structures being parallel to flight lines and we note examples of both acquisition artefact (c) and real geological structures (d) in the image.

Much of the shallower structural information is best seen in the greyscale 1st VD image, but we should be aware that some of the measured signal has been filtered out of this image. In particular, the field intensity amplitudes are suppressed in the 1st VD, as are longer-wavelength variations. In the latter stages of our observation phase, we should change images in order to capture information which is not visible in the 1st VD image. The composite TMI–1st VD drape image (Fig. 11.7) is chosen for this purpose because it clearly presents the field intensity variations while preserving much of the structural detail. The field intensity information, portrayed in colour, highlights the boundaries of the broad rock packages and shows local differences. We have seen from Chapter 5 that the extreme intensity values need to be identified from an image with a linear stretch, and the inset in Figure 11.7 clearly shows that the strong low in the central/southern part of the intensely magnetic ultramafic belt (marked in blue on Fig. 11.8) is indeed highly anomalous. Further scrutiny of the composite image shows several other unusual areas of lower magnetic intensity (also marked in blue). These areas do not show extreme variations of intensity, but they are anomalous in the context of the surrounding magnetic patterns. When we consider the common association of mineralising systems with the alteration of magnetic minerals (see Chapter 3), these unusual magnetic lows become features of interest. We have also noted from our assessment of the linear stretch image (inset, Fig. 11.7), that the most westerly of the linear magnetic rock units in the ultramafic belt shows very high magnetisation, particularly near the discordant circular feature. We have recorded this by using a thicker red line to delineate this magnetic rock unit.

Although more time could be spent capturing finer levels of detail in our observation layer, we recognise that analysis of 200 m spaced airborne data at 1:250 000 will almost certainly result in information overload and the limited viewing space does not allow all this information to be portrayed effectively. Hence, we choose to be somewhat selective in our observations. We find that getting the best balance between capturing the critical detailed observations, and generalising features which are of less relevance, is rarely an easy task. Our white paper test (see Section 6.3), which requires us to assess the geological sensibility of our observations, is of great assistance in this judgement. Applied regularly during the observation phase and, most importantly, at its completion, this test gives a firm foundation on which to build the integrated geological picture.

11.3.6 Solid geology layer – lithostratigraphic packages

The first task in constructing the solid geology is to define the distribution of lithostratigraphic packages over the entire study area. This will be straightforward in some areas, but will require a degree of educated guesswork in others. Introducing faults, folds and other structural information will occur progressively as we infer the polygons of lithostratigraphy.

The solid geology layer is compiled onto a new blank overlay placed on the observation layer. It is important to remember that the observation layer must be preserved and kept (as far as practicable) free of interpretive information. The magnetic rock units and breaks recorded on the observation layer will largely constrain the definition of contacts and structures in the solid geology layer. We will find that the compilation of the solid geology layer presents many challenges; it invariably involves much erasing and revision as we deal with areas of scant outcrop, areas where the aeromagnetic patterns appear to conflict with mapped exposures and areas of indistinct magnetic signature.

Where to start?

Once again, select an area that looks clear and simple and, in this case, is important to the overall interpretation. The strongly magnetic ultramafic belt is an obvious choice as the first package to define. Start the solid

geology layer by overlaying the observation layer on an image which emphasises the field intensity information. As with the observation layer, we will normally use more than one image in the solid geology phase of our work, but the total magnetic intensity is likely to be our best initial guide in defining rock packages. In the study area, we commence with and make most use of the composite TMI–1st VD image (Fig. 11.7), but also make reference to the other images to clarify particular problem areas.

We also make regular reference to the geology, but in this area, at this scale, we find that the geological map is only useful in localised areas. One very important point – it is counterproductive to commence the solid geology layer by transposing the known geology onto the overlay. We should expect the integration of the aeromagnetic data with the geology to involve some revision of the pre-existing mapping and at the broad scale of our current work we also anticipate the need for a degree of generalisation.

The following commentary outlines the sequence in which the solid geology layer (Fig. 11.9) was compiled. The commentary makes regular reference to the observation layer (Fig. 11.8) and the coloured TMI–1st VD composite image (Fig. 11.7), and we emphasise that the construction of the solid geology requires these two images to be co-displayed for much of the process. We build the solid geology on the framework of the observation layer while referring to the aeromagnetic imagery and the geology.

Delineating contacts

We commence with the ultramafic package because it is clearly defined in the aeromagnetic imagery; there is enough exposure to link the magnetic belt to the mapped ultramafic unit and the package is influenced by many of the key structures in the study area. We take the contacts as the western and eastern edges of the linear magnetic package, using the magnetic rock units from our observation layer to trace these edges.

We note the clear disruption to the continuity of the ultramafic package by a near-circular magnetic feature. The limited outcrop confirms our suspicion that this is a granite body and its clear discordance with the NNW-striking greenstone belt suggests that it is intrudes the belt. The published geology and the accompanying legend (Fig. 11.4b) confirms that this body is unfoliated and regarded as late tectonic (Agmc – the Comet Vale Monzogranite).

The contact between this granite and the ultramafic belt is well defined, as is the eastern granite margin, based on the characteristic magnetic texture of the granite, but the western margin cannot be delineated unambiguously from the aeromagnetic imagery. After confirming that there is no exposure in this western area to assist us, we review the other available imagery only to find that the magnetic character of this granite is almost identical to that of the much broader granitoid area which dominates the western part of our study area.

The differences in structural form between the two granitoid areas lead us to infer that they are separate bodies; the circular body, Comet Vale Monzogranite, being later and discordant with the greenstone belt trends, and the larger, massive body being earlier as its contacts with the greenstones are much more concordant. Again, reference to the geological map and legend in Figure 11.4a, b confirms that the larger body (Agmg – the Goongarrie Monzogranite) shows evidence of regional foliation. On this basis we delineate the location of the western margin of the later granite using its circular form and conveniently located faults as our guides. It is important to stress that this segment of the intrusive granite margin has been estimated using some geological reasoning with limited direct evidence from our available data. Such situations are very common in the solid geology phase of aeromagnetic interpretation.

Outlining the edge of the extensive western granitoid is the next logical step. North from the Comet Vale Monzogranite we can trace a distinct contrast in intensity, first between the granitoid and the ultramafic package, where we have already defined a contact, and then between the granitoid and a narrow zone of lower magnetic intensity which appears to terminate or lens out near the northern limit of our study area. With no exposure to help in this area, our approach is to look at similar settings in the study area and we find that, in the southern part of our study area, there is a weakly magnetic interval separating the ultramafic package from the western granitoid. Very limited exposure and a distinct linear texture in this weakly magnetic zone strongly suggest that it is part of the greenstone belt and likely composed mainly of mafic rocks. This would

also be the simplest interpretation of the narrow magnetic low in the north. An alternative interpretation would be that it is due to a marginal, more weakly magnetic phase of the granite.

The southern wedge of inferred mafic rocks between the western granitoid and the ultramafic package is next to be defined. We note that it is relatively well defined in the south, particularly if we follow the patterns of linear magnetic rock units from our observation layer. We note an abrupt termination of this belt of linear units at its northern limit. North of this belt, the magnetic character strongly suggests the presence of a granitoid. Further north, near the south-west margin of the Comet Vale Monzogranite, the magnetic intensities and textures would lead us to include this area as part of the western granitoid. However, ample mafic outcrop in the Comet Vale district indicates the further presence of the wedge of greenstone material and closer inspection of our observation layer shows subtle but credible linear magnetic features parallel to the exposed mafic rocks. Looking at the abrupt break in continuity of this mafic belt leads us to infer the presence of a second late granite body, and subtle circular trends in the aeromagnetic imagery in this area give some support to this. We emphasise that the evidence for this second younger granitoid is subtle and that its boundary is not clearly defined, but this interpretation does provide the most geologically sensible explanation of our observations.

We have now defined the gross geological polygons on the western side of our study area.

The eastern side presents greater challenges. East of the ultramafic package (particularly south of the Comet Vale Monzogranite) discrete linear magnetic rock units and occasional outcrops indicate that mafic rocks are dominant. We could infer that the individual magnetic rock units are specific lithologies (e.g. magnetic dolerite and gabbro are locally common within the greenstone sequence), but at this early stage it is more appropriate to simply define the package as dominantly mafic.

Further eastward we see a belt of very flat magnetic texture and relatively low intensity containing one or two weak but very continuous linear magnetic rock units. Limited exposures, combined with some local knowledge, lead us to infer that this package comprises dominantly sedimentary rocks. Progressing eastward we return to narrow belts with locally strongly magnetic linear rock units, and we have enough outcrop to confirm both mafic and ultramafic rocks.

The eastern margin of the study area shows a broad and moderately magnetic belt with a zoned linear texture. It has some similarities with the western granitoid zone and the sporadic outcrops within the belt are almost exclusively granite. While the texture of this zone is linear and broadly parallels the trends in the greenstone belt, the total magnetic intensity patterns of the zone have much stronger similarity with the western granitoid than the greenstones. We note from the geological map and legend that most granitoid outcrops are designated Agn (pervasively foliated granitoid gneiss). The linear texture we see in the aeromagnetic imagery is consistent with this gneissic foliation.

The far north of the study area comprises extensive exposures of mafic and ultramafic rocks but shows quite different structural patterns from the greenstone belt in the central part of the study area. Folding is apparent on N- to NNE-trending axes, and large areas of non-magnetic ultramafic rocks have been mapped. The boundary between this structural domain and the predominant NNW belt is relatively clear. Trends from the northern belt are discordant with the consistently NW-striking strong magnetic rock units.

After reviewing the array of lithological polygons and extending some of the reasoning applied above with some plausible guesswork, we can assign lithostratigraphic packages to our entire study area (Fig. 11.9). The main and broadly accepted geological references –Swager *et al.* (1990) and Witt (1993) – infer a local stratigraphic sequence that is reflected in our interpreted packages. The basal unit is dominanted by mafic rocks (ML), and this is overlain by both the thick interval of ultramafic volcanics (Ub) and a further sequence of mainly mafic rocks (Mu). The uppermost stratigraphic interval recognised comprises a mixed sequence of sedimentary rocks (Sf). While these stratigraphic assignments are not rigorous, they add a valuable dimension to our geological compilation. We now begin to map in the significant structures.

11.3.7 Solid geology layer – structures

The first task in defining structures is to integrate the above lithostratigraphic polygons with the features recorded on our observation layer.

Faults

The study area contains four main sets of faults (and/or shear zones), some of which are obvious and others that are more subtle. It is always advisable to deal with the most recent structures first, because by doing so we improve our ability to recognise and delineate older structures.

Apart from the E- to ENE-trending dykes and fractures in the north of the study area, which clearly post-date the granite-greenstone sequence, the youngest structures apparent are relatively short NE- and NW-trending faults (e.g. 'a' on Fig. 11.9). These clearly cut the ultramafic package with a consistent apparent NE dextral offset and apparent NW sinistral offset.

The set of curvilinear NNE to N–S fractures clearly seen in the western granitoid (e.g. 'b' on Fig. 11.9) seem to extend into the greenstone belts and are likely related to the main greenstone deformation phases. The timing of these faults appears ambiguous, with possible evidence for both earlier (pre-Comet Vale Monzogranite) and later (post-Comet Vale Monzogranite) displacements.

Broadly layer-parallel fault sets are evident as discordances in the lithological and tectonic layering within the greenstone sequence (e.g. 'c' on Fig. 11.9). These largely predate the Comet Vale Monzogranite and, although subtle, are regional-scale structures. They are likely to be part of the main deformation of the greenstone belt.

Folds

In Figure 11.6 we can see possible fold structures are seen in the north-eastern greenstone sequence, near the gneissic granite-greenstone contact south-east of the Comet Vale Monzogranite and internally within the ultramafic sequence. Inferred fold axes are oriented NNW to N–S, parallel to the regional structural grain, reinforcing the notion that ENE–WSW to E–W-directed shortening has been a major component of the regional deformation in the region.

We can now extend our observation layer on the basis of the above into a structural framework (Fig. 11.10) which allows us to exercise some interpretive licence ahead of our main phase of structural analysis and targeting. This phase of interpretation requires some level of confidence in structural geology and may be thought of as a more advanced level of analysis than the preceding work. The structural framework incorporates and largely honours our observation layer, but we add a degree of inferred continuity consistent with our reading of the patterns that became apparent in our first two layers.

11.3.8 Analysis of our solid geology map

We now have a 2-D solid geology map and a structural framework that can be interrogated and tested with field investigations and used to stimulate ideas on areas of interest for exploration or for advancing the general geological understanding. The solid geology map should not be seen as an end product. Before field testing, it remains a working hypothesis and a starting point for exploration. Having compiled the 2-D solid geology we can extend our interpretation in two directions.

a) What is the form of the geology at depth? Can we draw cross-sections?
b) What is the geological/structural history? How did the geometry we now see evolve?

Rather than attempting cross-sections 'cold', we first address the structure and geological history using the 2-D solid geology. There may be dip and plunge indicators in the surface mapping, and geophysical modelling may help to assess geometries in the third dimension but, in the authors' experiences, thoroughly interrogating the 2-D geometry is an important first step in creating cross-sections.

Stratigraphy

Extensive geological mapping in the region shows that the ultramafic volcanic (komatiite) interval is located in the lower part of the Archaean succession, and is commonly underlain by a basalt-rich interval (Witt 1993). Another major, dominantly mafic unit overlies the komatiites and the upper unit in the main Archaean sequence is a thick interval of mixed sedimentary, felsic extrusive and volcaniclastic rocks. These two upper stratigraphic intervals contain many coarse-grained mafic rocks (dolerites and gabbros) regarded as sills. These

sills are one of the most prolific host rocks for gold mineralisation. Nickel mineralisation in the region is commonly found near the basal contact of the komatiite unit and is almost always hosted by the komatiites.

While the massive granitoid areas are generally considered to be intrusive, local evidence suggests that they, at least in part, represent an older felsic basement on which the greenstone sequences evolved. Because most stratigraphic contacts in the Yilgarn Block are faulted, it is rarely possible to clearly define the entire sequence of deposition of the rocks. However, the hypothesis that the greenstone sequence outlined above evolved from rift-like sutures developed in a granitic basement is a useful framework for our interpretation.

Considering our solid geology map, we see that the southern section presents an almost intact sequence and broadly suggests a synclinal structure. The eastern side of the study area appears more intensely folded and sliced up, consistent with the stronger foliation seen in the eastern granitoid and the presence of the large-scale NW fault zone (the Menzies Shear Zone) noted in our initial regional overview.

We can now construct some critical cross-sections (Fig. 11.11). While these are somewhat diagrammatic, they express our view that the greenstone belt has a broadly synclinal form and is segmented with major belt-parallel faults.

11.3.9 Structural analysis

So far our interpretation has highlighted a series of key structural elements, with (in many instances) relationships that provide some relative timings on deformation events. Analysis of this information is best done by a specialist structural geologist, but it is useful for the non-specialist, project interpreter to develop a working structural model ahead of or in lieu of specialist input.

Some of the key structures are listed below and indexed on Figure 11.10 with an interpreted sequence of deformation phases, and with observed and/or inferred movements.

D1/D2 – first and second phases of deformation, E–W to ENE–WSW compression

There are a number of key structures.

1. Development of the primary N- to NNW-trending structural grain of the greenstone belts. N- to NNW-trending folds probably include both early recumbent folding (D1? – see points labelled ‘a’ on Fig. 11.10) and superimposed tight upright (D2? – ‘b’ on Fig. 11.10) folds. The present broadly synclinal form of the greenstone belt in the south of the area was likely to have been developed during D2 folding.
2. Belt-parallel, strike-continuous faults (and/or shear zones) form most of the contacts between the main lithological packages. These are interpreted as dominantly compressive (thrust to high-angle reverse faults), but with some possible component of wrench movement (‘c’).
3. The curvilinear NNE- to NE-apparent dextral fault zones (‘d’) are consistent with this early E–W compressive deformation. Smaller-scale WN- to NW-trending (‘e’) apparent sinistral faults evident in the southern part of the belt are interpreted as conjugate to the larger NE faults.
4. In the belt of NW-trending fabric north of the Comet Vale Monzogranite, the rotation of the layering and F1/F2 fold trends near the deformation zone (‘f’) may indicate significant sinistral wrench deformation. This is part of the crustal-scale Menzies Shear Zone, which is inferred to have been active since the early development of the greenstone depositional basin (see Fig. 11.3 and comments below on the delineation of major structural/lithological subdomains). The Menzies Shear Zone appears to merge with the NNW-trending shear zones bounding the main ultramafic belt in the NW of our area (and likely becoming more compressive in this area, ‘g’). Its SE extension is less obvious (‘h’), as complex interaction between the shear zone and at least two significant N–S faults occurs east of the Comet Vale Monzogranite.

D3 – continued E–W to ENE–WNW compression, with some belt-parallel sinistral wrench

1. The two circular granitoid intrusions (‘i’) straddle the main contact between the greenstone belt and the western granite terrane. Both granitoids truncate D2 fold and fault structures within the greenstone belt. The more northerly intrusion, the Comet Vale Monzogranite, marks a subtle but clear anticlockwise bend

in the greenstone belt and this location is near the Menzies Shear Zone. Intrusion of these two granitoids is consistent with the development of a major dilation zone at this bend during E–W compression, with a sinistral wrench developed along NNW- and NW-trending structures.

2. The NNE- to NE-trending dextral and small-scale NW-sinistral faults developed during D1/D2 were likely to have been reactivated during this phase. Some NE (apparent) dextral faults cut the northern part of the Comet Vale Monzogranite ('j'), suggesting continued deformation post emplacement of the Comet Vale Monzogranite. This is supported by:

   a) the thickened zones of ultramafic rocks near the north and south margins of the Comet Vale Monzogranite ('k', likely dilation strain shadows);
   b) variable strain and warping of fabrics around the eastern margin of the Comet Vale Monzogranite ('l');
   c) the intersection of the Comet Vale Monzogranite and greenstone belts by E–W apparent sinistral and extensional faults 'm').

D3–D4?? – is there another deformation??

There is one N–S fault complex interpreted on the eastern margin of the Comet Vale Monzogranite ('n'). It separates the SE margin of the magnetic Comet Vale Monzogranite from a small, less magnetic block with similar fuzzy magnetic texture ('o') and includes possible arcuate fault segments. Scattered outcrop very near this block suggest it may be part of the mafic package but the strong textural similarities with the Comet Vale Monzogranite favour its interpretation as a detached sliver of the Comet Vale Monzogranite. At this regional interpretation scale, and in the absence of definitive outcrop, it is not possible to confidently decide which alternative is correct.

Two possible structural models can be proposed for this fault complex.

1. The N–S fault is part of the D3 compressive to sinistral N- to NNW-trending fault system, and that the arcuate fault complex and fuzzy block SE of the Comet Vale Monzogranite is part of a compressive pop-up structure adjacent to the Comet Vale Monzogranite margin. This interpretation of the area is portrayed in Figure 11.12.
2. The N–S fault is a later (D4) fault, with dextral displacement. In this interpretation, the fuzzy block represents the SE corner of the Comet Vale Monzogranite, displaced to the south by roughly 3–4 km. This second interpretation is not obvious at this scale, but it could help explain why the regional Menzies Shear Zone is so difficult to trace SE of the Comet Vale Monzogranite. A more detailed review of the data at a larger scale may help – we will examine this in the next section.

Comparison of our structural analysis from the aeromagnetic data with that previously derived principally from field geological mapping by Witt (1993) and others, highlights the level of detail obtainable from the aeromagnetic data, even at a relatively coarse scale.

The published mapping and geological analysis by Witt (1993) show that four main deformation phases can be recognised in the field:

1. D1 – subhorizontal thrusting and recumbent folding;
2. D2 – upright regional folds with NNW axial planes and shallow plunges (implying E–W to WSW–ESE compression);
3. D3 – sinistral strike slip movement on NNW shear zones and continued regional shortening (E–W to WSW–ESE compression);
4. D4 – dextral movement on (largely pre-existing) NNW shear zones forming N- to NNE-trending dextral shears.

Our structural framework and tectonic history interpreted using the aeromagnetic data (Fig. 11.12) is very consistent with that developed from field observations. Perhaps the only ambiguities or missing elements are:

1. the late-stage ENE to E–W mafic dyke(s) in the north of the area do not fit into any of these events, and would provide evidence for a further but probably much later deformation phase. The dykes may well

occupy tensile fractures developed during the prolonged ENE–E–W compression. They are locally referred to as the post-cratonisation dykes (Isles and Cooke 1990);
2. is the N–S fault complex east of the Comet Vale Monzogranite part of the D3 or D4 event? Our more detailed look at the aeromagnetic data in Section 11.4 may solve this.

In a relatively short time span, our regional interpretation has both captured the regional-scale lithostructural architecture of the area and formed a credible analysis of the tectonic history of the area. Both are consistent with observations and conclusions from pre-existing field geological mapping. While the above analysis requires specialist skill and experience in structural geology, the recognition of the structures and basic assessment of likely displacements and timing relationships is well within the realm of routine aeromagnetic interpretation. In the next section we progress to the definition of exploration target areas and will see the benefit of extending our solid geology layer to a working structural interpretation.

11.3.10 Exploration targeting

Our starting point in exploration targeting is always to consider what is known within the study area, then within the surrounding district and progressively more broadly across the geological region. Having done this, it is most important to open the focus to 'what might be found' in the study area. The history of major discoveries shows that broad, lateral and courageous thinking are key ingredients. If we confine ourselves to finding more of what is already known, we run a serious risk of overlooking sometimes obvious clues to a significant discovery. We should remind ourselves that by taking on exploration in an area, we have the expectation that new and often better discoveries are a real possibility.

Known mineralisation in the Menzies–Goongarrie study area

Gold

Three gold-producing districts are known in the study area. Their locations are shown in Figure 11.13 and each is described in Witt (1993). We will not describe them in detail, but will focus on the perceived key geological characteristics in each mineralised area. Our emphasis will be on the characteristics that we may be able to recognise in the aeromagnetic data. Hence we consider generalised district- and prospect-scale features more than discrete ore body-scale features.

1. The **Menzies** district is a 10 km long by 1 km wide, NW-trending zone of gold workings in which there are six modern but small-scale open pit mines. Total production to 2009 from this district was less than 1 Moz. The envelope of workings is contained within, and was likely to have been controlled by, the major NNW-trending Menzies Shear Zone that we have identified as a regionally significant structure.
2. The **Comet Vale** gold district lies on the western contact of the ultramafic package near the southern margin of the Comet Vale Monzogranite. The mafic/ultramafic contact, which we have identified as a major layer-parallel fault, has bent sharply anticlockwise under the influence of the intrusive Comet Vale Monzogranite. This may be partly a D3 deformation-associated strain shadow at the southern end of the Comet Vale Monzogranite. The bend in the major fault, the associated strain shadow and the rheology contrast between the ultramafic rocks and the western (lower) mafic package are all likely to have contributed to the formation of gold deposits.
3. The **Goongarrie** gold district lies near the eastern edge of the ultramafic package where it is in faulted contact with the eastern (upper) mafic package. In the Goongarrie area, local cross-cutting fractures disrupt this very extensive layer-parallel fault contact, and the combination of multiple faults and the rheology contrast between the two rock packages are the features likely to have localised the gold.

While none of these established gold districts is a major producer, each has had modern, shallow open-pit production and each is subject to continuing exploration.

Nickel

The only historic nickel mine in the study area is Scotia, which lies in the SE part of our study area. Like most of the nickel deposits in this region, Scotia lies at the basal contact of the ultramafic package and does not

show diagnostic, district-scale local controls along this contact. It was a significant producer through the 1970s (~1.4 Mt at 2.2% Ni). Numerous nickel showings throughout the central ultramafic belt in the study area are recorded in open file databases.

Deposit characteristics in the Norseman–Wiluna Belt

Our study area is part of the Norsemen–Wiluna Belt (Groves *et al.* 1989), which is a world-class producer of both nickel and gold. A summary of the common characteristics of the significant deposits is presented below. We will use these general characteristics as guidelines for targeting, along with those identified in the local district above, and will also consider any unusual magnetic features which may have links to mineralising processes. Isles *et al.* (1990) describe the aeromagnetic features frequently associated with gold mineralisation in this region and François *et al.* (2005) outline the permissive features for gold deposits in the Archaean granite-greenstone environment in general.

These include:

1. deposits are close (1–2 km) to major, greenstone belt-parallel faults or shear zones;
2. they are hosted by or adjacent to mafic or ultramafic lithologies;
3. the structural trap is within a tectonic corridor, such as a jog in a major fault or a 2nd-order splay;
4. rheological contrast is a mechanism for enhancing entrapment;
5. the chemical favourability (reactivity) of some rocks, especially iron-rich rocks, in particular iron-rich phases of the mafic intrusions (dolerites and gabbros) that are common in the greenstone sequences;
6. the gold deposits were predominantly formed late in the deformation process, so that structures of all ages are worth considering as conduits and traps for mineralisation.

The characteristics of nickel deposit in the Yilgarn Craton are detailed in Barnes (2006):

1. they are hosted in ultramafic rocks;
2. Kambalda-style deposits are associated with extrusive rocks, and the base of a flow is the favoured location;
3. perseverance-style deposits are associated with sills within the ultramafic package;
4. a mantle-tapping crustal suture is an important ingredient in the conventional model.

The targeting process

So far our interpretation is speculative and untested by field work. We cannot therefore expect our targeting to be definitive. Our task is to identify areas of initial interest and plan field testing programs for these areas. It is almost certain that we will not have enough time or money to carry out exhaustive, definitive, scientific follow-up work on our targets. We normally identify a combination of broad areas of potential interest and more local areas where specific features attract our attention. We are therefore forced to use our best educated guesswork to rank the targets technically then assign them priorities for testing based on practical issues such as cost and accessibility.

Targets for our study area are presented in Figure 11.13 and shown in Table 11.1.

Most targets outlined are areas of several km^2, meaning that field testing will require much more than one or two drill holes. We should expect this, considering the broad scale of our analysis to date. Field testing will typically comprise reconnaissance mapping, geochemical sampling and possibly ground geophysical surveys over the target area. Extreme weathering and superficial transported cover in the Menzies district means that the area is not conducive to definitive geological mapping. The areas shown as outcrop on the published map are best described as coherent groupings of highly weathered subcrop. Both continuity of exposure and fresh rock are rare, such that the most common form of initial field exploration is shallow bedrock drilling, which can be rapid, inexpensive and quite definitive both geologically and geochemically.

11.3.11 Reducing the search space

At this stage of our evaluation we choose to reduce our search space and focus on areas of prime interest for analysis at more detailed scales. We (arbitrarily) restrict ourselves to an area of ~400 km^2, or one quarter of

Table 11.1: Exploration targets: Menzies–Goongarrie–Comet Vale region

Target no.	Description	Rationale	Ranking
T1a	Likely basal ultramafic contact.	Prospective for nickel.	High
T1b	NE dextral fault cuts the mafic and ultramafic sequences.	Gold may be on the tectonic mafic/ultramafic contacts. Similarities to Goongarrie and Comet Vale districts, and close to the Menzies Shear Zone and Menzies gold district.	Very high
T2	Dilational bend in Menzies shear zone in a mafic package.	Along strike from Menzies gold district.	High
T3	2nd-order dilational shear zone bending around Comet Vale Monzogranite.	A local magnetic high (ultramafic or mafic rocks?) which may provide permissive rheological and chemical contrasts. Also strongly influenced by late NE dextral faults.	Very high
T4	Northern contact between the Comet Vale Monzogranite and the ultramafic package.	Dilation strain shadow area, also influenced by NNE to N–S faults.	Moderate
T5	Zone of lower magnetic intensity at contact of Comet Vale Monzogranite and western granitoid.	Lies on dilational bends in N–S to NNE dextral fault zones. Reduced magnetisation may be reflect alteration.	Moderate
T6	Southern contact between the Comet Vale Monzogranite and the ultramafic package.	Strain shadow area and dilational bend on NNW sinistral shear zone which forms the (basal) mafic/ultramafic contact. Extension of Comet Vale gold district. Basal contact also favourable for nickel.	Very high
T7	Mirror image of T6, eastern part of strain shadow.	Late N–S (dextral) fault evident.	Moderate
T8a, b	Similar setting to T1a, T1b.	Late fault cutting mafic/ultramafic contact. T8a (basal ultramafic contact) favourable for nickel.	Moderate
T9	Highly anomalous magnetic low within ultramafic package.	Possibly remanently magnetised ultramafic sill. Potential for Perseverance-style nickel deposits.	Moderate
T10	Discrete and unusual magnetic low at contact between late granite intrusion and lower mafic package.	Possible alteration.	Moderate
T11	Major NE dextral fault cuts basal mafic/ultramafic contact.	Gold and nickel potential.	Moderate
T12a, b	NW sinistral fault cuts basal and upper mafic/ultramafic contacts.	Similar model to T1, T8 and T11. Known nickel occurrence on basal contact in 12a.	Very high
T13	Fault at mafic/ultramafic contact.	Analogous to T1, T8, T11, T12.	Moderate

our initial study area, and our next task is to select an area of this size which includes our highest-ranking targets. For the sake of this exercise we may consider the size of this area as a condition imposed by a joint venture partner or by state regulations. Not surprisingly our favoured area (shown in Fig. 11.13) is centred on the Comet Vale Monzogranite. It includes the two strain shadow areas where the Comet Vale Monzogranite abuts the ultramafic package, one of which includes the Comet Vale gold district. It also includes many interesting structural sites east of the Comet Vale Monzogranite where regional-scale faults bend around the intrusion. Of particular interest is the regional Menzies Shear Zone. Our selected area includes this corridor as it extends SE beyond the known Menzies goldfield into an area of complete sand

cover and limited prior exploration. Other target areas captured within this 400 km^2 area are specific magnetic anomalies:

1. an intriguing low with strong structural associations;
2. a distinct localised magnetic high lying in the Menzies Shear Zone corridor near the NE shoulder of the Comet Vale Monzogranite.

Having selected this Comet Vale Monzogranite-focused subarea (containing our highest-ranking targets) we will recast our imagery to enable us to analyse the area in much the same way as before, but in more detail. Once again, for the practicalities of space in this book we confine ourselves to an A4 page size, whereas in real life at least double the size would be preferable.

11.4 CAMP-SCALE (1:100 000) ANALYSIS

Our chosen scale (1:100 000) and the size of our viewing space allow us to look at specific relationships between outcrop (Fig. 11.14) and the aeromagnetic images, while at the same time maintaining aspects of the big picture. We do need to redo our imagery. If we simply resize the 1:250 000 scale images, we will undoubtedly restrict the recognition of possibly crucial features. In particular, the colour or greyscale histogram stretches suitable for larger areas are rarely optimal for subareas (see Section 5.4).

11.4.1 Imagery

We select the same basic set of images with one important exception. At the enlarged scale and at the prevailing Earth's magnetic field inclination (~60° south), the differences between TMI and RTP imagery will be quite noticeable. We recall that the RTP imagery should better reflect magnetic rock unit contact locations and generally more closely depict the geometry of the underlying geology. As a consequence, our choice of imagery is:

1. TMI (Fig. 11.15), presented here as colour contours to more clearly show local intensity variations;
2. RTP 1st VD (greyscale) (Fig. 11.16);
3. RTP magnetic intensity (colour) draped on RTP 1st VD (Fig. 11.17).

11.4.2 Interpretation process

The observation and interpretation steps we follow at 1:100 000 scale are essentially the same as at 1:250 000 and, indeed, these steps are necessary at most scales. At the present (enlarged) scale we need to take more care and spend more time in accurately recording the location of our magnetic rock units and contacts because these locations may become sites for field investigation. In particular, it is important to resist the temptation to record inferred continuity and interpretive generality on the observation layer. The subsequent solid geology layer gives us ample scope to express interpretive features. The observation layer we compile (Fig. 11.18) contains significantly more detail than its 1:250 000 scale predecessor, but our approach and methodology are much the same as before.

The important difference between our observations at 1:100 000 scale and those at 1:250 000 is that the enlarged imagery reveals more information on width and shape of individual magnetic rock units and the fault or fracture zones and contacts. Comparing Figure 11.18 with the equivalent part of Figure 11.8 emphasises this. We can now extend these observations to form a structural framework (Fig. 11.19), which fine-tunes the structural picture developed at the more regional scale.

As we progress to the solid geology layer and seek to delineate lithostratigraphic boundaries, we encounter many of the same quandaries and uncertainties as before. However, we can now effectively integrate outcrop and (limited) drill-hole data, and so compile a solid geology map with much more detail (Fig. 11.20). We can recognise that the contact of the Comet Vale Monzogranite is more complex, noting particularly the existence of a major and quite late N–S dextral fault (previously suggested tentatively in our regional interpretation). Within the more detailed imagery, this fault appears more angular (brittle) than most of the other N–S

curvilinear (ductile/brittle) faults, suggesting it is part of a later (D4) deformation event. We see the sediment-dominated package extend well to the north of the Comet Vale Monzogranite, and our definition of the fracture patterns becomes more detailed and precise. Our structural synthesis evolves with a clearer recognition of the influence of the late N–S fault at the eastern margin of the Comet Vale Monzogranite and the local expression of the regional-scale Menzies Shear Zone. Our overall interpretation of the deformation history does not change but we reiterate several key features and can refine our exploration targets.

Figure 11.21 shows our structural summary and the revisions to our set of exploration targets. We have elected to concentrate on gold exploration. The revised targets are now:

1. T1–3, which reiterates and amalgamates targets identified at the regional scale. It is the SE extension of the Menzies gold district, taking in the Menzies Shear Zone and extending SE to where it bends around the northern part of the Comet Vale Monzogranite and intersects our inferred late N–S fault. It includes several discrete magnetic rock units in association with local-scale structures. The absence of gold occurrences in this zone coincides with the beginning of total cover that will have greatly restricted historic exploration;
2. T4–5, which takes in the strain shadow at the northern margin of the Comet Vale Monzogranite and includes the major N–S to NNE shear zones at its NW limit. This area also shows local evidence of magnetite destruction;
3. T6, which is the Comet Vale gold district. It is the southern strain shadow and also an area where the major shear zone separating the ultramafic package from the lower mafic package bends anticlockwise under the influence of the Comet Vale Monzogranite. It is intersected by a series of (D2–D3?) E–W faults/fractures that could be dilational;
4. T1–3 'extended', which includes the late N–S dextral fault at the eastern margin of the Comet Vale Monzogranite and the SE extension of the Menzies Shear Zone;
5. T8, which covers a specific late-stage dextral fault cutting the ultramafic package and including both the western and eastern contacts with mafic packages.

Within each of these broad areas there are local features that attract our attention, but our targeting criteria are not sufficiently constrained to allow us to confidently identify these areas and exclude others within the target zones. However, we are invariably compelled to make judgements and commit to areas of highest priority for early exploration, even though each of the target zones we have identified has the potential to host a significant deposit. In a standard exploration program we would propose reconnaissance work covering each of the four target zones. For the purposes of the current exercise we select our highest-ranking zone and, within it, a favourite feature on which to focus our initial effort and expenditure. The target TMW (named after a local geographic feature – Moriarty Well) has the following special attributes:

1. it is in the zone of inflection of the Menzies Shear Zone at the shoulder of the Comet Vale Monzogranite;
2. it features a discrete and locally strong magnetic high;
3. it is cut by two well-defined late NE dextral faults.

This target satisfies almost all the criteria for gold mineralisation in the region.

Having highlighted this target area based on a 1:100 000 scale analysis of the 200 m spaced aeromagnetic data, and knowing that the next major exploration step will be field investigations, we can carry out a final phase of interpretation to ensure that we have captured all the relevant detail in the existing data before we go into the field.

11.5 PROSPECT-SCALE (1:25 000) ANALYSIS

As we zoom into the area of target TMW we discover that there is yet more (mainly structural) detail in the aeromagnetic data which has not been clearly recorded in our 1:100 000 scale analysis. The outcrop geology map (Fig. 11.22), now enlarged to 1:25 000 from its publication scale of 1:100 000, indicates substantial exposure of Archaean rocks in our main area of interest. From experience, we have learned that to extract the

maximum level of geological detail from aeromagnetic data it should be processed and interpreted at the scale where 1 cm represents one line spacing, so our current dataset may be worked down to a maximum scale of 1:20 000. Once again, simply enlarging our existing imagery is unlikely to provide maximum detail on the zoomed area and it is prudent to redo the imaging. We choose a similar set of three images as before (Figs 11.23–25) with one significant exception – the RTP 1st VD (Fig. 11.24) is in this case presented as a colour contour map. We discovered in Section 5 (Figs 5.3a, b) that pixel images lose resolution as we zoom in to maximum scale and that the contour format becomes much more suitable. Despite the busy appearance of the contour image, the information content is comprehensive and provides us with the means to extract maximum resolution from the aeromagnetic data. While the extra level of detail gained by reprocessing the data to 1:25 000 scale is not overwhelming, we can locate contacts more accurately and see structures more clearly. This becomes important when we are in the field searching for hard evidence to test our interpretation.

Having worked with the data for some time at the coarser scales and having progressively reduced our study area from 6500 km^2 to 430 km^2, and now to ~40 km^2, our layers of observation, solid geology and structural interpretation can be compiled relatively quickly.

With a few hours of focused work we can produce an interpretation (Figs 11.26a, b) at a scale suitable for use in the field along with the existing surface geological mapping to plan our traverses and key observation locations.

We note areas where our interpretation is inconsistent with the mapped exposures. Of particular interest is the discrete magnetic anomaly. When we scrutinise the data closely we find that the trace of the magnetic rock unit partly coincides with mapped ultramafic rocks, partly with sediment, partly with granite and partly with basalt (see Fig. 11.27). The high intensity of the anomaly is consistent with the serpentinised ultramafic rocks that occur nearby. Strongly magnetic variants of the other lithologies are not known within our study area but magnetic examples of each may be found in the broader region. This quandary cannot be resolved in the office. Field investigation is required. Ahead of this we choose to make an interpretation using the following logic.

1. The magnetic rock unit is most likely to have a single source – it is unlikely to be caused partially by four different adjacent lithologies.
2. The geological mapping we are using (at ~1:25 000 scale) has been enlarged from a published 1:100 000 scale map. A slight mis-positioning of the exposures (~100 m, or 1 mm on the map face) in the published map could render the magnetic anomaly coincident with either the ultramafic or basalt unit.
3. Magnetic basalt is rare in our study area, whereas most of the ultramafic rocks are strongly magnetic.

On this basis we have interpreted the feature as a sliver of serpentinised ultramafic rocks, caught up in the regional shear zone. Other slivers of ultramafic rocks occur east of the main anomaly (Fig. 11.22), and we feel comfortable with our pre-field interpretation. As with our prior interpretations, we have inferred lithostratigraphic packages to account for the relationships between magnetic zonation and the lithological distribution.

Our structural picture appears clearer at this scale and we can infer quite specific locations for contacts, faults, shear zones and fractures, subject of course to the limitations of our 200 m line spacing and 70 m flying height. We examine the magnetic gradients (ideally accessing measured profile data) to assess approximate depth to magnetic source and look at the nature and location of outcrop. We conclude that there is a strong likelihood that the source of our main magnetic anomaly of interest is exposed at surface.

Our field test plan is relatively simple. We need to establish the cause of the TMW magnetic anomaly and to look for evidence of structures and mineralising processes such as alteration or gossans. We will not confine our attention to the magnetic anomaly, because we have established that the entire corridor of the Menzies Shear Zone is structurally permissive for gold. However, the TMW area gives us a place to begin, where many of the exploration criteria listed in Section 11.8 are interpreted to be present.

11.6 TMW TARGET AREA – FIELD INVESTIGATION

Having highlighted the magnetically anomalous ultramafic (?) body within the 1:25 000 scale interpretation as an interesting exploration target, detailed mapping traverses are planned to ground-truth our interpretation.

Field work by the authors yielded the following observations.

1. The mapping by the GSWA (Swager and Witt 1990) appears accurate and generally consistent with the magnetic interpretation (allowing for some inaccuracies due to enlargement of 1:100 000 scale maps to 1:25 000).
2. Some outcrops were inconsistent with the 1:100 000 scale mapping, but consistent with the structural grain of the magnetic interpretation. This can be due to photo-interpretation of some areas during mapping with only minor field control, particularly in areas with little or no outcrop and intensely weathered units.
3. Our anomalous magnetic body is part of a porphyritic basalt (mapped unit 'Abp', see legend, Fig. 11.4b), locally hosting strata-bound but N- to NE-trending magnetite alteration veins. This is an exciting observation, as the porphyritic basalt elsewhere hosts significant gold mineralisation (e.g. the Ora Banda mine). The combination of a known preferential host for mineralisation, combined with a complex structural locus *and* anomalous alteration, makes this a high-priority target for detailed exploration.

A revised solid geology interpretation of the TMW target area (Fig. 11.27, panel c) area is produced using a focused integration of detailed aeromagnetic observations (Fig. 11.27, panel a), the published mapping (Fig. 11.27, panel b) and our new field observations. With the confirmation of this high-priority target, it is now time to fully test our interpretation and exploration ideas. Planned drill traverses across the magnetic anomaly, which is probably the altered porphyritic basalt, are shown (in red) on the revised interpretation. The traverses are oriented N–S to test both the stratigraphic contacts (NW–SE-oriented) and the interpreted and observed alteration and fault/fracture structures. This drilling program is designed to sample the regolith and the upper few metres of fresh bedrock. It should provide adequate geochemical information to assess the possibility that the target area hosts significant mineralisation. The drilling of this target and others that we have identified remains to be done.

11.7 REVISED INTERPRETATION MAP

Having started our analysis at 1:250 000 scale and worked down to a prospect scale we have learned and inferred a great deal of new information on the geology. In this chapter our worked example has taken us to one specific target in the field with an initially encouraging outcome. We have made changes and improvements to our interpretation as we have zeroed-in on increasingly smaller areas. In a typical interpretation campaign we would expect to visit several target areas and anticipate that changes and improvements to our interpretation would result from each visit. These changes can then be incorporated into our overall work and we can produce a revised interpretation map.

At this point, with the results of field testing included in our map, it is appropriate to present the map in a professional cartographic form. Figure 11.28 is our 'final' project interpretation map and represents a major advance on previously published maps of the area. We emphasise, however, that this map is likely to require periodic revision as further mapping and field exploration take place. We urge all interpreters to consider their work as dynamic rather than as a final and finished product. While it is important to finalise each phase of our work, to present it in a professional manner and to actively promote the implementation of the recommendations from the work (e.g. exploration target testing), we should always be prepared to embrace new information and ideas. The changes caused by these new facts or ideas may invalidate our existing map and necessitate a revision, but in the majority of cases this leads us closer to our discovery objectives.

11.8 SUMMARY FOR THE MENZIES–COMET VALE–GOONGARRIE CASE STUDY

We have progressively analysed detailed aeromagnetic data and geological mapping from regional (1:250 000) to prospect (1:25 000) scales. The process of absorbing the known geology, carefully observing and recording

aeromagnetic features, integrating these into a separate solid geological interpretation then applying structural principles to propose a sequence of geological events and infer areas of interest for exploration, has been illustrated at each scale of analysis. We have experienced the profound extensions to our geological understanding created by the integration of aeromagnetic data with the previous mapping, resulting in the definition of at least one as a prime exploration target. The process has been entirely qualitative to this stage. We emphasise the value of *time* taken to carefully observe, digest and record the wealth of geological information contained in the aeromagnetic imagery.

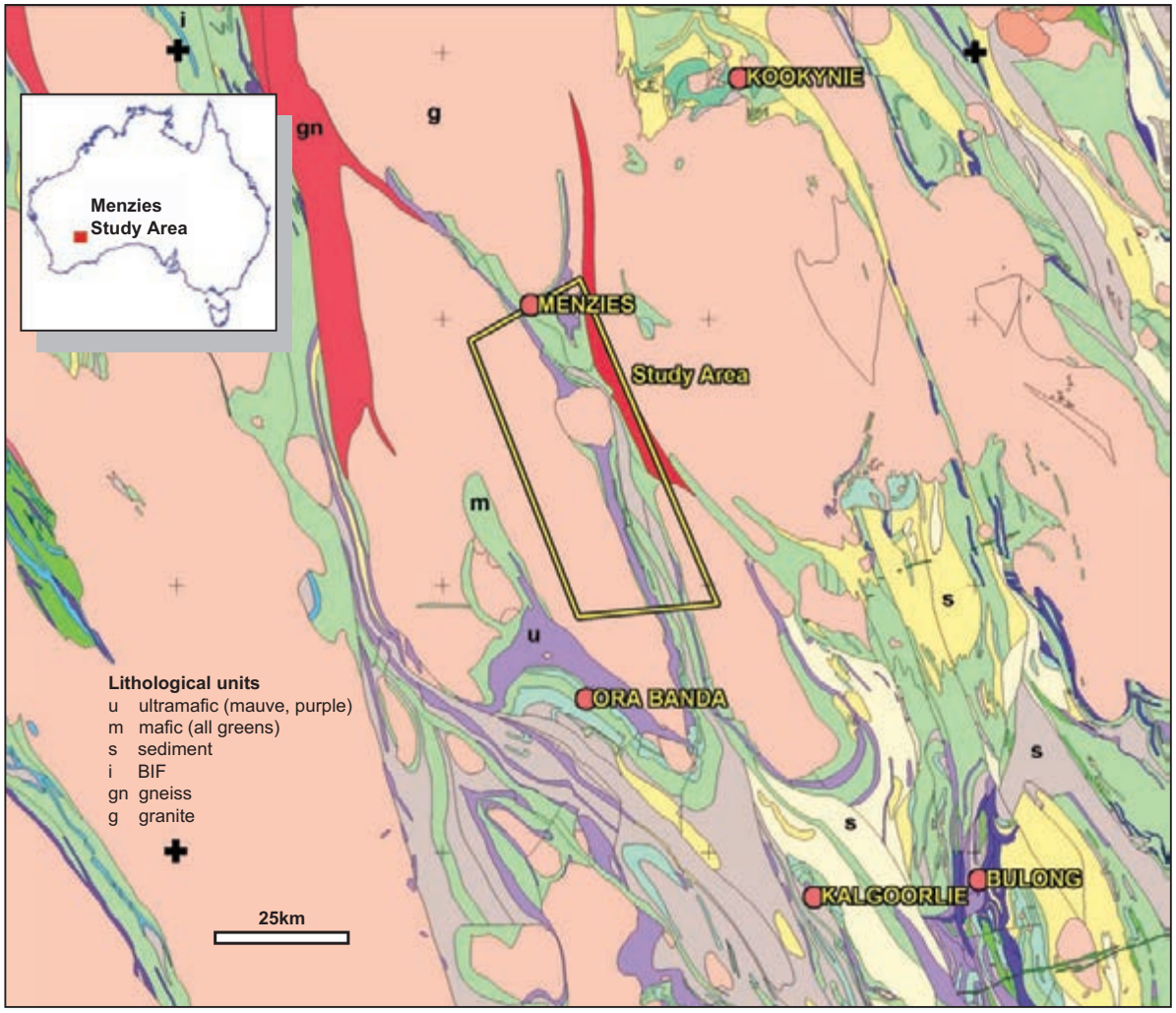

Figure 11.1: Geological Survey of WA regional solid geology (from 1:500 000 state-wide digital compilation). Note that the region has less than 5% outcrop, so the solid geology includes a considerable component of aeromagnetic interpretation. Crosses are Lambert projection metric grid points and are the same for Figures 11.2 and 11.3.

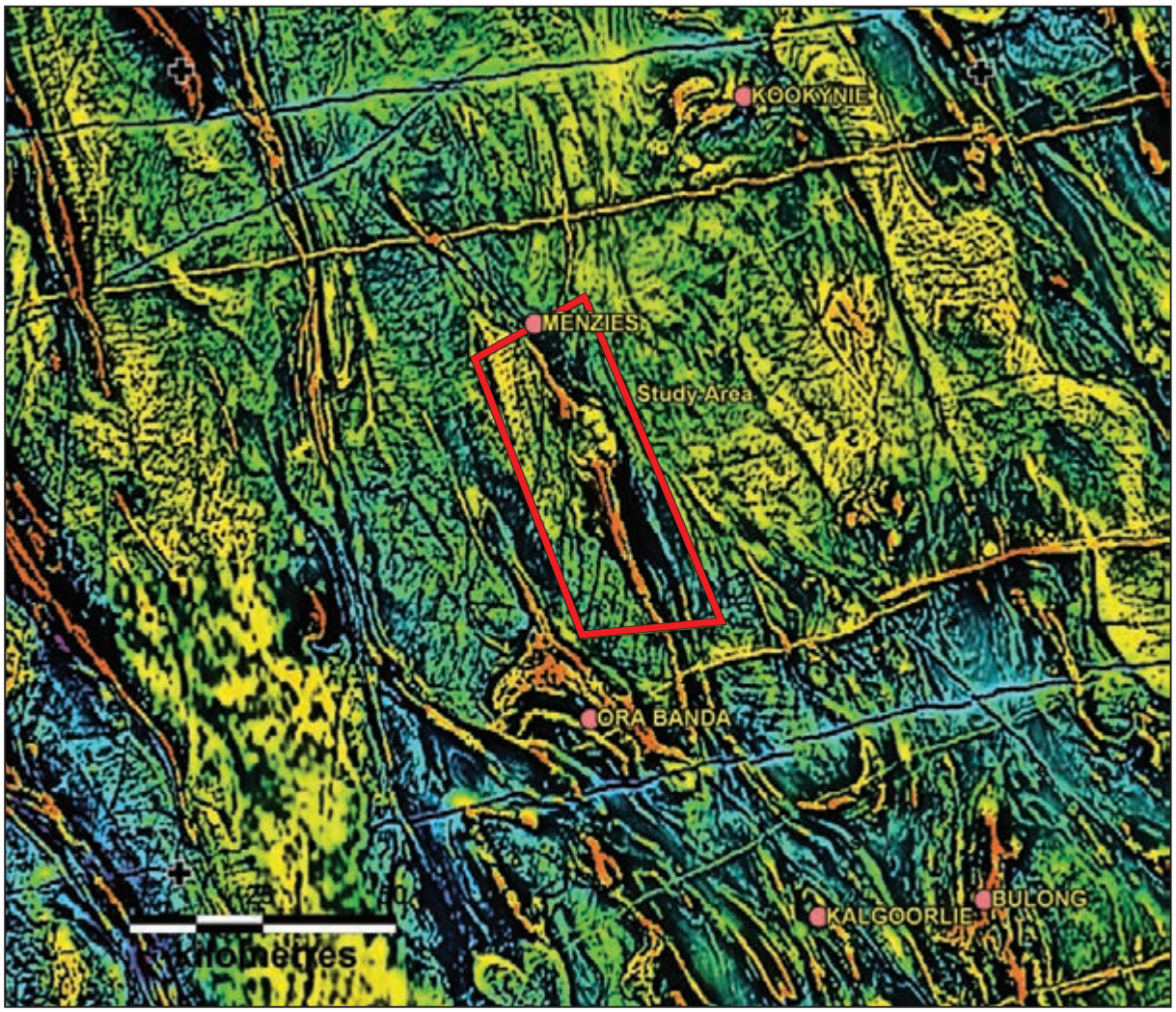

Figure 11.2: Composite regional aeromagnetic image (TMI draped on 1st VD). Derived from the Geoscience Australia nation-wide 250 m grid.

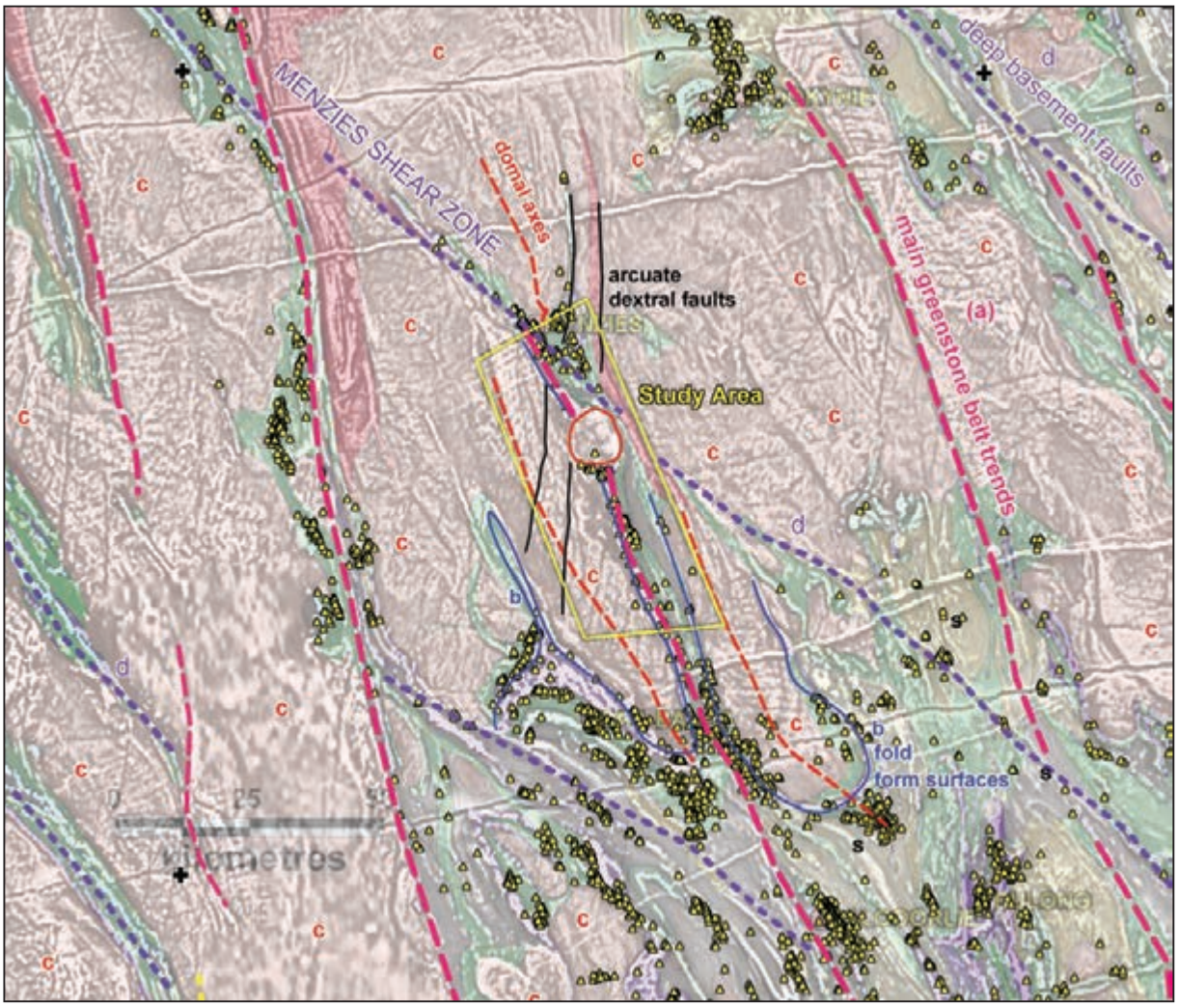

Figure 11.3: Regional summary interpretation sketch showing mineral occurrences. Refer to text for key to labelled features.

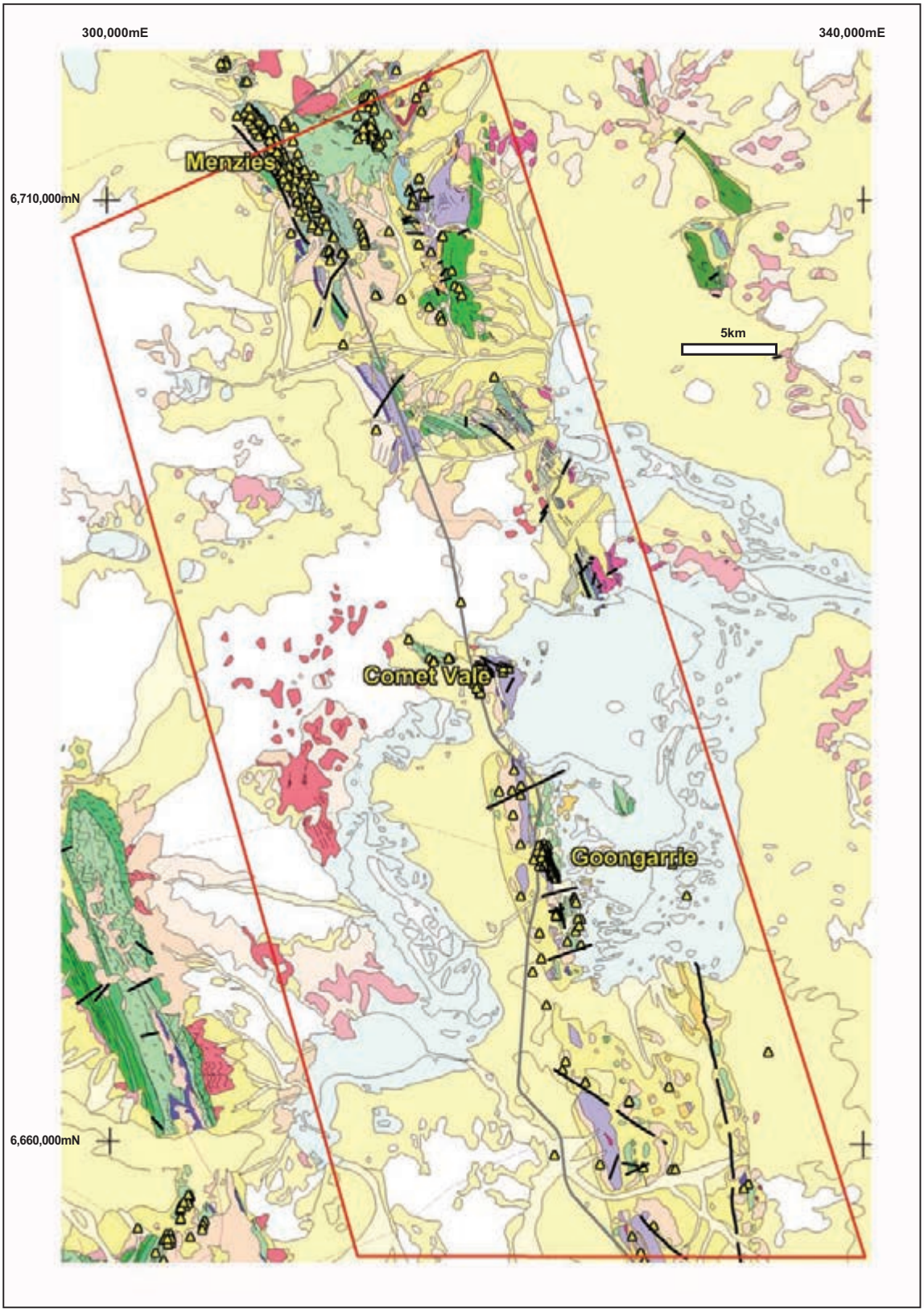

Figure 11.4a: Outcrop geology from Geological Survey of WA digital files. See Figure 11.4b for legend, yellow symbols are mineral (predominantly gold) occurrences. The localities labelled are the main gold districts. The metre coordinate system is Australian Map Grid 1984 (AMG Zone 51, AGD84). This coordination is followed for all subsequent maps and images.

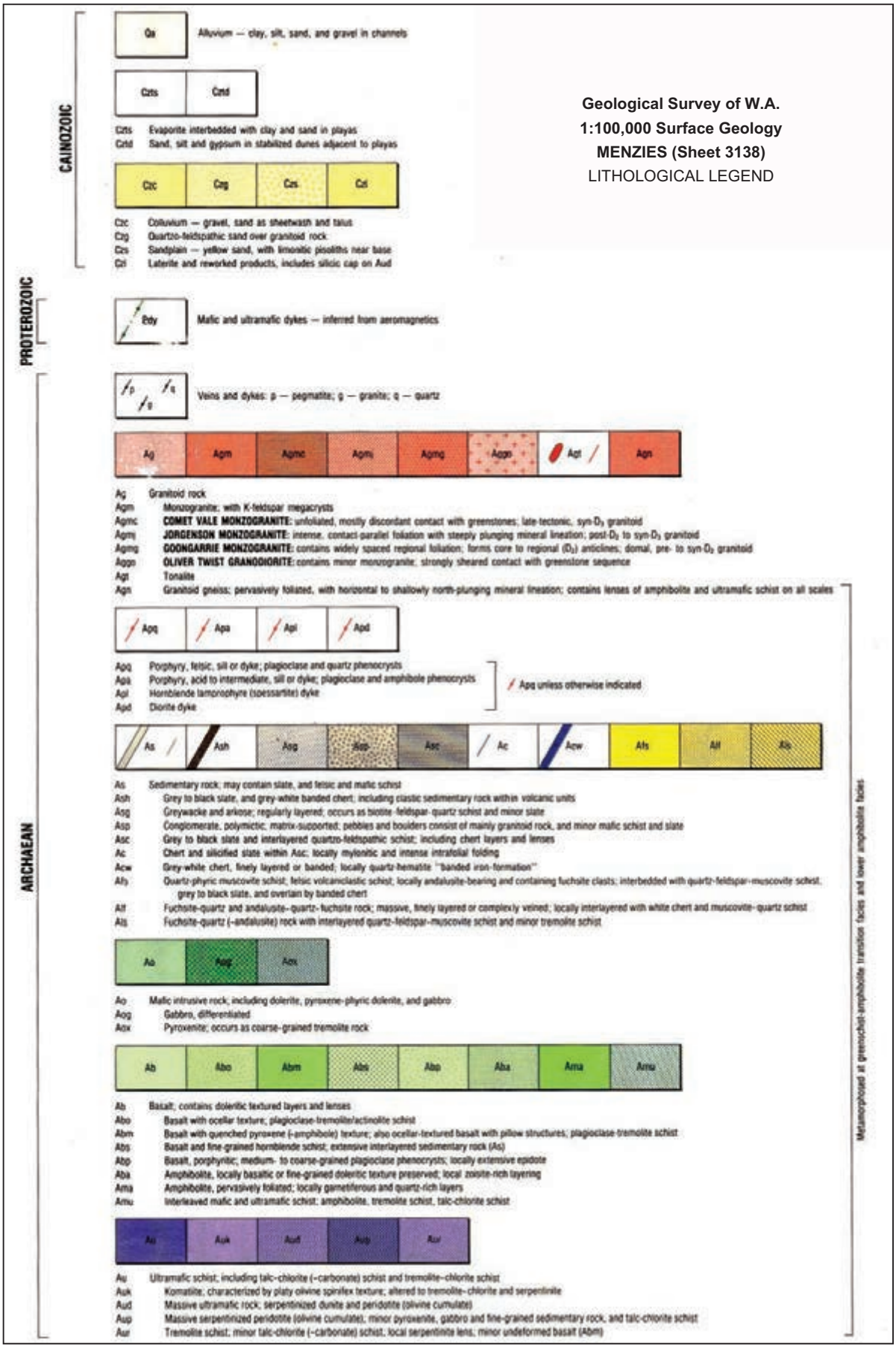

Figure 11.4b: Lithological legend for Geological Survey of WA geology.

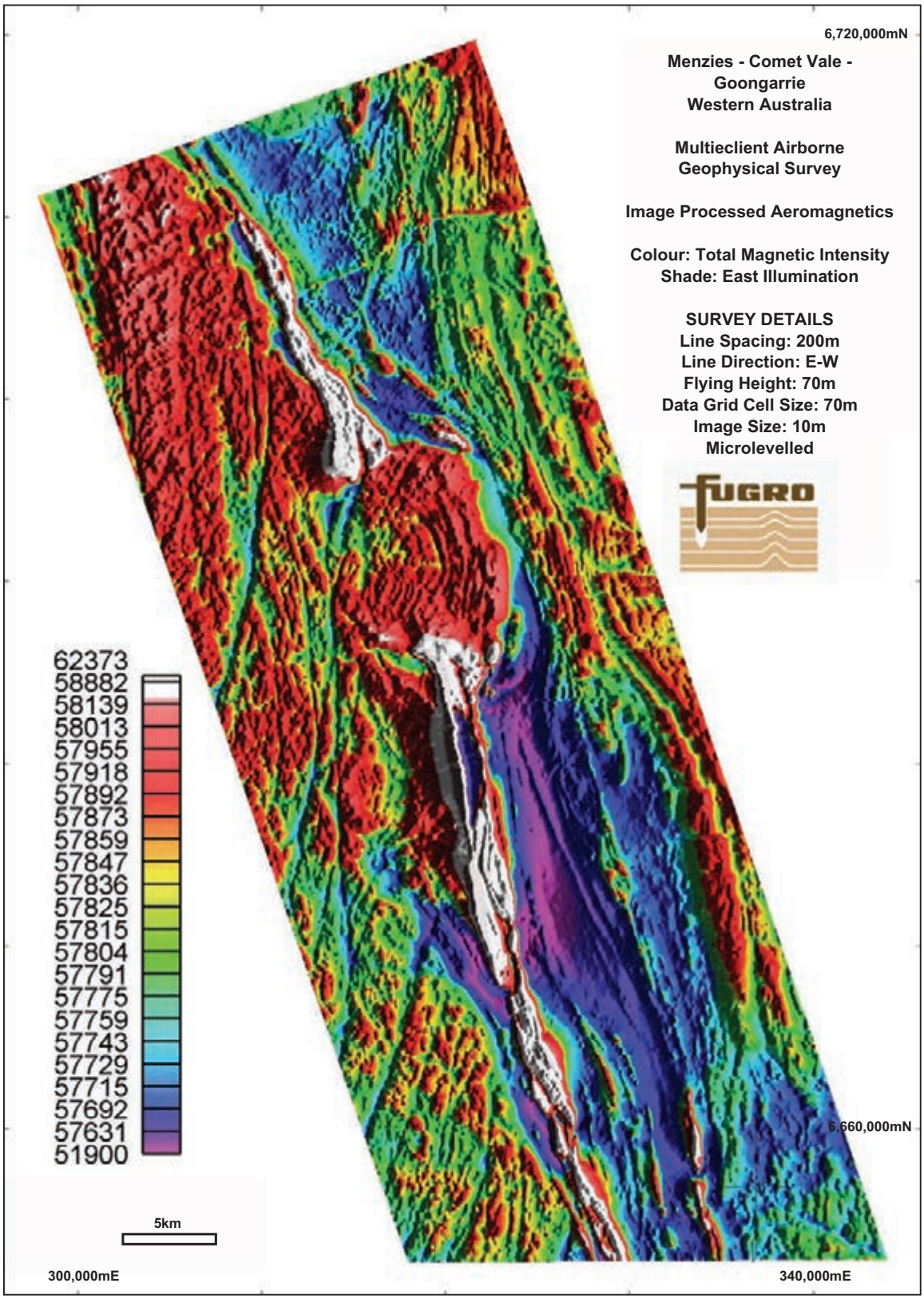

Figure 11.5: TMI. Equalised colour stretch and shaded from the east. Data and imaging courtesy Fugro Airborne Surveys.

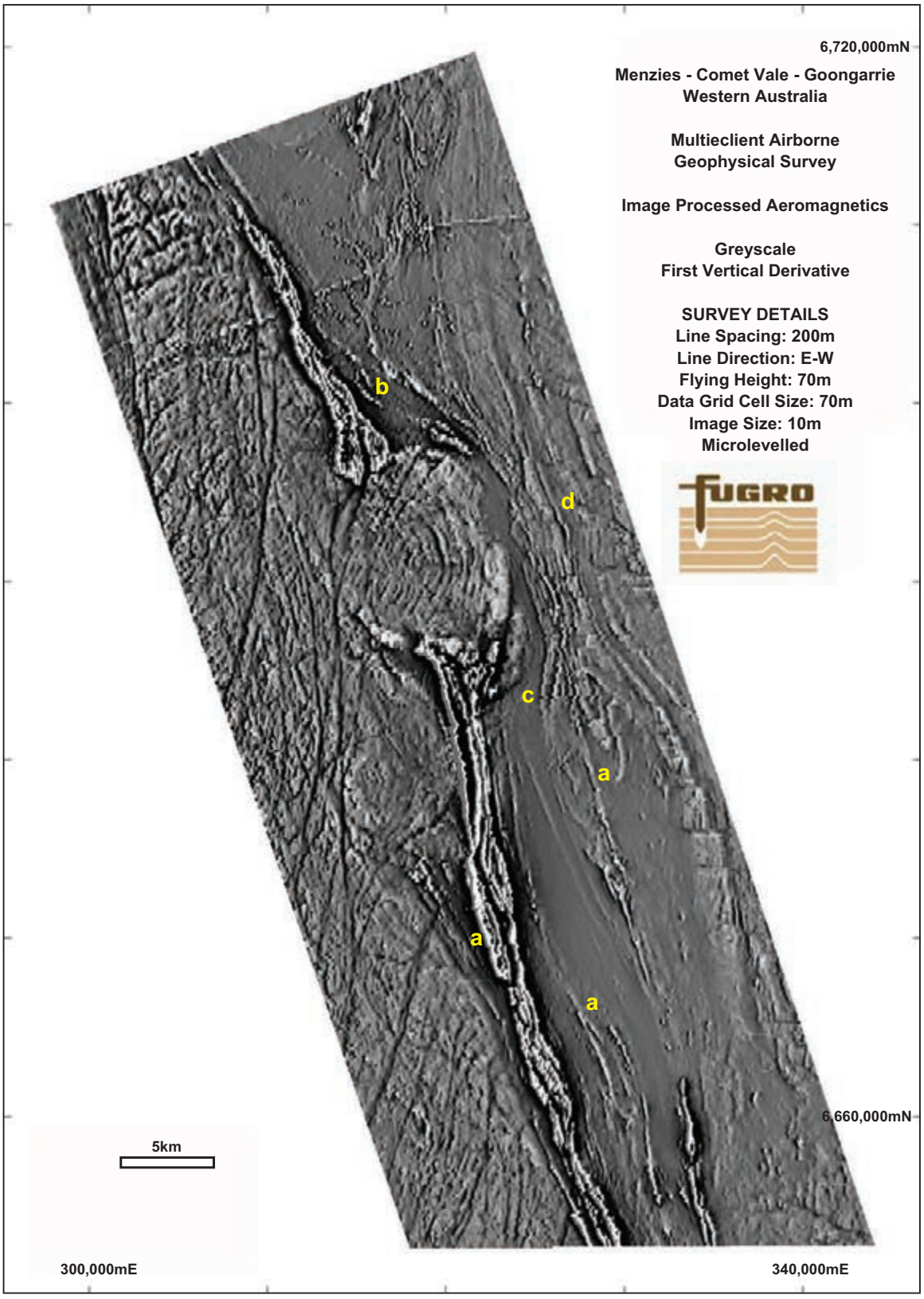

Figure 11.6: 1st VD. Non-linear stretch shade from the east. Data and imaging courtesy Fugro Airborne Surveys.

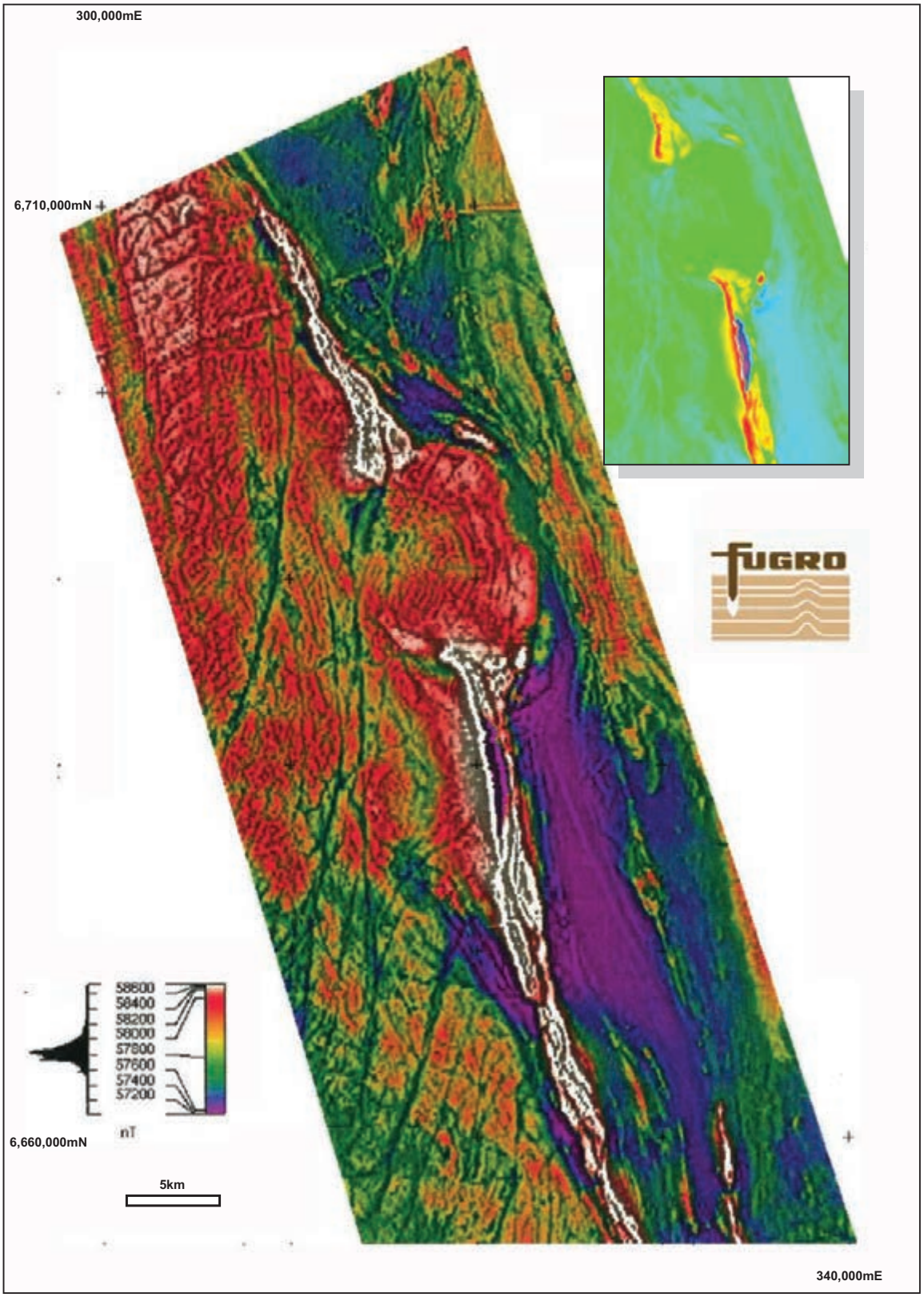

Figure 11.7: Composite image of TMI (colour) draped on 1st VD (grey). The inset shows a linear stretch on a section of the data highlighting the extreme magnetic low. The low has intensity values down to 52 000 nT against a background level of ~58 000 nT. The strongest highs adjacent to the west are around 62 000 nT. Data courtesy Fugro Airborne Surveys.

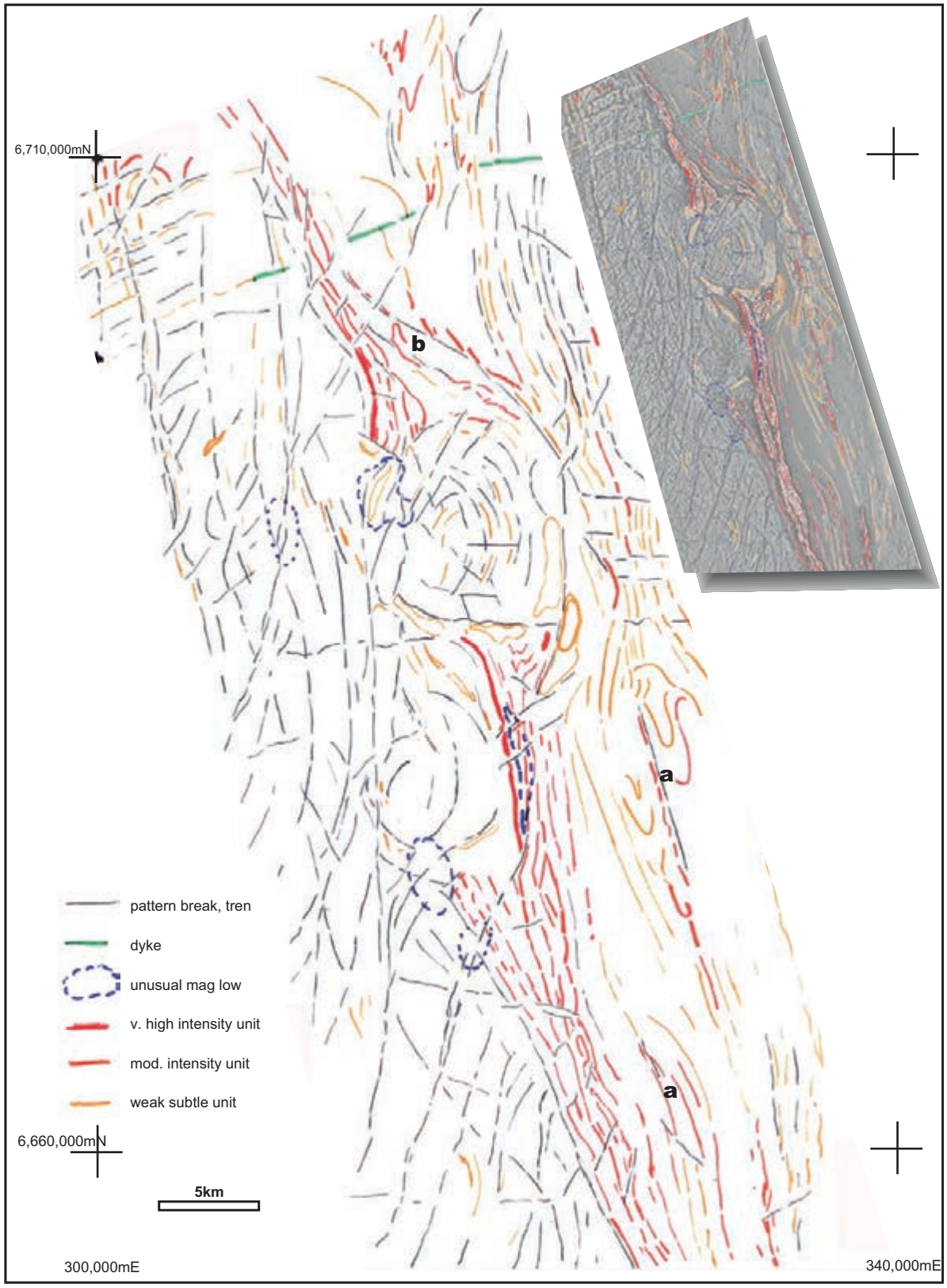

Figure 11.8: Observation layer. Inset shows observations superimposed on the 1st VD.

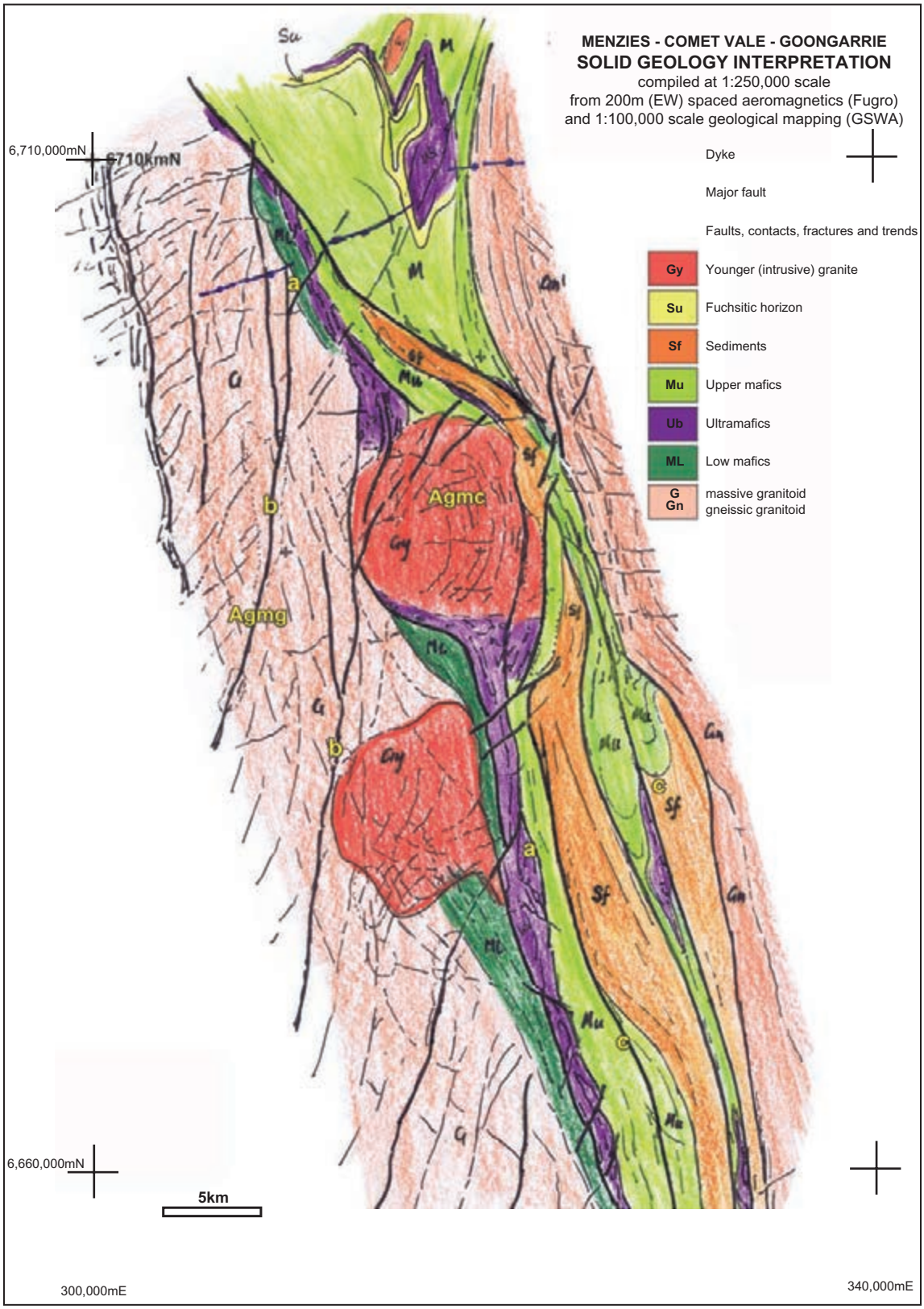

Figure 11.9: Initial solid geology compilation. Agmc is the younger Comet Vale Monzogranite and Agmg the Goongarrie Monzogranite (see legend, Fig. 11.4.b). Agmg is referred to as the 'western granitoid' in the text. Su, the fuchsitic horizon, is an unusual marker unit evident in outcrop but not clearly expressed in the aeromagnetics.

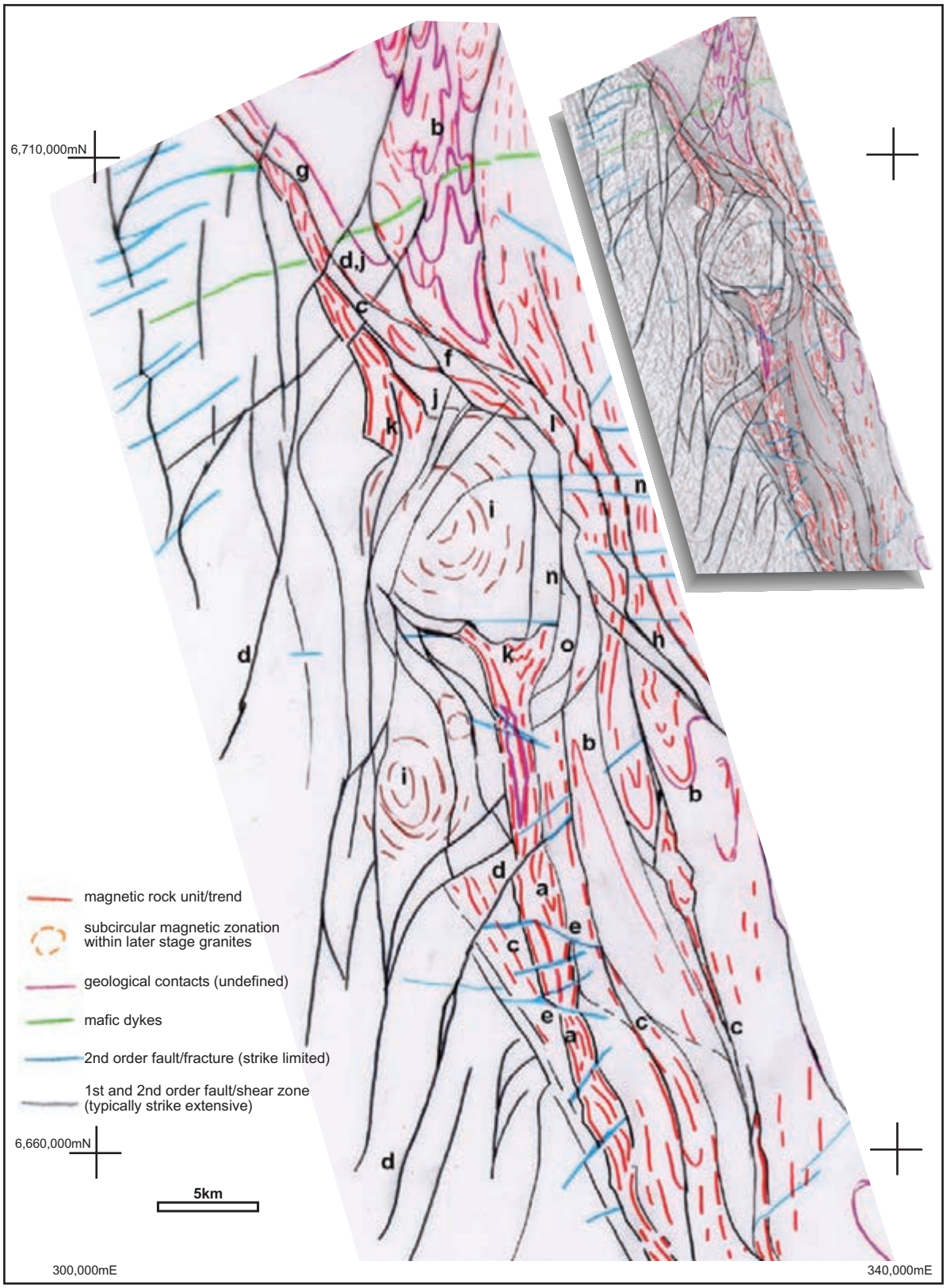

Figure 11.10: Structural framework – an extension of the observation layer incorporating initial ideas on structural continuity. Registration points are the same as in Figures 11.8 and 11.9. The inset shows how this layer relates to the 1st VD image.

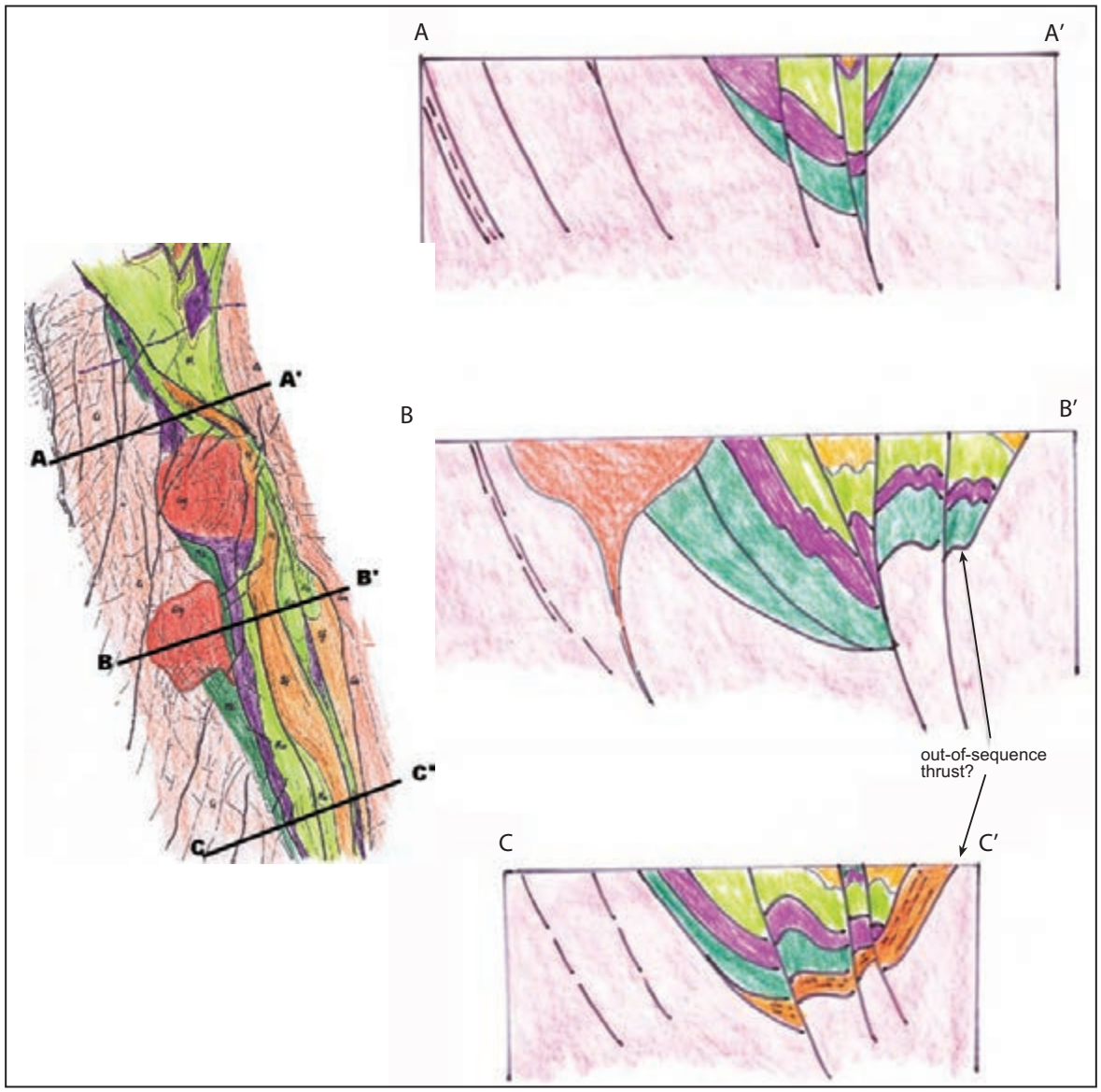

Figure 11.11: Interpretive cross-sections. See Figure 11.9 for legend.

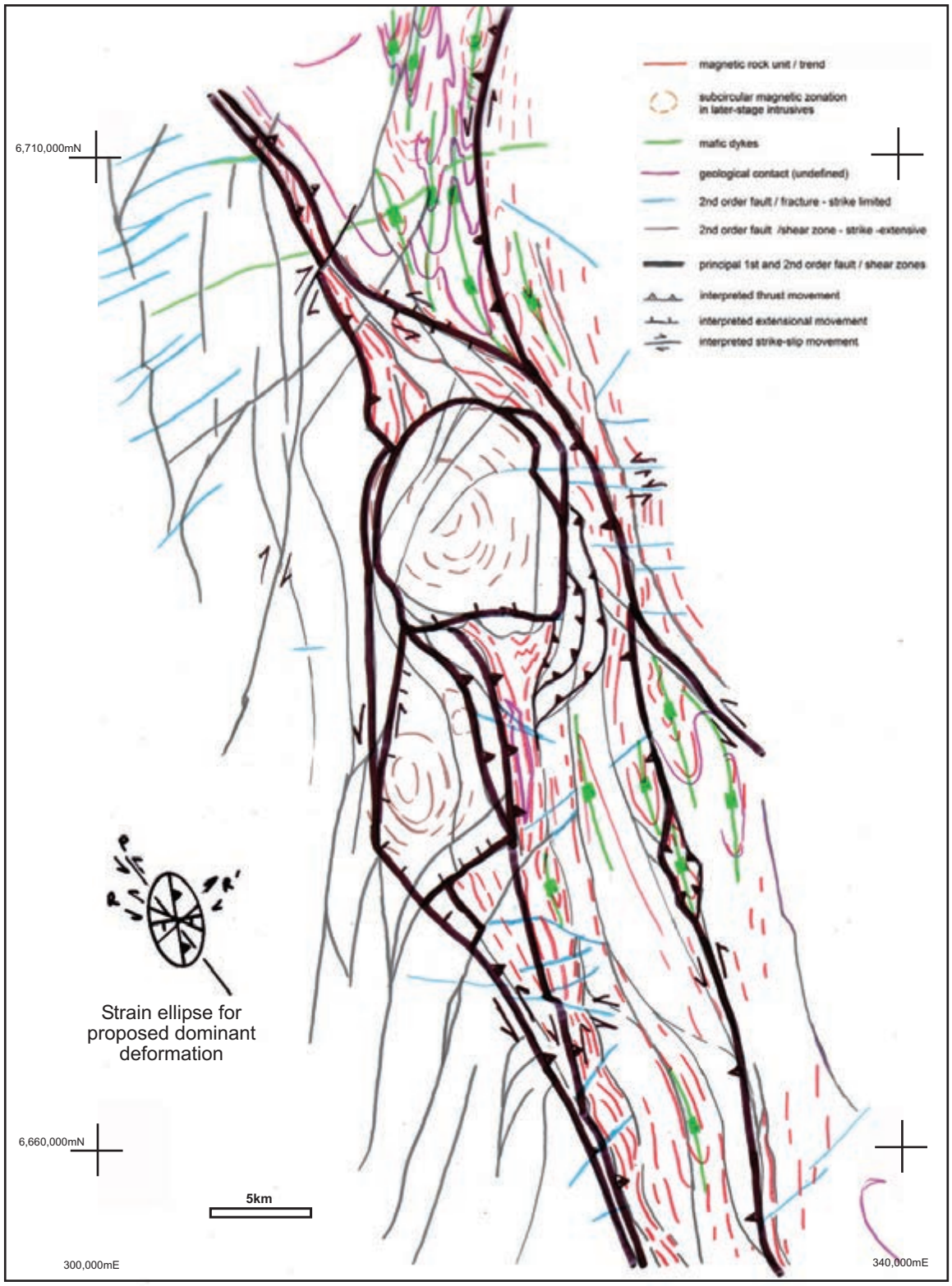

Figure 11.12: Structural interpretation and synthesis.

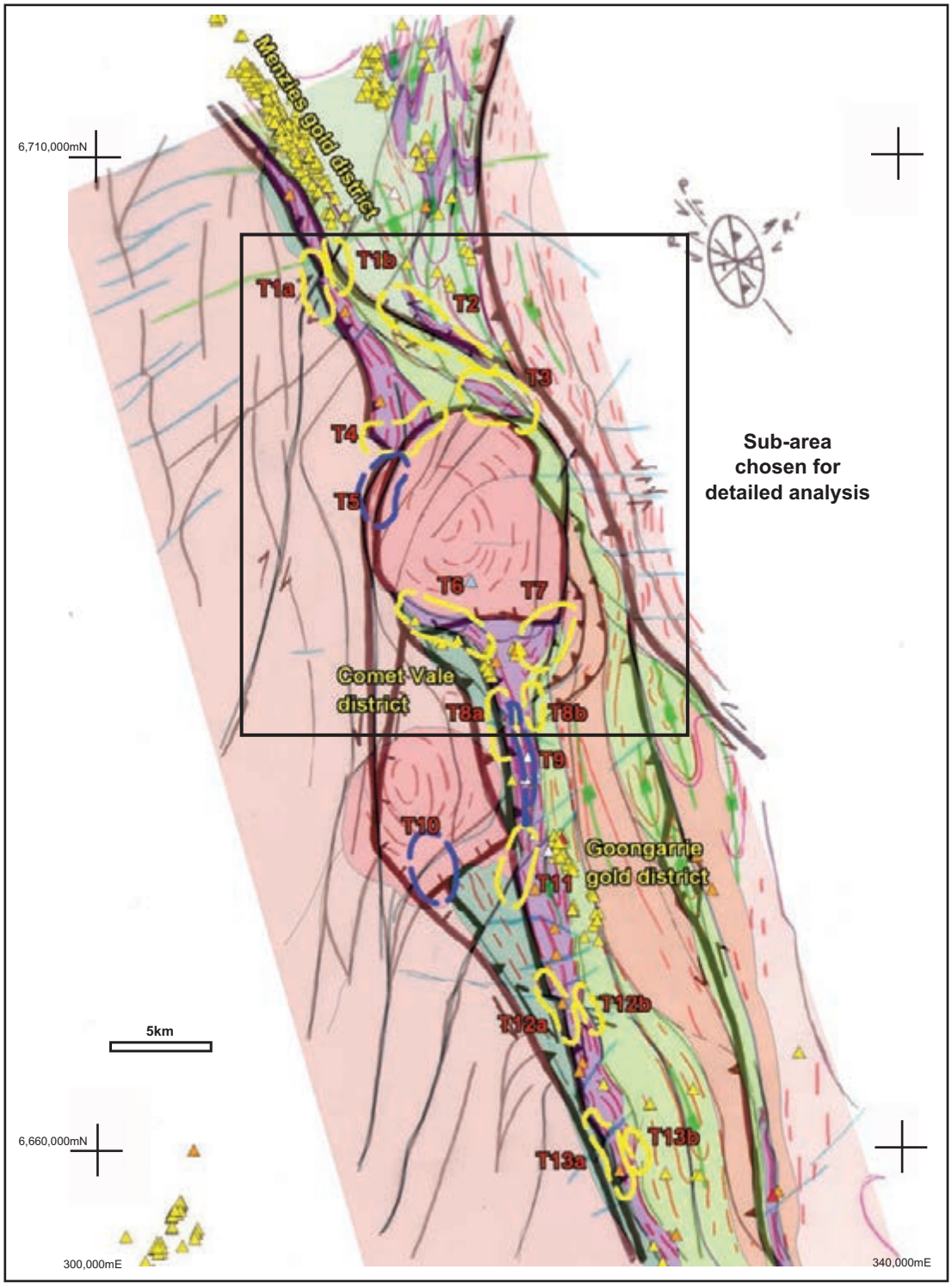

Figure 11.13: Exploration targets – showing gold and nickel occurrences. The target areas are described in Table 11.1.

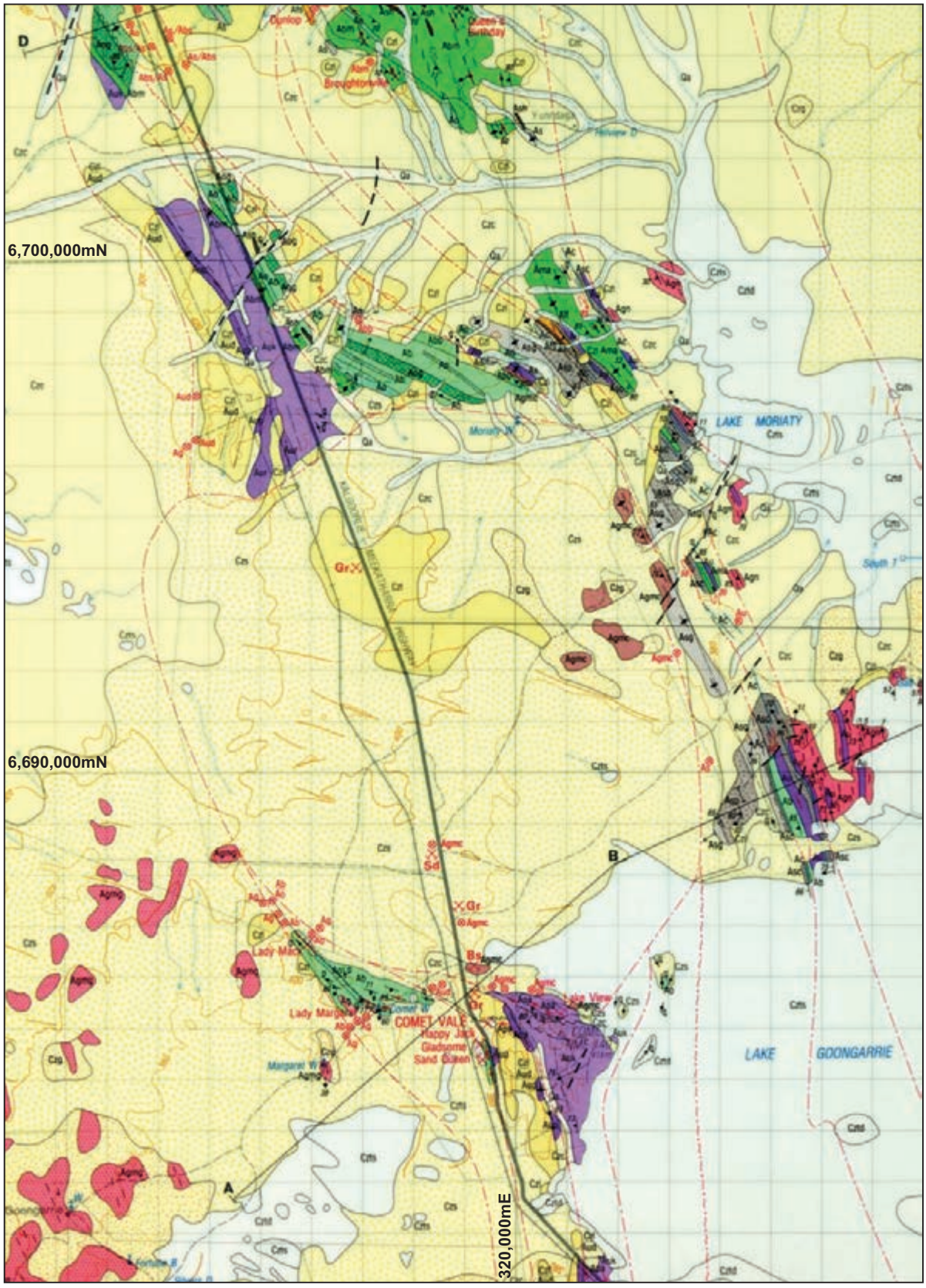

Figure 11.14: Geological Survey of WA outcrop geology of the Comet Vale subarea (part 'Menzies' 1:100 000 sheet). See Figure 11.4b for the legend.

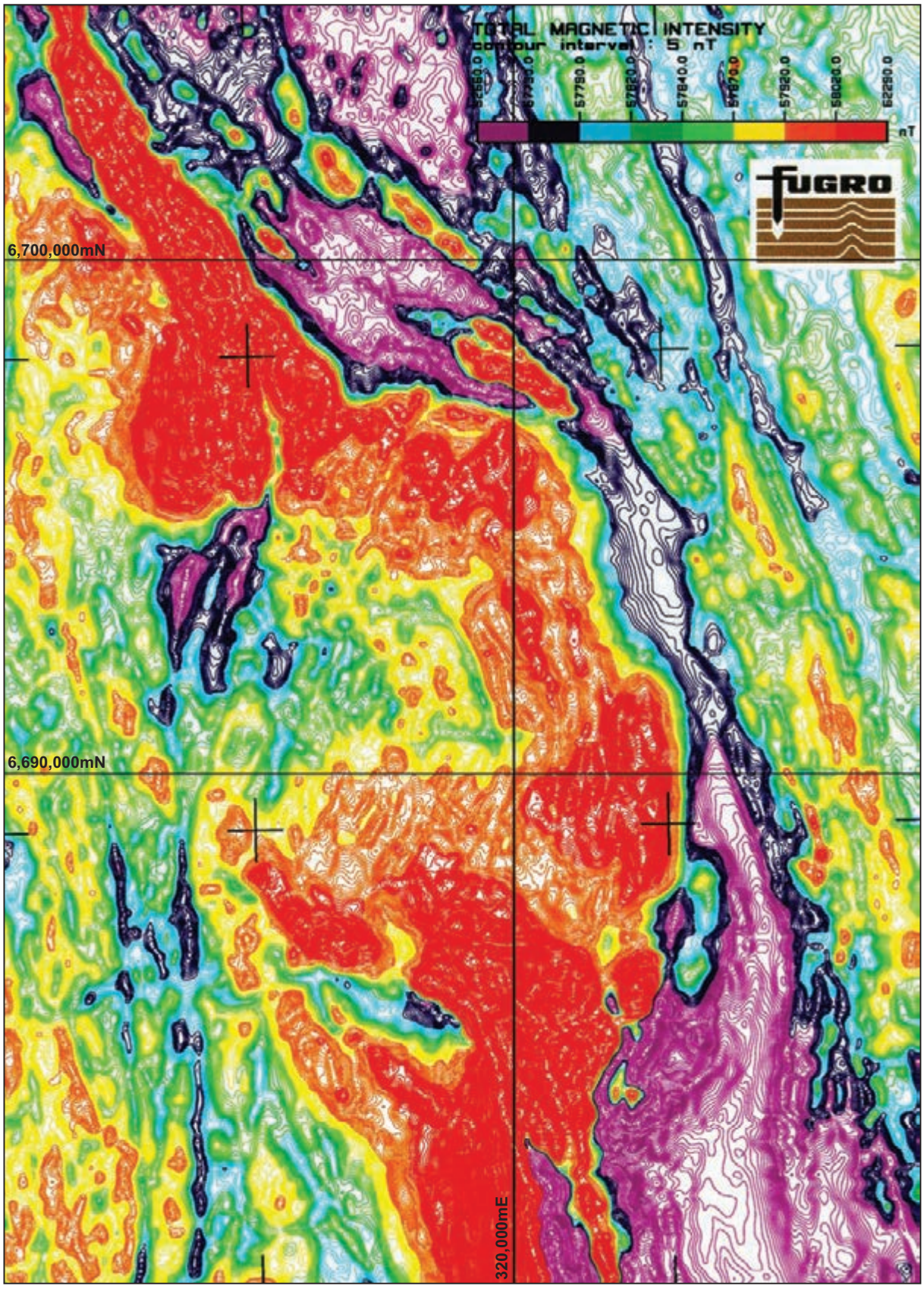

Figure 11.15: TMI contours (contour interval 10 nT).

Figure 11.16: 1st VD (RTP and re-enhanced).

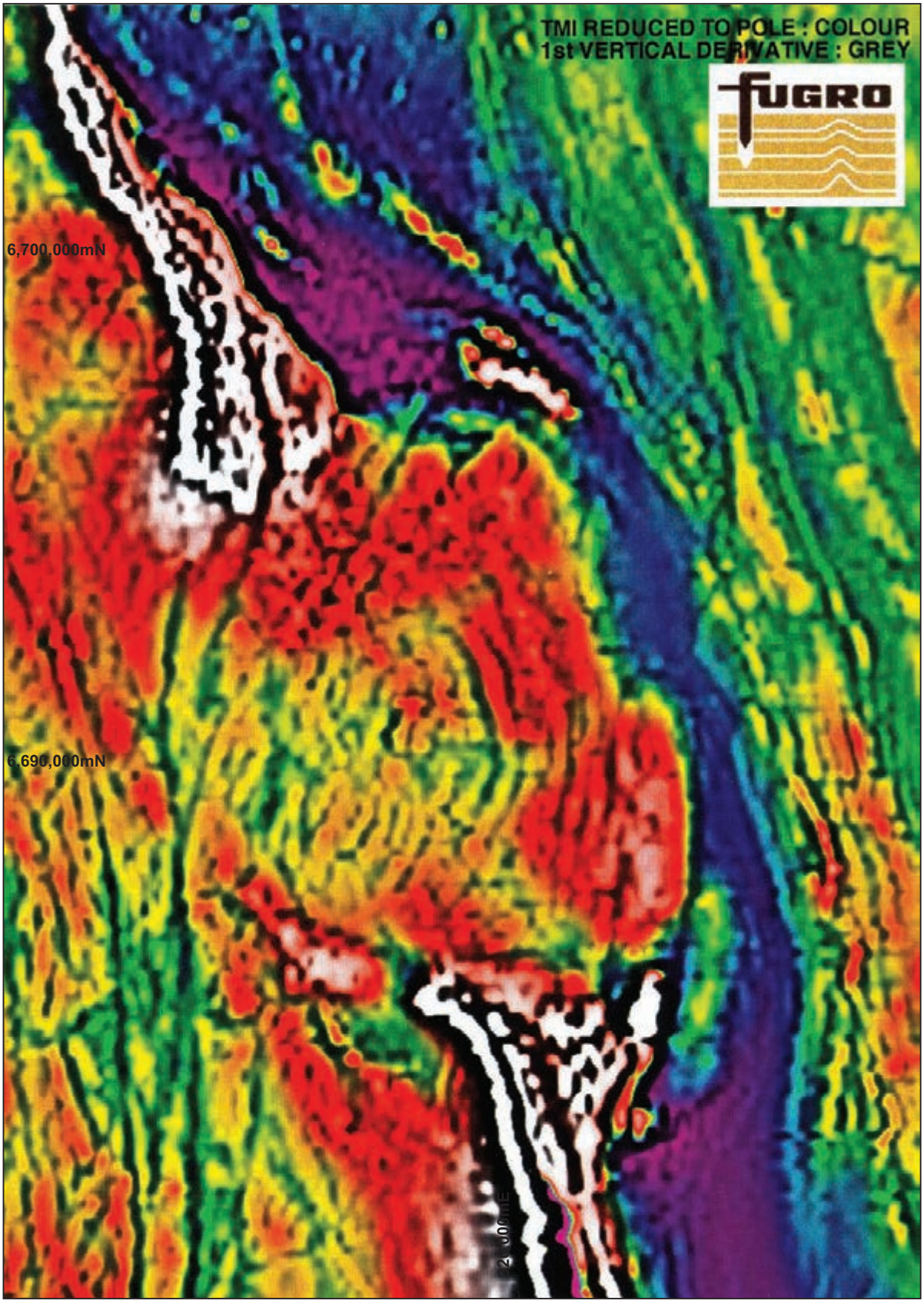

Figure 11.17: Composite image of RTP (colour) draped on RTP 1st VD (greyscale).

Figure 11.18: Observations layer (legend follows Figure 11.8).

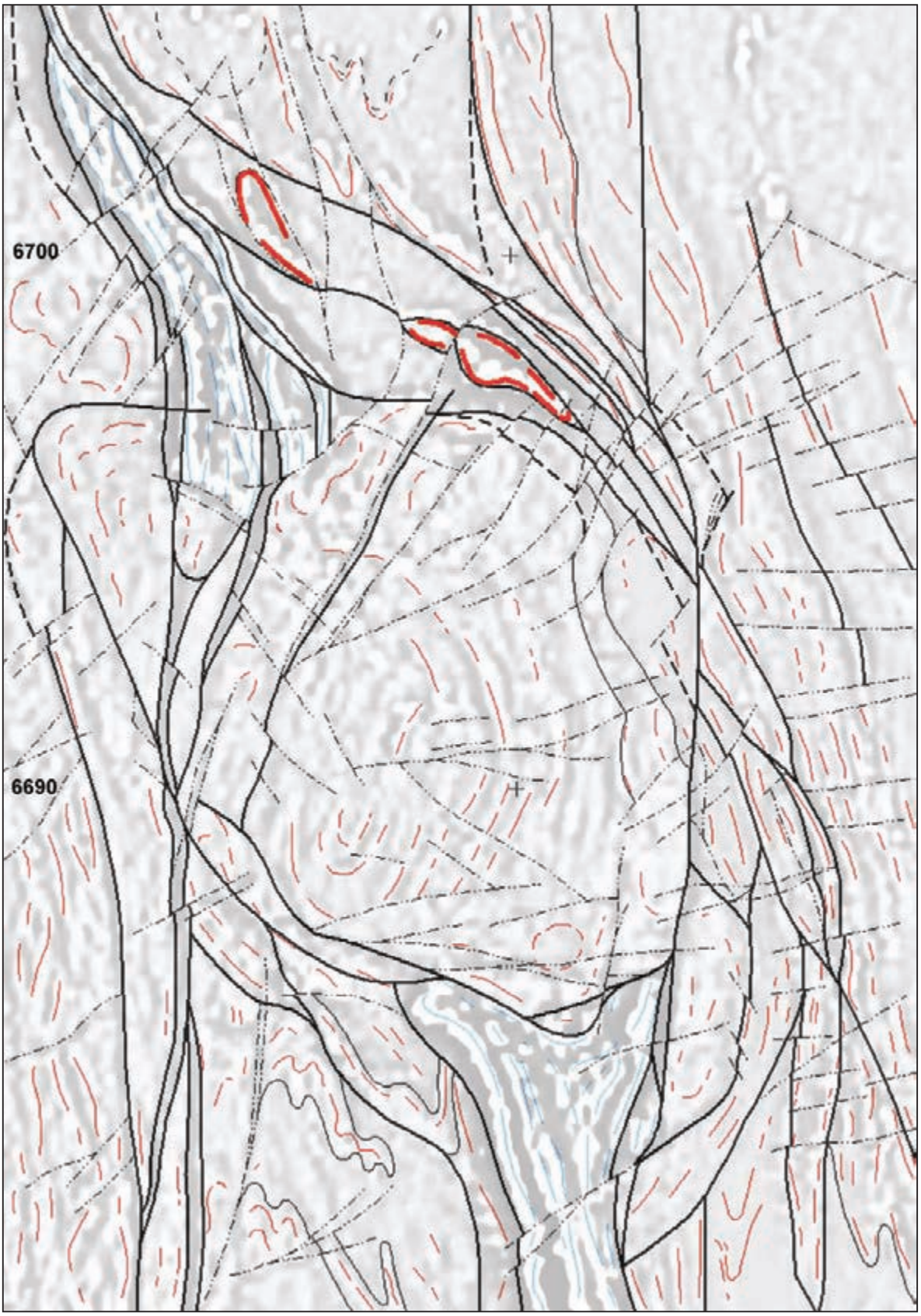

Figure 11.19: Structural framework (combination of initial observations and interpretation of structure) superimposed on RTP 1st VD. The solid black lines are first-order faults and contacts, dotted lines are second-order fractures and trends, blue lines are magnetic horizons in the ultramafic sequence, brown lines are magnetic rock units in other lithologies, thick red lines highlight an inferred anomalous magnetic rock unit.

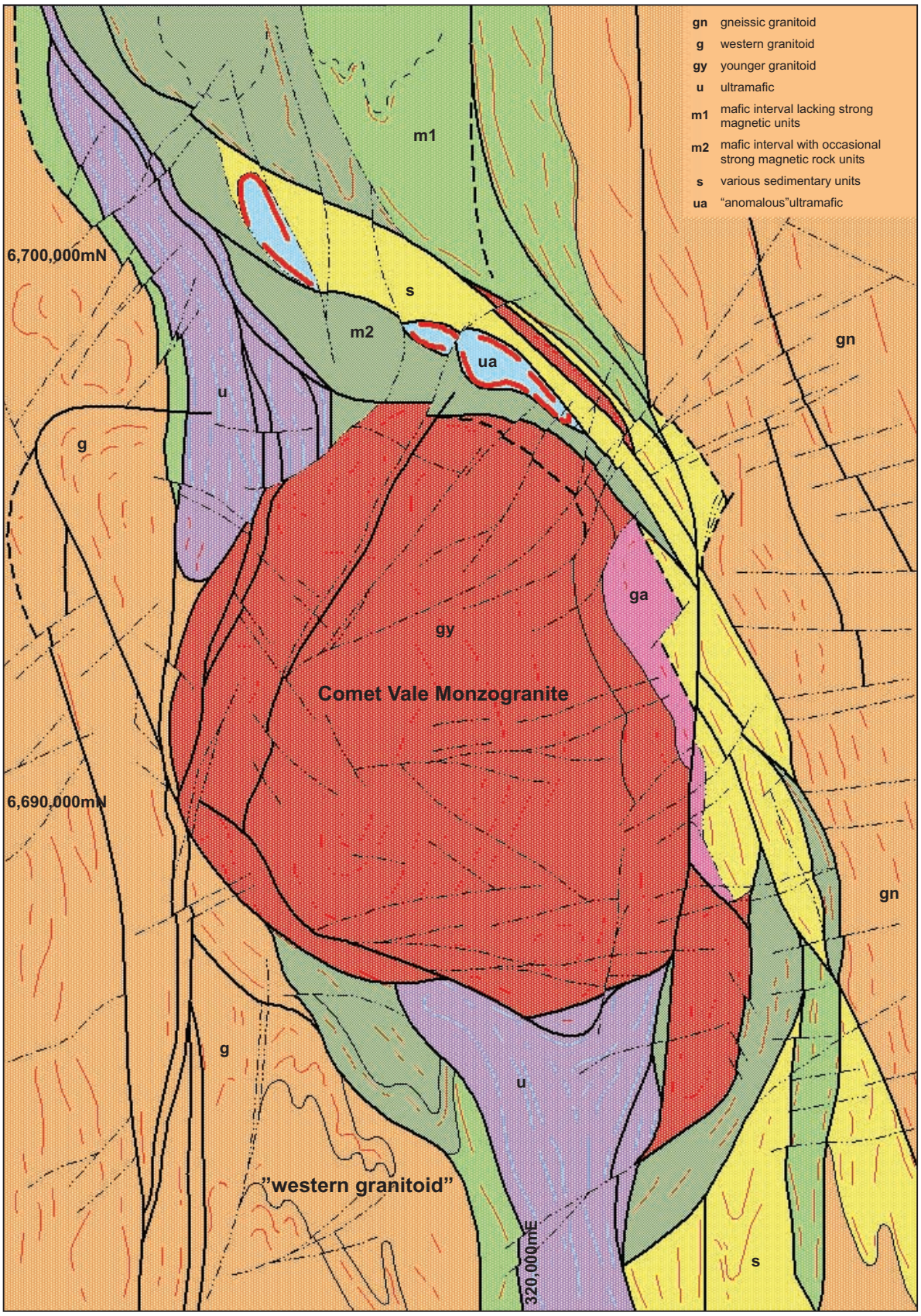

Figure 11.20: Solid geology compilation.

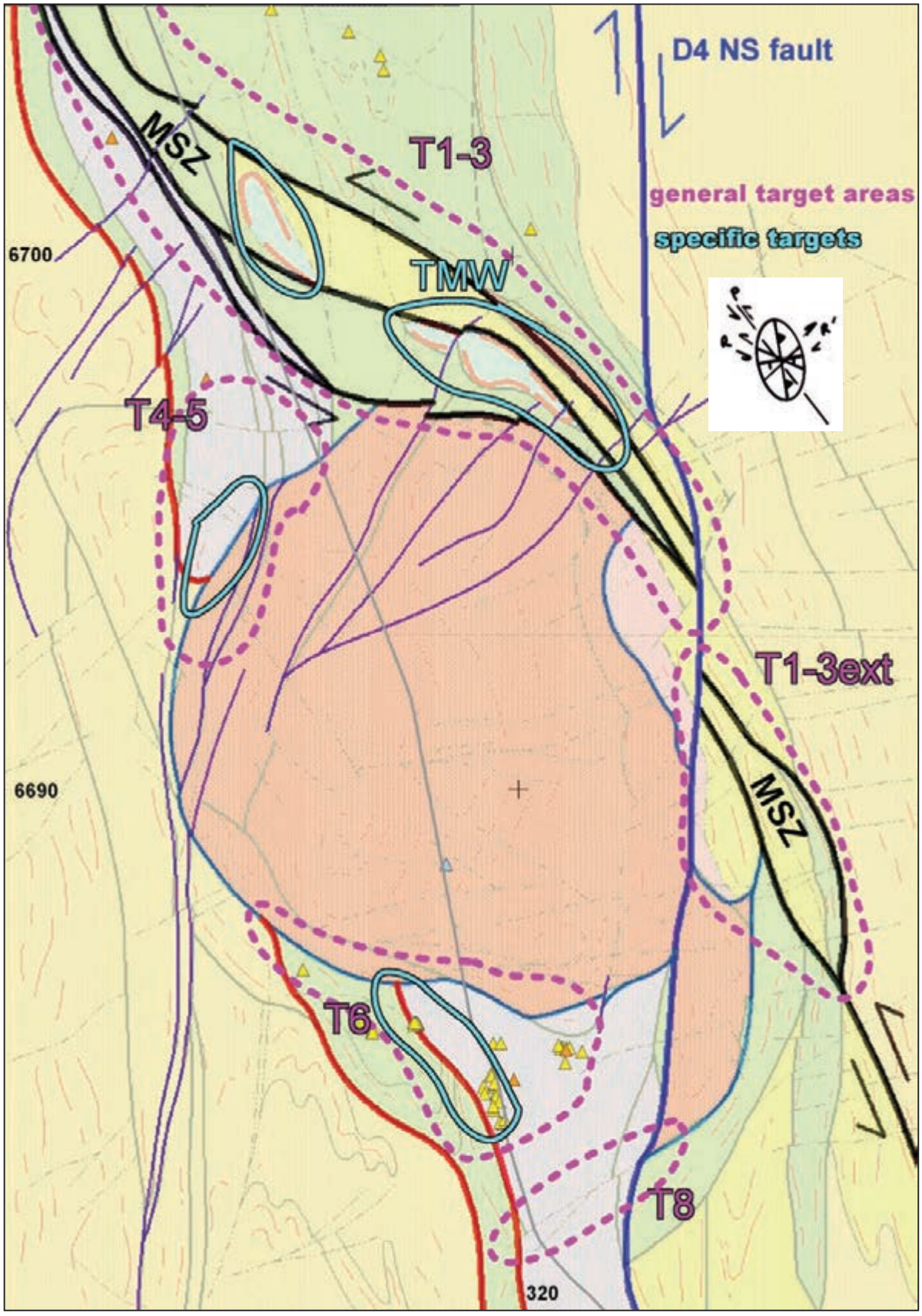

Figure 11.21: Structural summary and targets. The strain ellipse in Figure 11.12 describes the interpreted main deformation phases (see Section 11.3.9). The NS (?D4) fault appears to be a distinct, later event.

Figure 11.22: Moriarty Well area 1:25 000 scale study: Geological Survey of WA outcrop geology (part 'Menzies' 1:100 000 sheet, refer to Fig. 11.4b for legend). Grid is 1 km.

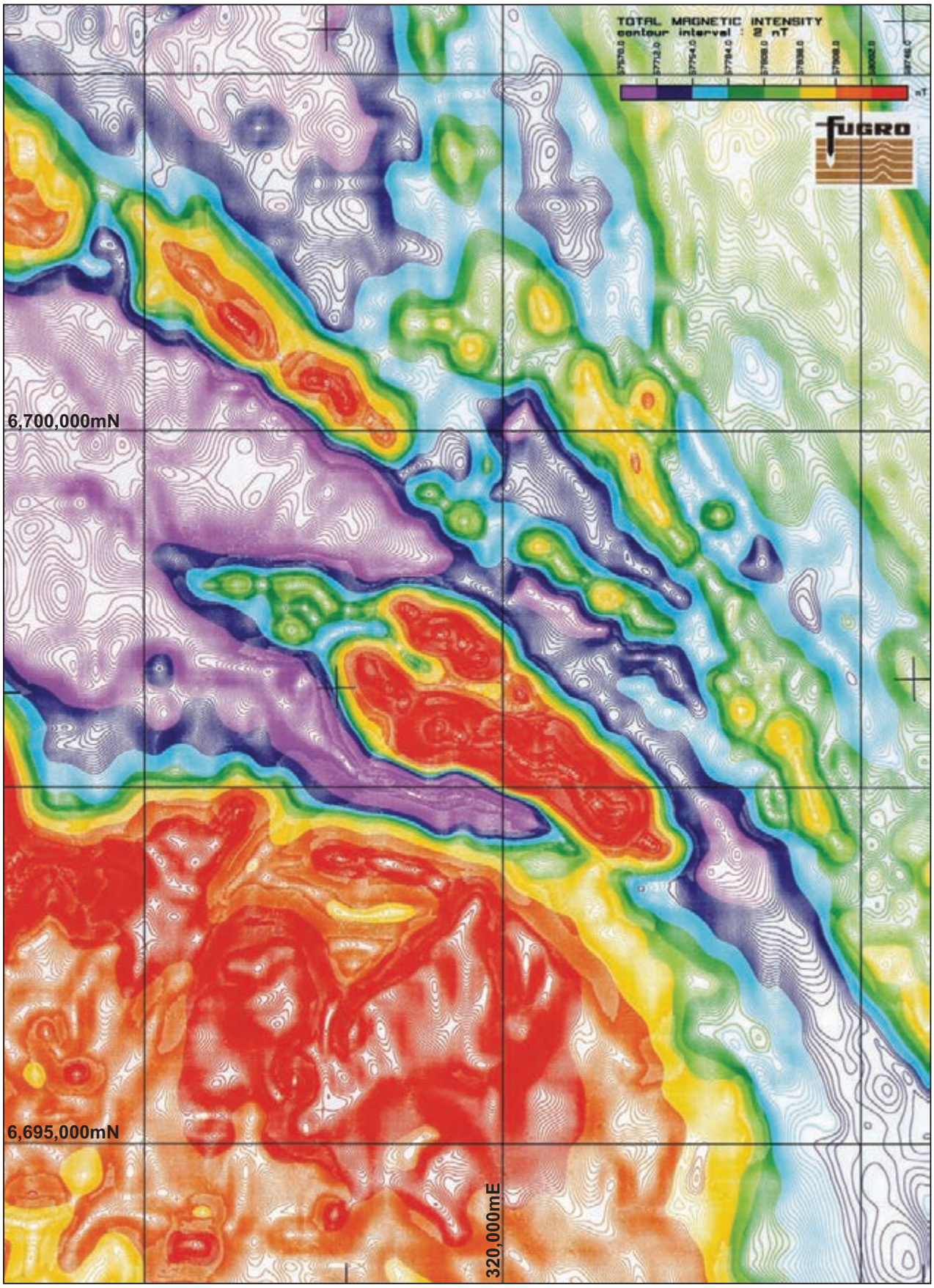

Figure 11.23: Moriarty Well area 1:25 000 scale study: TMI. Grid is 2500 m, smallest contour interval is 2 nT.

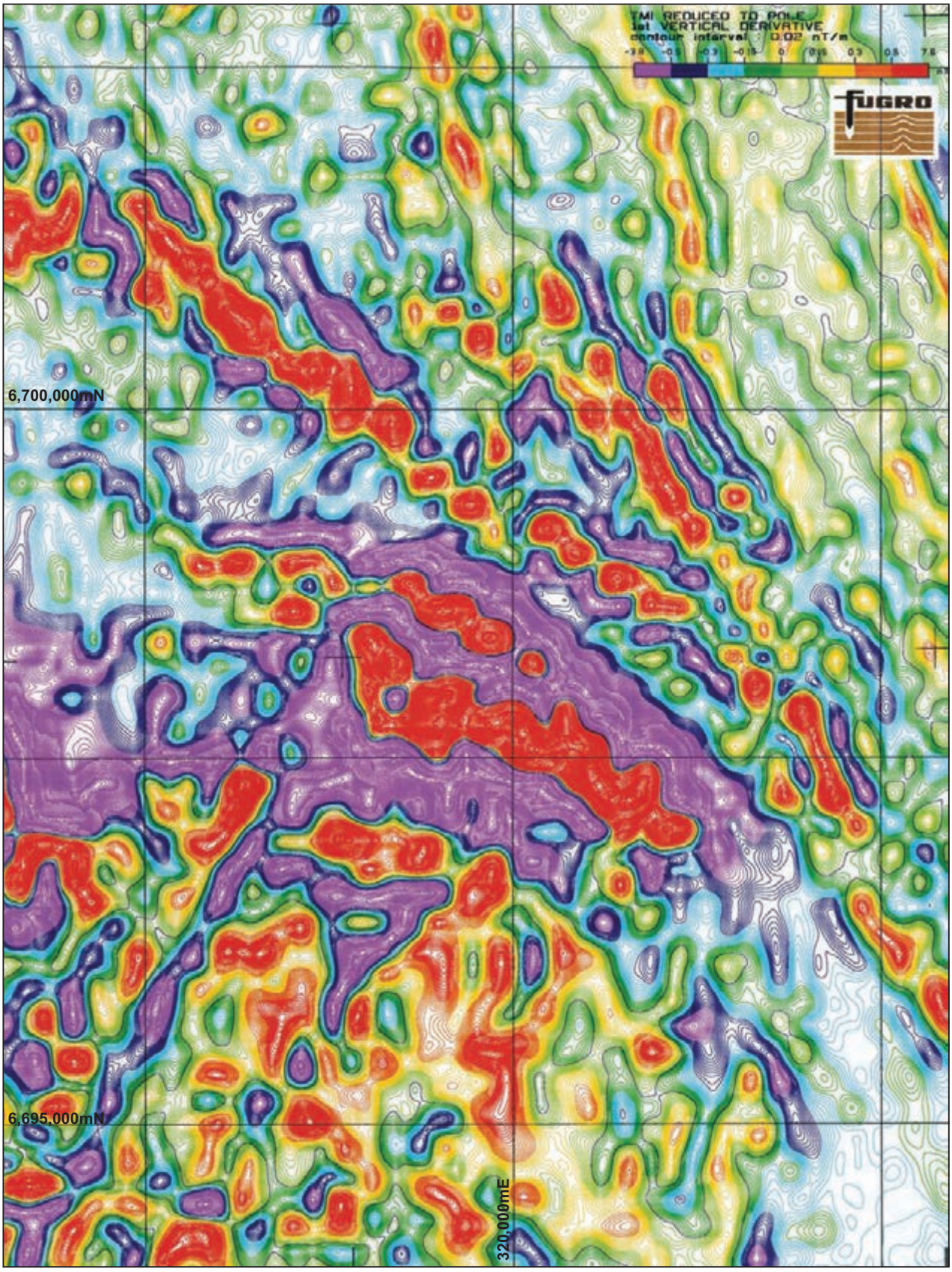

Figure 11.24: Moriarty Well area 1:25 000 scale study: 1st VD RTP. Non-linear contour interval.

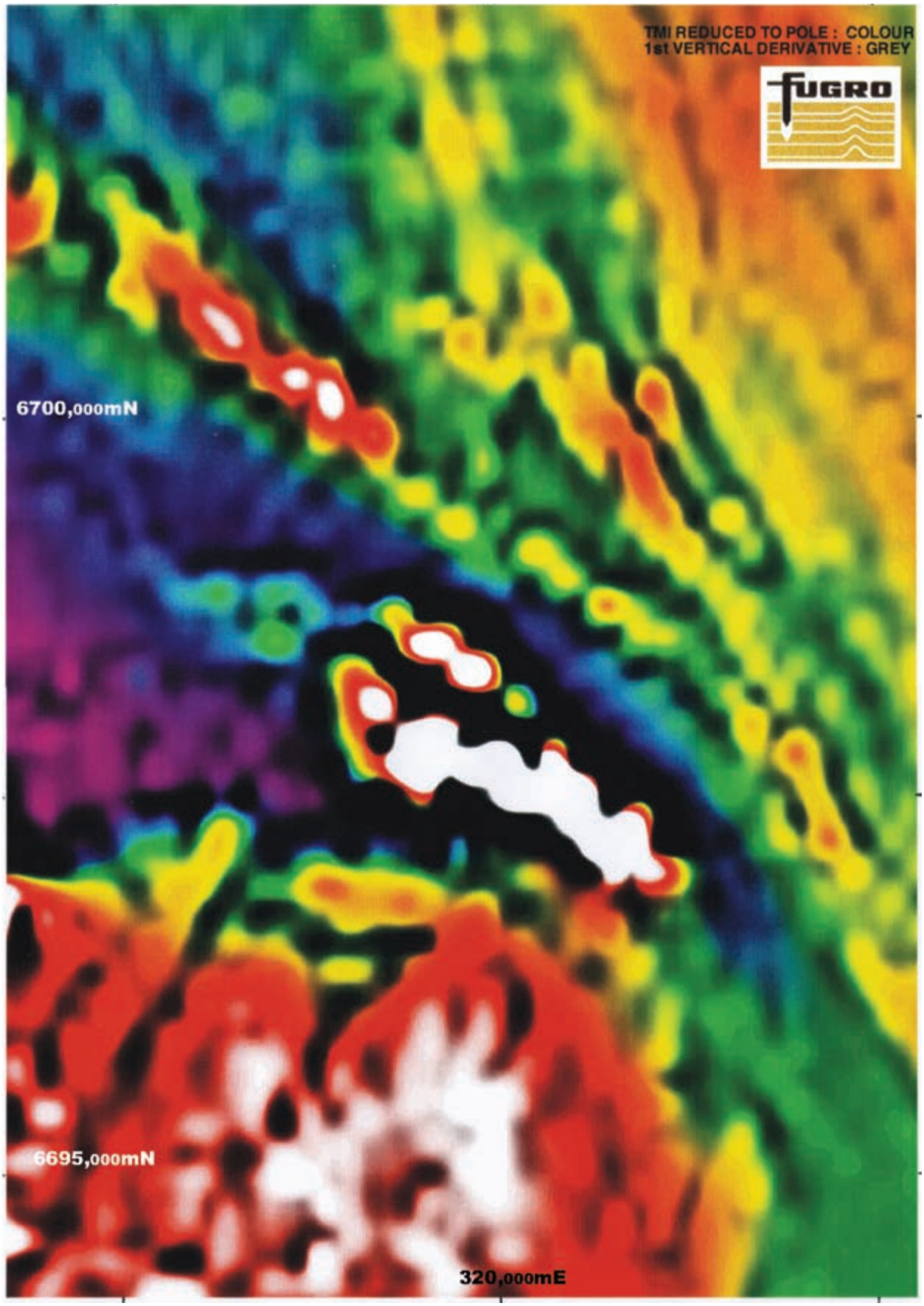

Figure 11.25: Moriarty Well area 1:25 000 scale study: composite image of TMI RTP and 1st VD RTP (grey).

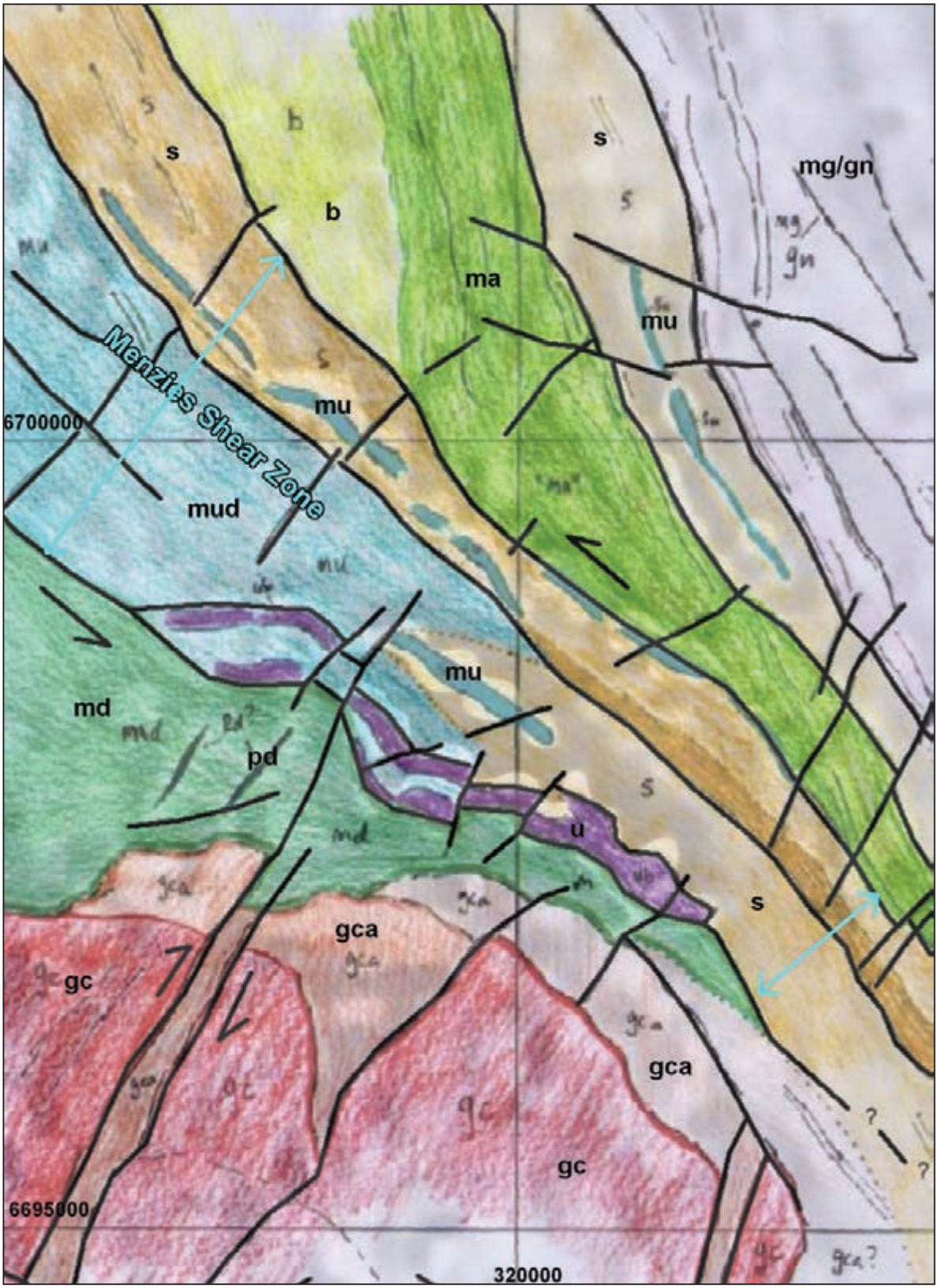

m	ultramafic	**ma**	amphibolitic mafic interval
mud	mafic interval with likely ultramafic and mafic rocks	**mg/gn**	mixed mafic & gneissic interval
mu	local mafic/ultramafic magnetic rock units	**gc**	Comet Vale Monzogranite
md	mafic unit containing basalt, dolerite and gabbro	**gca**	altered/marginal/non-magnetic variant of gc
s	mixed sedimentary interval	**pd**	late mafic dyke
b	basaltic interval		

Figure 11.26a: Solid geology and structural interpretation before field mapping, superimposed on RTP 1st VD.

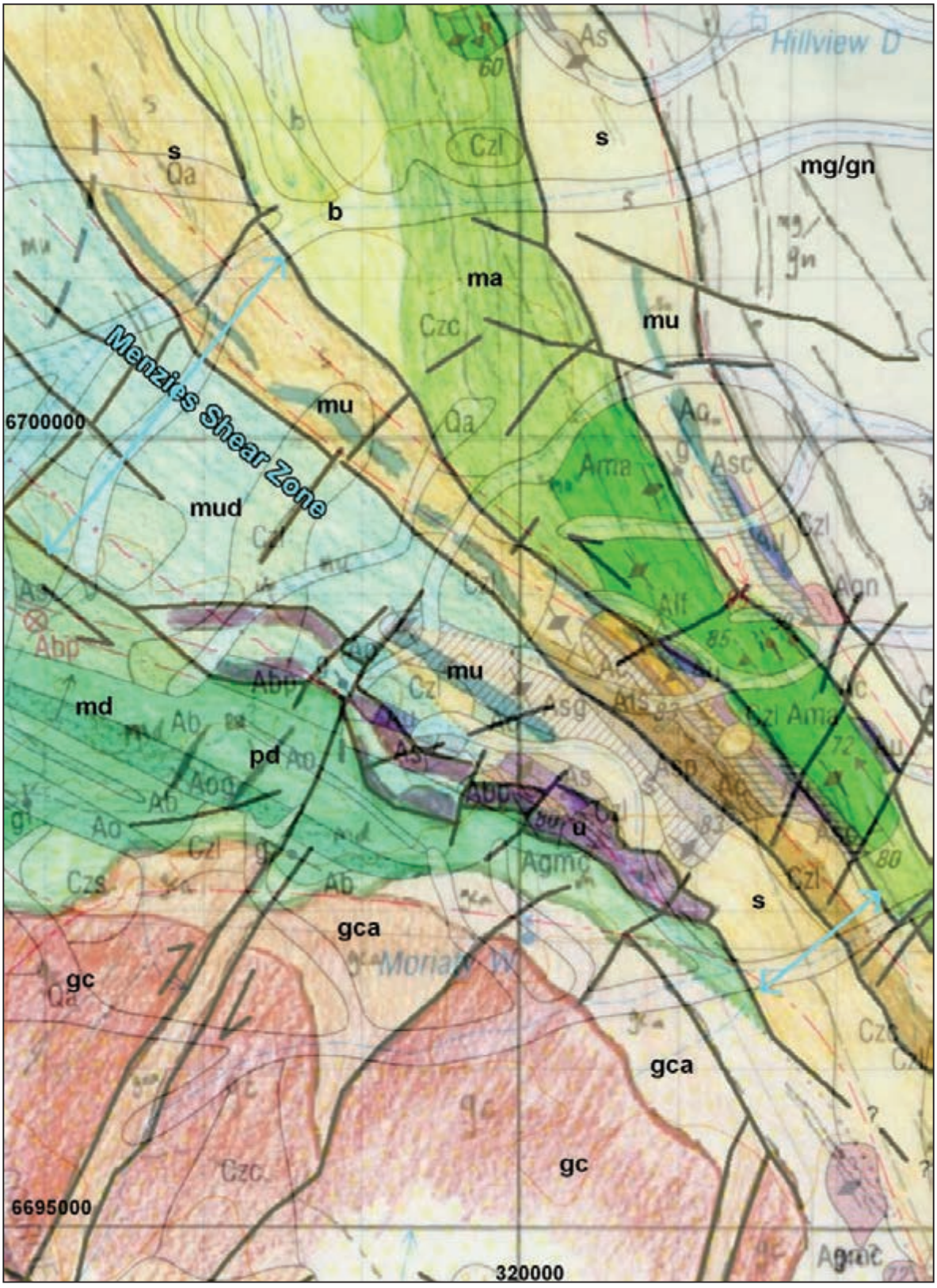

m	ultramafic	**ma**	amphibolitic mafic interval
mud	mafic interval with likely ultramafic and mafic rocks	**mg/gn**	mixed mafic & gneissic interval
mu	local mafic/ultramafic magnetic rock units	**gc**	Comet Vale Monzogranite
md	mafic unit containing basalt, dolerite and gabbro	**gca**	altered/marginal/non-magnetic variant of g
s	mixed sedimentary interval	**pd**	late mafic dyke
b	basaltic interval		

Figure 11.26b: Solid geology and structural interpretation before field mapping, superimposed on outcrop geology.

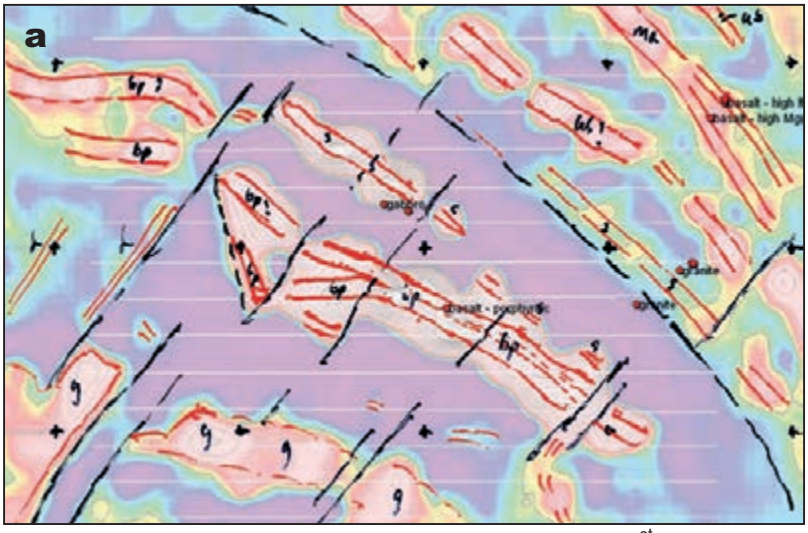

Detailed aeromagnetic observations, superimposed on RTP 1st VD image, line spacing is 200m

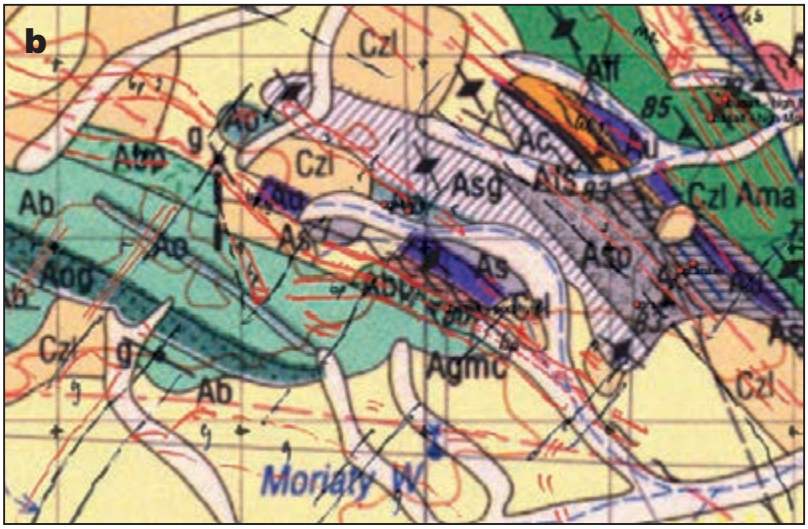

Detailed aeromagnetic observations, superimposed on outcrop geology, Grid is 1km

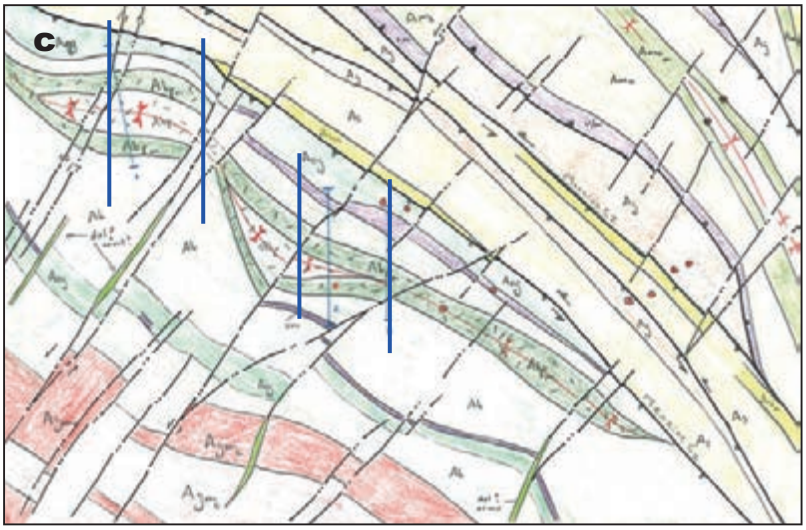

Revised, local geological interpretation. Red dots are the main field observatio points, blue lines are proposed bedrock geochemical drill traverses

Figure 11.27: Target Area TMW: detailed observations and local interpretation sketches, revised following field work and showing proposed geochemical drilling traverses.

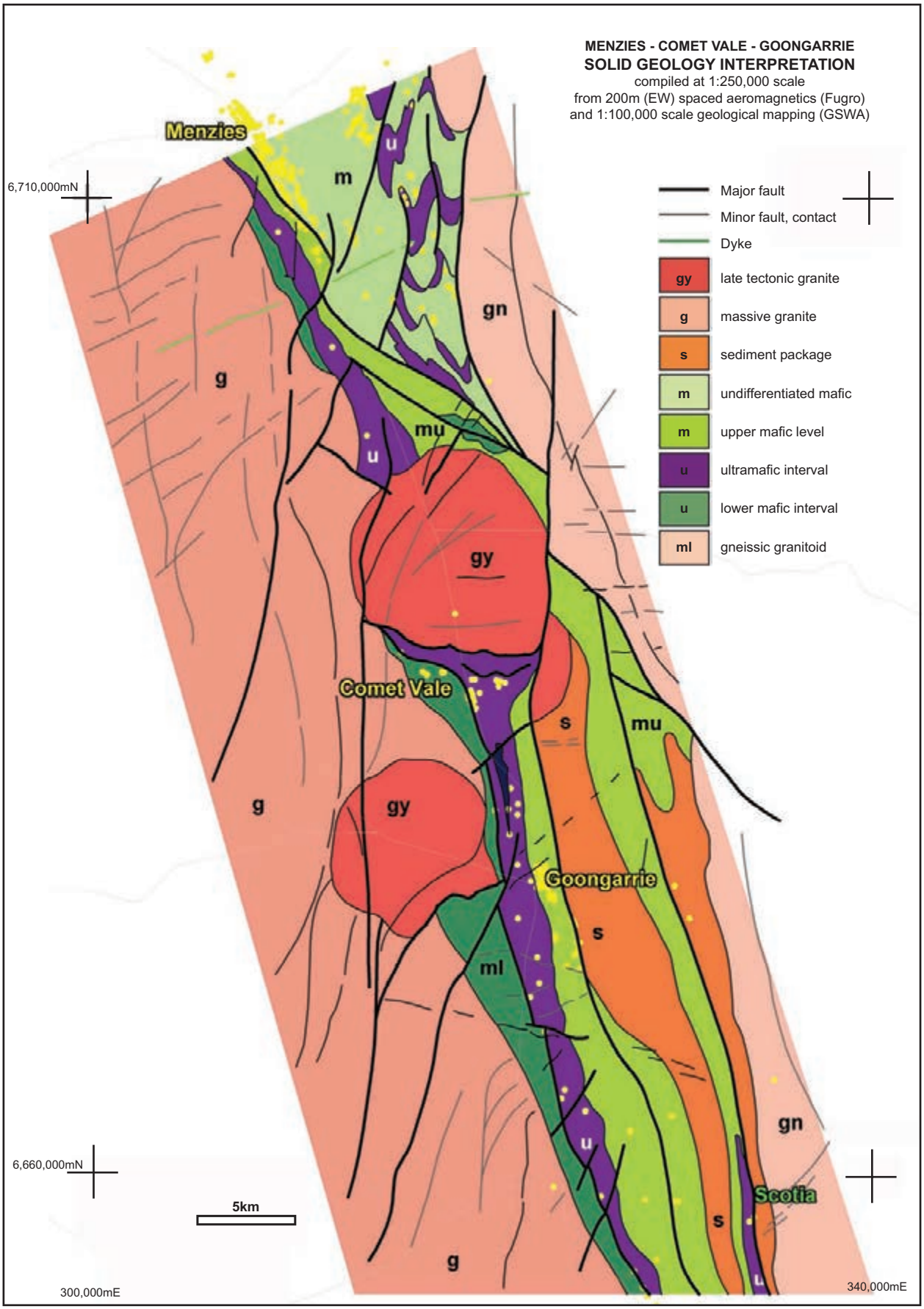

Figure 11.28: Revised 'final' solid geology interpretation map. This will be the working, district-scale project map. It will require review and likely revision after each main phase of field investigation.

12 Pine Creek–Golden Dyke case study – folded sedimentary sequence with mineralising granites

The following gold and base metal exploration study emphasises the value of aeromagnetic survey data in well exposed areas and illustrates the use of radiometric and aerial photography in forming a comprehensive interpretation. We will integrate semi-detailed (200 m spaced) aeromagnetic and radiometric data with good-quality government geological mapping and 1:50 000 scale aerial photography. The main area of interest is 7 × 10 km and it is prospective for gold, base metals and uranium. Both structure and stratigraphy play a role in controlling mineralisation in the area, and the aeromagnetic data provide key information on each of these attributes.

Our main task will be to prepare a revised geological interpretation at ~1:35 000 scale. This will integrate the aeromagnetic (and radiometric) data with geological mapping and emphasise both key structures and likely exploration target areas. An initial plan for on-ground exploration will be formulated and we will conduct an initial geological field reconnaissance to test our interpretation. We will then conclude the study by producing a revised field-tested solid geology map which will be the basis for the next phase of field exploration.

Our study/exploration area has been selected because it very closely resembles the nearby Cosmo-Howley district which contains two significant gold deposits. Triggs (1995) presents a study comparing the Golden Dyke Dome area to the Cosmo-Howley district.

12.1 REGIONAL SETTING

The Pine Creek Inlier is one of Australia's major mineral provinces. It hosts world-class uranium resources (Ranger, Koongarra, Jabiluka and Nabarlek) and is a significant gold producer with deposits such as Cosmo Howley, Enterprise and Mount Todd. It also hosts base metal deposits. The regional geology of the Inlier (formerly known as the Pine Creek Geosyncline) is summarised in Needham and De Ross (1990) and the metallogeny is discussed in Wyborn *et al.* (2001).

Localised domal structures cored with late Archaean granitoids expose the basement to the inlier, which is dominated by a Palaeoproterozoic sedimentary sequence deposited in a shallow intracontinental rift. This predominantly clastic sequence also contains some highly reactive rock units including carbonaceous shale, banded iron formation, evaporite and carbonate, as well as mafic and felsic volcanic rocks. The sequence was broadly to tightly folded, metamorphosed (to lower greenschist grade) and intruded by granites at around ~1875 Ma. A sequence of predominantly rift-related felsic volcanic rocks was extruded unconformably over the deformed metasediments at around 1860–1830 Ma.

There were two main episodes of granite intrusions in the Pine Creek Inlier. The first major event (1865–1850 Ma) was coeval with and continued after the major deformation. The next major event, which included

the Cullen Supersuite, occurred from ~1830–1810 Ma. Both events were associated with felsic volcanism. The Cullen Supersuite, which occurs widely in our study area, is a felsic fractionated I-(granodioritic) type suite and it has demonstrated links to gold, tin and tungsten occurrences.

Figure 12.1 summarises the regional geology and Figure 12.2 shows the regional aeromagnetic data. Because the area is quite well exposed, the aeromagnetic data adds little to the geological picture at this scale, but it does provide key evidence of the influence of the Cullen granite intrusions on the sedimentary sequence. Not only can we see contact aureoles around the unroofed granites, but the broader pattern of aeromagnetic highs also strongly suggests that the granite intrusive event has resulted in the creation of magnetic minerals in the sediments. Detailed studies (Stuart-Smith *et al*. 1993) have shown that the granites have significantly affected a large volume of the sedimentary sequence. In particular, mineralisation in the Cullen Mineral Field is largely coeval with the Cullen granite event and is inferred to be genetically related to it (Budd *et al*. 2002). The addition of magnetic minerals through the sequence appears to relate to conversion of pyrite to pyrrhotite in iron-rich, fine-grained sediments, although limited BIF horizons are known to occur.

Figure 12.1 shows the dominant NW structural grain and NE–SW-directed shortening. Deep-seated NW controlling structures have been proposed in Figure 12.3. These are based more on the changes in geometry of the sedimentary structures than surface expressions of major faults. The rotation evident in fold axes strongly suggests that these NW structures are dominantly sinistral strike-slip zones and there is ample hard evidence in outcrop to support this (Stuart-Smith *et al*. 1993). The other large-scale fault set in the region is oriented NE and has clear and consistent dextral strike-slip movement. These are very likely to be conjugate to the dominant NW sinistral faults.

The mapped and inferred fault zones often occur near narrow, linear and strongly magnetic anomalies caused by post-deformation mafic dykes that have intruded into pre-existing zones of weakness. There seems to be two or three generations of dykes. The youngest is reversely magnetised and trends approximately NW, consistent with the regional sinistral trans-tension. It overprints normally magnetised dykes that trend NW and NE, which may be a Reidel set or may represent two different generations. These dykes give some insight into the late deformation of the region as well as highlighting the earlier structural fabric.

Gold mineralisation dominates the Cullen Mineral Field and is our main focus in this study. Currently known gold deposits occur throughout the sedimentary sequence and do not favour any particular host lithotype or stratigraphic interval. Apart from the established temporal link between the Cullen granite event and gold mineralisation, and the inference of a genetic link (e.g. Wall 2005), there is a strong tendency for deposits to occur in or very close to the axes of anticlines.

12.2 OBJECTIVES AND DATA

For the purpose of this study, we have a pre-defined, relatively small area of interest and our exploration focus will not extend beyond this. We can proceed on the basis that neighbouring areas, while potentially interesting, will not be accessible to us for exploration. Hence our task is to make the most of our 70 km^2 defined area. Initial assessment of the area will use existing open file data and a starting exploration action plan will be formulated from this analysis. Our emphasis is on gold; this area has been selected because it has remarkable geological similarities to the Cosmo Howley gold-mining district lying 15 km to the west.

The first step in our assessment will be, as always, to develop a firm appreciation of the broad district containing our area of interest.

Geology

The region is well exposed, well mapped geologically and it has freely available, semi-detailed aeromagnetic and radiometric data. Government geological mapping covers our study area (and much of the Pine Creek Inlier) at 1:100 000 scale (Stuart-Smith and Needham 1979). The portion of this mapping pertinent to our study is presented in Figure 12.4a.

Airborne data

Airborne magnetic and radiometric data acquired privately in 1988 were subsequently purchased by the Northern Territory Geological Survey (NTGS) and are now incorporated into the freely available,

nation-wide airborne geophysical database. The survey was flown with 200 m spaced, E–W traverse lines at a mean terrain clearance of 60 m. Radiometic data were also acquired as part of this survey and are of interest for mapping and exploration. Owing to the limitations of this book, our description and analysis of the radiometric data are not extensive, but we will find that the radiometrics contributes several key features to the final interpretation. In most mapping and exploration applications we strongly recommend that all the potentially useful data be acquired and interpreted as part of the analysis.

12.3 DISTRICT-SCALE (~1:150 000) ANALYSIS

Following the guidelines presented in Section 6.6, we select an enclosing area of ~20 times our main area of interest to provide a broad-scale but semi-detailed view of the main geological features. This is presented at a scale of four to five times that planned for our project analysis (~1:150 000 and 1:35 000 respectively) to allow us to effectively and rapidly integrate the aeromagnetic data with the mapped geology.

After considering a range of filters and enhancements of the aeromagnetic data, we have selected a single composite RTP/RTP 1st VD image (Fig. 12.5) as being suitable for our brief, district-scale analysis.

The first step, as always, is to become familiar with the mapped geology and mineralisation in the area.

12.3.1 Geology

The sedimentary section (Fig. 12.4a, b) largely comprises subunits of the South Alligator Group and the Burrell Creek Formation, which is the main unit of the Finnis River Group and conformably overlies the South Alligator Group. Extensive, largely concordant sills of the Zamu Dolerite postdate the Finnis River Group but predate the deformation and metamorphism of the sequence. The Zamu Dolerite occurs widely in the basal South Alligator Group units (Koolpin Formation and Gerowie Tuff) but is largely absent in the overlying sedimentary units.

The sequence is tightly folded with predominantly NW- to N–S-trending fold axes and was metamorphosed to lower greenschist grade during the deformation. I-type granites intruded this sequence during and slightly after the deformation. These are quite well exposed throughout the district.

Late Palaeoproterozoic platform sediments and thin Cainozoic and Quaternary surficial deposits cover the above rocks and older (Mt Partridge Group) clastic sediments are occasionally exposed in anticlinal cores.

The major structures evident from the published map are the Burnside Granite and associated dome, the Howley Anticline, the Burrundie Dome and our area of interest, the Golden Dyke Dome. The Howley Anticline and the Golden Dyke Dome are strikingly similar structures. Both are broader at the southern end as they approach the McMinns Bluff Granite and both become narrow anticlines to the north. Both largely expose Koolpin Formation and Gerowie Tuff.

Cosmo Howley (~2 Moz) is the major gold deposit in the district, but smaller mines have been developed at Chinese Howley, Big Howley, Brocks Creek, Zapopan, Woolwonga and Golden Dyke (the last of which lies within our exploration area).

12.3.2 Observation layer

Compiling a basic observation layer (Fig. 12.6) gives valuable new information on both structure and stratigraphy. There are strong magnetic rock units which appear to map out fold form surfaces and these add much continuity to the structural picture. These units are seen throughout the sequence but are best developed in the basal part of the South Alligator Group (Koolpin Formation and perhaps Zamu Dolerite) and in the Burrell Creek Formation.

Offsets and terminations on these magnetic rock units highlight fault sets, most notably the NE-oriented, apparent dextral faults in the north of the Golden Dyke Dome.

The aeromagnetic images also add continuity and structural detail in the deformed contact zone of the Burnside Granite.

12.3.3 Solid geology interpretation

The patterns of regional folds evident in the published geology maps are greatly extended by the regional aeromagnetic image. Placing the observations on the mapped surface geology allows us to form a useful working solid geology sketch (Fig. 12.7, upper panel). The rotation of the fold axes north of the Golden Dyke Dome is a striking feature not clearly apparent from the geological mapping. We can extend this to a structural summary sketch (Fig. 12.7, lower panel) which expresses some key features affecting our main area of interest.

Most importantly, our project area straddles a major structural domain boundary between a broad anticlinorium and a complementary synclinorium. The anticlinorium includes the Burrundie and Golden Dyke Domes and exposes the basal parts of the South Alligator Group. The synclinorium is dominated by the younger Burrell Creek Formation. The structural domain boundary in part coincides with the Hayes Creek Fault.

The Howley Anticline abuts the regional synclinorium to the west, almost as a mirror image of the Golden Dyke Dome anticlinal structure.

Rotation of fold axes north of the Golden Dyke Dome is consistent with the previous observation of sinistral strike-slip movement on the regional, NW-trending Pine Creek Shear Zone, which is the likely master fault in the Howley-Golden Dyke district. A related observation is the perception of anticlockwise rotation of the Burnside Granite, which suggests it has been caught up in a sinistral shear couple.

The gold deposits in the district occur almost exclusively on anticlines and, as previously mentioned, the similarities between the major mining district on the Howley anticline and our Golden Dyke project area are profound. The McMinns Bluff Granite is interpreted at shallow depths beneath cover within 1 km of the southern exposure of the Howley anticline. This granite is part of the Cullen Supersuite which is temporally and possibly genetically linked to the development of gold mineralisation throughout the Pine Creek Inlier.

Our brief, district-scale study has placed the Golden Dyke project area in a clear structural and mineral exploration context and we now progress to a detailed integration of the geology and aeromagnetic data over this project area.

12.4 PROJECT-SCALE (~1:35 000) ANALYSIS

Our project area is ~7 × 10 km and the geological and aeromagnetic information available is the same as that used for the district-scale analysis, i.e. 1:100 000 scale government mapping and 200 m (EW) spaced aeromagnetic survey data. Our imagery and interpretation will be presented in this book at a scale of around 1:35 000. The work was compiled at 1:25 000 scale and has been reduced in size for publication.

12.4.1 Geological mapping

Close scrutiny of the geological map (Fig. 12.8) highlights the level of detail in the compilation. Not only is exposure very good, but the various stratigraphic units are usually readily differentiable from aerial photography or Google Earth® imagery (Fig. 12.9). The terrain is gently undulating and quite accessible. The recording of structural measurements (strike/dip/plunge) on the map gives an indication of the location of field traverses while the drawing of trend lines indicates areas where mapping has relied more on the aerial photography.

The Golden Dyke Dome is our main structure of interest. It has a core (and minor exposure) of the older Partridge Group (Wildman Sandstone), but largely exposes the Koolpin Formation and the semi-concordant sills of the Zamu Dolerite. The main dome axis is slightly refolded and plunges to the NNE and to the SE. There is a minor parasitic anticlinal structure on its western side. NE-trending faults are mapped in the SW part of the dome. Gold mineralisation occurs widely on the dome with the Golden Dyke mine being the only one of these with significant production (1980s, ~40 000 oz).

There is a very similar domal structure in the SE of our project area. It is dominated by Koolpin Formation exposure, with minor Zamu Dolerite, but has no recorded mineral occurrences. This area will be referred to as the South East Dome.

A N–S trending anticline exposing Koolpin Formation, Zamu Dolerite and Gerowie Tuff forms the eastern margin of our project area. There is a major and relatively open synclinal structure between the Golden Dyke and South East Domes. Named the Margaret Syncline, this structure exposes the Mt Bonnie Formation with a minor core of Burrell Creek Formation. Outcrop diminishes to the north and there is a (largely inferred) NE-trending dextral fault that offsets the contact between the Mt Bonnie Formation and the underlying Gerowie Tuff by ~1 km. The Margaret Syncline hosts one minor gold occurrence and two polymetallic deposits, Iron Blow and Mt Bonnie, the latter having been mined in recent times (Eupene and Nicholson 1990).

West of the Golden Dyke Dome and the associated tight anticline, which is the extension of the dome to the north, we cross the Hayes Creek Fault and encounter the Mt Bonnie Formation. The Mt Bonnie Formation traces out a NE-plunging syncline and begins to form an anticline at the western margin of our area. The core of the syncline is very poorly exposed but intermittent outcrops of Burrell Creek Formation suggest that the stratigraphic section is intact. While largely in fault contact with the Golden Dyke Dome this North West Syncline shows a high degree of both structural and stratigraphic continuity with the Golden Dyke Dome area. A small amount of dextral offset is seen on the Hayes Creek Fault from the geological mapping, but referring back to our earlier regional-scale studies we note that the Hayes Creek Fault is part of a large-scale zone of dextral wrenching.

12.4.2 Aeromagnetic imagery

We have selected four basic images for our interpretation, in much the same manner as in Chapter 11. As with the prospect-scale analysis in Chapter 11, we have chosen contour format for the TMI image (Fig. 12.11) and pixel format for the merged RTP/RTP 1st VD image (Fig. 12.14). The chosen high-pass filters are RTP 1st VD, presented as colour contours (Fig. 12.12) as in Chapter 11, and a merged RTP 1st VD/RTP 2nd VD (Fig. 12.13). We have also produced a stacked profile plot of TMI, which gives a clear indication of the amount of aeromagnetic data in the project area and a useful quick look at the range of aeromagnetic intensities (Fig. 12.10). The total number of line kilometres is quite small (~400) and when we consider the extensive outcrop and good-quality geological mapping in the project area we may not expect the aeromagnetic data to add much value.

12.4.3 Observation layer

Each of the three images makes a contribution to our aeromagnetic observations, but it is clear that the contoured RTP 1st VD portrays the most detail. We start working with this image, adopting the established scheme of coloured magnetic rock units and black lines for contacts and breaks. As we have substantial outcrop and a reasonable understanding of the structural context from our district-scale study, we can plan our observations according to the geology. Five geological subdomains are recognised from our assessment of the outcrop mapping:

a) the Golden Dyke Dome;
b) the South East Dome area;
c) the Margaret Syncline;
d) the North West Syncline;
e) the McMinns Bluff Granite.

Following our strategy to commence work in an area of relative simplicity as well as importance to our interpretation, it makes good sense to start with the Golden Dyke Dome. The above list is in a sequence that we will follow throughout our analysis of the prospect area. The rationale for this sequence is as follows:

a) the similarities of the South East Dome to the Golden Dyke Dome are such that any lessons learned in the latter dome will assist with our thinking on the South East Dome;

b) the Margaret Syncline lies between the above two structures and is less well exposed. Features observed in the dome areas may help us to interpret through these covered areas;
c) the North West Syncline is very poorly exposed and our interpretation here will rely on projections and extrapolations from the neighbouring areas;
d) the McMinns Bluff Granite appears to be in simple intrusive contact with the sediments and so is unlikely to present difficulties in the interpretation.

The completed observation layer is presented in Figures 12.15a and b and we sequentially show the observations in the above subdomains in Figures 12.16a and b.

Golden Dyke Dome

Figure 12.16a shows our observations on the Golden Dyke Dome superimposed on both the RTP 1st VD contours and the mapped surface geology. The strong, narrow, layer-parallel magnetic feature is an obvious first focus. Matching its trace to the geology, we find that it mostly coincides with the Koolpin Formation but is also very close to the contact with a dolerite sill and partly overlies the sill. Allowing for limitations in the accuracy of positioning for the geology (enlarged from 1:100 000 map) and the aeromagnetic data (200 m lines, 60 m height, 50 m grid cell size), it is feasible that the magnetic feature is due to the dolerite, particularly when the likely dip of the dolerite sill is considered. Knowing that dolerite is very commonly magnetic we may be tempted to regard it as the source of the magnetic feature, but reviewing the composition of the Koolpin Formation we find that it contains a subunit described as 'massive ironstone'. Looking further afield, we see that there are few (if any) significant magnetic features associated with the extensively exposed dolerite but there is one or more persistent and strong linear magnetic features overlying the Koolpin Formation. We conclude that the ironstone unit in the Koolpin Formation is almost certainly the cause of the major linear feature in the Golden Dyke Dome.

This magnetic feature is not continuous around the entire dome. In the SW part of the dome the magnetic pattern changes abruptly and becomes a broad and diffuse magnetic high with a central zone of slightly lower intensity (see Figs 12.13 and 12.14). The Koolpin Formation continues through this area but the strong linear magnetic feature does not. Although there are weak linear magnetic trends which follow the strike of the Koolpin Formation, we must infer either the absence of or a change to the ironstone unit. The broad magnetic high is the dominant feature and it overlies areas of exposed dolerite and Gerowie Tuff as well as (mainly) Koolpin Formation. Reviewing the three aeromagnetic images, we see some suggestion (especially in the TMI, Fig. 12.11) that the broad high has a deep source. However, the gradients on the other images clearly indicate the presence of near-surface (albeit weak) magnetic sources. Hence, the absence or modification of the magnetic ironstone unit remains unexplained. We now revisit the geological mapping and note that this part of the Golden Dyke Dome has several faults and fractures but such fractures are scarce in other parts of the dome. This part of the Golden Dyke Dome is also in contact with the McMinns Bluff granite. Before postulating a cause for the broad, diffuse magnetic high and the disappearance or change in the Koolpin ironstone unit, we consider the physical nature of the magnetic mineral distribution in the Golden Dyke Dome. In the north and east there is a single, narrow, linear, magnetic massive ironstone subunit of the Koolpin Formation. The rest of the Koolpin Formation and the Zamu Dolerite in this part of the dome have negligible magnetic mineral content. In the SW, however, we appear to have low concentrations of magnetic mineral dispersed throughout the Koolpin Formation, Gerowie Tuff and Zamu Dolerite. One plausible cause for this would be an alteration system channelled through the observed fractures and likely driven by the intrusion of the granite. This could explain dispersion of magnetic minerals from the Koolpin ironstone through the greater rock volume and consequent alteration and loss of magnetisation from the ironstone unit itself. An alternative explanation would be that the source of the broad magnetic high is a tongue of (magnetic) granite underlying the sediments, and this has demagnetised the Koolpin ironstone unit. Given the presence of numerous gold occurrences within this broad and diffuse magnetic zone, and the nature of the two proposed possible causes, we should regard this feature as anomalous and flag the need to include it in later targeting considerations. One final observation to

reiterate on this broad magnetic high is the coherent, elongate N–S zone of lower magnetic intensity near the centre of the high, giving it a doughnut-like appearance (Fig. 12.13). Several gold workings lie on the western margin of this zone.

Several linear breaks are observed on the Golden Dyke Dome, the most notable being a N-trending break which appears to offset the Koolpin ironstone unit. This occurs near a parasitic fold on the western side of the dome. The other observed breaks do not have obvious structural implications.

There are two localised magnetic sources which appear anomalous in the context of the mapped geology. The first is a 600 m long N–S-trending high which coincides with the axis of the dome and has gold workings nearby to the west. The other occurs in the far SE of the dome and appears as a folded segment of the Koolpin Formation ironstone subunit, but it is quite discordant with the mapped form surfaces in this area.

Before moving to the next area of observation we should reflect on the new geological information contributed by the aeromagnetic imagery on the Golden Dyke Dome. In a small area of excellent exposure and good-quality mapping we have noted at least five new features of interest which will need consideration when we compile our integrated solid geology interpretation.

South East Dome

The South East Dome area (Fig. 12.16b) is very similar in structure and stratigraphy to the Golden Dyke Dome. The Koolpin ironstone subunit occurs throughout the structure, but appears much more segmented and structurally complex. We observe two parallel, strong magnetic rock units in the SW part of this dome, one of which overlies inferred Gerowie Tuff. There is strong disruption to the ironstone subunit on the axis of the dome at its northern closure. This disruption is not evident in the geological mapping. A local, parasitic, anticlinal(?) closure is also observed in the far SE of this dome. NE of this fold closure, the ironstone subunit closely follows the mapped outcrop trends.

West and north of the dome a weak but persistent linear unit correlates with a mapped dolerite sill.

In the core of the dome, coincident with the axis, there is a narrow linear magnetic rock unit, partly but not wholly coincident with mapped Zamu Dolerite. Referring to Figures 12.13 and 12.14, we see that the intensity of this feature is similar to that of the localised magnetic rock unit on the axis of the Golden Dyke Dome.

Once again, we see that the integration of the aeromagnetic data has yielded information that is likely to refine the geological interpretation.

Margaret Syncline

The exposure in the Margaret Syncline is good in the southern part of our study area, but becomes scarce in the north. The aeromagnetic data show an assemblage of disjointed linear units with moderate to low magnetic intensity and two bullseye magnetic anomalies (see Figs 12.11 and 12.14). Referring to Figure 12.16c, we note the mapped NE-trending dextral fault which appears exposed near the Port Darwin Camp alluvial gold workings, but is mostly inferred through an area of alluvial cover. The apparent displacement on this fault, judging by the offset on the Gerowie Tuff–Mt Bonnie Formation contact, is of the order of 1 km.

If we now carefully consider the stratigraphic location of the many linear magnetic rock units, we see a remarkable consistency. These units are almost exclusively in the Mt Bonnie Formation and are mostly located between 250 m and 300 m from the stratigraphic contact with the Gerowie Tuff. This raises the possibility of a magnetic marker unit in the Mt Bonnie Formation. Referring to the geological legend in Figure 12.4b, we note that this formation contains thin beds of banded iron formation. The postulated magnetic marker is labelled ‘m’ on Figure 12.16c and, while relatively weak and lacking in continuity, it provides some very useful structural information. If the quite well-defined magnetic rock unit in the far NE of the study is indeed the Mt Bonnie BIF marker and we match this to its equivalent on the western side of the syncline, we see symmetry about the mapped syncline axis and a distance of ~1.2 km separating the near-surface expression of the units. If we then move to the south side of the NE-trending dextral fault, we see that the Mt Bonnie BIF marker is again present and again showing symmetry with the syncline axis. However, the BIF marker unit traces on opposite sides of the syncline are now separated by ~1.5 km. Given the mapped dips on

the limbs of the syncline(50–65°), this difference in width of the syncline across the fault suggests a component of vertical movement on the fault. We will revisit this idea when we get to the structural interpretation stage of our work.

We have not classified the bullseye magnetic anomalies as part of our BIF marker unit, despite the fact that they occur close to segments of the marker. Reviewing the field intensity information in the TMI (Fig. 12.11) and composite RTP image (Fig. 12.14), we see that the intensities are locally anomalous and the sources have limited strike. The geological map shows both of these magnetic features to have a close spatial association with mineral occurrences. The more northerly bullseye is located near a deposit named Iron Blow and the more southerly near a recently worked open pit mine called Mt Bonnie. We suspect that the magnetic anomalies are linked in some way to the deposits, but the information that we have does not convince us that they are coincident with the mineralisation, so we will flag this for further investigation later in our interpretive work.

North West Syncline

A narrow strip of Mt Bonnie Formation is exposed west of the Hayes Creek Fault and Figure 12.16d shows that the proposed Mt Bonnie BIF marker is present and highly continuous in this area. The synclinal closure in the southern part of this area is projected to plunge to the NE and sporadic exposure of Burrell Creek Formation reinforces this interpretation. Within the areas of inferred Burrell Creek Formation there is a complex pattern of relatively continuous linear magnetic rock units. Two reasonably convincing fold closures that match the southerly synclinal closure observed in the Mt Bonnie Formation are evident and there appears to be more than one marker unit within the complex area. No simple fold interpretation is apparent and the absence of outcrop forces us to be cautious in inferring too much continuity in our observations of the magnetic rock units. In Figure 12.16d we have recorded the stronger and weaker magnetic rock units, shown closure on folded units only where it is unambiguous and marked linear breaks only where they are clearly observable. We anticipate that our solid geology and structural interpretation in this part of the study area will involve a degree of educated guesswork. We expect that the lessons learned from compiling the better-defined areas to the east will assist us in this task.

Additional observations

Additional data over our study area that are not reproduced in this book include an earlier generation of geological mapping and detailed aerial photography. We have recorded some critical (including structural) observations from each of these datasets as well as mineral occurrence locations and key structural observations from the published mapping to enhance our observation layer. Significant drainage patterns have also been traced to assist in registration of the earlier mapping and the aerial photos, because these were not accurately rectified or geo-registered. We see from some discrepancies in the match between our observation layer and the published geological map that the degree of positioning consistency between the aeromagnetic data and the other datasets is not much better than ±100 m. This is primarily due to the manual rectification of the published 1:100 000 scale geological map (published in 1987).

12.4.4 Radiometric data

We have so far focused firmly on analysis of the aeromagnetic data because of the wide range of new geological information it provides. We have acknowledged in Chapter 7 that most aeromagnetic surveys also record gamma ray spectrometer data (radiometrics) and that these additional data can make a significant contribution to our final integrated interpretation. The abundant exposure in the Golden Dyke area makes the use of the radiometrics a must, and we take this opportunity to digress and expand on the description of the method in Section 7.2.2.

Outline of the data and processing method

Four channels of radiometric data are derived from the recording of counts of gamma rays emanating (mainly) from the top few centimetres of the Earth's surface. Each of these channels includes a range of

gamma ray energies (see Hansen 1980) and three of the channels relate to the specific daughter products of potassium (K), thorium (Th) and uranium (U). The fourth channel records counts over a broad energy interval and is called the total count channel. Each channel is compiled in line and grid format, in much the same way as aeromagnetic data, but the processing is somewhat different. Individual radio-element grids are imaged to show extreme values (usually a linear stretch) and subtle changes in concentrations (non-linear, equalised stretch). Most commonly, the three elemental channels are combined into composite ternary images. These use the red gun in the image display to portray K variations, the green gun to show Th variations and the blue gun to show U variations. The combined ternary images are an indication of the relative concentrations of the three radio-elements. Where all three are abundant, the ternary image will show brightly coloured to white tones, where all are low, dark to black tones and where there is a mixture of relative concentrations, the colour and brightness in the ternary image will reflect this.

Golden Dyke radiometric data

The airborne survey covering our project area included standard recording and processing of radiometric data. We will not present the entire dataset, but will focus on the images that provide key new information for our interpretation.

The ternary image (Fig. 12.17a) shows several clear subdivisions but, as expected, these do not have distinct boundaries – the image is fuzzy. We note the similarities between the radiometric patterns and the geology, and we sense that we could spend time delineating the colour/intensity variations and arrive at some form of surface lithological subdivision. Since the area is well exposed and is relatively well mapped we should first compare this mapping with the radiometrics. Figure 12.17b shows the mapped boundaries superimposed on the ternary image. We observe the following.

a) The McMinns Bluff Granite shows a bright, pink-toned pattern in the image, indicating moderate enrichment in radio-elements, with slight enhancement in K. This is consistent with its Adamellite composition.
b) The Zamu Dolerite areas are predominantly low in all radio-elements. This is expected from mafic rocks in general.
c) The Burrell Creek Formation shows moderate intensity with pink hues, suggesting mild enrichment in K. This is consistent with its siltstone/shale composition.
d) The Mt Bonnie Formation and the Gerowie Tuff both show moderate–high intensity and cannot be readily differentiated in the radiometrics. Note the variation in the ternary image tones in the areas where these units outcrop. While there is a consistent general radio-element response, the variability is such that we would not expect to be able to classify stratigraphic units on the basis of a radio-element signature.
e) There is a distinct U-rich marker at the top of the Koolpin Formation which is broadly coincident with the narrow, strongly magnetic marker unit. This uranium- and iron-enriched horizon within the carbonaceous shale unit is potentially geochemically reactive and should be considered of interest, particularly for gold and uranium exploration. The remainder of the Koolpin Formation is more subdued and certainly not distinct.
f) The small exposure of Wildman siltstone in the centre of the Golden Dyke Dome shows moderate intensity with a slight K enhancement, consistent with its composition.
g) The strongest radio-element responses (white areas) lie on the west side of the Golden Dyke Dome and anticline. There is one anomalous spot high (arrowed) that lies on an inferred fault and should be flagged for field investigation.
h) Two cover types are present. Cz comprises colluvium and partly *in situ* weathered products of the bedrock. It shows a moderate intensity consistent with adjacent bedrock. Qa is transported alluvial cover and often shows a lower intensity than the adjacent bedrock in our study area. However, it would be unwise to use this as a generalisation because alluvial material derived directly from radio-element-enriched rocks would be expected to show high intensity. The drainages in the granite at the southern end of the area exemplify this.

Structures mapped largely from aerial photography are also well expressed in the ternary image.

The individual K and Th images do not add significantly to the commentary above, but the U image is of interest in light of the known uranium endowment of the Pine Creek Inlier and the suggestion of some U enrichment in the ternary image. Figure 12.18 shows the U enrichment in the upper Koolpin Formation and patchy areas of slightly elevated U in the overlying sedimentary intervals. The strongest response (arrowed) is approximately two to three times local background and this is not particularly unusual. Uranium anomalies identified in airborne surveys most commonly show intensities greater than five times background. The intensity range histogram shown in the inset in Figure 12.18 indicates that there are no extreme or truly anomalous uranium counts in the study area.

Notably, the area of highest U counts does not coincide with the (nearby) area of highest composite response (Fig. 12.17b).

We need to record the *significant* observations from the radiometric data. We could delineate the radioelement variations in some detail from the ternary and individual channel images, but as seen in Figure 12.17b, these variations relate almost exclusively to the previously mapped surface geological subdivisions. Hence, it makes more sense to focus on the radioelement features that *add new information* to the geological picture. Figure 12.19 illustrates these features:

a) the white polygon is the composite K–Th–U high;
b) the blue polygons are the strongest local U highs;
c) PskU indicates the areas of the upper Koolpin Formation enriched in U;
d) the yellow line is a possible revision of the Koolpin–Gerowie contact. This takes on some significance when we integrate our aeromagnetic observations with the geological mapping.

We can imagine that if good-quality geological mapping did not exist, the radiometric data would be invaluable in defining the variations in exposed bedrock lithology and the cover types. We could use this, plus MSS imagery such as ASTER, to form a surface geology interpretation that could then be the basis for field observation leading to completion of the geology map. In this case, however, we rapidly see that the radiometrics is largely confirming information that already exists and it would be unproductive to spend too much time on analysis of the radiometric imagery. This is not an uncommon situation, and our advice is to always pay attention to the interrelationships between available geology and the radiometrics, but not to get bogged down in the large volume of information in this multi-channel dataset. Most importantly, we should actively focus on the aspects of the data that add new and valuable information to our interpretation. In all cases, we should ensure that appropriate radiometric imagery is produced and closely scrutinised.

In the Golden Dyke case, we can conclude that the radiometrics adds excellent value to our interpretation by confirming aspects of the prior geological mapping and by identifying several unusual or anomalous features requiring further investigation.

12.4.5 Solid geology layer

We will now compile the solid geology using the same subdivisions and in the same order that we approached the observation layer. The legend that we form for the new solid geology map closely follows the published geological mapping, but adds the new features we have identified from the aeromagnetic and radiometric data (Fig. 12.20). We show and discuss the solid geology in Figures 12.21a–e – readers may also wish to refer to the complete map (Fig. 12.22) and the published geology map (Fig. 12.8) during this discussion.

Starting in the Golden Dyke Dome we trace the well exposed upper contact of the Koolpin Formation where it is conformable with the Gerowie Tuff. The massive ironstone subunit of the Koolpin Formation allows us to slightly refine the trace of this boundary, the most significant adjustment being the inference of a N–S fault and the associated adjustment of the Koolpin–Gerowie contact on the NW side of the dome (Fig. 12.21a). We can also define an uppermost subdivision of the Koolpin Formation using this ironstone marker and the U-enriched zone that lies between the marker and the Koolpin–Gerowie contact (sku).

We have added the discrete magnetic anomaly just east of the Davis Camp gold workings and the observed broad area of diffuse, elevated magnetic response. The coincidence of the discrete magnetic anomaly with the

anticlinal axis, plus its narrow linear nature, suggest it may be due to magnetic mineralisation which has migrated into or formed in the anticline axial plane. This magnetic anomaly certainly does not fit the pattern of stratigraphic magnetic marker units observed elsewhere in the study area. After considering the proximity of the granite contact, the greater frequency of fracturing and the nature of the magnetic mineral distribution, we infer that the diffuse magnetic zone is most likely due to alteration driven by the granite intrusion and the contemporaneous deformation and low-grade metamorphism.

The remainder of the revised solid geology on the Golden Dyke Dome is inherited directly from the mapping. The dolerite sills are depicted as much narrower in our revised interpretation than in the original mapping. This interpretation has been sourced from discussions with the geologists who conducted the original mapping. They noted that the sills were often apparent from aerial photos over a much wider area than their true surface exposure due to the resistant nature of the dolerite and the consequent spreading of dolerite rubble at surface. This highlights the value of interaction between the aeromagnetic interpreter and those who have done the field work needed to establish the geological framework. This interaction is often not possible, but it is always worth pursuing when the source of the geological mapping is potentially accessible.

Similar, new structural and potential alteration information is added by the integration of the aeromagnetic and radiometric data in the South East Dome area (Fig. 12.21b). In particular, the Koolpin ironstone subunit shows the northern closure of the dome to be structurally disrupted: the simplest interpretation here is to extend the mapped fault and the associated, small, parasitic syncline from the north through the axis of the dome. Another structural addition is the inference of a high-angle reverse fault on the south-west side of the dome. This elegantly explains the apparent repetition of the Koolpin ironstone subunit (see cross-section D-D′ in Fig. 12.24). Although the westerly segment of this magnetic marker appears to coincide with Gerowie Tuff, the degree of uncertainty in rectification and registration of the geological mapping gives us latitude to propose this interpretation.

As recorded in our observation layer, there is a discrete linear magnetic anomaly almost coincident with the axis of the dome. Although it correlates largely with mapped dolerite outcrop, it extends beyond the dolerite exposure and has a much higher intensity than any of the magnetic features associated with dolerite in the study area. In addition, the response is narrow, linear and symmetrical, suggesting a narrow, steeply dipping source, which counts against the magnetic anomaly being due to dolerite. The dolerite sill exposed at the core of the dome would likely have flat dips and, if we recall that many of the sills are quite thin, it is plausible that the source of the magnetic anomaly either underlies the sill at shallow depth, or is unmapped and cuts across the sill. Hence we interpret it as a similar feature to the Davis Camp anomaly on the Golden Dyke Dome.

The inferred BIF marker in the Mt Bonnie Formation allows us to add significant detail to the fault patterns and the stratigraphic contact locations in the Margaret Syncline, particularly in the extensive areas of alluvial cover in the north. We can amend the location and nature of the syncline axis and confirm our suspicion that the major NW dextral fault also has a component of vertical movement. A simple, graphical construction (Fig. 12.21d) suggests ~500 m of south block down movement in addition to around 1 km of dextral strike-slip movement. The bullseye magnetic anomalies are presented on our solid geology map; after closely scrutinising positioning on the Google Earth® image (Fig. 12.9) and dismissing the possibility that these features might be due to mine infrastructure, we conclude that they are directly associated with the mineralisation at Iron Blow and the Mt Bonnie mine. We record these as anomalous features on our solid geology layer and flag them for further research when we consider exploration targets.

In the poorly exposed North West Syncline area (Fig. 12.21e) we start by working with the Mt Bonnie BIF marker through the fringing strip of outcrop. There is a significant (~400 m) apparent dextral offset on the marker unit near the Sandy Creek alluvial gold workings and we note that this is consistent with the offset of the Koolpin ironstone subunit to the south and apparent dextral offset on magnetic rock units in the covered area to the north. This leads us to infer a N–S-trending fault complex extending from the Golden Dyke Dome, across the Hayes Creek Fault to the central part of the syncline area, which we infer to be occupied by the Burrell Creek Formation.

The fold patterns here are complex and the 200 m flight line spacing in the aeromagnetic survey makes them hard to resolve. Two likely fold limbs close to the south, consistent with the exposed synclinal closure in the Mt Bonnie Formation in the south-west of the study area. These are both almost certainly synclinal closures, indicating tighter folding within the Burrell Creek Formation than in the underlying stratigraphic units east of the Hayes Creek Fault. This form of disharmonic folding is not uncommon where there is a viscosity contrast between layers. The more sandy Burrell Creek Formation is more prone to buckling than the more silty/shaley layers underlying it.

As noted during our observation stage, there appear to be two magnetic rock units within the Burrell Creek Formation, one higher in intensity and more continuous than the weaker, less continuous parallel unit. We have highlighted the stronger unit as a stratigraphic marker and used this to separate the Burrell Creek Formation into a lower (fbl) and upper (fbu) unit. This assists us in visualising the structural features in the solid geology map. The final enhancement in the solid geology layer is to review the more subtle offsets and bends in the Mt Bonnie BIF marker and the Burrell Creek markers and infer a series of N–S to NNW faults with consistent apparent dextral displacement. A central group of these faults penetrates south to the Golden Dyke Dome while the others appear to splay from the general location of the Hayes Creek Fault.

12.4.6 Structural interpretation

We recall from our district-scale analysis that our study area includes a major structural domain boundary, broadly in the form of the Hayes Creek Fault (Fig. 12.7). We also note from Figure 12.7 that the fold patterns form NNW to N–S axes with a Z-vergent style kink from north to south. As recognised from mapping at the regional scale (Fig. 12.3), the sinistral Pine Creek Shear Zone is the master fault affecting the Golden Dyke Dome area even though it does not occur within our specific study area. The Hayes Creek Fault, which is the largest-scale structure in our study area, is mapped regionally as a dextral strike-slip fault and, although we see some evidence of this locally, there is no evidence of significant displacement across the mapped fault in outcrop mapping or in our solid geology interpretation. In the northern part of our study area the published geology map (Fig. 12.8) shows a discrete dextral fault with ~250 m of apparent dextral displacement, but in the southern part the inferred fault zone shows no evidence of movement and is more likely to be a zone of high strain, and perhaps bending without discrete detachment.

The orientation of the fold axes infers broadly E–W compression under the influence of the Pine Creek Shear Zone and the doming of folds, seen only near the granite margins, is likely due to buttressing by the earlier or contemporaneous granite intrusion. The fault patterns are highly consistent with the notion that the Pine Creek Shear Zone is the master fault affecting deformation in our study area. As illustrated in Figure 12.23, the Hayes Creek Fault fits the conjugate R′ orientation and the N–S–NNW faults fit the compressive, high-angle reverse fault direction with minor/secondary dextral movement being consistent with the X direction. The E- to ENE-trending faults show some dextral movement, but also vertical movement in response to the tensile stress caused by the regional NNW shear regime.

These observed structural and stratigraphic patterns can be interpreted as part of a single progressive deformation driven by the Pine Creek Shear Zone. We emphasise that this is put forward as our working hypothesis. It is the simplest interpretation that explains the bulk of our observations at both local and regional scales. The cross-sections shown in Figure 12.24 reinforce the solid geology and structural interpretations and provide a very useful third-dimensional perspective on our study area as we progress to the consideration of exploration targets.

12.4.7 Targets

The Mt Bonnie and Iron Blow polymetallic deposits have distinct associations with local magnetic anomalies, but positioning uncertainty in the published mapping causes some doubt as to the coincidence of magnetic rock units and mineralisation. Eupene and Nicholson (1990) describe the deposits and indicate that pyrrhotite is the dominant sulphide in the mineralised zone. As mentioned above, careful reference to the Google Earth® image indicates that the magnetic anomalies are indeed coincident with the mineralisation. Review of

prior exploration and mining indicates that both deposits have been soundly evaluated and, considering the very short strike length of both of the magnetic anomalies, we judge that they do not constitute suitable targets for our early exploration.

Major uranium deposits occur in the Pine Creek Inlier but none are known in the vicinity of our study area and most occur in a geological setting not present in our area. We have, however, noted one area of enhanced (three to four times background) uranium count intensity and we should investigate this further. Literature research on current exploration activity reveals that this area constitutes the Thunderball uranium prospect (Thundelarra Ltd 2011), so that uranium anomaly is explained. Other radiometric features are regarded as indicative of stratigraphic variations, and no further anomalies are present. Our original focus on the Golden Dyke Dome was driven by its close similarity to the Howley Anticline and the associated gold mineralisation and for simplicity we will concentrate our targeting effort on gold.

Recapping the key elements associated with gold in the Pine Creek Inlier, we find that significant deposits occur in all stratigraphic intervals, from the Koolpin Formation to the Burrell Creek Formation. All the named deposits in Figure 12.3 occur in anticlinal structures. The main gold mineralising event is broadly contemporaneous with the Cullen granite suite, which is the main intrusive event affecting our study area. We have also noted magnetic aureoles at the margins of the granites (Fig. 12.2) and might anticipate some association between mineralising processes and generation of magnetic minerals (e.g. Wall 2005). In addition to these locally observed factors, we will look for structural settings where fracturing and folding is likely to have facilitated flow and entrapment of mineralising fluids.

Our targets are described in Table 12.1 and illustrated in Figure 12.25. The target areas are between 0.5 and 2 km^2 in area and our ranking is, at this early stage, relatively crude and subjective. However, we now have a firm focus for our field exploration and, given the extensive exposure and good accessibility, we should initially plan to map and sample the target areas. On completion of this work and receipt of our sample analyses we would review our interpretation and our targets, then plan the next phase of more detailed field exploration.

12.4.8 Magnetic source depth estimation

As we plan our field investigations it is imperative to assess the surface environment of the key localities that need field observation. The Google Earth® imagery (Fig. 12.9) should allow us to gauge the likelihood of *in situ* outcrop, and the general 'map-ability' of local areas. Mapping in poorly exposed or covered areas will be unlikely to provide answers to questions raised in our interpretation. Where direct observation of magnetic rock units is desirable, we should always carry out depth estimates before trekking to the field. In Figure 12.26 we illustrate the use of the straight slope graphical method, that allows us to rapidly estimate depths with an uncertainty of around ±25%. We have done this on the east flank of the Golden Dyke Dome in order to determine the best locations to observe the inferred Koolpin ironstone marker unit. We note that there is a 600 m section of the marker that yields depths to top of 80–100 m below the aircraft. Given the nominal 60 m survey flying height and the uncertainty in our estimation method, this section has a reasonable chance of exposing the magnetic rock unit and will be our starting point for observation and identification of its source. Elsewhere the depths are greater, suggesting that marker does not exist at surface in a fresh, unweathered state.

We have highlighted the potential of the Davis Camp magnetic anomaly in our targeting discussion, and as this is of more direct exploration interest than the Koolpin ironstone marker it deserves closer attention in depth estimation. Figure 12.27 illustrates a basic modelling effort using simple geometric shapes. The modelling takes into account altitude and terrain variations and indicates that the Davis Camp anomaly (in this area) is unlikely to be seen in its unweathered state at the surface.

Despite the depths-to-top inferred, we can remain hopeful that the high degree of outcrop and the considerable age of the weathering surface may allow preservation of the weathered equivalents of the magnetic rock units we are seeking to identify in the field.

12.4.9 Field investigation

Our field work focused on the resolution of geological questions raised in our interpretation. Geochemical sampling and analysis, and the broader spectrum of exploration of the area, are topics beyond the scope of this book. Our integrated interpretation aims to provide the best possible geological platform for this exploration. The main questions raised by our interpretation to be addressed in our field work are as follows.

a) Is the strong magnetic unit apparently lying in the Koolpin Formation a marker horizon?
b) Is the magnetic unit in the Mt Bonnie Formation similarly a marker?
c) What is the source of the Davis Camp magnetic anomaly?
d) Is the Hayes Creek Fault a simple planar fault as depicted on the published geology map?
e) Does the N–S fault complex we have inferred on the western flank of the Golden Dyke Dome exist?
f) Does the ENE dextral/normal fault cutting the Margaret Syncline have the location and form inferred from our interpretation?
g) Is our proposition that the structures observed could be due to one progressive deformation consistent with field structural observations?

There are several further questions that could, and perhaps should, be addressed by field work. The above questions provided the main focus for the available time, constrained (as is often the case) by limitations of access. The narrative below is necessarily brief. Our purpose in this book is to convey the methodology of aeromagnetic interpretation, so our description of the field work concentrates on the process and results, rather than on too much detailed observations and geological implications.

General field environment

The area is hilly and lightly timbered, with occasional steep scree slopes and long grass masking exposures. Where exposure is accessible the amount of genuinely *in situ* outcrop is far less than anticipated from the Google Earth® image. Hill-creep, where large bodies of outcrop tilt downhill under the influence of gravity, is common. However, as anticipated from the published geology map, there is sufficient good-quality exposure to support confident mapping. The weathering environment limits the continuity of information and impacts adversely on our ability to clearly identify structure.

Koolpin Formation ironstone marker

As anticipated from the depth estimates, despite its continuity evident in the magnetics, this unit is hard to find in the field. Extensive dolerite rubble often obscures it and it appears to be commonly deeply weathered. The dolerite is essentially non-magnetic. Our observations concluded that it is likely to be a stratigraphic interval, possibly as little as 10 m thick, where magnetic mineral is enhanced, within a generally iron-rich, silty to shaley sediment. No fresh samples were found and the distinctive, weathered variants appear as massive, limonitic, gossanous ironstone. The measured magnetic susceptibilities of these weathered samples (0.002–0.006 SI) were ~1/10th of that anticipated from the modelling, reinforcing the notion that such surface measurements, particularly in deeply weathered environments, can be a poor representation of the bulk susceptibility of the magnetic rock unit.

Davis Camp magnetic anomaly

While our modelling made us pessimistic about observing the source of this feature in outcrop, we were successful in locating a subcropping quartz-ironstone breccia within the expected footprint of the feature. Measured magnetic susceptibilities (~0.005 SI) were again much lower than those expected from fresh rock, but they contrasted sharply with nearby siltstone exposures that consistently registered near zero values. Pyrite pits observed in the samples could be indicators of a weathered mineralised body and the brecciation may indicate a fault in the anticlinal hinge. We concluded that the source of the anomaly was not definitely demonstrated, but there were positive indications as to its possible association with mineralisation.

Table 12.1: Golden Dyke Area – exploration targets

Target no.	Description	Rationale	Ranking
T1	Interplay zone of Hayes Creek Fault (shear zone) with N–S fault/fold complex. N–S fault zone extending to core of Golden Dyke Dome. Some suggestion of magnetic mineral destruction (Fig. 12.12). Includes alluvial gold occurrences and radiometric anomalies.	Enhanced fracturing and likely dilation associated with the intersection of the Hayes Creek Fault and the 2nd order N–S faults provide both fluid path and trap sites for gold. The target zone taps the central part of the Golden Dyke Dome. The radiometric anomalies are odd but potentially interesting.	Very high
T2	Discrete magnetic anomaly coincident with anticline axis. Davis Camp gold workings very close to this anomaly.	Anticline axes host most known significant gold mines in the region. Granite intrusion linked to magnetic mineral creation and possibly gold mineralisation.	Very high
T3	Axis of anticline fold nose in Koolpin Formation. Includes one gold occurrence (Good Shepherd).	Closely analogous setting to Cosmo Howley mine.	High
T4	Interplay of Hayes Creek Fault with major ENE dextral/normal fault. N–S compressional faults also splay from Hayes Creek Fault here.	Major zone of accommodation of the movement on the ENE fault. Key zone of change from transpressive to transtensional structural environment; dilation and fluid entrapment likely.	High
T5	Very similar setting to T4, but both fault zones less well developed.	As for T4.	Moderate
T6	SW part of Golden Dyke Dome. Lies within the inferred alteration zone and includes the Golden Dyke gold occurrences, N–S and NE fault sets, and a coherent magnetic low which may indicate mag-destructive alteration.	Enhanced fracturing and evidence of granite-related alteration, plus proximity to both the granite and a local parasitic anticline provide many opportunities for gold fluid source, movement and entrapment.	Very high
T7	Anticline axis/nose in Koolpin Formation near granite contact. Includes a small discrete and discordant magnetic anomaly.	Anticline axes host most known significant gold mines in the region. Granite intrusion linked to mineralisation and magnetic mineral creation. Another setting simialr to Cosmo Howley.	High
T8	Complex anticlinal closure with an axial planar fault.	Sructural and stratigraphic setting similar to Cosmo Howley, with enhanced fluid flow likely due to axial planar fault.	High
T9	Small discrete magnetic anomaly on anticline axis and coincident with the inferred axial planar fault (see T8).	Very similar to T2. Magnetic anomaly correlates with Zamu Dolerite outcrop but dolerite sill may be thin and should be flat-lying, so could be covering the magnetic anomaly source.	Moderate
T10	Anticline axis/closure in Burrell Creek Formation.	General Pine Creek region anticline model. Several significant gold deposits in the region hosted in Burrell Creek Formation.	Moderate
T11	Anticline axis/closure in Burrell Creek Formation.	General Pine Creek region anticline model. Several significant gold deposits in the region hosted in Burrell Creek Formation.	Moderate

Hayes Creek Fault

A quite exhaustive search for evidence of faulting in and around the inferred trace of this fault west of the Golden Dyke Dome revealed only a minor fault-parallel quartz blow. This work was supported by a close analysis of detailed aerial photography and it was concluded that the existence of a discrete fault in this location was unlikely.

N–S faults on the western side of the Golden Dyke Dome

Structural measurements to the north and south of the line of the Hayes Creek Fault, combined with detailed scrutiny of aerial photography, give firm support to the interpretation of this N–S fault complex.

ENE fault cutting the Margaret Syncline

The revised location of this fault based on the aeromagnetic interpretation was in conflict with the previous geological mapping in an area of good outcrop. Our new field observations on the continuity of the Mt Bonnie ironstone marker confirmed that the revised location is correct.

One progressive deformation?

We observed abundant local field evidence to support the inference (e.g. Stuart-Smith *et al*. 1993) of an F2 folding event comprising broadly N–S directed compression. Hence our attempt to simplify the deformation history to one progressive event is inappropriate, and this is reflected in our final, revised interpretation map.

12.4.10 'Final' presentation

The final task before we become consumed with the rigours and demands of field exploration is to compile our revised interpretation into a presentable, readily usable and editable form. Although we have done all the hard work of integrating the aeromagnetic data with mapped geology and produced a very useful new map, our hand-drawn interpretive work has a temporary draft appearance, which may discourage those who are likely to support our exploration endeavours. While we, as the interpreters, recognise that our work is dynamic and will require review and likely amendment after each new phase of information gathering (e.g. drilling), the professional presentation of our work plays an important part in portraying confidence and enthusiasm in our interpretation. Figure 12.28 shows the final (digital) product for this phase of our interpretation on the Golden Dyke area.

12.5 SUMMARY FOR THE PINE CREEK–GOLDEN DYKE STUDY

It is instructive to compare our revised interpretation (Fig. 12.28) to the original outcrop mapping (Fig. 12.8), and to recall that we did not anticipate that the small amount of aeromagnetic and radiometric data (400 line km) would greatly modify the existing good-quality mapping. While this proved to be largely correct, we can now reflect on the valuable modifications and enhancements that our interpretive work have yielded. We list these below.

Golden Dyke Dome

a) Identification of the Koolpin ironstone subunit, likely to be a stratigraphic marker.
b) Associated with this marker, there is an uppermost interval in the Koolpin Formation that is enriched in uranium.
c) Recognition of a likely alteration zone in the south-west part of the dome.
d) Recognition of a likely significant N–S fault system on the west side of the dome.
e) Identification of a high-priority target magnetic anomaly near Davis Camp.

South East Dome

a) Recognition of strong structural complexity in the north of the dome.
b) Recognition of a likely high-angle reverse fault on the west side of the dome.
c) Identification of a possible target magnetic anomaly underlying a thin dolerite sill in the core of the dome.

Margaret Syncline

a) Identification of a likely magnetic BIF stratigraphic marker in the Mt Bonnie Formation.
b) Addition of structural detail (especially faults) in areas of alluvial cover.
c) Identification of magnetic anomalies associated with Iron Blow and Mt Bonnie mineralisation.

North West Syncline

a) Mapping of fold and fault patterns through this extensively covered area.

Structure

a) Enhancement of the pre-existing structural interpretation by recognition of previously unseen fault and fold patterns.
b) Proposition of a simplified structural interpretation that proved to be incorrect, but facilitated useful discussion on the evolution of the study area.

Exploration targets

a) Identification of 11 initial target areas, most of which could not have been identified without the aeromagnetic data.

In conclusion, we have succeeded in integrating two moderately detailed datasets to produce a working interpretation that will provide our initial field exploration with a high degree of focus, compared to that which may have arisen in the absence of the aeromagnetic data. This study area is not unusual in the way that the aeromagnetic data provide critical new information in a well exposed and well mapped area. Interpreters should be aware that the presence of abundant geological control gives us more opportunity to understand the aeromagnetic (and radiometric) data and to focus on features that are genuinely anomalous and potentially important in achieving our exploration or mapping goals.

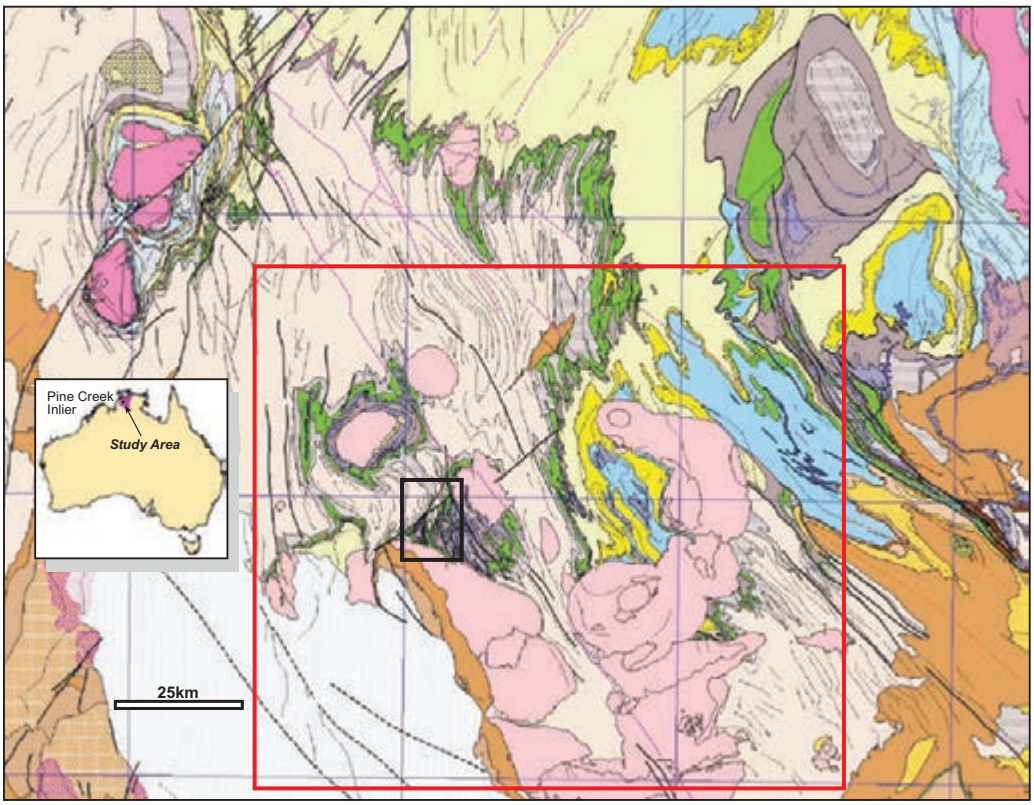

Figure 12.1: Southern Pine Creek Inlier – published solid geology (from NT Geological Survey digital database). See legend in Figure 12.4b, black rectangle indicates main study area, red outline shows the Cullen Mineral Field.

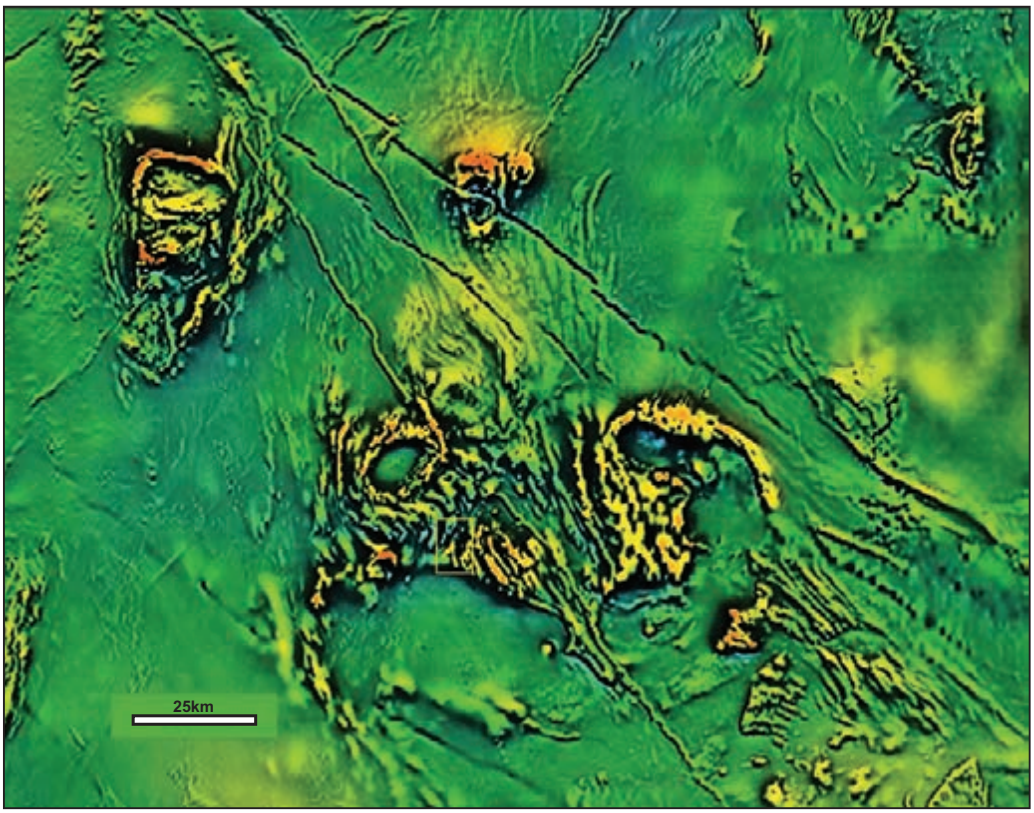

Figure 12.2: Composite TMI/1st VD aeromagnetic image covering the same area as Figure 12.1. High intensities in red are around 1000 nT above background. Image derived from Geoscience Australia national grid.

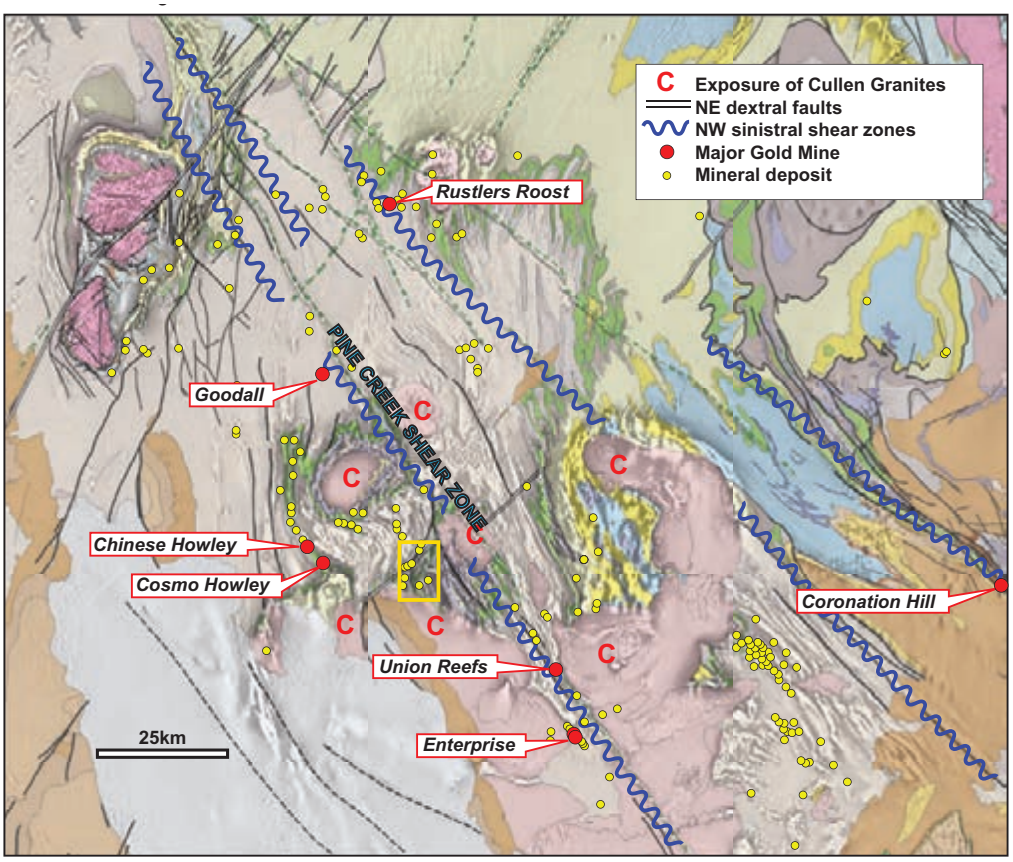

Figure 12.3: Merged geology/TMI images showing major gold deposits and key structures. Images derived from Geoscience Australia national grid.

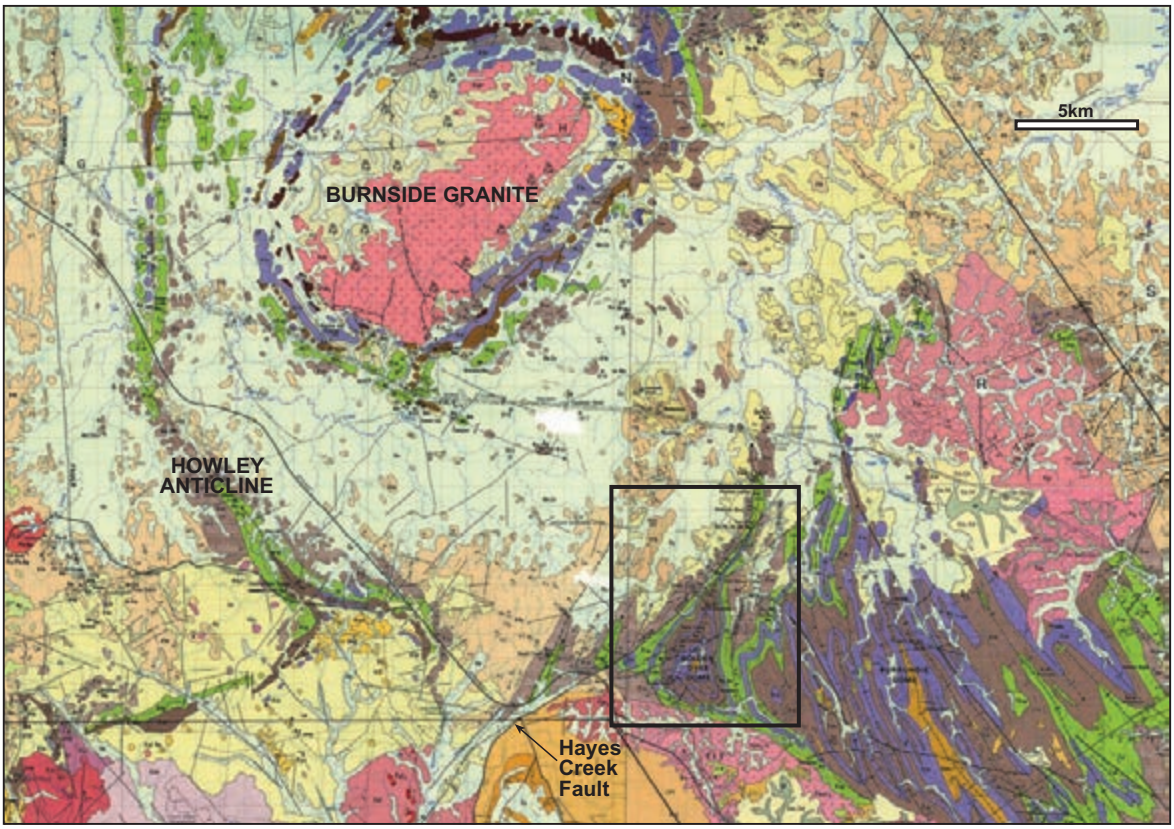

Figure 12.4a: Howley-Golden Dyke district geology (1:100 000 scale mapping by BMR in the 1970s (Stuart-Smith and Needham 1979).

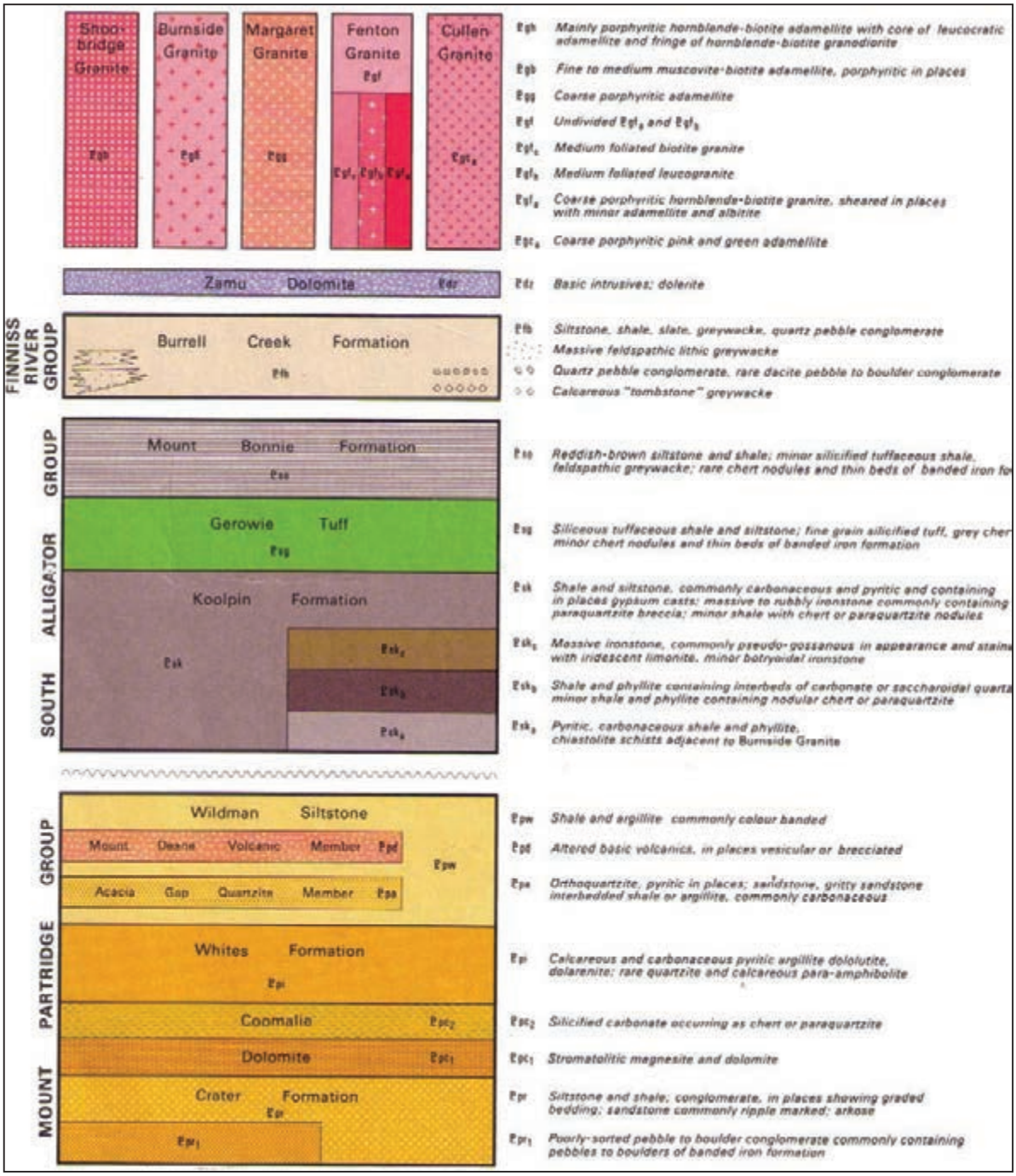

Figure 12.4b: District geology legend (from Batchelor 1:100 000 sheet).

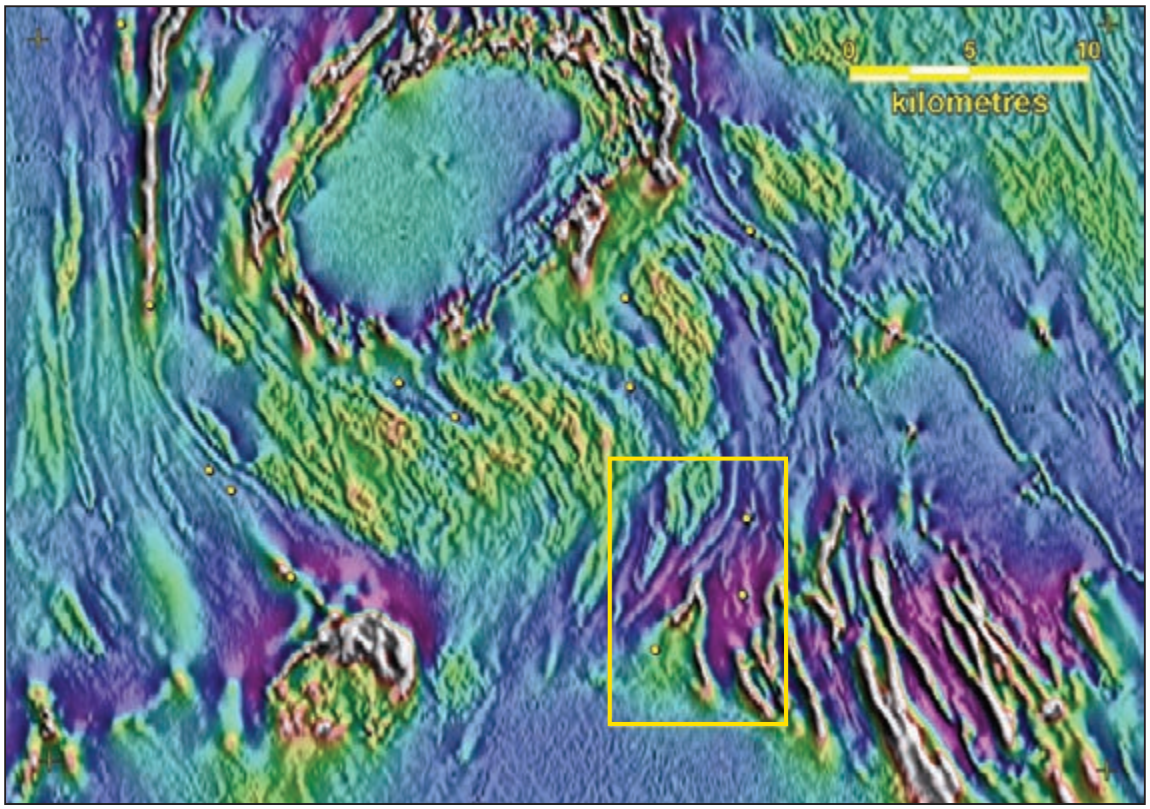

Figure 12.5: Composite RTP/1st VD aeromagnetic image, Howley-Golden Dyke district (identical area to that in Fig. 12.4a). Data from NT Geological Survey and Geoscience Australia.

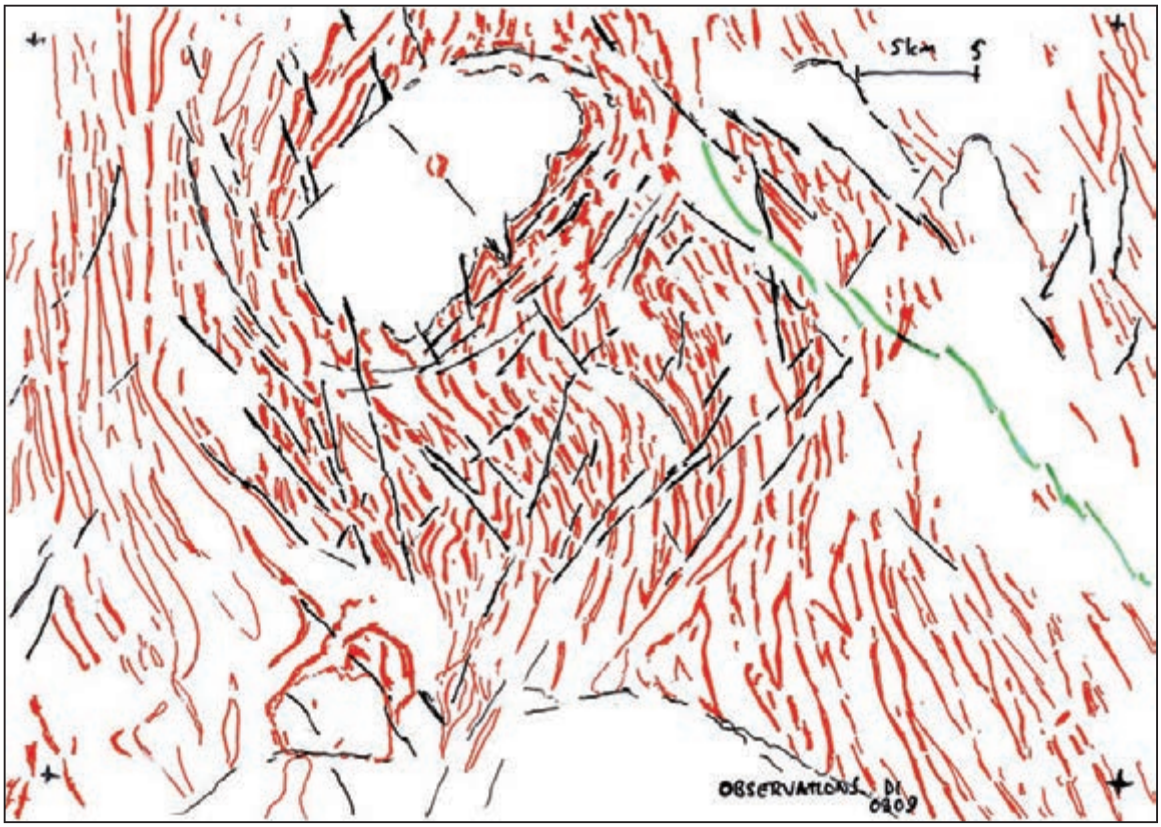

Figure 12.6: Observation layer, Howley-Golden Dyke district. The red lines represent (probably stratigraphic) magnetic rock units, green lines are post-deformation mafic dykes and black lines are faults, fractures and contacts.

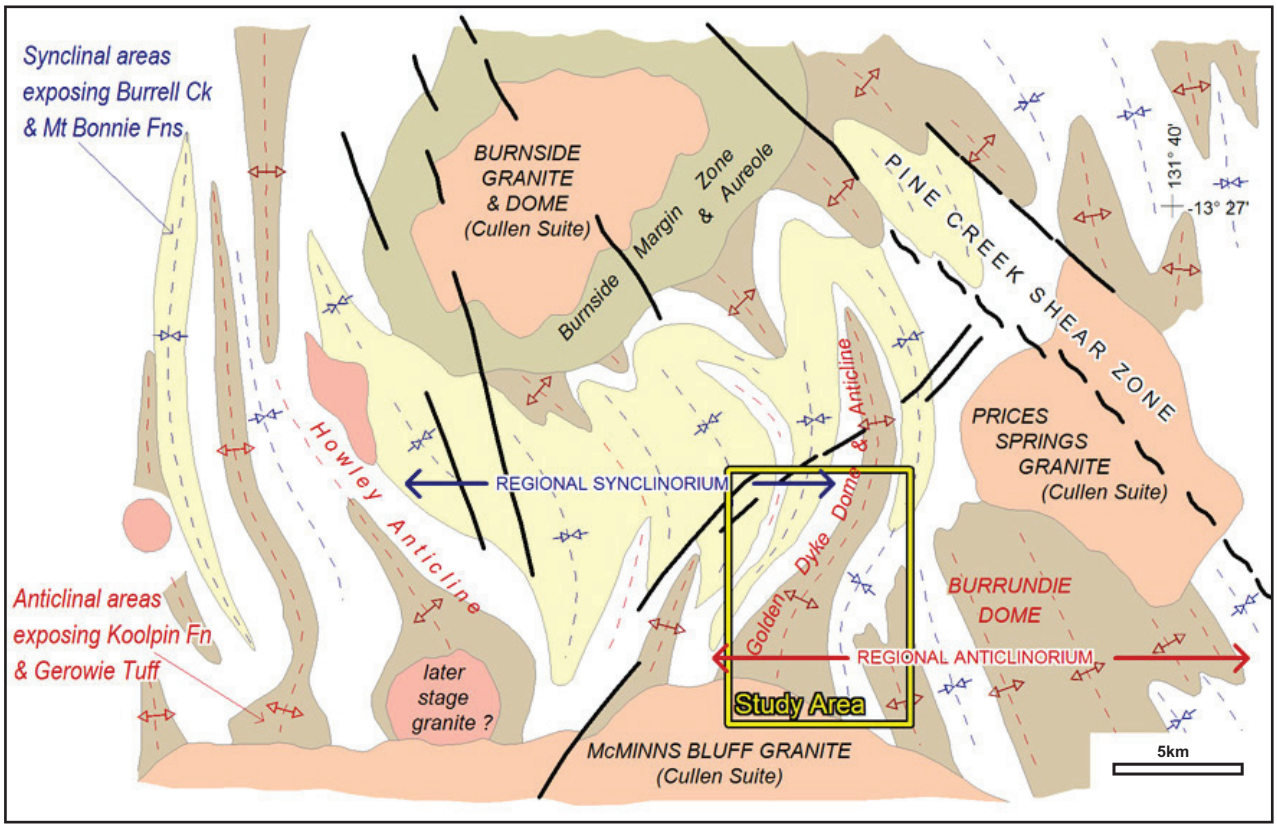

Regional Tectonic Sketch

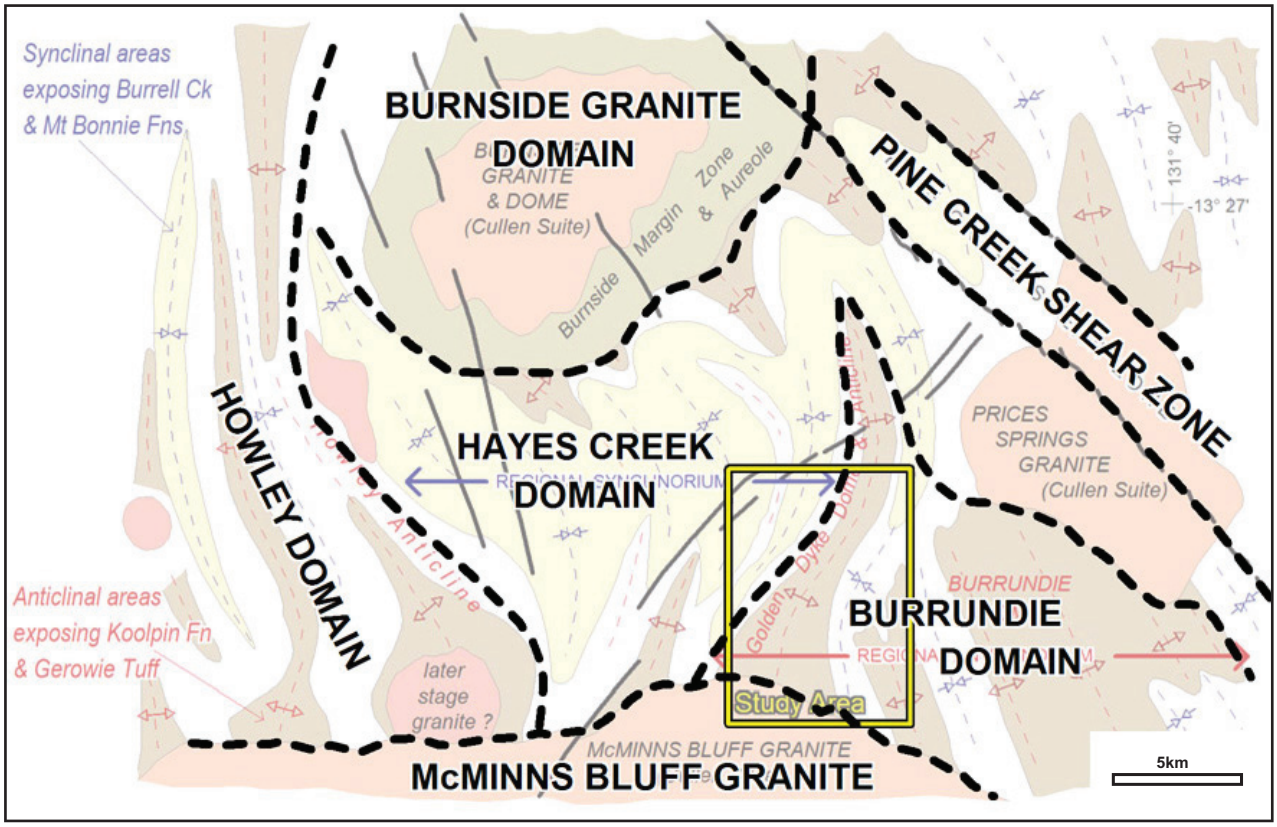

Broad Structural Domains

Figure 12.7: Howley-Golden Dyke district overview.

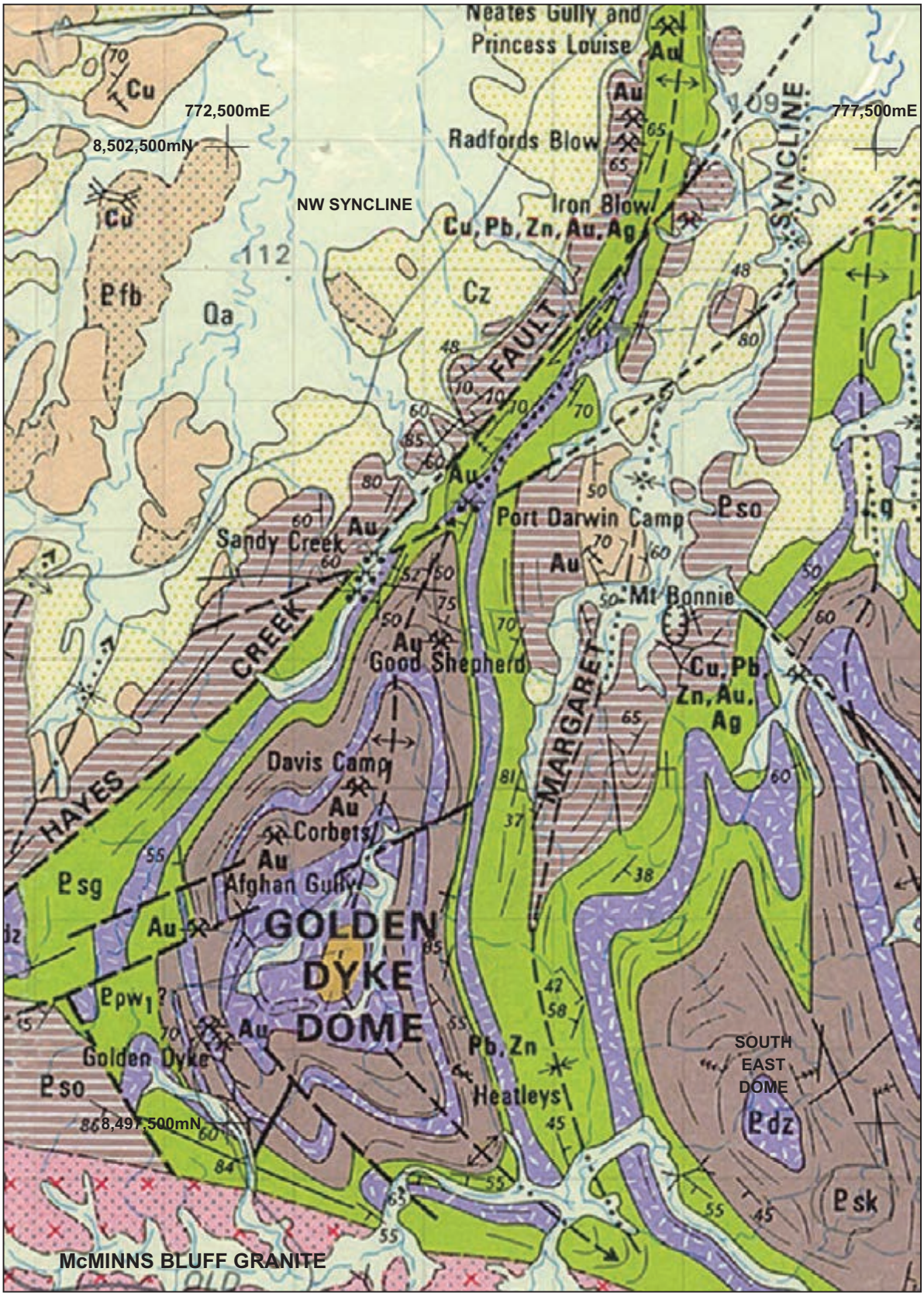

Figure 12.8: Golden Dyke area – geology (part of published Pine Creek 1:100 000 mapsheet; Stuart-Smith and Needham 1979) The faint grid lines are 1 km apart and are an older coordinate system (AGD66, AMG zone 52). The four labelled registration points match the aeromagnetic imagery and the GoogleEarth image and these are all coordinated in the AGD84 (zone52) system.

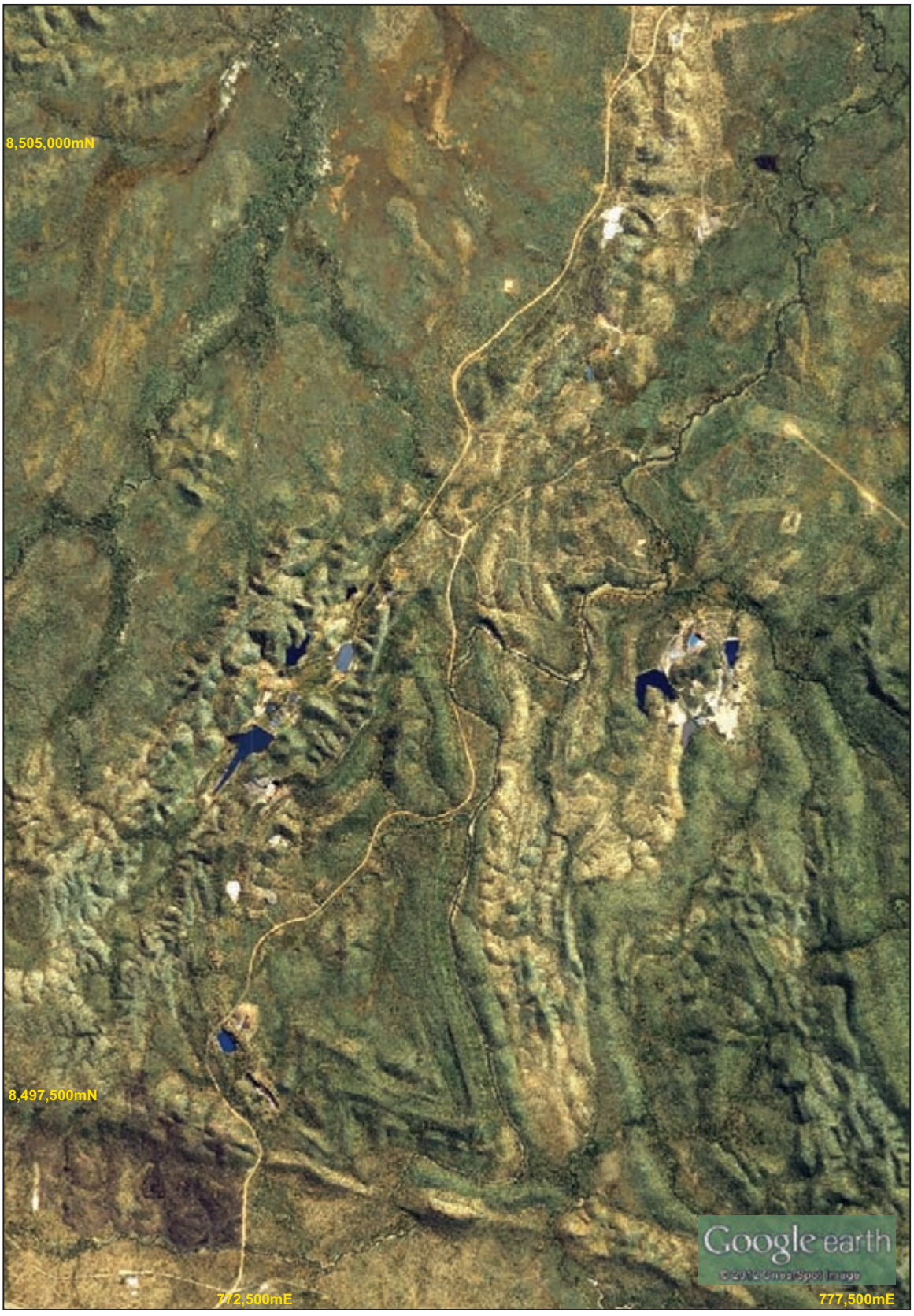

Figure 12.9: GoogleEarth Image of the Golden Dyke Study area. Coordinates in the AGD84, AMG zone 52 system.

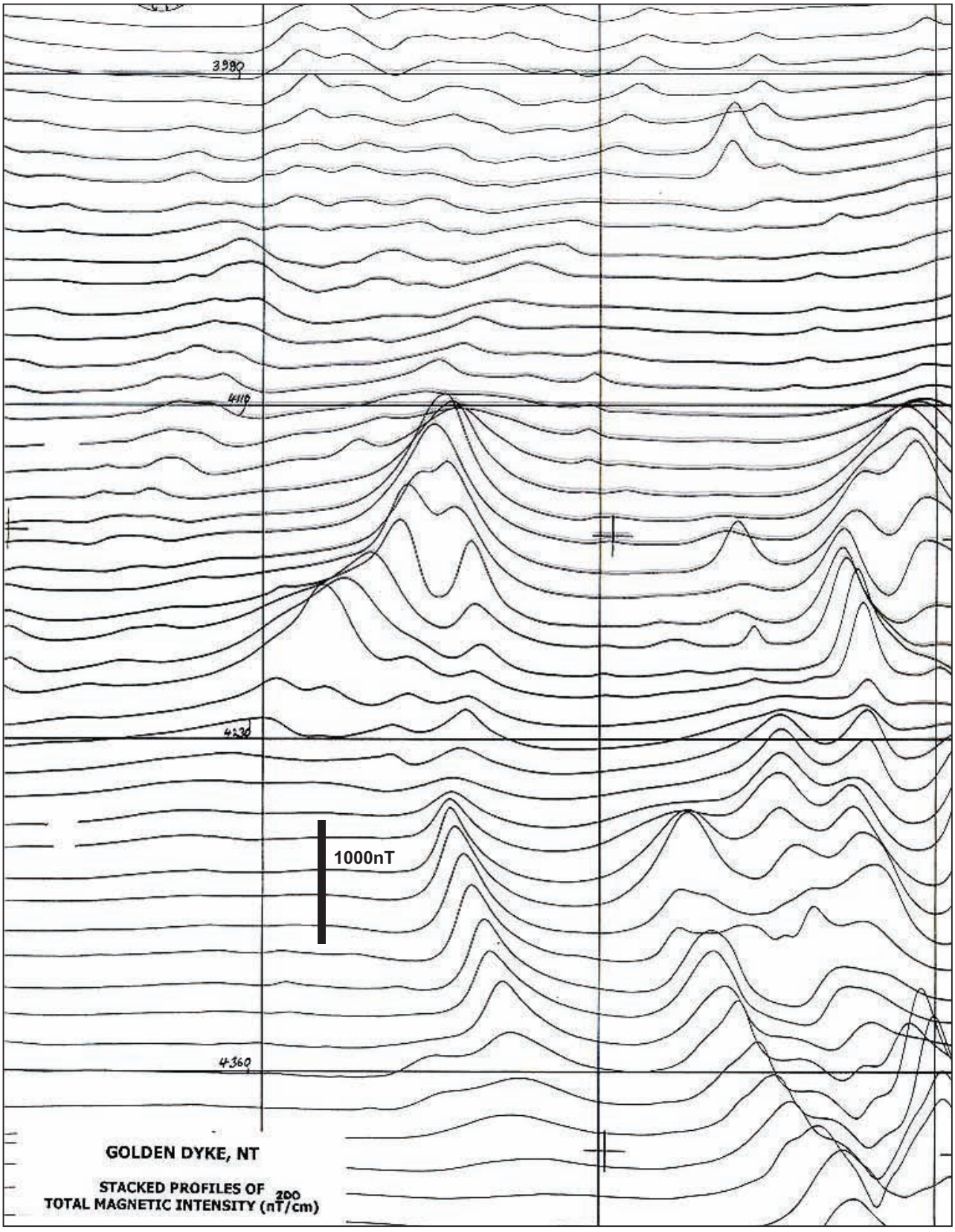

Figure 12.10: TMI profiles. Grid markers match Figure 12.9. Open file data from NT Geological Survey and Geoscience Australia, same data as in Figure 12.5.

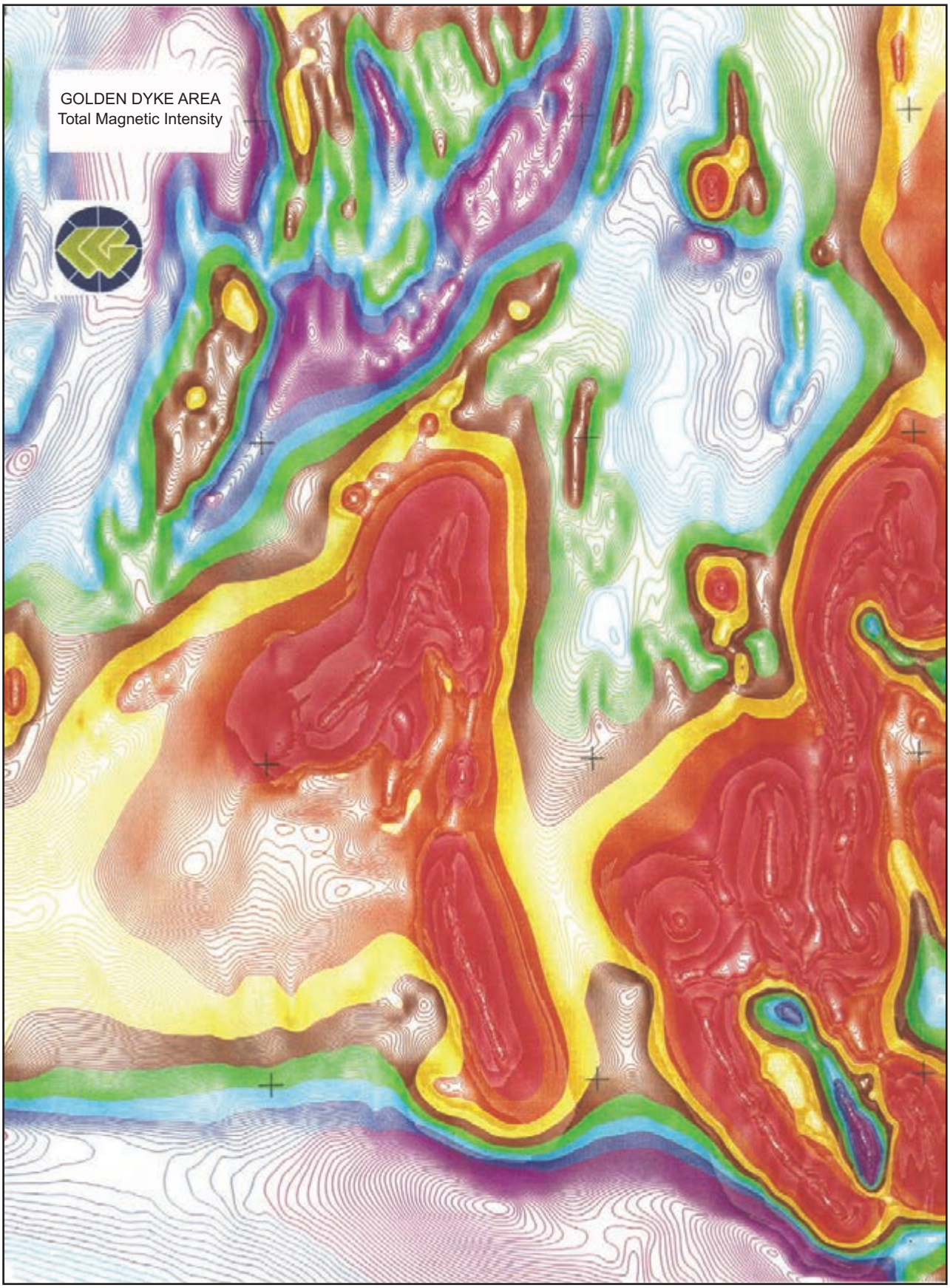

Figure 12.11: TMI contours (contour interval 2 nT). Grid markers match Figure 12.9. Data from NT Geological Survey and Geoscience Australia. Imaging by World Geoscience (now Fugro Airborne Surveys).

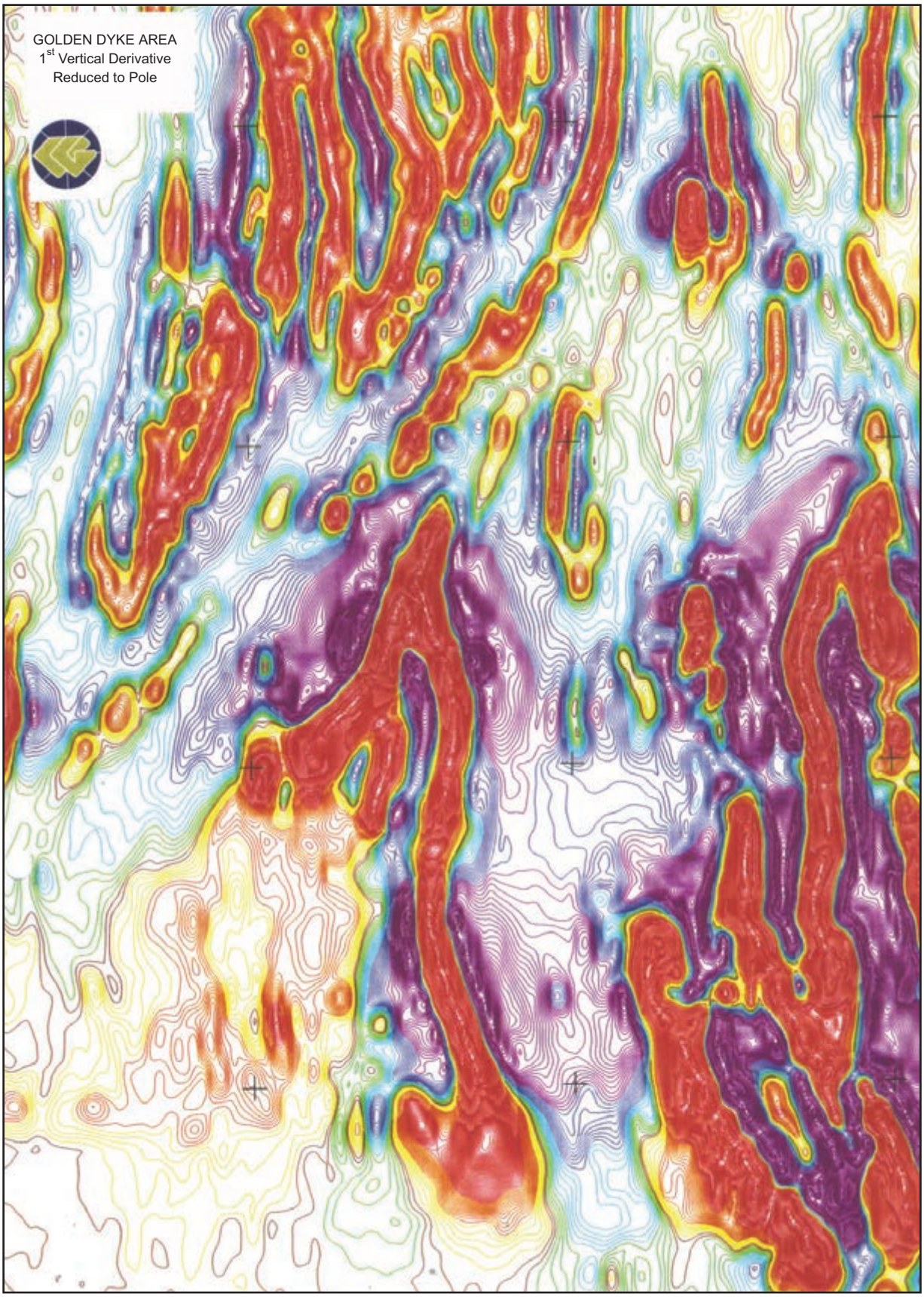

Figure 12.12: RTP 1st VD contours. Data from NT Geological Survey/Geoscience Australia, Imaging by World Geoscience (now Fugro Airborne Surveys). Grid markers match Figure 12.9.

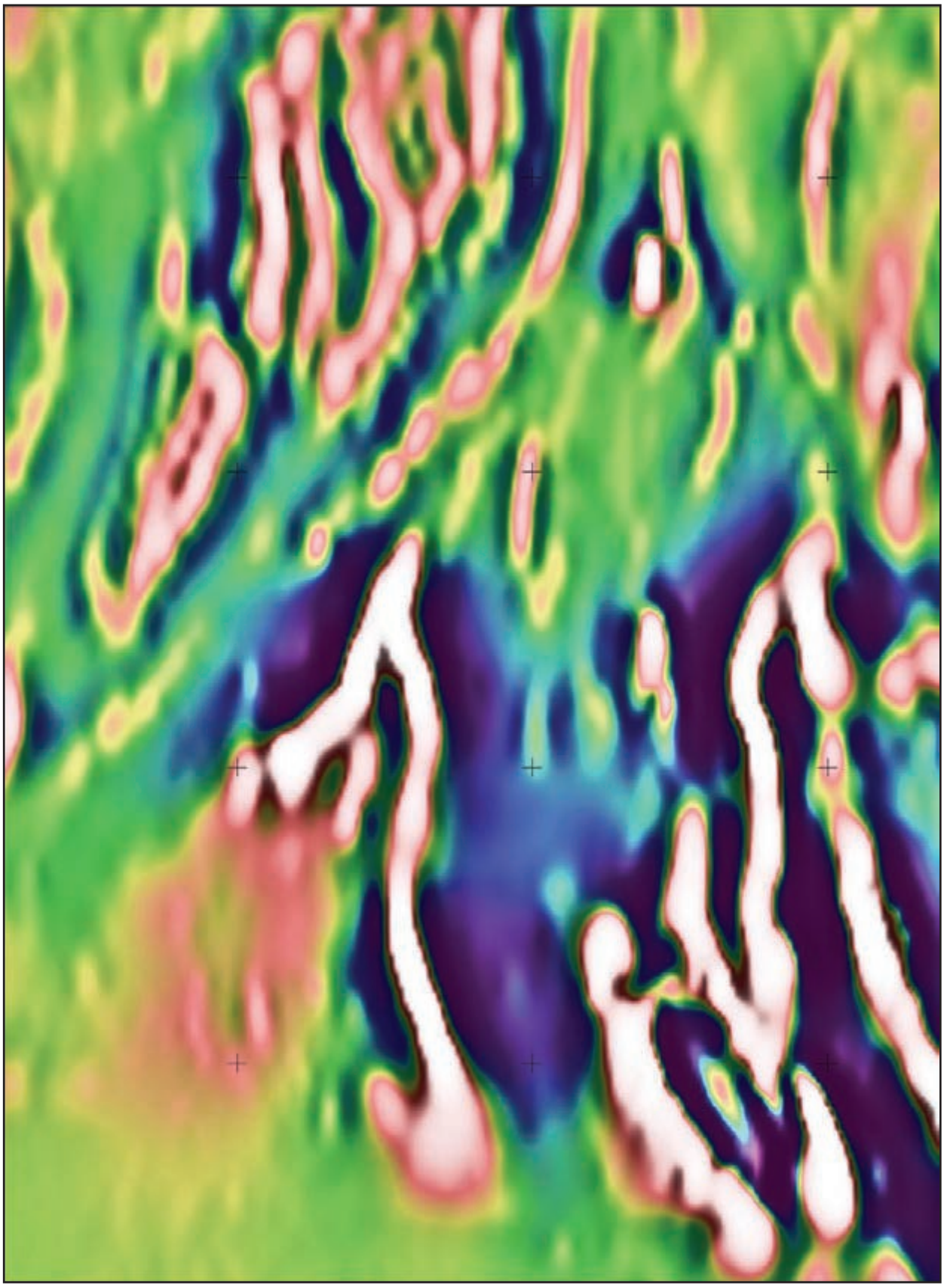

Figure 12.13: RTP 1st VD (colour) draped on RTP 2nd VD (intensity). Grid markers match Figure 12.9. Data from NT Geological Survey and Geoscience Australia. Imaging Andy Roberts, Southern Geoscience Consultants.

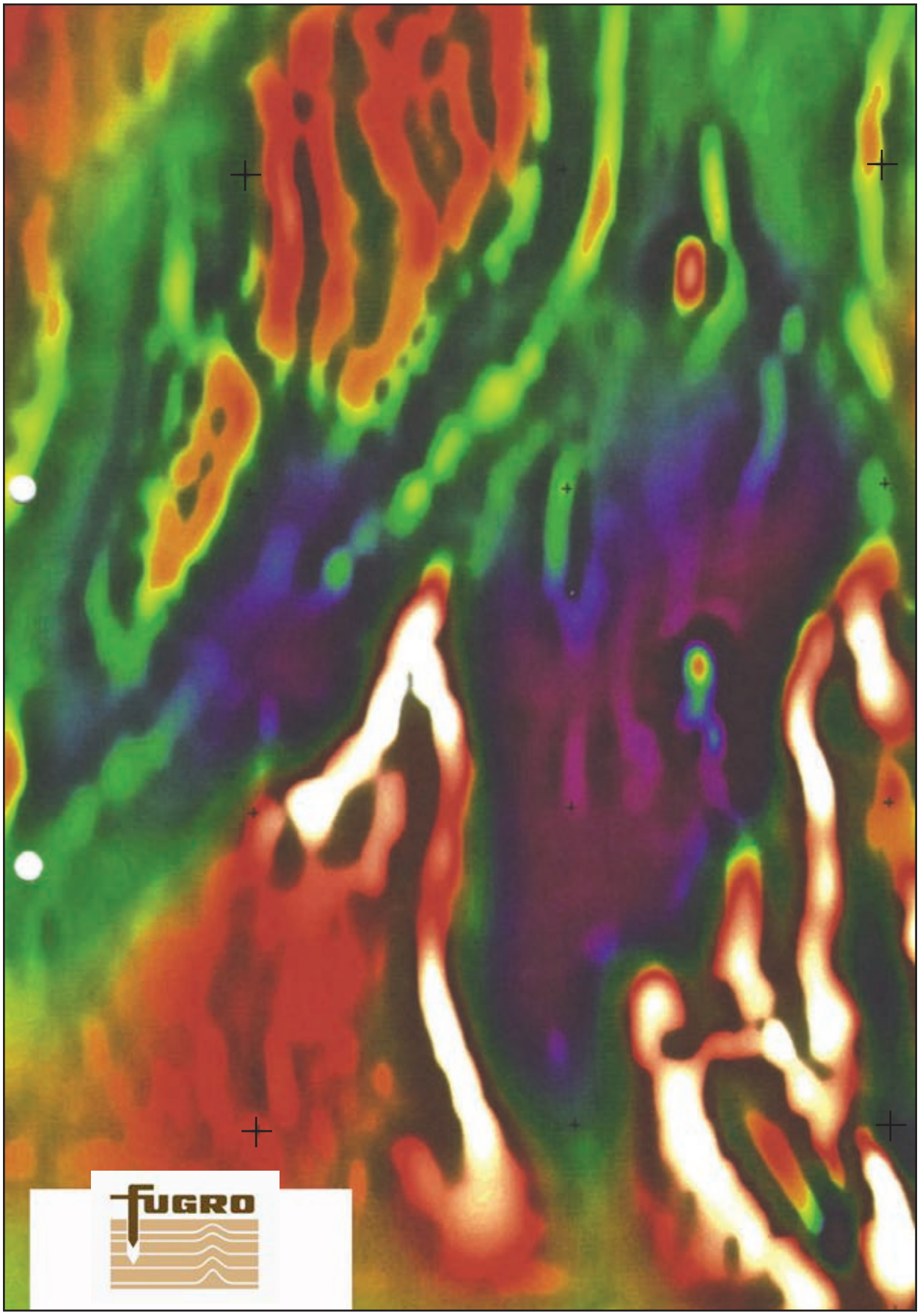

Figure 12.14: Composite RTP/RTP 1st VD image. Grid markers match Figure 12.9. Data from NT Geological Survey. Imaging by World Geoscience (now Fugro Airborne Surveys).

Figure 12.15a: Aeromagnetic observations layer. Grid markers match Figure 12.9.

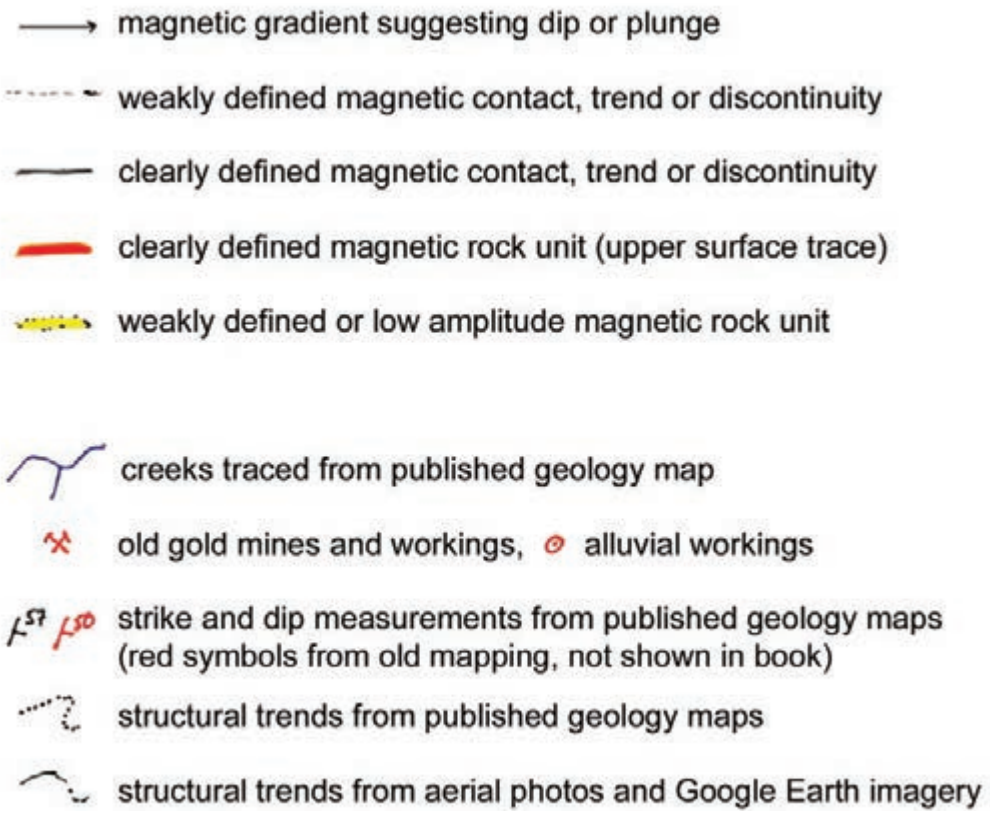

Figure 12.15b: Legend for aeromagnetic observations layer.

Figure 12.16a: Golden Dyke Dome – aeromagnetic observations on RTP 1st VD (left) and outcrop mapping (right). Refer to Figures 12.8, 12.12 and 12.14 for originals.

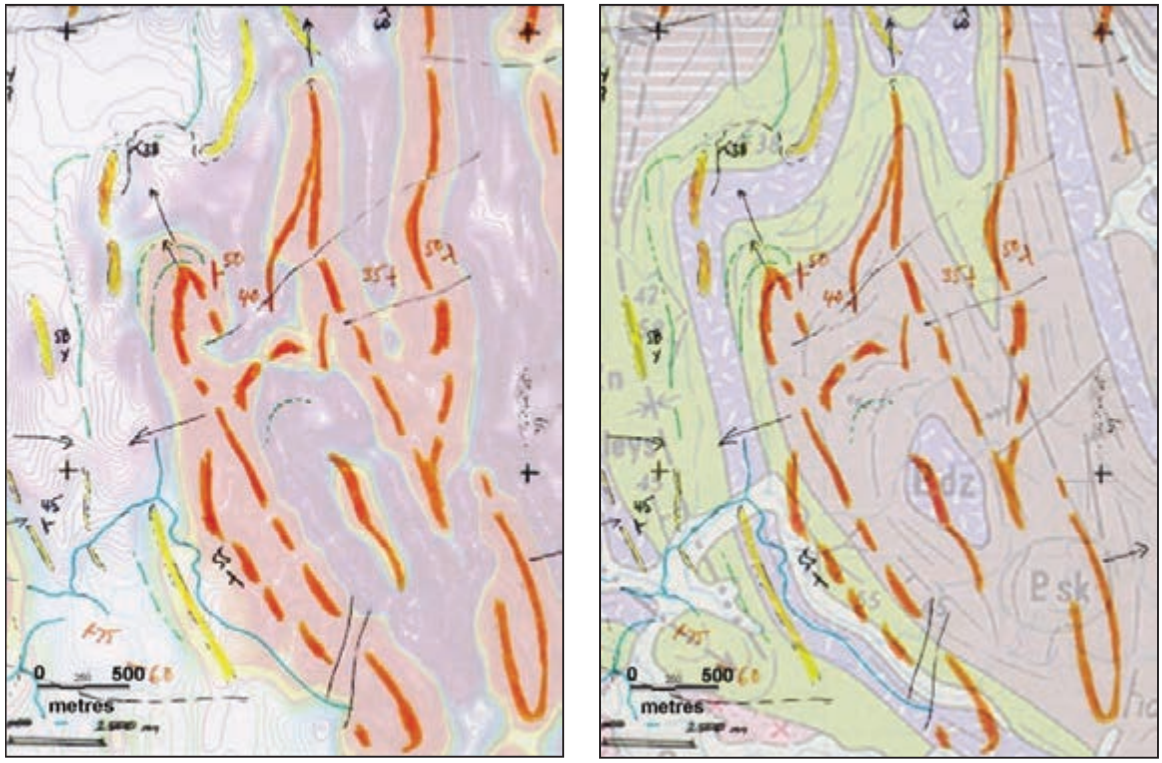

Figure 12.16b: South East Dome – aeromagnetic observations on RTP 1st VD (left) and outcrop mapping (right).

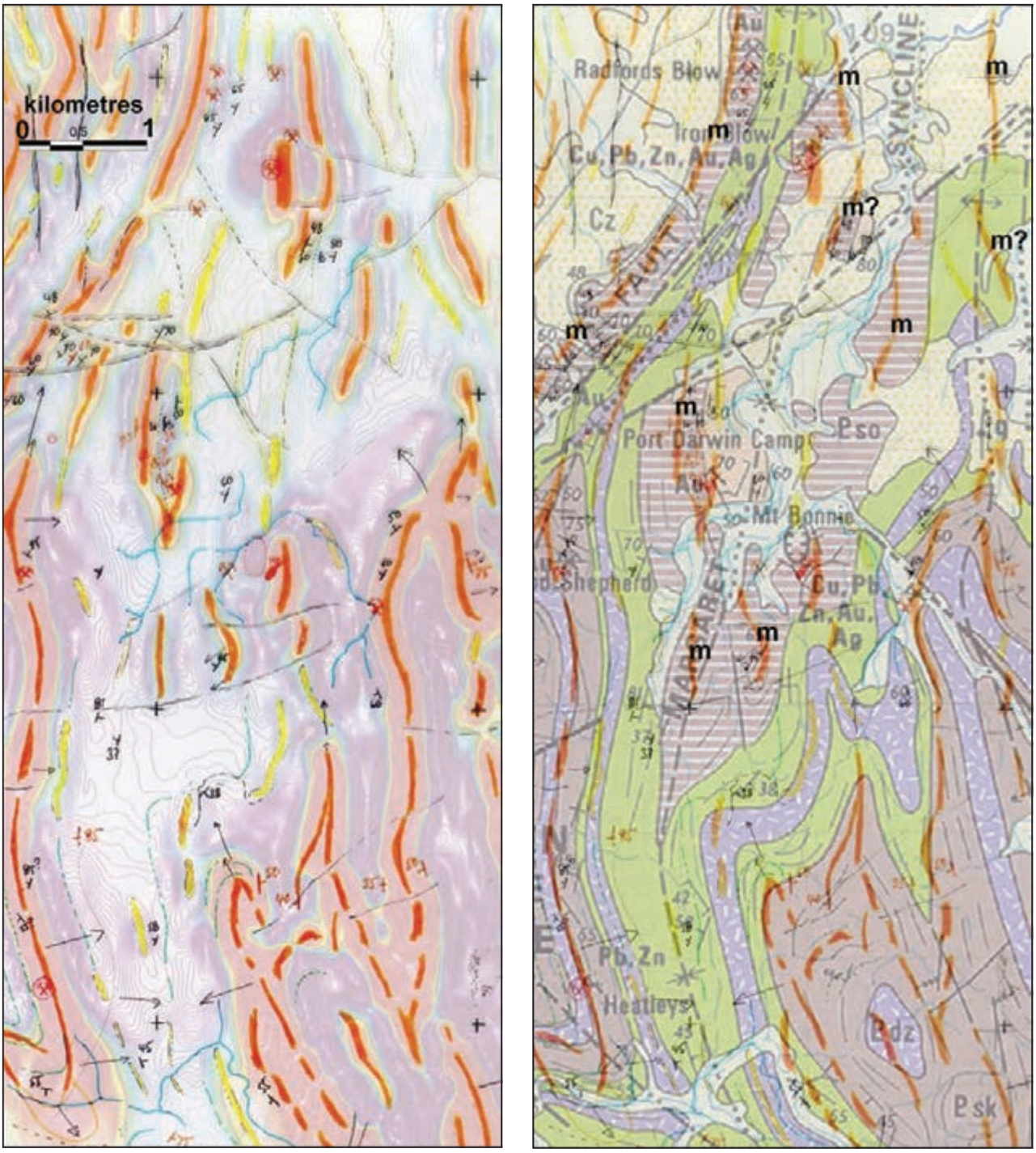

Figure 12.16c: Margaret Syncline area – aeromagnetic observations on RTP 1st VD (left) and outcrop mapping (right).

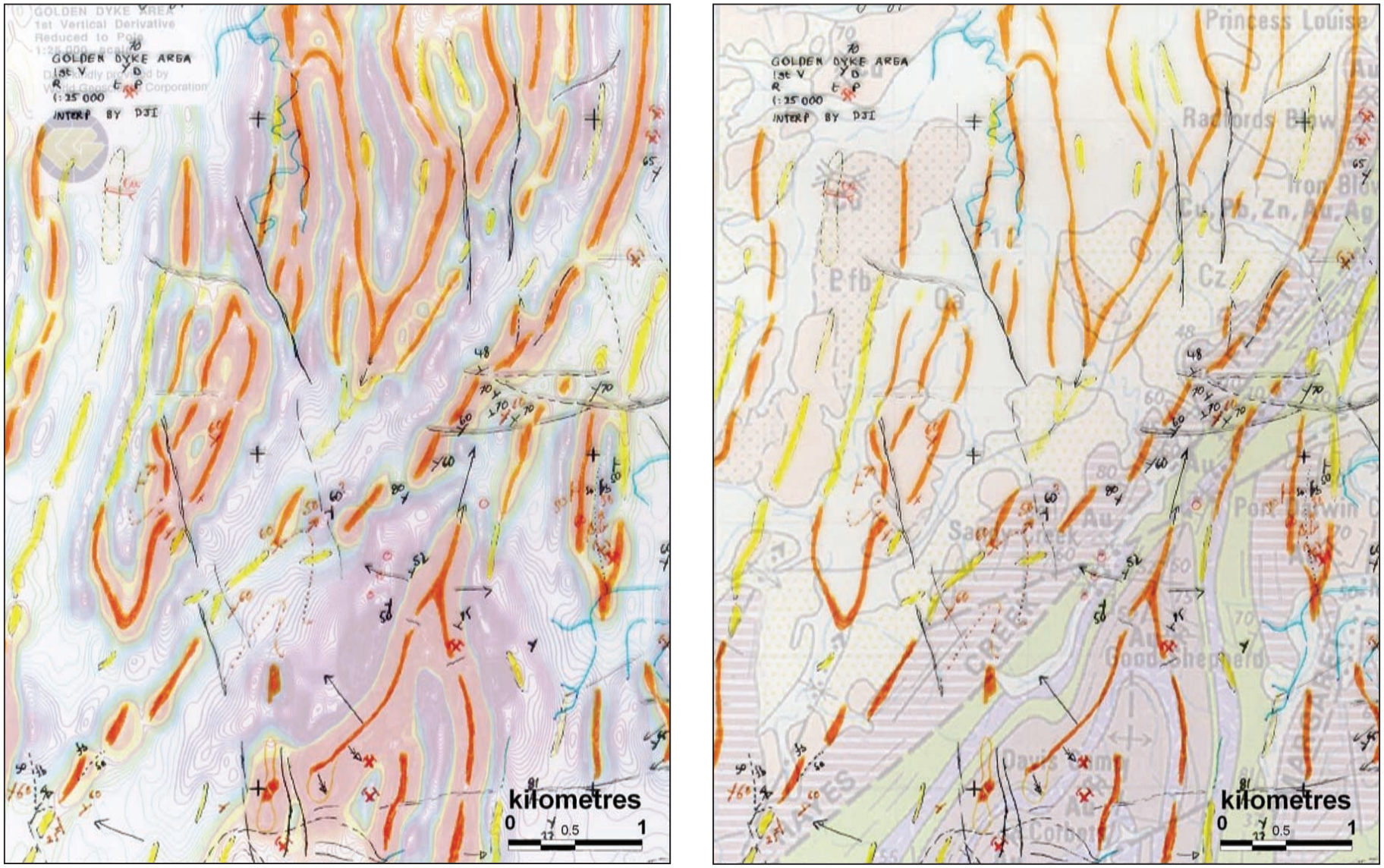

Figure 12.16d: North West Syncline area – aeromagnetic observations on RTP 1st VD (left) and outcrop mapping (right).

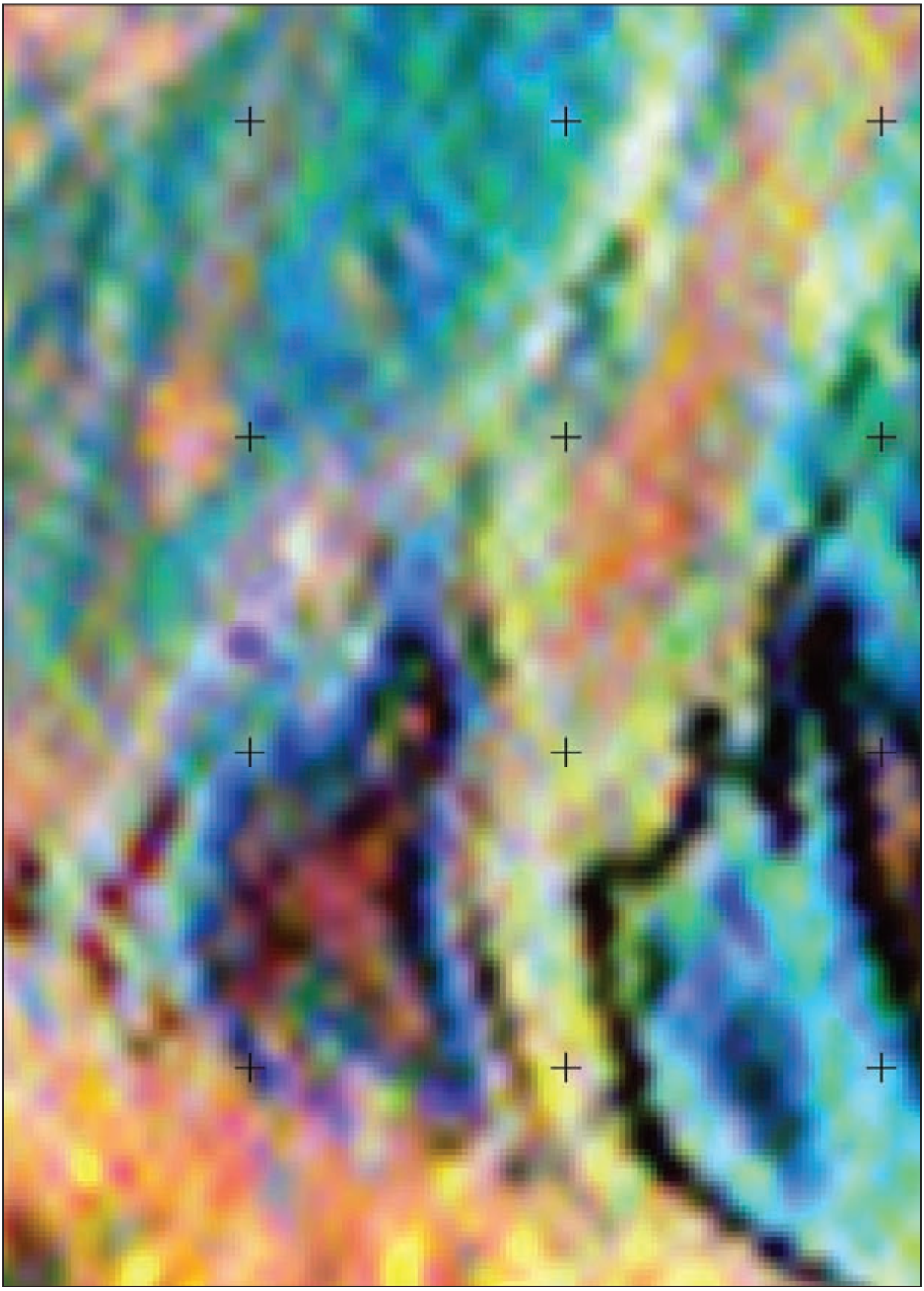

Figure 12.17a: Ternary radiometric image. Each of the K, Th and U channels has a non-linear stretch to optimise subtle variations in concentrations.

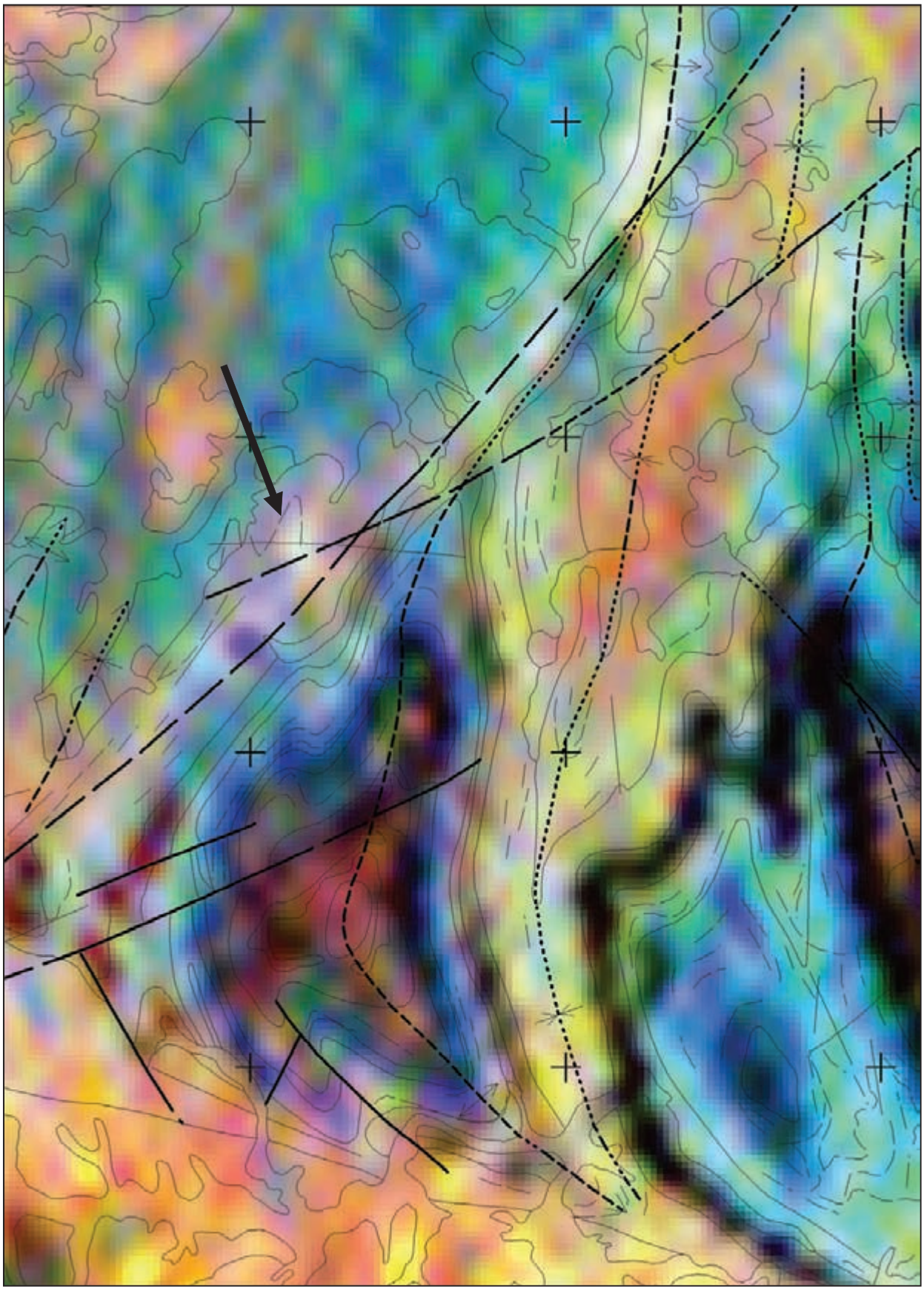

Figure 12.17b: Ternary radiometric image with mapped (pre-airborne survey) geological boundaries superimposed. The complete surface geology map is shown in Figure 12.8. The arrowed feature is the strongest composite K,Th and U response in the area, at around two times background in all channels.

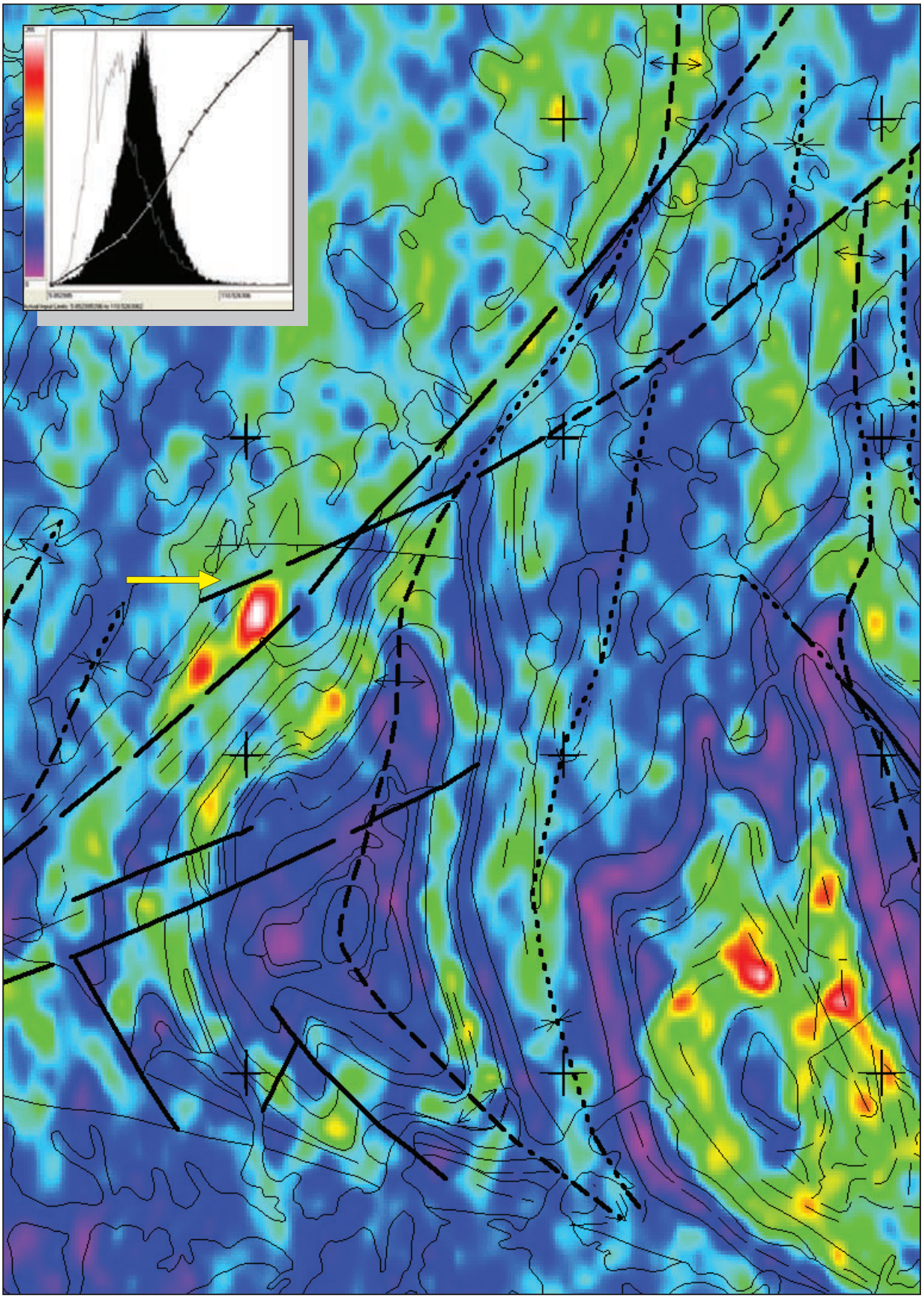

Figure 12.18: Uranium channel image. The inset shows the stretch of the colour look-up table against the U count intensities (in counts-per-second). The intensity range is 5–110 cps with a common background range of ~30–60 cps. The arrowed feature is the strongest response (two to three times local background) and relates to subcropping uranium mineralisation (see text).

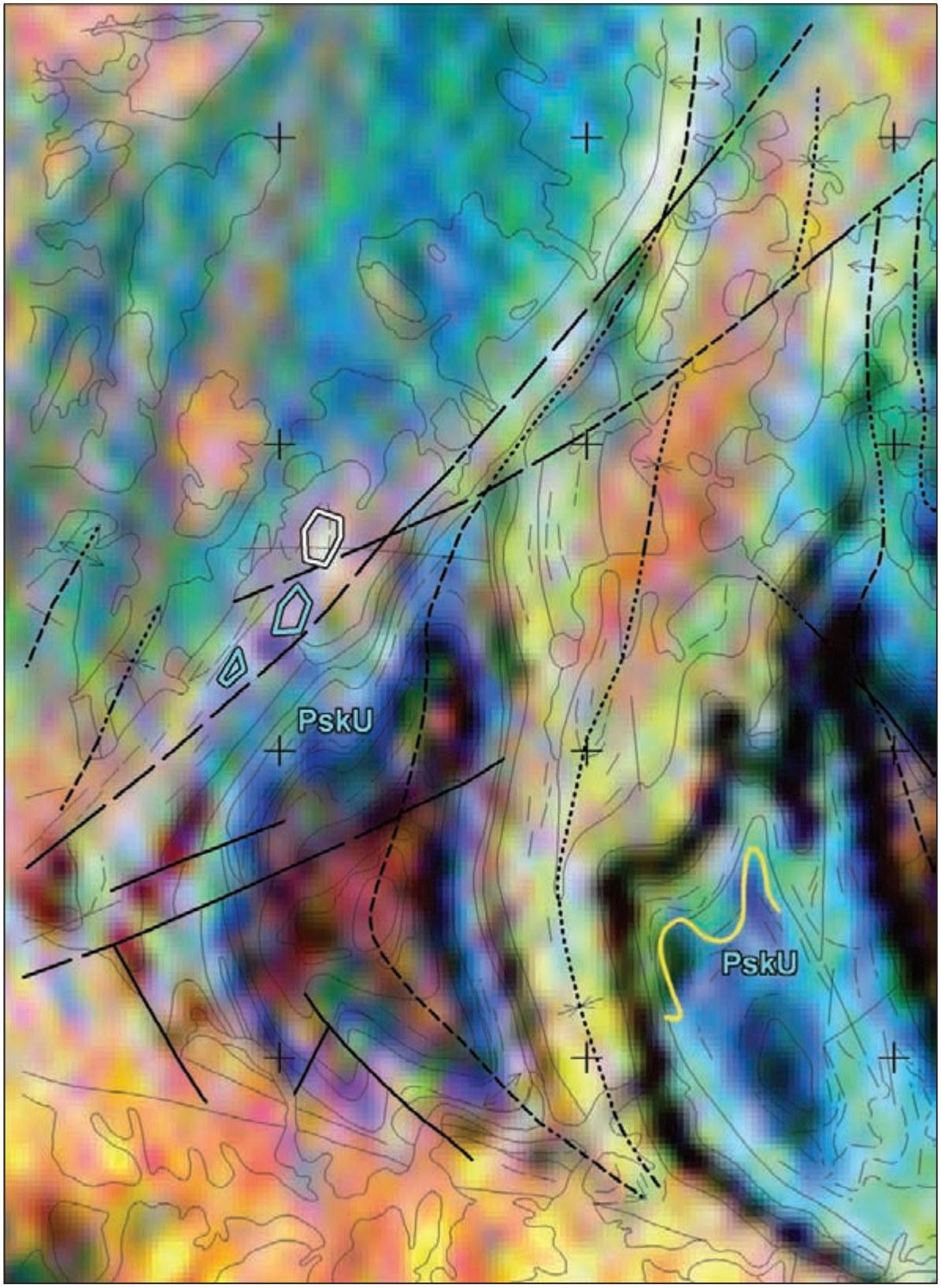

Figure 12.19: Ternary radiometric image showing mapped geological boundaries and significant radiometric features. Refer to text for description.

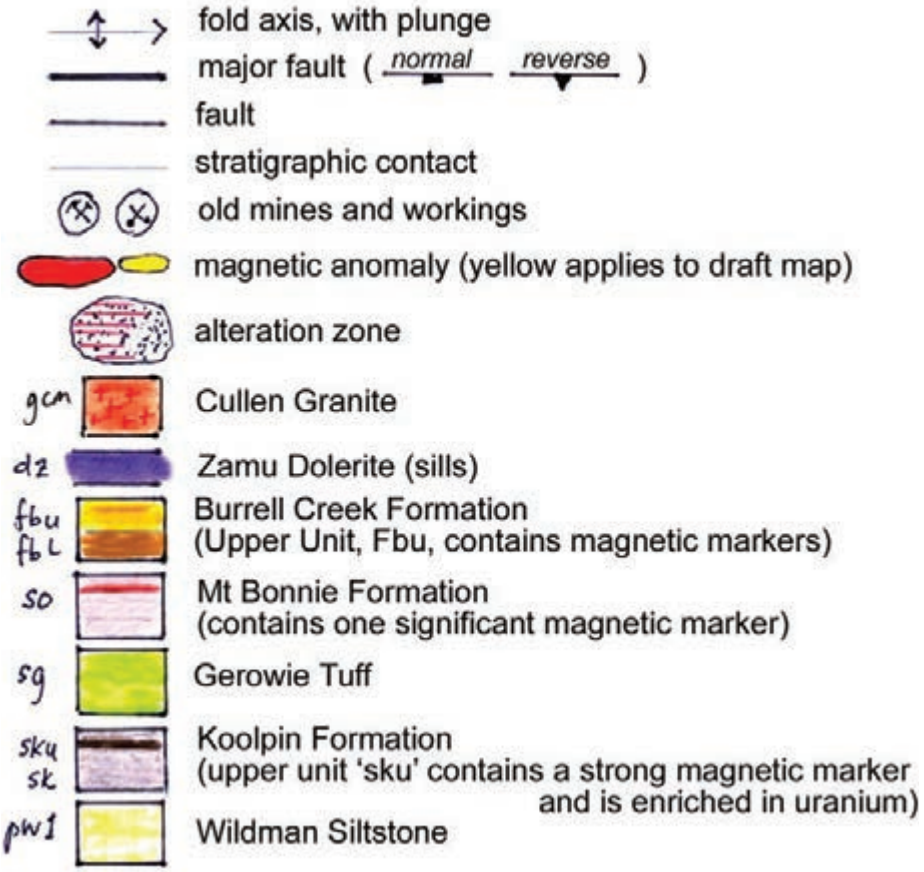

Figure 12.20: Legend for solid geology layer (Figs 12.21 and 12.22), cross-sections (Fig. 12.24) and final interpretation map (Fig. 12.28). Refer to Figure 12.4b for full (published) descriptions of stratigraphic units.

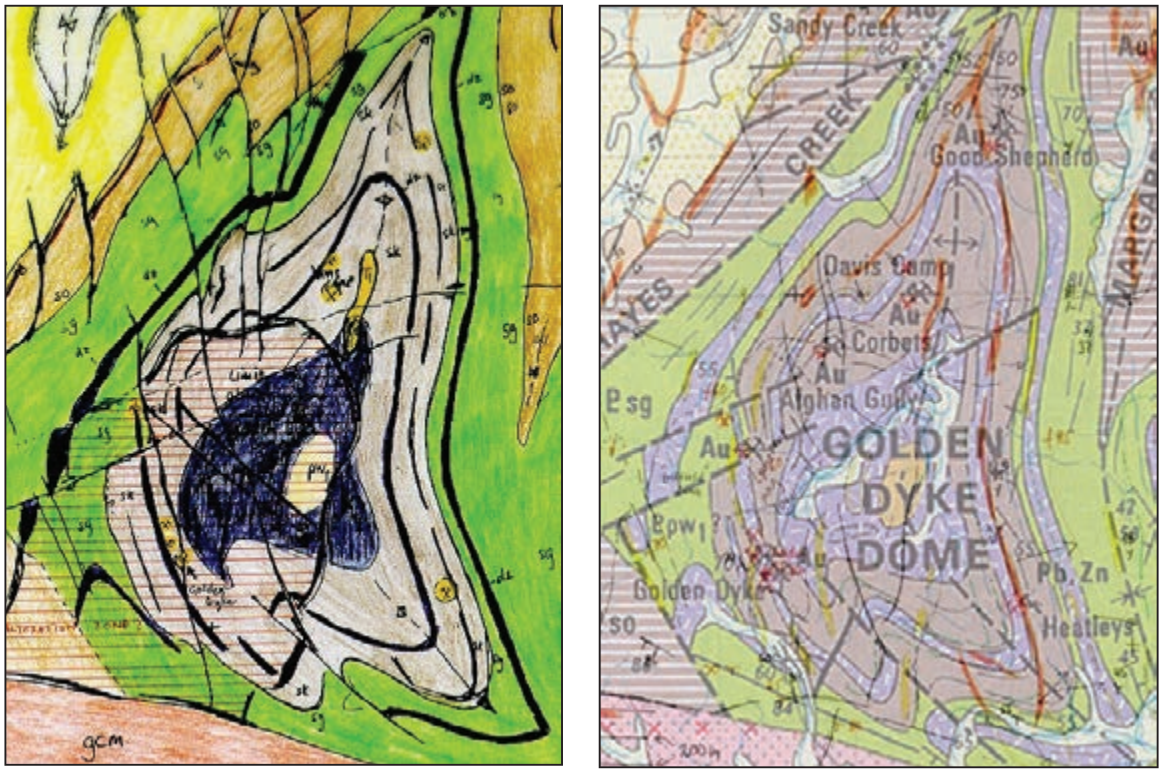

Figure 12.21a: Golden Dyke Dome – draft solid geology (left) and mag observations on outcrop mapping (right).

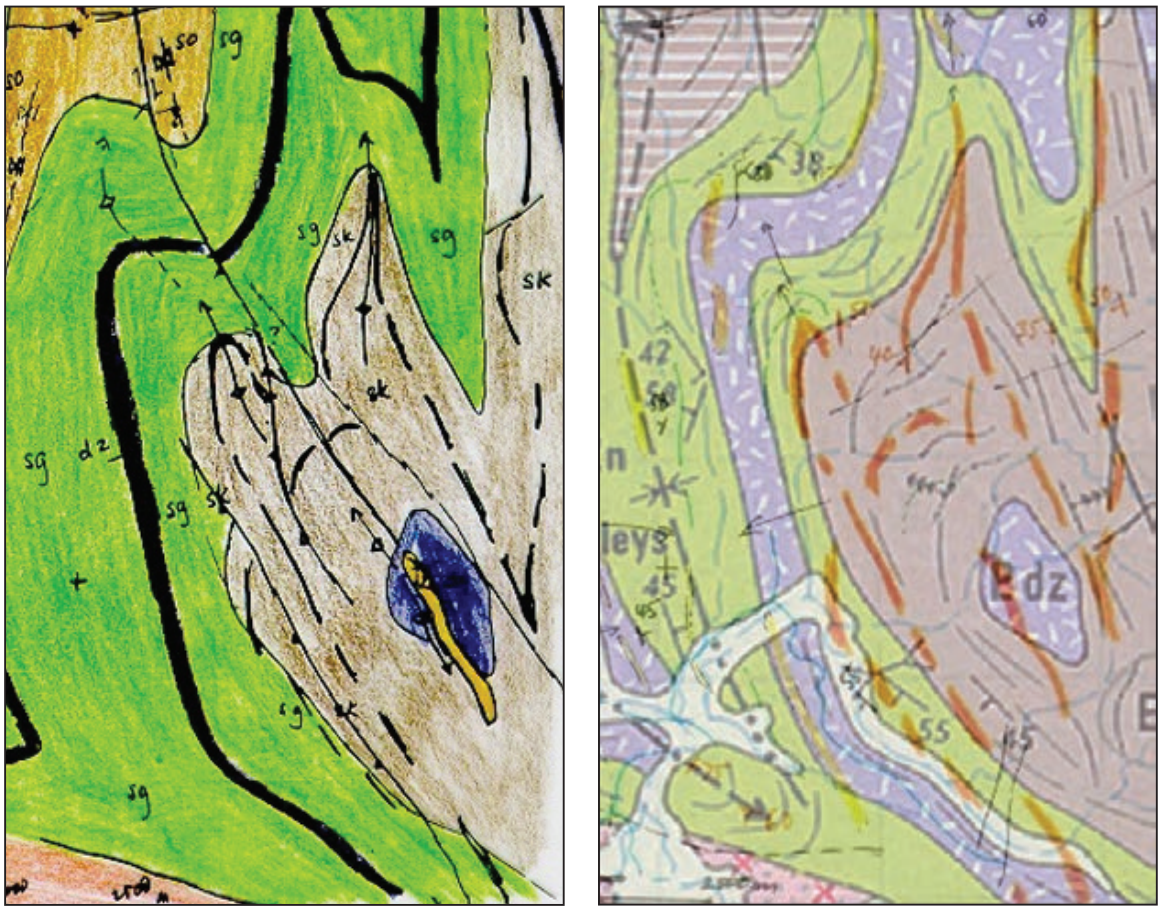

Figure 12.21b: South East Dome – draft solid geology (left) and mag observations on outcrop mapping (right).

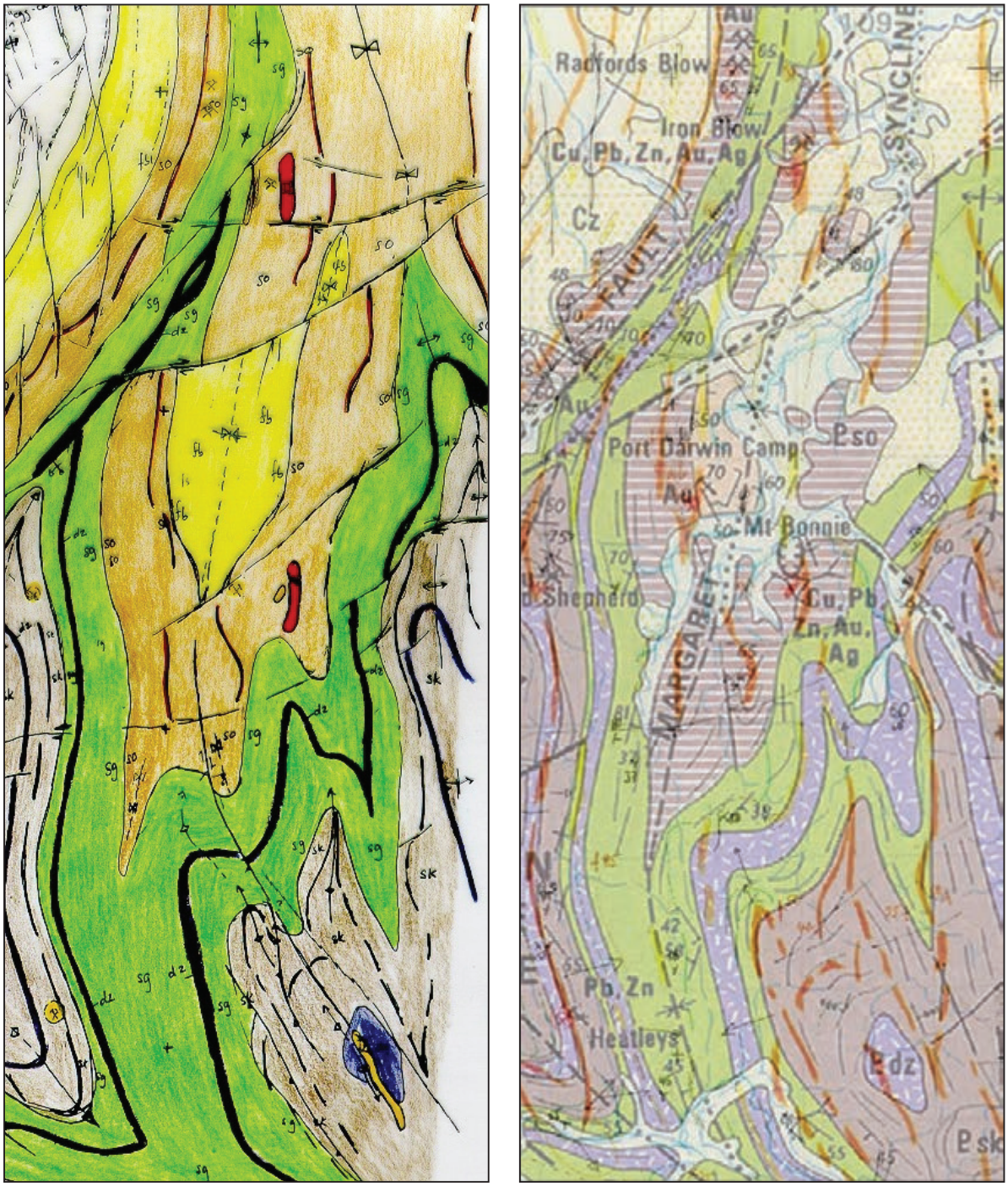

Figure 12.21c: Margaret Syncline – draft solid geology (left) and mag observations on outcrop mapping (right).

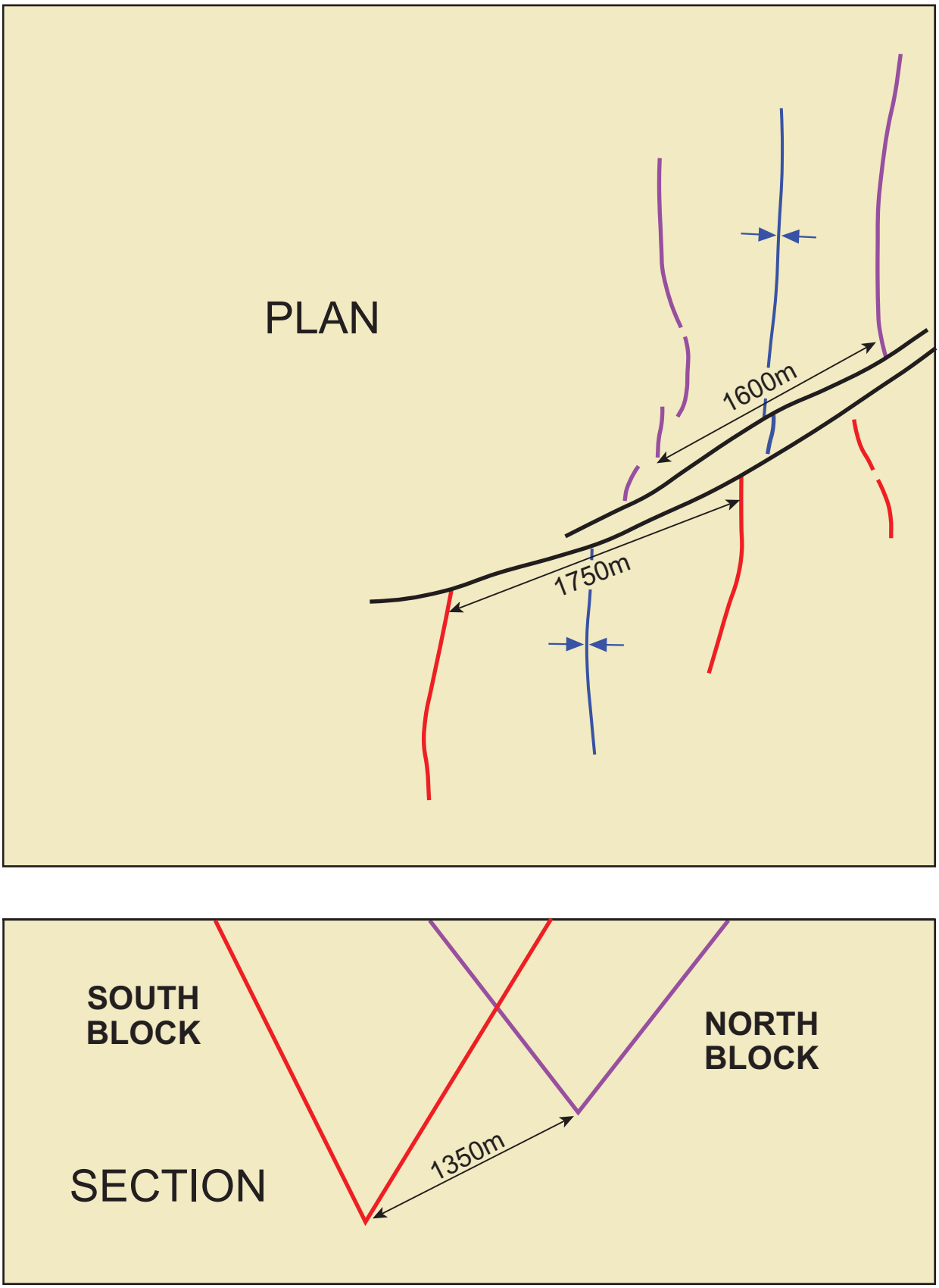

Figure 12.21d: Graphical construction showing the approximate total displacement on the ENE-trending fault in the Margaret Syncline. The red and magenta lines represent the Mt Bonnie BIF marker, black lines represent the surface traces of the fault.

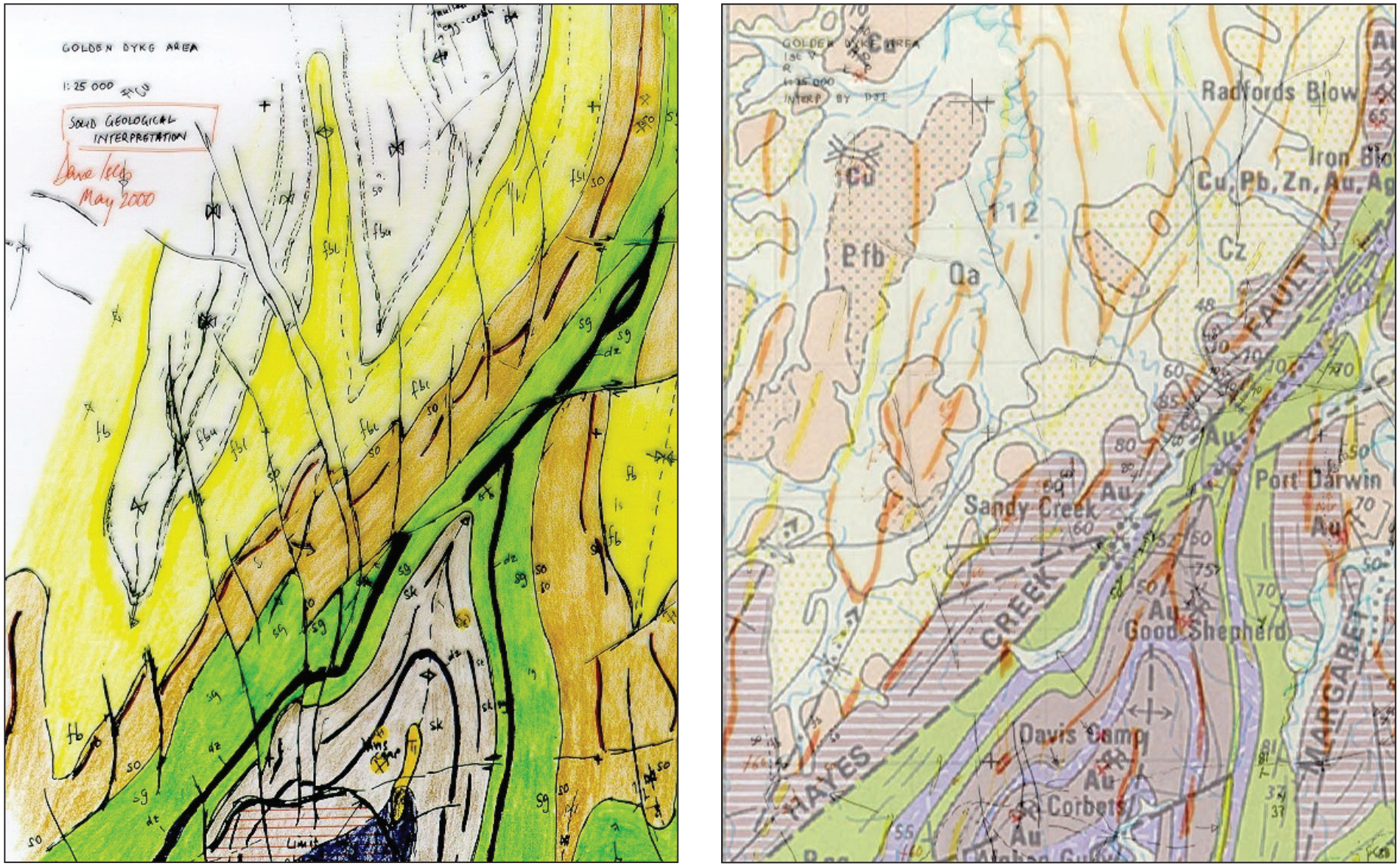

Figure 12.21e: North West Syncline area – draft solid geology (left) and mag observations on outcrop mapping (right).

Figure 12.22: Working (draft) solid geology layer, showing cross-section locations. See Figure 12.20 for legend.

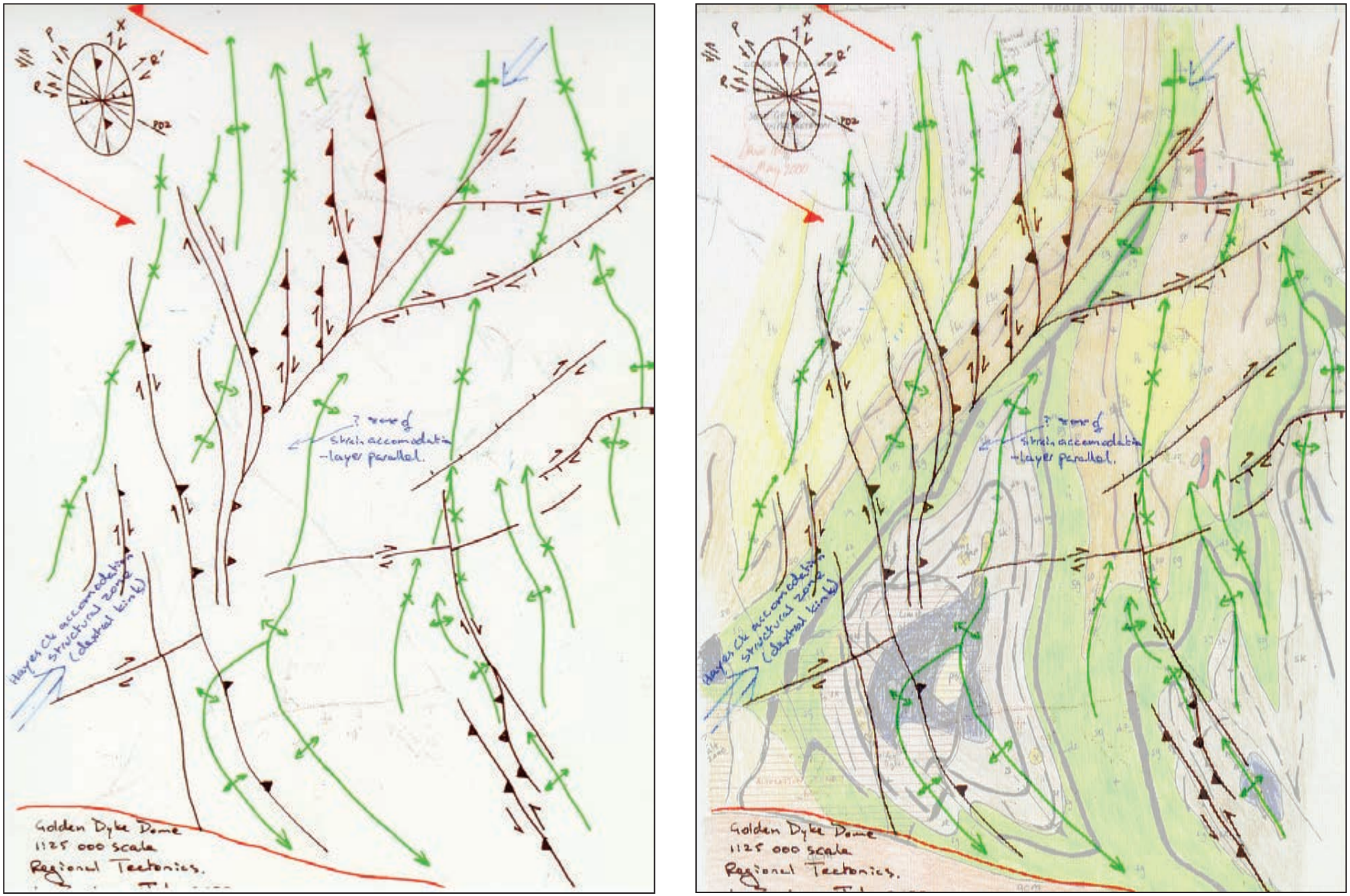

Figure 12.23: Initial structural framework/summary sketch.

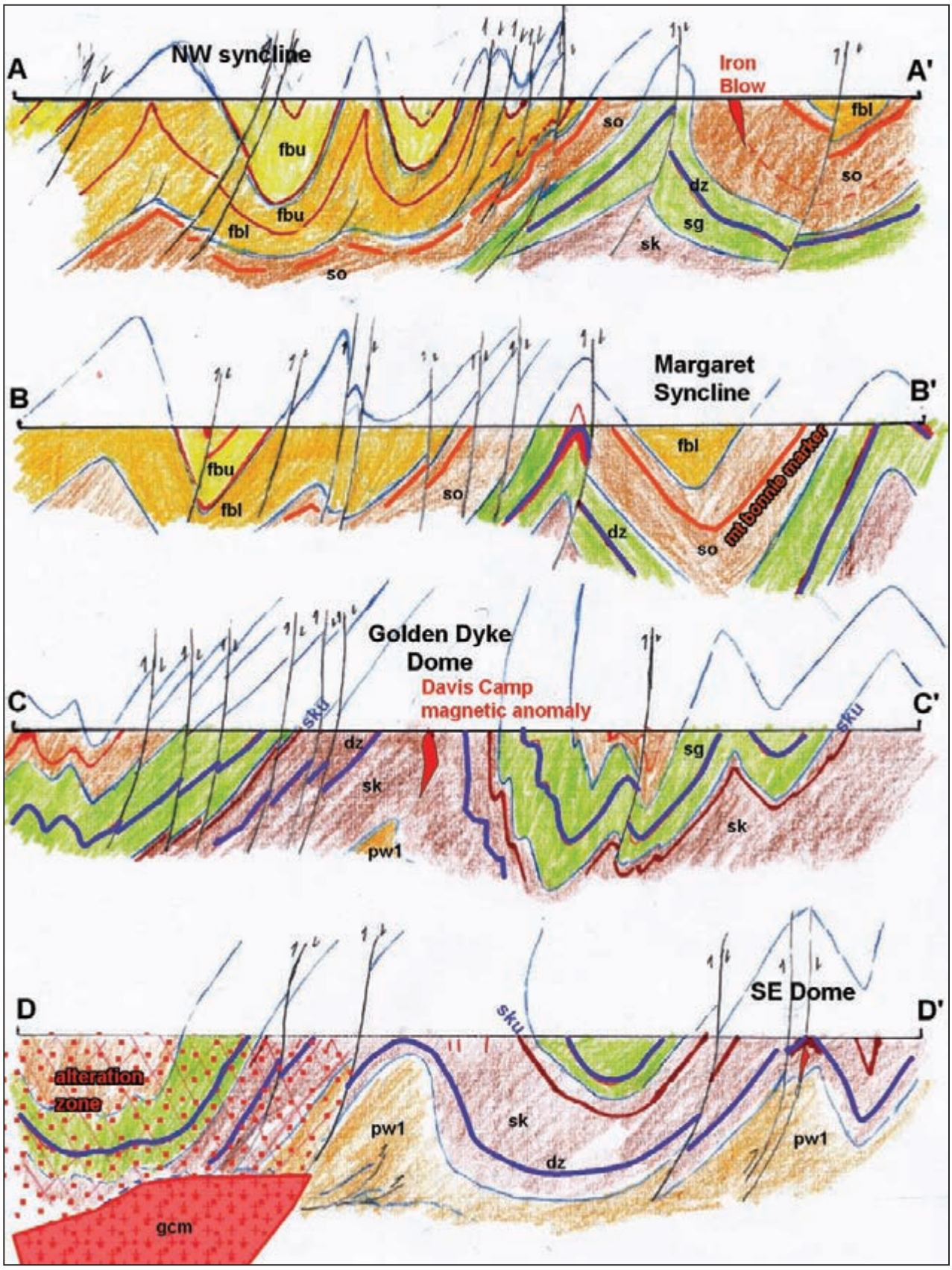

Figure 12.24: Cross-sections. See Figure 12.20 for legend and Figure 12.22 for location.

Figure 12.25: Working exploration targets map.

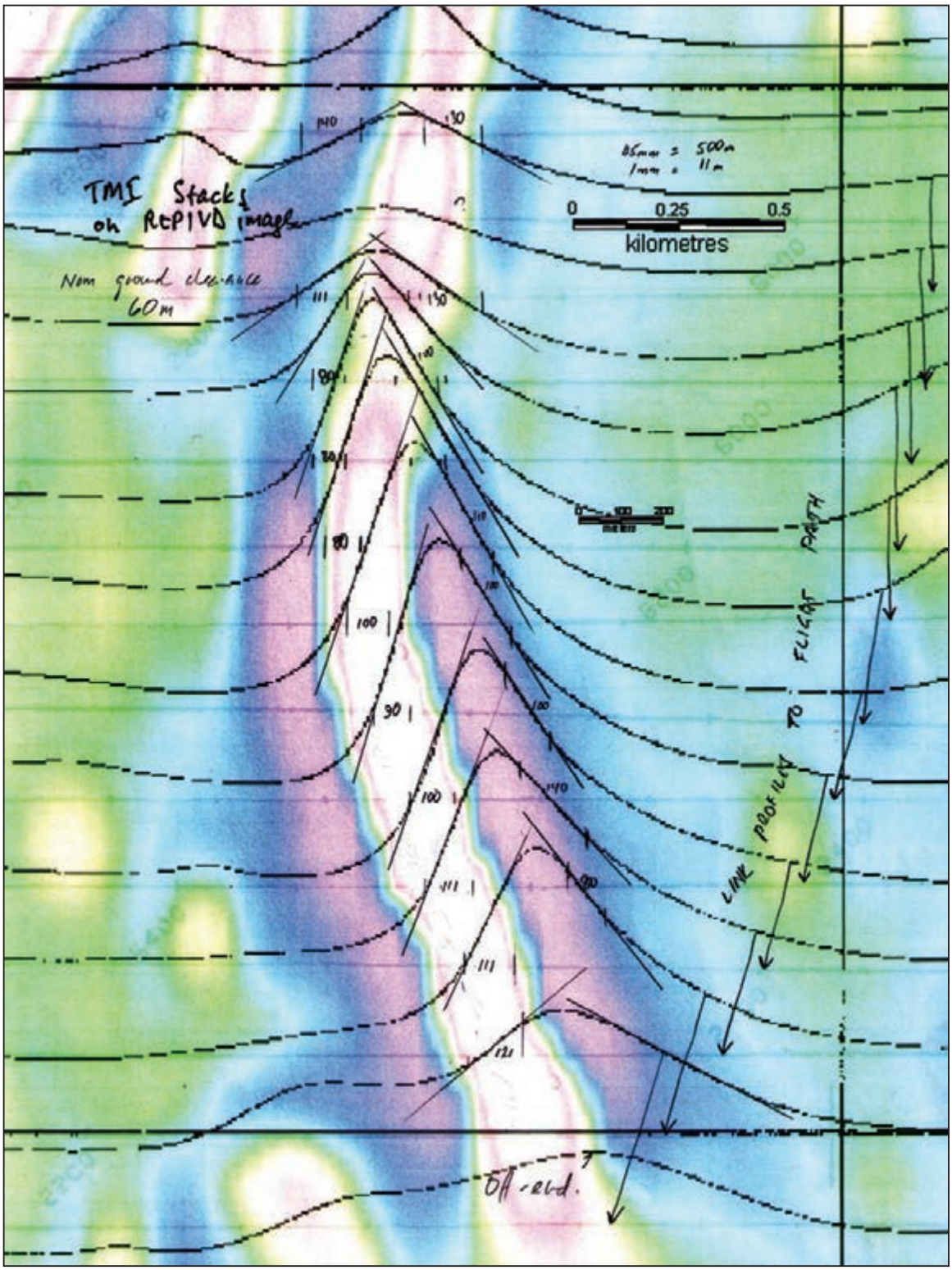

Figure 12.26: Straight-slope depth calculations for the Koolpin ironstone marker. Depths are below aircraft. Arrows relate profiles to the image and flight path. As the nominal flying height is 60 m, the calculations suggest that the source of the magnetic anomaly may not be seen at surface.

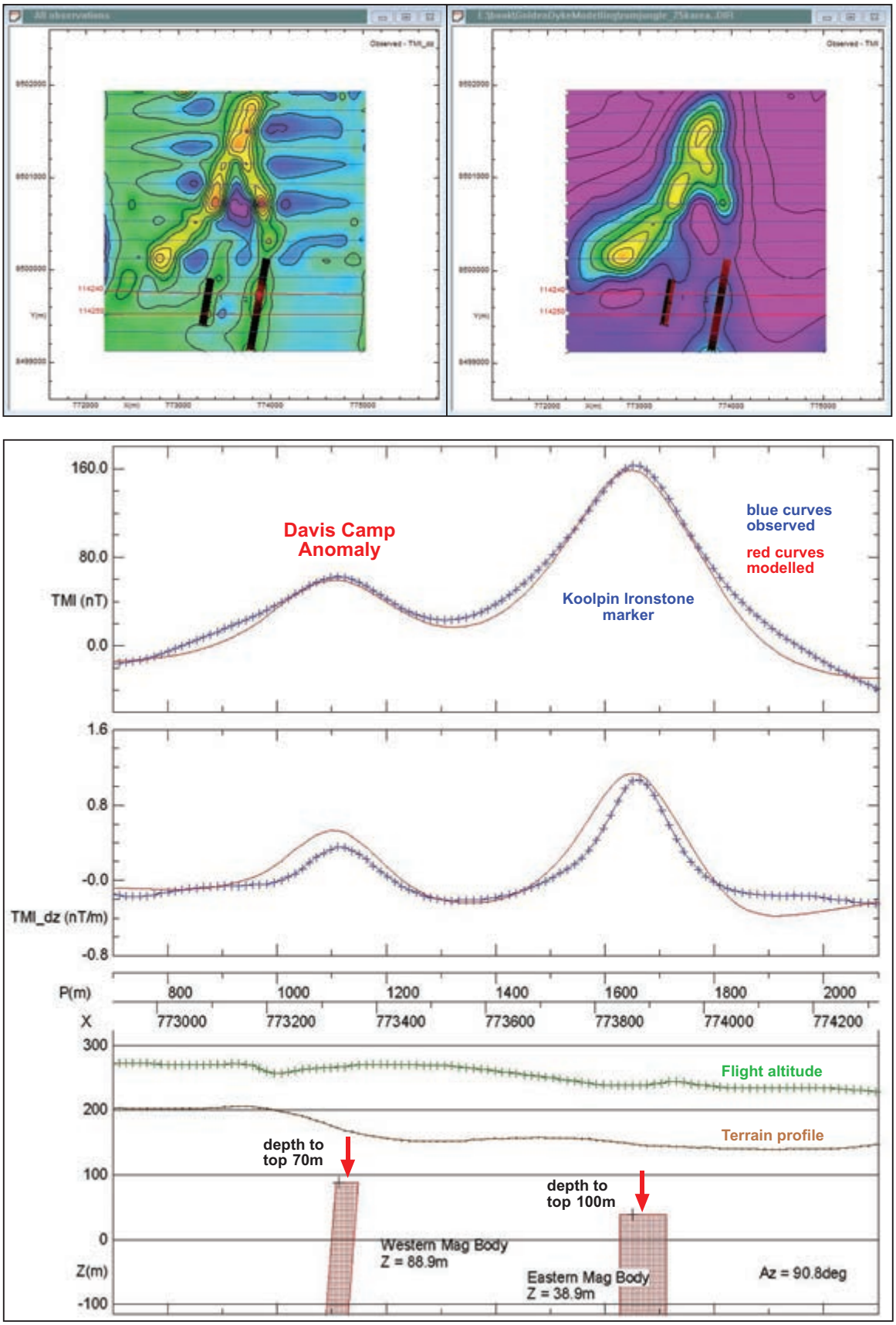

Figure 12.27: Models for magnetic rock units in the Golden Dyke Dome. The models support the estimated depths from the straight-slope graphical method and suggest that the magnetic rock units may not be exposed. Modelling by Greg Maude, Southern Geoscience Consultants, using Potent Software.

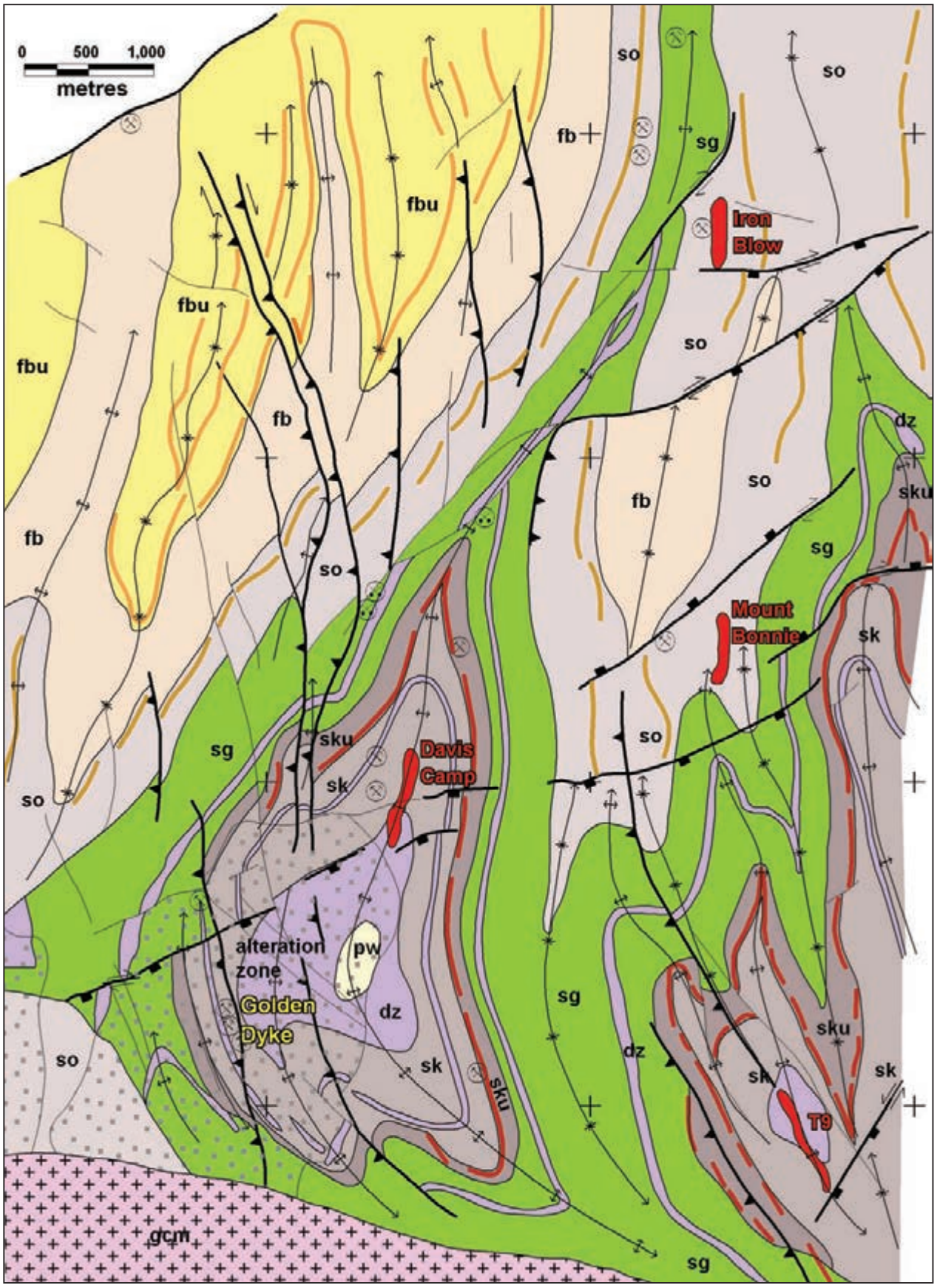

Figure 12.28: Final integrated solid geology interpretation map. See Figure 12.20 for legend. The grid markers are the same as those in all images, refer to Figure 12.9 for coordinate values.

13 Amadeus Basin case study – Palaeozoic sedimentary basin with complex thrust margin

13.1 INTRODUCTION

The southern sector of the Amadeus Basin (Fig. 13.1) provides an excellent example of a sedimentary basin with magnetic sources of various ages, geological affinities and depths. These include the strongly magnetic basement, forming the southern margin of the basin (and extending below the basement sediments), several intra-basin sedimentary and volcanic sources, plus post-basin weathering and palaeo-channel sources.

The sector of the basin chosen for this study includes a complex thrust interface between basin and basement, providing the opportunity to examine inversion-style structures. This allows us to illustrate how aeromagnetic data can elucidate complex structures before implementation of seismic surveys.

This study is not designed as a definitive integrated interpretation. Rather, it is intended as a guide to the methodology used to maximise the extraction of geology from aeromagnetic data in sedimentary basins. The authors have selected a sector of the Amadeus Basin to illustrate this process, and have worked through the data in sufficient detail to identify the key geological elements contained within it. They have not, however, conducted exhaustive research into previous geological mapping and exploration and, because of time and space restrictions, have not attempted to produce a comprehensive interpretation. Such an interpretation would require in-depth integration of all available geology, satellite imagery, seismic and gravity data and would take several months (as a minimum). The material presented here should therefore be regarded as an illustrative guide, focusing on the aeromagnetic data, rather than a definitive analysis of the study area.

We worked this interpretation at two scales in order to simulate the scales and style of interpretation that would be carried out at the early stages of assessment of a poorly or under-explored sedimentary basin. The entire study area was analysed at ~1:1 000 000 scale and we then selected a subarea for more detailed analysis at roughly 1:250 000 scale (Fig. 13.1). The Amadeus Basin has some hydrocarbon resources and perceived exploration potential (Ambrose 2006; Marshall 2004), but our study area has very coarse gravity coverage and almost no seismic data. Dentith and Cowan (2009) present an enlightening introduction to the importance of aeromagnetic and gravity data in early-stage targeting in the far western part of the Amadeus Basin.

Importantly, we acknowledge the considerable contributions to this chapter made by Zhiqun Shi and Ian Campbell. Their capabilities and experience in the data processing, enhancement and quantitative modelling of aeromagnetic data in sedimentary basins has been an essential part of the work presented here. The contributions of Zhiqun and Ian exemplify the benefits of enlisting specialist assistance for some of the data manipulation tasks that require advanced (and often expensive) software and considerable experience in application.

13.2 DATA PROCESSING, FILTERING AND DEPTH DETERMINATION APPROACHES

The aeromagnetic data comprise a merger of mostly recent government surveys, with 400 m N–S line spacing. There is one 16 × 20 km section in the centre of the study area which has only historical 2-mile spaced coverage. This is very obvious in the derivative images, but the area is small enough to have minimal impact on our interpretation. Gridded data (80 m native cell size) was downloaded from the GADDS website (Geoscience Australia 2011). The high quality of the merging and levelling of the various surveys into one grid by Geoscience Australia made recourse to the measured line data unnecessary for our purposes. A shaded, colour image of the TMI grid is presented in Figure 13.2.

13.2.1 RTP

Chapter 10 emphasises the need to use RTP imagery in sedimentary basins owing to the increasing shift in anomaly shapes with increasing depth to source. Figure 10.9 shows the TMI–RTP comparison in part of the study area, and highlights the large shift in some of the primary deep sources. Hence, we have used the RTP imagery exclusively for the qualitative interpretation, while retaining the use of the TMI data for the quantitative modelling. The RTP image (Fig. 13.3) shows subtle but highly continuous, shallow magnetic units trending NW–SE in a very discordant relationship with stronger, broader (and likely deeper), predominantly NE-trending magnetic units. We will aim to view and assess the shallower and deeper features separately.

13.2.2 Derivatives

Conventional first (1st VD) and second vertical derivatives (2nd VD) would be expected to emphasise the shallower sources at the expense of the deeper ones. Figures 13.4 and 13.5 show our best images of these derivatives, computed from RTP data.

13.2.3 Separation filtering and wavelength filtering

The need to assess the deeper and shallower magnetic sources separately is a critical factor in sedimentary basin studies. The two main approaches to this are separation filtering and wavelength filtering, as discussed in Chapter 10. Separation filtering for our study area was carried out for this study by Campbell (2011) and wavelength filtering by Shi (2010). Both methods achieved a valuable separation of deeper and shallower magnetic sources and we comment briefly here on the similarities and differences between the two approaches.

The radially averaged power spectrum (Fig. 13.6) is the essence of separation filtering. We observe strong signal from around 400 m, 2000 m and 7500 m with weaker signal at apparent depths of around 80, 700 and 18 500 m. Note that 80 m is the predominant flying height for the survey data in the area, indicating the presence of near-surface magnetic sources. Matched filtering and inverse transformation of these apparent depth segments in the radially averaged spectrum yields filtered grids which we refer to as spectral depth windows. We emphasise that each of these windows highlights a range of magnetic depth sources, but we expect that the average or dominant depth will be close to the nominal depth calculated from the spectrum and that sources much shallower and deeper than this nominal depth will be poorly represented in that window. Assessment of the geological content in each of the spectral depth windows resulted in selection of the 7500 m (Fig. 13.9) window as the best representation of deep magnetic sources. The 2000 m (Fig. 13.8) and 700 m (Fig. 13.7) windows are useful indicators of source geometries at moderate depths. Although the 400 m window (not shown) presented a very strong signal, it was dominated by shallow basement sources in the south of the study area and added little to our view of the basin area. Similarly, the 80 m window gave a robust view of the near-surface magnetic rock units, but was inferior to the RTP 2nd VD in the clarity it provided on shallow features. The 18 500 m window (also not shown) displayed no well-defined geometries, appearing to reflect the deeper component of features evident in the 7500 m window.

Wavelength filtering was conducted as follows:

a) low-pass filtered grids were generated for wavelengths greater than 10 km, 20 km and 60 km respectively;
b) high-pass filtered grids were generated for wavelengths less than 10 km, 20 km and 60 km respectively;
c) a band-pass filtered grid was generated to retain wavelengths of between 10 km and 60 km.

Once again, assessment of the geological content of each grid was carried out; this resulted in selection of the 10–60 km band-pass filtered grid (Fig. 13.10) and the >20 km low-pass filtered grid (Fig. 13.11) as the most useful for the interpretation.

Comparisons between the spectral depth windows and the wavelength filtered images resulted in the above choices. The greyscale RTP 2nd VD (Fig. 13.5) clearly showed most clarity in portraying the shallow features. The mid-depth spectral depth windows (700 m, Fig. 13.7 and 2000 m, Fig. 13.8) provided better geological resolution that the high-pass wavelength filters. For the deeper section, the 10–60 km band-pass filter, Figure 13.10 clearly resolved the geometries of magnetic sources within the basin and added clarity to the picture portrayed in the 7500 m spectral depth window. Both these images were used in the qualitative observation stage. The >20 km wavelength image served to reinforce the main elements of the deep geometry in the basin.

Overall, the study shows that separation filtering provides better depth focus and more robust geometry in the magnetic field patterns than wavelength filtering, but the simplicity of application of the latter and the resolution achieved in the selected images makes wavelength filtered images valuable additions to the interpretation set.

13.2.4 Modelling

Neither separation filtering nor wavelength filtering gives precise depths. Similarly, depth-to-basement software schemes (see Section 8.3) rarely yield useful results when responses from sources at different depths are superimposed. Careful direct application of conventional forward modelling can solve this problem, and greatly reduce the need to apply these somewhat imprecise 'automatic depth' techniques. The initial phase of modelling, carried out in our study area by Shi (2011) using the ModelVision Pro™ software system, incorporated forward modelling, local anomaly inversion and automatic depth calculation. This aimed to better quantify the range of depths to magnetic sources within the basin and to provide some localised indication of dips on major contacts. Selected single and multi-profile line data were extracted from the TMI grid and simultaneous multi-profile modelling was performed in each area to provide realistic estimates of deep magnetic rock unit depths and geometries. Figure 13.14 shows the spread of segments selected to achieve this and Figure 13.15 shows one example of a modelled profile, which suggests the possibility of basement slices with high-angle reverse or thrust fault relationships to the basin sediments (Section 13.4.3). In a broader sense, the modelling has been used to identify depths to specific basement magnetic bodies. These were picked from the modelled profiles and transferred to the deep observation layer to form the basis for the basement interpretation discussed in the next section (Fig. 13.17).

13.2.5 AUTOMAG

AUTOMAG (Shi and Boyd 1993) is an automatic depth computation scheme designed to focus on a particular, predefined (and relatively narrow) depth range. It is based on the method developed by Naudy (1971) and has been successfully used in mapping cover thickness in poorly exposed hard-rock terrains (e.g. Moore 1997). It is now incorporated into the modelling software package mentioned above. However, as noted above, automatic depth-to-basement techniques do not perform well where responses from sources at multiple depths overlie one another. Hence, we have not attempted application of this technique for our greater study area. We have, however, applied AUTOMAG to the deep sources in the detailed study in the northern subarea (Shi 2011) with very useful results (Figs 13.30 and 13.31).

13.3 BROAD-SCALE (1:1 000 000) STUDY

The broad-scale study covers an area of 320 km by 215 km in the central/southern part of the Amadeus Basin and includes the basin's interface with the Musgrave Block basement to the south (Fig. 13.1). Analysis of the area at a scale of 1:1 000 000 was carried out to establish a structural framework that related the poorly exposed but clearly folded Palaeozoic sediments to the deeper geometry of the basin/basement contact zone. The basin includes modest hydrocarbon resources but has attracted limited historic exploration (Burgess *et al*. 2002). A recent basin-wide data compilation and analysis (Munroe *et al*. 2004) expands on the structural evolution of the region and provides a useful basis for more local-scale studies.

Published 1:250 000 scale geological mapping from the Alice Springs (Young *et al*. 2002), Kulgera (Edgoose *et al*. 1993), Henbury (Ranford *et al*. 1968) and Lake Amadeus (Wells *et al*. 1968) map sheet areas provides a sound basis for evaluating the area. These maps cannot be legibly reproduced at the presentation scale of this book, but can be downloaded from the Geoscience Australia website at http://www.ga.gov.au/products-services/maps/maps-of-australia.html. Figure 13.36 gives a representative sample of the style of outcrop and the extent of (mainly sand dune) cover in the study area, and Figure 13.13b summarises the main stratigraphic intervals and deformation events.

13.3.1 Regional setting

The Amadeus Basin is an E–W-trending Neoproterozoic to mid-Palaeozoic sedimentary basin, bounded to the north and south by crystalline basement of the Arunta Inlier and Musgrave Blocks respectively (Korsch and Kennard 1991; Wells *et al.* 1970). Lindsay and Korsch (1991) and Shaw (1991) interpreted that the basin underwent roughly N–S compression with fold and thrust deformation during the Petermann Orogeny (~550–520 Ma) and the Alice Springs Orogeny (~400–350 Ma). Broad, open E-trending folds are common throughout the basin, with more intense deformation adjacent to both the northern and southern margins. Some of the intense deformation is due to salt tectonics localised mainly in the lower part of the sedimentary sequence and interpreted to occur during both the Petermann and Alice Springs Orogenies.

The southern margin of the basin was significantly modified during the Petermann Orogeny, when the Musgrave Block basement was thrust to the N–NNE. This was accompanied by development of the Petermann Nappe Complex (with intercalated Musgrave Block metamorphics and Neoproterozoic sediments and volcanics), and the deposition of foreland molasse basin sedimentary rocks. Contacts between the Musgrave Block and Amadeus Basin sequences are commonly thrusts or high-angle reverse faults. The E–W to ESE–WNW folds and faults north of the nappes and foreland basin sequences probably include both Petermann Orogeny and Alice Springs Orogeny structures.

13.3.2 Imagery

Standard colour shaded relief images were generated for the TMI (Fig. 13.2) and RTP (Fig. 13.3). However, the derivative and separation filtered grids provided the main images for interpretation. The extreme high and low magnetic intensities in the study area lie wholly within the near-surface Musgrave Block and appear to be a mixture of metamorphic (dominant) and intrusive (subordinate) sources.

The RTP 1st VD image (Fig. 13.4) is presented as a lightly shaded (from NE) colour image. This provides a useful blend of higher frequency, shallow features and broader deeper features allowing the interrelationships of the two to be clearly viewed. The greyscale RTP 2nd VD image (Fig. 13.5) has no shading and has a customised, optimum stretch. This image provides the clearest view of the nearer surface magnetic rock units and was the main image used to compile the shallow observation layer.

Separation and wavelength filtering enable us to view the various deeper components in the aeromagnetic data and, as discussed, a selection of these spectral depth windows allows us to progressively define the geometry of subsurface magnetic rock bodies with increasing depth. Figures 13.7 to 13.11 illustrate our choice of images for the deeper aeromagnetic features, all being displayed in colour with very light shading.

13.3.3 Observation layers

The qualitative interpretation phase was subdivided into three layers corresponding to the shallow (0–~500 m), the mid-level (2000 m) and the deep (7500 m) spectral depth windows. Observation layers and structural framework interpretations were compiled for each of the three windows, but for simplicity, the shallow and mid-level windows have been combined into one layer for presentation (Fig. 13.12).

Shallow to mid- structural levels

The shallow-level imagery highlights magnetic units from surface to around 500 m. This provides an excellent view of the regional distribution of the main lithostratigraphic units and the detailed fold and fault deformation structures in the upper part of the basin. The scattered nature of outcrop and extensive cover prevents

regionally comprehensive, detailed surface mapping in the basin. The magnetic units delineated on our observation layer (Fig. 13.12) are associated with at least four separate geological subdomains and/or structural levels, as listed below.

a) Musgrave Block (Proterozoic crystalline basement).

This dominates the southern and south-western sectors of the study area. The basement rocks are strongly magnetic, with many complex sources associated with folded high-grade metamorphic rocks and variably magnetic intrusions. The patterns of the Musgrave Block sources are recorded in yellow on Figure 13.12. The regional structural grain changes from broadly NNW to NNE-trending in the south, to a more ESE to E–W belt along the northern margin of the block. This is associated with overprinting of an earlier Palaeoproterozoic–Mesoproterozoic structural grain by N-vergent thrust and shear structures associated with the Mesoproterozoic Musgravian and Cambrian Petermann Orogenies. Comprehensive interpretations of aeromagnetic surveys and geology in the Musgrave Block can be found in Rankin and Newton (2002) and Slater (2004). A broader-scale interpretation of the Musgrave Block in relation to reconstruction with the North American Grenville Orogen is outlined by Aitken and Betts (2008).

A more NNW-trending elliptical subdomain is also evident on the western margin of the study area (labelled 'P' on Fig. 13.12). This coincides with the eastern edge of the Petermann Nappe Complex (Young *et al*. 2002).

The mid-level observations (scarlet line-work in Fig. 13.12) show the trends in the deeper blocks of strongly magnetic Musgrave Block material immediately north of the exposed basement in the eastern part of the study area. The abrupt variations in magnetic gradient indicate that the basement–basin margin is a series of fault blocks, with increasing thicknesses of non-magnetic cover to the north, rather than simple unconformable on-lap of the Amadeus Basin sediments.

b) Amadeus Basin.

The southern margin of the Amadeus Basin is structurally complex, with thick-skinned thrusting of Musgrave Block metamorphic rocks to the north. The margin of the basin is interpreted as the line where the magnetic expression of the Musgrave Block rocks changes from clear to fuzzy (best shown in Fig. 13.5), indicating an abrupt change in frequency content of the magnetic data consistent with significant increase in thickness of non-magnetic sedimentary cover.

The sediments and possible volcanic rocks in the SW sector of the basin, adjacent to the Musgrave Block metamorphic rocks, are characterised by weak to moderate magnetic intensities and variable structural grain (recorded as magenta lines in Fig. 13.12). Sediments within the overall area of the foreland molasse basin (Mt Currie Conglomerate, Young *et al*. 2002) are non-magnetic to weakly magnetic, and have a well defined, broadly NW–SE linear structural grain. Deeper expressions of these molasse basin magnetic units suggest the presence of up to 1 km thickness of non-magnetic cover.

To the north and east of this main foreland molasse basin, in the central to western part of the study area (labelled 'B' on Fig. 13.12), there is a broad zone dominated by a volcano-sedimentary sequence with a characteristic blobby magnetic signature (seen clearly in Figs 13.5 and 13.7). While the magnetic bodies in this area appear irregular and scattered, Figure 13.5 strongly suggests the presence of broad regional fold trends. The magnetic units appear to have significant volume and appear at varying depths, suggesting that they are not caused by surficial remnants of the known Tertiary laterite profile. To the east, in the Mt Connor area (Fig. 13.13a), the blobby magnetic units can be seen at increasing depth below non-magnetic Neoproterozoic sediments.

The eastern and northern sectors of the study area (subdomains AB-2, AB-5 and AB-6 in Fig. 13.13a) are dominated by non-magnetic to very weakly magnetic sediments and possible volcanic rocks. The RTP 2nd VD image (Fig. 13.5) shows a series of narrow, weakly magnetic units (red line-work in Fig. 13.12) within the sequence, with strike-extensive NW- to WNW-trending folds evident in the west and north, changing to more strike-limited 'dome and basin' style folds in the SE; the latter are best developed in subdomain AB-2 in the vicinity of Mt Connor. The fold styles and magnetic character are strikingly different from the foreland basin and the blobby magnetic sediments in the south-west.

c) Tertiary palaeo-channels and laterite.

Very narrow, high-frequency, weakly magnetic anomalies in the east and north-east of the area (black units on Fig. 13.12) are probably due to localised residual laterite (mainly ferricrete) surfaces and dendritic palaeo-channels. These are likely to be of Tertiary age.

d) Mid- structural levels.

The 700 m and to a lesser extent the 2000 m spectral depth windows show the complex nature of the Musgrave Block–Amadeus Basin interface, particularly in the eastern part of the study area (scarlet units in Fig. 13.12). The step-wise deepening of the Musgrave Bock material is apparent, as is the progressive thrusting of ESE-trending sequences over predominantly NE basement.

There are three prominent ESE-trending linear magnetic anomalies in the SE of the basin that occur at a depth of 500–700 m (visible in Fig. 13.5 and highlighted by green arrows in Figs 13.12 and 13.13a). These units may define a concealed fold in rocks similar to the blobby magnetic sequence, or they may represent further thrust slices of Musgrave Block material (with associated folding). The near-surface folds in this zone appear structurally anomalous. No other folds of this orientation at this depth are conspicuous in the magnetic data. It is possible that they are related to localised salt tectonic effects associated with salt-bearing members of the Bitter Springs Formation (and therefore of potential interest for hydrocarbon exploration – see Section 13.5).

To the east and north-east, deeper (1–2 km) magnetic bodies trend NE and begin to parallel the basement trends in the central part of the basin. There is clear expression of the E-trending Musgrave Block metamorphic complex thrust over these deeper bodies (plus intervening Amadeus Basin sediments). These NE-trending magnetic features in the deeper basement reflect the more primary Musgravian Orogeny structural grain, whereas the strong E–W structural grain within the shallower Musgrave Block thrust to the north reflects intense overprinting by the Petermann Orogeny.

13.3.4 Shallow structural framework interpretation

The shallow and mid-level magnetic data highlight both the detailed fault margin of the basin–basement zone and broad subdomain partitioning of the basin defined by distribution of differing magnetic signatures and regional structural grains. Figure 13.13a shows these broad solid geology subdomains.

a) Musgrave Block.

The northern margin of the Musgrave Block is sharply defined in the magnetic data for most of its strike extent, with an overall ESE-trending thrust or high-angle reverse fault geometry (N-verging). In the far east of the area, the overall basement–basin contact swings to the east, but individual fault blocks have an ESE orientation. The contact zone is further complicated by numerous linear to arcuate NE- and NW-trending faults (post-thrusting?). Apparent movements along these faults vary, suggesting they have a combination of significant vertical and strike-slip movements.

A second structural level of Musgrave Block basement occurs immediately north of the near-surface basin–basement contact. This is very narrow in the west, but appears up to 20 km wide in the east. This represents a belt of concealed basement blocks overlain by the Amadeus sediments. Modelling (e.g. Fig. 13.15) suggests the blocks are bounded by moderate to steep south-dipping faults. This agrees with the known development of N-vergent thrusting or reverse faulting associated with the Petermann Orogeny within the northern Musgrave Block (see Young *et al*. 2002).

A NE-trending structural corridor (dashed red lines in Fig. 13.13a) appears to partition the broader section of concealed basement in the east from the narrow belt in the west. This structure parallels the structural grain of the concealed (pre-Musgravian?) metamorphic basement rocks, and may therefore reflect reactivation of early primary structures during basin extension and inversion.

b) Petermann Nappe Complex.

In the far west of the area, a partly elliptical magnetic subdomain (PNC) overprints the ESE trend of the Musgrave Block margin. This is part of the NE- to NNE-verging thrust and nappe complex of the Wankeri Detachment Zone and Petermann Nappe Complex (see Young *et al*. 2002).

The exposed part of the Musgrave Block, shown in Section A-B (Fig. 13.20), coincides with subhorizontal thrust sheets and nappes of the Petermann Nappe Complex. The published Ayers Rock 1:250 000 geology map (Young *et al*. 2002) shows scattered outcrops of complexly intercalated Musgrave Block metamorphic rocks and Neoproterozoic sediments within this region. The thickness of the exposed nappe/thrust complex has yet to be determined.

c) Amadeus Basin.

The Amadeus Basin sedimentary sequences within the study area have been subdivided into seven structural and stratigraphic subdomains on the basis of the aeromagnetic imagery. The boundaries between some of these subdomains are broad transitional zones, and probably reflect the presence of underlying basin–basement structures rather than discrete mappable contacts in the field. The simplified stratigraphic column (Fig. 13.13b) shows the major units, unconformities and deformation events and this relates broadly to the interpreted subdomains, but the link from this column to our interpretation is better seen in the (interpretive) cross-section in Figure 13.20.

Subdomain AB-1

This comprises a near-rhombic belt of sediments with weak magnetic signatures. The belt is dominated by the Cambrian Mt Currie Conglomerate (coeval with the Petermann Orogeny), folded in a broad syncline with the underlying Neoproterozoic sediments. This folding is outlined by dark green lines in the Mt Connor area in Figure 13.13a. The south-western margin of the subdomain is a thrust contact with the structurally-overlying Petermann Nappe Complex. At depth, the thrust probably roots into a steeper reverse fault. The subdomain largely represents a foreland molasse basin developed during the Petermann Orogeny.

Subdomain AB-2

This is an irregular belt of broadly E–W folded, weakly magnetic sediments to the eastof the study area. Folding appears broader than that within AB-1, and may reflect:

i) subdomain AB-2 was possibly less affected by the Petermann Nappe Complex deformation;
ii) variations in deformation across the basin due to variations in thickness of salt within the sediments, with consequent variations in salt tectonics during deformation.

The subdomain includes a series of subcircular to elliptical folds with relatively short fold axial trends. The best developed of these is the Mt Connor structure. This fold style is anomalous within the southern Amadeus Basin, where strike-extensive, linear folds predominate. The zone of irregular folds form a broad structural corridor (red lines in Fig. 13.13a), centred on a deeper NE-trending fault corridor evident in the deep-level magnetic data (highlighted by black arrows in Figs 13.18 and 13.19 – see also Section 13.3.5). This structural corridor extends into subdomain AB-5, where it is also coincident with irregular folds.

Subdomain AB-3

This is a broadly ESE-trending belt of sediments and volcanics with irregular, blobby magnetic signatures. The sequence is broadly folded and appears to plunge gently to the east. Possible continuation of the magnetic units below the Inindia beds at Mt Connor to the east suggests the sequence is a regional facies equivalent of the Neoproterozoic Bitter Springs Formation or Dean Quartzite, the basal units of the Amadeus Basin sequence. Rare outcrops of the Dean Quartzite are shown on the Ayers Rock 1:250 000 map sheet.

Subdomain AB-4

This comprises a roughly ESE-trending belt of folded non-magnetic to weakly magnetic sediments, including Neoproterozoic Dean Quartzite, Bitter Springs Formation, Inindia beds, Winnall beds and Cambrian Mt Currie Conglomerate. The contact with the variably magnetic AB-3 sediments is interpreted as an unconformity, with the AB-4 sequence overlying AB-3.

Subdomains AB-5 and AB-6

These are two ESE-trending belts dominated by layered non-magnetic to weakly magnetic sediments with overall ESE- to E-trending strike-extensive folds. Both the magnetic character and fold styles within these two belts are significantly different from those within the southern subdomains. The sediments in this area include units of the Cambro-Ordovician Pertaoorrta and Larapinta Groups, the Silurian-Devonian Mereenie Sandstone and the Devonian-Carboniferous Pertinjara Groups.

The boundaries to AB-5 and AB-6 are broad zones across which fold style and structural grain subtly vary (Fig. 13.13a). The structural corridors possibly overlie deeper-seated intra-basin or basement faults. These deep-seated structures may have partitioned both:

i) sedimentation and development of significant unconformities;

ii) postsedimentation deformation strain.

As previously noted in the description of AB-2, AB-5 also includes a zone of irregular folding, coincident with a zone of broad NE-trending features evident in the 7500 m spectral window (see Fig. 13.17). This is interpreted as a deep, basement-related fault corridor (black arrows in Figs 13.18 and 13.19).

Subdomain AB-7

This comprises a magnetically bland belt of broadly folded Palaeoproterozoic sediments in the SE of the basin. There are no obvious magnetic layers in the sediments in this area. The boundary between AB-7 and AB-5 is a broad, NE-trending structural corridor parallel to but slightly offset from a major NE basement trend partitioning the mid-level Musgrave Block basement. This structural corridor is marked by the change from magnetic to non-magnetic sequences to the SE, and appears to influence the distribution (development and preservation?) of magnetic palaeo-channels and residual ferricrete zones of likely Tertiary age (see Figs 13.5 and 13.13a). This suggests the structural corridor has influenced the Amadeus Basin from early Neoproterozoic deposition to Cainozoic weathering events.

Our analysis of the shallow and mid-level aeromagnetic imagery has added significantly to the recognition of regional stratigraphic and deformation subdomains within the study area, and has outlined the gross geometry of the near-surface and mid-level basin and basement contacts.

Localised low-angle discordances between some of the magnetic layers within the strongly folded sediments of the AB-5 and AB-6 subdomains suggest either localised faults (reverse or thrust?) and/or a significant unconformity not evident in the published regional maps. More detailed integration of the regional mapping with the aeromagnetic data at finer scales is likely to outline further thrust-related structural complexity and may provide insights into stratigraphic variations.

One early observation from our interpretation is an apparent quasi-regular spacing of the four WNW-trending domain-bounding structures across the basin and basement, beginning with the Wankeri Detachment Zone–Petermann Nappe Complex in the west and extending to the east with the NW-trend of the AB-5–AB-6 structural corridor boundary. This may reflect a regular spacing of (early?) deep basin or basement fault zones across the basin (oblique to the primary E–W basin architecture). Very regional-scale gravity data (Fig. 13.16), which will be discussed in the next section, lends support to this observation.

Before moving on to discuss the deeper-level interpretation, we emphasise that observations and interpretation at different levels are interdependent. We have drawn on deeper-level information to compile the shallow interpretation and will certainly reference the shallow work when trying to understand the deeper levels. While we normally form our interpretations in increasing depth order, we must always interrelate and integrate all available data at each stage.

13.3.5 Deep-level interpretation – observation layer

The deep (7500 m) spectral depth window (Figs 13.9 and 13.17) delineates a clear pattern of basement magnetic trends beneath the basin sediments. Selective, localised modelling by Shi (2011, Fig. 13.14) indicates predominant depths of around 6 km, with shallower sources near the Musgrave Block margin and deeper (7–8 km) sources in the north of the study area (Fig. 13.18). The 7500 m spectral depth window includes long wavelength responses over the exposed Musgrave Block which may be a reflection of volumetrically large magnetic bodies and structures within the block rather than deeper, underlying basement.

The exposed Musgrave Block includes both ESE- and NE-trending magnetic belts, reflecting the interaction of earlier (Palaeoproterozoic) NE- trending protoliths and later (Mesoproterozoic–Neoproterozoic) deformational fabrics. The ESE- to E-trending structural grain that dominates the northern margin of the Musgrave Block is repeated within a belt of magnetic sources ~20 km wide, beneath the Amadeus Basin sediments, immediately north of the near-surface Musgrave–Amadeus contact zone. This magnetic fabric is more sharply defined in the 2000 m spectral depth window (Fig. 13.8), suggesting that the dominant depth to these marginal Musgrave sources is of that order.

The more arcuate SE- to SSE-trending magnetic rock units in the west of the area appear related to the NE limit of the NE-verging Wankeri Detachment Zone and Petermann Nappe Complex, together with the foreland basin associated with the Mt Currie Conglomerate. This highlights the depth extent of the thick-skinned NE-verging thrust deformation prevalent in the northern part of the Musgrave Block.

The central and northern parts of the study area are dominated by a series of elongate magnetic features trending dominantly NE. This structural grain contrasts with that of the overlying E–W trending folds of the shallow basin sediments. The intensity and orientation of the deep magnetic sources suggest they reflect the structural grain of the Musgravian Orogeny, relatively unaffected by the strong E–W Peterman Orogeny deformational grain evident along the northern margin of the exposed Musgrave Block. This deep-level structural grain is also seen south of the Musgrave Block in the basement to the Officer Basin (Fig. 13.1).

A series of conjugate NE- and NW-trending faults is evident throughout this structural subdomain.

13.3.6 Gravity data

The study area has sparse gravity coverage, mainly the ~11 × 11 km station program completed Australia-wide in the 1980s. While the variations within the study area appear quite simple, in the broader context, extreme (hundreds of milliGals) variations are associated with the predominantly E-trending Musgrave–Amadeus–Arunta–Ngalia Proterozoic basement and basin provinces (see Fig. 13.1). These are the largest gravity variations in continental Australia and cannot be simply explained in terms of the density distributions attributable to these basement and basin sequences. Analysis and explanation of these variations is beyond the scope of this chapter, but is best expressed as being sourced in lower crustal and upper mantle structures (Fig. 10 in Shaw *et al*. 1991).

Within our study area, extreme low gravity values coincide with outcropping Musgrave crystalline basement, and peak gravity values occur in the central parts of the basin where the thickness of sedimentary cover is over 5 km. The predominant gravity trends are discordant with most of the shallow and deep aeromagnetic trends. However, second-order gravity variations evident in gradient trends do appear to relate to structures seen in the aeromagnetic data and the geology, such that we would anticipate that better gravity quality data could be used to advantage in studying the basin/basement architecture.

13.3.7 Deep structural framework

Integration of our qualitative observations with the local modelling facilitates the compilation of a structural framework for the basement at depths of around 6–7 km (Fig. 13.18).

At the deeper structural levels, attributing particular lithologies or stratigraphic intervals to specific magnetic signatures is seldom achievable, as shown by the complex magnetic sources in the exposed Musgrave Block (Rankin and Newton 2002). Hence, the framework interpretation concentrates on the structural grain, depth to magnetic sources and fault distribution in the basement.

Figure 13.18 highlights the regional faults affecting the exposed and concealed Musgrave Block and possible older basement rocks. These faults have been subdivided into mid-level structures (blue lines) and deeper-level structures (>6 km, magenta lines).

The mid-level faults are dominated by ESE- to E-trending thrust to high-angle reverse faults, forming regional steps in the basement/basin contact (see cross-section, Fig. 13.20). There are several regionally significant NE-trending fault corridors that appear to partition both the more arcuate structures associated with the Petermann Nappe Complex in the west, and other anomalously arcuate structures in the SE. NW-trending structures are minor and subsidiary in this southern part of the study area and may relate to Musgravian age granite intrusions, as suggested in Figure 13.1.

The deeper basement to the north is dominated by weakly arcuate NW-trending faults. These are offset by or partitioned between major NE fault corridors. Although there is no indication in the qualitative interpretation, quantitative modelling suggests the faults are SW-dipping, moderate to high-angle reverse faults. These match the reverse fault geometry along the northern margin of the Musgrave Block. The NE-trending faults are interpreted as normal faults based on their roughly orthogonal geometry to the reverse fault, and evidence of significant vertical displacements of magnetic basement from the quantitative modelling. The vergence of the normal faults in the cross-section is based on the modelled offsets (e.g. Fig. 13.15).

13.3.8 Summary – broad-scale study

A comparison of the structural framework maps for the shallow and deep levels (Fig. 13.19) highlights significant coherent interrelationships between the shallow and deeper basement structures in the southern part of the study area. In the northern sector, interrelationships between the shallow and deeper structures are not particularly obvious. We infer a significant detachment surface between the basal section of the basin and the upper-level fold system in this sector, probably within the Bitter Springs Formation (illustrated in the cross-section, Fig. 13.20). The degree to which the basement faults extend into the sedimentary pile cannot be determined from the aeromagnetic data and there is insufficient outcrop to give tighter constraints. Seismic data would be required to detail these relationships. The coincidence of anomalous fold patterns in the near-surface geology with deep-seated (basement-related?) faults (e.g. the irregular folds associated with the NE-trending fault corridor in subdomains AB-2 and AB-5) indicates that the basement faults have influenced and partitioned the deformation of the sediments throughout the basin.

A brief, qualitative interpretation, combined with some focused quantitative modelling of the aeromagnetic data, has provided an informative, first-pass model of both the detailed near-surface structure and the discordant basement/deep-basin architecture of the southern sector of the Amadeus Basin. This model gives us a solid basis on which to further study the basin and, in particular, to plan the location and extent of seismic surveying.

13.4 DETAILED (1:250 000 SCALE) STUDY AREA

A subarea of the Amadeus Basin study area was reprocessed and reinterpreted at ~1:250 000 scale to examine in more detail the degree of interaction between shallow-level geology and the deep basement structural architecture. We selected an area of ~100 km by 75 km in the north (shown in Fig. 13.19) that featured good definition of layering in the shallow sediments and a range of coherent basement magnetic sources to enable delineation of fault architecture. This area is of potential interest for hydrocarbon exploration because it is likely to contain favourable source and reservoir stratigraphy and may include fold and thrust-related structural traps. Proximity to the Mereenie Oil Field (50 km to the north) and the Palm Valley gas field (80 km to the NE) raises the level of exploration interest (Central Petroleum Ltd 2011). Both the oil and the gas fields lie within the Ordovician Larapinta Group (Pegum 1997; see also Fig. 13.13b) and this interval is well represented within our subarea of more detailed study.

13.4.1 Data processing

The approach to data processing was very similar to that used in the main study area, based on RTP and RTP derivatives. Separation filtering was once again applied, yielding a very clear distinction between deep (9500 m) and shallow (0–400 m) magnetic sources (see spectrum in Fig. 13.21). Three key images were selected for the qualitative assessment. As with the full study area, the greyscale RTP 2nd VD (Fig. 13.24) shows the clearest definition of near-surface magnetic rock units and structures. A coloured RTP 1st VD (Fig. 13.22) gives a useful blend of shallower and deeper sources, while the 1st VD of the 9500 m spectral depth window (Fig. 13.23) best defines the form of the deeper magnetic sources and discontinuities. Note the use of contour lines in this image to provide clearer definition of magnetic gradients.

A more comprehensive program of combined forward and inversion modelling was carried out on the detailed study area, once again by Shi (2011). Twenty-five N–S section lines were defined to co-display model results and observed TMI data. An array of 3-D block models was created in order to achieve a close match between survey and model data (Figs 13.28 and 13.29). The match criteria were based solely on the deep sources. One of the key features of the modelling is the predominance of extensive, strongly magnetic rock bodies at depths of 10–14 km, with significant but more localised subordinate sources at 5–8 km. This gives a valuable insight into and confidence in the patterns defined in the 9500 m spectral depth window. The other striking feature of the modelled sections is the consistency of southerly dip on

the magnetic rock body contacts, in keeping with the tectonic style of the region (Fig. 10 in Shaw *et al*. 1991).

The AUTOMAG software was once again applied to the 9500 m spectral depth window to provide an alternative estimate of depths to magnetic sources. The resulting solutions and depths to source are superimposed on Figure 13.31a. The consistency between the depths derived from AUTOMAG and those inferred from modelling is generally good but, as with most automated depth schemes, there are occasional rogue solutions, and there is a need to evaluate the solutions in the context of both the magnetic data and the geological model for the area.

Our approach to interpretation in this subarea is the same as before with the compilation of shallow and deep observation layers, a thorough interpretation of the shallow section and finally an attempt to link the shallow to the (necessarily) more vague features identified at depth.

13.4.2 Shallow interpretation

The shallow observation layer is shown in the context of the aeromagnetic image and the surface geology in Figs 13.25 and 13.26. The abundance of strike extensive coherent magnetic horizons within the sedimentary sequence provides a sound basis for greatly extending both the stratigraphic and structural picture in the subarea. The interpreted stratigraphic and structural framework is presented in Figure 13.27.

The structure in the shallow-level sediments is dominated by relatively open, ESE-trending folds, with variable (but commonly large) strike extent. Discordances in magnetic layering provide evidence for localised thrusts, asymmetric fold limbs or unconformities. A possible lateral thrust ramp occurs locally near the centre of the area (structural zone oblique to and intersecting fold axial trends), and is coincident with a significant gravity gradient. This is also associated with localised zones of irregular bedding trends in the magnetic data, suggestive of disrupted layering. In the exploration context, it is possible that this is related to localised salt diapirism at depth, given that this tectonic style is known in the NW part of the Amadeus Basin (Dentith and Cowan 2009). This is highlighted as Zone A in Figs 13.25 and 13.26. Two similar zones of locally disrupted bedding trends (Zones B and C) have also been highlighted.

Localised and strike-limited NE-trending mafic dykes are interpreted from a series of linear weakly magnetic anomalies; these are parallel to underlying deep-basement normal faults, and may represent late-stage reactivation of the basement structures.

13.4.3 Deep-level interpretation

Observations on the deep-level magnetic data and reference to the depth determinations (Figs 13.31a,b) show two N–S to NNE-trending strongly magnetic zones within the basement, truncated to the north by NW- and ENE-trending faults. In addition, there are several lower-intensity magnetic zones and/or magnetic gradients forming an ENE- to E-trending structural grain; these are more closely related to the upper level fold trends, and may reflect some partial linking of deep basin structure and upper level folding.

Key model-body depths have been transcribed onto the observation layer. While there is considerable ambiguity and uncertainty surrounding the nature of the deep magnetic sources, the structural patterns and depth variations do provide a basis for interpretation of the deep structure. The range of depths and the nature of the models strongly suggest the existence of a deeper and strongly magnetic basement terrain at depths of 10–15 km (depths marked in black) and a shallower, more weakly magnetic terrain at depths of 5–9 km (depths marked in blue). Depths to this shallower basement terrain increase to the NE, probably reflecting north side down movement on the above-mentioned faults. The interpreted NNE-trending fault shows consistent E block down movement in both the shallower and deeper basement.

The Bouguer gravity data (Fig. 13.32), based on sparse (1 station per ~120 km^2) measurements, show limited correlation with either the deep or the shallow magnetic features. The decrease in gravity to the north is consistent with the thickening Palaeozoic sedimentary section but, as evident in Figure 13.16, the gravity variations are most likely to reflect deep-crustal/upper-mantle structures which do not have clearly related structures in the near surface.

Integration of quantitative modelling of the deep aeromagnetic features with our qualitative observations, and the interpretation of the shallow geology in this subarea, is shown in Figure 13.33. The features of the deep interpretation are:

a) the NW- to ENE-trending faults have likely N-block down, moderate- to high-angle reverse geometries, with displacements on the order of 1.5–2 km;
b) a NNE-trending fault separates the two NNE-trending magnetic bodies, with an E-block down displacement of ~3 km in the south and ~1 km in the north. This is interpreted as a normal fault developed as a transfer structure during NE–SW compressive deformation;
c) the deeper basement blocks modelled show consistent southerly dip on contacts and likely N block up movement, suggesting that the NNE-vergent thrust/high-angle reverse fault tectonics evident near the Musgrave–Amadeus boundary persists into this area.

13.4.4 Summary – detailed study

Our interpretation of the magnetic data suggests there is not a strong similarity in structural trends within the basin sediments and the underlying basement; this is reflected in the cross-section in Figure 13.34, with an inferred decollement either at the sediment–basement contact or within the lower section of the Bitter Springs Formation. The basement geometry defined from the deep magnetic patterns appears to predate basin development but may have undergone some reactivation during both basin deposition and inversion. The NNE-trending normal fault evident from modelling may have acted as a growth fault during early deposition and is probably a regional structure that partitioned strain and fold morphology in the upper-level sediments. The interpreted NW- and NE-trending reverse faults in the basement may also be pre-basin structures reactivated during basin inversion and may have played a role in early basin development (although evidence for this from the aeromagnetic data is minimal). As illustrated in Figures 13.20 and 13.34, the almost complete discordance between the deeper-level reverse faults and the upper-level folding probably reflects the development of a low-angle detachment zone (decollement) within the lower basin sequences that is not directly observable in either the surface mapping or the aeromagnetic data. This may lie within the salt-bearing Bitter Springs Formation, or lower – at the sediment–basement contact.

13.5 WHERE TO FROM HERE? A BRIEF TARGETING EXERCISE FOR HYDROCARBONS

The historic oil and gas fields in the Amadeus Basin are hosted in the Ordovician Larapinta Group, and current thinking (Pegum 1997; Central Petroleum 2011) is that the source rocks are also within this stratigraphic group. Recent exploration (Young and Ambrose 2005) has expanded to include the salt-bearing Bitter Springs Formation and the underlying quartzite units that occur much lower in the basin sequence (Fig. 13.13b). We reiterate that we have not attempted to assess and integrate all available data for this study. There are very limited seismic data and only three wells (located in the eastern part of our study area) which, along with more detailed gravity and satellite data (plus a more in-depth study of the exposed stratigraphy), would form an integral part of the assessment and interpretation of the basin for hydrocarbon exploration. Our purpose in this chapter has been to focus on the aeromagnetic data and highlight their contribution to sedimentary basin assessment.

Our broader-scale interpretation (Fig. 13.19) highlighted the presence of significant, deep fault corridors both within the Amadeus Basin sedimentary section and the underlying crystalline basement. Near the southern margin of the basin, we noted a major change in fold styles across a NE-trending, basin transfer fault corridor, from relatively open ‘dome and basin’ style folds in the Mt Connor area to the west to more linear ESE- to E-trending folds to the east (dashed red lines in Fig. 13.13a). This change in fold style suggests thickness and possibly facies variations within the sedimentary section, across the fault (including variations in salt thickness within the sequence). The transfer fault is inferred to have been active both as a growth fault during sedimentation, and a partitioning structure during basin deformation. It could therefore have acted as a locus for complex faulting within the basin sediments and facilitated salt diapirism.

To the east of this inferred transfer corridor, we have noted the presence of an ESE-trending fold at a depth of ~500–700 m (highlighted by green arrow in Fig. 13.12). This fold is unique in the area, both in its appearance in the magnetic data and its modelled depth. This anomalous structure might also be associated with localised fold and thrust-related salt tectonics that could, if the appropriate source and trap rocks were present, form a localised hydrocarbon trap.

We focus on the subarea of more detailed interpretation for this targeting exercise, making the assumption that this area is available to us, perhaps through acquisition of tenure or grant of access. The area is within 50–80 km of the known hydrocarbon fields at Mereenie and Palm Valley and includes similar stratigraphic sequences as well as a permissive structural style, interpreted from the aeromagnetic data. It can therefore be considered potentially prospective for hydrocarbons. The numerous fold-axial trends evident in both outcrop and in our detailed magnetic interpretation (Fig. 13.33) provide a means to infer potential anticlinal hydrocarbon traps. However, we emphasise that, away from the (very limited) areas of outcrop, our inference of anticlines or synclines becomes tenuous, particularly if there are unrecognised, intervening thrusts within these areas. The likely presence of thrusts within the folded sediments, as proposed in the detailed interpretation, may also enhance the prospectivity of the area, creating potential for blind-thrust-related fold development and localisation of salt-diapir structures. Thrusts may, of course, also breach suitable traps and cause hydrocarbon leakage. Analogous structures with inferred exploration potential have been highlighted from aeromagnetic and gravity data within the western part of the Amadeus Basin (Dentith and Cowan 2009).

One particular zone stands out when the shallow and deep structural level subarea interpretations are compared (Zone A in Figs 13.25, 13.26 and 13.27).

The shallow observations and interpretation show Zone A to be characterised by localised, irregular bedding trends, in marked contrast to the surrounding ESE-trending and more strike-extensive folds. Zone A also coincides with the inferred shallow- to mid-level NW-trending transfer fault zone or accommodation corridor, and overlies the intersection of NW- and NE-trending faults evident in the deep-level interpretation (Fig. 13.35). The obvious structural complexity of Zone A, combined with the likely presence of the Cambro-Ordovician Larapinta group, makes this a worthy starting point for exploration in the study area.

Two other dominantly structural target zones (B and C) associated with irregular bedding trends and changes in structural orientation evident in the shallow magnetic data have been identified.

Zone B lies along the SE extension of the main fold/thrust corridor coincident with Zone A and features an anticlinal structure located between two inferred thrusts. This zone also includes an E–W structural trend evident in the deep interpretation and some indication of local NE-trending structures. The favourable Larapinta Group is present in thrust contact with older rocks that form an anticline potentially cored with the salt-bearing Bitter Springs Formation.

Zone C is associated with a relatively subtle zone of irregular bedding trends and local NNW-trending faults in the near-surface geology underlain by NNE trends in the deep (~10 km) basement. The stratigraphic interpretation here infers the likelihood of Bitter Springs Formation occurring in complex anticlinal structures beneath younger sediments.

Zone D comprises two en-echelon anticlinal structures in the Bitter Spring Formation and Zone E takes in an area along strike to the SE where much the same stratigraphic intervals interact with our inferred oblique transfer zone.

We selected these areas as potential target zones for hydrocarbons using simple and quite general structural and stratigraphic criteria in an area of very limited outcrop and almost no prior exploration. We acknowledge that more in-depth analysis of local 'play-styles' would normally take place as part of the targeting process: However, using our interpretation of the shallower and deeper geological features from the aeromagnetic data, we now have a basis on which to plan on-ground exploration. The next phase of exploration would be acquisition of reconnaissance seismic reflection data: We have laid out an initial plan (shown in Fig. 13.35) that covers our target areas with dip lines, and is linked by lines more parallel to the regional strike. This line layout (totalling 350 km) would provide a wide range of information on structure and stratigraphy in addition to investigating the key structures and target areas inferred from our aeromagnetic interpretation.

13.6 CONCLUSION – AMADEUS BASIN STUDY

We have illustrated the range of geological inference and interpretation that can be sourced from basic analysis of good-quality aeromagnetic survey data in a complex sedimentary basin. The area chosen for the illustration has poor outcrop, very limited gravity and almost no published seismic data. Our quantitative analysis of the aeromagnetic data has been integrated with qualitative observations and a focused geological rationale. More intense modelling of the aeromagnetic data could be applied to refine the geometries of the (abundant) magnetic rock units, but at this stage this would add little to our integrated working hypothesis on the geology and structure of the study area. While acknowledging that more in-depth assessment of the exposed geology, possibly including integration of airborne radiometric and satellite data, would normally take place along with the aeromagnetic interpretation, our work highlights the key role that aeromagnetic data can play in defining an initial framework for exploration.

Analysis of the shallow and deep structures within both the regional and detailed areas has highlighted preliminary target areas for hydrocarbon exploration. Our concluding graphic (Fig. 13.36) shows the small amount of exposed basin geology, with our target areas and proposed first-pass seismic program superimposed. Comparing Figures 13.35 and 13.36 gives a measure of the amount of new geological information provided by the aeromagnetic data and the degree to which it extends our view of the subsurface.

Testing of the interpretations and further advancement of both the geological understanding of the area and hydrocarbon prospectivity will require seismic surveys and, ultimately, drilling. These are high-cost exploration activities, so optimisation of their location is very important. The cost of the aeromagnetic survey coverage used in this study was less than the cost of one 1000 m-deep drill-hole and considerably less than the cost of the proposed initial seismic program. We contend that a modest amount of interpretive work, such as was carried out in this study, provides a sound basis for locating such seismic surveying, highlighting the cost-effectiveness of high resolution aeromagnetic surveys in sedimentary basins.

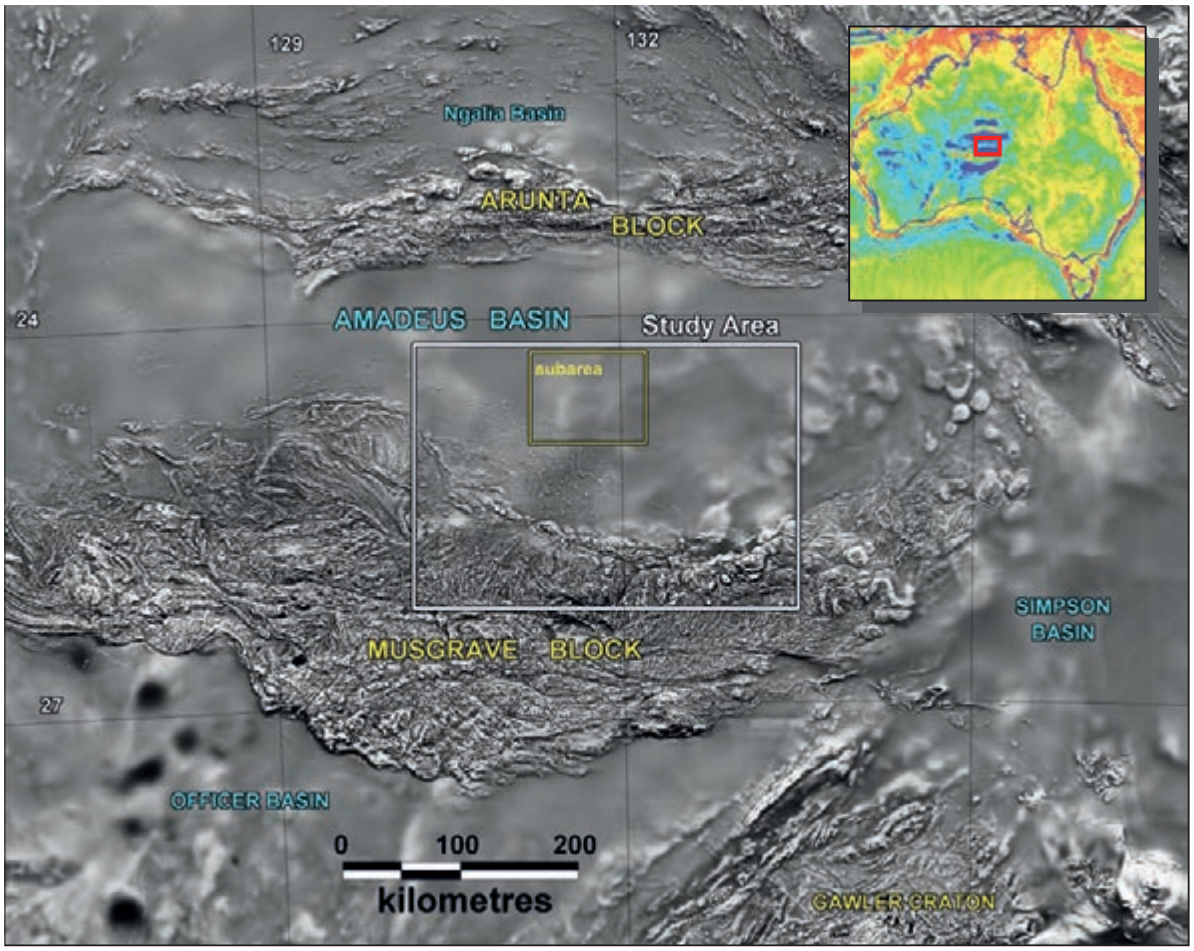

Figure 13.1: Location diagram, Amadeus Basin study area. Underlay is the TMI aeromagnetic grid of Australia. Inset shows the location in the continental context; underlay is the Bouguer gravity grid of Australia. Note the extreme gravity variations in and near the study area. Data courtesy Geoscience Australia.

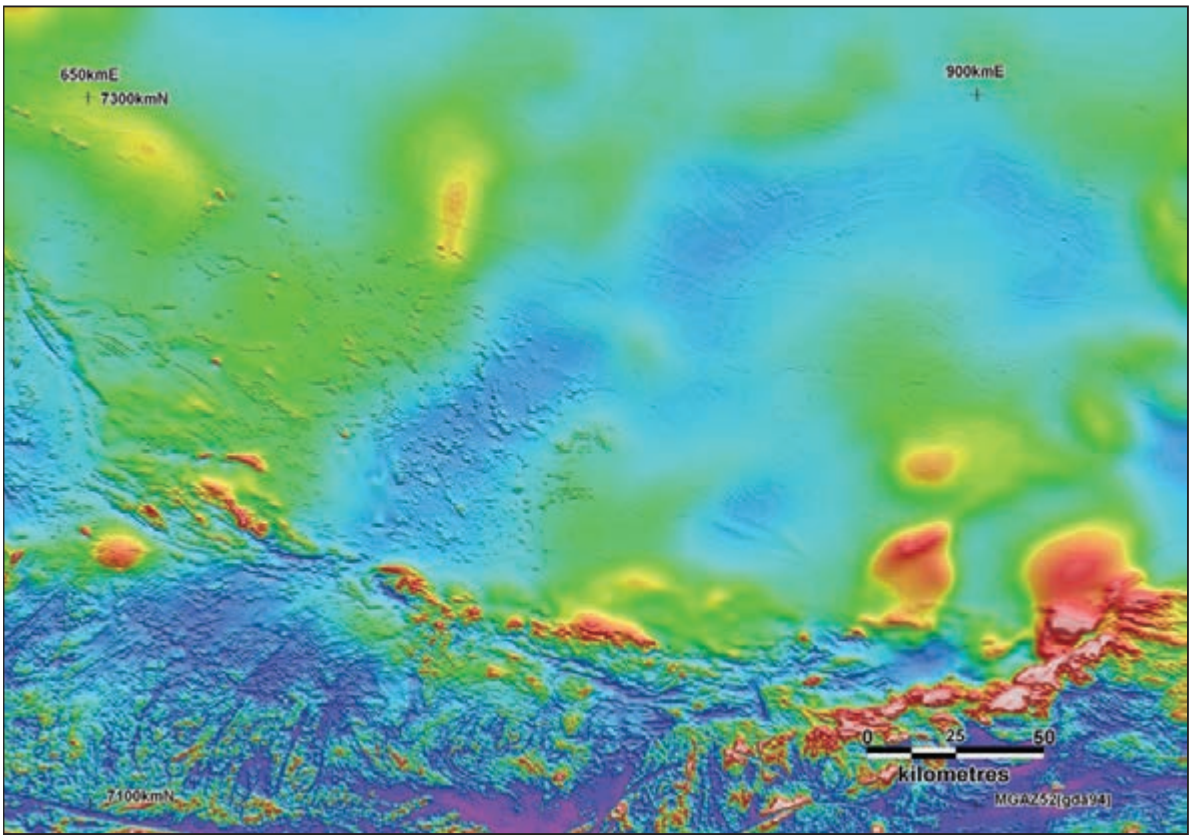

Figure 13.2: Amadeus Basin study area, TMI image, shaded (NE), optimised colour stretch. Data range is 3700 nT. Image derived from the same grid as that in Figure 13.1.

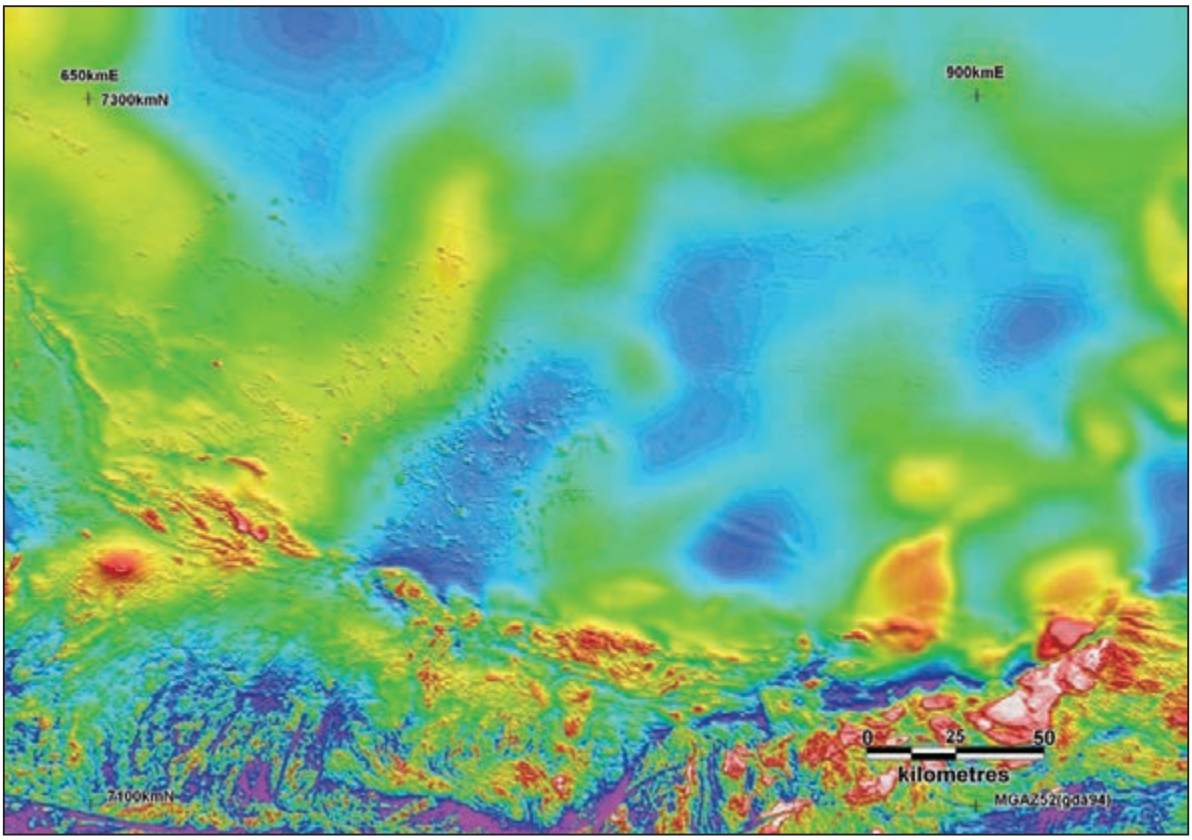

Figure 13.3: Amadeus Basin study area, RTP image, shaded (NE), optimised colour stretch. Data range is 3300 nT.

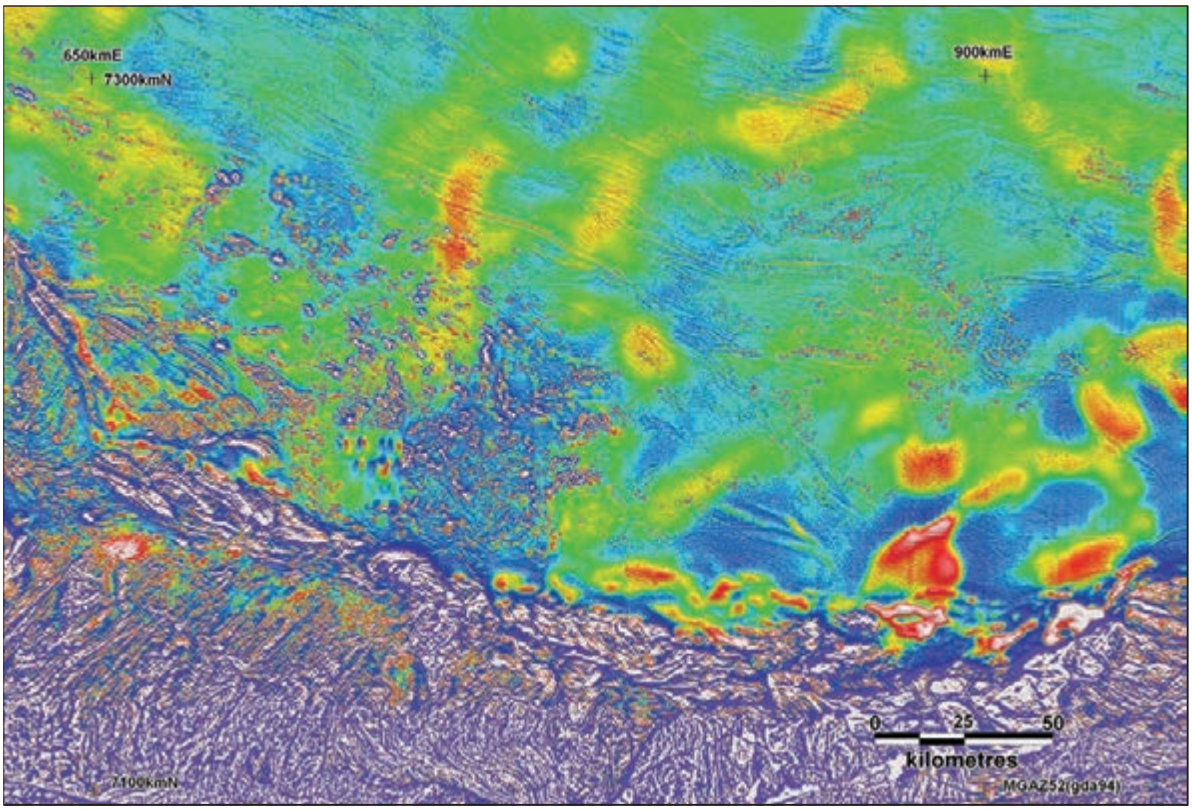

Figure 13.4: Amadeus Basin study area, RTP 1st VD image, shaded (NE), optimised colour stretch.

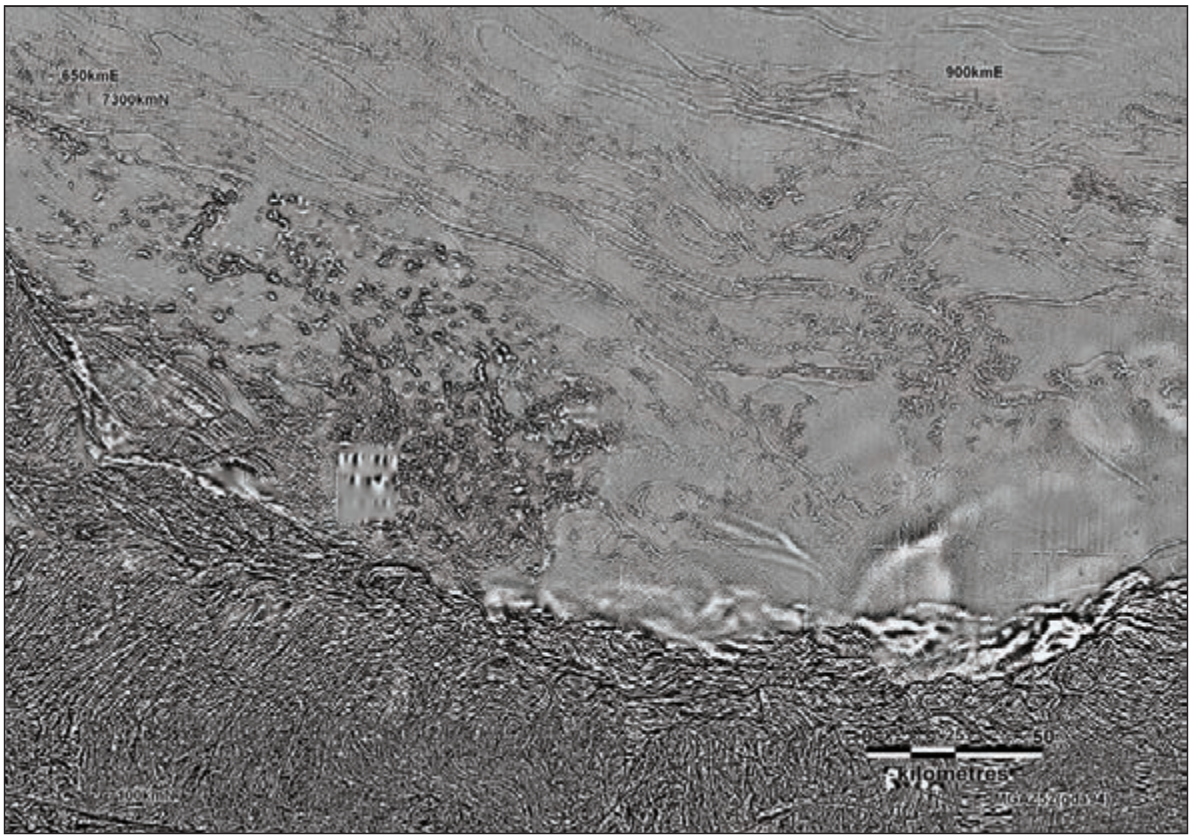

Figure 13.5: Amadeus Basin study area, RTP 2nd VD image, greyscale, optimised stretch.

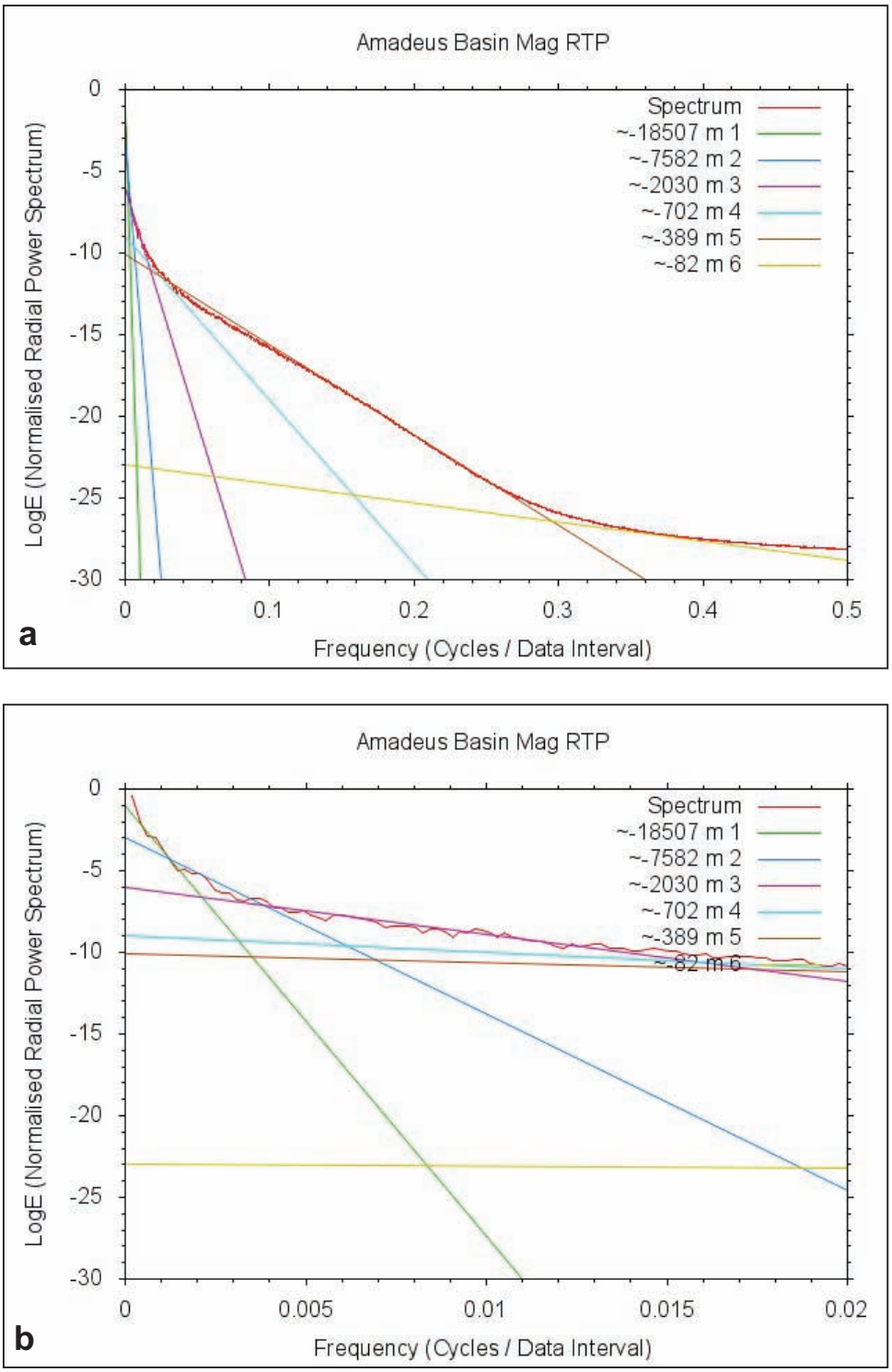

Figure 13.6: Radially averaged power spectrum of the Amadeus Basin study area, RTP grid. a) The entire spectrum. b) An enlargement of the low-frequency (deeper) part of the spectrum.

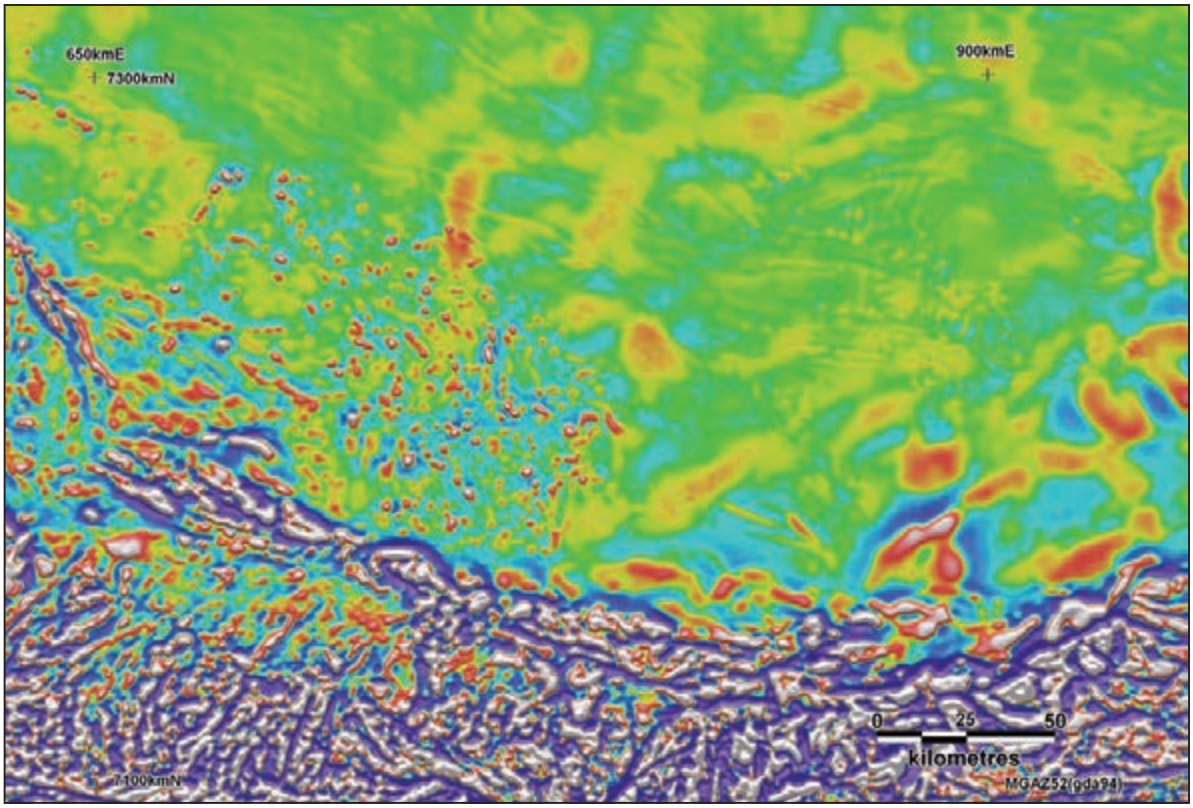

Figure 13.7: Spectral depth window 700 m, RTP 1st VD optimised colour image.

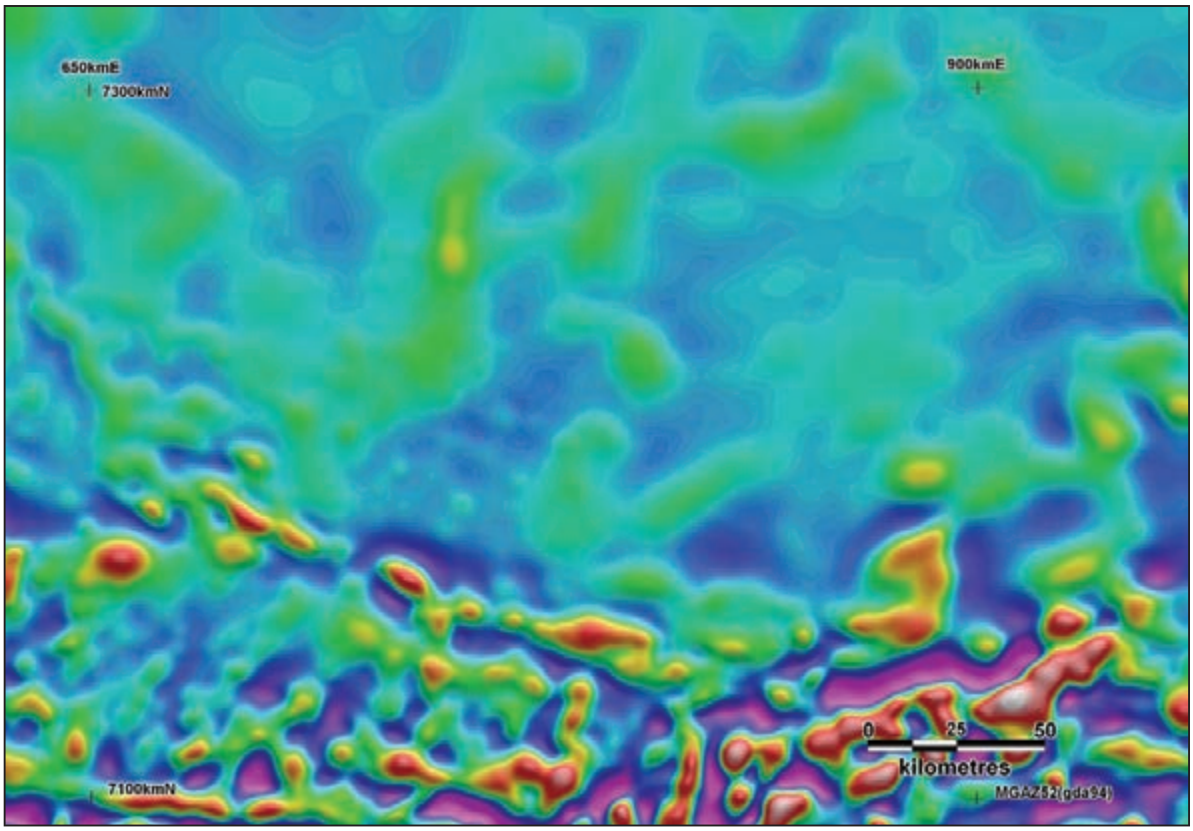

Figure 13.8: Spectral depth window 2000 m, RTP 1st VD optimised colour image.

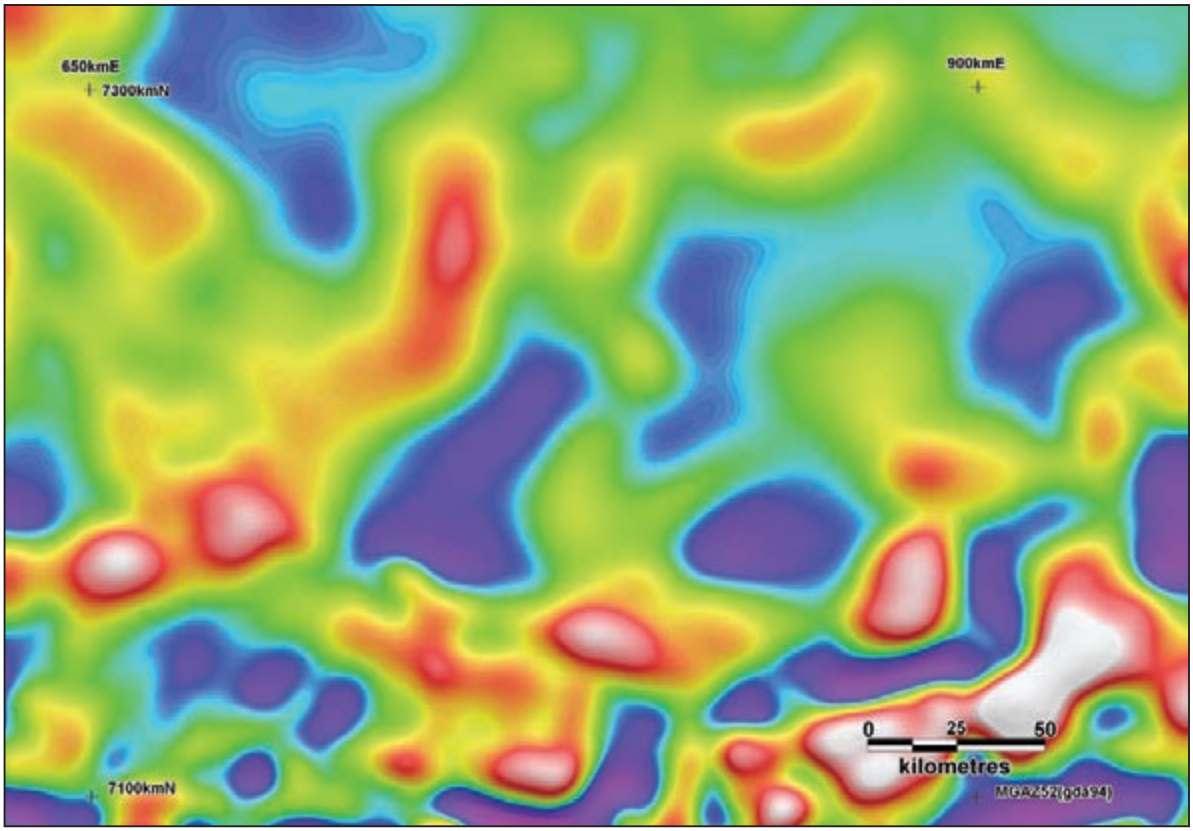

Figure 13.9: Spectral depth window 7500 m, RTP 1st VD optimised colour image.

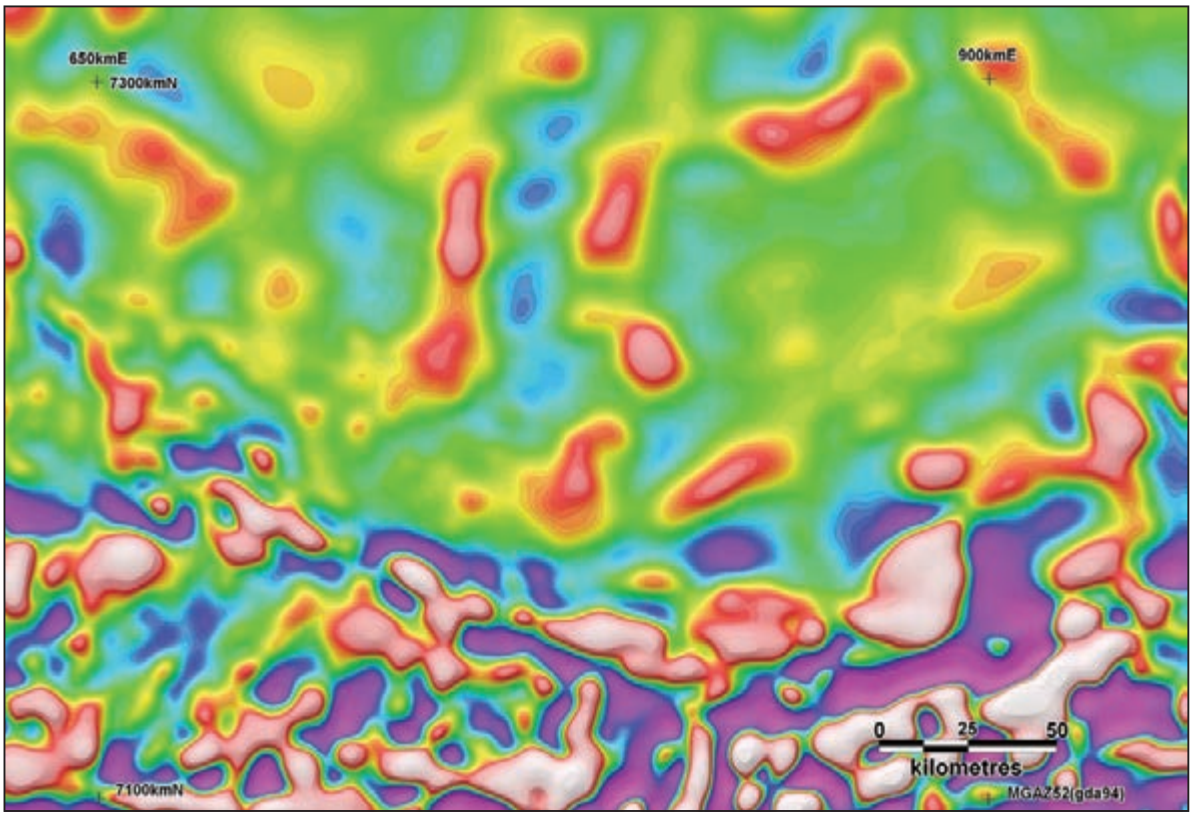

Figure 13.10: 10–60 km wavelength band-pass filter on RTP grid, optimised colour image.

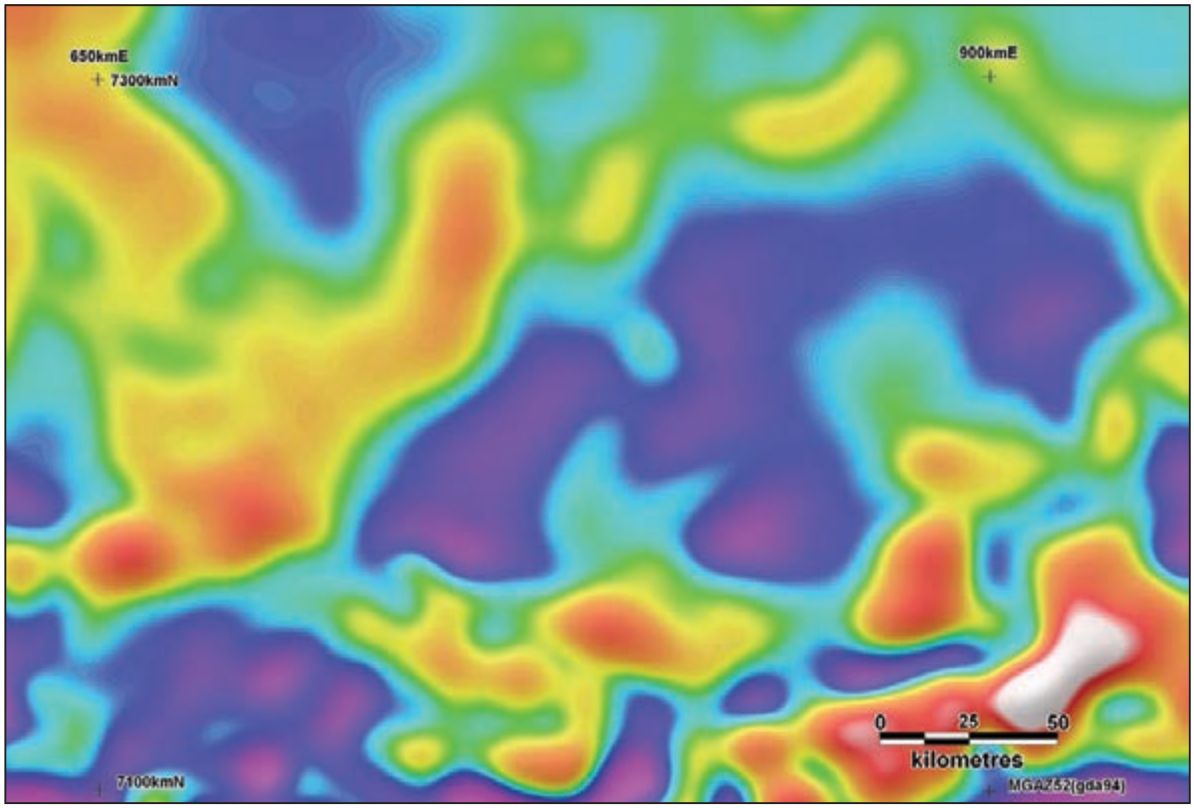

Figure 13.11: >20 km wavelength low-pass filter on RTP grid, optimised colour image.

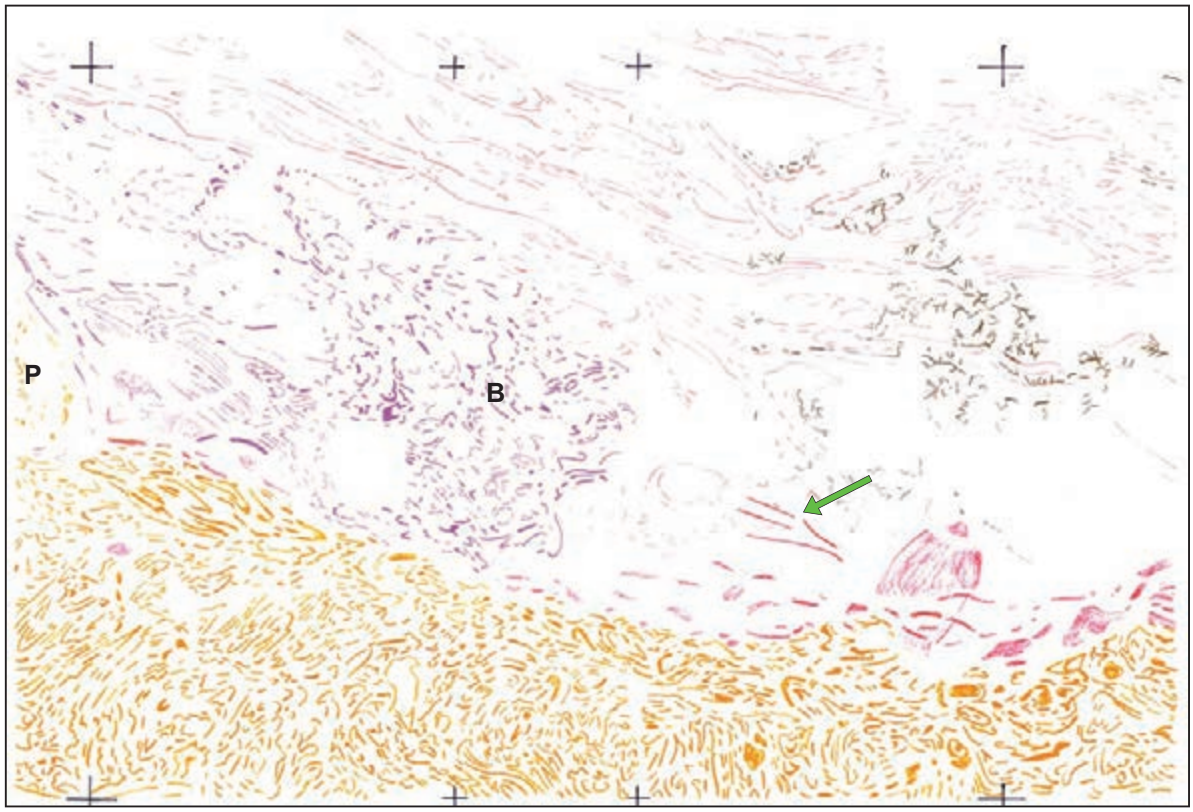

Figure 13.12: Shallow observation layer, based mainly on RTP 2nd VD image. Refer to text for key to observation.

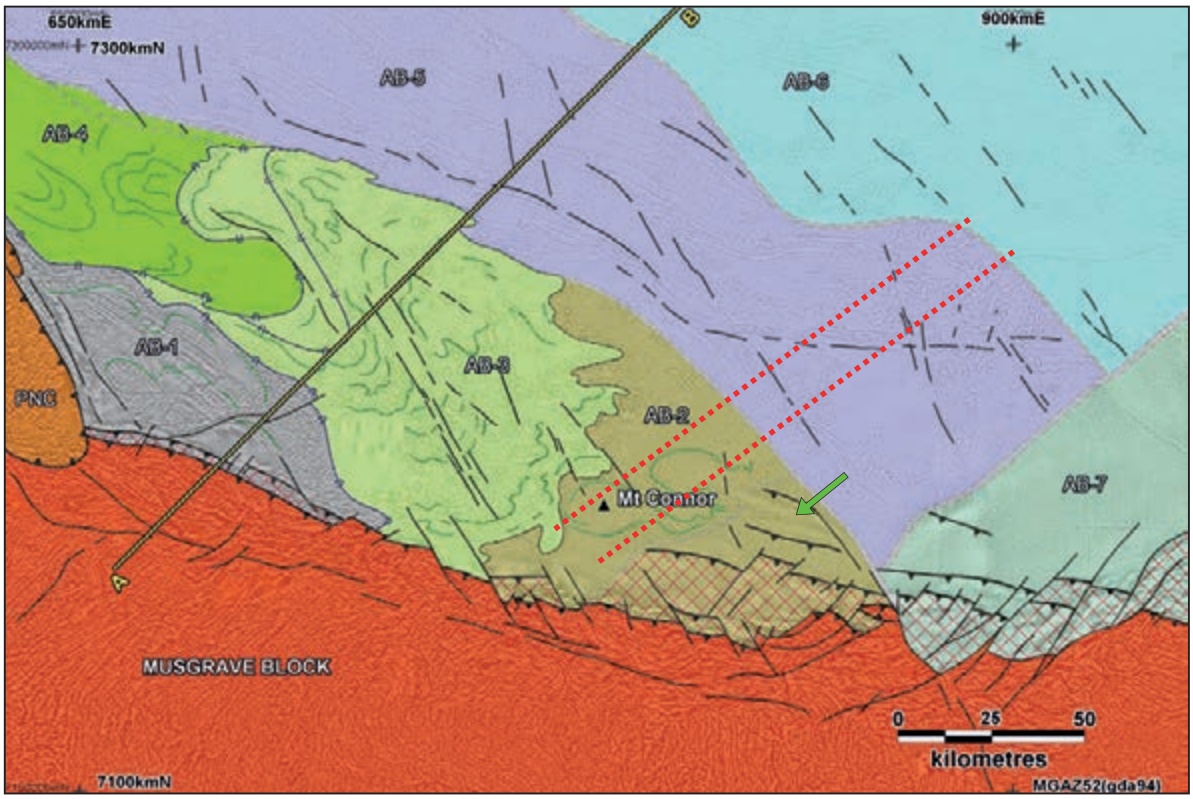

Figure 13.13a: Shallow solid geology interpretation with RTP 2nd VD underlay. A–B is the cross-section line (see Fig. 13.20). Refer to text for description of structural domains.

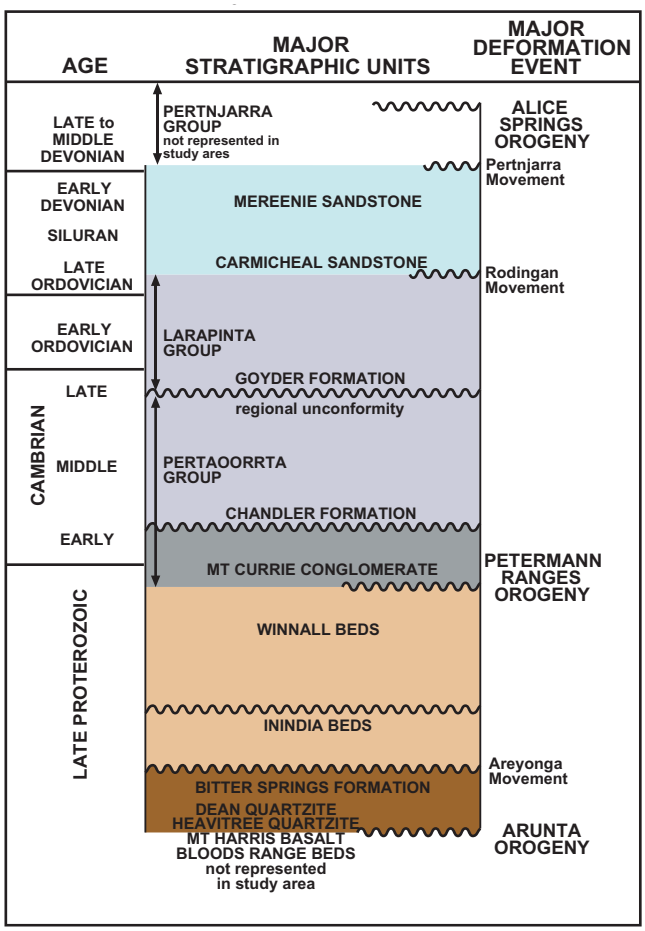

Figure 13.13b: Simplified stratigraphic column (adapted from Shaw 1991). The colouring of intervals relates directly to the interpreted cross-section in Figure 13.20 and in a more general sense to the structural subdomains in Figure 13.13a.

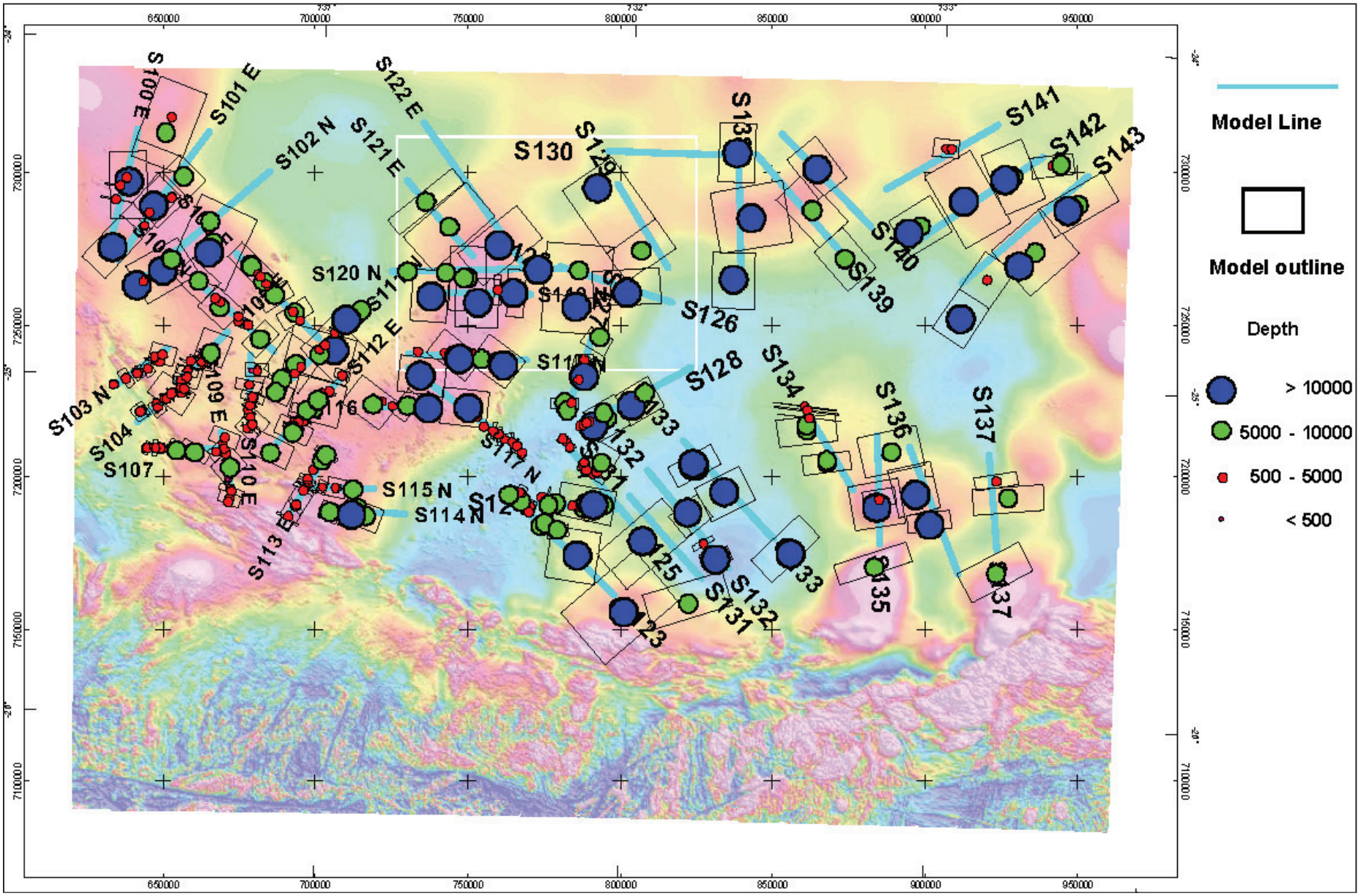

Figure 13.14: Summary of regional modelling by Shi (2011).

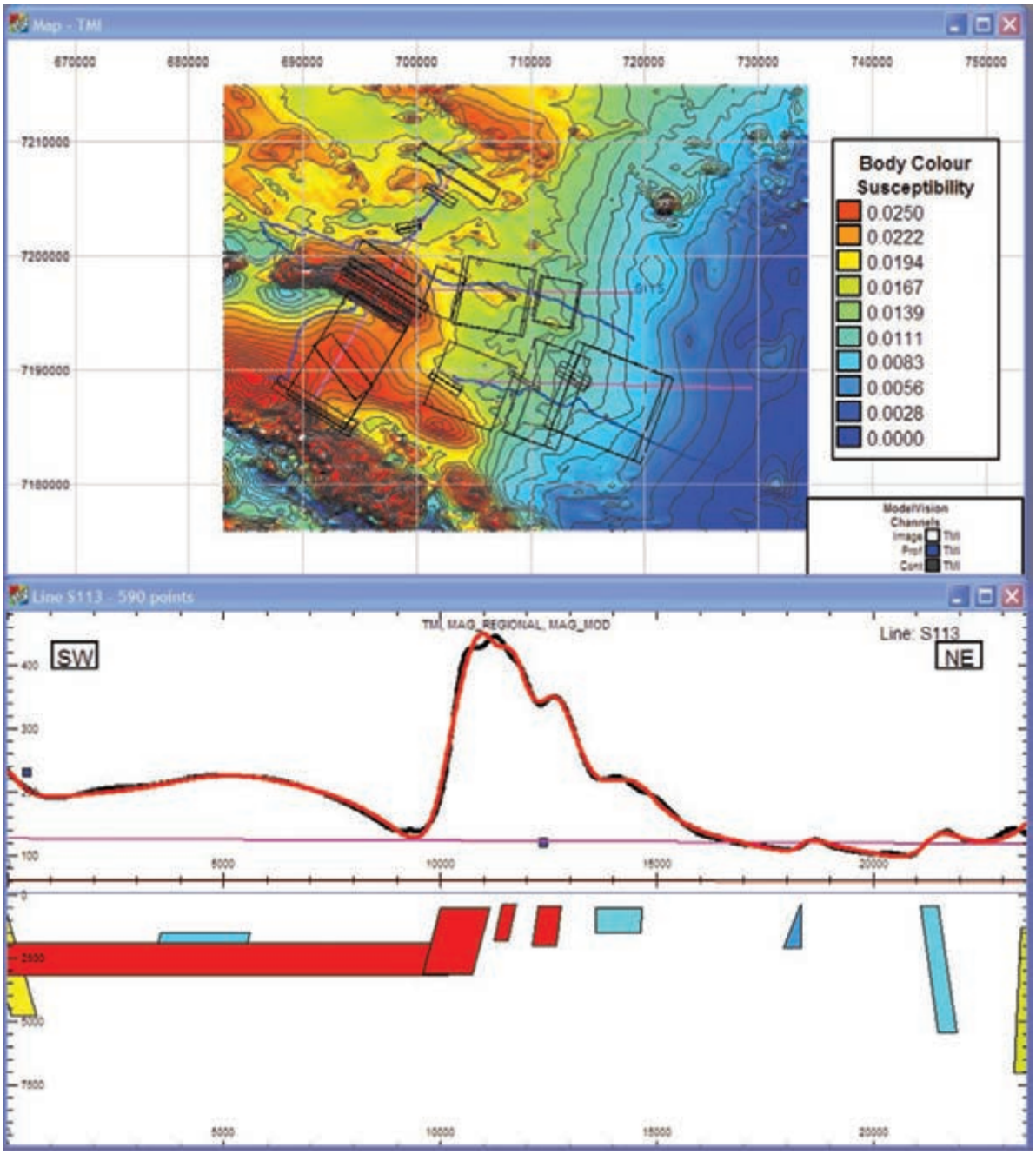

Figure 13.15: Example of modelled profile (S113 from Shi 2011).

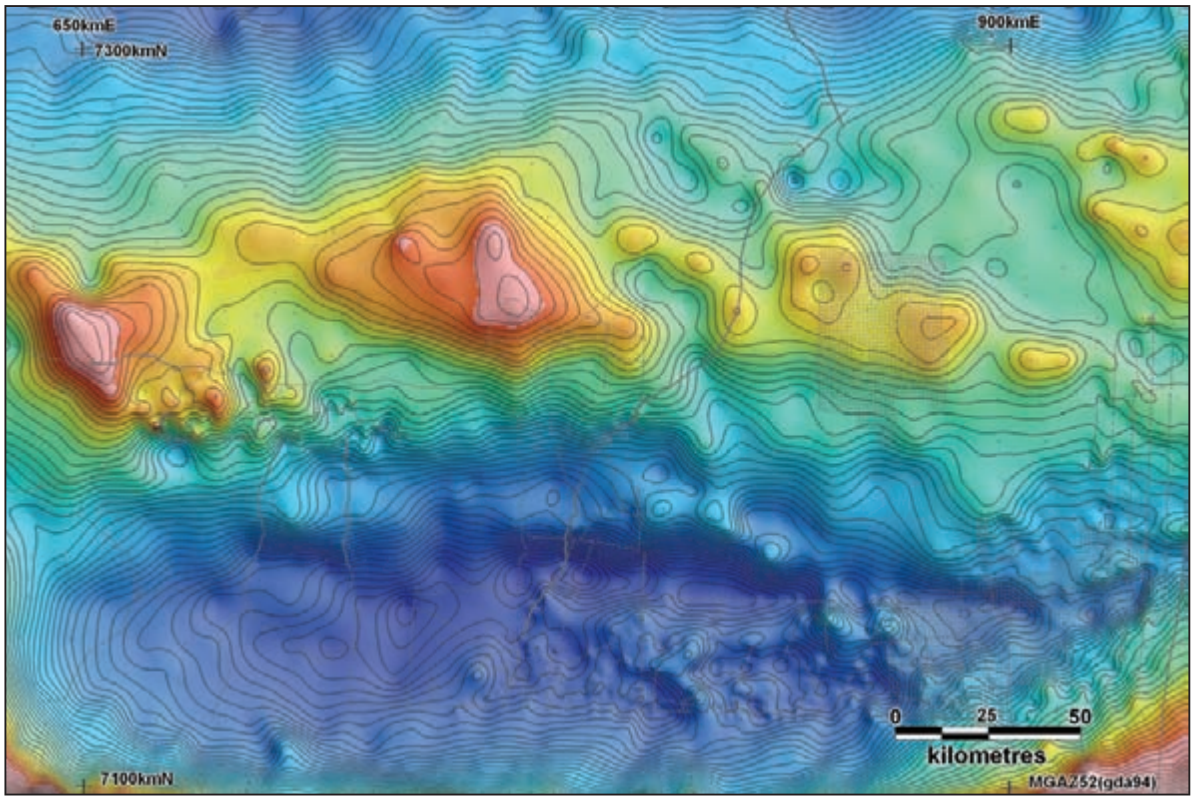

Figure 13.16: Bouguer gravity (contour interval 2 milliGals, 20 gu). Grey dots are station locations. Data courtesy Geoscience Australia.

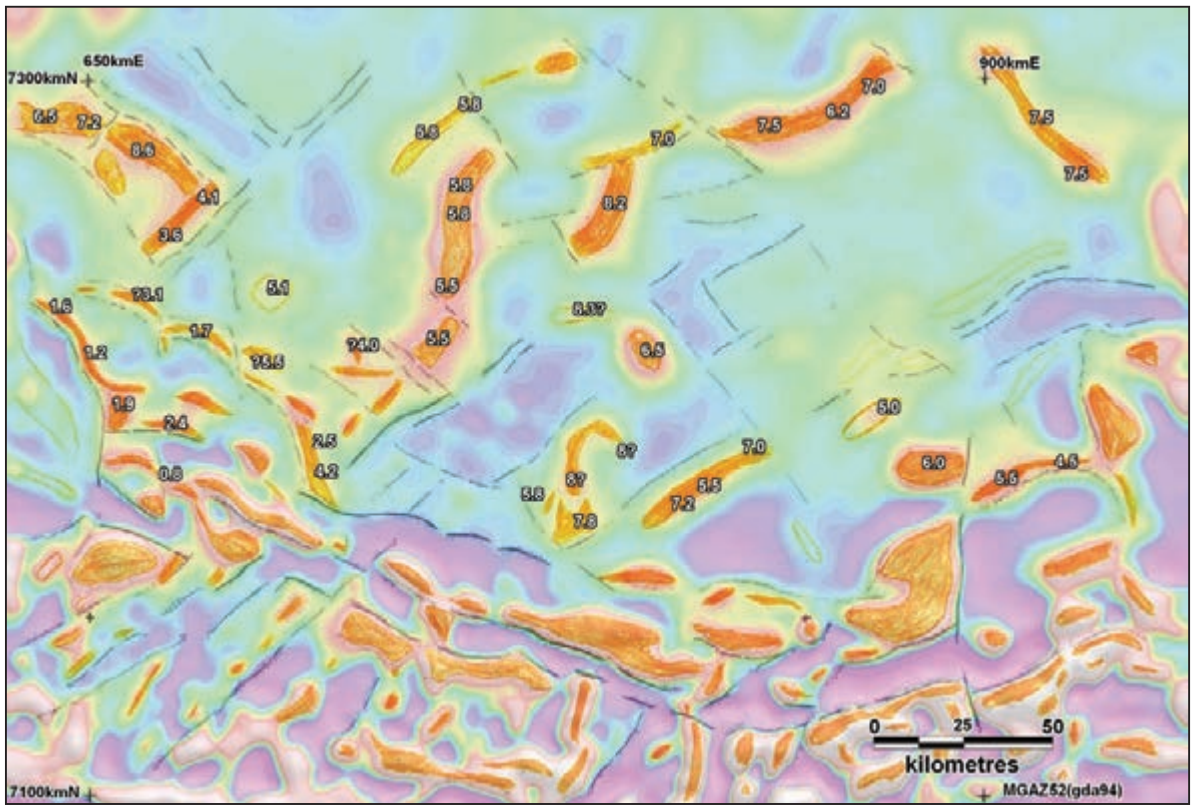

Figure 13.17: Deep aeromagnetic observation layer on 7500 m spectral depth window. Depths in km from modelling shown in Figure 13.14.

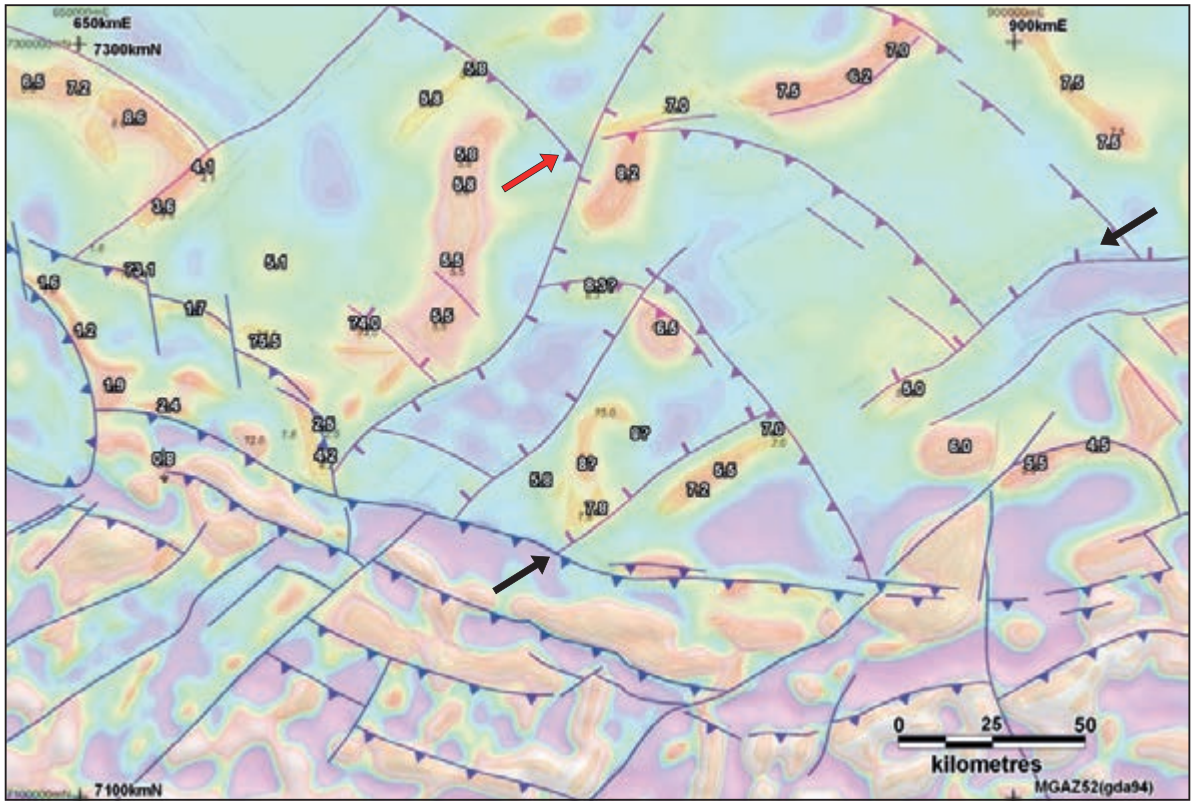

Figure 13.18: Deep structural framework on 7500 m spectral depth window.

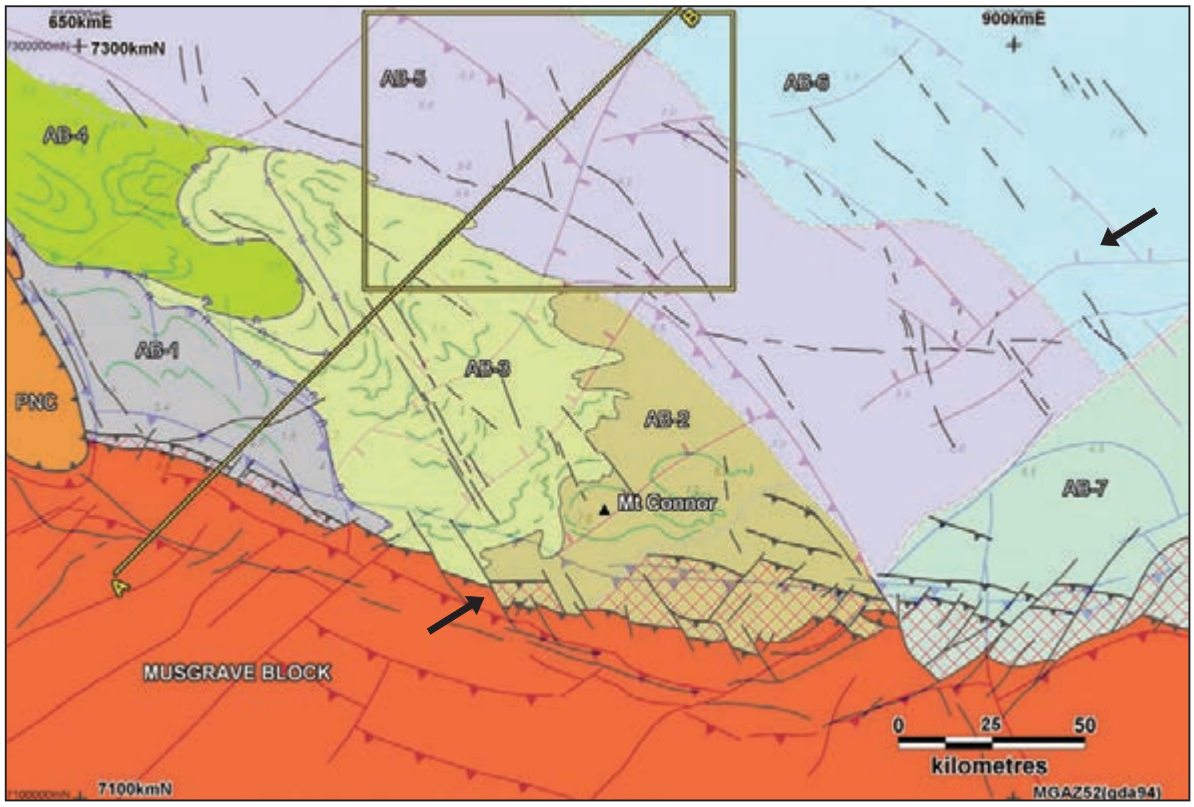

Figure 13.19: Shallow and deep interpretations superimposed. A–B is the cross-section line shown in Figure 13.20 and the yellow rectangle shows the detailed subarea analysed later in this chapter.

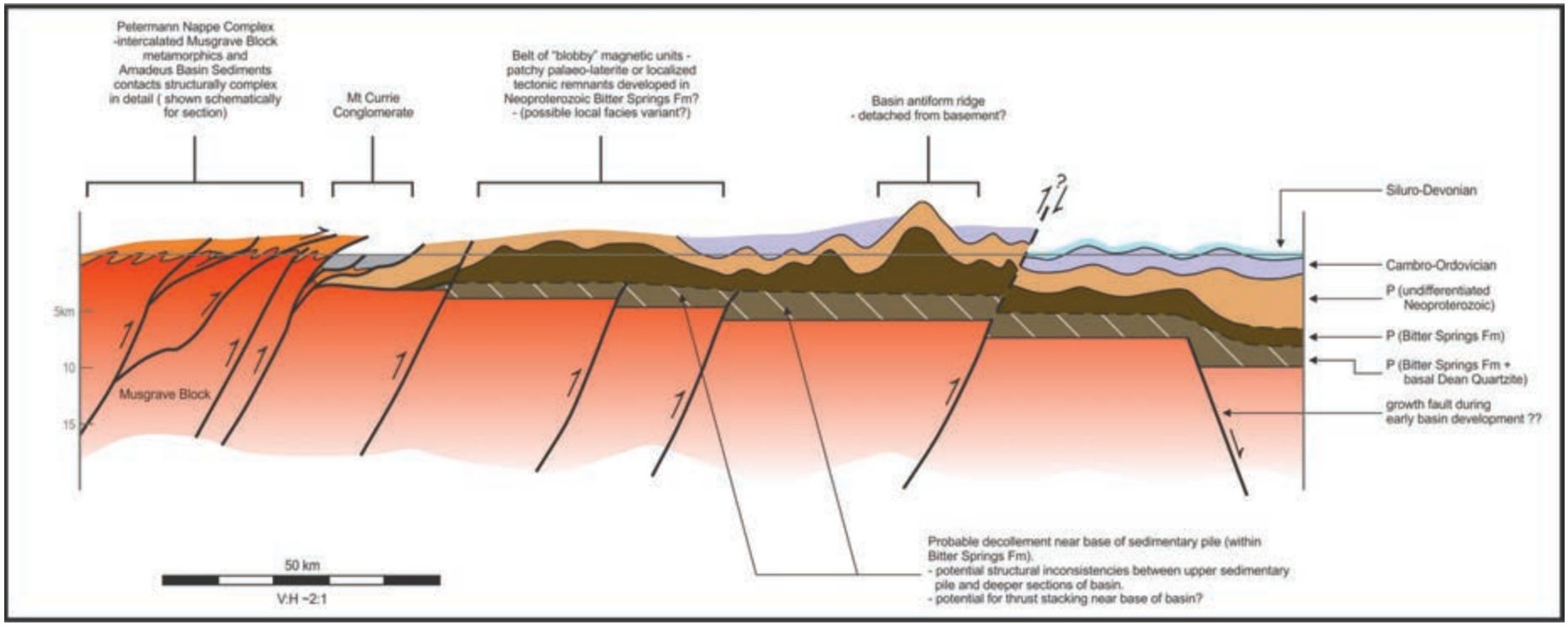

Figure 13.20: Interpreted cross-section A–B. See Figure 13.19 for location.

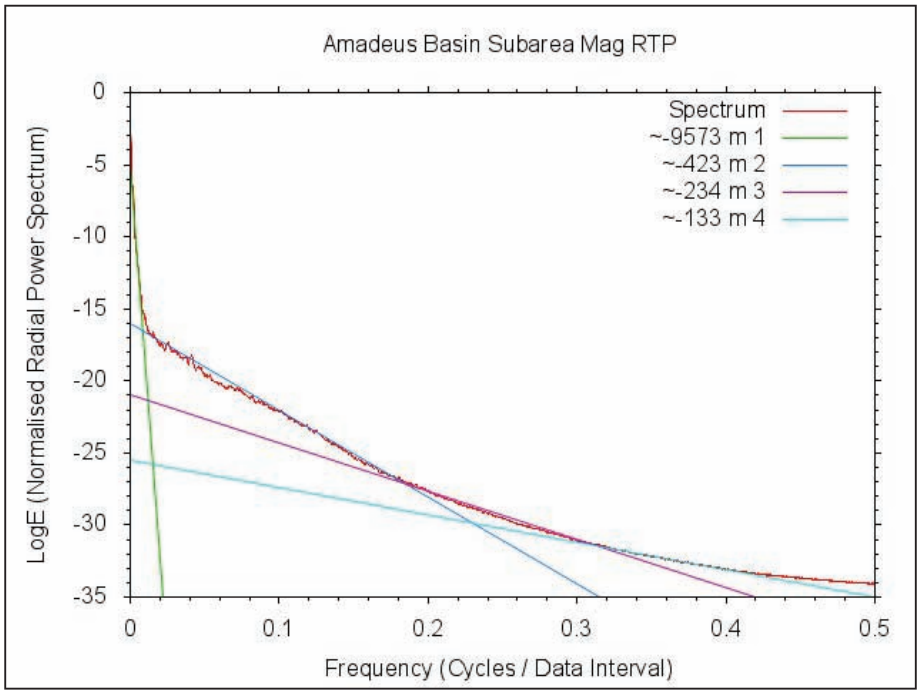

Figure 13.21: Detailed study subarea. Radially averaged power spectrum, RTP grid.

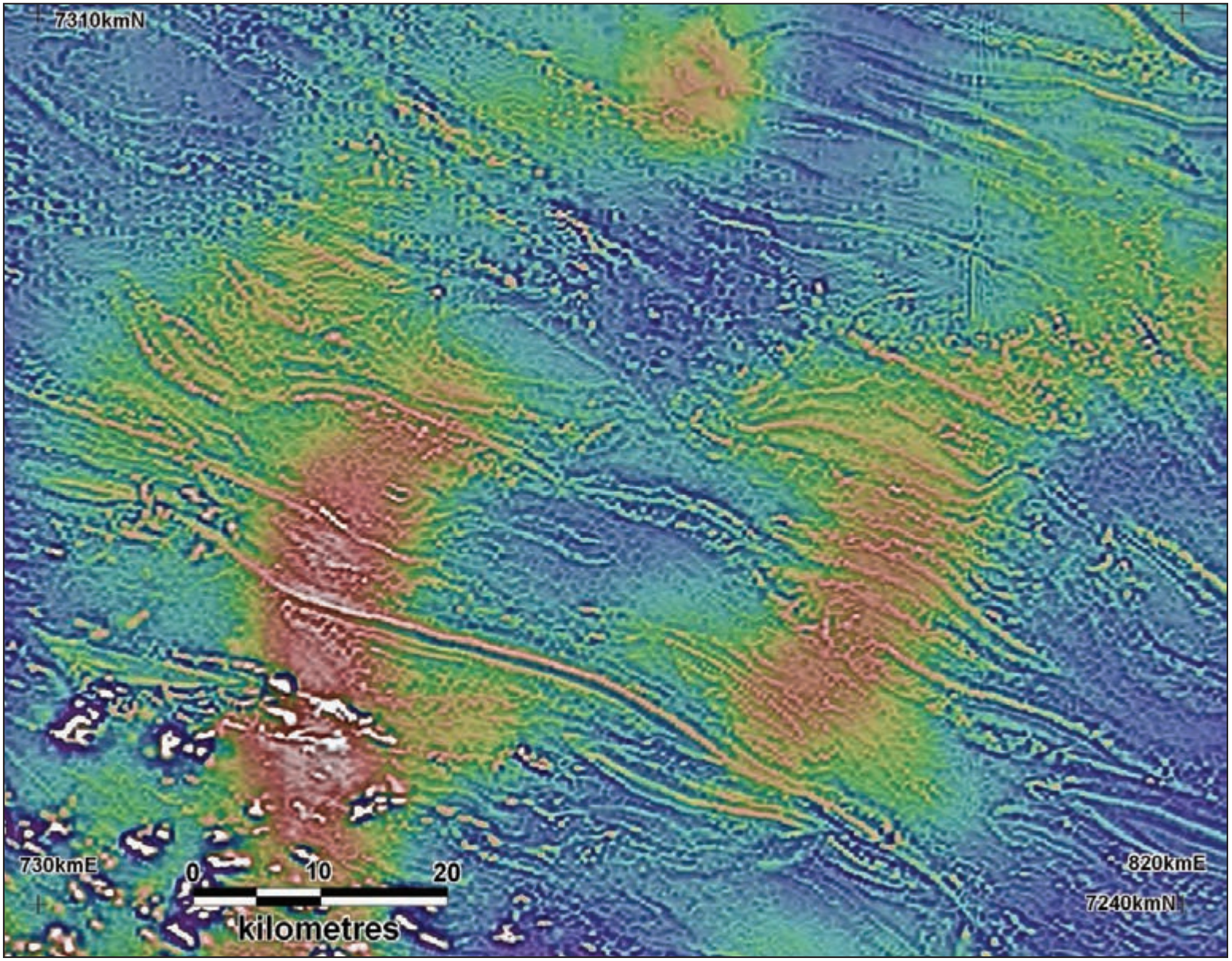

Figure 13.22: Detailed study subarea. RTP 1st VD image, shaded, optimised colour stretch.

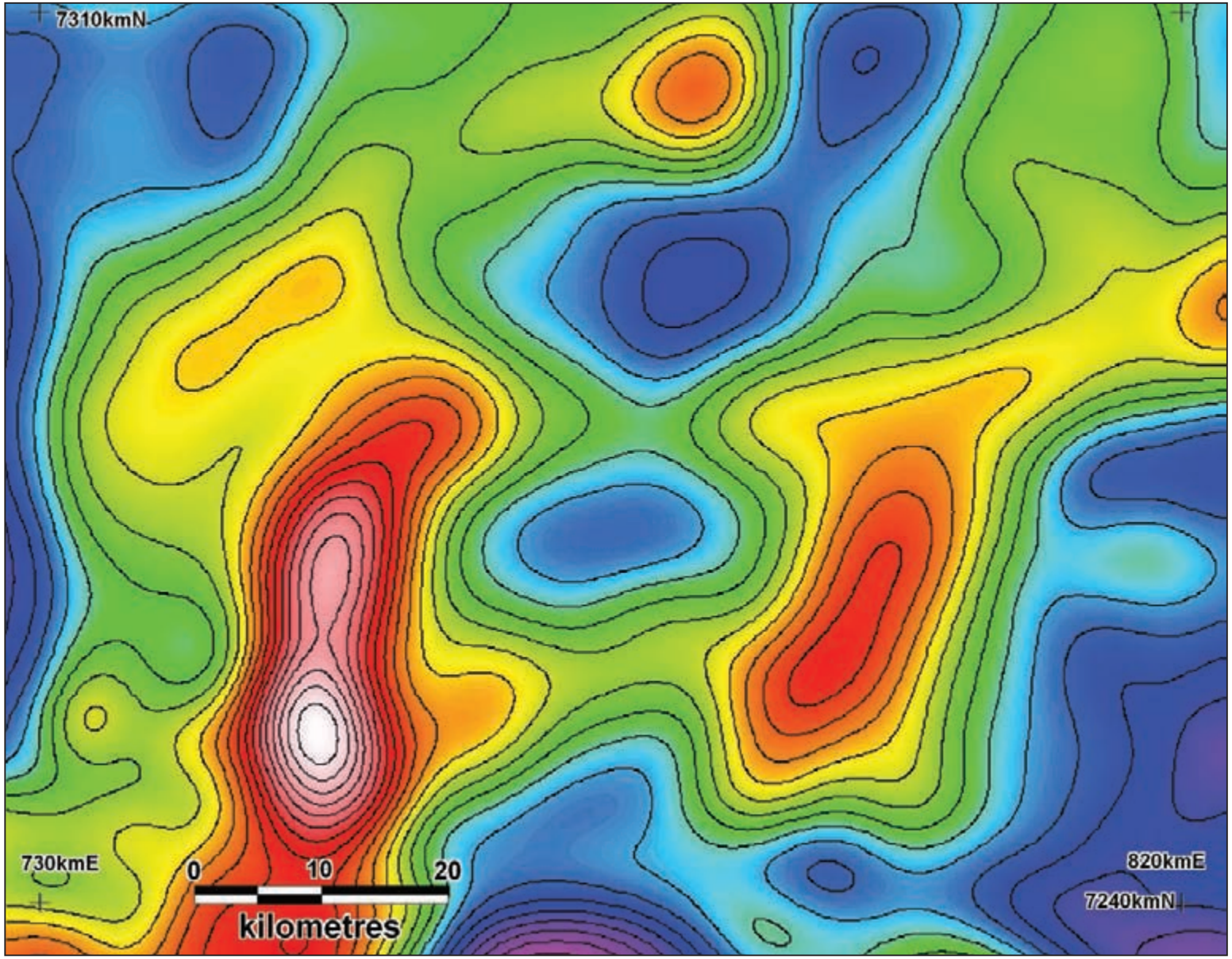

Figure 13.23: Detailed study subarea. Spectral depth window 9500 m, RTP 1st VD image.

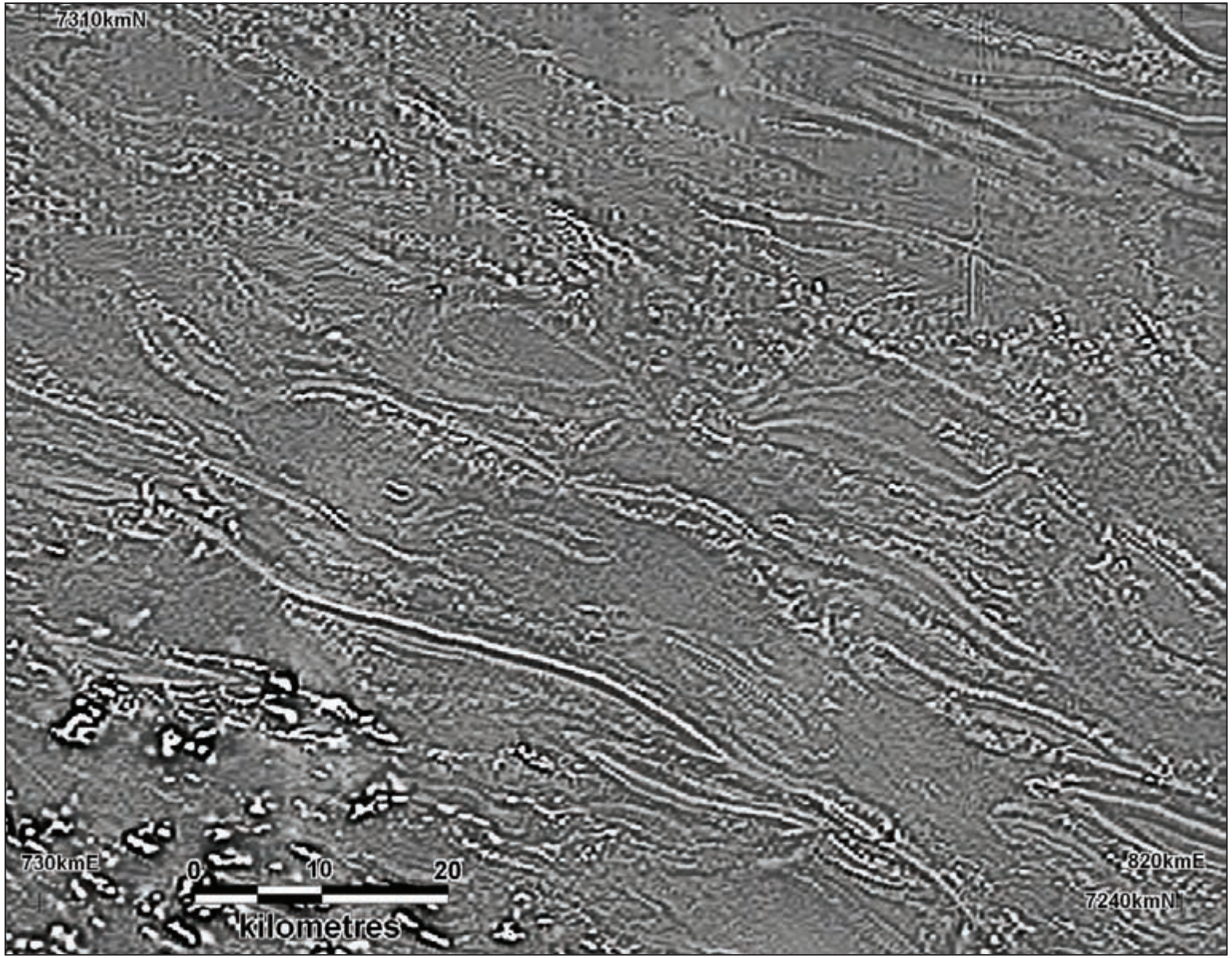

Figure 13.24: Detailed study subarea. RTP 2nd VD image, greyscale, optimised stretch.

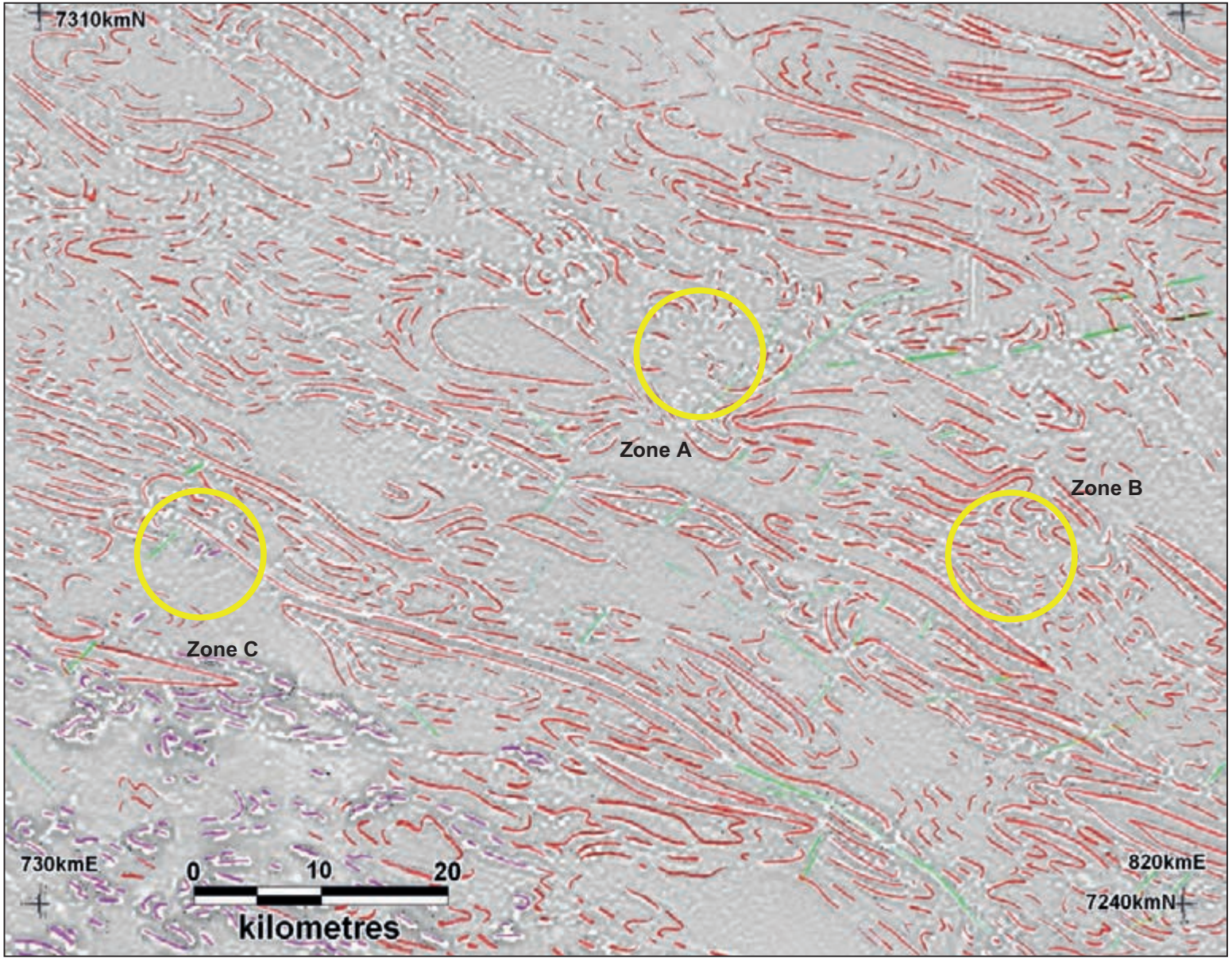

Figure 13.25: Detailed study subarea. Shallow aeromagnetic observations on RTP 2nd VD image.

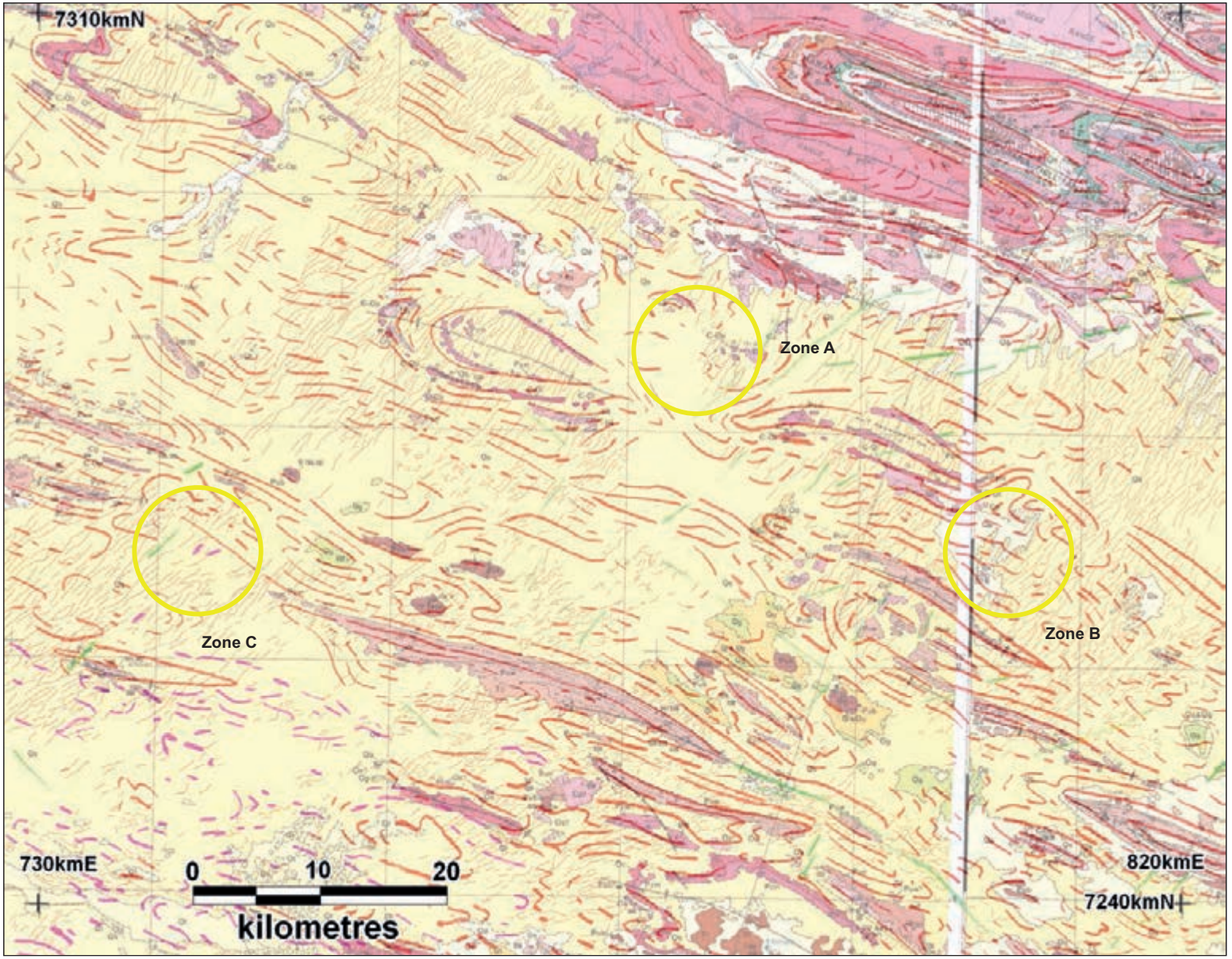

Figure 13.26: Detailed study subarea. Shallow aeromagnetic observations on outcrop geology.

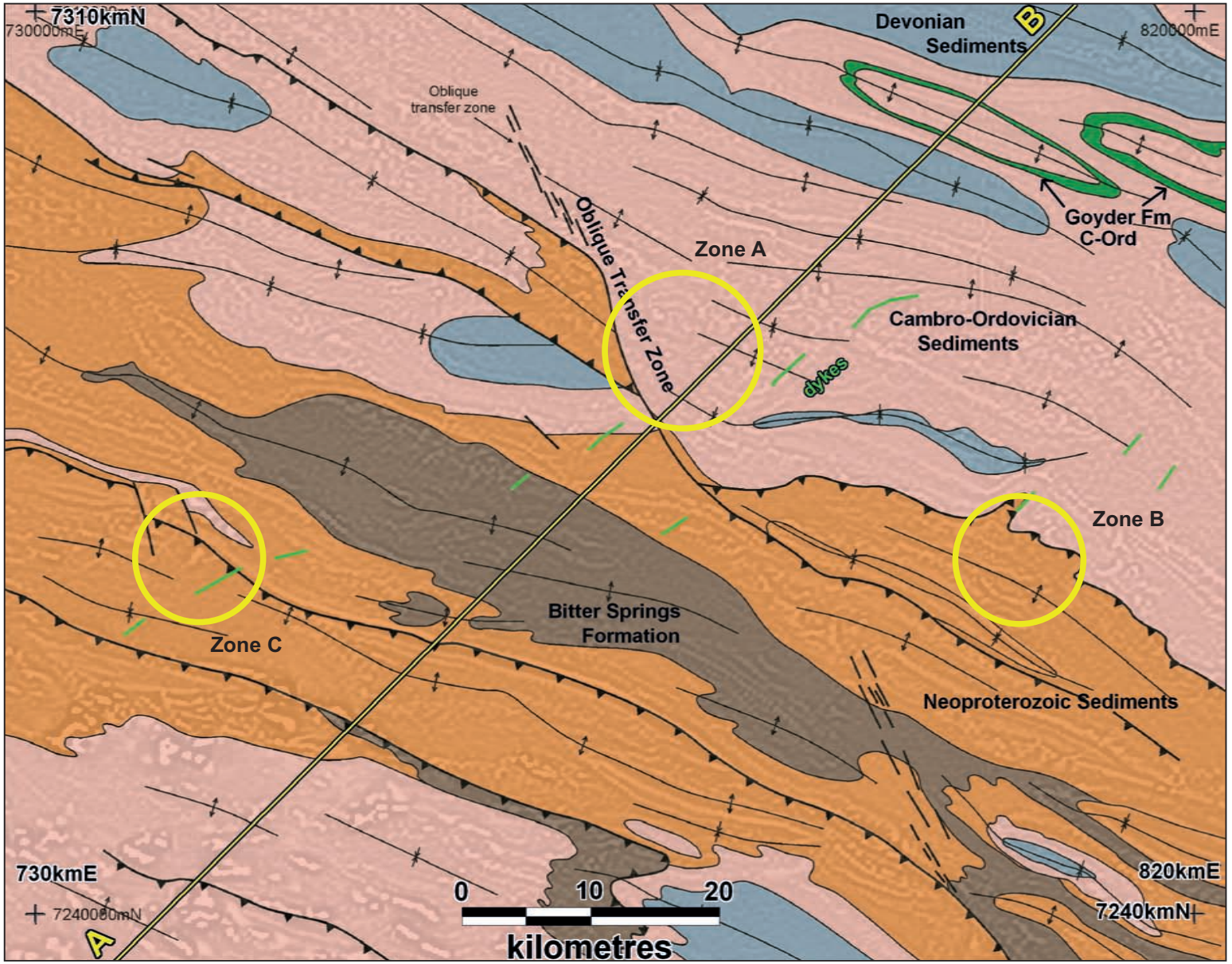

Figure 13.27: Detailed study subarea. Shallow solid geology with RTP 2nd VD underlay (see Fig. 13.34 for cross-section).

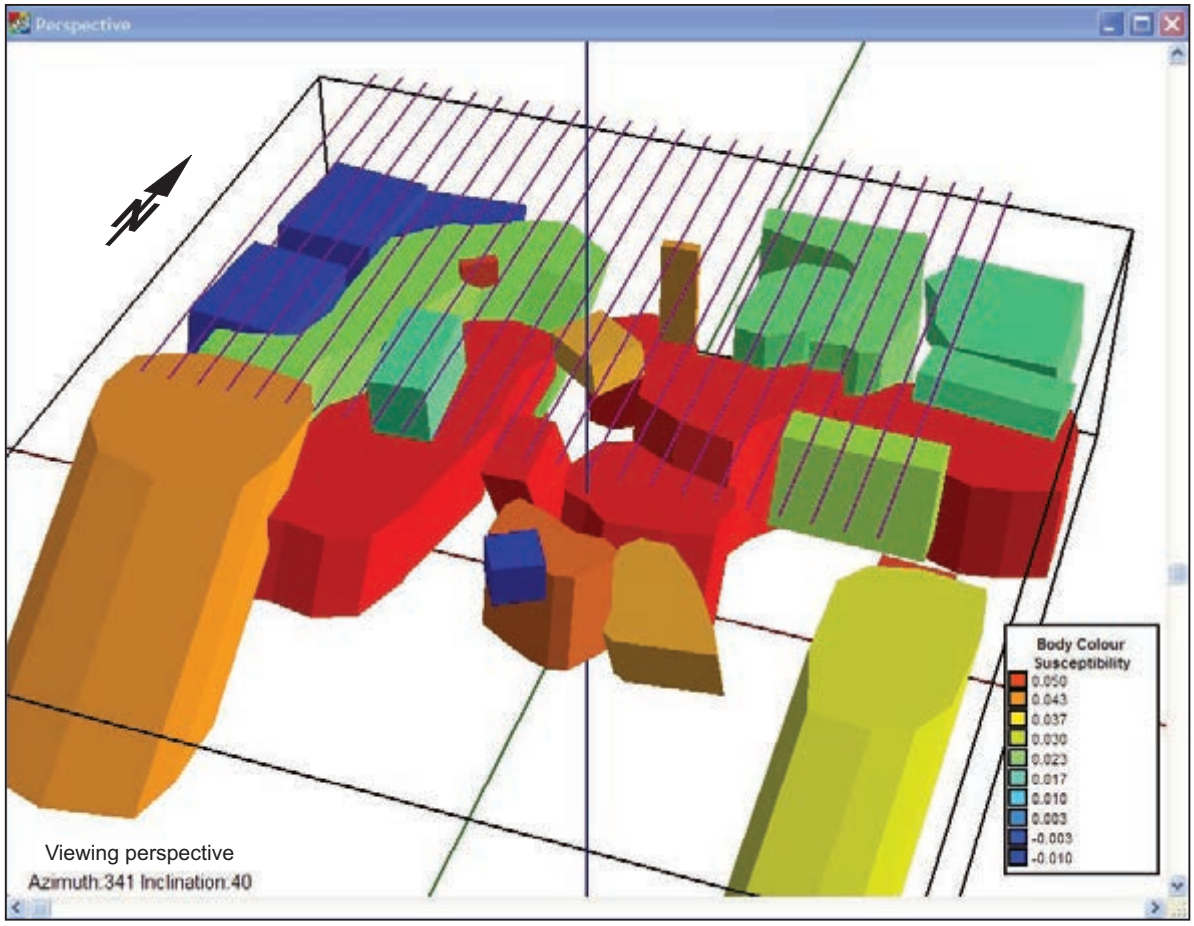

Figure 13.28: Detailed study subarea. Location of initial modelling lines and first-pass 3-D model bodies. Modelling by Z. Shi.

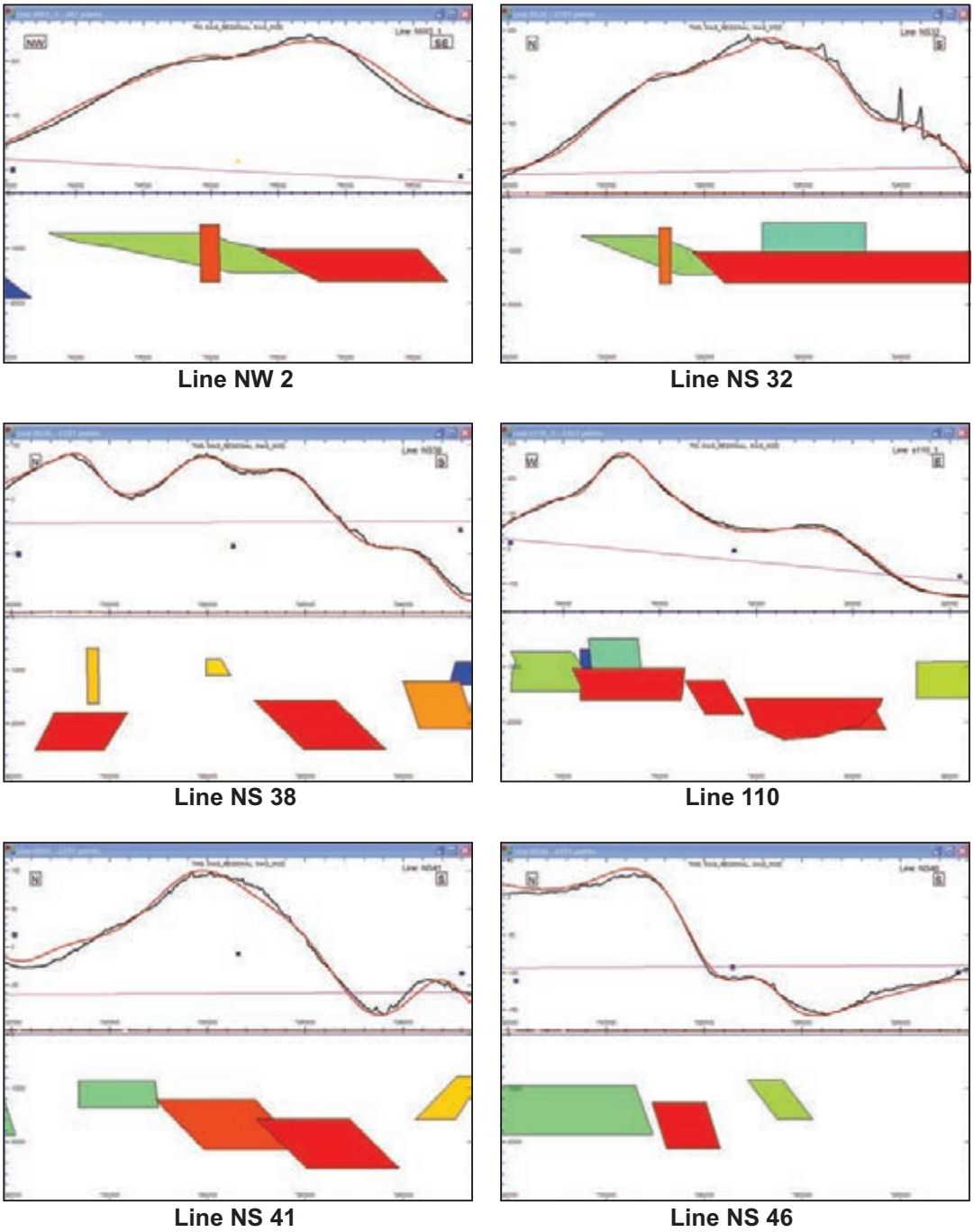

Figure 13.29: Detailed study subarea. Key modelled profiles; see Figure 13.31a for line locations and Figure 13.28 for 3-D geometry and magnetic susceptibility key. The labelled ticks on the vertical depth scale are 10 km apart. Modelling by Z. Shi.

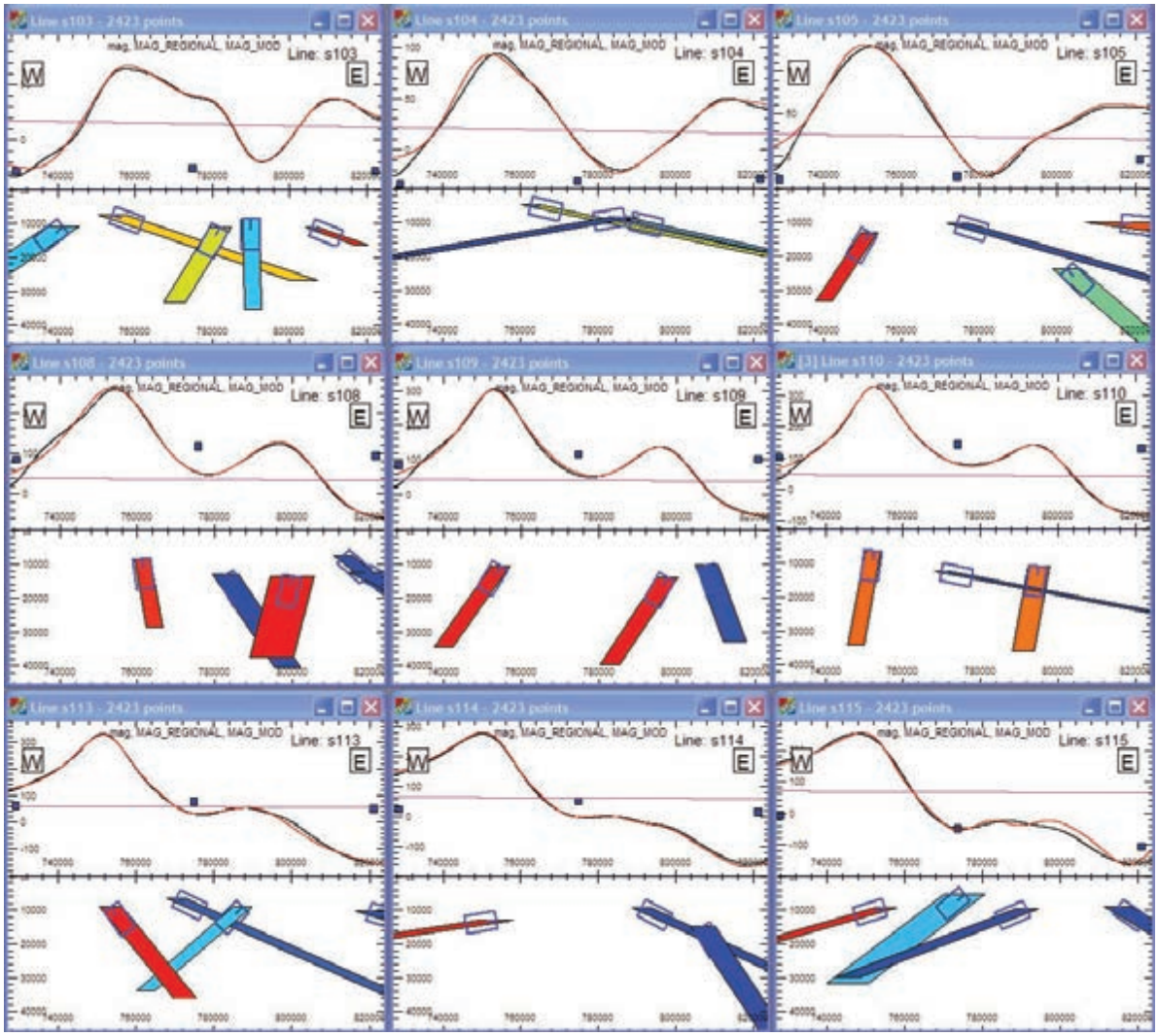

Figure 13.30: Detailed study subarea. Selected E–W section lines processed with AUTOMAG. The symbols depict solutions for 2-D dyke-like bodies, and the corresponding tabular bodies are shown. The black profile line is the measured data, the red line is computed from the tabular models. The line locations are shown with red numbers in Figure 13.31a.

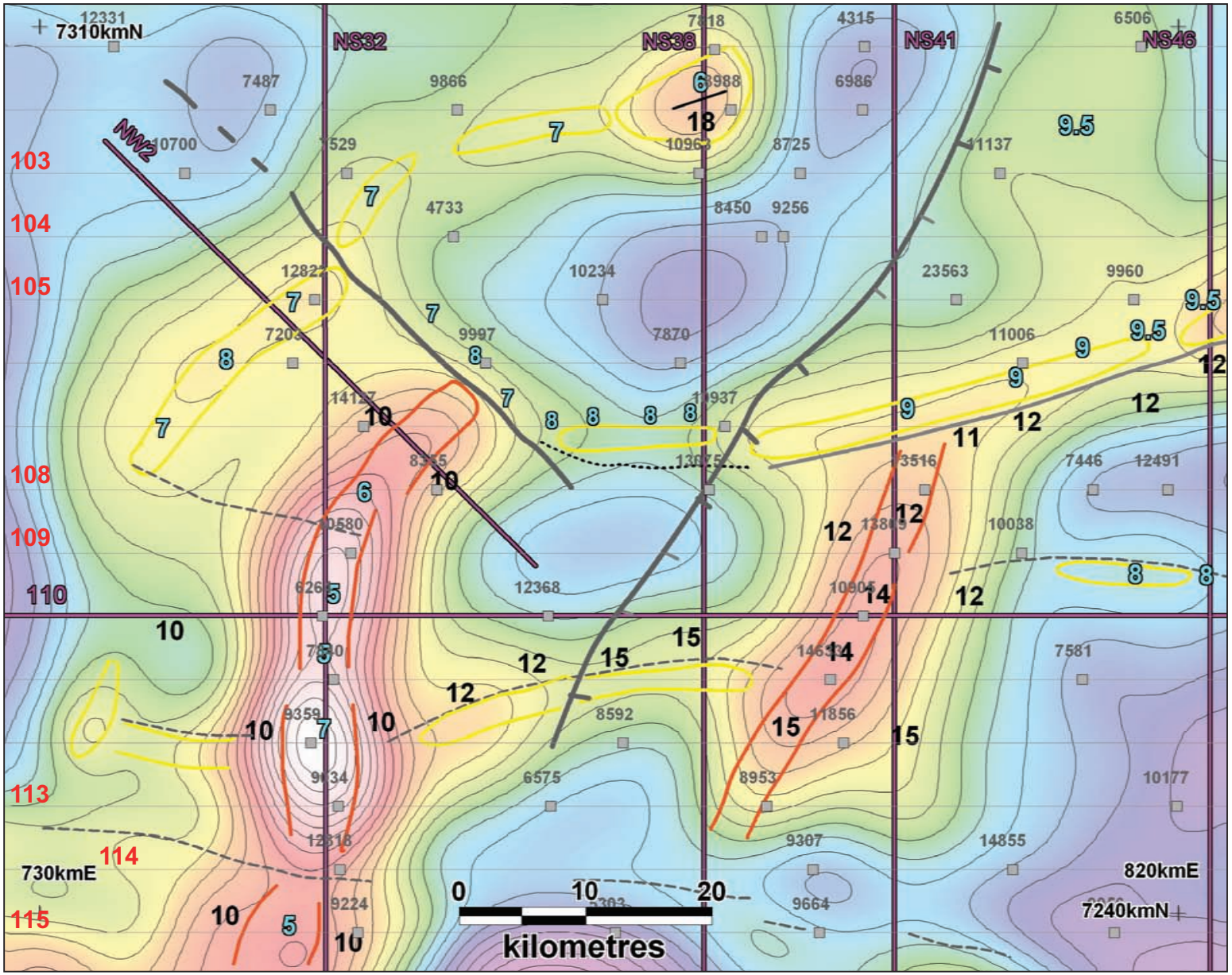

Figure 13.31a: Detailed study subarea. Deep interpretation on 9500 m spectral depth window.

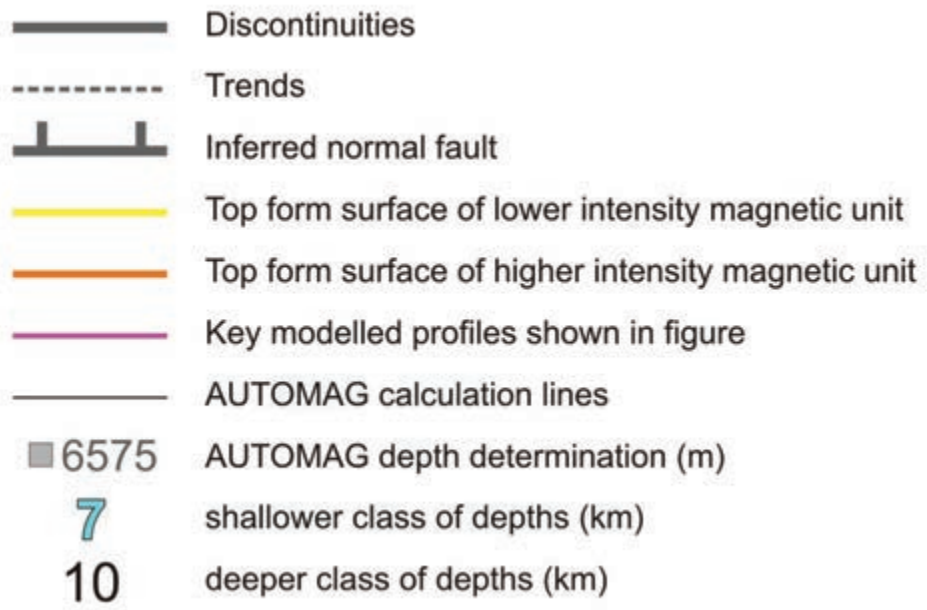

Figure 13.31b: Legend for deep-level interpretation.

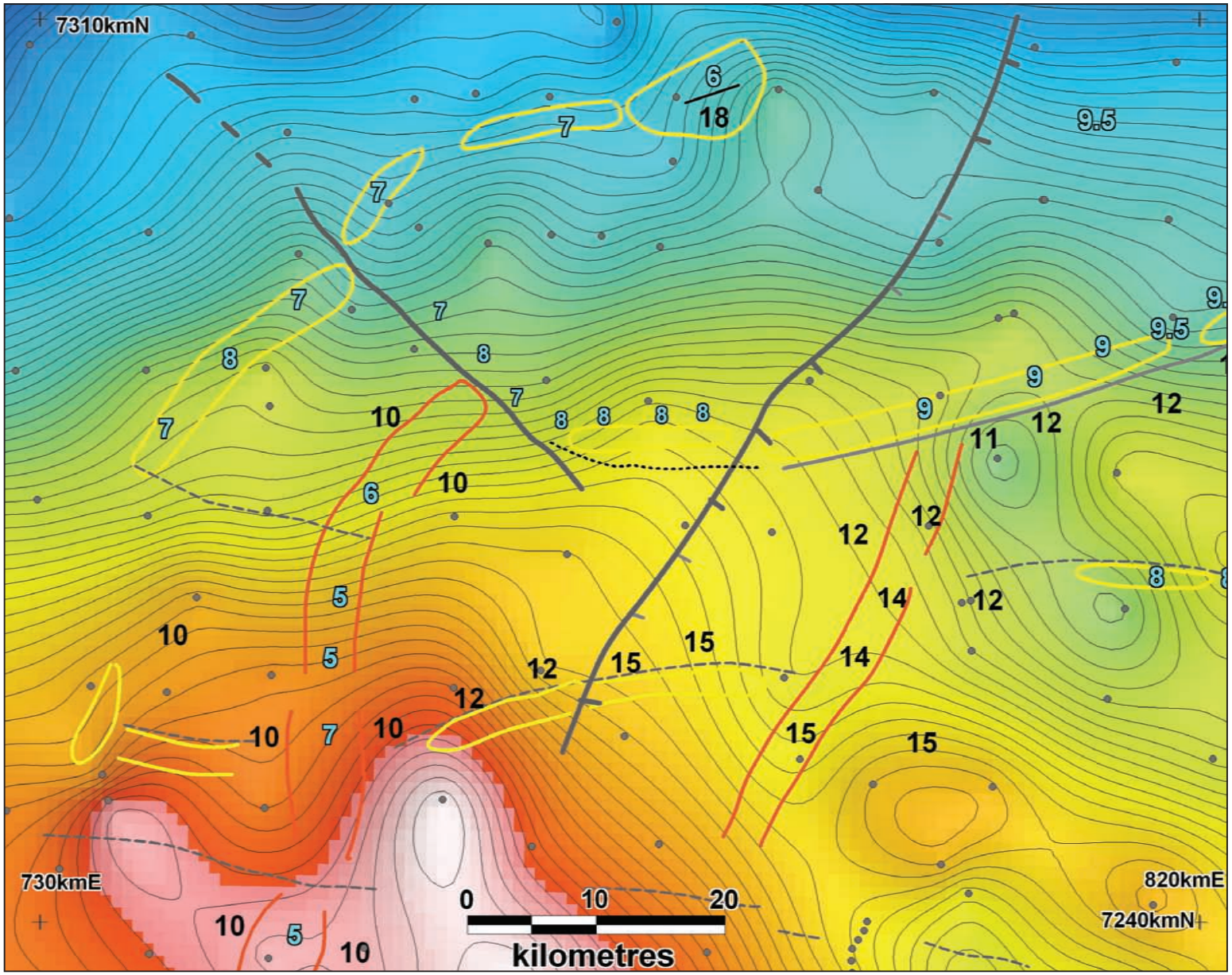

Figure 13.32: Detailed study subarea. Deep interpretation on Bouguer gravity. The grey dots are gravity station locations.

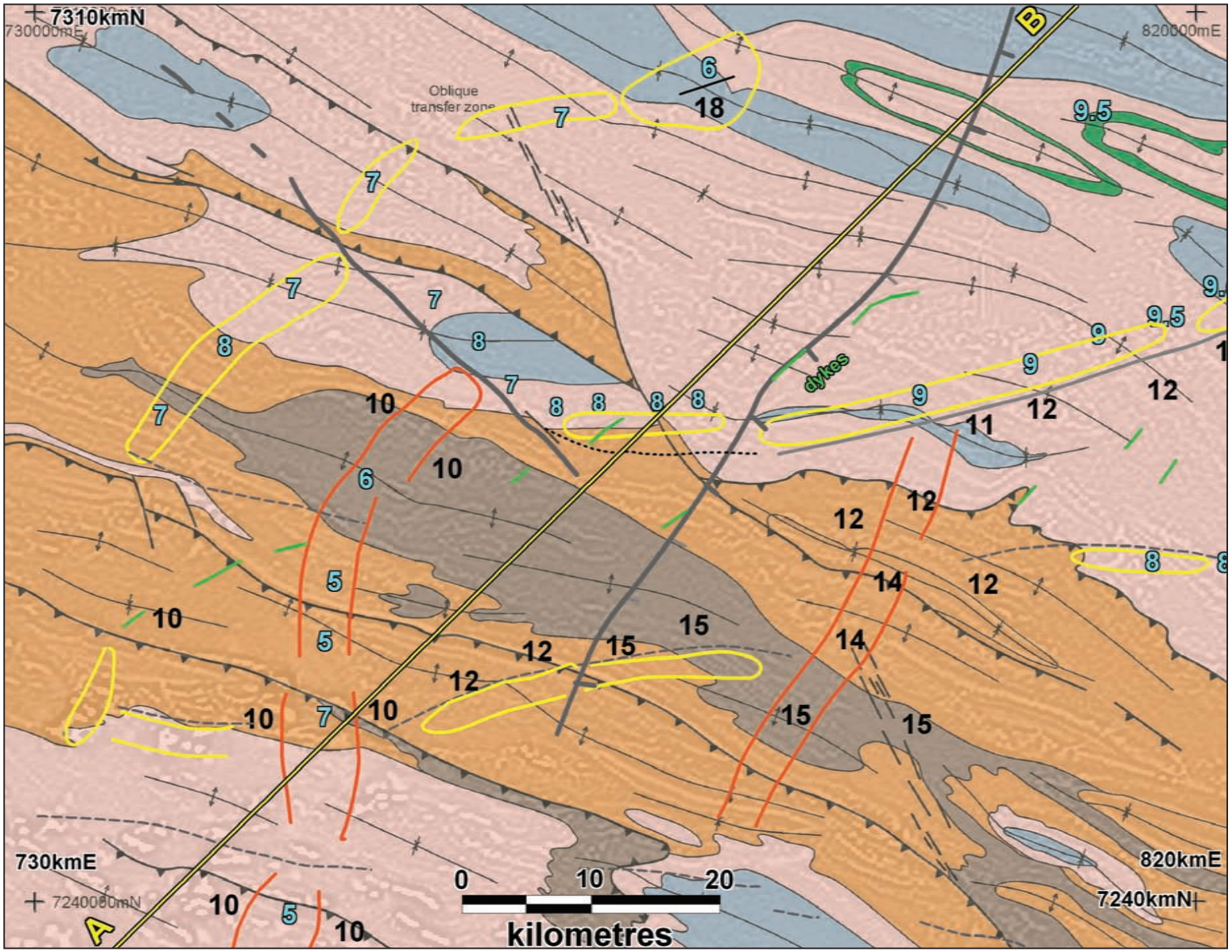

Figure 13.33: Detailed study subarea. Shallow solid geology interpretation and deep structural framework.

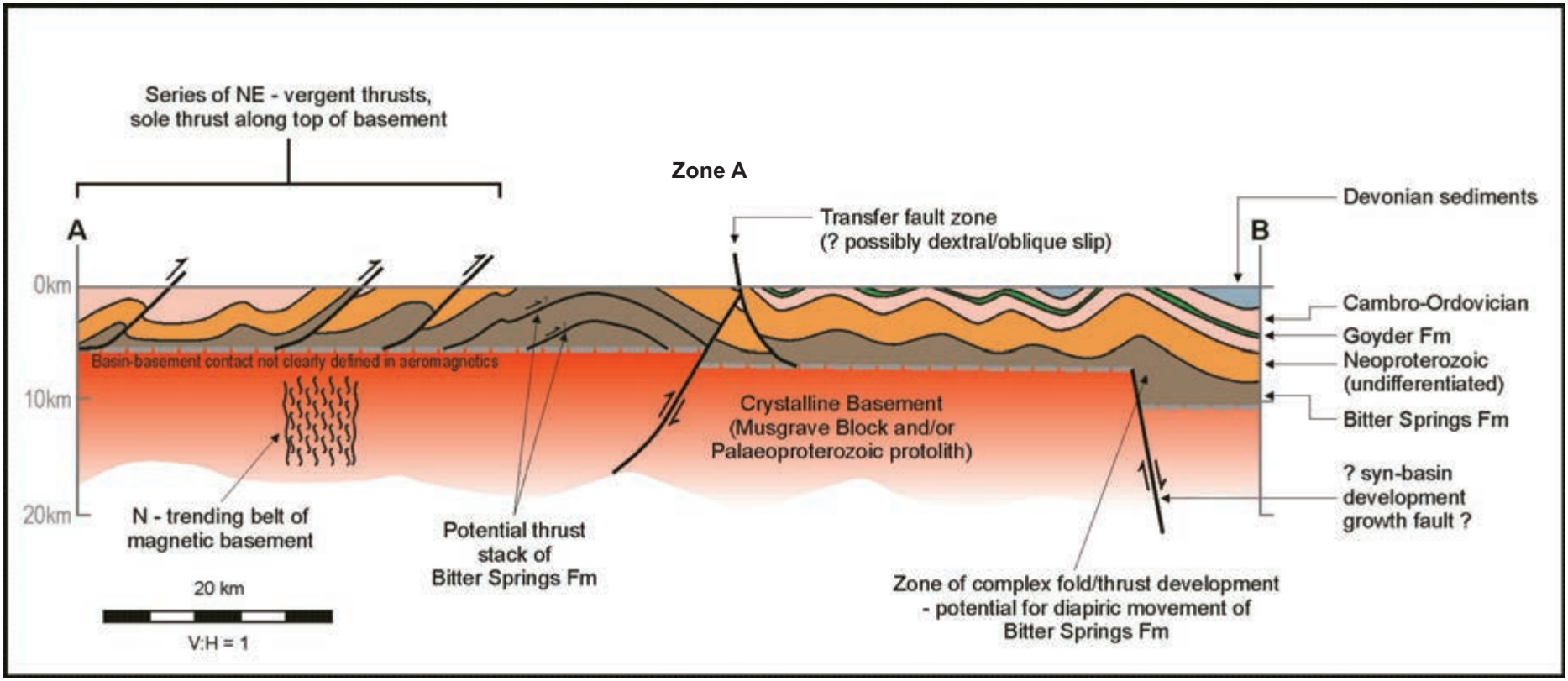

Figure 13.34: Detailed study subarea. Interpreted cross-section A–B.

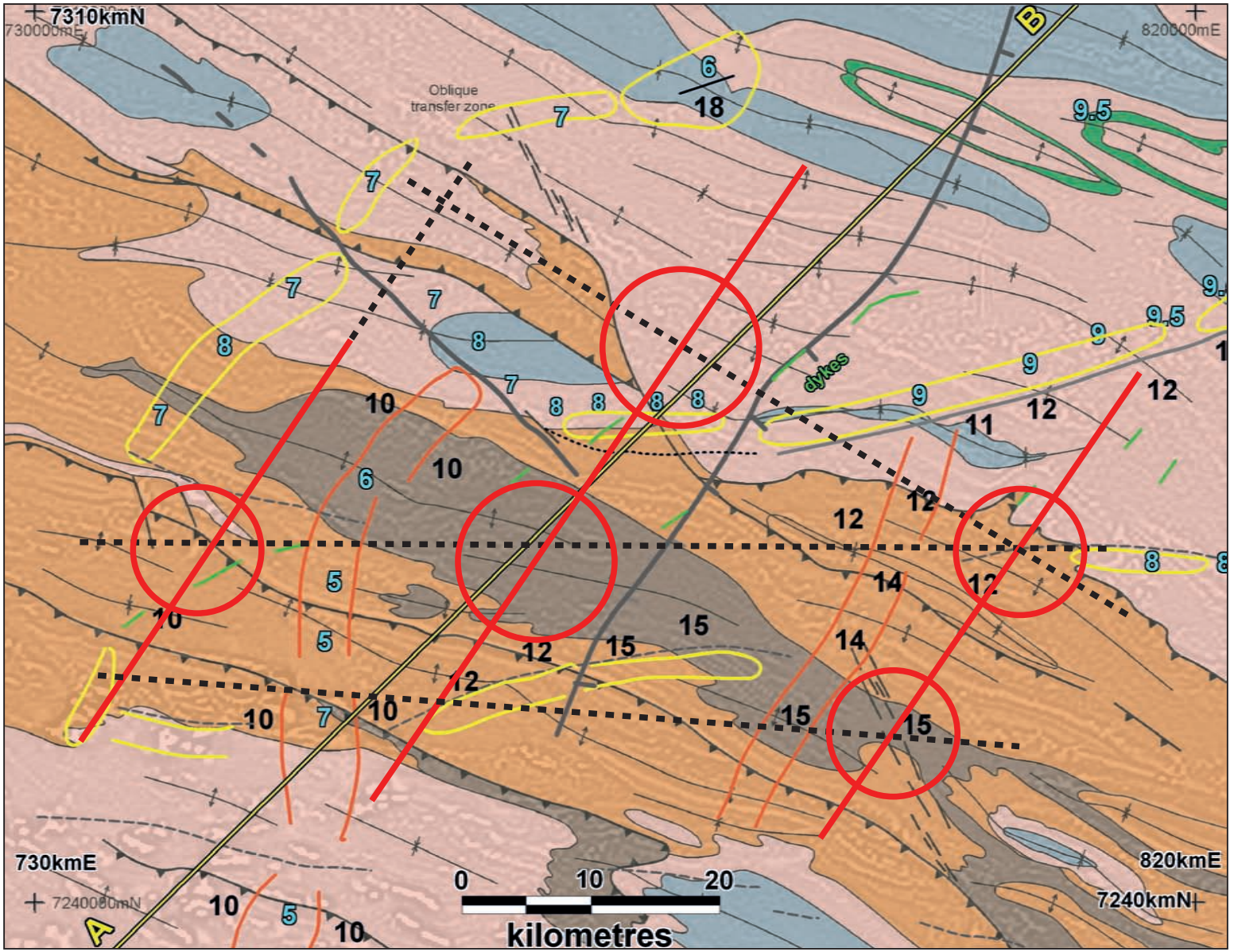

Figure 13.35: Consolidated aeromagnetic interpretation showing target zones and a proposed initial seismic program. The potential structural trap target zones (A–C) are covered with reconnaissance dip lines (red). The dashed blue lines are planned to tie these lines together and to elucidate the deep N–S to NNE-trending magnetic features.

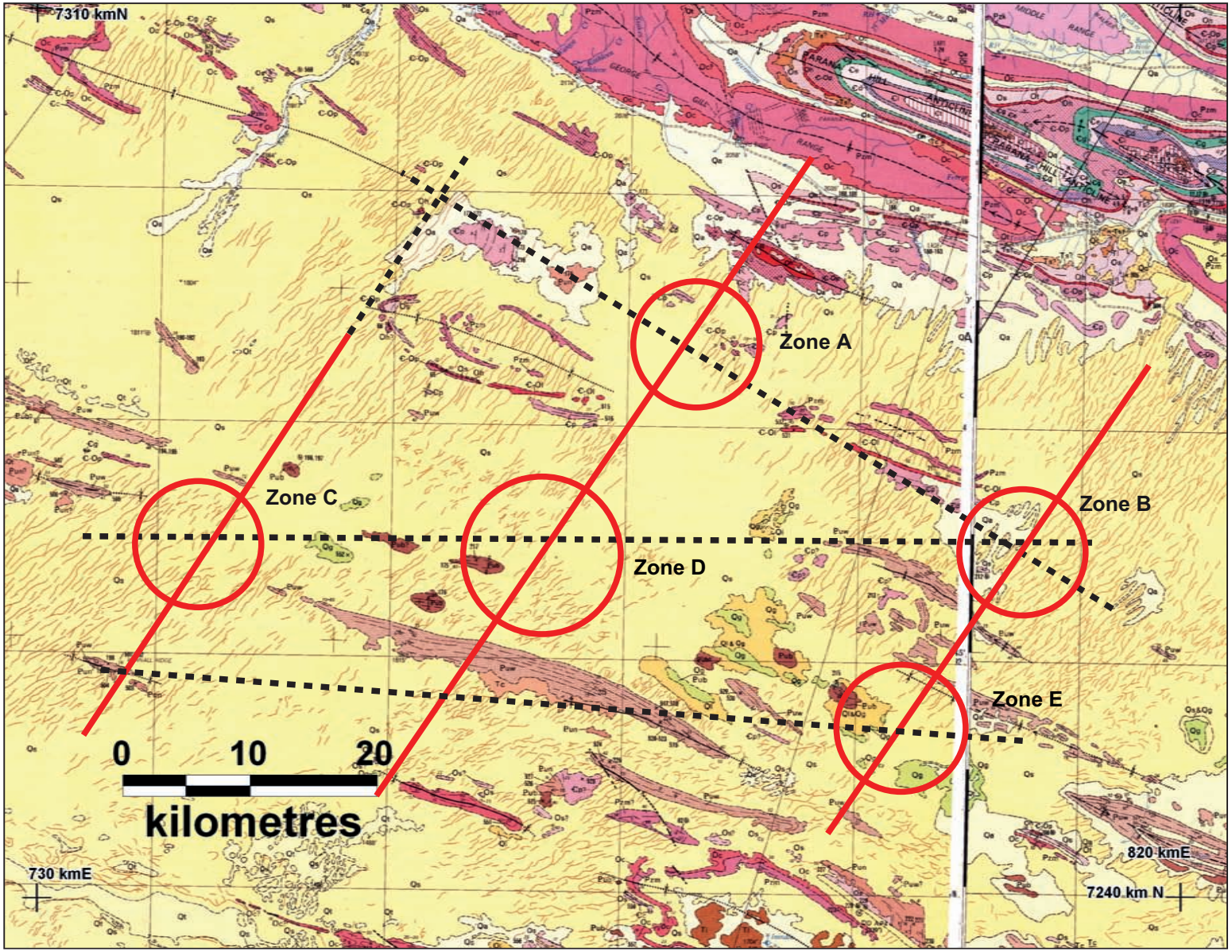

Figure 13.36: Proposed seismic program superimposed on surface geology. The red dip lines are focused on specific target zones. The dashed lines are designed to tie the program together and to provide information on deeper basement structures evident in the aeromagnetics.

References

Aitken AR, Betts PG (2008) High-resolution aeromagnetic data over central Australia assist Grenville-era (1300–1100 Ma) Rodinia reconstructions. *Geophysical Research Letters* **35**, L01306.

Al Azry H, Webster SS, Isles D, Al Zubaidy H, Witham W (1993) Exploration for Cyprus style copper deposits, Sultanate of Oman: a case history. *Exploration Geophysics* **24**(4), 315–322.

Ambrose GJ (2006) Northern Territory of Australia, onshore hydrocarbon potential, 2006. Northern Territory Geological Survey. *Record* **2006–003**.

Anderson H, Nash C (1997) Integrated lithostructural mapping of the Rossing area, Namibia, using high-resolution aeromagnetic, radiometric, Landsat and aerial photographs. *Exploration Geophysics* **28**(2), 185–191.

Anderson H, Jones N, Ameglio L (2006) Reducing seismic risk from the air: utilising airborne geophysics to assist petroleum exploration. *6th Conference and Exposition on Petroleum Geophysics*. 9–11 January, Kolkata. Abstracts. http://www.spgindia.org/conference/6thconf_kolkata06/326.pdf.

Arato B, Posfai M, Dunin-Borkowski RE (2001) Magnetic minerals produced by magnetotactic bacteria. *7th Conference European Ceramic Society*. 9–13 September, Brugges. Abstracts.

Baranov V, Naudy H (1957) Numerical calculation of the formula for reduction to the magnetic pole. *Geophys ics* **22,** 359–383.

Barley M (2009) Evidence for the origin of Palaeoproterozoic banded iron formations in the Hammersley Province of Western Australia. University of Western Australia Centre for Exploration Targeting. February 2009 workshop notes (unpublished).

Barnes SJ (ed.) (2006) *Nickel Deposits of the Yilgarn Craton: Geology, Geochemistry and Geophysics Applied to Exploration*. Society of Economic Geologists Special Publication 13.

Berger Z, Fortin D, Wang X (2004). High-resolution aeromagnetic (HRAM) surveys: exploration applications from the western Canada sedimentary basin – exploration in highly deformed terrains using fixed-wing aircraft and helicopter-mounted systems. *American Association of Petroleum Geology. Search and Discovery Article 40123*.

Bhathal RS (1971) Magnetic anisotropy in rocks. *Earth-Science Reviews* **7**, 227–253.

Bird D (1997) Primer: interpreting magnetic data. *Explorer. Geophysical Corner*, May 1997.

Boyd D (1969) The contribution of airborne magnetic survey to geological mapping. Mining and Groundwater Geophysics 1967. Geological Survey of Canada. *Economic Geology Report* **26**, 213–227.

Boyd A (2009) New generation helicopter time domain systems. A decade in Australia. *New Exploration Technologies Symposium*. Sydney. Abstracts. http://www.smedg.org.au/Sym09/Boyd.pdf.

Boyd DM, Isles DJ 2007. Geological interpretation of airborne magnetic surveys – 40 years on. In *Exploration 07: Fifth Decennial International Conference on Mineral Exploration. Proceedings*. (Ed. B Milkereit) pp. 491–505.

Breiner S (1999) Applications manual for portable magnetometers. GeoMetrics. Unpublished manual. Sunnyvale, California.

Budd AR, Wyborn LAI, Bastrakova IV (2002) The metallogenic potential of Australian Proterozoic granites. *Geoscience Australia Record* 2001/12.

Buddington AF, Lindsay DH (1974) Iron-titanium oxide minerals and synthetic equivalents. *Journal of Petrology* **5**, 310–357.

Bullock S, Isles D (1994) Airborne geophysics in Western Australia. In *Geophysical Signatures of Western Australian Mineral Deposits*. (Eds MC Dentith, KF Frankcombe, SE Ho, JM Shepherd, DI Groves and A Trench) pp. 85–103. Australian Society of Exploration Geophysicists. Special Publication 7.

Burgess JM, Johnstone AL, Schaefer BF, Brescianini RF, Tingate PR (2002) New perspectives of the Amadeus Basin, Northern Territory. *Petroleum Exploration Society of Australia Journal* **29**, 14–23.

Butler RF (2004) Palaeomagnetism: magnetic domains to geologic terranes. Electronic edition, September 2004. www .pmc.ucsc.edu/~njarboe/pmagresource/ButlerPaleomagnetismBook.pdf.

Campbell WH (1997) *Introduction to Geomagnetic Fields*. Cambridge University Press, Cambridge.

Campbell JB (2002) *Introduction to Remote Sensing*. Guilford Press, New York.

Campbell I (2011) Separation filtering of Geoscience Australia gridded data, Amadeus Basin, Northern Territory. Unpublished report.

Campbell I, Saul S, Isles D, Pridmore D (1992) Case studies in the application of the reduction to pole operator in aeromagnetic surveys. *9th Geophysical Conference and Exhibition Handbook*. Abstracts, pp. 25–26. Australian Society of Exploration Geophysicists.

Camus F, Sillitoe RM, Petersen R (1996) *Andean Copper Deposits: New Discoveries, Mineralization, Styles and Metallogeny*. Society of Economic Geologists. Special Publication 5.

Central Petroleum Ltd (2011) Annual Report to Shareholders. ASX Melbourne.
Chinner GA (1960) Pelitic gneisses with varying ferrous/ferric ratios from Glen Clora, Angus, Scotland. *Journal of Petrology* **1**, 178–217.
Clark D (1997) Magnetic petrophysics and magnetic petrology: aids to geologic interpretation of magnetic surveys. *Australian Geological Survey Organisation. Journal of Australian Geology and Geophysics* **17**(2), 83–104.
Clark DA, Emerson DW (1999) Self-demagnetisation. *Preview*, April–May, 22–25.
Clark DA, Schmidt PW (1994) Magnetic properties and magnetic signatures of BIFs of the Hamersley Basin and Yilgarn Block, Western Australia. *Exploration Geophysics* **25**(3), 169–169.
Corbett G (2009) Geological models in epithermal – porphyry exploration: Terry Leach's legacy. *Geological Society of Australia. Specialist Group in Economic Geology. Newsletter* **1–2**, 3–14.
Corbett G, Leach T (1998) *Southwest Pacific Rim Gold – Copper Systems: Structure, Alteration and Mineralization.* Society of Economic Geologists. Special Publication 6.
Core D, Buckingham A, Belfi ld S (2009) Report on structural analysis: detailed analysis of magnetic data – done quickly and objectively. *Geological Society of Australia. Specialist Group in Economic Geology. Newsletter* **1–2**, 15–20.
Corner B, Wilsher WA (1989) Structure of the Witwatersrand Basin derived from interpretation of aeromagnetic and gravity data. In *Exploration '87. Proceedings.* (Ed. GD Garland) pp. 532–546.
Cowan D, Cowan S (1993) Separation filtering applied to aeromagnetic data. *Exploration Geophysics* **24**(4), 429–436.
Cowan D, Dentith M (2003) Appendix: data processing and presentation. In *Geophysical Signatures of South Australian Mineral Deposits.* (Ed. M Dentith) pp. 283–289. Australian Society of Exploration Geophysicists. Special Publication 12.
Cudahy T, Jones M, Thomas M, Laukamp C, Caccetta M, Hewson R, Rodger A, Verrall M (2008) Next generation mineral mapping: Queensland airborne HyMap and satellite ASTER surveys 2006–2008. CSIRO Report P2007/364.
Dentith M, Cowan D (2009) Using potential fi ld data for petroleum exploration targeting, Amadeus Basin, Australia. 11th International Congress, Salvador. Extended Abstracts, pp. 1–4. Brazilian Geophysical Society.
Department of Mines and Petroleum (2010) *Petroleum in Western Australia, September 2010.* Department of Mines and Petroleum. Perth, Western Australia.
Dobrin MB, Savit CH (1988) *Introduction to Geophysical Prospecting.*4th edn. McGraw-Hill, New York.
Doyle E, Bowden AA, Jones GV, Stanley G (1992) The geology of the Galmoy Zn-Pb deposits, Co. Kilkenney. In *The Irish Mineral Industry 1980–1990.* (Eds AA Bowden, G Earls, PG O'Connor and JF Pyne) pp. 211–225. Irish Association of Economic Geology, Dublin.
Dransfi ld M (2007) Airborne gravity gradiometry in the search for mineral deposits. In *Exploration in the New Millenium. Decennial Mineral Exploration Conferences*. Toronto. Abstracts. (Ed. B Milkereit) pp. 341–354. http://www.dmec.ca/ex07-dvd/E07/pdfs/20.pdf.
Dunlop DJ, Özdemir Ö (1997) *Rock Magnetism: Fundamentals and Frontiers.* Cambridge University Press, Cambridge.
Edgoose CJ, Camacho A, Wakelin-King GA, Simons BA (1993) *Kulgera, Northern Territory. 1:250 000 Geological Map Series. Explanatory Notes, SG 53–5.* Northern Territory Geological Survey, Darwin.
Eupene GS, Nicholson PM (1990) Iron Blow and Mt Bonnie polymetallic deposits. In *Geology of the Mineral Deposits of Australia and Papua New Guinea.* (Ed. FE Hughes) pp. 751–754. Australian Institute of Mining and Metallurgy.
Farr TG, Rosen PA, Caro E, Crippen R, Duren R, Hensley S, Kobrick M, Paller M, Rodriguez E, Roth L, Seal D, Shaffer S, Shimada J, Umland J, Werner M, Oskin M, Burbank D, Alsdorf D (2007) The Shuttle radar topographic mission. *Reviews of Geophysics* 45: RG2004.
Foss C, McKenzie B (2009) Strategies to invert a suite of anomalies due to remanent magnetisation: an example from the Georgetown area of Queensland. Australian Society of Exploration Geophysicists. Extended Abstracts 2009 (1).
Foss C, McKenzie B (2011) Inversion of anomalies due to remanent magnetisation: an example from the Black Hill Norite of South Australia. *Australian Journal of Earth Sciences* **58**(4), 391–405.
François RK, Poulsen H, Cassidy KF, Hodgson CJ (2005) Gold metallogeny of the Superior and Yilgarn Cratons. In *Economic Geology: One Hundredth Anniversary Volume 1905–2005.* (Eds JW Hedenquist, JFH Thompson, RJ Goldfarb and JP Richards) pp. 1001–1034.
Gabell A, Tuckett H, Olson D (2004) The GT-1A mobile gravimeter. In *Airborne Gravity 2004.* (Ed. RJL Lane). Geoscience Australia. Record 2004/18.
García-Lobón JL, Rey-Moral C (2004) Magnetismo y radiación gamma natural de la República Dominicana. *Boletín Geológico y Minero* **115**(1), 153–168.
Gay SPJr (2004) Glacial till: a troublesome source of near-surface magnetic anomalies. *The Leading Edge* **23**, 542–547.
Geological Survey of Queensland (2000) North-West Queensland mineral province report (GIS and atlas).
Geoscience Australia (2011) Geophysical Archive Data Delivery System (GADDS). http://www.geoscience.gov.au/gadds.
Gibson RI, Millegan PS (eds)(1998) Geologic applications of gravity and magnetics: case histories. Society of Exploration Geophysics Geophysical Reference Series 8. American Association of Petroleum Geology. Studies in Geology 43

Gidley PR (1988) The geophysics of the Trough Tank gold-copper prospect, Australia. *Exploration Geophysics* **19**(2), 76–78.
Grant FS (1985) a Aeromagnetics, geology and ore environments, I. Magnetite in igneous, sedimentary and metamorphic rocks: an overview. *Geoexploration* **23**, 303–333.
Grant FS (1985) b Aeromagnetics, geology and ore environments, II. Magnetite and ore environments. *Geoexplorat ion* **23**, 335–362.
Grant FS, West GF (1965) *Interpretation Theory in Applied Geophysics*. McGraw-Hill, New York.
Grauch VJS, Hudson MR (2007) Guides to the understanding of the aeromagnetic expression of faults in sedimentary basins: lessons learned from the central Rio Grande rift, New Mexico. *Geosphere* **3**(6), 596–623.
Grauch VJS, Hudson MR (2011) Aeromagnetic anomalies over faulted strata. *The Leading Edge* **30,** 1242–1252.
Groves DI, Barley ME, Ho SE (1989) Nature, genesis and tectonic setting of mesothermal gold mineralisation in the Yilgarn Block, WA. In *The Geology of Gold Deposits: The Perspective in 1988.* (Eds RR Keays, WHR Ramsay and DI Groves). Economic Geology Monograph 6.
Gunn PJ (1997) a Quantitative methods for interpreting aeromagnetic data: a subjective review. *Journal of Australian Geology and Geophysics* **17**(2), 105–113.
Gunn PJ (1997) b Application of aeromagnetic surveys to sedimentary basin studies. *Journal of Australian Geology and Geophysics* **17**(2), 133–144.
Gunn PJ (1998) Aeromagnetics locates prospective areas *and* prospects. *The Leading Edge* **17**(1), 67–69.
Gunn PJ, Borodie R, Mackey T, O'Brien GW (1995) Evolution and structuring of the Joseph Bonaparte Gulf as delineated by aeromagnetic data. *Exploration Geophysics* **26**, 255–261.
Guo WW, Li Z-X, Dentith MC (2011) Magnetic petrophysical results from the Hamersley Basin and their implications for interpretation of magnetic surveys. *Australian Journal of Earth Sciences* **58**, 317–333.
Haederle M (1992) The resolving power of the aeromagnetic method. World Geoscience Corporation. Perth, Western Australia. Unpublished report.
Haggerty SE (1976) Oxidation of opaque mineral oxides in basalts. In *Oxide Minerals*. (Ed. D Rumble). Short course notes, Hg 1–Hg 100. Mineralogical Society of America.
Haney M, Johnston C, Li Y, Nabighian MN (2003) Envelopes of 2D and 3D magnetic data and their relationship to the analytic signal: preliminary results *SEG Expanded Abstracts* **22**, 596–599.
Hansen DA (1980) Radiometrics: geological applications for portable gamma ray spectrometers. In *Practical Geophysics for the Exploration Geologist.* (Comp. R Van Blaricom). North West Mining Association, Spokane.
Hart J, Freeman H (2003) Geophysics of the Prominent Hill prospect, South Australia. *16th Geophysical Conference.* Adelaide. Extended Abstracts 2003(3), pp. 93–100. Australian Society of Exploration Geophysicists.
Hegarty R (2011) Interpretation of aeromagnetic and gravity data from western New South Wales – identifying basin and basement geology. *Australian Society of Exploration Geophysicists Conference.* Brisbane. Extended Abstracts, pp. 1–4.
Hill RET, Gole MJ, Barnes SJ (1988) Physical volcanology of komatiites. A fi ld guide to the komatiites between Kalgoorlie and Wiluna, Eastern Goldfi lds Province, Yilgarn Block, Western Australia. *Excursion Guide Book* 1. Geological Society of Australia (Western Australia Division).
Hillan D, Foss C (2012) Correction schemes for self-demagnetisation. *Australian Society of Exploration Geophysics, 22nd Conference.* 26–29 February, Brisbane. Extended Abstracts.
Hobbs BE, Means WD, Williams PF (1976) *An Outline of Structural Geology.* John Wiley and Sons, New York.
Hoschke T (2008) Geophysical signatures of copper-gold porphyry and epithermal gold deposits. *Arizona Geological Society Digest* **22**, 85–100.
Hoschke T (2011) Geophysical signatures of copper-gold porphyry and epithermal gold deposits and implications for exploration. ARC Centre of Excellence in Ore Deposits, University of Tasmania.
Hudson MR, Grauch VJS, Minor SA (2008) Rock magnetic characterization of faulted sediments with associated magnetic anomalies in the Albuquerque basin, Rio Grande rift, New Mexico. *Geological Society of America Bulletin* **120**, 641–658.
Hutchins D, Robson D, Wackerle R (2007) The impact of government pre-competitive geophysical data to the exploration community. In *Exploration 07: Fifth Decennial International Conference on Mineral Exploration. Proceedings.* (Ed. B Milkereit) pp. 507–512.
Irvine RJ, Robertson I (1987) Interpretation of airborne geophysical data over the Ok Tedi porphyry copper-gold orebody using image processing techniques. *Exploration Geophysics* **18**(2), 103–107.
Irvine RJ, Smith MJ (1990) Geophysical exploration for epithermal gold deposits *Journal of Geochemical Exploration* **36**, 375–412.
Ishihara S (1977) The magnetite-series and ilmenite-series granitic rocks. *Mining Geology* **27,** 293–305.
Ishihara S (1981) The granitoid series and mineralization. In *Economic Geology 75th Anniversary Volume*. (Ed. BJ Skinner) pp. 458–484.

Isles DJ (1983) A regional geophysical study of the Broken Hill Block, NSW. Unpublished PhD thesis. University of Adelaide.

Isles DJ, Cooke AC (1990) Spatial associations between post-cratonisation dykes and gold deposits in the Yilgarn Block, Western Australia. In *Mafic Dykes and Emplacement Mechanisms.* (Eds AJ Parker, PC Rickwood and DH Tucker). A.A. Balkema, Rotterdam.

Isles DJ, Moody IW (2004) Examples of FALCON® data from diamond exploration projects in Northern Australia. In *Airborne Gravity 2004.* (Ed. RJL Lane). Geoscience Australia Record 2004/18.

Isles DJ, Rankin LR (2011) Geological interpretation and structural analysis of aeromagnetic data. TGT Consulting/ Geointerp unpublished workshop manual (current edition).

Isles DJ, Harman PG, Cunneen JP (1989) The contribution of high resolution aeromagnetics to Archaean gold exploration in the Kalgoorlie region, Western Australia. In *The Geology of Gold Deposits: The Perspective in 1988.* (Eds RR Keays, WHR Ramsay and DI Groves). *Economic Geology Monograph* **6**, 389–397.

Isles DJ, Cook A, Hallberg JA (1990) Aeromagnetic evaluation. In *Gold Deposits of the Archaean Yilgarn Block Western Australia: Nature, Genesis and Exploration Guides.* (Eds SE Ho, DI Groves and JM Bennett). Geology Key Centre and University Extension, University of Western Australia. Department of Geology Publication 20, 342–347.

Isles DJ, Saul SJ, Spencer GA (1992) Relationships between geological resolution and flight line spacing in low level aeromagnetic surveys. *Sampling Practices in the Minerals Industry Conference. Proceedings.* Brisbane. pp. 67–72. Australian Institute of Mining and Metallurgy.

James PR (1975) A deformation study across the northern margin of the Limpopo Belt, Rhodesia. Unpublished PhD thesis. University of Leeds.

Jessell MW (2002) *The Atlas of Structural Geophysics II. Journal of the Virtual Explorer.* Vol. 5. http://virtualexplorer .com.au.

Kligfi ld R, Lowrie W, Dalziel IWD (1977) Magnetic susceptibility anisotropy as a strain indicator in the Sudbury Basin, Ontario. *Tectonophysics* **40**, 287–308.

Korhonen JV, Fairhead JD, Hamoudi M, Hemant K, Lesur V, Mandea M, Maus S, Purucker M, Ravat D, Sazonova T, Thebault E (2007) *Magnetic Anomaly Map of the World. 1:50,000,000 scale.* 1st edn. Commission for the Geological Map of the World, Paris. http://www.cidpusa.org/map.htm.

Korsch RJ, Kennard JM (1991) Geological and geophysical studies in the Amadeus Basin. Bureau of Mineral Resources, Canberra. Bulletin 236.

Lane R (2004) Integrating ground and airborne data into regional gravity compilations. In *Airborne Gravity 2004.* (Ed. RJL Lane). Geoscience Australia Record 2004/18.

Laukamp C, Caccetta M, Cia J, Cudahy T, Gessener K, Haest M, Liu YC, Ong C, Rodger A (2010) The uses, abuses and opportunities for hyperspectral technologies and derived geoscience information. Australian Institute of Geoscientists. Bulletin 51.

Li X (2006) Understanding 3D analytic signal amplitude *Geophysics* **71**(2), L13–L16.

Lindsay JF, Korsch RJ (1991) The evolution of the Amadeus Basin, central Australia. In *Geological and Geophysical Studies in the Amadeus Basin, Central Australia.* (Eds RJ Korsch and JM Kennard). Bureau of Mineral Resources, Canberra. Bulletin 236, 7–32.

Lowther JM, Balding AB, McEvoy FM, Dunphy S, MacEoin P, Bowden AA, McDermott P (2003) The Galmoy Zn-Pb orebodies; structure and metal distribution – clues to the genesis of the deposits. In *Europe's Major Base Metal Deposits.* (Eds JG Kelly, CJ Andrew, JU Ashton, MB Boland, G Earls, L Fusciardi, G Stanley) pp. 437–454. Irish Association of Economic Geology.

Marshall T (2004) A review of the source rocks in the Amadeus Basin. Northern Territory Geological Survey. *Record* **2004–008**.

McIntyre JI (1980) Geological significance of magnetic patterns related to magnetite in sediments and metasediments – a review. *Australian Society of Exploration Geophysics. Bulletin* **11**, 19–33.

Merrill RT, McElhinny MW (1983) *The Earth's Magnetic Field.* Academic Press, New York.

Miller HG, Singh V (1994) Potential fi ld tilt – a new concept for location of potential fi ld sources. *Journal of Applied Geophysics* **32**, 213–217.

Milligan PR, Gunn PJ (1997) Enhancement and presentation of airborne geophysical data. *Journal of Australian Geology and Geophysics* **17**(2), 63–75.

Minty BRS (1991) Simple micro-levelling for aeromagnetic data. *Exploration Geophysics* **22**, 591–592.

Moore DH (1997) A geological interpretation of the geophysical data for the Ouyen 1:250 000 map sheet area. Department of Natural Resources and Environment. Victorian Initiative for Minerals and Petroleum. Report 39.

Moore DH (2004) St Arnaud 1:250 000 map: a geological interpretation of the geophysical data. Department of Natural Resources and Environment. Victorian Initiative for Minerals and Petroleum. Report 82.

Morgan R (1998) Magnetic anomalies associated with the North and South Morcombe Fields, U.K. In *Geologic Applications of Gravity and Magnetics: Case Histories*. (Eds RI Gibson and PS Millegan). Society of Exploration Geophysics. Geophysical Reference Series 8: American Association of Petroleum Geology. *Studies in Geology* **43**, 85–91.

Mørk MBE, McEnroe SA, Olesen O (2002) Magnetic susceptibility of Mesozoic and Cenozoic sediments off mid Norway and the role of siderite: implications for interpretation of high-resolution aeromagnetic anomalies. *Marine and Petroleum Geology* **19**, 1115–1126.

Morrell A (2004) Geophysical characteristics of low-sulphidation epithermal gold-silver deposits in the Waihi-Waitekauri region, New Zealand. Unpublished MSc thesis. University of Auckland, New Zealand.

Morrell A, Locke CA, Cassidy J, Mauk JL (2011) Geophysical characteristics of adularia-sericite epithermal gold-silver deposits in the Waihi – Waitekauri region, New Zealand. *Economic Geology and the Bulletin of the Society of Economic Geologists* **106**, 1031–1041.

Moskowitz BM (1991) Hitchhiker's guide to magnetism. Institute for Rock Magnetism, University of Minnesota. www .irm.umn.edu/hg2m/hg2m_index.html.

Munroe S, Ham A, Griffi S (2004) Amadeus Basin SEEBASE™ Project. Northern Territory Geological Survey. *Record* **2004–010**.

Musgrave RJ, Grewar J, Vega M (2006) Significance of remanence in Stawell goldfi ld aeromagnetic anomalies. *Australian Journal of Earth Sciences* **53**, 783–797.

Musgrave R, Poudjom Djomani YP, Greenfi ld J, Hegarty R, Sick S (2007) Potenial fi ld 'worms' and models as the basis of a 3D tectonic model of the Koonenberry Belt, north-western NSW. *Australian Society of Exploration Geophysicists Conference*. Perth. Extended Abstracts, pp. 1–3.

Nabighian MN (1972) The analytic signal of two-dimensional magnetic bodies with polygonal cross-section: its properties and use for automated anomaly interpretation. *Geophysics* **37**, 507–517.

Nabighian MN, Grauch VJS, Hansen RO, LaFehr TR, Li Y, Peirce JW, Phillips JD, Ruder ME (2005) The historical development of the magnetic method in exploration. *Geophysics* **70**(12), 33ND–61ND.

Naudy H (1971) Automatic determination of depth on aeromagnetic profiles *Geophysics* **36**(4), 717–722.

Needham RS, De Ross GJ (1990) Pine Creek Inlier – regional geology and mineralisation. In *Geology of the Mineral Deposits of Australia and Papua New Guinea*. (Ed. FE Hughes) pp. 727–738. Australian Institute of Mining and Metallurgy.

Norman C (1993) New developments in the aeromagnetic technique for sedimentary basin exploration. *Preview* **42**, 11–16.

Norman C (2011) Personal communications to authors concerning aeromagnetics in sedimentary basins.

Oldenburg DW, Pratt DA (2007) Geophysical inversion for mineral exploration: a decade of progress in theory and practice. *Exploration in the New Millenium. Decennial Mineral Exploration Conference. Proceedings.* Toronto. (Ed. B Milkereit). http://www.dmec.ca/ex07-dvd/E07/pdfs/5.pdf.

Osborne EF (1962) Reaction series for subalkaline igneous rocks based on diffe ent oxygen pressure conditions. *The American Mineralogist* **57**, 211–226.

Paine JW (1986) A comparison of methods for approximating the vertical gradient of one-dimensional magnetic fi ld data. *Geophysics* **51**, 1725–1735.

Pegum DM (1997) An introduction to the petroleum geology of the Northern Territory of Australia. Northern Territory Geological Survey, Darwin.

Poudjom Djomani YP, Musgrave R, Hegarty R (2007) 'Worming' in New South Wales. *Australian Society of Exploration Geophysicists Conference*. Perth. Extended Abstracts 1.

Pratt DA, McKenzie KB, White AS (2012) The remote determination of magnetic remanence. *Australian Society of Exploration Geophysics. 22nd Conference*. 26–29 February, Brisbane. Extended Abstracts.

Prieto C (1996) Gravity/magnetic signatures of various geologic models – an exercise in pattern recognition. *Footnotes on Interpretation. Integrated Geophysics Corporation Footnote Series* 4(4).

Prieto C (1998) Gulf of Mexico continental slope – understanding the magnetic response due to salt intrusion. In *Geologic Applications of Gravity and Magnetics: Case Histories*. (Eds RI Gibson and PS Millegan). Society of Exploration Geophysics. Geophysical Reference Series 8: American Association of Petroleum Geology. *Studies in Geology* **43**, 14–17.

Prieto C, Grow T, Curtis C (1993) Gulf of Mexico continental slope – understanding the magnetic response due to the salt intrusion. Footnotes on Interpretation. Integrated Geophysics Corporation Footnote Series 1(1).

Rajagopalan S (1987) The use of 'automatic gain control' to display vertical magnetic gradient data. *Exploration Geophysics* **18**(2), 166–169.

Rajagopalan S (2003) Analytic signal vs. reduction to pole: solutions for low magnetic latitudes *Exploration Geophysics* **34**(4), 257–262.

Rajagopalan S, Milligan P (1994) Image enhancement of aeromagnetic data using automatic gain control. *Exploration Geophysics* **25**(4), 173–178.

Rajagopalan S, Schmidt P, Clark DA (1993) Rock magnetism and geophysical interpretation of the Black Hill Norite, South Australia. *Exploration Geophysics* **24**(2), 209–212.

Rajagopalan S, Clark DA, Schmidt P (1995) Magnetic mineralogy of the Black Hill Norite and its aeromagnetic and palaeomagnetic implications. *Exploration Geophysics* **26**(3), 215–220.

Rajaram M, Anand SP (2003) Crustal structure of south India from aeromagnetic data. *Journal of the Virtual Explorer* **12**, 72–82.

Ranford LC, Cook PJ, Wells AT, Stewart AJ (1968) *Henbury, Northern Territory. 1:250 000 Geological Map Series.* Geoscience Australia.

Rankin LR, Newton CA (2002) Musgrave Block, central Australia: regional geology from interpretation of airborne magnetic data. Primary Industries and Resources South Australia. Report Book 2002/031.

Reeves C (2005) Aeromagnetic surveys. Principles, practice and interpretation. Geosoft E-publication. www.geosoft .com/media/uploads/resources/technicalpapers/Aeromagnetic_Survey_Reeves.pdf.

Reford MS, Sumner S (1964) Aeromagnetics. *Geophysics* **29**(4), 482–516.

Reid AB (1980) Short note. Aeromagnetic survey design. *Geophysics* **45**, 973–976.

Reynolds RL, Rosenbaum JG, Hudson MR, Fishman NS (1990) Rock magnetism, the distribution of magnetic minerals in the Earth's crust, and aeromagnetic anomalies. *Proceedings of the US Geological Survey Workshop on Geological Applications of Modern Aeromagnetic Surveys.* 6–8 January 1987, Lakewood, Colorado. (Ed. WF Hanna). US Geological Survey Bulletin 1924, pp. 24–45. http://pubs.er.usgs.gov/publication/b1924.

Reynolds RL, Fishman NS, Hudson MR (1991) Sources of aeromagnetic anomalies over Cement oil fi ld (Oklahoma), Simpson oil fi ld (Alaska), and the Wyoming-Idaho-Utah thrust belt *Geophysics* **56**(5), 606–617.

Riedinger N, Pfeifer K, Kasten S, Garming JFL, Vogt C, Hensen C (2005) Diagenetic alteration of magnetic signals by anaerobic oxidation of methane related to a change in sedimentation rate. *Geochimica et Cosmochimica Acta* **69**(16), 4117–4126.

Robinson SH, Belford SM (1991) The Scuddles massive sulphide discovery: an exploration case history. *Exploration Geophysics* **22**(2), 315–320.

Rowe JD (1998) High resolution aeromagnetic data as a salt mapping tool, Genesis Field, Gulf of Mexico. 1998 Society of Exploration Geophysics Annual Meeting. New Orleans. Extended Abstracts.

Rutter H, Esdale DJ (1985) The geophysics of the Olympic Dam discovery. *Exploration Geophysics* **16**(3), 273–276.

Schmidt PW, Clark DA (1998) The calculation of magnetic components and moments from TMI: a case study from the Tuckers igneous complex, Queensland. *Exploration Geophysics* **29**, 609–614.

Schmidt PW, McEnroe SA, Clark DA, Robinson P (2007) Magnetic properties and potential fi ld modelling of the Peculiar Knob metamorphosed iron formation, South Australia: an analog for the source of the intense Martian magnetic anomalies? *Journal of Geophysical Research* **112**, B03102

Sexton M, Morrison GW, Orr TOH, Foley AM, Wormald PJ (1995) The Mt Leyshon magnetic anomaly. *Exploration Geophysics* **26**(3), 84–91.

Shaw RD (1991) The tectonic development of the Amadeus Basin, central Australia. In *Geological and Geophysical Studies in the Amadeus Basin, Central Australia.* (Eds RJ Korsch and JM Kennard). Bureau of Mineral Resources, Canberra. Bulletin 236, pp. 429–461.

Shaw RD, Korsch RJ, Wright C, Goleby BR (1991) Seismic interpretation and thrust tectonics of the Amadeus Basin, central Australia, along the BMR regional seismic line. In *Geological and Geophysical Studies in the Amadeus Basin, Central Australia.* (Eds RJ Korsch and JM Kennard). Bureau of Mineral Resources, Canberra. Bulletin 236, pp. 385–409.

Shi Z (1993) Automatic interpretation of potential fi ld data applied to the study of overburden thickness and deep crustal structures, South Australia. Unpublished PhD thesis. Department of Geology and Geophysics, University of Adelaide.

Shi Z (2010) Enhancement processing of GA 2010 V5 magnetic grid, Amadeus Basin, Northern Territory. FrOG Tech unpublished report.

Shi Z (2011) Magnetic basement depth modelling, detailed area, Amadeus Basin. FrOG Tech unpublished report.

Shi Z, Boyd D (1993) *AUTOMAG* – an automatic method to estimate thickness of overburden from aeromagnetic profiles. *Exploration Geophysics* **24**, 789–794.

Shive PN (1986) Suggestions for the use of SI units in magnetism *Eos, Transactions, American Geophysical Union* **67**(3), 25–26.

Slater KR (2004) *Musgrave Block Special, Northern Territory. Integrated Interpretation of Geophysics and Geology, 1:500 000 Scale Map.* Northern Territory Geological Survey, Darwin and Alice Springs.

Smith PM, Whitehead M (1989) Seismic, gravity and magnetics, a complementary geophysical study of the Palanquin Structure, Timor Sea, Australia. *Exploration Geophysics* **20**, 25–29.

Spector A, Grant FS (1970) Statistical models for interpreting aeromagnetic data. *Geophysics* **35**(2), 293–302.
Spencer GA, Pridmore DF, Isles DJ (1989) Integration of exploration data using colour space on an image processor. *Exploration Geophysics* **20**(2), 31–35.
Stuart-Smith PG, Needham RS, Page RW, Wyborn LAI (1993) Geology and mineral deposits of the Cullen Mineral Field, Northern Territory. *Australian Geological Survey Organisation. Bulletin* **229**, 1–145.
Stuart-Smith PG, Needham RS (1979) *Geology of the Batchelor-Hayes Creek Region. Australian 1:100 000 Geological Map Series*. Bureau of Mineral Resources, Canberra.
Swager CP, Witt WK (1990) *Menzies Geological Map. 1:100 000 Scale Map Series. Sheet 3138*. Geological Survey of Western Australia.
Swager CP, Griffen TJ, Witt WK, Wyche S, Ahmat AL, Hunter WM, McGoldrick PJ (1990) *Geology of the Archaean Kalgoorlie Terrane:an explanatory note*. Geological Survey of Western Australia, Report 48.
Tapley IJ (2002) Radar Imaging. In *Geophysical and Remote Sensing Methods for Regolith Exploration*. (Ed. E Papp). CRCLEME Open File Report 144, pp. 22–32.
Tapponnier P, Peltzer G, Le Dain AY, Armijo R, Cobbold P (1982) Propagating extrusion tectonics in Asia: new insights from simple experiments with plasticine. *Geology* **10**, 611–616.
Tauxe L (2009) Essentials of paleomagnetism. Web edition 1.0 (18 March 2009). http://magician.ucsd.edu/Essentials/.
Thomson S, Fountain D, Watts T (2007) Airborne geophysics – evolution and revolution. *Exploration in the New Millenium. Decennial Mineral Exploration Conferences. Proceedings. Toronto.* (Ed. B Milkereit).
Thundelarra Ltd (ASX code THX) (2011) Annual Report to Shareholders. Australian Stock Exchange, Perth.
Triggs DM (1995) An integrated study of the Golden Dyke Dome, Northern Territory. Unpublished BSc (Hons) thesis. Department of Earth Sciences, Monash University.
Tucker DH (1983) The characteristics and interpretation of regional magnetic and gravity fi lds in the Broken Hill district. *Australasian Institute of Mining and Metallurgy Conference*. Broken Hill, NSW. Extended Abstracts, pp. 81–114.
Turner SP (1991) Late-orogenic, mantle-derived bi-modal magmatism in the southern Adelaide Foldbelt, South Australia. Unpublished PhD thesis. Department of Geology and Geophysics, University of Adelaide.
Urquhart WES (1989) Field examples of controls on magnetite content. *Exploration Geophysics* **20**(2), 93–97.
Urquhart WES, Strangway DW (1985) Interpretation of an aeromagnetic survey of the Qian'an Archean metamorphic rock series in China. *The Utility of Regional Gravity and Magnetic Anomaly Maps. Society of Exploration Geophysicists Conference. Proceedings*. Tulsa. (Ed. WJ Hinze) pp. 439–449.
Wall VJ (2005) TAG: thermal aureole (pluton-related) gold systems. *Australian Institute of Geoscientists. AIG News. Quarterly Newsletter* **79**, 1–7.
Webb M, Rowston P (1995) The geophysics of the Ernest Henry Cu-Au deposit (NW) Qld. *Exploration Geophysics* **26**, 51–59.
Wells AT, Ranford LC, Cook PJ, Stewart AJ, Forman DJ (1968) *Lake Amadeus, Northern Territory. 1:250 000 Geological Map Series*. Geoscience Australia.
Wells AT, Forman DJ, Ranford LC, Cook PJ (1970) Geology of the Amadeus Basin, central Australia. Bureau of Mineral Resources, Canberra. Bulletin 100.
White AJR, Chappell BW (1988) Granites. In *Geology of Victoria*. (Eds JG Douglas and JA Ferguson) pp. 427–439. Geological Society of Australia, Victorian Division, Melbourne.
Whiting TH (1986) Aeromagnetics as an aid to geological mapping – case history from the Arunta Inlier, Northern Territory, Australia. *Australian Journal of Earth Sciences* **33**, 271–286.
Witt WK (1993) Gold mineralisation of the Menzies-Kambalda Region, Eastern Goldfi lds, Western Australia. Geological Survey of Western Australia. Report 39.
Wones DR, Eugester HP (1965) Stability of biotite: theory and application. *The American Mineralogist* **50**, 1228–1272.
Wyborn L, Jagodzinski E, Bastrakova I, Budd A (2001) Pine Creek Inlier synthesis. In *The Metallogenic Potential of Australian Proterozoic Granites*. (Ed. AR Budd). Geoscience Australia. Record 2001/012.
Young IF, Ambrose GJ (2005) Petroleum geology of the southeastern Amadeus Basin: the search for sub-salt hydrocarbons. *Central Australian Basins Symposium. Proceedings*. (Eds TJ Munson and GJ Ambrose). Northern Territory Geological Survey, Darwin and Alice Springs.
Young DN, Duncan N, Camacho A, Ferenczi PA, Madigan TLA (2002) *Ayers Rock, SG 52–8. 1:250 000 Geological Map Series*. 2nd edn. Northern Territory Geological Survey, Darwin and Alice Springs.